UNIVERSITY OF SOUTHAMPTON

FACULTY OF ENGINEERING AND THE ENVIRONMENT

Materials and Surface Engineering

Biomechanical analysis of the lower limb amputee socket interface

by

Jinghua Tang

Primary Supervisor: Professor Liudi Jiang

Co-Supervisor: Professor Dan Bader

Industrial Supervisor: Dr David Moser

Thesis for the degree of Doctor of Philosophy

March 2018

ABSTRACT

FACULTY OF ENGINEERING AND THE ENVIRONMENT
Materials and Surface Engineering

Doctor of Philosophy

BIOMECHANICAL ANALYSIS OF THE LOWER LIMB AMPUTEE SOCKET INTERFACE

The lower limb prosthetic socket provides a critical interface, which transfers loads between the ground and the residuum. Many amputees report issues related to residuum pain primarily induced by poor socket fit, leading to unsatisfactory rehabilitation outcomes. From a scientific perspective, residuum and socket have been treated as a rigid body. Effective methods, which could provide quantitative measurements of multi-directional loads (i.e. the kinetics) and relative motion (i.e. kinematics) at the residuum/socket interface, are not currently available. The *in-situ* measurement of kinematic and kinetic parameters and indeed their correlations during amputee walking would help to obtain a comprehensive understanding of the biomechanics at the critical residuum/socket interface.

In this thesis, means of assessing residuum/socket interface mechanics has been developed, incorporating the kinematics and kinetics, to comprehend the interface biomechanics. A novel kinematic model was developed to evaluate the interface kinematics based on a 3D motion capture system. The model was applied on both knee disarticulation and trans-tibial participants. Repeatable interface kinematic waveforms (coefficient of multiple correlation of up to 0.988) were obtained on level walking studies over a 2-year period. The model is highly sensitive to walking speed, terrain and prosthetic components. For example, a 21% of increase in walking speed led to an increase in angular and axial displacements of approximately 23% and 6%, respectively. In addition, a novel tri-axial pressure and shear (TRIPS) sensor system, capable of measuring both dynamic pressure and shear stresses, was used to evaluate the interface kinetics as a function of gait cycle (GC). The multi-directional stresses obtained from key loading bearing locations of the residuum suggested that the interface loading is dependent on walking speed, terrain, prosthetic components and socket suspension system. For example, changes to the latter by the removal of one sock resulted in a reduction of the stresses at the proximal location of approximately 30% and an increase of stresses at the distal location of the residuum of up to 28%. Subsequently, the combination of the novel kinematic model and the body interface sensor system was applied to study their correlation, providing a first-of-its-kind approach which shed light on the in-situ interface biomechanics. The method for assessing socket interface mechanics established here therefore provides a stepping stone to quantitatively assist in the socket fitting process and the monitoring of residuum tissue health.

By Jinghua Tang

Contents

List of Figures

List of Tables

Declaration of Authorship

I, Jinghua Tang, declare that the thesis entitled *Biomechanical assessment at residuum/socket interface for lower limb amputees* and the work presented in the thesis are both my own, and have been generated by me as the result of my own original research.

I confirm that:

- This work was done wholly or mainly while in candidature for a research degree at the University;
- Where any part of this thesis has previously been submitted for a degree or any other qualification at this University or any other institution, this has been clearly stated;
- Where I have consulted the published work of others, this is always clearly attributed;
- Where I have quoted from the work of others, the source is always given. With the exception of such quotations, this thesis is entirely my own work;
- I have acknowledged all main sources of help;
- Where the thesis is based on work done by myself jointly with others, I have made clear exactly what was done by the others and what I have contributed myself;
- Parts of this work have been published as:

Signed:.....

Date:.....

Acknowledgements

I would like to express my gratitude to my supervisors, Professor Liudi Jiang (primary supervisor), Professor Dan Bader (co-supervisor), and Dr. David Moser (industry supervisor) for their excellent management of the project, advice and support.

I would like to thank Chas. A Blatchford and Sons Ltd., the industrial partner of their project, for continuous help and support throughout this project. In particular, I would like to express my sincere gratitude to Dr. David Moser, your expertise was invaluable for this project. I also would like to thank Mr. Joe McCarthy for sharing the clinical knowledge in the field of prosthetics and Mr. Richard Bradbury for his assistance in amputee walking tests in the gait laboratory.

In addition, I would like to thank the team in the University of Southampton – my colleagues and friends – Dr. Michael McGrath, Dr. Piotr Laszczak, Dr. Jiangliang Gao, Dr. Maria Valero and Mr. Nick Hale. In particular, I would like to thank Dr. Piotr Laszczak for the contribution of the TRIPS sensor system, Dr. Michael McGrath for sharing the expertise in amputee walking tests, Dr. Jianliang Gao for helping with testing the TRIPS sensor system and development of the data acquisition software, Mr. Nick Hale for assisting design improvement of the TRIPS sensor system, Dr. Maria Valero for providing her expertise on signal processing.

I also would like to thank the technicians: Dr. Andrew Robinson (Testing and Structures Research Laboratory laboratory), Mr. Dave Beckett and Ms. Heather Potter, the Chief Technician for the Health Tech Lab and Mr. Chris Malcholm (Design Studio), where majority of the research was taken place, whose support at different stages of this work was invaluable.

Furthermore, I would like to thank the support from University of Southampton and China Scholarship Council (CSC) for providing PhD studentships.

Lastly, I would like to thank my family for all their love and encouragement. For my parents who raised me with a love of science and supported me in all my pursuits.

Jinghua Tang

University of Southampton

Chapter 1 Introduction

1.1 Motivation

For lower limb amputees, a well-fitting prosthetic socket plays an important role in rehabilitation outcome. It serves the medium through which the residuum is connected to the rest of the prosthesis.

Prosthetic socket designs and fitting are primarily based on the subjective evaluations of stump movement inside the socket and the corresponding stress profiles [1-3], during ambulation. Sockets made by different prosthetists can thus vary significantly due to different levels of clinical experience of the prosthetist, and/or different amputee/prosthetists relationships. There is also a lack of objective measures to assess quality of socket fit. Physiologically, the volume of the lower limb residuum can vary considerably as a function of physical activities, weight fluctuations and/or comorbidities. Thus, socket fit is only based on a snapshot of the stump shape and volume in the clinic. In addition, there is no self-monitoring system that amputees could use to assess socket fit during their daily living activities. Consequently, a poorly fitted socket can result in discomfort, pain, tissue damage leading, in severe cases, to a higher level amputation. All these issues may well lead to the rejection of the prosthesis, affecting the individual's quality of lives. Addressing the issues relies heavily on the measurements to analyse the biomechanical state of the residuum/socket interface. This includes the measurement of both dynamic loads and movements.

From a scientific perspective, the dynamic residuum movement inside the socket and the multi-directional interface loads could provide guidance to the bioengineers to predict the tissue viability at the stump, under complex loading conditions [4]. An outcome of the examination of the stump tissues could then be implemented into the daily life monitoring, thus further improving the socket comfort and amputee satisfaction. In addition, the interface biomechanics, combined with a conventional lower limb musculoskeletal model, the gait analysis protocol for a lower limb amputee can be improved [5].

From the prosthetic industry perspective, the understanding of the interface biomechanics could influence the assessment standards of the lower limb prosthetics as a whole, for example ISO 10328 where socket interface is treated as a rigid body [6]. By incorporating translational and rotational mechanics at the socket interface, assessment of the prosthetic componentry can be conducted in a more realistic condition. In addition, biomechanical measures at the interface could also be used as inputs to existing prosthesis design, leading to a fully body-machine integrated prosthesis.

Recognising the need to evaluate the interface kinematics, various imaging techniques, such as X-ray and Dynamic Roentgen Stereogrammetric Analysis have been exploited. The overall findings suggested that up to 57mm of stump axial movement [7] and 10° of stump angular movement [8] can be observed. Equally, in order to evaluate the interface kinetics, a range of interface stress sensors, such as strain gauge-based sensors and magneto-resistive sensors, have been inserted into the residuum/socket interface to be used in walking tests. The resulting pressure and shear values of up to 350kPa and 80kPa, respectively, were recorded during amputee walking [9, 10].

Despite all these studies, the imaging-based technologies for kinematic evaluation is only applicable in laboratory settings for research purposes. They also require large (1.9m x 1.2m x 2.3m) and expensive facilities (up to 250,000 euros) with the risk of exposing amputees to ionising radiation. Thus, they are not suitable to use at prosthetic clinics. For assessing interface kinetics, most stress sensors reported to-date were only sensitive to measure pressure, including a few commercial systems such as Tekscan™ F-Socket System and Novel Pliance System. Other reported sensors, which can measure combined pressure and shear, require permanent socket modifications (i.e. drilling holes), or are bulky and constructed on rigid substrates, which are not appropriate for clinical use at a tight socket interface. There is thus an unmet need to develop clinically accessible approaches to evaluate dynamics residuum movement in the socket and the corresponding interface loading profile during amputee walking.

This thesis aims to address these challenges by developing a dynamic interface coupling model for the interface kinematics and applying TRIPS sensors for measuring and analysing interface kinetics. These novel interface kinematic and kinetic techniques can then be potentially combined to form a biomechanical assessment platform for lower limb amputees. It is predicted that such an assessment platform could enhance the understanding of the socket interface biomechanics and therefore could be potentially used to aid the socket design, fitting, daily life fit monitoring, in-depth scientific research and prosthetic componentry design and assessment.

1.2 Aim and objectives

Aim of the thesis

The aim of this thesis is to develop a comprehensive biomechanical assessment at residuum/socket interface. This includes the development of a 3D motion capturing method to evaluate residuum movement (kinematics) in the socket and application of the TRIPS sensor system to assess the mechanical interaction (kinetics). Further analysis is enabled by preliminary work using combined kinematic and kinetic approaches, with a view to obtain initial understanding of their biomechanical relationships.

Objectives of the thesis

To achieve this aim, four primary objectives are included:

- Objective 1: To investigate human joint biomechanics of both able-bodied participants and lower limb amputees, highlighting the effects of residuum/socket interface on gait profiles.
- Objective 2: To develop a 3D motion capturing-based technique to evaluate relative stump motion in the socket. The repeatability and sensitivity of the technique will be assessed to evaluate its clinical applicability.
- Objective 3: To assess multi-directional stresses at the key locations of a stump. The sensitivity of the developed sensor system and stress profiles as a function of walking speed, terrains and prosthetic components will also be assessed.
- Objective 4: To assess the interface biomechanics by combining the relative motions and multi-directional stresses.

1.3 Overview of research activities and chapters

To meet the aim and the objectives of the project, a range of research activities have been formulated, as all chapters are outlined in Figure 1.1.

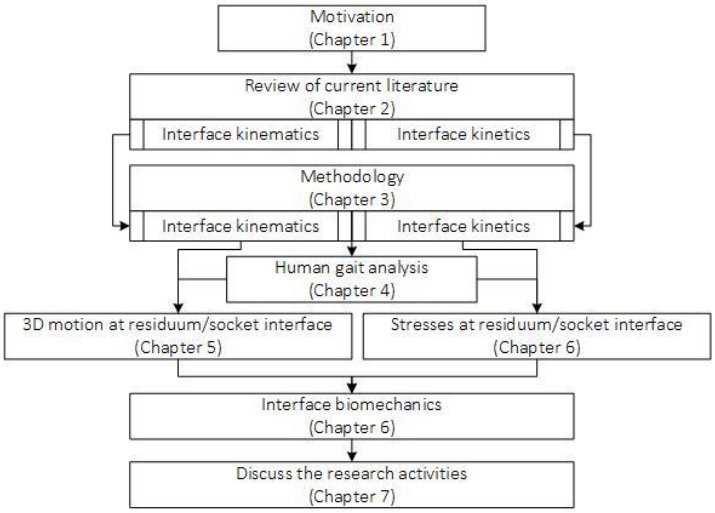

Figure 1.1: Chapter overview

The key results have been published in two peer-reviewed journals and presented at eight national and international conferences. Two prizes were awarded at national and international conferences. An overview of each individual chapters are described below:

Chapter 1: This chapter describes the motivation for assessing the mechanics at the residuum/socket interface, including the kinematics and kinetics.

Chapter 2: This chapter reviews both assessment techniques and biomechanical results of the 3D motion and the stresses at residuum/socket interface. It highlights the need to develop clinical-friendly techniques for assessing the biomechanics at socket interface.

Chapter 3: This chapter describes the two key experimental facilities that have been employed in the project. A 3D motion capture system to evaluate the residuum motion and a sensor system to measure the stresses at socket interface.

Chapter 4: This chapter focuses on the understanding of the human lower limb joint biomechanics. The joint biomechanics obtained on lower limb amputee highlights the need and can be used to study of the biomechanics at socket interface.

Chapter 5: This chapter describes the development of a technique to evaluate the 3D motion at the socket interface. The repeatability and the sensitivity of the technique is evaluated based on amputee case studies.

Part of the content in this Chapter was published as an article on a peer-reviewed journal (**Tang J**, McGrath M, Laszczak P, Jiang L, Bader D, Moser D, et al. Characterisation of dynamic couplings at lower limb residuum/socket interface using 3D motion capture. Med Eng Phys. 2015; 37:1162-8.).

Chapter 6: This chapter describes the use of the TRIPS sensor system to evaluate the loading at socket interface. The repeatability and the sensitivity of the technique is evaluated based on amputee case studies. The interface biomechanics is assessed using the 3D motion (Chapter 5) and stresses (Chapter 6) obtained at the socket interface.

Part of the content in this Chapter was published as an article on a peer-reviewed journal (**Tang J,** McGrath M, Hale N, Jiang L, Bader D, Laszczak P, Moser D, et al. A combined kinematic and kinetic analysis at the residuum/socket interface of a knee-disarticulation amputee. Med Eng Phys. 2017; 49:131-9.

Chapter 7: This chapter summarises the work carried out and highlights its contributions to the field of prosthetics. Additionally, it describes the limitation of the research and identifies the pathways for the future work.

Chapter 2 Literature review

2.1 Lower limb amputation and prosthetics

2.1.1 Lower limb amputation

It is estimated [11-13] that the current worldwide amputee population is approximately 15 million or 0.2% of the world population. It is also forecasted that the amputee population will increase by 47% from 1995 to 2020. In the UK, there are approximately 63,500 lower limb amputees [11] and 83% of these are unilateral lower limb amputees [12].

An amputation, sometimes considered to represent a failure of management by hospital professionals, is actually a significant step in recovery or rehabilitation for a patient whose upper/lower limb cannot be salvaged by other medical treatment/therapy [13]. There are four most common reasons for performing an amputation procedure, namely, gangrenous tissue from disease associated with diabetic foot ulcer, cancer, trauma, such as occurs in war scenarios and congenital malfunction. The relative proportions of these occurrences are shown in Figure 2.1a.

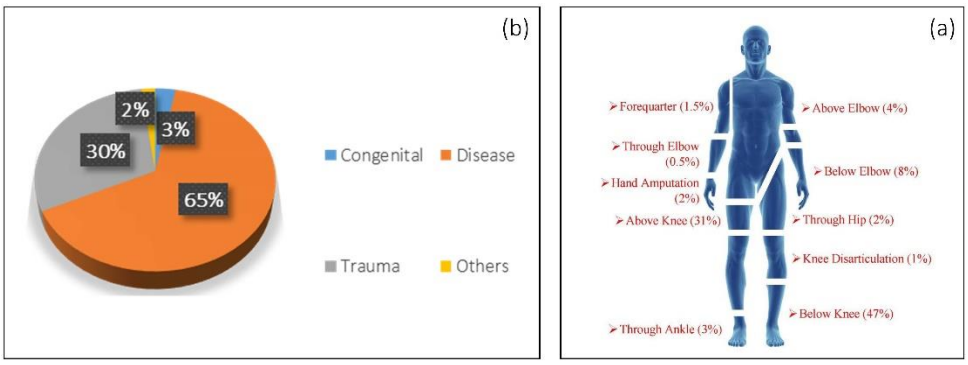

Figure 2.1: (a) Common cause of amputation [14] worldwide and (b) a schematic showing the levels of amputation.

Figure 2.1b indicates the common levels of amputation and its prevalence according to the World Health Organization [14]. The majority of amputation procedures were performed on the lower limb with 47% trans-tibial, 31% trans-femoral, and 22% other levels of amputation. Overall, lower limb amputation accounts for nearly 80% of the amputees worldwide.

Several common surgical techniques are commonly adopted for the amputation below the knee, including the long posterior flap technique [15] (Figure 2.2a) and skew flap technique [16] (Figure 2.2b). The former technique is well known for preserving blood supply to the soft tissue in the lower leg during loading [15]. In addition, the skew flap technique is based on the thermographic mapping of the lower limb. A higher temperature region is often recorded at anterior-medial and posterior-posterior lateral regions, suggesting an improved circulation and nutrition of the soft tissue [17].

During an amputation surgery, retaining the maximum amount of functioning muscle (gastrocnemius and soleus) is one of the key criteria for ensuring muscle strength, shape and blood circulation. In addtion, the stabilisation of the muscle is also the key to retain the muscle fucntion. Historically, there are three common techniques to achieve this, namely, myofascial closure, myoplasty and myodesis. Myofascial closure encases the remaining mucle using the outer fascial envelop, which proves not to be effective and only recommended for people with severe ischemea. Myoplasty approach involves the attachment of the muscle over the end of the bone and sew them to opposing muscle group. It is known that unless the muscles are firmly attached the scar tissue, they muscle tend to slide back and forth against the distal end of the bone. This may induce brusal tissue and discomfort. It is therefore often recommended that muscle groups should be directly attached to the bone, namely myodesis.

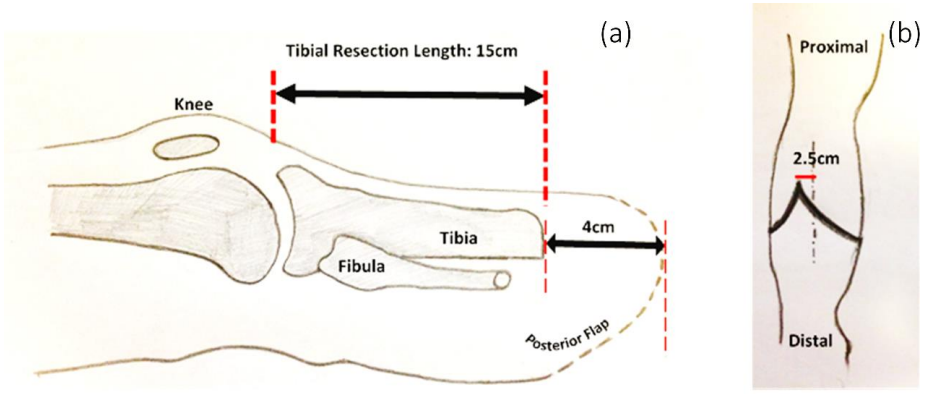

Figure 2.2: Schematics showing the (a) long posterior flap technique and (b) skew flap technique.

The length of residuum varies, depending on the cause of the amputation and the surgical technique. It is reported that a short residuum (less than 10cm) is likely to heal quicker with a reduction in re-amputation rate than a long residuum (greater than 10cm) [18]. In addition, amputees who have longer residuum (approximately 19.3cm) appears to have a greater postural stability, comparing to the ones with shorter residuum (approximately 9.2cm) [19]. Further, a greater walking speed and reduction in energy consumption were evident on amputees with longer residuum length, comparing to the ones with shorter ones [20].

2.1.2 Lower limb prosthesis and rehabilitation

From surgery to rehabilitation

A suitable rehabilitation process is often prescribed to patients after amputation surgeries as it is critical to the subsequent quality of life. The patient will be subjected to wound healing (Phase 1), mostly involving pain control. In particular, Phase 2 or the pre-prosthetic phase involves the process of residual limb shaping from an initial cylindrical shape (post-operative)

to a more conical shape. During this period, studies have shown that a reduction in residual limb volume of up to 9.7%, equivalent to up to 200mL of tissue [21]. Muscle strength will likely increase coincident with an increase in activity during this phase of rehabilitation. Phase 3 involves the prosthetic prescription and fabrication. It is worth noting that the changes in shape and volume of the residual limb affect the quality of socket fit. Intensive rehabilitation training with the patient is conducted by an increase in wearing time and familiarisation with the functions of the prosthesis. Lastly, the wearing of the prosthesis is a life-long challenge which requires constant adjustments, which are performed in clinics by prosthetists.

Lower limb prosthesis

A common lower limb prosthesis typically consists of a socket, liner, knee (for trans-femoral amputee only), shin tube, an ankle-foot device as shown in Figure 2.3. The socket is bespoke for each individual, and attaches tightly to the residual limb which itself is often draped a prosthetic liner.

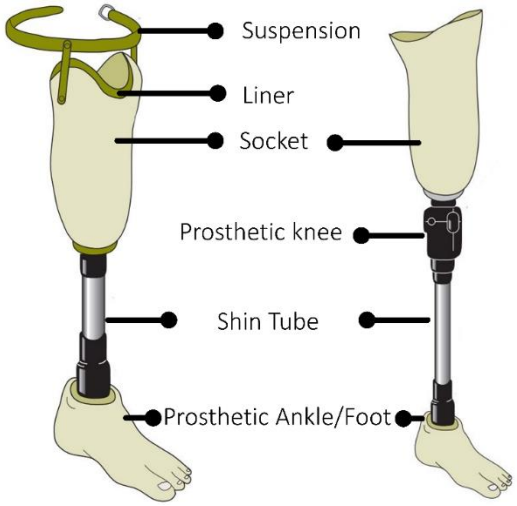

Figure 2.3: Typical prosthesis used on trans-tibial amputee (left) and trans-femoral amputee (right).

A prosthetic knee and foot are used to replace the natural knee and foot. For trans-tibial amputees, normally a pylon is rigidly connected to the socket which acts to accommodate the loss of the shank length. A prosthetic foot/ankle unit will then be fixed to the distal end of the pylon, using a bolted connection. For trans-femoral amputees, a prosthetic knee will be used to provide articulation, mimicking the biomechanical function of the biological knee joint.

Common types of prosthetic knee or limb systems are illustrated in Table 2.1. A successful prosthetic knee ensures a loading symmetry between the prosthetic side and the intact side [22-24], therefore reducing the chance of developing joint arthritis due to excessive loading on the non-affected limb. At the same time, limb safety and comfort, which is associated with knee

flexion/extension motion, needs to be maintained when walking on different terrains [25-27]. In most of the reported studies, gait analysis have been used as a technique to evaluate the performance of the prosthetic knees [28-30]. Biomechanical parameters, such as joint angles, joint moment and work done have been commonly used to quantify the performance of the prosthetic knee. However, the socket comfort as a function of the different types of prosthetic knee is not well understood due to the lack of measurement tools at the residuum/socket interface.

Table 2.1: Summary of three common types of prosthetic knees.

Knee Type	Description	Examples		
Mechanical	Polycentric knee with swing and stance knee flexion & extension control. Flexion and extension resistance can be tuned manually.	 KX06 knee*	 Pheon Knee**	 Total Knee 2100***
MPK	Adjustment of knee flexion and extension resistance, depending on walking speed, change of terrain and different phase of GC.	 Orion 3 knee*	 C-leg**	 Rheo Knee***

**Products from Chas A Blatchford & Sons Ltd.: http://www.blatchford.co.uk/*

*** Products from OttoBock: https://professionals.ottobockus.com*

****Products from Ossur: https://www.ossur.co.uk/*

Table 2.2 illustrate the different types of the prosthetic foot/ankle units, all of which play a key role during ambulation of an amputee. In particular, it assists in the smooth advancement of the prosthesis (tibial advancement in a biological shank), providing comfort and stability in stance, and ensuring shock absorption during loading [31]. The correct choice of a prosthetic foot is critical, and may affect key characteristics of the patient's gait, such as cadence, velocity and stride length [32], hence enhancing the entire biomechanical response of the prosthesis. It is worth noting that for MPF, the hydraulic ankle resistance can be dynamically tuned, which may affect the load transfer from the foot to the residuum/socket interface. Here, load transfer is defined as the flow of loads from the ground interface, via the prosthetic feet, thought the pylon to the prosthetic knee and finally reached the socket interface. To date, the advantage of using MPF has been illustrated by the resulting improvement in gait performance [33-36], involving smoother progression of centre of pressure, increased toe clearance and greater

prosthetic ankle work. However, no clinical evidence has been reported to illustrate the advantage of the MPF for the health of the residuum. This could be an important outcome measure, which affects the overall governmental funding on prosthetic devices.

Table 2.2: Summary of three common types of prosthetic foot.

Foot Type	Description	Examples		
SACH foot	No ankle joint movement			
Energy storing	No ankle joint movement. Use of heel and toe spring to store energy in early stance and release energy in late stance	 Eprit Foot*	 Triton Foot**	 Flex-foot***
Hydraulic	On top of the energy-storing feature, hydraulic ankle allows ankle dorsi/plantar-flexion movement.	 Echelon Foot*		 K2 Sensation***
Microprocessor controlled foot (MPF)	Adaption of the ankle dorsi/plantar-flexion.	 Elan Foot*	 Meridium Foot**	 Proprio Foot***

**Products from Chas A Blatchford & Sons Ltd.: http://www.blatchford.co.uk/*

*** Products from OttoBock: https://professionals.ottobockus.com*

****Products from Ossur: https://www.ossur.co.uk/*

Apart from prosthetic foot, an axial and torsional shock absorber can also be attached to the prosthetic foot and can be used to reduce the shock and shear forces caused by vertical and twisting motion, affecting the load transfer to the residuum/socket interface.

2.1.3 Prosthetic socket design and fitting

The prosthetic socket connects the residuum to the rest of the prosthesis and fulfils an important function, namely, to ensure both optimum adhesion and the proper fit of the prosthesis. Although there are different types of sockets, most design concepts are based on the management of load distribution over the residuum and movement of the residuum within the socket [2, 3].

Trans-tibial sockets

Common trans-tibial sockets involve PTB, TSB and the hydrostatic designs. One of the key criteria for trans-tibial socket design is the selection of loading bearing and load-relieving

locations. As illustrated in Figure 2.4a and b, for a trans-tibial amputee, the patellar tendon ligament, anterior compartment, medial flare of the tibia, distal end, shaft of the fibula and popliteal fossa are the key load tolerant locations [37]. Of these, the patellar tendon ligament area is often selected as the key location to distribute load, as it is composed of relatively inextensible collagenous fibres, which stretch minimally under normal tensile loads along their axial direction. This arrangement is particularly suited to bearing anterior-posterior compressive loads [38].

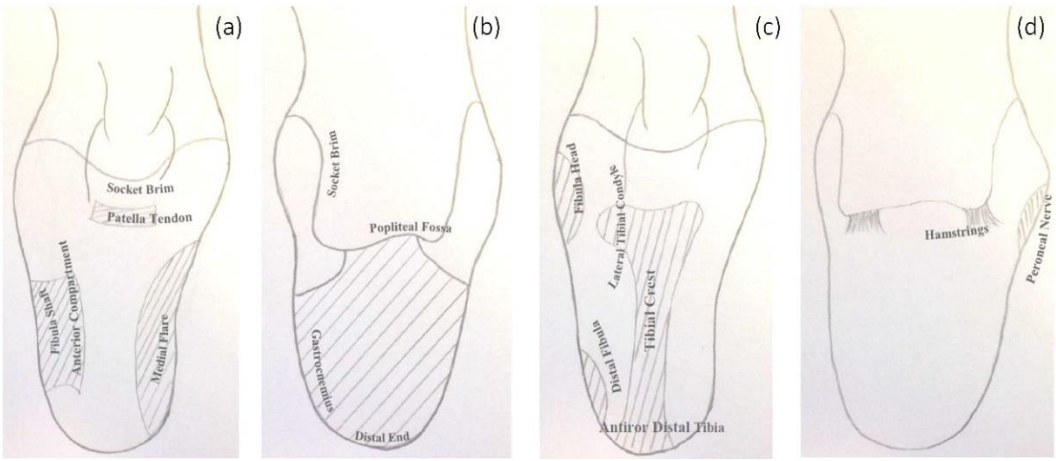

Figure 2.4: Load tolerance regions on trans-tibial residuum, (a) anterior view and (b) posterior view; load sensitive region on trans-tibial residuum, (a) anterior view and (b) posterior view

The common load sensitive regions, as identified in Figure 2.4c and d, include the fibula head, tibial crest, peroneal nerve, distal cut of the fibula and the lateral tibial condyle. When designing load bearing features for trans-tibial sockets, these areas must be avoided.

The PTB socket (Figure 2.5a), was designed to bear body weight primarily on the patella tendon region of the residuum [39]. In the TSB socket design, weight is distributed over the entire surface of the residuum, as shown in Figure 2.5b, as opposed to specific regions. In recent years, moderate load bearing over the patella tendon bar on a TSB socket has been introduced to distribute some load at the patella tendon bar, thereby relieving load in more sensitive areas.

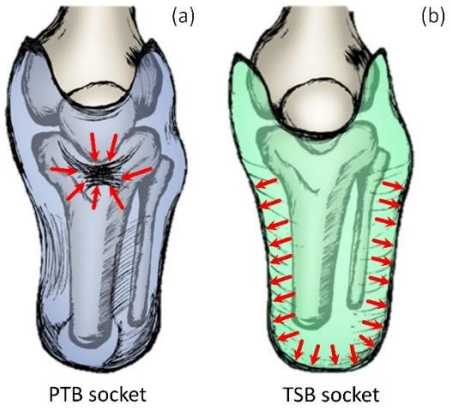

Figure 2.5: Schematics showing (a) a conventional PTB socket and (b) a TSB socket.

A hydrostatic socket [40] represents a special case of total surface bearing socket as the weight is also distributed over the residuum. The rationale for this design is based on Pascal's law. The magnitude of uniform pressure based on the well-established Reswick and Rogers' curve [41], which defines the relationship between tissue tolerance threshold and time of continuous loading.

To date, there is still debate when selecting the type of trans-tibial socket at the fitting stage. When fabricating a PTB socket, there is lack of guidance on the magnitude and duration of load that should be borne on the patella tendon region. This is primarily due to the lack of tissue viability data to guide the fitting process. When fabricating a non-PTB socket, as the tissue composition and its biomechanics vary between amputees, the exact load threshold that should be uniformly distributed over the stump is difficult to determine. In addition, due to the change in socket fit during the course of the day, the load distribution profile, designed at the socket fabrication stage, may no longer be appropriate. Therefore, an interface load monitoring system, together with the knowledge on the tissue viability are needed to guide the socket fabrication for the prosthetist and for self socket fit adjustments during daily activities.

Trans-femoral socket

The first trans-femoral socket was made of aluminium with a rounded plug shape, or the plug socket. However, the ischial tuberosity tends to drift up and down in the socket, due to fluctuations in the residuum volume [42]. Accordingly, the key design consideration for a trans-femoral socket is the stabilisation of the soft tissues inside the socket. This requires a quantification of soft tissue movement inside the socket to assess socket design and performance. Currently, common trans-femoral sockets include Quadrilateral (QUAD), Contoured Adducted Trochanteric-Controlled Alignment Method (CAT-CAM) and High-Fidelity (Hi-Fi) designs.

The QUAD socket (Figure 5a) was developed by Radcliffe and colleagues [2, 43, 44]. Its design was based on the conceptualised pressure, created between the socket interface and the movement of femur within the stump, as shown in Figure 2.6. It is also worth noting that the ischium is not contained in the socket, as shown in Figure 2.7a.

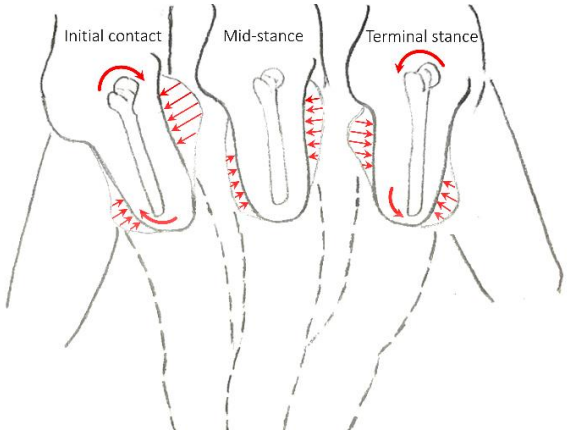

Figure 2.6: Radcliffe's conceptualised socket interface pressure and residual femur movement with the stump. Image adapted from [44].

The QUAD socket offered a major improvement in functionality over the earlier plug socket, although abduction of the femur was observed in over 90% of its users. This would lead to an instability in walking, which could be caused by the shape of the socket (wide in the medial-lateral dimension and tight in the anterior-posterior dimension). The lateral socket wall was designed to be located at least 25mm away from the femur and when the femur exerts loads against the lateral wall during weight bearing, the QUAD socket can move laterally without any resistance. Reconsideration of the QUAD socket design was initiated by Long [45].

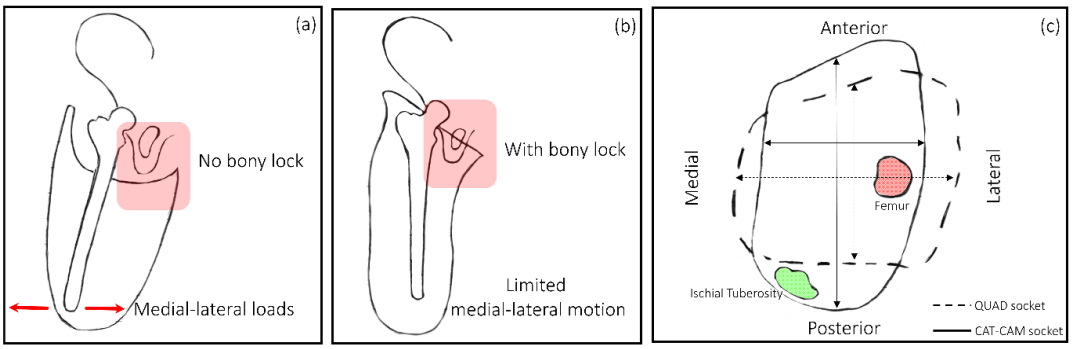

Figure 2.7: (a) An illustration of QUAD socket, (b) an illustration of CAT-CAM socket and (c) cross-section view at

A CAT - CAM socket, is one type of the ischial containment socket developed by Sabolich [46], as shown in Figure 2.7b. It is designed to be narrower in the medial-lateral dimension compared with the quadrilateral sockets as shown in Figure 2.7c , such that it fits intimately with the ischial ramus, thus 'locking' onto the pelvis, and encapsulating the ischial tuberosity. In addition, the

anterior-posterior brim dimension at the proximal region was reduced compared with the QAUD socket design, to relieve the pressures at both anterior and posterior proximal regions of the residuum.

The concept of the Hi-Fi socket design, as shown in Figure 2.8a, involves depressions added onto the socket walls in the anterior, posterior, medial and lateral regions with open release areas between these features to receive the displaced tissue [47]. The theory behind this design involves 'grabbing' the femur mechanically using the four depression features built on the socket [47]. The femoral motion relative to the residuum tissue was restricted, improving the spatial awareness and proprioception of the limb. However, as mentioned by the developers of the Hi-Fi socket, the amount of tissue that need to be depressed or released has not been quantified with respect to its tolerance to withstand local pressures and shear forces.

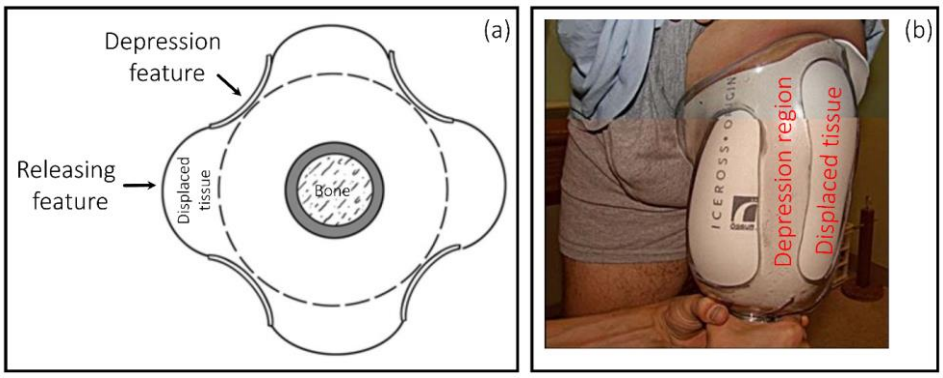

Figure 2.8: (a) The concept of HI-FI socket design and (b) illustrations of tissue depression region and tissue releasing region

Socket-fitting in current clinical practice

The quality of socket fitting directly influences the kinematic and kinetic characteristics at the residuum/socket interface. It is thus important to briefly review current fitting practice. In most prosthetic clinics, the socket fitting iterative process is performed by a prosthetist. An example of a socket fitting flow chart is illustrated in Figure 2.9. However, due to human error and complex geometry, differences will exist between prosthetists, as exemplified by one report highlighting a difference of up to a 35mm in stump circumference between two prosthetists [48] Residuum shape capturing is often a manual process, involving applying several lays of Plaster of Paris over the stump. With the negative cast obtained, a positive cast can be made for the subsequent rectification process.

The rectification process involves first, the selection of socket type. However, there is no unified option on the choice of a socket for a specific amputee. This is largely due to the lack of measurement tool. Padding and reduction is performed on the positive cast with a selected socket design. The amount of plaster that needs to be added or removed is based on the experience of the prosthetist with no tool to guide them in this process. This is followed by the drape of a transparent socket, such that when the stump is donned the colour of the skin can be noted by a prosthetist. The skin colour will usually indicate whether the stump is in contact with the socket and will also provide an approximation of relative loading at a particular stump region. The rectification process is manual and iterative, which requires considerable experience, skill and knowledge about socket interface biomechanics. Thus this process is predominantly based on the subjective views of the individual prosthetist [49] with some feedback from the amputee. Therefore, the experience of the prosthetist will also inform the adjustments on the positive cast, repeating the rectification process until the amputee is reasonably happy with the fitting.

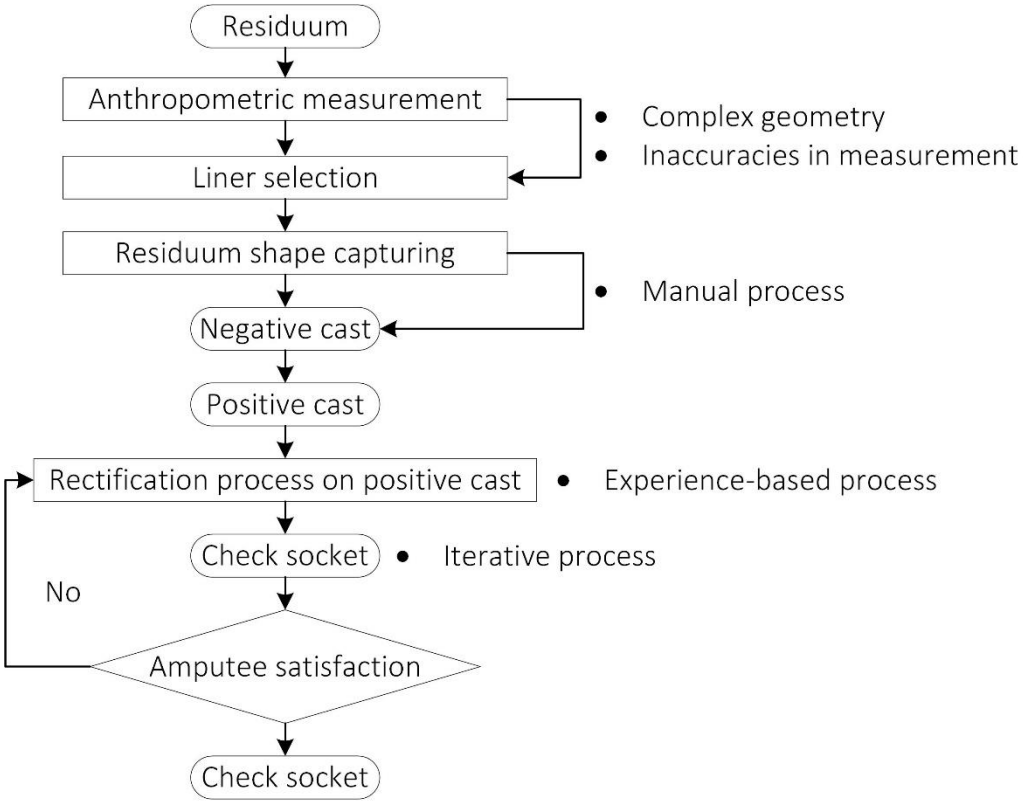

Figure 2.9: Socket fitting flow chart

A key to a successful prosthetic limb fitting is the assessment of the socket fit. However, in current clinical practice, prosthetists use limited tools or technologies to quantitatively assess the socket fit. Patient feedback or satisfaction plays an important role in the socket fitting

process. However, for patients with neuropathy, abnormal loads at the socket interface cannot be directly translated to pain due to the loss of sensation. Therefore, in this case, patient feedback can be unreliable and misleading [50]. Therefore, technologies are required for the evaluation of the socket fit to aid the prosthetist. Although prosthetic manufacturers, based on their experience, have published their own guidelines for the liner selection and socket fitting process, there is still no unified standard that is agreed by prosthetic industry. This is largely due to the lack of means to evaluate the socket design, socket fitting process and socket fabrication process. In addition, the lack of understanding in tissue damage thresholds under multi-directional stresses also play an important role in the socket rectification process.

2.1.4 Socket interface

The trans-tibial socket interface is typically formed by a stump, a liner and a socket (Figure 2.10a). Key bony landmarks, the fibula head, patella tendon bar and cut-end of the tibia, are typically covered by a thin layer of skin that has been created at surgery (Figure 2.10a). A liner is then typically worn over the stump to aid cushioning and suspension. The stump together with the liner will then be donned into a socket. A socket interface is formed as a contact interface between the socket and residuum. For a knee disarticulation amputee (Figure 2.10b), the socket interface is typically formed by a socket, a Pelite liner and a residuum. Socks are often worn as a means to adjust socket fitting.

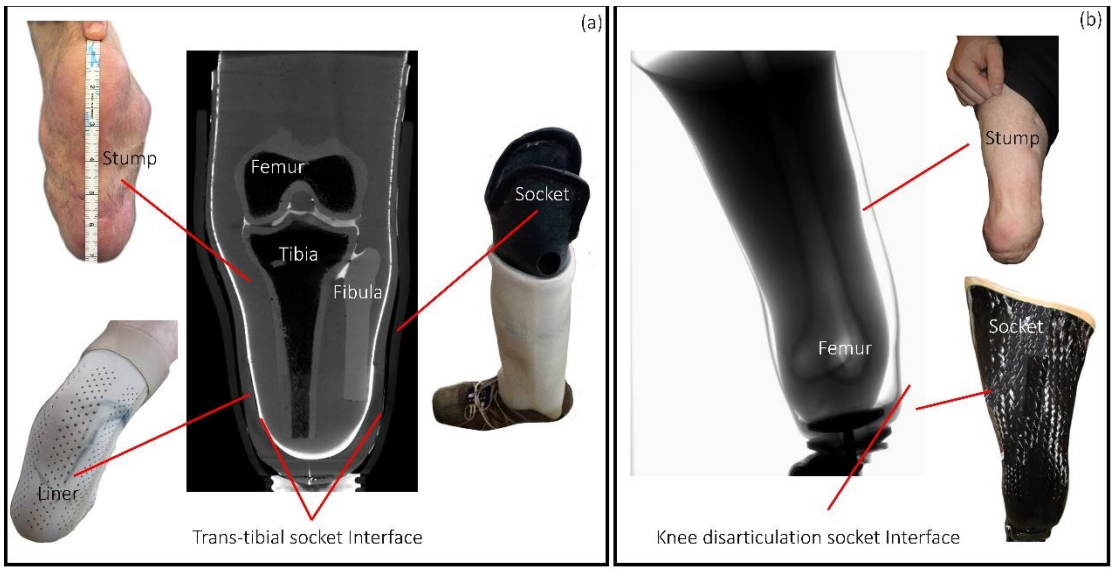

Figure 2.10: Typical socket interface for a (a) trans-tibial and (b) a knee disarticulation amputee.

Attachment between residuum and socket

The mass of a typical trans-femoral prosthetic limb, incorporating a socket, a prosthetic knee, a pylon and a prosthetic foot is just under 4kg [51]. When the prosthetic limb is attached to the

residuum, in the non-load bearing state, the weight of the prosthesis will be supported by the friction at residuum/socket interface. It has been reported that, the extra mass of the prosthetic limb could result in a reduction in forward impulses on the body, resulting from push-off and deceleration of the swing leg [52]. In addition, the mass of the prosthesis could also affect the proprioception and stability of the overall limb.

Socket attachment directly links to comfort at the interface. The first type of suspension technique relied on the features built on the socket. As an example, Supra-Condylar (SC) [53] and Supra-Condylar Supra-Patellar (SCSP) [54] features were built on PTB socket. The SC feature (Figure 2.11a) suspends the prosthesis on the residuum by extending the socket brim above the medial femoral condyle. Furthermore, an SCSP feature (Figure 2.11b) has an anterior trim line proximal to the patella, which enhances the stability in the sagittal plane.

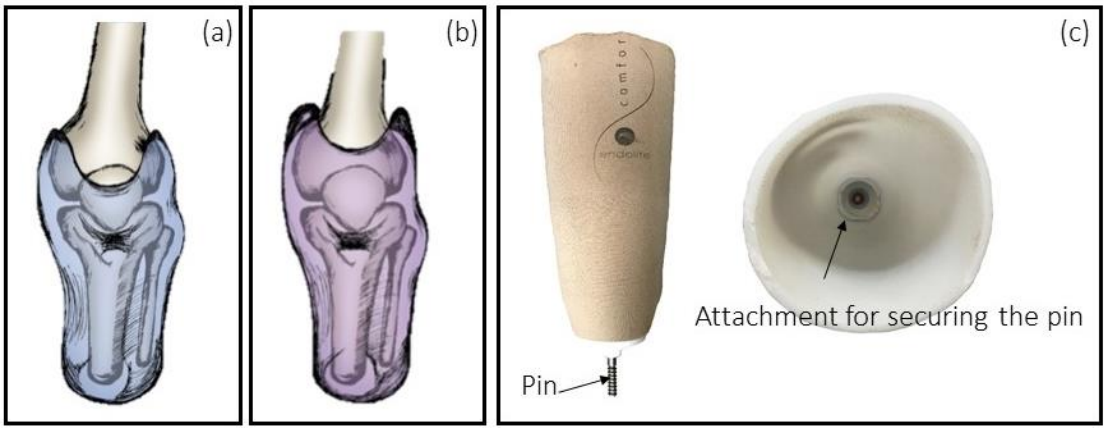

Figure 2.11: (a) PTB socket with SC suspension, (b) PTB socket with SCSP suspension (Image taken from: https://www.physio-pedia.com/Prosthetics) and (c) pin lock suspension.

An alternative type of suspension technique is based on the pin lock feature built on the prosthetic liner and the socket (Figure 2.11c). A pin projecting from the bottom end of the gel (elastomer, urethane or silicone) liner is forced into a locking mechanism at the distal end of the socket. As the pin enters the shuttle lock in the socket, the residuum together with the liner attaches to the socket. Studies have showed an advantage of the pin lock suspension technique in gait performance, in terms of increases in step length, walking speed and knee range of motion, leading to enhanced overall satisfaction rates [55].

The third type of technique involves vacuum suspension. A vacuum pump is used to remove air molecules from the thin, sealed air space between the socket and the liner. The resulting state of vacuum holds the residuum firmly to the socket. Theoretically, the liner, and therefore the skin are no longer able to be separated from the socket. This mechanism helps to prevent

volume loss of the residuum. However, there is still no consensus as to the appropriate vacuum level that should be applied to the socket interface [56, 57].

Interface compliance

It is evident that the residuum/socket interface has its own compliance, which will be highly dependent on individual factors, such as the nature of the amputation surgery, design of the socket, location on the residuum, choice of the liner and suspension technique. The compliance of the interface is directly associated with the load transfer to the stump and its relative motion. Therefore, a review of the socket interface compliance is provided. The Young's modulus of each of the elements which make up the interface are shown in the schematic (Figure 2.12) [58]. It is evident that, depending on the location of the residual limb, the value of tissue stiffness is variable. When there is a bony prominence subjacent to the stump soft tissues, higher tissue stiffness will be observed resulting in the stump being exposed to higher loads. This could potentially lead to stump tissue damage under repetitive and continuous loading. By monitoring loads at a bony prominence location, the potential of stump tissue damage could be reduced. Several research groups has quantified the tissue stiffness at various locations of the residuum. As an example, Sengeh and Herr [59] expressed the stiffness as a function of distance between the socket and the bone. This distance varies from 1mm to 50mm on the trans-tibial residuum, representing a large variation of stiffness from 10.4kPa to 89.2kPa [60, 61].

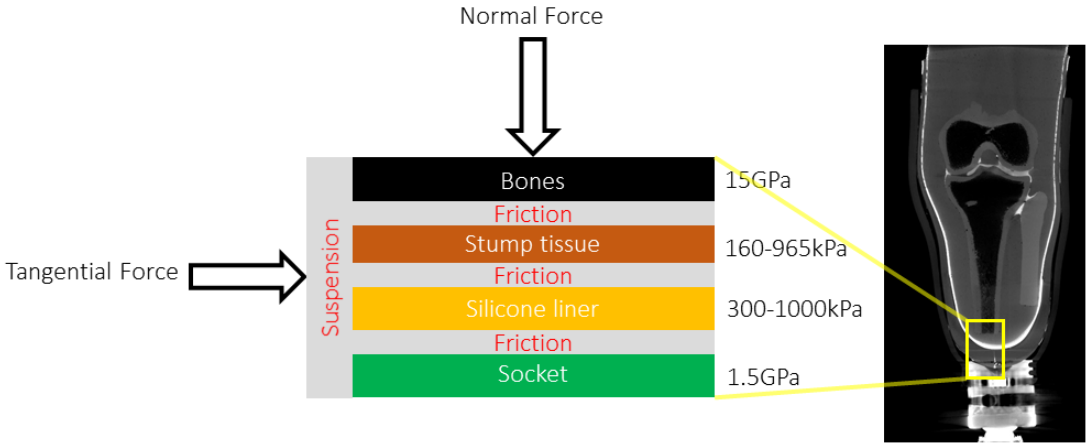

Figure 2.12: Schematic showing a section view of a trans-tibial residuum/socket interface

In the vertical direction, the two consecutive layers are constrained by the nature of the attachment of the prosthesis to the residual limb. In the horizontal direction, the movement between the two consecutive layers are constrained by friction. Upon application of a normal force, the largest displacement may be seen in the stump tissue and silicone liner, which

represent the low stiffness elements at the interface. In the horizontal direction, upon application of a tangential load, deformation of the tissues may occur and could be associated with damage of the stump tissues. While interface biomechanics are closely linked to ambulation i.e. gait performance of the amputee, it is therefore important to review typical gait characteristics for both able-bodied and amputee groups.

2.2 Challenges related to residuum/socket interface

2.2.1 Clinical observations

Residuum volume fluctuation

Once a socket is fitted by the prosthetist, amputees go home and continue with their daily life. At this stage, the socket fit is optimal to the current status of the stump. It has been reported that amputee typically takes up to 9130 ± 4420 steps per day associated with 7.5 ± 3.7 hours of walking [62]. These physical activities may cause residuum volume fluctuation. According to Zachariah et al [63], the residuum volume increased by up to 10.9% after a short period of walking. From a long term point of view, Fernie reported up to 21% of residuum volume fluctuation over a year, which may be associated with a loss of body weight [64]. In addition, up to 3.5% difference in residuum volume was found when the stump is contracted compared to it being relaxed [65].

In addition to physical activities, a change in body weight [66] and muscle composition [67] are important factors. For example, atrophy of the muscles will reduce residual limb volume. A prosthetic socket can be treated as a rigid body, usually made of carbon fibre or thermoplastic, which will not deform significantly during normal ambulation. On the other hand, if volume of the residuum changes up to 15% [68] in a day, it could significantly alter the quality of socket fitting or the coupling between the residuum and the socket.

Socket alignment

There are several key locations on the prosthetic limb to ensure appropriate alignment including the connection between the prosthetic components [69-71] for lower limb amputees. For a trans-tibial amputee (Figure 2.13), in addition to the normal angular alignment (Figure 2.13a), socket flexion (Figure 2.13b) and extension (Figure 2.13c) in relation to the pylon can also be applied to the limb in sagittal plane. In the coronal plane, normal alignment (Figure 2.13d), socket abduction (Figure 2.13e) and socket adduction (Figure 2.13f) are the three possible factors to consider by the prosthetists.

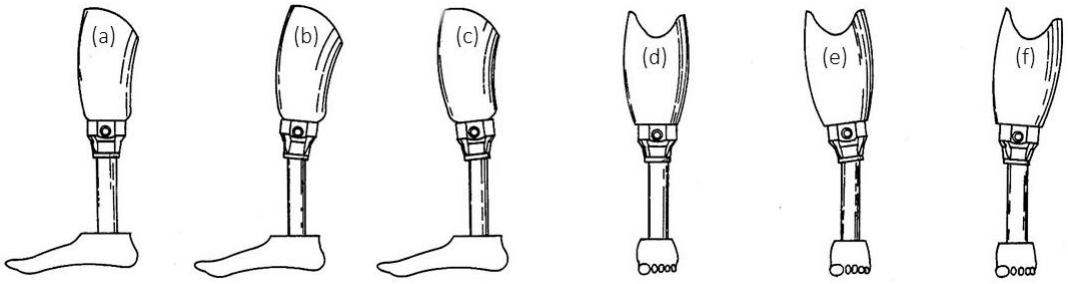

Figure 2.13: (a) – (c) Socket angular alignment in sagittal plane and (d) - (f) socket angular alignment in coronal plane. Figure adopted from [72].

According to a study conducted by Zahedi et al [73] with 3 prosthetists, 183 trans-tibial and 100 trans-femoral amputees, it was established that amputees can tolerate several alignments settings. Indeed the alignment settings range in some parameters by as much as 148 mm in translation and 17° in rotational. Different studies indicate that the prosthesis alignment influences both distribution as well as the magnitude of the stress imposed on the residuum [73-75]. Although the most significant pressure change due to prosthetic component was reported to be approximately 285kPa [9], usually much smaller pressure re-distribution have been reported. One study [76] reported that aligning the prosthetic foot in plantar-flexion setting consistently increases pressures in the patellar tendon area with a corresponding decrease at the distal tibia. However, aligning the foot in dorsiflexion has the opposite effect. Despite this specific finding, many studies lack consistency, and, to-date, research does not provide a comprehensive and systematic view of the impact of alignment on the kinetics and kinematics at the residuum/socket interface.

Skin problems

According to two studies conducted by Levy [4, 77], up to seven types of skin problems (Figure 2.14) have been identified on the stumps of lower limb amputees. For minor conditions, redness will be evident at bony prominences whereas for major conditions, pain and tissue break down will occur, leading to a pressure ulcer (Figure 2.14a). Contact dermatitis, as shown in Figure 2.14b and Figure 2.14c, is commonly observed with redness and itching reported by amputees. In severe conditions, blistering will be induced due to scratches. Figure 2.14d shows negative pressure hyperaemia, which may be associated with the negative pressure at the interface and limb volume change. In this condition, suspension techniques must be altered and in severe cases, a new socket required to accommodate the stump volume change.

Figure 2.14: Skin problems on lower limb amputees.

Folliculitis (Figure 2.14e) is also a common condition where hair follicles become inflamed due to bacterial or fungal infection. The acute management for folliculitis is to reduce the heat and surface friction at the socket interface. Figure 2.14f shows the typical symptoms associated with an abscess. It usually occurs with/after tissue break down with bacterial infection. Xerosis, as shown in Figure 2.14f, is usually caused by dry skin.

Among the seven commonly observed skin problems, four of them may be associated with the loading, pressure, shear and frictional forces, at the socket interface leading, in some cases, to the replacement of the socket with a new design. Therefore, a loading monitoring system is needed for prosthetist use for socket fitting purposes and for amputee use during daily activities.

Residuum pistoning motion

The axial movement of the residuum relative to socket is commonly termed, pistoning, by prosthetists. There are three possible types of movement between the residuum and the socket, labelled D1, D2 and D3 in Figure 2.15a. D1 describes the movement between the cut-end of the tibia and the distal end of the socket. D2 describes the axial movement between the cut-end of the tibia and the prosthetic liner. D3 describes the axial movement between the prosthetic liner and the distal end of the socket.

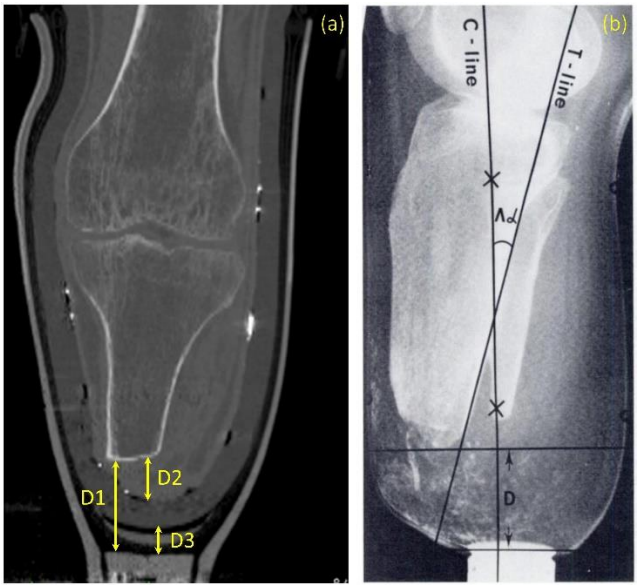

Figure 2.15: Pistoning motion at residuum/socket interface of a trans-tibial amputee. Image adopted from https://www.ors.org/Transactions/59/PS2--096/1667.html. (b) A photo showing the angular movement (α) and axial movement (D) at a trans-tibial residuum/socket interface.

Excessive D1 movement causes lack of proprioception or spatial awareness of the residuum in relation to the rest of the prosthetic limb [7, 78, 79]. This can compromise the walking stability. Excessive D2 movement may induce internal tissue damage [80-82] which can cause pain, discomfort and, in severe condition, secondary amputation may be required. Excessive D3 movement may induce poor blood circulation leading to increase susceptibility of soft tissue damage at the distal tip of the stump. Appropriate means to quantify the amount of pistoning is needed to aid both the socket fitting process and the understanding of the interface mechanics.

2.2.2 Residuum movement relative to socket

As shown in Figure 2.12, the residuum/socket interface is commonly composed of bone, soft tissue, a prosthetic liner and the rigid prosthetic socket. The stump, including the rigid bone and the soft tissues, is enclosed by the rigid socket. During amputee daily activities, loads including forces and moments will be transferred to the socket interface. Due to the compliance between the rigid bone and the rigid socket with soft tissues in between, movement at the residuum/socket interface will be induced. This complex movement, incorporating both the angular [83] and axial movement [7], are commonly observed in clinical settings.

In most of the previously reported studies, angular movement at the residuum/socket interface is defined as the moment of the cut-end of the tibia (for trans-tibial amputee [84] [83]) or cut-end of the femur (for trans-femoral amputee [8]) in relation to the socket (α in Figure 2.15b).

Axial movement (D in Figure 2.15b), also known as pistoning motion, is commonly defined as the vertical movement between the cut-end of the bone and the distal end of the socket.

It is well known that the amount of angular and axial movement of the residuum relative to the socket can be associated with the degree of stability during ambulation [84-86]. Excessive movement at the interface could induce the reduction in spatial awareness of the stump with respect to the rest of the prosthesis. This could potentially pose safety issues, especially for elderly amputees, as they tend to exhibit reduced soft tissue stiffness. In addition, additional work is needed to compensate for this movement resulting in increased energy expenditure during daily activities[87]. Therefore, understanding the movement between the residuum and the socket for lower limb amputee could potentially improve the overall amputee satisfaction [31, 88-90].

From an industrial perspective, the understanding of the movement at residuum/socket interface could potentially improve the functionality of the product. The structural assessment of existing prosthetic products is based on mounting the prosthetic against a rigid socket interface, as recommended in ISO 10328: 2016. By incorporating a non-rigid socket interface, the test load exerted on the prosthetic components can be more realistic and improve the overall assessment quality.

The residuum movement against the inner socket wall would induce intensive kinetic interactions at the residuum/socket. In next section, this intensive dynamic interaction will be introduced.

2.2.3 Residuum/socket interface loading

Due to the dynamic movement between the residuum and the socket, load will be induced at the interface, which may be directly associated with damage of the stump tissues. The load applied to the tissue surface can be resolved into two directions, namely, a normal force perpendicular to the skin surface and a shear force applied tangential to the skin surface (Figure 2.16a). Interface pressure is defined as the normal force acting on the unit area of the skin. When the pressures are uniformly distributed over wide area of the skin, damage is less likely when compared to loading applied to localised areas [91], such as the bony prominences on trans-tibial amputees. It is well established that an inverse relationship exists between the intensity of external loads and the duration of the loading application required to produce residuum tissue damage [41, 92], such as pressure ulcer [93], as shown in Figure 2.16b. In particular, Reswick and Rogers [41] formulated tissue tolerance guidelines of allowable

pressure levels on tissue overlaying bony prominences, against time of sustained pressures, as indicated in Figure 2.16c.

Figure 2.16: (a) A schematic showing the normal and tangential forces, (b) a photo, showing residuum ulceration and dermatitis and (c) Reswick and Rogers' curve [41, 94, 95] (dotted line) and further by Linder-Ganz[75, 76] (red curve).

Interface shear stress is defined as the tangential force acting on a unit area of skin. A few studies have attempted to establish the relationship between shear stress thresholds for skin breakdown. Naylor [96] defined the work needed to produce a friction blister as the product of frictional force and the number of cycles needed to cause a blister. The results suggested that, in general, to cause rupture of the skin epidermis greater cycles are needed at lower frictional forces. Sulzberger [97] demonstrated that less time and work are required to produce a blisters on thin skin compared to thick skin, because of the adapted load-tolerance structure exists in thick skin. In addition, the formation of a skin blister is also related to elevated skin temperature [98] and moisture [96], as is common at the stump/prosthetic interface..

From a clinical perspective, the combined measurement of both pressure and shear stress can be used during the socket fitting stage to avoid excessive loading bearing at sensitive locations. In addition, the measurement of load applied at stump tissue could further enhance the understanding of the biomechanical and biological behaviour of the tissue. Such tissue behaviour could be further implemented in the next-generation socket systems to improve comfort and thus the overall rehabilitation outcome.

2.3 Able-bodied gait biomechanics

The excessive movement (Section 2.2.2) and the stresses at the socket interface (Section 2.2.3) can be directly induced from ambulation, involving load transfer from the ground to socket interface. A review of able-bodied gait biomechanics will be provided with a view to aid in the understanding of amputee gait biomechanics.

A typical GC consists of both stance and swing phases (Figure 2.17). The beginning of the stance phase is defined as initial contact (IC) in the GC. This is followed by a loading response, during which the foot flattens with respect to the ground. At approximately 30% of GC, the body is supported by one single leg and the propulsive phase is initiated. After mid-stance, the heel starts to lift off from the ground. After the terminal stance (TS) phase, the heel continues to lift up and finally clears the ground, during toe-off (TO) occurring at approximately 62% of GC. The swing phase typically occupies from 62% to 100% of a GC.

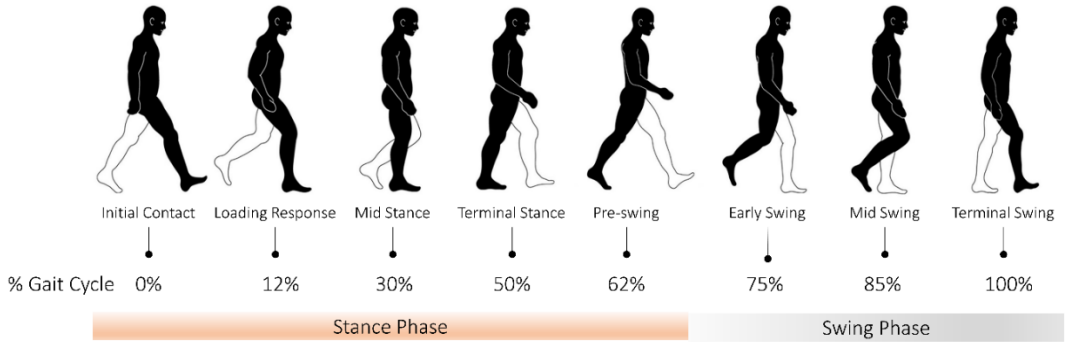

Figure 2.17: Definition of able-bodied GC

The GC is a repetitive pattern, involving loading in the stance phase and unloading when foot clears the ground in the swing phase. Understanding the load transfer from the ground to the limb is critical in the clinical decision-making process for pathological gait.

2.3.1 Ground reaction forces

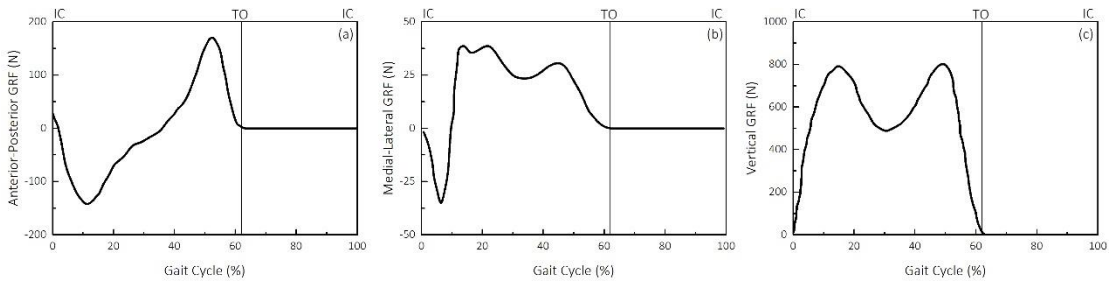

Figure 2.18: Reference set of (a) anterior-posterior, (b) medial-lateral and (c) vertical component of GRF, as a function of GC.

GRF presented in Figure 2.18 was collected by Winter [99]. The anterior-posterior (Figure 2.18a) and the medial-lateral (Figure 2.18b) component provides adequate friction between the foot and the ground. This could reduce or prevent the potential threats to walking stability [100]. In early stance phase (approximately 12% of GC), the ground exerts a posteriorly-directed force onto the foot, serving the purpose of brake (Figure 2.18a). Minimal shear force is observed in mid-stance phase (approximately 32% of GC). Just before heel-rise, the ground exerts an anteriorly-directed force to the foot to propel the body in upward and forward directions. In the medial-lateral direction (Figure 2.18b), from IC to approximately 8% of GC, a laterally-directed force is evident. During the remainder of the GC, a positive force is evident as the ground exerts a medially-directed force on the foot.

The vertical component of GRF (Figure 2.18c) is composed of two peaks, separated by a small trough. The first peak occurs between the loading response and mid-stance phase, in the response of weight acceptance. The mid-stance valley trough at approximately 30% of GC, results from the elevation of the body's centre of gravity. The second peak occurs in TS phase and is modified by pushing the ankle plantar-flexors against the floor. All three components of the GRF are further transferred proximally to the ankle, knee and hip joint. Joint mechanics, including joint kinematics and kinetics, has been used to describe the biomechanics during walking.

2.3.2 Ankle joint biomechanics

Figure 2.19-Figure 2.21 show the normative set of gait analysis data obtained from 16 able-bodied participants (male, adult), walking at their natural cadence [99]. From 0-5% of GC, up to 5° of ankle plantar-flexion is evident (Figure 2.19a), whereas from 5% to approximately 45% of GC, ankle dorsi-flexion is evident. The rapid decrease of the body weight on the foot at IC initiates an ankle dorsi-flexion motion, achieving foot flat after the loading response phase. Further dorsi-flexion motion is aided by the tibial progression. As the pre-swing phase is initiated, a plantar-flexion motion was evident and approximately -20° ankle angle is observed at TO. In the swing phase, a minor decrease in the plantar-flexion is experienced as the foot is preparing for the next stance phase.

Ankle moment (Figure 2.19b) is presented in loading response, acting to control the rate of foot lowering. The GRF vector passes anteriorly to the ankle joint after the loading response and the ankle dorsi-flexion moment returns to zero. This is followed by an increase in ankle plantar-flexion, which peaks in TS. During this period, the ankle plantar-flexes to help the limb to achieve an upward and forward push-off, preparing for the swing phase.

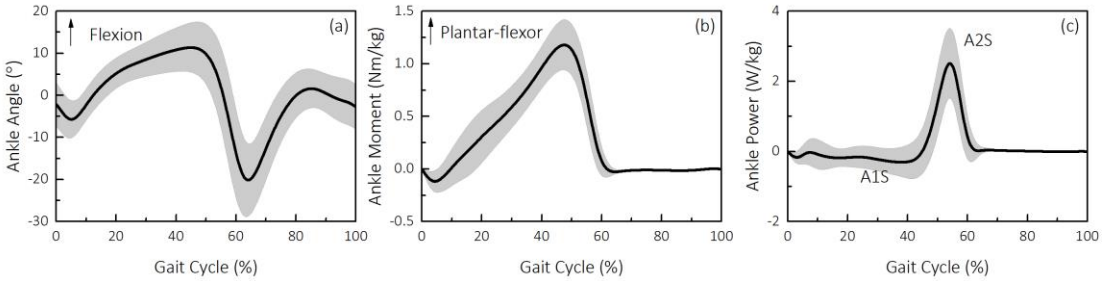

Figure 2.19: Reference set of (a) ankle joint angle, (b) moment and (c) power as a function of GC.

Figure 2.19c shows the ankle joint power as a function of GC. In the loading response, the rapid response of the dorsi-flexor muscles eccentrically controls the foot lowering, generating an immediate peak negative power (A1S). There is a surge of positive power at approximately 53% of GC, which corresponds to the concentric activation of propulsive plantar flexor activity (A2S) during the pre-swing phase.

2.3.3 Knee joint biomechanics

Two waves of knee flexion motion can be seen during each stride (Figure 2.20a). The first wave spans between the loading response and mid-stance phase, aiding the knee to absorb impact from the ground. The second wave occurs in the initial swing phase to assist the foot clearance.

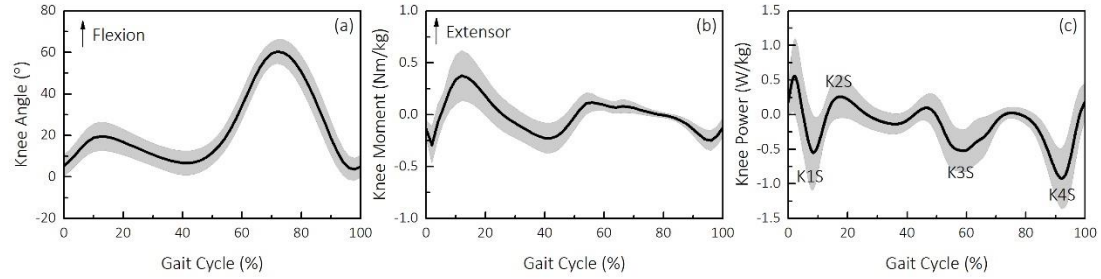

Figure 2.20: Reference set of (a) knee joint angle, (b) moment and (c) power as a function of GC.

Figure 2.20b shows the knee joint moment as a function of GC. A peak extensor moment was evident in early stance phase. Figure 2.20c shows the knee joint power as a function of GC. During the loading response, power absorption (K1S) is presented and this corresponds to the eccentric knee activity. K2S corresponds to the concentric knee activity (K2S) in the mid-stance phase. Thereafter a negligible joint power is generated, between about 35-40% of GC, when the ground reaction force stabilises the knee in a state of extension. In TS, an eccentric activity (K3S) was evident resulting from the rectus femoris. Finally, a period of negative power was activated towards the end of the GC. This corresponds to the eccentric activity in the hamstrings muscles to control knee extension.

2.3.4 Hip joint biomechanics

Figure 2.21 shows the hip joint angle as a function of GC. During the loading response, the hip angular position remains relatively stable and only begins to extend after the loading response. Up to 38° of change in the form of extension in hip angle was observed in the stance phase. During the pre-swing phase, the hip begins to flex until the terminal swing phase (90% of GC), eventually ending with the hip retracted during the terminal swing.

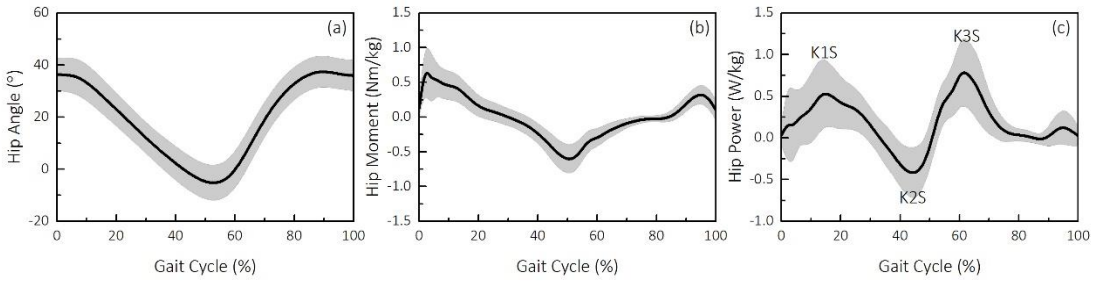

Figure 2.21: Reference set of (a) hip joint angle, (b) moment and (c) power as a function of GC.

Figure 2.21b illustrates the hip joint moment as a function of GC. Hip extension moment was presented in the first half the stance phase and hip flexor moment was presented during the remainder of the stance phase. The former hip extension moment acts to support and stabilise the posture of the trunk. The latter, hip extension moment assists the knee extensor in preventing the possible collapse of the knee joint. During the second half of the stance phase, the hip flexion moment helps to stabilise the posture of the trunk from flexing backward and counteract an anterior reaction force is acting on the hip joint centre.

The muscle is generating energy (H1S) during the first 15% of the GC, which corresponds to the concentric hip extensor activity during the loading response (Figure 2.21c). This is followed by a region of negative power, which is caused by the eccentric hip flexor activity (H2S) after 40% of GC. During the TS phase or the pre-swing phase of the GC, a period of power generation (H3S) is evident, corresponding to the concentric activity in the hip flexors. This is considered to be the second largest contribution from the muscular system to achieve a propulsive power during the GC.

2.4 Lower limb amputee gait biomechanics

For lower limb amputees, appropriate prosthetic fitting offers improved control over its position and alignment, possibly by improving proprioception and force transfer to the prosthesis. It is believed that with optimal fitting of the socket, the degree of gait asymmetry can be reduced. Hence, the characteristics of amputee gait can be considered to represent one

of the key parameters, which reflect the biomechanical conditions at the residuum/socket interface.

2.4.1 Ankle joint mechanics

Figure 2.22, Figure 2.23 and Figure 2.24 show joint mechanics for lower limb amputees, as a function of GC. The reference set of data was extracted from eight trans-femoral amputees [101] (7 male and 1 female, age: 28-60 years) and five trans-tibial amputees [102] (all male, age: 32-77 years).

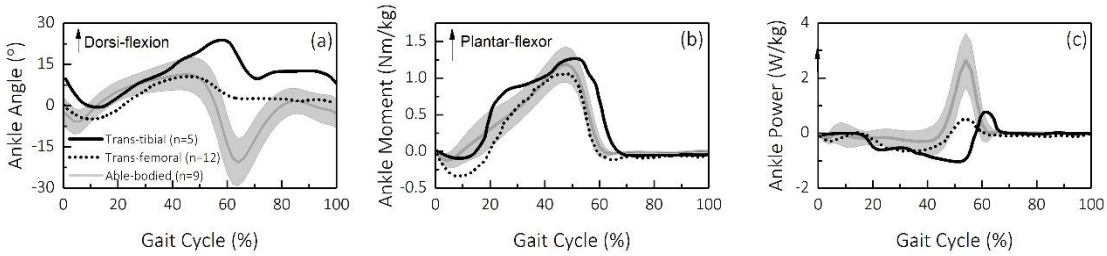

Figure 2.22: A reference set of ankle joint mechanics on prosthetic side. Data from [101] and [102] was re-produced.

From IC to approximately 10% of GC, up to 10° and 5° of ankle plantar-flexion movement (Figure 2.22a) was evident for trans-tibial and trans-femoral amputee, respectively. It is followed by ankle dorsi-flexion movement of up to 25° and 15° for trans-tibial and trans-femoral amputees, respectively. During the remainder of the stance phase, ankle angle in sagittal plane restores to a value slighter higher than the value obtained at IC. In swing phase, little ankle movement was observed.

In the early stance phase (approximately 12% of GC), a peak plantar-flexion moment of up to 0.30Nm/kg and 0.05Nm/kg was evident on the trans-tibial and trans-femoral amputee (Figure 2.22b), respectively. Peak dorsi-flexion moments of up to 1.3Nm/kg and 1.1Nm/kg were measured on trans-tibial and trans-femoral amputees, respectively.

The peak ankle eccentric power (Figure 2.22c) of up to 1.0W/kg (at approximately 55% of GC) and 0.6W/kg (at approximately 30% of GC) was evident on trans-tibial and trans-femoral amputees, respectively. The corresponding peak ankle concentric power values of up to 0.8W/kg and 0.5W/kg was recorded.

2.4.2 Knee joint mechanics

Up to 25° of knee flexion movement was reported in early stance phase for trans-tibial amputees (Figure 2.23a). However, little knee flexion movement was measured in stance phase

for trans-femoral amputees. In TS phase, up to 54° and 78° of knee flexion angle was observed for trans-tibial and trans-femoral amputees, respectively.

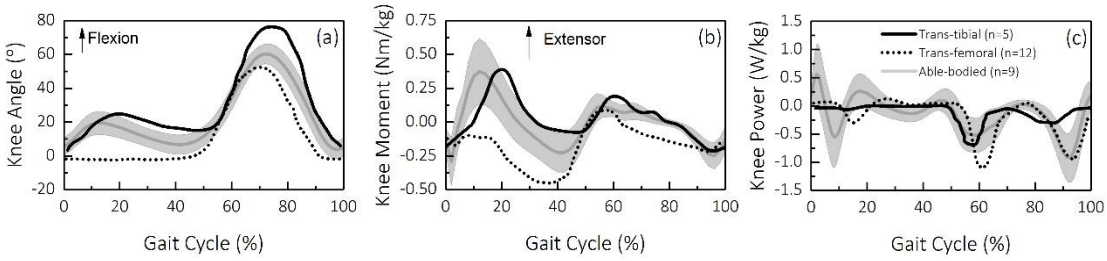

Figure 2.23: A reference set of knee joint mechanics on prosthetic side. Data from [101] and [102] was re-produced.

Up to 0.4Nm/kg and -0.1Nm/kg of knee extension moment in early stance phase was evident on trans-tibial and trans-femoral amputees (Figure 2.23b), respectively. This indicates the difference between the functioning of a biological and prosthetic knee.

Little knee eccentric power, in early stance, was observed for trans-femoral amputees (0.0W/kg) while up to 0.25W/kg was evident for the trans-tibial amputee (Figure 2.23c). At TO, a greater knee eccentric power was observed for trans-tibial amputees (1.1W/kg), compared to the value obtained for trans-femoral amputees (0.6W/kg).

2.4.3 Hip joint mechanics

Up to 35° and 40° of hip ROM was evident on trans-tibial and trans-femoral amputees (Figure 2.24a), respectively. A greater hip extension moment (Figure 2.24b) was evident for trans-tibial amputees (1.0Nm/kg), compared to that for trans-femoral amputee (0.25Nm/kg). However, in TS phase, a greater hip flexor was observed for trans-tibial amputees (1.24Nm/kg) compared to that for trans-femoral amputees (0.2Nm/kg).

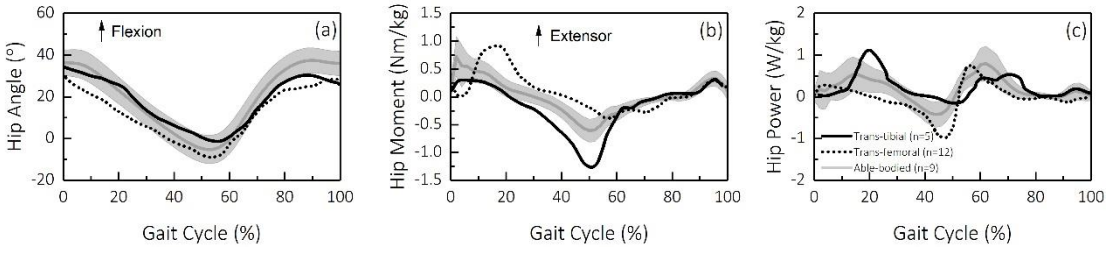

Figure 2.24: A reference set of hip joint mechanics on prosthetic side. Data from [101] and [102] was re-produced.

A greater hip power generation (Figure 2.24c) was observed in early stance phase for trans-tibial amputees (1.1W/kg), compared to that for trans-femoral amputees (0.1W/kg). There was a reduction in hip power absorption for trans-tibial amputees (0.0W/kg), compared to that for trans-femoral amputees (-1W/kg).

2.4.4 Comparison with able-bodied group

Temporal-spatial parameters

It is recognised that lower limb amputees have a less efficient gait pattern and one of the key contributors is the asymmetries in temporal-spatial parameters. Therefore, it is a dilemma to decide whether the load should borne on the prosthetic or the contra-lateral side. If excessive load was distributed over the residuum, there is an increases risk of developing tissue damage. By contrast, the emphasis of relieving the load on the prosthetic side could result in gait compensation, which may, in turn, lead to an over-use of the contra-lateral side. Therefore, developing a means to assess the load distribution at the residuum/socket interface is critical to achieve a more balanced weight bearing on both prosthetic and contra-lateral sides.

Table 2.3 illustrates a selection of these parameters that are frequently used in amputee gait analysis studies. A greater swing time is observed on the prosthetic side, compared to the contra-lateral side, which may be associated with the long step length demonstrated on the prosthetic side.

It is also worth noting that the contra-lateral side experiences a longer percentage during the stance phase, compared with both the prosthetic side and the able-bodied group. This may be further associated with the increased joint loading on the contra-lateral side, resulting in the increased risk of osteoarthritis in hip and knee joints [103, 104]. Therefore, it is a dilemma to decide whether the load should borne on the prosthetic or the contra-lateral side. If excessive load was distributed over the residuum, there is an increases risk of developing tissue damage. By contrast, the emphasis of relieving the load on the prosthetic side could result in gait compensation, which may, in turn, lead to an over-use of the contra-lateral side. Therefore, developing a means to assess the load distribution at the residuum/socket interface is critical to achieve a more balanced weight bearing on both prosthetic and contra-lateral sides.

Table 2.3: Comparison in temporal-spatial parameters for lower imb amputee.

	Prosthetic VS contra-lateral	Prosthetic VS Able-bodied	Contra-lateral VS able-bodied
Step length	+ [105]		
Stride length		+ [105], [106]	
Walking speed	N/A	Comparable [107] or slightly higher in the able-bodied [108]	N/A
Stance %	+ [108]	+ [105], [109]	+ [110]
Swing %	+ [109]	+ [105], [109]	
Swing speed		+ [105]	
+: higher			

Ground reaction force

- Trans-tibial amputees

In comparison to the non-amputated side, a reduction in peak anterior-posterior braking force, peak medial-lateral GRF and the 2nd peak of vertical GRF in TS phase was observed [111] on the amputated side. The reduction in peak vertical GRF may suggest that the amputated side is less capable of weight bearing. The reduction in peak vertical GRF may suggest that the amputated side is less capable of weight bearing. Also, the reduction in the peak medial-lateral GRF may indicate that the exchange of body weight from one limb to the other may be impaired. In addition, the reduction in peak braking force in the anterior-posterior direction may be associated with the lack of stability during loading. Greater peak medial-lateral GRF and vertical GRF were evident on the contra-lateral side of the amputees, compared with the values for able-bodied participants [111-113].

- Trans-femoral amputees

For trans-femoral amputees, GRF obtained on the prosthetic side showed reductions in 2nd peak of the vertical GRF, peak braking force, compared to both the contra-lateral side of the amputees and the able-bodied [114]. This is likely caused by hip hiking in coronal plane, which may induce a more vertical landing of the prosthetic limb in early stance phase.

With regards to the medial-lateral GRF, a greater peak GRF value was obtained on the prosthetic side, compared to the values obtained for both contra-lateral side of the amputee and the able-bodied group. It is likely that, due to the higher vertical displacement of the centre of mass for trans-femoral amputees, a greater body movement in the frontal plane is needed to smooth out the centre of mas displacement [101, 115]. This could result in the higher values of peak medial-lateral GRF.

When comparing the GRF obtained on the contra-lateral side of amputee to the value obtained for the able-bodied, a reduction in 2nd peak of vertical GRF and peak braking force was evident. However, a greater braking impulse in early stance phase was observed on the contra-lateral side of trans-femoral amputees

Ankle joint mechanics

A reduced and delayed plantar-flexion movement in early stance phase was evident for trans-femoral amputees (Figure 2.22a), when compared with the able-bodied (Figure 2.19a). This is likely due to the fact that plantar-flexion motion is primarily a result of heel compression in the

absence of the ankle joint movement. The reduction in plantar-flexion movement could potential lead to a delayed foot-flat phase, increasing the risk of limb instability during the load response phase. A reduced dorsi-flexion movement, equivalent to up to 38%, during mid to TS phase was additionally reported and is likely due to the inability of the prosthetic foot spring to bend [116, 117].

Plantar-flexion moment was developed over 0-12% of GC for lower limb amputees (Figure 2.22a) which is significantly higher than that on the able-bodied (up to 5% in Figure 2.19b) [101, 102]. This suggests a lack of ability to rapidly achieve foot flat in stance phase for lower limb amputees. The prolonged duration of plantar-flexor moment may increase stress-time integral at the residuum/socket interface. The peak dorsi-flexion in TS phase, was considerably lower i.e. a 60-70% reduction for lower limb amputees compared to the able-bodied [101, 102].

When the carbon fibre heel blade deflects during early stance phase, energy will be absorbed in the blade, resulting in an ankle power absorption or eccentric power for a lower limb amputee. During TS phase, the stored elastic energy in the blade will be released, generating a power that propels the prosthetic limb. It has been reported that, for lower limb amputees, the power generation (Figure 2.22c) was up to four times less than that for able-bodied (Figure 2.19c), which may be directly associated with the deflection capability of the prosthetic foot blades [101, 102].

Knee joint mechanics

Knee flexion in early stance phase is reduced (Figure 2.22a) for trans-tibial amputees, thus limiting the shock-absorbing capacity [118], comparing to the value for the able-bodied (Figure 2.20a). This could result in abnormal loads exerted through the residuum/socket interface, which may result an increased risk of tissue damage. For trans-femoral amputees, the knee flexion (Figure 2.22a) in early stance phase is either absent or negative [101]. This could be associated with the prevention of both knee buckling and the collapse of the limb.

Knee flexor moments in early stance phase appears to show the greatest difference between the lower limb amputee and able-bodied [106]. The knee extensor moments associated with trans-tibial amputees (Figure 2.23b) was significantly smaller than the value for the able-bodied (Figure 2.20b) [106]. However, EMG data indicted the opposite findings with a 25% increase in vastus lateralis intensity compared to the able-bodied [106]. Hence, caution is needed when assessing residuum/socket interface using joint kinetic data alone. It is therefore proposed that measurement needs to directly record at the residuum/socket interface. For trans-femoral

amputees, even smaller knee flexor moments were recorded in early stance phase, when compared to both trans-tibial and able-bodied individuals.

For trans-tibial amputees, a reduction of knee joint power (up to 53%) absorption in early stance phase (Figure 2.23c) have also been reported [119], compared to values for able-bodied (Figure 2.20c). A similar finding was observed for trans-femoral amputees with the absence of both energy absorption and energy generation on knee joint power [120], until TO. It is therefore proposed that the prosthetic knee joint plays little role in the shock absorption during both the loading response and limb propulsion TS phase.

Hip joint mechanics

It is reported that, the range of the motion on the both prosthetic side (Figure 2.24a) and contra-lateral side for trans-femoral amputee is almost doubled, when compared to the able-bodied (Figure 2.21a) [121]. This is likely due to the loss of biological knee and foot with muscle loss around the residuum. Extra movement was required by the hip to control the limb. When comparing among amputees, the hip range of motion for trans-femoral amputees, was found to be reduced when fitted with the ischial containment socket[122]. During hip extension, the ischial lock feature built on the socket, limits the physiological motion on the prosthetic side, which may trigger a compensatory mechanism on the pelvis on the sound side. This suggests that different type of prosthesis, in this case involving socket design can influence the joint kinematics.

No active control of prosthetic ankle and knee joint is allowed with passive prosthetic components. This could result in high moments at the hip, assisting the limb progression [120]. It is reported that, for lower limb amputees, hip moments at IC (Figure 2.24b) is two-fold greater than for the able-bodied (Figure 2.21b) [115]. This finding was observed for both the prosthetic side and the contralateral side.

Both trans-tibial and trans-femoral amputee rely on the hip to absorb and generate power. There is no doubt that, from various studies, a large surge of hip joint power generation just before TO is evident [119, 120, 123]. This serves as a compensatory mechanism in response to the lack of generation of prosthetic ankle and knee joint power. The over-use of the hip on the prosthetic side will then contribute to the excessive femoral movement inside the socket. This may result in the reduction of limb stability and proprioception.

In this section, differences in temporal-spatial parameter, ground reaction forces and joint mechanics have been highlighted between the amputee group and able-bodied group. The

greatest difference was evident in knee joint mechanics for trans-tibial amputees and hip joint mechanics for trans-femoral amputees. This was primarily due to the loss of the biological joint and the presence of a residuum/socket interface. Therefore, a comprehensive understanding of the load transfer mechanism from the ground to the socket interface is critical for the biomechanical assessment of the socket interface.

2.5 Load transfer mechanism for lower limb amputee

With presence of the residuum/socket interface, abnormal load transfer to each of the joint was revealed in previous studies (Section 2.4.4). In addition, with the issue illustrated in Section 2.2, a biomechanical understanding of the interface requires an examination of the load transfer mechanisms from the ground, through the prosthetic limb to the socket interface. This will be addressed in the following section.

2.5.1 Theory of lower limb load transfer

Able-bodied group

The theory of lower limb load transfer can be demonstrated, using a linked-segment model. As shown in Figure 2.26a, the skeletal model for an able-bodied group consists of three segments and four key anatomical landmarks. Up to three gait models (Figure 2.25) have been commonly used in human gait analysis, based on a review incorporating 51 studies [5]. They are namely, a linear segment representation model, a Helen Hayes conventional model [124] and a lower limb musculoskeletal model with three degrees of freedom at each of the joint [125]. Each of the models assume that all segments are rigid and their centre of mass is located along their length, as defined by de Lava [126]. Furthermore, no movements are assumed between the tissue and the underlying skeleton [127].

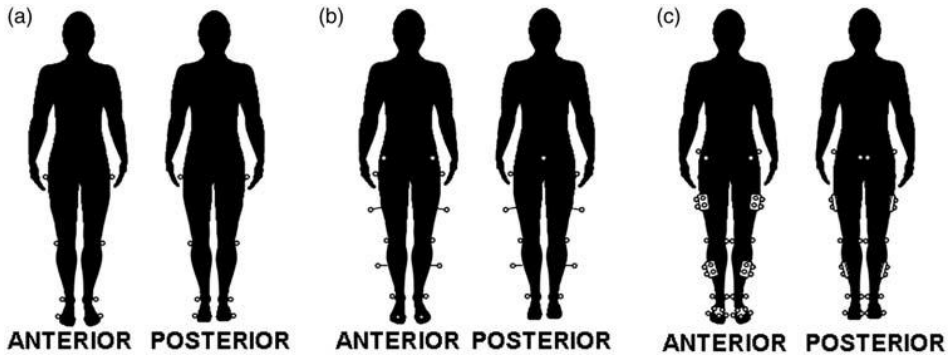

Figure 2.25: Marker placement protocol for (a) linear segment model, (b) Helen Hayes conventional model and (c) a lower limb musculoskeletal with three degrees of freedom at each of the joint model. Image adopted from [5].

Three internal forces are acting on the foot segment (Figure 2.26b), including the foot gravitational force $m_{Foot}\mathbf{g}$, ankle joint force $\mathbf{f}_{Ankle}$ and inertial force $\mathbf{a}_{Foot}m_{Foot}$. The external force and internal forces can be represented by:

$$\boldsymbol{f}_{Ankle} = m_{Foot}\boldsymbol{a}_{Foot} - \boldsymbol{f}_{GRF} - m_{Foot}\boldsymbol{g} \tag{2.1}$$

Where $\mathbf{f}_{ankle}$ is the force vector experienced by the ankle joint, $\mathbf{f}_{GRF}$ is the ground reaction force vector, $\mathbf{m}_{foot}$ is the mass of the foot segment, $\mathbf{g}$ is the gravitational constant and $\mathbf{a}_{Foot}$ is the linear

acceleration of the foot segment in vector form. The ground reaction force vector can be obtained from a force platform, while the mass of the foot segment can be obtained from published cadaveric studies.

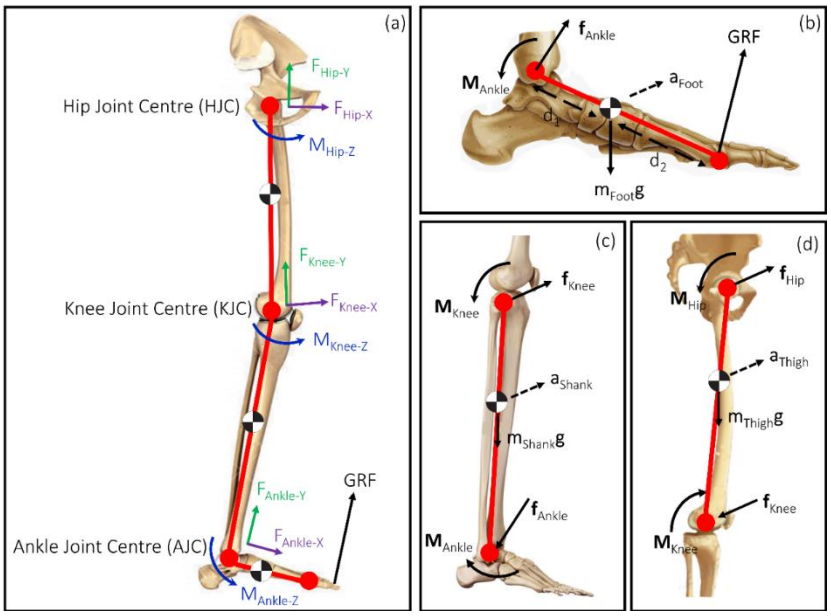

Figure 2.26: Lower limb musculoskeletal model and its free body diagram for able-bodied person

By taking the moments about the centre of mass of the foot segment, the vector form of ankle joint moment can be expressed by:

$$\boldsymbol{M_{Ankle}} = I_{Foot}\boldsymbol{\alpha_{Ankle}} - (\boldsymbol{d_1} \times \boldsymbol{f_{Ankle}}) - (\boldsymbol{d_2} \times \boldsymbol{f_{GRF}}) - \boldsymbol{T} \qquad (2.2)$$

Where $\mathbf{M}_{Ankle}$ is the moment vector experienced by the ankle joint, I_{Ankle} is the second moment of inertia of the foot segment, $\boldsymbol{\alpha}_{Ankle}$ is the angular acceleration vector of the foot segment, $\mathbf{d}_1$ is the vector linking the centre of mass of the foot to the ankle joint centre, $\mathbf{d}_2$ is the vector linking the centre of the mass of the foot segment to the proximal end of the foot and $\mathbf{T}$ is the GRF torque in vector form.

Having calculated the joint moment, the joint power, can be estimated from the product of joint moment and the joint angular velocity. For example, the ankle joint power can be expressed as:

$$\boldsymbol{P_{Ankle}} = \boldsymbol{M_{Ankle}} \times (\boldsymbol{\omega_{Shank}} - \boldsymbol{\omega_{Foot}}) \qquad (2.3)$$

The same approach can be repeated to estimate the force, moment and power at knee joint (Figure 2.26c) and hip joint (Figure 2.26d). This technique has been commonly applied in gait analysis and typical results are presented in Section 2.3.

Amputee group

In the context of amputee clinical gait analysis, the introduction of both prosthetic components and the residuum poses new challenges to the definitions of joint centre, segments, and the protocol for marker placement as well as the reporting of meaningful clinical data. Jia et al [128, 129] proposed an analytical calculation of the knee joint force within the socket, based on Newton's 2nd law of motion for trans-tibial amputee. Figure 2.27 shows the free body diagram of a trans-tibial residuum donned onto a prosthetic limb.

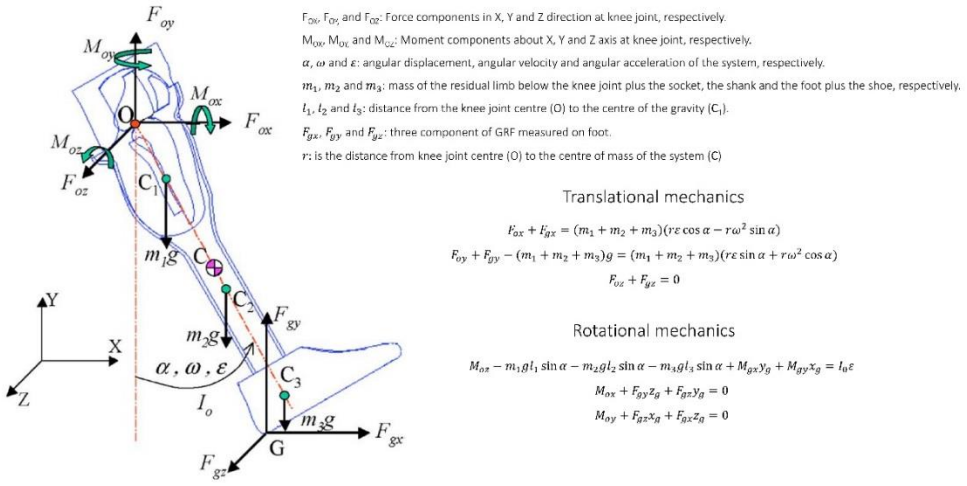

Figure 2.27: Free body diagram for the calculation of loads at knee joint.

By substituting raw data from 3D motion analysis system, including the angular displacement, angular velocity, angular acceleration and ground reaction force as a function of GC, three components of force and moment can be calculated. Figure 2.28 shows the force and moment applied to the knee joint centre over one GC.

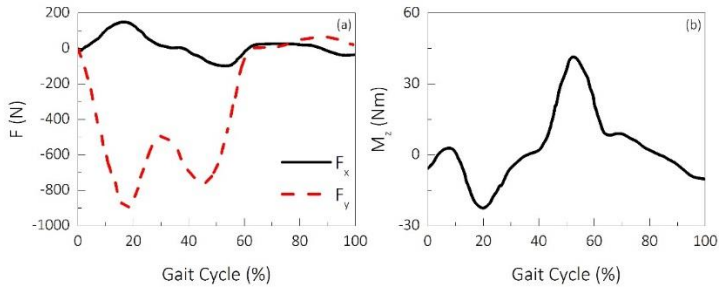

Figure 2.28: (a) Forces and (b) moment applied at knee joint, over a GC. Data was extracted from [128].

In the stance phase, from IC to approximately 20% of GC, an anteriorly-directed force is observed (Figure 2.28a), leading to the knee joint pressing against the socket. By contrast, in the TS phase, a posteriorly-directed force is evident and this can lead to increased interaction

between the stump and the posterior brim of the socket. In the vertical direction, a double-hump force profile is evident.

Figure 2.28b shows the bending moment in the sagittal plane. At approximately 20% of GC, a negative bending moment is observed. This can lead to the interaction between the cut-end of the tibia and the posterior-distal location of the socket, to achieve a braking effect. Positive bending moment is observed in the TS phase (approximately 55% of GC). This may result in the interaction between the cut-end of the tibia and the anterior-distal location of the socket. A number of factors, however, question the aforementioned assumption of many of the models including,

- Prosthetic components (Section 2.1.2), such as the prosthetic foot, has a deformable keel, which violate the rigid body assumption [130, 131]. Indeed, only two of the 50 studies modelled the deformable keel separately as an elastic structure [132, 133].
- Any relative movement at the residuum/socket interface may violate the rigid body assumption of the standard model for example, the shank segment for the trans-tibial amputee and thigh segment for the trans-femoral amputee [134].

2.5.2 Direct measurement of load transfer

Understanding the load transfer distal to the prosthetic socket is critical for the assessment of socket fit, prosthetic componentry design and associated finite element analysis [135]. Instrumented load cells have been commonly placed underneath the socket (Figure 2.29) to measure the forces and moment transferred to the interface [69, 136-142]. By using load cells, load transfer at a certain location along the prosthesis, typically located just below the socket, can be measured.

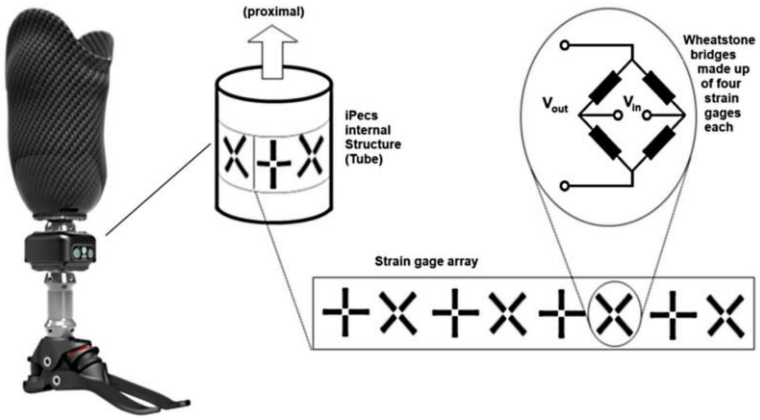

Figure 2.29: The placement of an iPecs load cell underneath the socket. Image adopted from [138].

Figure 2.30 shows the waveform and peak values of the forces observed just below the socket for both trans-tibial [140] and trans-femoral amputee [137, 139, 142]. In the anterior-posterior direction, a posteriorly-directed force is acting on the socket in early stance phase while an anteriorly-directed force is evident towards the end of the stance phase (Figure 2.30a). In the medial-lateral direction, the medially-directed force dominates most of the stance phase (Figure 2.30b). In Figure 2.30c, a peak compressive force is observed at approximately 82% of GC.

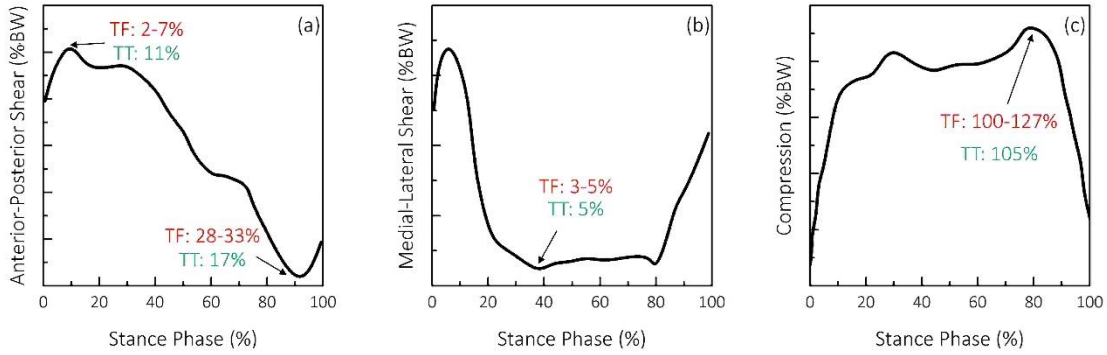

Figure 2.30: Forces measured just below the socket in (a) anterior-posterior direction, (b) medial-lateral direction and (c) vertical direction. Data present in the figure can be found in [137, 139, 140, 142] .

Figure 2.31 shows the waveform and peak values of the corresponding bending moments for both trans-tibial [70, 140, 143] and trans-femoral amputees [137, 139, 142]. The highest bending moment is observed in the sagittal plane, a peak plantar-flexor moment is evident at approximately 80% of the stance phase. The bending moments observed in both coronal and transverse planes are low compared with those measured in the sagittal plane.

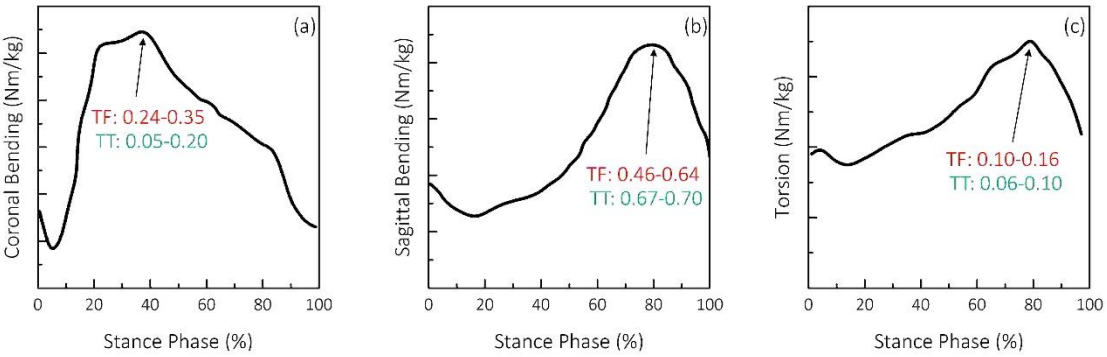

Figure 2.31: Bending moments measured just below the socket in (a) coronal plane, (b) sagittal plane and (c) transverse plane. Data present in the figure can be found in [70, 140, 143] for trans-tibial amputee and [137, 139, 142] for trans-femoral amputee.

To date, two measurement techniques for load transfer have been reported. It is evident from a theoretical point of view that the walking speed and the terrain can influence the load transfer from the ground to the distal end of the socket. For example, the walking speed can affect the

rotational kinematics of the segment distal to the socket (Equation (2.2) and Equation (2.3)), thus resulting in a change of load transfer. These factors are most conveniently discussed separately.

2.5.3 Key parameters affecting load transfer

Speed

With a passive prosthetic devices (Section 2.1.2), optimal performance can be obtained at customary walking speed. Accordingly, at other speeds, the performance of the prosthetic device will be sub-optimal. In addition, Fey [144] reported an increase in both knee joint force and moment with walking speed. It is worth noting that, the knee joint moment was not normalised to walking speed in their study. In addition, an enhanced value of positive hip joint power was obtained when walking at an increased speed to that recorded at a self-selected speed.

Terrain

It is well known that when walking on a descending ramp, the stability of the prosthetic limb stability needs to be ensured to prevent a fall. Furthermore, when engaging with an ascending ramp, the ease of tibial progression in early stance and an adequate power generation in TS are critical for improving gait stability. Therefore, there is a need to understand load transfer through the prosthetic limb when engaging with different terrains.

Several studies have reported the influence of the terrain on the joint biomechanics. When walking on a descending ramp, a higher knee flexion motion was reported in both TS and swing phases for trans-tibial amputees [145]. However, for trans-femoral amputees, the terrain does not seem to have an effect on the knee joint kinematics. When walking on an ascending ramp, a reduction in ankle dorsi-flexor was evident in early stance phase compared with that on a descending ramp [146]. In TS phase, a greater ankle plantar-flexor was revealed when walking on descending ramp, comparing with that on ascending ramp. A significant reduction in knee extensor was observed when walking on the ascending ramp, in early stance phase, comparing with that on descending ramp. The hip extensor moment was approximately doubled in early stance phase when on the descending ramp, comparing with that on the ascending ramp [147].

Prosthetic components

As introduced in Section 2.1.2, different types of prosthetic components have been developed depending on the level of amputation and operating procedures. The examination of the

influence of prosthetic components on joint biomechanics can provide guidance on the optimal design of these prosthetic components.

It has been reported that a smooth/rapid change in load transfer profile is evident when using a hydraulic ankle-foot device compared to a non-hydraulic foot [34]. When fitted with a hydraulic foot both a rapid progression of centre of the pressure (CoP) beneath the prosthetic hind foot and an increase in walking speed when fitted were observed. With same type of prosthetic knee, Genium knee showed a greater knee flexion motion in swing phase compared with the value obtained on a C-leg [26]. Peak values of ankle dorsi-flexor were reduced significantly with a hydraulic foot compared with a non-hydraulic [33]. Segal et al [101] reported that the C-leg enhanced the knee flexor moment significantly compared with a conventional mechanical knee. Nickel [147] linked the socket comfort with the adaptation and the adjustment of prosthetic ankle on ramped surface. In addition, an enhanced energy storing capacity and restoration of the prosthetic ankle were observed with an adjustable ankle compared with fixed-ankle devices.

De Asha, Johnson [148] reported that hydraulic ankle device reduced the magnitude of the posteriorly directed CoP displacement, greater shank angular velocity and comfortable walking speed on trans-tibial amputees. In addition, the speed-related changes in the compensatory contra-lateral joint kinetics was minimised when using hydraulic ankle device, comparing to those with rigid ankle [33].

The alignment between prosthetic components was also reported to have significant effect on load transfer through the prosthetic limb. As an example, peak knee extensor was increased when the socket was translate posteriorly or in a more flexed position in relation to the distal components [149]. In coronal plane, a reduction in Varus moment was observed in mid stance by adduction or medial translation of the socket.

Interface mechanical properties

Prosthetic liners, as introduced in Section 2.1.2, with different thickness were reported to affect the load transfer mechanism. Walking with a thicker liner reduced the force and vibratory feedback to the residuum and contributed to a higher vertical GRF [150]. Furthermore, the way of attaching residuum to the rest of prosthesis (Section 2.1.4) can also load transfer through prosthetic limb. A reduction in the 1st peak of vertical GRF and an increase peak braking GRF was reported using pin-lock suspension comparing to that with suction suspension [55]. When friction coefficient was altered by two different liners, the polyurethane liner resulted in a

faster walking speed and a greater symmetry in kinematic variables [151]. Furthermore, by altering the prosthetic mass and its distribution, higher efficiency in knee joint work was observed when the mass was distributed in a proximal position, comparing to the value obtained in a distal position.

Based on the review above, walking speed, terrain, prosthetic components and interface mechanical properties can alter the load transfer to prosthetic limb. According to Figure 2.27, these factors would subsequently affect the load exerted at the knee joint within the socket interface for trans-tibial amputee and the hip joint for trans-femoral amputee proximal to the socket interface. Conventional gait analysis treats the socket interface as a rigid segment due to the lack of assessment techniques to provide in-situ measurement of kinematics and kinetics at the socket interface. This lack of biomechanical understanding at the socket interface could potentially also lead to the tissue damage (Section 2.2.3) and stability (Section 2.2.2) at the socket interface.

2.6 Residuum/socket interface kinematic assessment

A range of studies have been reported to measure real time stump movement and loading at the socket interface with a view to understanding *in-situ* biomechanics as a function of amputee's GC. To date, a few well established techniques including medical imaging, motion capture and instrumented sensor will be briefly critiqued in the following section.

2.6.1 Techniques for kinematic assessment

X-ray radiograph

X-ray based techniques have proved the most popular with researchers to investigate the kinematic coupling between the residuum and the socket [83, 85, 152-159]. The accuracy of RSA has been reported to present 0.3° and 0.2mm rotational and translational resolutions, respectively [160]. From the 1970s to 1990s, x-rays were used to produce 2D radiographs [85, 154-157]. Participants were asked to perform different stride positions statically, (Figure 2.32a and Figure 2.32b), while the radiological images were recorded (Figure 2.32c). Prostheses were prepared with a thin steel wire, running along the inner surface of the external prosthetic socket [156], in order to obtain high contrast radiograph between bone and sockets. These techniques were further developed [158] [83] by introducing several tantalum markers attached to the truncated bones to accurately measure the bone displacement relative to socket, under local anaesthesia [83]. This was followed by a-10-week recovery before actual experiments. The experiment often involves a static protocol, including full weight bearing, half weight bearing and non-weight bearing.

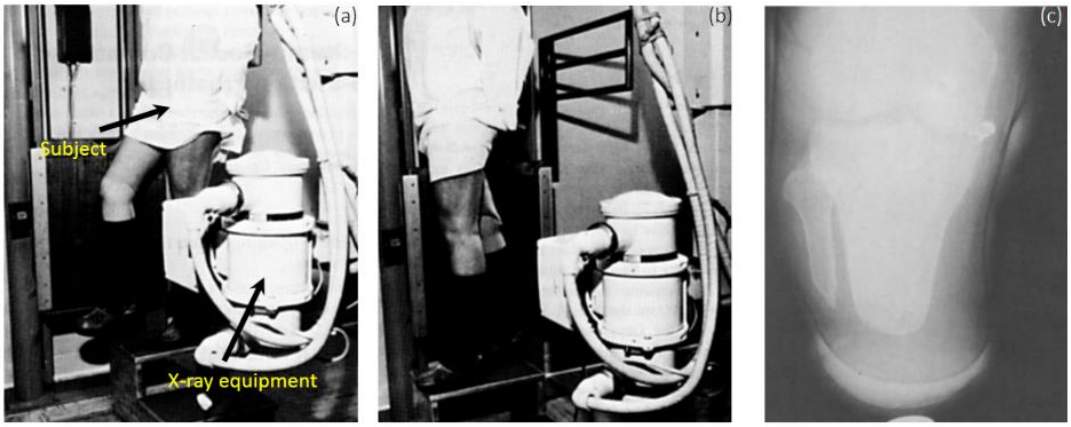

Figure 2.32: An illustration of participant performing different stride positions: (a) mid-swing and (b) foot-flat. (c) An example of radiograph taken from a trans-tibial amputee. All images were taken from Grevsten and Erikson [155].

Volumetric spiral x-ray computed tomography (SXCT)

SXCT was developed to investigate the movements at the residuum/socket interface [152, 153, 159]. The SXCT can produce 3D volumetric images of the socket interface. Therefore, a 6-degree-of-freedom motion of the residuum can be extracted. Participants were typically asked to lie supine on the platform. Metal markers were adhered to the surface of the stump, before donning the prosthesis [152, 153, 159]. Subsequently, an external load applicator was attached to the participant to apply load (up to body weight) to the socket interface [152, 153, 159]. CT scans were performed at different load levels. The 3D volumetric image of the socket interface were produced (Figure 2.33b) and subsequently sliced to form 2D images (Figure 2.33c).

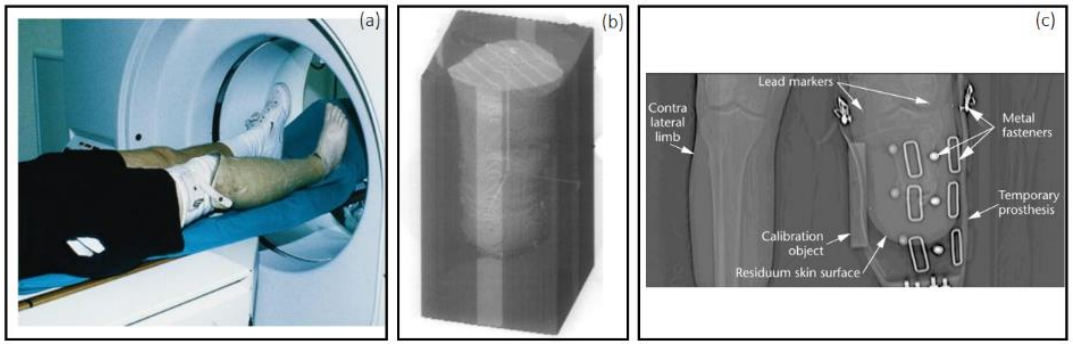

Figure 2.33: (a) Patient lying supine and preparing from the CT scan, (b) Volumetric rendering of 3D stump, output from the CT scanner and (c) an example of the cross-section of the intact and prosthetic limb, sliced from the volumetric 3D image. Note: (a) and (c) were taken from Vannier [159], (b) is taken from Commean [152].

Dynamic Roentgen Stereogrammetric Analysis (DRSA)

Papaioannou and colleagues used DRSA [161-165], combined with laser-based 3D digitiser with CT imaging equipment, to investigate the angular and linear couplings. Several tantalum markers (Figure 2.34a) and tantalum pigment paint (Figure 2.34b) were employed on the surface of the internal surface of the socket and surface of the stump, respectively. The laser scanner is subsequently used to obtain the internal and external surface of the socket, while reconstructed geometry of the residual bone with the 3D geometry of the stump and the 3D socket surface data were obtained by the CT imager. Participants were asked to perform dynamic activities (Figure 2.34c) and tantalum marker (and painted meshes), bone edges, were tracked. 3D motion at the socket interface were registered using multiple software, including Matlab, 3Ds Max studio, AutoCAD, Geomagic studio and Mimics.

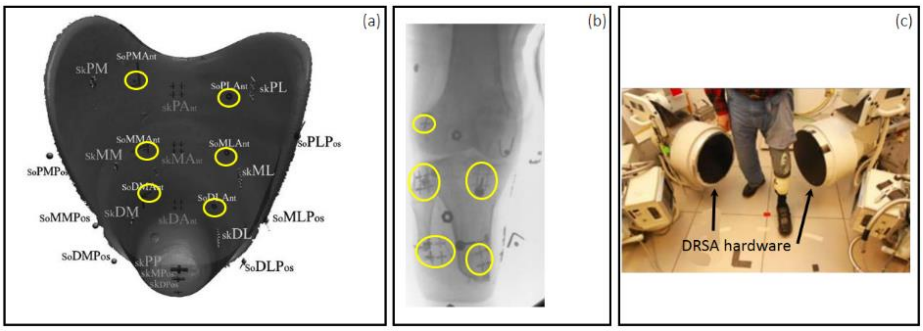

Figure 2.34: (a) Tantalum markers (yellow circle) placed over the internal surface of the socket, (b) tantalum meshes (yellow circles) painted on the stump and (c) DRAS imaging hardware. All images can be found in [164].

Ultrasound transducers

As an alternative to radiation-based equipment, Murray and Convery [8, 166, 167] used ultrasound transducers to investigate residuum/socket interface kinematic couplings. These study involved three stages, calibration of the ultrasound transducer [167], pilot amputee level walking tests [8] and amputee daily living activity tests [166]. Two rectangular openings were introduced on the lateral socket wall (Figure 2.35a) to mount the two ultrasound transducers (Figure 2.35b). Subsequently, each participant was asked to perform different activities. Videos, showing the movement of the femur relative to the socket, were recorded by the ultrasound transducer. Such movement were analysed using a video playback. This technique was reported to have the resolution of less than 1°.

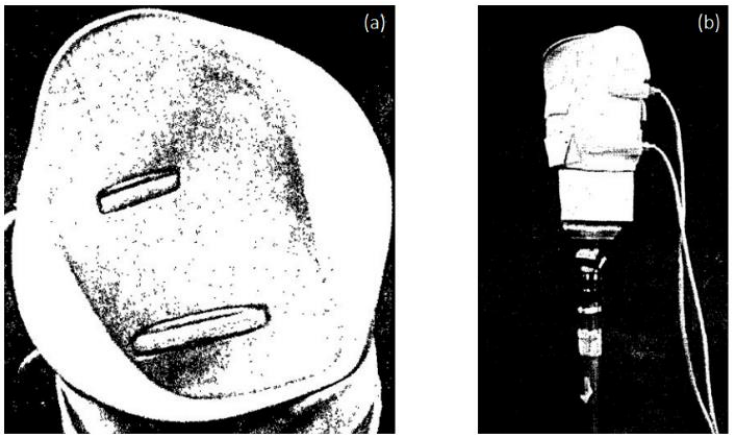

Figure 2.35: (a) Two openings made on the lateral socket wall for mounting the two ultrasound transducers and (b) two ultrasound transducer mounted on the lateral socket wall. Note the images were taken from Convery and Murray [8].

Motion capture technique

Cameras has been used to investigate the 2D translational movement between the residuum and the socket [78]. Four stickers can be placed over the greater trochanter (marked as A in Figure 2.36a), proximal lateral end of the liner (marked as B in Figure 2.36a), proximal lateral

end of the socket (marked as C in Figure 2.36a) and distal end of the socket (marked as D in Figure 2.36a). Four images were taken by a DSRL camera, corresponding to, non-weight bearing posture, half-weight bearing posture, full-weight bearing posture and posture with weight attached to the prosthetic feet. Corresponding images were analysed by measuring the change in the 2D distance between A and D stickers, representing the residuum axial movement.

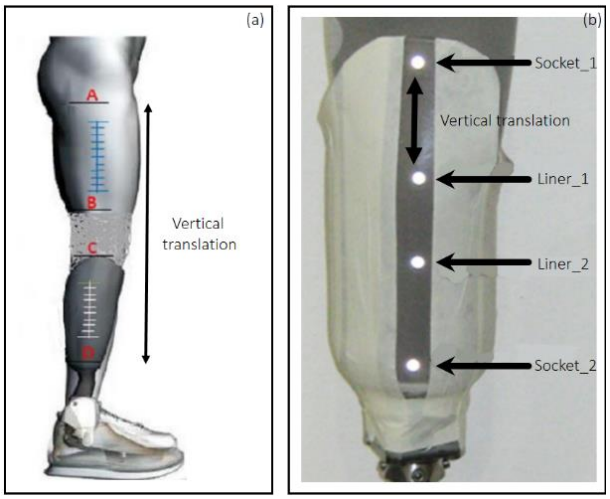

Figure 2.36: (a) Schematic showing the DSLR Camera based method, adopted from Gholizadeh et al. [78] and (b) gait laboratory 3D motion capture based method for the evaluation of residuum/socket vertical translational movement, adopted from Gholizadeh et al. [168].

3D motion capture technique

Gholizadeh et al. [168] used 3D motion capture to quantify the vertical displacement between the liner and socket (Figure 2.36b) for trains-tibial amputees. Four paper-thin reflective markers were used with two placed over the lateral proximal (marked as Socket_1 in Figure 2.36b) and lateral distal (marked as Socket_2 in Figure 2.36b) location of the socket, two placed over the liner and below the knee (marked as Liner_1 and Liner_2 in Figure 2.36b). The 3D marker co-ordinates of each of the marker were extracted. The 3D distance, between the Socket _1 and Liner_1 marker, was used as a representation of residuum axial motion.

A more sophisticated marker model was developed by Childers and Siebert [169] to investigate the residuum angular and translational movements for trans-tibial amputees. Two 40mm-diameter holes were drilled on the socket (LFE and AD location in Figure 2.37a) to accommodate the marker placement. Five real markers (marked as green in Figure 2.37a) were placed at the residuum/socket interface. Soc_1 and Soc_2 were placed along the lateral aspect of the socket. ADT_1 and ADT_2 were rigidly connected and placed over the AD location, through the hole. Similarly, a LFE marker were placed over the stump, via the hole. Both holes, one at LFE location and one at AD location, were subsequently sealed.

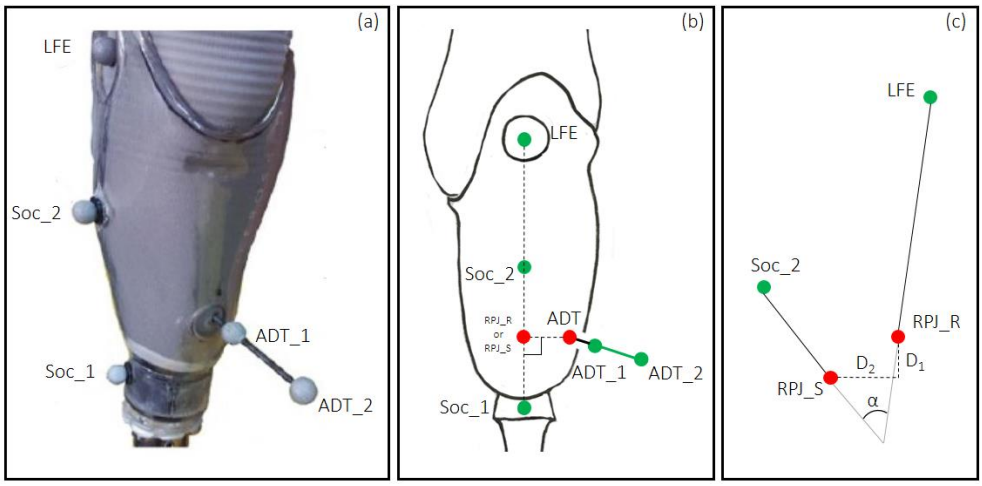

Figure 2.37: (a) Marker placement, adopted from [169] (b) A schematic showing real and virtual marker definition and (c) the definition of relative angular and translational movement between the residuum and the socket.

Two virtual markers (red in Figure 2.37b), ADT and RPJ, were defined using the real markers. The ADT marker is tracked with the ADT_1 and ADT_2 marker. In addition, the residual-prosthesis joint (RPJ) was defined at the intersection of a line between Soc_1 and LFE markers and a second line perpendicular to the first line and through the ADT virtual marker. In dynamic motion capture, the RPJ virtual marker was tracked relative to the socket markers (Soc_1 and Soc_2) and labelled RPJ_S. In addition, the RPJ marker is tracked relative to residuum makers (LFE and ADT) and labelled RPJ_R.

Figure 2.37c shows the definition of the translational and rotational movement between the residuum and the socket. The translational movement is defined as the movement between RPJ_R and RPJ_S marker. The angular movement between the residuum and the socket is defined by the angular different between LFE and RPJ-RL markers for the residuum and Soc_1 and RPJ_S markers for the prosthesis.

Sensor technologies

A non-contact photoelectric sensor system (Figure 2.38) was developed to measure the translational residuum motion at the distal location [170], adding an extra 70g of mass and 8.9mm thickness to the prosthesis. The reported sensor has a measurement range of 60mm and root mean square (RMS) error of less than 1.95% of full-scale output.

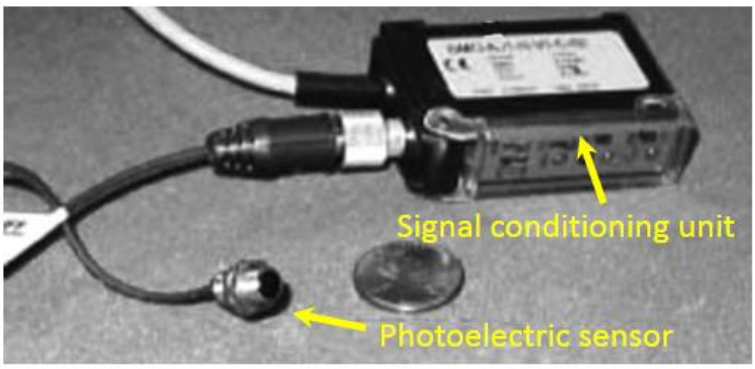

Figure 2.38: the photoelectric sensor with its signal conditioning unit, image taken from Sander et al [170].

Childers and his colleague [171] developed a limb/socket measurement (LSM) device (Figure 2.39a), incorporating an aluminium frame and two linear variable differential transformers (LVDTs), to measure the residuum translational motion in the sagittal plane. The aluminium frame was attached to a bracket via a hole made through the socket as shown in Figure 2.39b. In addition, the other side of the bracket was adhered to the lateral-distal location of the residuum, close to the cut-end of the tibia. The reported LSM had a measure ranged of 100mm and resolution of ±0.2mm.

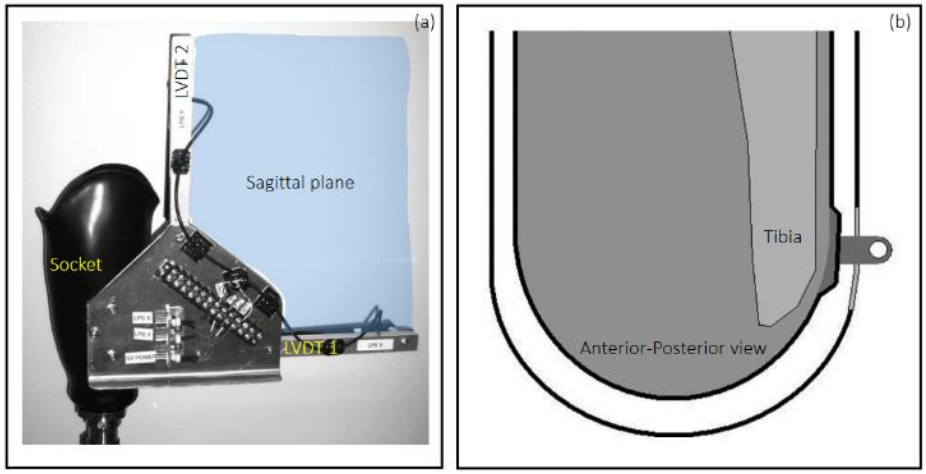

Figure 2.39: (a) The aluminium frame, including two LVDTs attached to the lateral side of the socket wall and (b) the bracket used for aluminium frame attachment.

Summary of techniques for assessing 3D motion at socket interface

- The cost of using or purchasing medical imaging equipment, such as an SXCT and a DRSA machine, in clinical settings is high. Availability of such machine in middle or low-income country may prove an issue.
- X-ray radiograph, SXCT, DRSA technique involves radiation exposure to the amputees, which could prove harmful for repeated use.

- Digital image acquisition and processing skills, computer-aided design skills and programming skills are required to acquire process and analyse the image. As an example, up to four pieces of software are required to use the DRSA technique.
- For the SXCT technique, in some cases, metal wire needs to be inserted at the residuum/socket interface. In extreme cases, surgical operation may be needed for the insertion of reference markers. Both could result in a secondary injury and infection at the residuum.
- For both ultrasound and DRSA techniques, modifications to the socket are required. For the former, two openings at lateral socket are needed to mount the transducer. For the DRSA technique, the insertion of a tantalum mesh and markers is required, leading to an altered mechanical behaviour at the tight socket interface.

Several types of instrumented sensors have been developed for incorporation into the prosthesis to measure the residuum motion. Although they have proved accurate in measuring movement, there are limitations namely:

- For both photoelectric sensor and the LSM device, an instrumented socket is required with openings cut on the socket. This will affect the structural integrity of the socket, thus limiting their usage for monitoring purpose in daily life.
- For both photoelectric sensor and the LSM device, extra weight are added to the prosthesis. This can lead to unnatural gait and thus measurement will not be representative.

The motion capture technique for socket interface kinematic assessment is well known for its capability of capturing the dynamic movement, compared to the x-ray radiograph. In addition, the radiation exposure to amputee is minimal. However, there are several drawbacks associated with their usage namely:

- For the camera-based technique, a transparent socket is required. This limits its use for amputees who are fitted with a non-transparent socket, such as carbon fibre socket. In addition, the insertion of the reflective sticker at the tight socket interface can result in residuum discomfort, leading to an unnatural gait. Further, only axial motion can be derived from this technique.
- For the 3D motion capture-based technique, a new marker placement protocol is required involving the palpation of the key landmarks on the residuum. This could introduce the variations in marker placement between different investigators. Also, a new calculation protocol needs to be developed in the gait analysis software.

The studies have been mostly conducted as research case studies in laboratories. A proof-of-concept technique needs to be developed that can be translated in to a daily monitoring device, alarming the amputee when excessive motion occurs at the residuum/socket interface. Based on the measured movements at the interface, clinical interventions either through a prosthetist or via an adaptive socket system can be triggered.

The feasibility of using 3D motion capture system as a tool to assess the kinematics at residuum/socket interface has not been extensively studied. However, it has the potential to be partially replaced by the inertial measurement unit (IMU) [172, 173]. Wearable devices, based on IMUs, can be then be developed to acquire the 3D motion at the critical interface. Via this technique, devices can be worn on the amputee and the motions occurring at the socket interface can be monitored during daily activities. The interface mechanics can then be examined with amputees in both research laboratories and a larger cohort of amputees during their daily life.

2.6.2 3D motion at trans-femoral residuum/socket interface

To author's best knowledge, despite the wide use of the medical imaging based technique, only two studies from the same research group have reported the dynamic characterisation of the residuum/socket interface kinematics [8, 166]. Both studies utilised ultrasound transducers to report dynamic movements of the residuum movement relative to the socket. However, the reliability of the technique, including the repeatability on the same day and reproducibility across different days, has not been reported. The review of the two studies can, however, provide a benchmark for the comparison of socket interface kinematics. Clearly, more studies need to be performed on both trans-femoral and knee disarticulation amputees, in order to gain a comprehensive understanding of the socket interface kinematics.

Level walking

According to Convery and Murray [8], at IC, the distal end of the femur extended up to 7° until mid-stance phase (Figure 2.40). After mid-stance, the distal end of the femur started to transfer into a flexion positon in relation the lateral socket wall and approximately 7° was reached at TO. In swing phase, it stabilised and returned to the position seen at IC. Up to 14 of femoral ROM was obtained in relation to the lateral socket wall. In the coronal plane (Figure 2.40), from IC to mid stance of the GC, up to 9° of femoral abduction was obtained in relation of the socket. From mid-stance to TO, it decreases such that femur was 3° adducted relative to the socket. Up to 12° of femoral motion was observed in the coronal plane in relation to the socket.

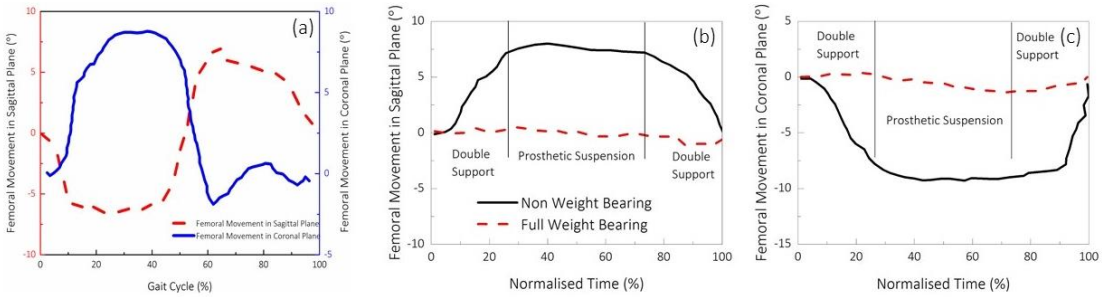

Figure 2.40: (a) Femoral movement relative to the socket as a function of GC during level walking. (b) Femoral movement relative to the socket during weight bearing activities in (b) sagittal plane (c) coronal plane. Raw data was extracted from Convery and Murray [8] using WebPlotDigitiser Version 3.8.

Weight bearing activities

Apart from the results obtained from level walking trials, femoral motion relative to the socket was also evaluated when performing varies daily activities [166]. When lifting the prosthetic limb above the ground (non-weight bearing), up to 8° of flexion motion of the femur was evident. The position of the femur relative to socket showed little difference when performing full weight bearing activities (Figure 2.40b). In coronal plane, as shown in Figure 2.40c, up to 9° of femoral adduction was obtained during non-weight bearing activity. Little movement of femoral when during full-weight bearing activity.

Sit-to-Stand activities

Figure 2.41a shows the femoral motion in sagittal and coronal planes when performing a sit-stand activity. During the transition from seated position to a standing position, up to 13° of femoral extension was evident in order to propel the trunk upward. Up to 10° of femoral flexion was observed during the transition between standing posture to seated posture. This may be associated with the deceleration of the limb to slow the trunk due to body weight. In the coronal plane, up to 7° of adduction was evident during the transition from seated position to standing position. Figure 2.42b shows the femoral motion in sagittal and coronal plane when performing step up-down trials. Up to 13° and 15° of femoral motion was observed in the sagittal and coronal planes, respectively.

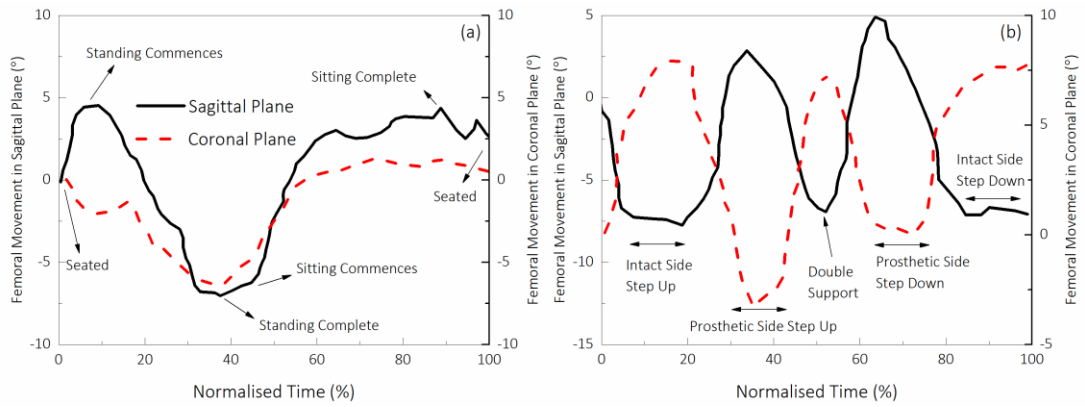

Figure 2.41: Femoral movement relative to socket obtained during (a) sit-stand activities and (b) step up-down activity. Flexion and abduction of the femur is defined as positive. Raw data was extracted from Convery and Murray [166] using WebPlotDigitiser Version 3.8.

Walking on inclined surfaces

Figure 2.42a and Figure 2.42b shows the femoral motion relative to the socket when walking on different terrains. Similar waveforms, in both sagittal and coronal planes, were reported by the authors [166]. It is also reported that, no difference was found in the peak to peak values of the femoral motion relative to the socket. However, in sagittal plane, less femoral motion was observed from IC to approximately TS phase when walking on a descending surface, compared to that on the ascending surface.

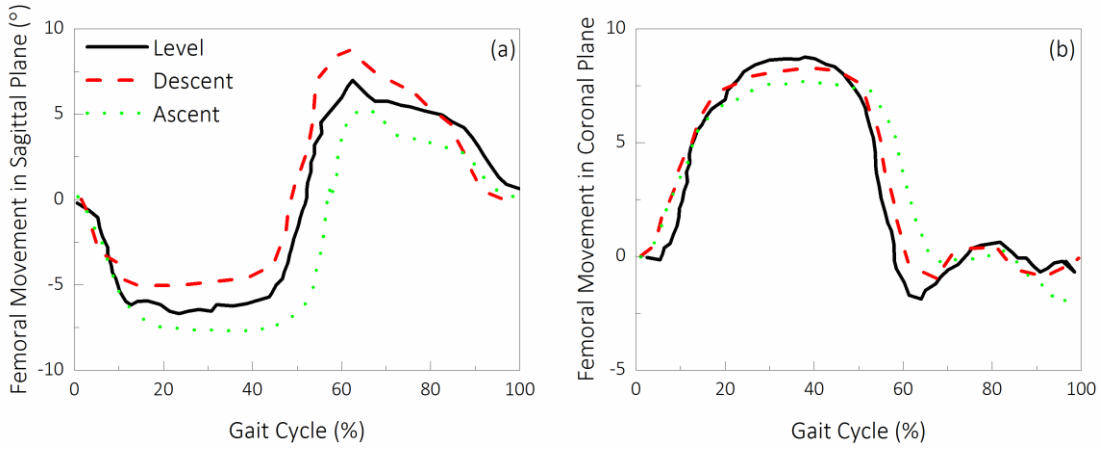

Figure 2.42: Femoral movement relative to the socket when walking on different terrains in (a) sagittal plane, flexion is defined as positive and in (b) coronal plane, abduction is defined as positive. Raw data was extracted from Convery and Murray [166] using WebPlotDigit.

2.6.3 3D motion at trans-tibial residuum/socket interface

Table 2.4 shows the 2D and 3D motions obtained at socket interface. 16 studies were identified for the assessment of 3D motion at the trans-tibial socket interface, 10 of them are limited to static loading conditions while the other six studies were from two research groups. For most

of the static study, a medical imaging technique was chosen as means to quantify residuum movement in relation to socket.

Static weight bearing results

For this type of study, a reference zero was typically chosen during non-weight bearing condition, the subsequently tibial movement in full-weight bearing posture was reported based on this reference value. For the tibial translational movement, displacement in a range between 16mm [83] and 22mm [156] was obtained in anterior-posterior direction. In medial-lateral direction, tibial movement of up to 6mm [83] was reported from only one study. Up to 35mm of tibial axial movement was also measured [83]. When changing postures, including IC posture, TO posture and full weight bearing posture, up to 1mm difference was observed in tibial vertical displacement. It is worth noting that the angular movement of the distal tibia ranges from 0.7° [155] to 8° [83]. This large variation may potential results from the different imaging equipment used and protocols used for defining tibia angle in relation to the socket. It is also worth noting that for all static studies, PTB socket was used, which is not commonly used now in prosthetic clinics. Cautions needs to be taken when comparing these results with the ones obtained in recent studies.

Apart from the weight bearing activities, tensile force was applied to the prosthesis by hanging weights at 30N, 60N and 90N to simulate the force experienced during swing phase. 14mm, 17mm and 18mm of elongation of the residuum were reported [78], at the three tensile force. However, this method is questionable as it neglects the contribution of muscle functionality in the prosthesis suspension. Therefore, the results obtained using this technique may be an over-estimation. In order to evaluate the performance of the prosthesis in swing phase, a more natural swing trial may be needed. It is also worth noting, when the tensile force change from 30N to 60N, 3mm of residuum elongation was reported. Whereas only 1mm elongation was measured when tensile force increased from 60N to 90N. This reduction in the elongation at higher tensile load may suggest complex visco-elastic behaviour of the interface.

Two of the studies highlighted the reduction (up to 80%) in tibial vertical movement in using the suction suspension, compared with strap suspension [83] [154]. This may suggest that, in static condition, suction suspension offers better suspension, comparing to the strap suspension technique. Apart from the evaluation of the suspension technique, choice of liner was also assessed. In comparison of the cushion line, a suction liner revealed a 3mm reduction during weight bearing activities [168].

Dynamic walking results

Papaioannou reported, as one of the dynamic studies, up to 151mm and 15mm of dynamic tibial motion when performing stepping down and fast stop activities, respectively. The results obtained in this study is questionable as 151mm of the tibial axial movement was measured with a mean stump length of 148mm. This is equivalent to the de-attachment of the whole prosthetic from the residuum. Therefore, the reliability of the study may be considered when performing comparisons. It is also worth noting that no level walking data was reported from this research group. Apart from the results obtained when performing stepping down and fast stop, the 3D translational motion during cycling was also reported with an instrumented socket. Up to 4mm of axial and sagittal translation of the residuum was reported. When switching from cuff suspension to pin suspension, a reduction of 2mm of axial movement was evident.

Childers and Siebert [169] reported the only study involving the movement of the residuum in relation to socket during level walking activities, using 3D motion capture system. Up to 3° of tibial flexion movement from IC to mid-stance phase, which is recovered just before TO. In addition, up to 15° of tibial flexion was evident during the swing phase. With regards to residuum axial motion, little movement was observed in the stance phase and 30mm was measured during swing phase. It is therefore evident that most of the residuum motion relative to the socket occurs during swing phase. In addition, as it is the only study reporting the kinematics at trans-tibial socket interface, more work is needed to study on a larger cohort of amputees.

Issues and limitations

- Only one dynamic study focusing on interface kinematics during level walking.
- For results obtained upon static trials, large inter-study variation was evident. This could due to the use of different imaging equipment and protocols for analysing the image data.
- There is a lack of reliability study on all the techniques.
- The sensitivity of the technique on other clinical parameters, such as walking speed, terrain, prosthetic components, has not been studied.

Table 2.4: Selected reports on interface relative movement for trans-tibial amputee

Techniques	Author	Year	Type	Subject and Prosthesis	Residuum/socket interface relative movement
x-ray radiograph	Erikson [154]	1973	static	TT (n=22) PTB socket	Tibia vertical movement relative to distal end of socket • Strap suspension: 22.5mm • Suction suspension: 11mm
x-ray radiograph	Erikson [155]	1975	Static	TT (n=22) PTB socket	Comparing with the tibial positon relative to distal end of socket obtained at no weight bearing: • 10.5mm change at IC posture • 11.3mm change at full weight bearing posture • 10.4mm change at TO posture • 1.7° change at IC posture • 1.4° change at full weight bearing posture • 0.7° change at TP posture
x-ray radiograph	Lilja [156]	1993	Static	TT (n=7) PTB socket	Tibia AP and PD movement relative to socket • AP: 22mm • PD: 28mm
SXCT	Commean [153]	1997	Static	TT (n=1)	Skin slippage and tibia movement relative to socket, under 133.5N of compressive load: • Skin slippage: 2-6mm • Tibia movement: 10mm vertical movement
SXCT	Commean [152]	1998	Static	TT (n=1)	>7mm of skin deformation
x-ray video fluoroscope	Bocobo [174]	1998	Static	TT (n=2)	Methodology study, highlighting the feasibility of using x-ray videofluroscope
x-ray radiograph	Tanner [158]	2001	Static	TT (n=1)	Neoprene sleeve suspension has 18mm more tissue displacement than silicone suction suspension

Techniques	Author	Year	Type	Subject and Prosthesis	Residuum/socket interface relative movement
x-ray radiograph	Söderberg [83]	2003	Static	TT (n=1)	Tibia vertical movement relative to distal end of socket • PTB strap suspension :35mm • Suction suspension: 7mm Tibia AP and ML movement relative to socket • AP: 16mm • ML: 6mm Tibia rotation relative to socket • Up to 8°
Instrumented socket	Sanders [170]	2006	Dynamic	TT (n=1) PTB socket	Residuum vertical displacement relative to socket • Up to 41.7 mm
DRSA	Papaioannou [163]	2009	Dynamic	TT (n=1)	Strain and skin displacement during FS and step down SDo with active vacuum suspension: • FS: 18% of strain or 15mm skin displacement • SDo: 10% strain or 12mm skin displacement
DRSA	Papaioannou [164]	2010	Dynamic	TT (n=10)	Skin-socket and skin-skin slippage during FS and SDo: • Skin-socket: 151mm for FS and 19mm for SDo • Skin-skin: 10mm for FS and 24mm for SDo
DRSA	Papaioannou [165]	2010	Dynamic	TT (n=3)	Vertical displacement between liner and socket: • Increased by 16% when vacuum pump de-activated
2D motion capture	Gholizadeh [78]	2011	Static	TT (n=5) Silicone liner and shuttle lock	Residuum vertical displacement relative to socket (value expressed with reference to full weight bearing) • Non-weight bearing: 10mm • 30N tension: 14mm • 60N tension: 17mm • 90N tension: 18mm
Instrumented socket	Childers [171]	2012	Dynamic	TT (n=2)	Residuum displacement relative to socket during cycling • PD: 2mm (pin) and 4mm (cuff) • AP: 4mm both suspension techniques

Techniques	Author	Year	Type	Subject and Prosthesis	Residuum/socket interface relative movement
3D motion capture	Gholizadeh [168]	2012	Static	TT (n=6)	Residuum vertical displacement relative to socket • Seal-In liner: 0mm in full, half and non-weight bearing posture. 1mm, 1mm and 2mm change in displacement when 30N, 60N and 90N of tension is applied, respectively. • Dermo liner: 0mm, 2mm in full, half and non-weight bearing. 2mm, 4mm and 5mm of change in displacement when 30N, 60N and 90N of tension is applied, respectively.
3D motion capture	Childers [169]	2016	Dynamic	TT (n=1) TSB socket Silicone liner Pin lock suspension	Residuum movement relative to socket during level walking • Vertical translation: 30mm • AP translation: 18mm • Sagittal rotation: 15°

Abbreviations: TT=trans-tibial amputee; PTB=patella tendon bearing socket; IC=initial contact; TO=toe-off; AP=anterior-posterior; PD=proximal-distal; SXCT=spiral X-ray computed tomography; TF=trans-femoral; ML=medial-lateral; DRSA= dynamic roentgen stereogrammetric analysis; FS=fast top; SDo=step down

2.7 Residuum/socket interface kinetic assessment

In this section, techniques used for the assessment of residuum/socket interface kinetics will be described with its corresponding limitations. This is followed by the description of the results obtained from these techniques on both trans-tibial and trans-femoral amputees. Subsequently, the state-of-the-art understanding of the interface kinetics will be critiqued.

2.7.1 Reported sensor techniques

A number of sensors have been developed to measure the stresses at the residuum/socket interface. It is most convenient to discuss each separately.

Strain-gauge based diaphragm sensors

For this type of sensor, strain gauges (SG), in a bridged configuration, are adhered to a deformable diaphragm. Upon exerting the pressure on the diaphragm, the diaphragm deforms which, in turn, changes the resistance in the SGs. The pressure, hence, can be correlated to the change in the resistance. This type of sensor commonly adopts the shape of flat cylinder disc, with diameters ranging from 3.2mm [175] to 6.4mm [176]. Indeed, the commercial Kulite™ sensor system is often used by researchers for clinical measurement of pressure at residuum/socket interface [9, 175, 177, 178]. However, SG-based sensors are not sensitive to monitoring shear stresses. It is well known that high sensitivity is one of the advantage of this type of sensing mechanism, which could potentially eliminate the usage of amplification, reducing the complexity of the electronics involved in the data acquisition system. In addition, this type of sensor is of small weight, adding minimum weight to the existing prosthesis. However, when placed against the liner/skin, discomfort has been reported by amputees due to it high rigidity. From a researcher perspective, its high rigidity can lead to stress concentrations, which cause measurement errors of up to 85% of full-scale output [179, 180]. In order to reduce the discomfort and stresses concentration issues, sensors can be placed flush with the socket or at socket/skin interface. However, this requires the manufacturing of an instrumented socket (Figure 2.43a), which limits its use in clinical settings.

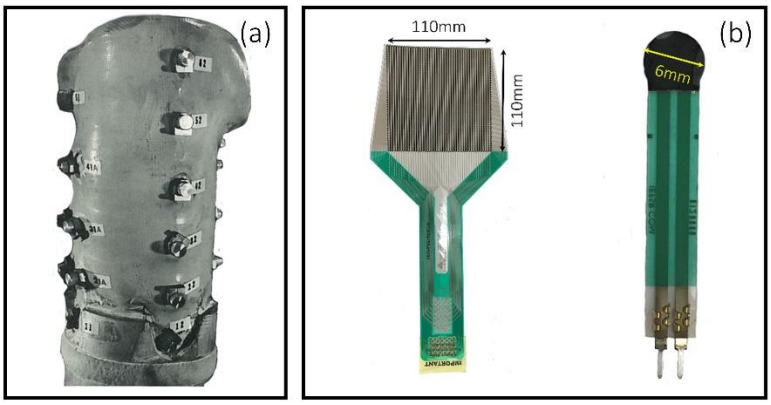

Figure 2.43: (a) An image of an instrumented socket, with strain gauge based diaphragm sensor mounted in flush to the socket wall. Image adapted from Apoldt and Bennett [176]. (b) Two examples of different sizes of TekScan FRSs.

Force sensing resistors

The force sensing resistor (FSR) is a resistance-based sensor. It incorporates a layer with printed carbon-based ink, conductive substrate layer and a spacer layer separating the two, with a total thickness of approximately 0.1mm. Upon application of a force, the link layer starts to contact with the conductive layer, thus reducing the resistance. The magnitude of the force can then be correlated to the resistance change between the ink layer and conductive layer. Commercial pressure sensing systems, such as Teckscan™, adopt this type of sensing mechanism and produce sensor arrays (Figure 2.43b) suitable for different applications, including measuring pressure at the residuum/socket interface. However, FSR technology is not capable of measuring shear forces.

FSR provides distinct advantages when comparing to other sensor systems, including:

- Thin profile and flexibility, thus reducing the measurement error due to localised stress concentrations.
- High spatial resolution involving 96 sensor cells in 203mm by 76mm sensing area, which gives approximately 0.6 sensor cells per square centimetre [181].
- Appropriate measurement ranges up to 517kPa of pressure [181].
- Appropriate sampling frequency of up to 165Hz, which is adequate for measurement of dynamic stresses during gait cycles [182].

In addition, TekScan™ report the sensor system performance in their commercial datasheet [183], including ±3% linearity error, ±2.5% repeatability error, up to 4.5% hysteresis error and up to 5% of drift error. However, inconsistency in these parameters were reported by laboratory-based tests. Indeed, on a flat bed, the FSR showed hysteresis and drift error of up

to 24% and 12%, respectively [182]. In addition, on a curved surface, accuracy, hysteresis and drift error amounted to 11%, 42% and 33%, respectively [182]. Furthermore, the typical TekScan system used by prosthetic researchers, F-Socket™, cost as much as $10,000, limiting its widespread use in prosthetic clinical settings.

By implementing the similar sensing mechanisms, pressure sensitive textiles have been developed by Infi-tex Ltd. and Sensing Tex Ltd. Instead of using rigid conductive substrates like FSRs, conductive fabrics has been used. The use of fabric greatly reduces the rigidity of the sensor, which is favourable when inserting at the tight residuum/socket interface. This could minimise the discomfort resulting from the rigid substrates. However, the technical specification are not available in the public domain, which makes it difficult to assess suitability for application at the residuum/socket interface for lower limb amputees.

Magneto-resistive and piezo-resistive sensor

Building on top of the SG-based diaphragm sensor, magneto-resistive components have been added in order to measure shear forces at residuum/socket interface [10]. There are two magneto-resistive elements, one for shear X measurement and one for shear Y measurement, separated by a rubber disc and a magnet (Figure 2.44a). Upon application of shear, relative displacement occurs between the magnet and coil, which, in turn changes the magnetic properties in the magneto-resistive element, inducing resistance changes. The magnitude of shear can then be correlated to the change in resistance in the magneto-resistive element. The pressure sensing technique is similar to that described in SG-based diaphragm sensor as shown in Figure 2.44b. The sensor system reported has a thickness of 4.9mm and a diameter of 16mmm mounted within the socket wall.

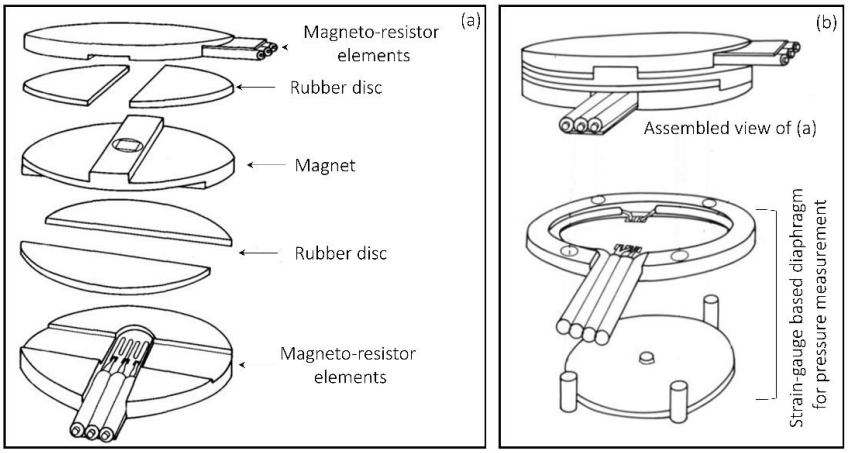

Figure 2.44: (a) An exploded view of parts responsible for shear measurement in a magneto-resistive sensor and (b) strain gauge based sensor responsible for pressure measurement in a magneto-resistor sensor. Image adapted from [10].

Sensor Product Inc. has developed Tactilus® Surface Pressure Mapping Technology that is capable of measuring pressure, based on a piezo-resistive mechanism. The Tactilus mat system, of 0.3mm thickness, has a measurement range of 0-1398kPa and a measurement frequency of up to 1000Hz. Its thin profile and measurement rate is suitable for the load measurement at residuum/socket interface. However, to author's best knowledge, no study has used this technology to assess interface loading in lower limb amputees. It is also worth noting that, such system is only capable of measuring pressure and is insensitive to shear stresses.

Capacitive sensors

The capacitive sensors utilise electrodes separated with a flexible material, which form a capacitor. Upon application of a normal load, the distance between the two electrodes is reduced, thereby inducing a change in capacitance. In the commercial field, Novel™ Pliance is one of the typical pressure sensing systems, which can be applied at the residuum/socket interface. The system presents a promising utilisation with its high flexibility, thin profile and multiple sensor array. Up to 16 sensors are included in one mat and the system can support up to 16 mats. However, similar to Tekscan™, only pressure can be measured by the Novel™ device.

Researchers have developed capacitive sensing systems that are capable of measuring both pressure and shear simultaneously [184-187]. Most of them, however, still employ costly materials and manufacturing techniques such as, Polydimethylsiloxane (PDMS) and moulding. Additionally, due to the use of polymer-based materials, their hyper-elastic properties may cause non-linearity, while the material viscoelasticity may result in hysteresis, each of which need to be accounted for during appropriate sensor designs.

Issues and limitations of current stress sensing technologies

From a clinical perspective, a stress sensing system is needed to provide a consistent way to fit into a socket, combined with experience from a prosthetist. This could minimise the variations in socket fit quality at the initial socket fitting stage. For example, interface stresses at key load bearing and relieving locations can be monitored, which guides a prosthetist during the fitting process. During subsequent daily activities, the stress sensing system can also be used as a monitoring device. For example, if excessive load was experienced at load relieving locations, warning signals can be provided to an amputee and subsequent intervention can be conducted. The stress monitoring system can also be used as an input to a smart prosthesis, which changes its shape based on the stresses measured at interface. This would potentially reduce the need

to visit a prosthetic clinic and minimise the risk of damaging stump tissue. It is also well known that both pressure and shear stress are critical in assessing tissue viability. Pressure ulcers and friction blisters can be directly associated with the multi-directional loads experienced at the interface. A comprehensive understanding of the interface kinetics, which underpins the socket design, fitting and stump tissue loading, is required. The use of an interface sensing technique provide a direct measure of interface kinetics.

Little was found in the existing literature that reported an appropriate interface stress sensing system that can be applied at the body-machine interface. For most of the studies, pressure sensors have been used, for example, TekScan F-Socket system. However, high hysteresis and drift error has been reported, which is not favourable when measuring dynamic stresses during gait. In addition to these limitations, the high cost associated with existing pressure sensor limits its frequent use in prosthetic clinics. Multi-directional stress sensors have also been reported in the literature. These stress sensors involve costly manufacturing techniques and the consistency between each of the sensor cannot be guaranteed. In addition, an instrumented socket, involving drilling holes on socket wall, needs to be manufactured. This could largely limit its use for monitoring purpose during daily activities. Furthermore, some of the sensors are bulky and rigid and when used at the tight socket interface, can lead to stress concentrations and discomfort. This will introduce inaccuracies of the measurement and at the same time, gait biomechanics could be altered due to the discomfort. Most of the multi-directional stress sensing systems remain as a research tool. This is because it requires large amount preparation work, such as the manufacturing of an instrumented socket before taking measurements. To characterise the multi-directional stresses at the residuum/socket interface, a sensor system that is capable of measuring both pressure and shear stresses simultaneously is needed. In addition, the sensor needs to be thin and flexible, which is critical for socket comfort purpose.

2.7.2 The unique multi-directional stress sensing system

TRIPS sensor system

In the University of Southampton, a multi-directional stress sensing system has been developed, which is capable of measuring pressure and two orthogonal components of shear stress acting at body/machine interface. The mechanism of the system is based on the change in capacitance upon application of both normal and tangential loads. The development of the sensor system was conducted by researchers from the University of Southampton and Chas A Blatchford & Sons Ltd. Three generations of sensor systems were designed, manufactured and characterised

in both laboratory and clinical settings. These were available for the current PhD project. Its design, manufacturing and characterisation of the sensor system is presented in Chapter 3.

Pilot amputee test

Pilot experiments were conducted on a single knee-disarticulation amputee, involving walking on level [188] and inclined surfaces. Dr. Piotr Laszczak, Dr. Michael McGrath, Dr. Jiangliang Gao participated this pilot study.

Three sensors were positioned at the anterior proximal, posterior proximal and distal end of the stump (Figure 2.45). The sensors were adhered to the outer surface of a liner with double-sided tape. To prevent damage to the sensors, a protective gel pad was placed between the sensor and the socket. During the tests, sensor signals corresponding to pressure, longitudinal and circumferential shear were simultaneously collected from all three sensors with a 100Hz sampling frequency. The participant was requested to walk at a self-selected speed on a level surface, as well as ramped surface (8 °). On each terrain, the participant was asked to traverse the walkway/ramp until at least 15 steps were recorded.

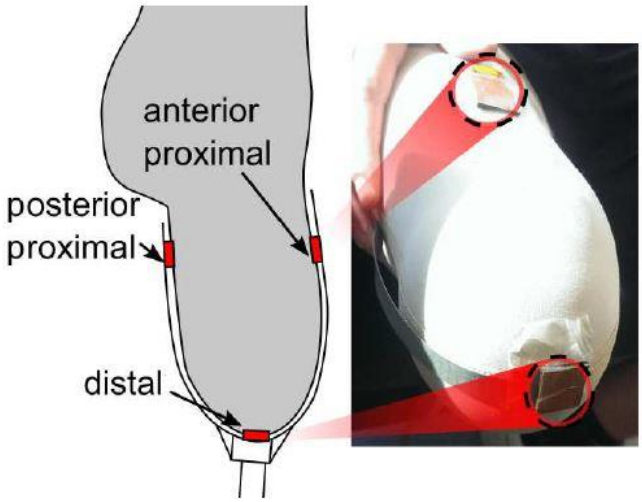

Figure 2.45: Positioning of the sensors during the preliminary amputee test.

When walking on level surfaces, approximately 30kPa and 3kPa of pressure and longitudinal shear were recorded at the anterior-proximal location, respectively. Up to 38kPa and 9kPa of pressure were recorded at the posterior-proximal location, respectively. The increasing trend of the longitudinal shear during early stance phase indicates that the residuum was pushed into the socket. The decreasing trend observed during TS phase suggested that the residuum was pulled out of the socket. It is worth noting that the circumferential shear obtained at the two proximal locations are small (<2kPa). Up to 80kPa, 20kPa and 3kPa of change in pressure,

longitudinal and circumferential shear were recorded at the anterior-distal location of the residuum (Figure 2.46c), respectively.

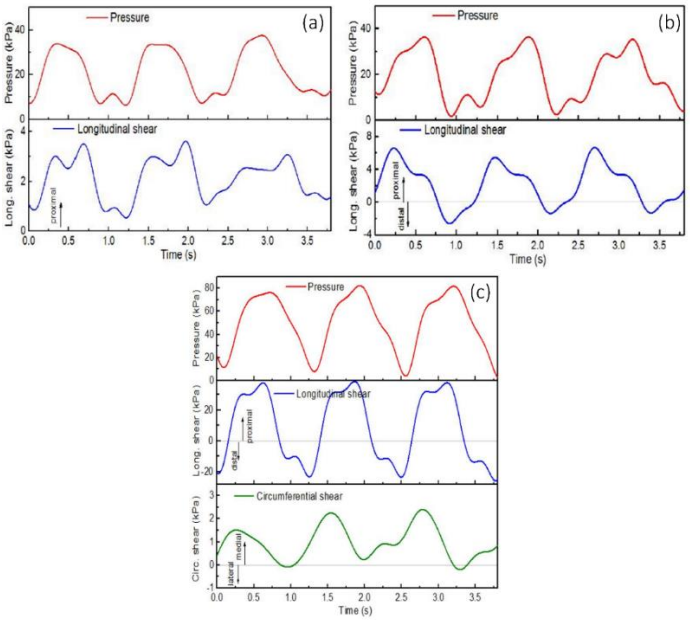

Figure 2.46: Stresses measured at (a) anterior-proximal, (b) posterior-proximal and (c) distal location of the residuum, as a function of time.

Up to a 5% increase and a 4% decrease in posterior-proximal pressure were evident in early stance phase, when walking on descending and ascending surfaces, comparing to that during level walking. Corresponding changes in the TS phase were up to a 3% decrease and a 4% increase in posterior-proximal when walking on descending and ascending surfaces, respectively. Little change was observed in the longitudinal component of shear stresses at the posterior-proximal location.

The results of the pilot walking tests provide preliminary validation of the 2nd generation sensor system for measuring dynamic pressure and shear stresses at a knee disarticulation prosthetic socket interface. This was encouraging as the complex geometries of trans-femoral and knee disarticulation sockets are known to cause many technical difficulties for interface measurements. Indeed, stress measurements at the distal region are frequently limited to transducers mounted within the socket wall [189, 190], due to interference with prosthetic knee mechanism, while fluid-filled sensors with over-long tubes have been reported to exhibit errors [29] [191]. To the best of our knowledge, simultaneous measurements of pressure and shear on knee disarticulation amputees have not been reported previously.

The pilot amputee tests mentioned were designed to test the performance of the sensor system and provide valuable stress profiles on non-trans-tibial amputees, which is currently

lacking in the field. Despite the effort made in this amputee test, more work is needed to investigate the sensor performance and interface biomechanics to investigate:

- The biomechanical aspect of the socket interface over a gait cycle. The data need to be synchronised with GRF, which is conventionally used to define gait cycles.
- Stress profiles at key load bearing locations on different days, in order to gain insights into variations of the socket fitting.
- Effect of factors e.g. walking speed and terrain, on the interface stresses need from a biomechanical point of view.
- The validity of use of the sensor system with trans-tibial amputees at loading bearing regions, which may be susceptible to tissue damage.

2.7.3 Multi-directional stresses at residuum/socket interface

Interface stresses at the trans-femoral socket interface

The conceptualised biomechanics between the residuum and the socket was first outlined by Radcliffe for trans-femoral amputees [44], as shown in Figure 2.47. For a trans-femoral socket, the majority of the body weight should be supported by the ischial tuberosity and with minor loads born by the flare of the anterior socket brim. Distal loading needs to be avoided, in order to prevent the stump oedema.

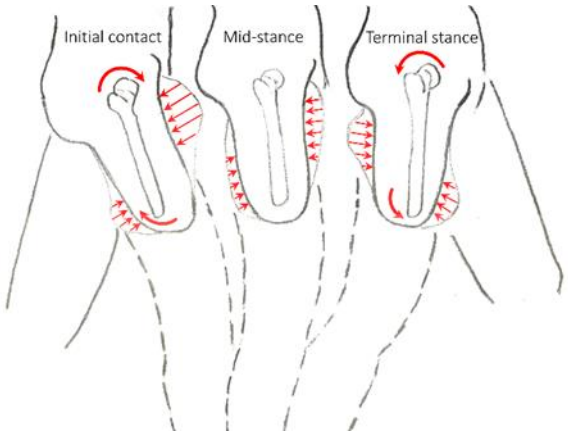

Figure 2.47: A representation of Figure 2.6, illustrating the conceptualised loading at residuum/socket interface for trans-femoral amputee. Image adapted from [44].

At IC, the socket should provide considerable support at anterior socket brim area to prevent the ischium from sliding forwards and downwards. It is also anticipated that the femur should press posteriorly against the posterior-distal soft tissues to maintain knee stability. In TS, the femur should move anteriorly against the anterior-distal soft tissues to initiate the knee flexion

in swing phase. At the same time, the ischial seat must provide sufficient support of body weight, resulting in high pressures at the posterior-proximal location.

As a special group of trans-femoral amputees, Hughes outlined the socket biomechanics of the knee disarticulation amputee [192]. Different from trans-femoral sockets, which emphasis the load bearing at ischial region, knee-disarticulation socket is designed to support the body weight in distal regions (Figure 2.48). Therefore, socket movement relative to femur is more evident at distal location for trans-femoral amputees. While proximal socket movement relative to the femoral head is more pronounced. In early stance phase, to maintain the stability of the limb, the GRF vector should pass in front of the knee rotational centre, avoiding knee flexion. Consequently, the socket must be designed to allow loading bearing at posterior-distal and anterior-proximal locations. In swing phase, the force acting on the residuum tends to pull the socket away from the residuum. However, this is not always the case as the pulling forces may be balanced by the fitting the socket over the flare the femoral condyles.

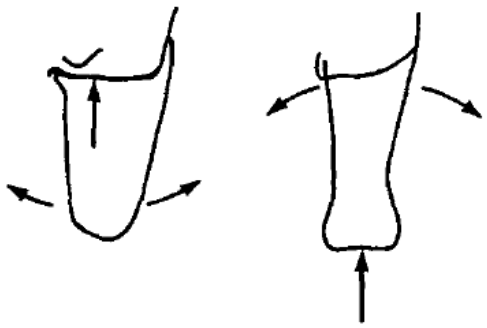

Figure 2.48: Comparison of trans-femoral (Left) and knee-disarticulation (right) socket with the rotational effect about of the point of support. Image adopted from [192].

The socket interface biomechanics, described by Radcliffe and Hughes, are the only two studies that provide the combined assessment of interface kinematics and kinetics. This is largely due to the lack of means to provide in-situ dynamic measurement of the residuum motion (Section 2.6.1) and stresses at socket interface, without the disruption of dynamic ambulation. In the majority of the studies, only one assessment, either kinematics or kinetics, was provided.

Apart from the conceptualised mechanics at residuum/socket interface of trans-femoral amputee, to author's best knowledge, up to nine reported studies have focused on the characterisation of interface kinetics for trans-femoral amputees [176, 188, 193-196] using direct measurement. Among them, four of the studies obtained experimental stress measurements from amputee participants, four studies used Finite Element Analysis (FEA) techniques as an estimation of stress profile over the residuum and the final study from the

1970s is based on the conceptualised guesswork. Peak stress, as one of the most important parameters in assessing the socket interface kinetics, is often quoted as an outcome measure to indicate the socket fitting qualities and as an indication of potential tissue damage.

Appoldt [176] reported a peak pressures of up to 8p.s.i (approximately 55kPa) at the posterior-proximal location of the residuum of a trans-femoral amputee. A separate transducer, sensitive to tangential stresses, was developed by the group and peak shear stress in a range of 1-3.6p.s.i (approximately 7-25kPa) were obtained at the anterior-distal location of the residuum [193] on two trans-femoral participants. A similar magnitude of peak pressure (58kPa) and longitudinal shear stress (27kPa) was obtained by Laszczak et al [188] at the posterior-proximal location and anterior-distal location, respectively. Lee et al [194], however, reported slightly higher peak pressure, in the range of 70-90kPa, at both the ischial tuberosity and lateral mid limb location of the residuum.

Apart from the experimental measurement using transducers, FEA is also common in characterising interface kinetics. Peak pressure, longitudinal shear stress and circumferential shear stress of 4kPa, 1.4kPa and 0.6kPa were predicted due to donning of the socket [195]. When simulating the stress profiles during walking, peak pressure of up to 119kPa, 90kPa and 101kPa were obtained at ischial bearing areas during foot-flat, mid-stance and heel-off phases of the GC [196], respectively. The corresponding longitudinal and circumferential shear stresses were approximately 26kPa and 104kPa, respectively, at the posterior-proximal region of the residuum.

As a summary, peak pressures and shear stresses within a range of 55-119kPa and 4-104kPa was reported, respectively, based on eight studies involving 12 participants. Of eight of the studies, three [176, 188, 194] presented the dynamic profiles of the stresses measured experimentally at the residuum/socket interface. Each of these reported the typical double-hump waveform in both the temporal profiles of pressure and shear. The first peak was reported to occur at the loading response of the gait cycle and the second peak was typically observed at TS phase of the gait cycle.

Interface stresses at the trans-tibial socket interface

The conceptualised biomechanics between the residuum and the socket was also first outlined by Radcliffe for trans-tibial amputees [3]. Force and moment diagrams were used to analyse the anticipated stress profile at residuum/socket interface with the aid of the GRF vector.

For trans-tibial amputees, at IC, the knee stability is maintained by active hip extension mechanics. The knee is forced to extend due to the external load exerted by the socket, as shown in Figure 2.49a. In the mid-stance phase, the GRF vector passes through the region, posterior to the KJC. In this case, if the knee is completely relaxed, a buckling effect might occur. However, an amputee can resist the buckling tendency by actively extending the knee, resulting in the loading pattern shown in Figure 2.49b. Stresses are expected to concentrate at the anterior-distal, patella-tendon and popliteal regions of the residuum. During the TS phase (Figure 2.49c), as the GRF vector still passes through the posterior region of the KJC, similar stress concentration regions are anticipated to those in mid-stance phase. However, as the amputee starts to initiate the swing phase, the knee extension becomes dominant. This may result in an increase in stresses at the anterior-distal region to 'kick' the prosthesis, initiating the swing. At the same time, the stresses at the patella-tendon would be reduced due to the active knee extension.

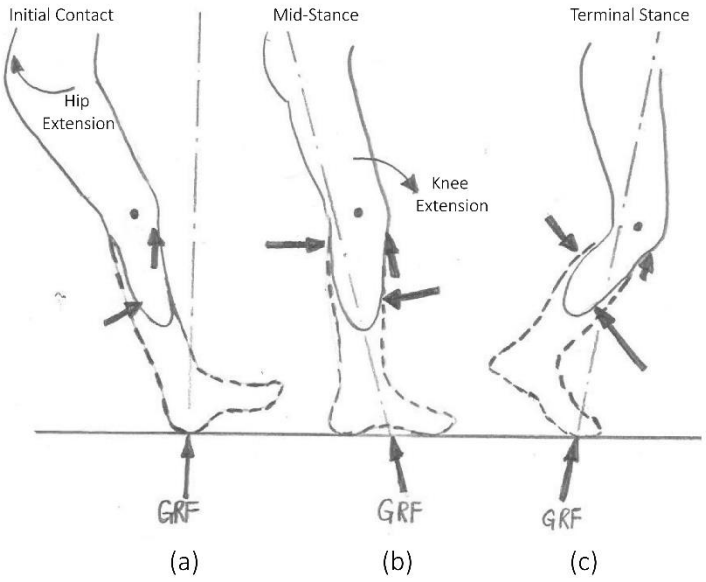

Figure 2.49: Conceptualised loading profile at residuum/socket interface at (a) initial contact, (b) mid-stance and (c) TS phase of a GC

One FEA study reported a similar stress profile, induced by the interaction between the residuum and the socket [128]. High pressure magnitudes were predicted at anterior-proximal and posterior-distal locations, with an associated decrease in pressure in anterior-distal and posterior-proximal locations. In TS phase, the pressure profile was the opposite.

To gain insight into the stresses developed over the residuum/socket interface, the characterisation of wave-shapes of normal and shear stresses is critical. Sanders and colleagues

[197] categorised these into five events in stance phase, based on the pressure and shear measurements on various regions of the residuum (Figure 2.50).

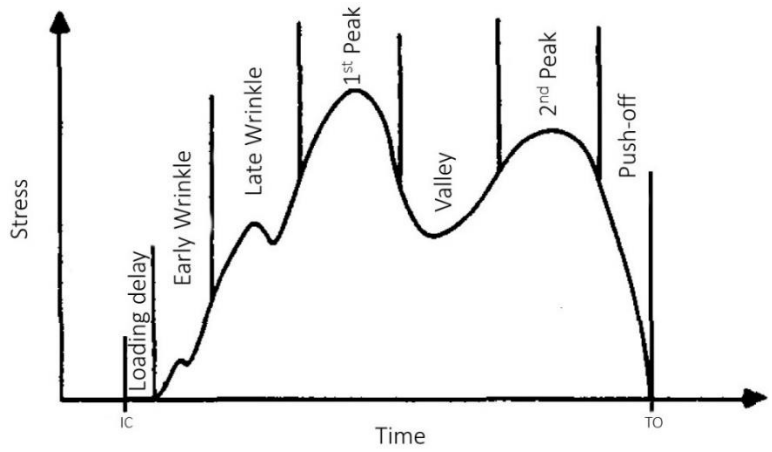

Figure 2.50: Waveform of the interface stresses observed in stance phase. Image adopted and edited from [197].

Loading delays: this represents the fact that an increase in stress at the transducer sites was not recorded immediately at IC, particularly evident at anterior locations. This loading delay is probably caused by the residuum axial/pistoning motion and the resultant shank force. The typical amount of loading delay ranges from 4% to 12% of stance phase, which is anteriorly-directed.

High-frequency events: marked as Early Wrinkle and Late Wrinkle in Figure 2.50. After IC, high frequency events typically occur during the loading response of the GC. However, it may not be present at all sites of the stump. There are several possible reasons that contribute to the presence of these events including, the foot being forced too fast to transfer to foot flat, deformation of the prosthetic heel spring, muscle activation and slippage at the interface. Stability during ambulation could be compromised if excessive high-frequency events are presented.

1st Peak: 1st peak usually occur after the high-frequency events. Timing of this peak at different locations, in the same step, may not be exactly the same. It is proposed that the difference in timings could be attributed to the non-linear viscoelastic behaviour of the residuum tissues.

Valley and 2nd peak: Valley and second peaks have relatively low frequency content compared to those in early stance phase.

Push-off: just before TO, the residuum/socket interface will be unloaded, which was not simply the reverse of that immediately after IC. During unloading, the results shear vectors were not opposite in magnitude and direction from the loading resultant shear vectors.

Issues and limitations

Despite the many studies involving trans-tibial amputees using different transducers, there are very few consistent findings. In the case of the PTB socket, four sites of high pressures were identified, namely, the patellar tendon, popliteal fossa, medial flare and fibular head. Among these regions on the residuum, the patellar tendon usually exhibits highest pressure at TO. Medial areas are less well examined, due to risk of making contact with the contra-lateral limb by a transducer.

Inconsistencies in reported results were observed, indicating large inter-study variability. For example, the mean and SD pressures at the patellar-tendon was 165±99kPa and 235±229kPa for the kick point region of the residuum. The pressure profiles at residuum/socket interface was found to be similar for amputees fitted with TSB and PTB sockets, although less pronounced peaks with lower magnitude were observed with TSB socket. Generally, in the PTB socket peak pressures reached values above 300kPa, while corresponding values in the TSB socket rarely exceeded 200kPa. In addition, variation in weight of the amputee may also contribute to the inconsistencies in the peak stress observed across studies. None of the studies reports the normalised stress values, possibly due to the lack of understanding of the factors that underpin the both temporal profiles and stress magnitudes. A comprehensive understanding of interface stresses is clearly needed and this could influence the choice of parameters. This, in turn, could aid the comparison between studies from different research groups.

Kick point, fibular head, popliteal fossa and posterior mid-tibia regions are frequently quoted as highly subjected to shear. There is no consistency in shear direction and magnitude. According to Sanders and colleagues [198] more than 65% of transducer sites were exposed to less than 10kPa of shear, while peak shear stresses may reach up to 80kPa. Studies have shown that shear stress distribution does not follow pressure distributions. The shear stresses are much more localised, thereby exposing part of the stump tissue to tensile forces [198].

Table 2.5: Selected reports on residuum/socket interface pressure and shear measurement

Techniques	Author	Year	Type	Subject	Pressure and shear measurement	
					Key statements	Peak values and where
SGD	Rae [177]	1971	P	TT (n=26)	Significant change in pressure due to different types of liners	P: Anterior distal (517kPa)
SGD	Pearson [9]	1973	P	TT (n=10)	Determined anterior-distal region as the sensitive region to alignment perturbation	P: Anterior distal (410kPa)
SGLS	Katz [199]	1977	P	TT (n=1)	Correlation between pain threshold and pressure	P: no pain (308kPa)
SGD	Winarski [200]	1987	P	TT (n=2)	Correlation between the socket moment and interface pressure	P: Posterior (320kPa)
FSR	Engsberg [201]	1992	P	TT (n=2)	Pressure difference between an adult and a child	P: PTB (120kPa)
SGB+SGD	Sanders [202]	1992	P+S	TT (n=3)	First study, measuring combined pressure and shear stress	P: 205kPa S: 54kPa
MR	Williams [10]	1992	P+S	TT (n=1)	Measurement of combined pressure and shear	P: Lateral (165kPa) S: Popliteal fossa (35kPa)
SGB+SGD	Sanders [189]	1993	P+S	TT (n=3)	Reported generalised pressure and shear waveforms	P: Anteriorial medial mid limb (185kPa) S: Anteriorial medial mid limb (45kPa)
SGB+SGD	Sanders [203]	1997	P+S	TT (n=2)	More on the generalised pressure and shear waveforms	P: anterior medial distal (224kPa) S: anterior lateral distal (60kPa)
MR	Zhang [204]	1998	P+S	TT (n=5)	Pressure and shear waveform characterisation	P: Popliteal fossa (320kPa) S: Anterior medial mid limb (61kPa)
FSR	Convery [205]	1998	P	TT(n=1)	Pressure distribution in hydrostatic socket	P: Patella tendon (417kPa)
SGB+SGD	Sanders [206]	1998	P+S	TT (n=1)	Significant change in pressure and shear due to socket alignment	P: Anterior lateral mid limb (215kPa) S: Anterior medial mid limb (80kPa)
SGB+SGD	Sanders [74]	1998	P+S	TT (n=3)	Significant change in pressure and shear due to foot alignment	P: Lateral (186kPa) S: Anterior medial distal (47kPa)
FSR	Convery [205]	1999	P	TT (n=1)	Significant change in pressure due to socket shapes (PTB and PCast)	P: Patella tendon (417kPa)

Techniques	Author	Year	Type	Subject	Pressure and shear measurement	
					Key statements	Peak values and where
SGD+SGB	Sanders [198]	2000	P+S	TT (n=3)	No significant change in peak stress due to cadence and componentry configurations	P: Popliteal fossa (160kPa) S: Anterior-medial mid limb (27kPa)
FSR	Beil [207]	2002	P	TT (n=9)	Significant change in peak stresses due to suspension technique (suction and vacuum assisted)	P: medial mid limb (155kPa)
SGD+SGB	Sanders [208]	2002	P+S	TT (n=2)	Significant alteration of peak stresses due to weight loss and stump volume fluctuation	P: Popliteal fossa (173kPa) S: Posterior mid limb (36kPa)
Cap	Chou [209]	2003	P	TT (n=15)	No significant change of peak stresses due to change in walking speed	P: Medial condyle (286kPa)
SGD	Goh [210]	2003	P	TT (n=4)	Pressure distribution in PTB socket. Significant variation in subjects' AP and ML pressure profile	P: Popliteal fossa (110kPa)
SGD	Goh [211]	2003	P	TT (n=5)	Pressure distribution in socket produced by pressure cast system. Raised concerns about the validity of hydrostatic socket environment	P: Lateral side (81kPa)
FSR	Seelen [76]	2003	P	TT (n=17)	Significant change in mean stresses due to perturbation of ankle alignment	P: Anterior-distal tibia (75kPa)
FSR	Beil [212]	2004	P	TT (n=7)	Significant change in peak stress due to suspension techniques (pin and suction), during swing	P: Medial mid limb (26.7kPa)
SGD+SGB	Sanders [190]	2005	P+S	TT (n=2)	Significant change in stresses across 6 months	N/A
Cap	Dou [213]	2006	P	TT (n=1)	Pressure distribution when walking on stairs, slops and non-flat road	P: Patella tendon (216kPa)
FSR	Dumbleton [214]	2009	P	TT (n=48)	Significant change in peak pressure due to tow of the socket manufacturing techniques (hands-on and hands-off)	P: Anterior (110kPa)
Cap	Wolf [215]	2009	P	TT (n=16)	Significant change in pressure profile due to the use of micro-processor controlled foot	P: Posterior mid limb (228kPa)
FSR	Ali [216]	2012	P	TT (n=9)	Significant change in pressure profile due to the use of two liners	P: Anterior mid limb (87kPa)
SGD	Sewell [217]	2012	P	TT (n=1)	Prediction of pressure using artificial neural network	P: Lateral mid limb (486kPa)
FSR	Ali [218]	2013	P	TT (n=11)	Significant change in peak pressure when engaging stairs, using two different liner	P: Popliteal fossa (82kPa)
FSR	Yeung [219]	2013	P	TT (n=5)	Significant change in peak pressure during long distance walking	P: Patella tendon (2.39kPa/kg)

Techniques	Author	Year	Type	Subject	Pressure and shear measurement	
					Key statements	Peak values and where
Cap	Shiraz [220]	2014	P	TT (n=1)	Significant change in peak pressure due to ankle alignment change	P: Popliteal fossa (500kPa)
FSR	Eshraghi [221]	2015	P	TT (n=12)	Signiant change in peak pressure when engaging stairs and ramps	P: 70kPa (no indication of where)
Cap	Safari [222]	2015	P	TT (n=6)	Correlation between socket comfort and interface pressure	P: Patella tendon (160kPa)
FSR	Gholizadeh [223]	2016	P	TT (n=1)	Significant change in pressure due to difference suspension techniques (pin and Velcro)	P: Proximal (120kPa)

Abbreviations: SGD=strain gauged diaphragm based sensor; SGB=strain gauge based beam type sensor; TT=trans-tibial amputee; TF: trans-femoral amputee; P=pressure; S=shear; FSR=force sensing resistor; Cap=capacitance based sensor; Pe=piezoelectric based sensor; SGLS=strain gauge based load socket; MR=magneto—resistive sensor; FF=fluid filled sensor

2.8 Summary

A lower limb residuum/socket interface is a complex mechanical and biological system involving the residuum, liner and socket with different compliances (Section 2.1.4). The biomechanics of amputee walking showed significant differences when compared to an able-bodied cohort (Section 2.4.4). This is primarily due to the change in load transfer mechanism (Section 2.5.1) in the prosthetic limb with presence of the socket interface. In addition, factors such as walking speed, terrain, and prosthetic components will also alter the load transfer mechanism (Section 2.5.3), leading to discomfort and loss of stability at the socket interface (Section 2.2). Despite the importance of assessing the interface biomechanics, to-date, the association between the load transfer mechanism and socket interface kinematics and kinetics is still not clear. This is primarily due to the lack of appropriate assessment techniques.

The current technique used for the evaluation of interface kinematics involves the usage of medical imaging equipment; sensors and motion capture (Section 2.6.1). They are either expensive, bulky and typically involve the use of an instrumented socket, which limits their use in daily activities for continuous assessment and monitoring purposes. Furthermore, the majority of studies only provide static data, which limits their use in the assessing dynamic load transfer. A comprehensive understanding of interface kinematics would benefit from a technique that can provide dynamic data without altering existing prosthesis, which can be easily translated to clinical settings.

Sensors have been developed to assess interface kinetics (Section 2.7.1). However, the devices are typically bulky, adding extra weight and length to prosthesis. Despite the importance of the role of shear stress acting on the residuum/socket interface, most of studies only report pressure values. In addition, the current pressure sensor systems exhibit low repeatability and accuracy when applied at residuum/socket interface. To date, only two research groups have reported multi-directional stress measurements at the socket interface. A comprehensive understanding of interface kinematics would benefit from a sensor system that is able to provide both pressure and shear stresses and can be easily integrated into existing prosthetic components.

In this PhD project, a technique for assessing socket interface kinematics will be proposed based on 3D motion capture system, which is commonly available in gait laboratory. The TRIPS sensor system, developed at the University of Southampton, will be used to provide *in-situ* interface kinetics. The combined interface kinematic and kinetic evaluation would provide a

comprehensive understanding of the biomechanics at the residuum/socket interface for lower limb amputee.

Chapter 3 Key experimental methodology

A range of methodologies have been involved in this PhD project including the use of a gait laboratory equipped with 3D motion analysis system, the TRIPS sensor system and a material test machine. The joint mechanics of an able-bodied participant, a trans-tibial participant and a knee disarticulation participant will be evaluated, using the 3D motion analysis system. The in-depth understanding of load transfer mechanism, at lower limb joints, could further aid the analysis of socket interface mechanics. An interface kinematic model will be first developed to assess the residuum 3D motion relative to the socket. The corresponding interface kinetics will be assessed using the TRIPS sensor system. The repeatability and sensitivity of both methods will be evaluated by performing repeated tests with different test conditions. The interface mechanics will be subsequently analysed by combing the residuum 3D motion and the dynamic stress at the socket interface.

Figure 3.1 provides an overview of the combined usage of gait laboratory and the TRIPS sensor system. The gait laboratory incorporates two optical sensor units, infra-red-based markers, and an 8m level walkway with a force platform integrated at approximately the half way point (Figure 3.1a). Motion analysis software then uses the both marker data and force data from the force platform to compute the joint biomechanics (Figure 3.1b).

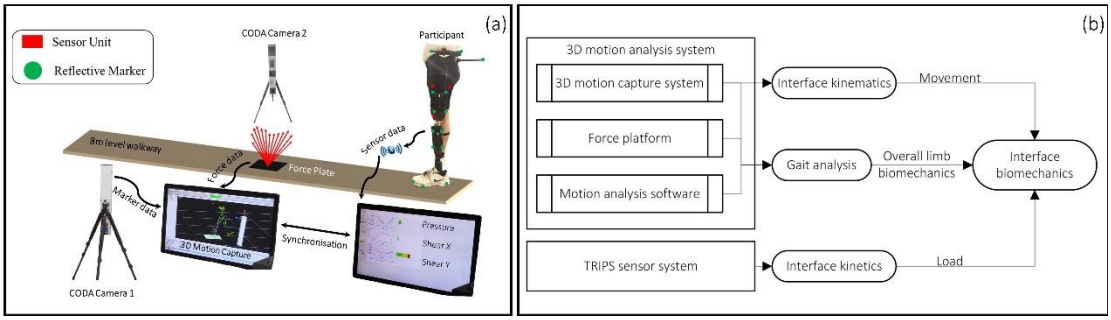

Figure 3.1: (a) Schematics showing the equipment in the gait laboratory. (b) Functionality of each piece of equipment.

3.1 The 3D motion analysis system

3D motion analysis system was used to analyse the gait characteristics of both able-bodied and amputee participants. Two raw inputs are needed in order to compute the gait biomechanics, the marker data from 3D motion capture system and the force data from the force platform. The marker data describe the trajectory of the key lower limb anatomical landmarks and the force data describes the loads between the foot and the surface of the walkway. The key anatomical landmarks, in the form of the marker data, were then used to construct a lower limb gait model with linked segment. The position of the linked segments together with the

force experienced at one end of the segment chain (foot), were subsequently used to calculate the loads at each of the joints (ankle, knee and hip) via an inverse dynamics technique. In most of the research involving human gait analysis, a gait laboratory is commonly used.

For all the data presented in this thesis, the gait laboratory at the Endolite Research Centre, Chas A Blatchford and Sons Ltd, was used. The gait laboratory is equipped with Codamotion (Charnwood Dynamics Ltd, Victoria Mills, Rothley, LE7 7PJ, UK) 3D motion capture system, a force platform (Kistler 9286BA, Kistler Instrument Ltd., Switzerland) and Odin motion analysis software. Two types of walkways are also available in the laboratory, including an 8m level (Figure 3.2a) and 5° ramped walkway (Figure 3.2b). The force platform was mounted in parallel with both walkways in all test conditions.

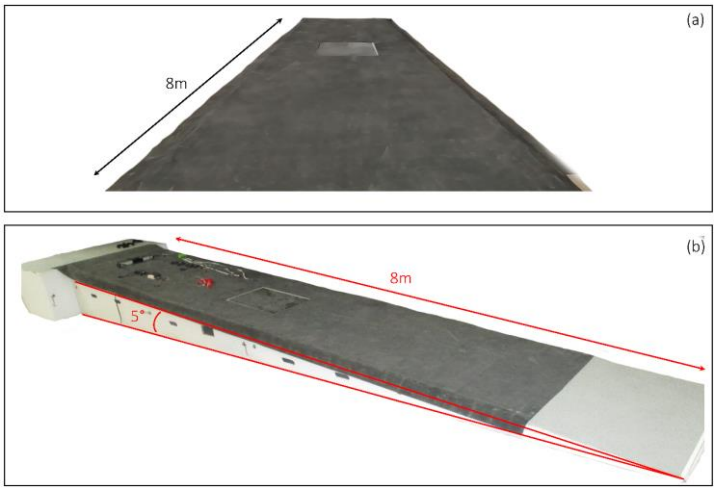

Figure 3.2: (a) Level and (b) ramped walkway available in the gait laboratory.

It is worth noting that the force platform was located at approximately half-way point of the level walkway. Approximately four steps needed to be taken in order to reach the force platform from the starting position. In addition, the force platform was integrated at approximately two-thirds of way up the ramped walkway. Up to three steps and six steps need to be taken in order to reach the force platform during descending and ascending, respectively.

3.1.1 3D motion capture system

The Codamotion 3D motion capture system combines high frequency infra-red-based technology and optical correlation algorithms to give the 3D location of a given infrared (IR) source. The high frequency IR LED emitter, which can be captured by one or more optical sensor units or camera(s), are designed to be enclosed in a black shell, which is commonly referred to as a marker.

Infrared-based markers

Figure 3.3a and c show two types of IR-based LED markers that have been used to capture key anatomical landmarks on the lower limb. The first type, a standard marker (Figure 3.3a), is used to calibrate the lab co-ordinate and track the key anatomical landmarks of the foot. Typically, three standard markers will be plugged into a marker drivebox (Figure 3.3c), which provides power and assigns a name to each of the marker. The second type of marker, termed the marker cluster, consists of four standard markers, mounted on one of two sizes of a rigid plate, as shown in Figure 3.3b. The marker clusters are used to provide 6-DoF movement information of a rigid body. No external drivebox is required for the marker clusters as the built-in battery powers the four markers.

Optical sensor unit

Two optical CX1 sensor units, one of which is shown in Figure 3.3d, are used to detect the IR source from each of the markers at every 40μs, regardless of the sampling rate user specified. Based on the optical correlation algorithm, the 3D location of each marker is measured and calculated.

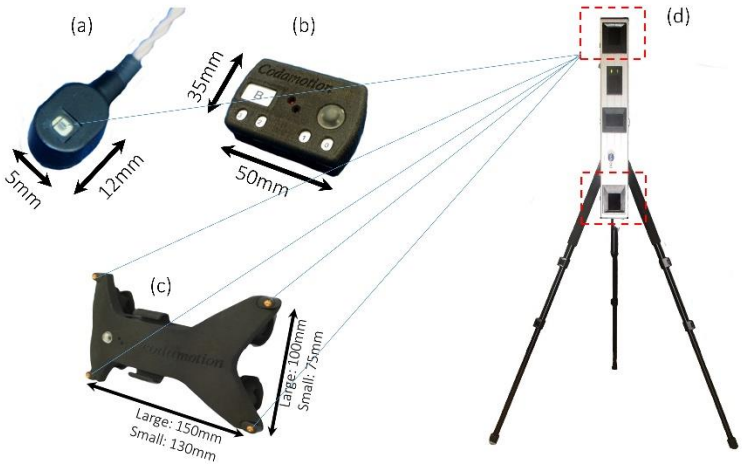

Figure 3.3: Optical sensing unit, the two individual camera highlighted by the red dashed line indicates the ones used for calculation of y component of co-ordinate.

The X and Z components or the anterior-posterior and distal-proximal components of the co-ordinate system are measured by the optical sensor, while the Y component or the medial-lateral component of the co-ordinate system is derived from triangular calculation of the signals from the two cameras. According to the Codamotion User Guide (Version 1.08, April 2016), the RMS amplitude of the noise generated from the X and Z components of the co-ordinate system are within 0.1mm. By contrast, the Y component of the co-ordinate system is more susceptible to noise and is typically within 0.4mm, (personal communication from Andrew Ward, the Senior Software & Support Engineer in Charnwood Dynamics Ltd). Other sources of inaccuracies could

arise from the photo-detector current noise in the two cameras and from the AC component of room lighting, which is typically at double of the mains frequency i.e. 100Hz.

3.1.2 Force platform

The three component of ground reaction forces and centre of pressure (CoP) are measured by a calibrated force platform (Kistler 9286BA, Kistler Instrument Ltd., Switzerland), as shown in Figure 3.4. The measurement directions (X, Y and Z-axis shown in Figure 3.4), are defined in relation to the force plate itself, acting on the foot.

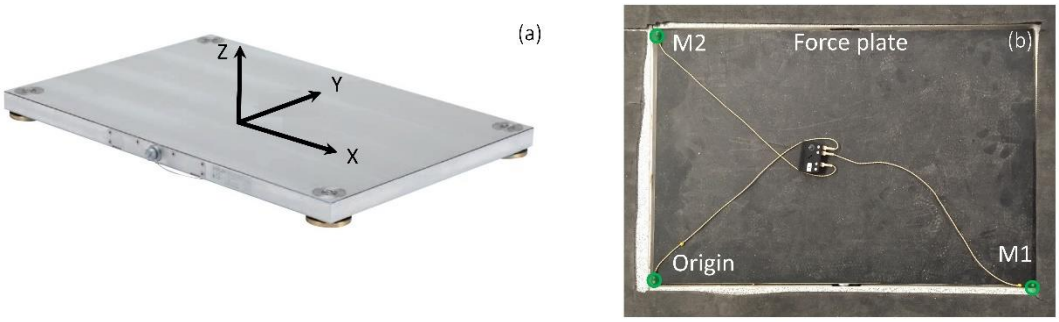

Figure 3.4: (a) Kistler 9286BA force plate with X, Y and Z-axis defined with reference to its own geometry and (b) an illustration of marker placement on the force plate to define GCS

The measurement range of anterior-posterior and medial-lateral component of ground reaction force are set at -1250N to 1250N, while the measurement range for vertical component of ground reaction force is set at 0 to 10,000N. A cable is used to connect the force plate to the CodaHub. The CodaHub records the analogue voltage outputs from the force plate and converts them to forces in newtons through a calibration matrix. Free moments generated on the force plate, together with the CoP were subsequently calculated. The calibration certificate, provided by the Kistler Instrument Ltd., is available in Appendix A2.

3.1.3 Calibration of the gait laboratory

Apart from providing GRF, moments and CoP, the force plate is also used to define a reference co-ordinate system – global co-ordinate system (GCS), such that the 3D marker co-ordinates are tracked in relation to the GCS. Three markers (marked as M1 M2 and Origin in Figure 3.4b) were used to define the GCS. The X-axis of the GCS or X_{GCS}, is defined by connecting Origin marker to M1. Z_{GCS}, is defined by the axis perpendicular to the plane formed by Origin, M1 and M2 marker, pointing upwards. The Y_{GCS} is defined orthogonal to the X_{GCS} and Z_{GCS}.

3.1.4 Data acquisition and processing

Data acquisition

CodaHub is a data acquisition hardware for the 3D motion analysis, with following functions:

- It provides power to the two optical sensor units and also receives the 3D marker co-ordinates from them via the two d-sub 25 pin cable connection (Figure 3.5a)

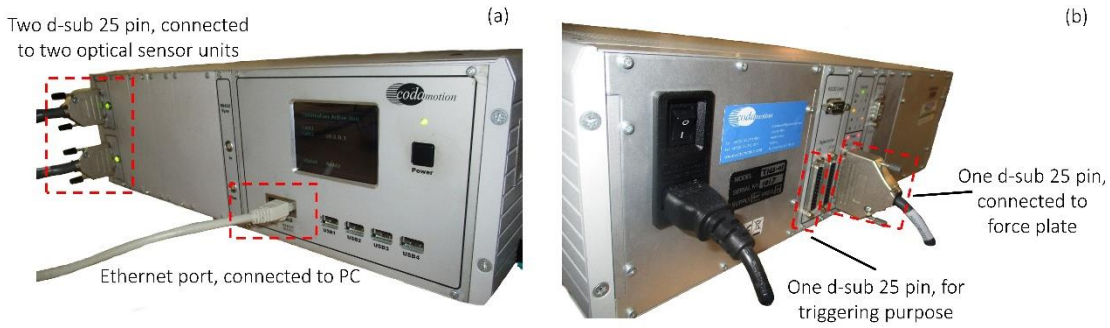

Figure 3.5: (a) Front and (b) back panel of the CodaHub.

- It collects and synchronises the datastream from 3rd party equipment, e.g. the voltage values from the force plate (Figure 3.5b)
- It interfaces with the dedicated software on an external PC, through an Ethernet cable, for extracting 3D marker data and force platform data (Figure 3.5a)
- It is also capable of sending or receiving synchronisation signals to trigger or to be triggered for initiation of data collection. This is achieved through the d-sub 25 pin connector on the rear side of the Codahub (Figure 3.5b).

Raw data processing

The raw marker data and the GRF data collected from the CodaHub were subsequently processed by Odin motion analysis software (Version 1.08). For the raw marker data, the sampling frequency was set at 100Hz for all data collection presented in this thesis. Subsequently, a low-pass zero-lag Butterworth filter was applied with cut-off frequency set at 50Hz. For the marker that was out-of-view during dynamic data collection, a linear interpolation method was used by Odin software. It is worth noting that the data presented in this thesis does not involves out-of-view markers. Both raw and filtered marker data are saved by the Odin motion analysis software. GRF was sampled and collected at a rate of 500Hz by the force platform. At the beginning of the data collection, the effect of walkway vibration to GRF was examined such that no clear spikes was presented when the foot is not in contact with the force platform. Subsequently, a low-pass zero-lag Butterworth filter was applied to the GRF with cut-off frequency set at 100Hz. Similarly, both raw and filter GRF data are saved by the motion analysis software. The analysis of human joint biomechanics involves the use of a 6-DoF

lower limb musculoskeletal model. In the next section, the marker placement protocol will be introduced.

3.2 Human gait analysis method

3.2.1 Marker placement

The configuration of marker placement on the able-bodied participant (Figure 3.6), the knee-disarticulation participant (Figure 3.7) and trans-tibial participant (Figure 3.8) during the motion capture process, was based on a 6-DoF model. The marker model follows the recommendations of the International Society of Biomechanics (ISB) for defining the bone orientations [224]. A total of 28 real markers, including a marker wand and a pelvic frame, are placed on the three groups of participants. A pelvic wand was mounted on the pelvic frame with P3 and P6 marker attached to the tail of the wand on the left and right aspect, respectively.

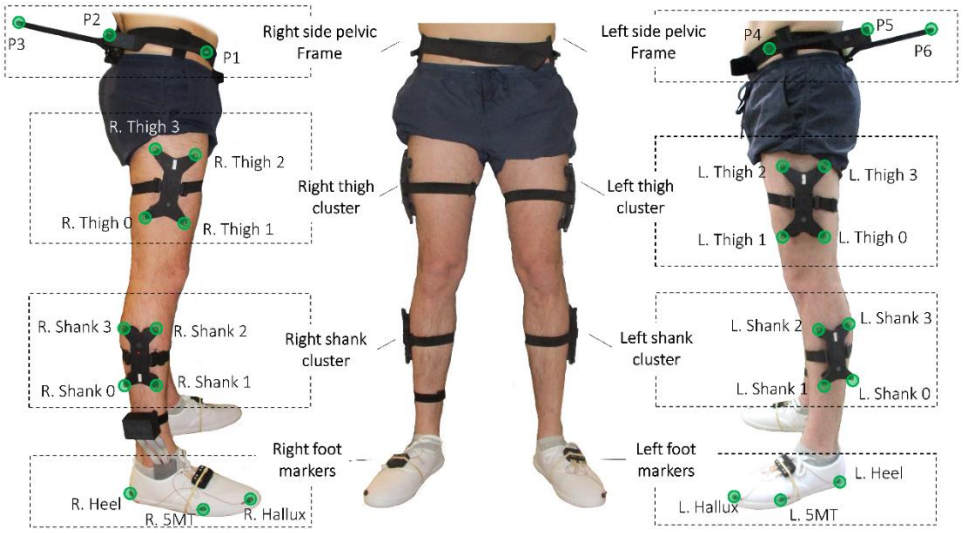

Figure 3.6: Real marker placement on the able-bodied participant.

Figure 3.7: Real marker placement on the knee disarticulation amputee.

Figure 3.8: Real marker placement on the trans-tibial amputee.

Having introduced the real marker placement, the key anatomical landmarks or virtual markers can be tracked and calculated in relation to the position of real markers. A Pointer (Figure 3.9), incorporating four real markers and a trigger, is used to define these anatomical landmarks.

Figure 3.9: A photo of the Pointer for defining virtual markers.

3.2.2 Lower limb musculoskeletal model

Pelvis

Prior to the placement of the pelvic frame, a belt with a Velcro strap was worn on the participant. Subsequently, a frame consisting of six markers (labelled as P1 to P6 in Figure 3.6, Figure 3.7 and Figure 3.8) was worn around the pelvis, sitting against the belt. Considerable care was taken to adjust the position of the frame, such that the sides lie in the plane of the anterior superior iliac spine (ASIS) and the posterior superior iliac spine (PSIS) landmarks.

The definition of the pelvic landmarks allows, firstly, the tracking of the orientation of the pelvis and secondly, the definition of the hip joint centres (HJC). In order to define pelvic anatomical landmarks, ASIS and PSIS are palpated and subsequently digitise using the Pointer. The palpation process of the left ASIS can be found in Appendix A3.

The motion of the pelvis was tracked using a pelvic frame. The orientation of left and right PSISs can be tracked using P2 and P5 on the pelvic frame. In addition, the left and right ASISs are defined through digitisation and further tracked in relation to the pelvic frame, during dynamic motion capture. Having defined all four virtual markers, a pelvic model with its local co-ordinate system (LCS), describing the orientation of the pelvic, can be constructed as shown in Figure 3.10.

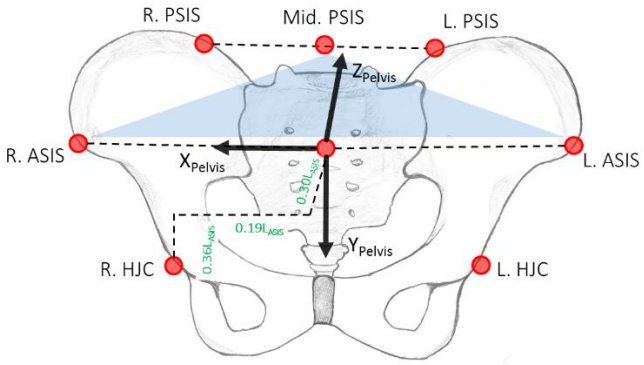

Figure 3.10: Pelvic virtual markers and the definition of hip joint centres

The origin of the pelvic LCS coincides with the midpoint of R.ASIS and L.ASIS virtual markers (Equation (3.1)). Medial lateral axis of the pelvic LCS or X_{Pelvis} can be defined as a unit vector starting from the Mid .ASIS, pointing towards R. ASIS. The anterior-posterior axis of the pelvic LCS or Y_{Pelvis}, can be defined as a unit vector orthogonal to the plane defined by Mid. PSIS, R. ASIS and L. ASIS, pointing in the anterior direction. The proximal-distal axis of the pelvic LCS can be defined as a unit vector orthogonal to both X_{Pelvis} and Y_{Pelvis}, pointing cranially.

$$Mid.ASIS_{x,y,z} = \frac{L.ASIS_{x,y,z} + R.ASIS_{x,y,z}}{2} \quad (3.1)$$

Having defined the LCS for the pelvis, the location of HJCs were defined in relation to a pelvic LCS using Roentgen Stereophotogrammetric Analysis (RSA) with a regression equation proposed by Bell et al [225, 226] and later adapted by Leardini et al [227]:

$$R.HJC_x^{Pelvis} = 0.36 \times L_{ASIS} \tag{3.2}$$

$$R.HJC_y^{Pelvis} = -0.19 \times L_{ASIS} \tag{3.3}$$

$$R.HJC_z^{Pelvis} = 0.3 \times L_{ASIS} \tag{3.4}$$

Where L_{ASIS} is the 3D distance between the left and right ASIS (Equation (3.5)), the superscript 'Pelvis' means that the calculated HJC location is defined in relation to pelvic LSC.

$$L_{ASIS} = \sqrt{(R.ASIS_x - L.ASIS_x)^2 + \left(R.ASIS_y - L.ASIS_y\right)^2 + (R.ASIS_z - L.ASIS_z)^2} \tag{3.5}$$

Regression method was chosen to determine the location of HJCs as the relative motion at socket interface may contribute to a larger error when using functional method.

Thigh

For the able-bodied participant, a cluster of four markers was placed on the lateral side of the left and right thigh as shown in Figure 3.6, respectively. These markers were numbered sequentially, starting with Thigh. 0 at the distal-posterior corner, and continuing anti-clockwise to Thigh. 3 at the proximal-posterior corner. A strap was tightened around the marker cluster to ensure stability.

For both knee disarticulation and trans-femoral participants, on the prosthetic side, a cluster of four markers was placed on the lateral socket wall (Figure 3.7). These markers were numbered sequentially, starting with Soc. 0 at the distal-posterior corner, and continuing anti-clockwise to Soc. 3 at the proximal-posterior corner. It is worth noting that, in order to account for the curvature and the rigidity of the socket, extra black non-reflective duct tape (Part Number: 6910, 3M PLC, Bracknell, UK) was wrapped around the cluster to father secure the cluster. For trans-tibial participants, a cluster of four markers was strapped over the suction sleeve, which extended over to the thigh (Figure 3.8). For trans-tibial participants, who do not require a suction sleeve, a cluster of four makers was placed on the lateral side of the thigh and secured with the strap.

Having defined the left and right HJCs, i.e. the proximal ends of the thigh segment, knee joint centre (KJC) needs to be defined in order to construct the thigh segment. For the able-bodied

participant, the lateral femoral epicondyles (LFE and MFE) were first digitised and the detailed process of palpation can be found in A3.

The KJC is defined as the midpoint between the LFE and MFE, see Equation (3.6).

$$KJC_{x,y,z} = \frac{LFE_{x,y,z} + MFE_{x,y,z}}{2} \tag{3.6}$$

On the knee-disarticulation participant, the prosthetic equivalent of LFE & MFE or lateral knee pivot (LKP) & medial knee pivot (MKP) are digitised at the prosthetic knee. An example of digitised LKP and MKP on a KX06 knee is shown in Figure 3.11a. On the trans-tibial participant, LKP and MKP are digitised at the medial and lateral point of the estimated knee axis of rotation over the socket (Figure 3.11b).

The prosthetic knee was securely fixed to the socket through a four-bolted connection. The location of prosthetic knee pivot centre (KPC) was subsequently defined as the midpoint of LKP and MKP, see Equation (3.7).

$$KPC_{x,y,z} = \frac{LKP_{x,y,z} + MKP_{x,y,z}}{2} \tag{3.7}$$

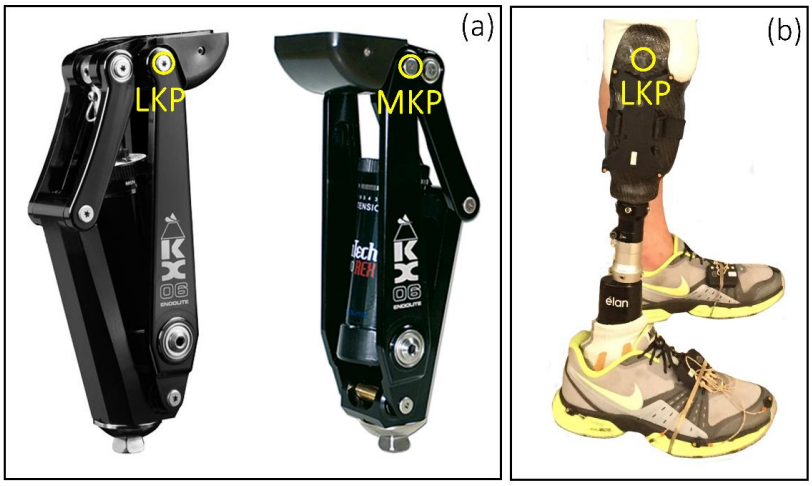

Figure 3.11: (a) Location of MKP and MKP on the KX06 knee for the knee disarticulation amputee and (b) the location of digitised LKP on a trans-tibia amputee, MKP is located on the media aspect of the socket, which is not shown.

These virtually digitised LFE & MFE on the able-bodied participant and LKP and MKP markers on the amputee participant were tracked by using the thigh and socket clusters as the reference, respectively.

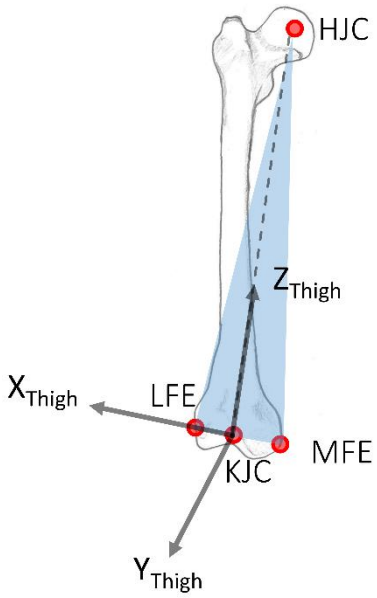

Figure 3.12: Thigh segment virtual markers and the definition of the thigh LCS

Having defined the knee rotational centre, i.e. the distal ends of the thigh segment, thigh segment and its LCS can be defined by linking the knee rotational centre (KJC for able-bodied participant and KPC for amputee participant) and the HJC. Figure 3.12 shows the key anatomical landmarks on the thigh segment and its definition of LCS. The origin of the thigh segment corresponds to the knee rotational centre. The proximal-distal axis of thigh LCS or Z_{Thigh}, is defined as a unit vector pointing from the knee rotational point towards the HJC. The anterior-posterior axis of thigh LCS or Y_{Thigh}, is defined as a unit vector orthogonal to plane form by LFE, MFE and HJC, pointing anteriorly. For the knee disarticulation participant, the prosthetic equivalent LFE and MFE, defined as LKP and MKP previously, are used to calculate Y_{Thigh}. The medial-lateral axis of the thigh LCS or X_{Thigh}, subsequently, is calculated as a unit vector orthogonal to both Z_{Thigh} and Y_{Thigh}.

Shank

For an able-bodied participant, a cluster of four markers was placed on the lateral side of the left and right shank, respectively, as shown in Figure 3.6. These markers were numbered sequentially, starting with Shank. 0 at the distal-posterior corner, and continuing anti-clockwise to Shank. 3 at the proximal-posterior corner. A strap was tightened around the cluster to ensure stability.

For amputee participants, a cluster of four markers was strapped to the prosthetic pylon using the non-reflective duct tape as shown in Figure 3.7 and Figure 3.8. The pylon was located distal

to the prosthetic knee for knee disarticulation amputee and distal to the socket for trans-tibial amputee.

The proximal ends of the shank segment is defined by the Lateral Tibial Condyle and Media Tibial Condyle (LTC and MTC) for the able-bodied participant as shown in Figure 3.14. It is worth noting that, the two virtual points previously digitised at medial and lateral aspects of the knee are further used, however tracked with the shank cluster. Therefore, the proximal end of the shank segment can be defined as Inter-Tibial Condyle (ITC), the midpoint between the LTC and MTC, see Equation (3.8).

$$ITC = \frac{LTC_{x,y,z} + MTC_{x,y,z}}{2} \tag{3.8}$$

The distal ends of the shank segment is defined by Lateral Malleolus and Medial Malleolus (LM and MM), as shown in Figure 3.14. The location of the LM and MM is superficial and easy to palpate and digitise. Subsequently, the ankle joint centre (AJC) is defined as the midpoint between the LM and MM, see Equation (3.9).

$$AJC_{x,y,z} = \frac{LM_{x,y,z} + MM_{x,y,z}}{2} \tag{3.9}$$

For amputee participants, the prosthetic equivalent of LM and MM are digitised on the prosthetic foot and they are termed as Lateral Ankle Pivot and Media Ankle Pivot (LAP and MAP). An example of the locations of LAP and MAP on Elan™ foot is shown in Figure 3.13. Therefore, the ankle pivot centre (APC) on the amputee Participant can be defined as the midpoint between LAP and MAP, see Equation (3.10).

$$APC_{x,y,z} = \frac{LAP_{x,y,z} + MAP_{x,y,z}}{2} \tag{3.10}$$

Figure 3.13: Locations of digitised LAP and MAP on the Elan foot

The digitised medial and lateral aspects of the ankle, LM & MM (for able-bodied Participant) and LAP & MAP (for amputee participants), are tracked relative to the shank cluster during the motion capture process.

Having defined the proximal and distal ends of the shank segment for both able-bodied and amputee Participants, the shank segment can be constructed by connecting the AJC (for able-bodied Participant) or APC (for amputee Participants) to ITC. Figure 3.14 shows the key anatomical landmarks on shank segment with its definition of LCS. The origin of the shank LCS coincides with the ankle rotational centre (AJC or APC). Proximal-distal axis of the shank LCS or Z_{Shank}, is defend by the unit vector starting from ankle rotational centre, pointing towards ITC. The anterior-posterior axis of the shank LCS or Y_{Shank}, is defined by the unit vector orthogonal to the plane formed by LM, MM and ITC, pointing anteriorly. Finally, the medial-lateral axis of the shank LCS or X_{Shank}, is defined as the axis orthogonal to both Y_{Shank} and Z_{Shank}, pointing laterally.

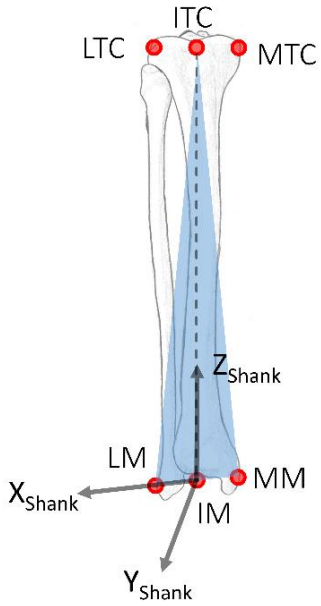

Figure 3.14: Shank segment virtual markers and the definition of the thigh LCS

Foot

For an able-bodied participant, three markers are placed over the shoe using double-sided tape and they are named as Hallux, 5MT and Heel in Figure 3.6, Figure 3.7 and Figure 3.8. Hallux marker was placed at the top surface of the Hallux, as recommended by Codamotion, such that the marker will always be in the view of the Coda camera. The heel marker was placed at the lateral side of the calcaneus at the same height of the Hallux marker. 5MT marker was placed at the equivalent positon of the fifth metatarsal head, laterally.

For amputee participant, Hallux, 5MT and Heel markers were placed at their equivalent positons, on their prosthetic side, over the shoe as indicated by F1, F2 and F3 in Figure 3.7 and Figure 3.8.

Based on three real markers placed on the foot (top of the foot, 5MT and lateral aspect of the heel), the motion analysis software Odin computes two virtual markers inducing, 1MT and calcaneus. It is worth noting that the Mid. MT virtual maker labelled in Figure 3.15 is calculated as the midpoint between the 1MT and 5MT, see Equation (3.11).

$$Mid.MT_{x,y,z} = \frac{1MT_{x,y,z} + 5MT_{x,y,z}}{2} \tag{3.11}$$

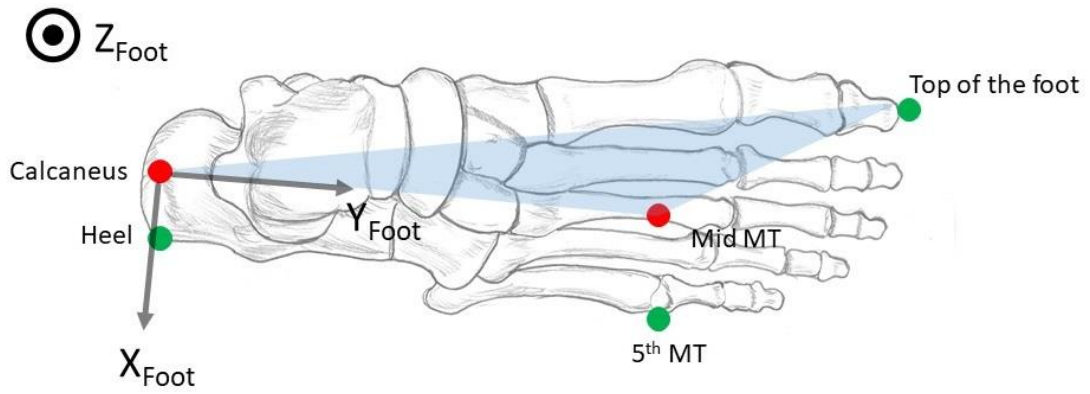

Figure 3.15: Real (green) and virtual (red) markers on the foot and the corresponding foot LCS.

Having defined the virtual markers on the foot, the foot segment and its LCS can be constructed, as shown in Figure 3.15. Three are three real markers placed on the foot, namely, 'heel', 'top of the foot' and the '5th MT'. 'Heel' marker is placed at the lateral side of the calcaneus. 5th MT marker is placed at the 5th MT anatomical landmarks and the 'top of the foot' marker is placed approximately at the location of big toe. The 'Calcaneus' virtual marker is defined based by offsetting the 'Heel' real marker by half of the ankle width towards medial direction. Similarly, the location of the 'Mid MT' virtual marker is defined by offsetting the '5th MT' real marker by half of the ankle width towards medial direction. The ankle width is defined as the distance between the LM and MM.

The foot segment is defined by connecting the 'Calcaneus' virtual marker to the 'Mid MT' virtual marker. The origin of the foot LCS coincides with the Calcaneus virtual marker. The anterior-posterior axis of the foot LCS or Y_{Foot} is defined as a unit vector pointing from 'Calcaneus' virtual marker towards 'Mid MT' marker. The proximal-distal axis of the foot LCS or Z_{Foot} is defined as a unit vector orthogonal to the plane formed by 'Calcaneus', 'Mid MT' and '5th MT', pointing

cranially. Finally, the medial-lateral axis of the foot or X_{Foot}, is defined by the unit vector orthogonal to both Y_{Foot} and Z_{Foot}, pointing laterally.

The joint biomechanics, incorporating joint kinematics and kinetics was calculated by the Odin motion analysis software according to the theory described in 2.5.1. The reference zero of joint angle was defined as the angle obtained in a standing trial.

3.3 The TRIPS sensor system for socket interface kinetic assessment

3.3.1 Overview of the sensor system

Figure 3.16 shows the latest generation of the TRIPS sensor system [188, 228], incorporating a sensor unit and data acquisition (DAQ) unit. The sensor unit has a dimension of 20mm by 20mm by 1mm thickness, including a top electrode, a bottom electrode and a deformable silicone material sandwiched in the middle. The DAQ unit has a dimension of 650mm by 420mm by 280mm, incorporating a Printed Circuit Board and three AAA Nickle-Metal Hydride batteries (3.6V and 730mAh). Upon application of a multi-directional load on the sensor unit, one pressure signal and two shear signals (S_L and S_C marked in Figure 3.16) are acquired by the DAQ unit and further transmitted via Bluetooth to a Personal Computer (PC).

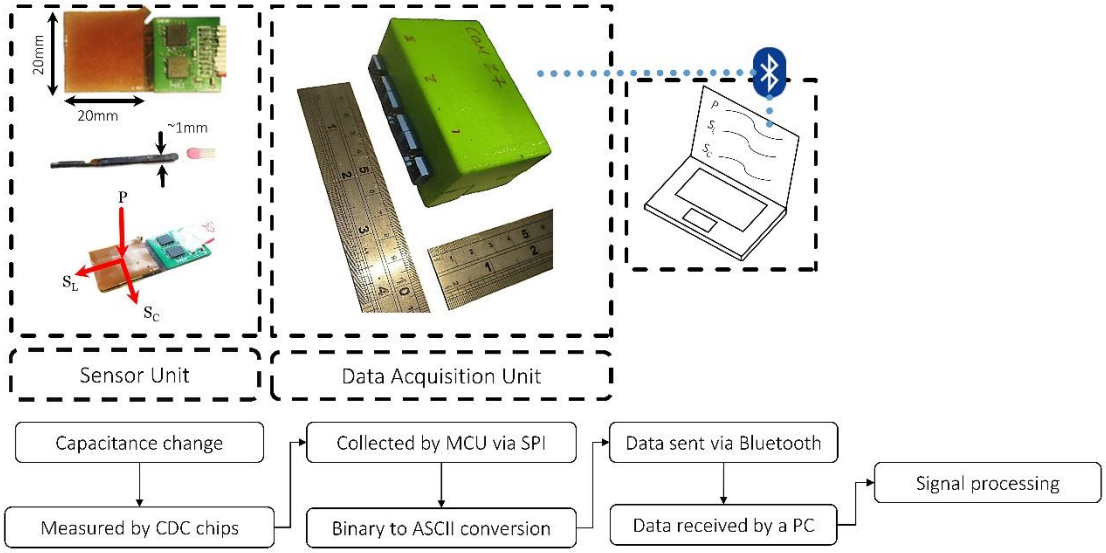

Figure 3.16: Photos and schematics showing the pressure and shear sensor system.

3.3.2 Design and fabrication of the sensor unit

Sensor unit design

The application of normal pressure and tangential shear to the sensor unit will induce the change in geometry of the deformable silicone material, in both normal and tangential directions. As the silicone material is sandwiched between the two electrodes, the deformation

of the silicone produces a change in capacitance between the two electrodes. In the next section, the electrode arrangement and the calculation of de-coupled pressure and shear signal, induced from the multi-direction load, will be introduced.

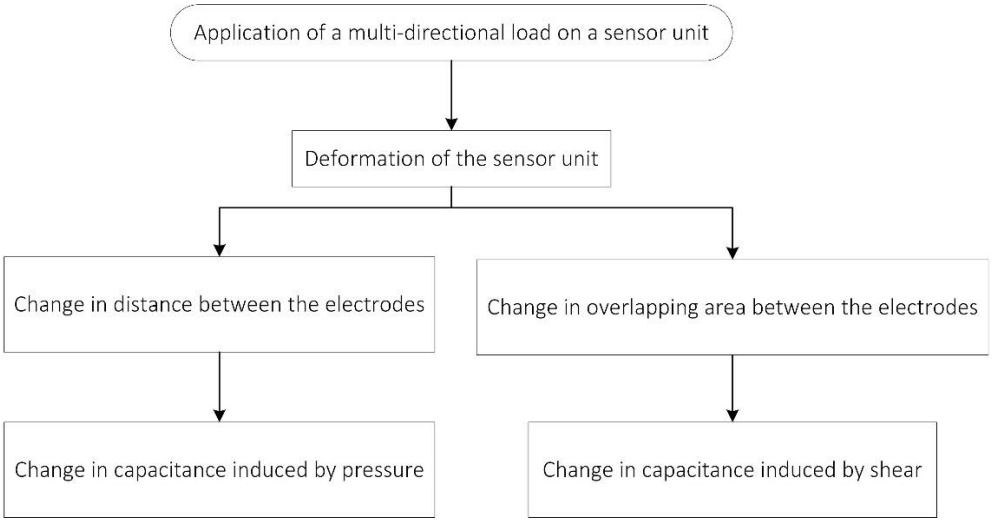

Figure 3.17: A flow chart showing the sensing mechanism on the sensor unit

The pressure and shear sensing system was designed based on the capacitance sensing mechanism. In order to explain how it works in detail, basic knowledge of capacitor will be briefly introduced here. A capacitance sensing mechanism relies on using two parallel electrical conductors (top and bottom in Figure 3.18a) which are separated by an insulator (transduction medium in Figure 3.18a).

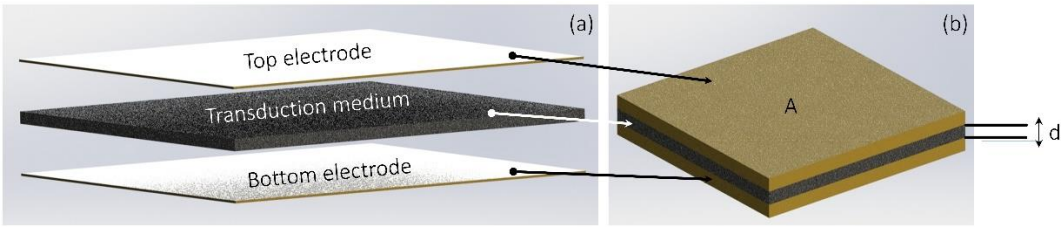

Figure 3.18: (a) An exploded view and (b) an assembled view of a capacitor formed with two electrodes and a transduction medium.

Capacitance (C), form by the two parallel electrodes with a transduction medium (Figure 3.18b), is governed by:

$$C = \varepsilon_0 \varepsilon_r \frac{A}{d} \tag{3.12}$$

Where ε_0 is the relative permittivity of a vacuum. ε_r is the relative permittivity of the transduction medium which can be assumed as a constant, 'A' is the effective or overlapping

area of the two parallel electrodes (Figure 3.18b) and 'd' is the separation between the two parallel electrodes (Figure 3.18b).

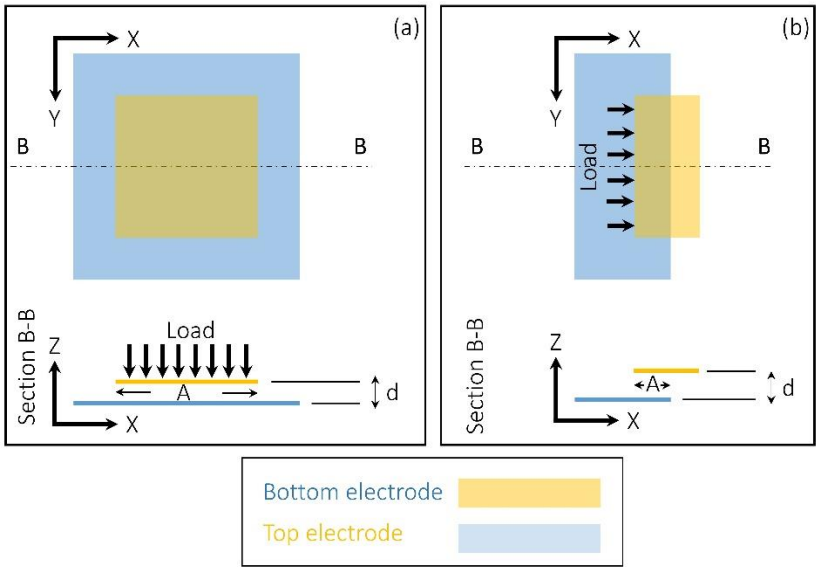

Figure 3.19: Mechanism of change in capacitance induced from (a) Pressure and (b) shear.

According to Equation (3.12), assuming the dielectric property of the transduction medium as a constant, the change in C could be induced from either the change in 'd' or 'A'. The change in d or Δd and change in A or ΔA can be further induced from the pressure, shear or combined pressure and shear loads acting on the electrodes. Figure 3.19a illustrates the basic pressure sensing mechanism. This involves a top electrode paired with a bottom electrode, forming a capacitance. In this case, the surface area of the bottom electrode is significantly larger than the one on the top electrode. Therefore, upon application of a normal load (perpendicular to the surface of electrode), the overlapping area between the top and bottom electrode ('A' in Figure 3.19a) remains as a constant, whereas the distance between the top and bottom electrode ('d' in Figure 3.19a) changes in relation to the magnitude of the load applied.

Figure 3.19b illustrates the basic shear sensing mechanism. Upon application of a load parallel to the surface of the electrode, the overlapping area between the top and bottom electrode ('A' in Figure 3.19b) changes in relation to the magnitude of the load applied. It is worth noting that, a certain load, perpendicular to the electrode surface, needs to be applied in order to transfer the shear force. Therefore, in this case, the distance between the top and bottom electrodes ('d' in Figure 3.19b) changes as well.

Having introduced the pressure and shear sensing mechanisms based on capacitance. The design of electrode, capable of sensing both pressure and shear will be introduced.

Upon application of pure pressure (loads acting normal to the electrodes), the overlapping area (A_z) of the capacitor C_z remains as a constant. The change of capacitor C_z could be only induced by the change in d, which is dependent on the applied pressured. Therefore, the change in C_z due to pure pressure can be expressed by:

$$\Delta C_z = \varepsilon_0 \varepsilon_r \frac{A_z}{d_0} - \varepsilon_0 \varepsilon_r \frac{A_z}{d_0 - \Delta d} \tag{3.13}$$

Where d_0 is the separation distance between the top and bottom electrode when it is at unloaded state and Δd is the change in separation distance between the top and bottom electrodes due to pure pressure. By re-arranging Equation (3.13) and assuming d >> Δd, we have:

$$\Delta C_z = \varepsilon_0 \varepsilon_r \frac{A_z \Delta d}{d_0^2} \tag{3.14}$$

There are three electrodes responsible for sensing the transduction of shear in the x-direction, which are marked as E3, E4 and E5. E3 at the bottom electrode, and E4 and E5 on the top electrode. In simple terms, when the electrode is subjected to pressure and shear in the x-direction, the separation distance d between top (E3) electrode and bottom electrode (E4 and E5) changes, as well as the overlapping areas, A_4 and A_5. The change in capacitor in C4 (parallel plate formed by E4 and E3) can be expressed by:

$$\Delta C_x = \varepsilon_0 \varepsilon_r \frac{A_x}{d_0} - \varepsilon_0 \varepsilon_r \frac{A_x - \Delta A}{d_0 - \Delta d} \tag{3.15}$$

Where A_0 is the overlapping area when the electrode is in the unloaded state, d_0 is the separation distance between the E3 and E4, ΔA and Δd are the change in overlapping area and distance between E3 and E4 due to combined pressure and shear, respectively.

By re-arranging Equation (3.15) we have:

$$\Delta C_{x-4} = \varepsilon_0 \varepsilon_r \frac{d_0 \Delta A_x - \Delta d A_x}{d_0 (d_0 - \Delta d)} \tag{3.16}$$

The change in capacitance recorded E5 and E3 can be obtained using similar principle:

$$\Delta C_{x-5} = \varepsilon_0 \varepsilon_r \frac{-d_0 \Delta A_x - \Delta d A_x}{d_0 (d_0 - \Delta d)} \tag{3.17}$$

Equation (3.16) and Equation (3.17) may be used to evaluate the differential capacitance ΔC_x, as expressed by:

$$\Delta C_x = \Delta C_{x-4} - \Delta C_{x-5} = \varepsilon_0 \varepsilon_r \frac{2\Delta A_x}{(d_0 - \Delta d)} \tag{3.18}$$

It is evident that under the assumption of small deformations ($\Delta d \ll d$), the electrode separation remains virtually unaltered and hence, the differential capacitance ΔC_x corresponding to the sensor shear signal should theoretically be independent of pressure:

$$\Delta C_x = \varepsilon_0 \varepsilon_r \frac{2\Delta A_x}{d_0} \tag{3.19}$$

Sensor unit fabrication

The silicone rubber (Room Temperature Vulcanization (RTV) 4420, Bluestar Silicones, France) was selected as the material for the sensor frames. In the prosthetic industry, silicone rubber represent the material of choice for liners and vacuum sleeves, due to its durability and the matching mechanical property to the soft tissue. Moreover, the use of silicone rubber also provides the potential to integrate the sensor frame with the existing liner product on the market.

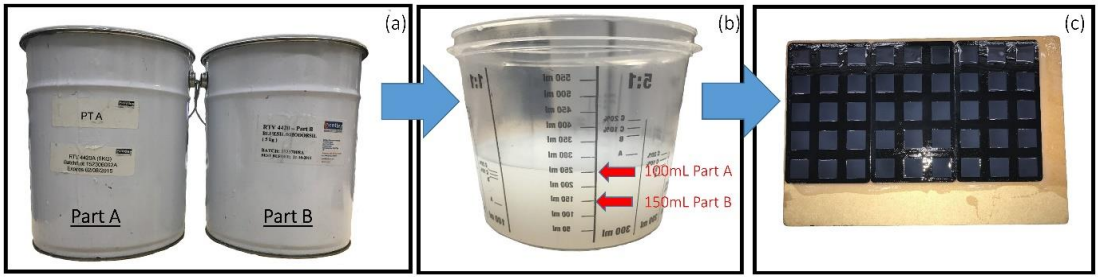

Figure 3.20: Sensor frame manufacturing process. (a) illustration of the two components of liquid silicone material, (b) Mixed part A and part B silicone material with volumetric ratio of 1:1.5 in graduated plastic cup and (c) batch injection moulding process (45 pieces of silicone square).

According to the data sheet of Bluestar Silbione RTV 4420, the A and B components of the liquid silicone material (Figure 3.20a) are recommended to be mixed at 1:1 ratio, producing a semi-rigid silicone material. However, in order to match the compressive modulus of the silicone liner, the part A and part B of the Bluestar Silbione RTV 4420 liquid silicone are mixed at 1:1.5 ratio (Figure 3.20b). A simple injection moulding process, involving pouring the liquid silicone material in to a designed 3D printed mould as shown in Figure 3.20c, was chosen. The curing process for the liquid silicone takes up to four hours.

A custom made 3D printed alignment jig (Figure 3.21a) was used to ensure the repeatability of the assembly process. Initially, the cured silicone square was placed in the indent of the

alignment jig (Figure 3.21b), designed with a matching geometry of the footprint of the electrode (flexible PCB). Then silicone adhesive (Momentive Performance Materials GmbH, Germany) was applied on the surface of the bottom electrode using a brush (Figure 3.21b) and the silicone square is subsequently place over it (Figure 3.21c). This was followed by application of the glue on the top surface of the electrode (Figure 3.21c) which was subsequently folded over to cover the top surface of the silicone square (Figure 3.21d). A rectangular aluminium block with dimensions of 19mm x 19mm x 25mm was manufactured. It was placed on the top surface of the flexible PCB as a compression weight to ensure a uniform load distribution of the glued area during curing (Figure 3.21e).

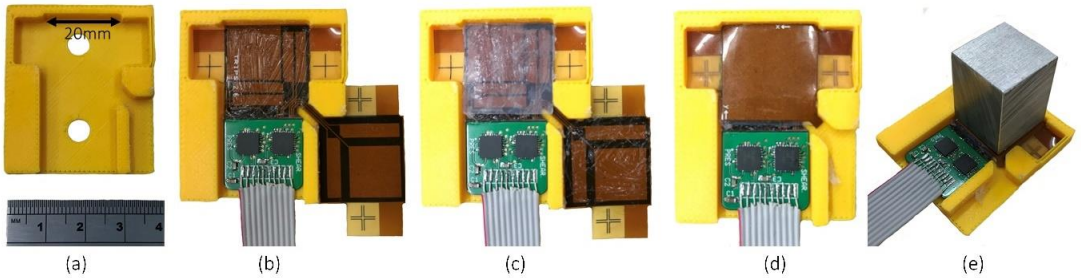

Figure 3.21: Sensor frame assembly

Thickness of each sensor unit is measured at three locations along the edge (at approximately 0mm, 10mm and 20mm location) and up to 1.2mm±0.2mm of thickness was obtained at all three locations.

3.3.3 Design and fabrication of sensor data acquisition unit

The capacitance change, in analogue form, is then collected and digitised by two 24-bit Capacitance-to-Digital Convertor (CDC) chips (ACAM PCap02). The PCap CDC chip is selected because it offers minimal noise, high sampling rate and its capability of measuring capacitance in both parallel and floating configuration. One of the CDC chips is in charge of the collection of signal induced from the normal loads and the other CDC chip is in charge of the collection of signals induced from the two orthogonal tangential loads. The DAQ unit supports up to three sensor units, including synchronised nine channels of signal (three from each of the sensor unit).

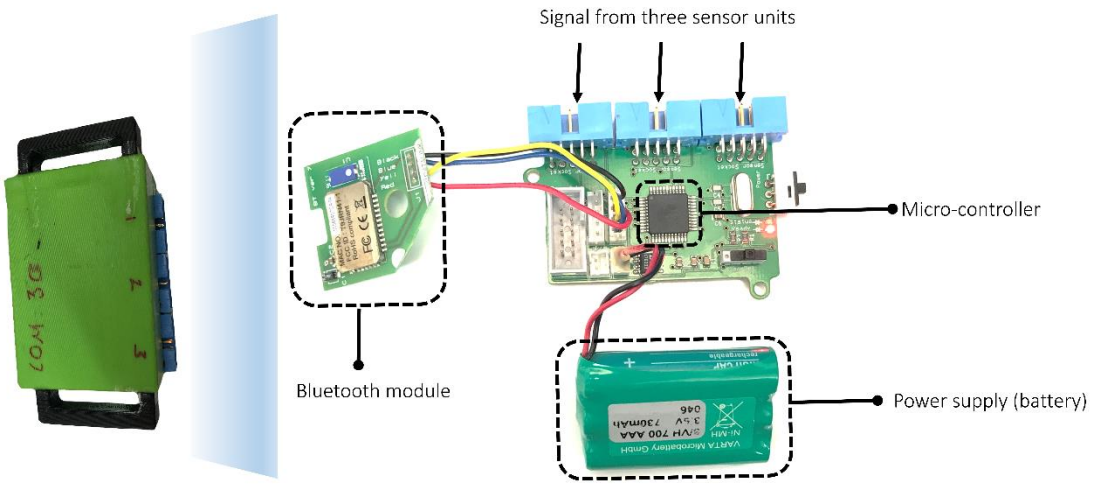

Figure 3.22: Photos showing the PCB of the DAQ unit.

The microcontroller (32-bit, AVR ATmega32 shown in Figure 3.22) on the PCB then started the data acquisition from the two CDC chips sequentially, one at a time. It is assumed that the lag between the two data acquisition from each of the CDC chip was negligible (a few Nano seconds). Data acquisition was set at 100Hz. At this stage, the data collected by the micro-controller was in machine readable binary form. The data was further converted to decimal numbers (ASCII form) by the micro-controller. Then, the signal in decimal form was further sent to a PC-based software.

The PC software displays the received data as a function of time and further saved in the format of comma separated values (.csv). Before the usage of the sensor system in clinical tests, each of the sensor unit, together with the DAQ unit needs to be calibrated, such that the capacitance signal can be converted to stress values.

3.4 Calibration of the sensor system

The sensor system calibration was designed to convert the measured capacitance signal to physical values, for example stress, that are relevant to both researcher and prosthetists. Figure 3.23 summarises the process of sensor system calibration. Each of the sensor unit was connected to the DAQ unit and subsequently mounted on a material test machine. Two type of load profiles, in both static and dynamic form, were applied via the test machine to each of the sensor unit in pressure and two orthogonal shear directions. The sensor system response, induced from the mechanical loads was recorded and used as an input for a signal-processing model. The signal processing model was designed to translate the capacitance values to stresses values in the unit of kilo Pascal in both pressure and shear directions.

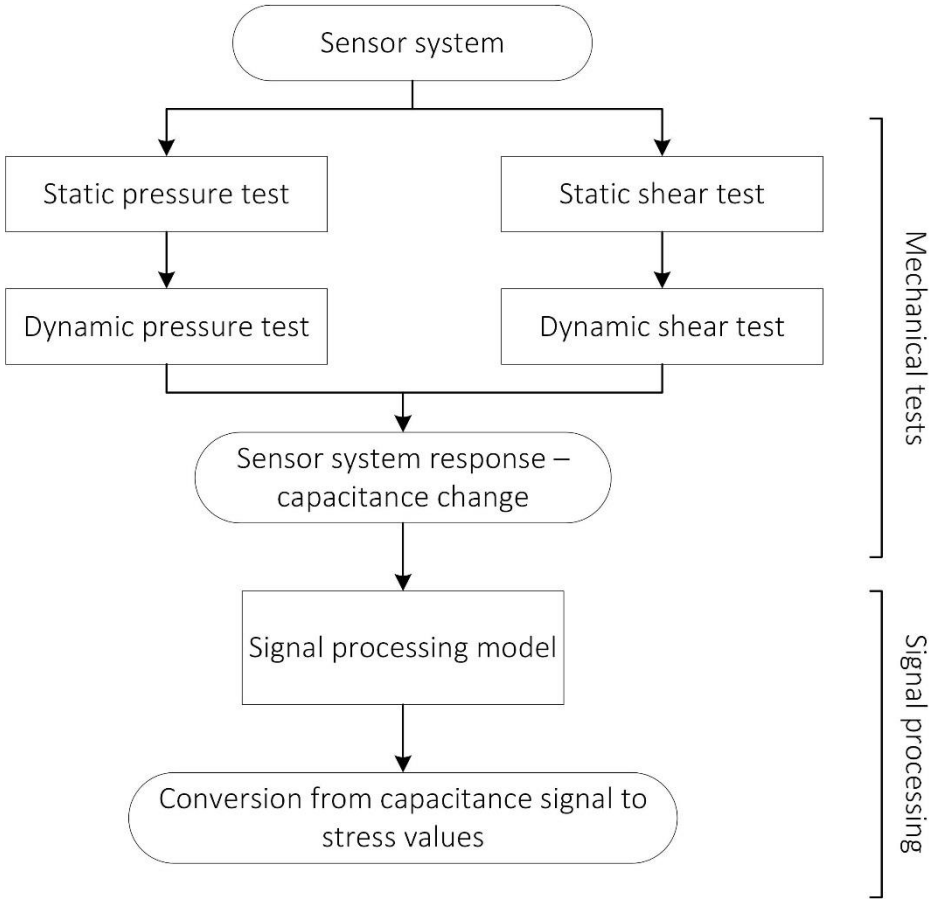

Figure 3.23: A flow chart showing the sensor system calibration process.

3.4.1 Test machine for sensor system calibration

Figure 3.24: A photo showing the Instron ElectroPuls™ E1000 material test machine[229].

The Instron ElectroPuls™ E1000 (Instron Ltd, High Wycombe, UK), the uni-axial material test machine, was used to conduct mechanical tests. The test machine (Figure 3.24) incorporates a load cell (measurement range: ±2kN and measurement accuracy: 0.5N) and an actuator (movement range: 60mm and movement accuracy: 0.015mm), which was controlled via an electromagnetic mechanism.

(a) (b)

Figure 3.25: Custom-made (a) compression platens and (b) shear platens

In order to test the sensor performance in pressure and shear channels, two sets of attachments (Figure 3.25a and Figure 3.25b) were designed and manufactured by Dr. Piotr Laszczak in the Engineering, Design and Manufacturing Centre (EDMC) in the University of Southampton. The detailed engineering design was detailed in Dr. Laszczak's PhD thesis [230]. The compression platens (Figure 3.25a), were then attached to the test machine. The bottom platen was fixed to the machine while the top platen applied the pre-programmed compression force profile (Figure 3.26a). The shear platens were assembled first and then mounted on the test machine (Figure 3.25b), and the sensor placed in the gap between the two aluminium hemi-spheres. Similarly, the bottom platen was fixed, while the top platen applies the pre-programed load through the sensor unit (Figure 3.26b).

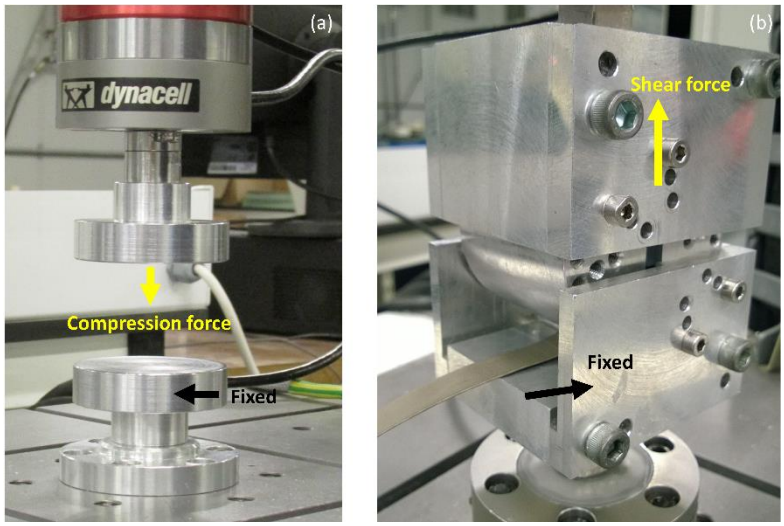

Figure 3.26: Assembled (a) compression platens and (b) shear platens on the Instron material test machine.

3.4.2 Mechanical test protocols

In order to characterise the static and dynamic behaviour of the sensor system, six sets of test protocols (two for each channel: pressure, shear X and shear Y channel) were designed in the Instron WaveMatrix software.

Static pressure test protocol

Figure 3.27a shows the load in newtons, applied by the Instron machine, during the static pressure calibration test. The loading profile was designed such that it incorporates two phases, loading (0N-200N) and unloading (200N-0N). It is worth noting that, during loading phase, a 2N/step was adopted between 0N to 60N in order to improve sensor system accuracy, while 20N/step was adopted between 60N to 200N. A similar protocol was adopted during unloading phase. The peak force of 200N, corresponded to the peak pressure of 500kPa. A peak value of 500kPa was chosen, as it represents the peak value obtained in pilot amputee test. This value also covers the highest reported peak pressure of 350kPa [9, 10].

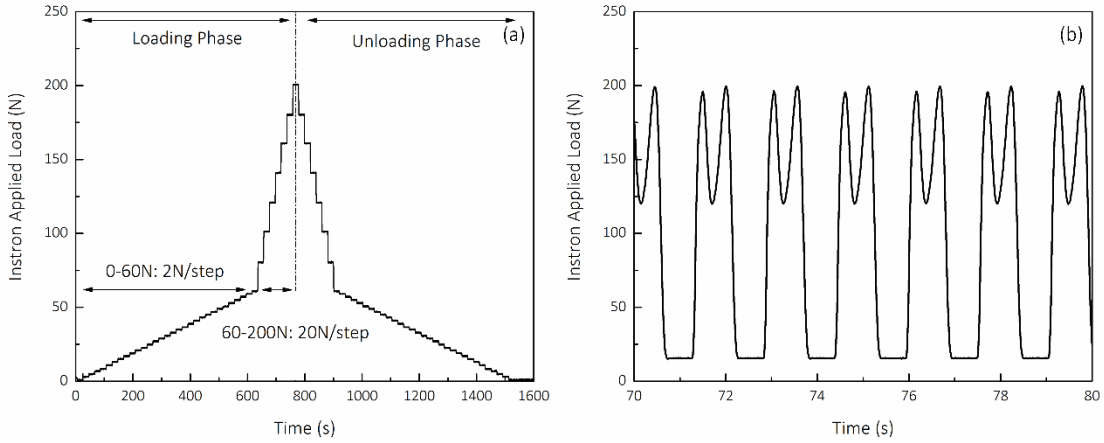

Figure 3.27: Applied load from Instron machine for (a) static and (b) dynamic pressure calibration test.

Dynamic pressure test protocol

Figure 3.27b shows the load in newtons, applied by the Instron machine, during the dynamic pressure calibration test. A double-hump profile over 60% of the cycle was used to represent the typical vertical load transfer from the ground interface to socket interface. A peak value of 200N was used, which represents a peak pressure of 500kPa. For the remaining 40% of the cycle, peak value of 20N was used, which typically represents the force experienced by the residuum during swing phase (5-90N) [128, 168].

Static shear test protocol

Figure 3.28a shows the load in newtons, applied by the test machine, for the static shear calibration test. Step loading was applied by the test machine to the each of the sensors. In total, four steps (8N/step) were applied in both positive and negative directions, therefore a peak load of 32N (equivalent to 80kPa) was applied. A peak value of 80kPa was chosen as it covers the highest shear value reported in the literature [10].

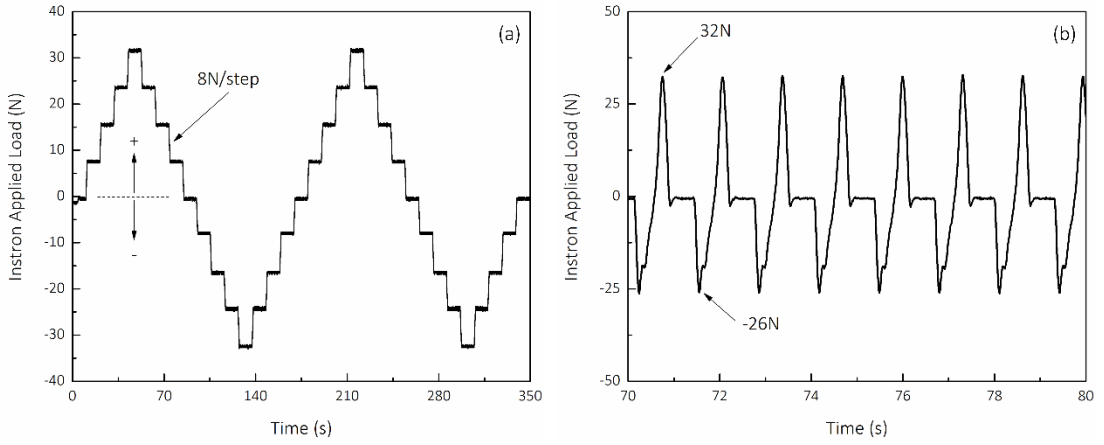

Figure 3.28: Applied load from Instron machine for (a) static and (b) dynamic shear calibration test.

Dynamic shear test protocol

Figure 3.28b shows the load in newtons, applied by the test machine, for dynamic shear calibration test. Profile obtained from the anterior-posterior component of GRF over 60% of the cycle, was used in the dynamic shear calibration test, as it represented the typical anterior-posterior shear force transfer from the ground interface to socket interface. Peak value of 32N was used in the profile, which represented peak shear value of 80kPa.

Sensor system response to mechanical tests

Figure 3.29 shows the sensor system response when performing static pressure and dynamic pressure calibration tests. With the same peak load applied to the sensor unit, changes in capacitance unit of up to 7900 and 5800 were observed during static and dynamic pressure calibration tests, respectively. It is also evident in the inset to Figure 3.29a that the sensor system response under step loading follows typical non-linear behaviour[231]. When an applied load reached the pre-programed value, the stress recorded by the sensor unit starts to decrease indicating stresses relaxation behaviour. In order to compensate for the stress relaxation behaviour, the test machine automatically applied more load to the sensor unit to reach the pre-programed target load. It is also worth noting that when comparing the first loading cycle (at approximately 15s) and the last loading cycle (at approximately 290s), signal drift was observed which is time-dependent.

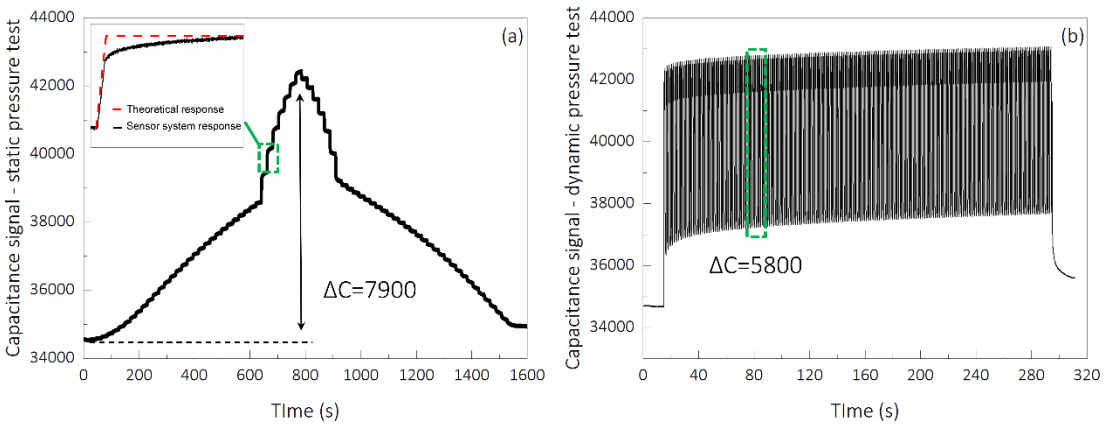

Figure 3.29: Sensor system response induced from (a) static and (b) dynamic pressure calibration tests.

Figure 3.30 shows the sensor system response when performing static pressure and dynamic shear calibration tests. In a similar manner to that during the pressure calibration test, when the same peak load is applied on the sensor unit, changes in capacitance units of up to 1200 and 800 were observed when performing static and dynamic calibration tests, respectively. This suggests that the sensor system exhibits different non-linear time-dependent responses

under static and dynamic loading conditions. In the next section, a material model, used to compensate the non-linear sensor system behaviour will be introduced.

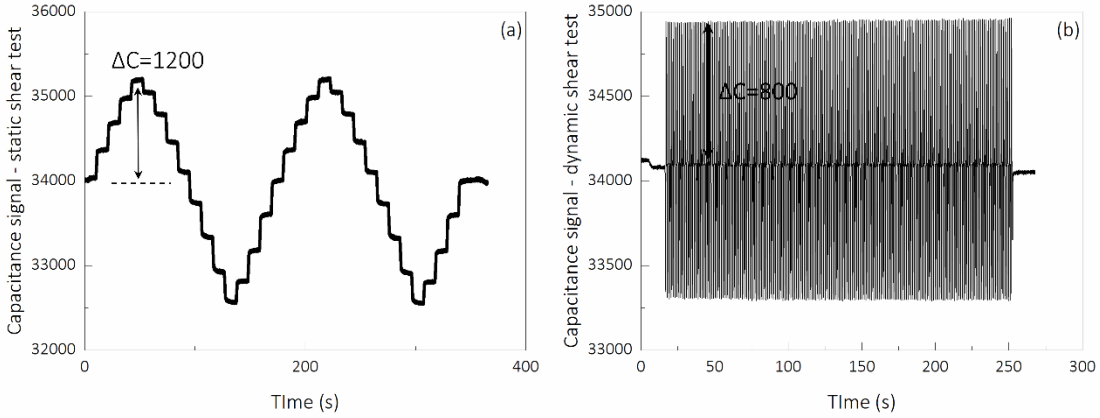

Figure 3.30: Sensor system response induced from (a) static and (b) dynamic shear calibration tests.

3.4.3 Signal processing model for the sensor system

Note, the implementation of the signal processing model on the current sensor system originate from Dr. Piotr Laszczak's work.

The non-linear viscoelastic material model – Wiechert Model

In order to compensate for the non-linear visco-elastic material behaviour of the sensor system output, a generalised material model, the Wiechert Model, was introduced. It consists of a series of spring and dashpot pairs to characterise the sensor system. This Wiechert model was chosen as it represents the general form of the linear model for characterising viscoelasticity. Other material models, such as a Maxwell model, can be derived from the Wiechert model by defining the value of 'n' in Figure 3.31. In this study, the value of 'n' was set to two, as it represents an optimum value when considering the performance of the model and the computational time.

Figure 3.31 shows the generalised structure of a Wiechert model, which contains a single spring (k_0) in parallel with n pairs of spring-dashpot arm (for example k_j and c_j). The single spring (k_0) in the Wiechert model accounts for the non-linearity of the material behaviour, while the spring-dashpot arm accounts for the visco-elastic behaviour of the material behaviour.

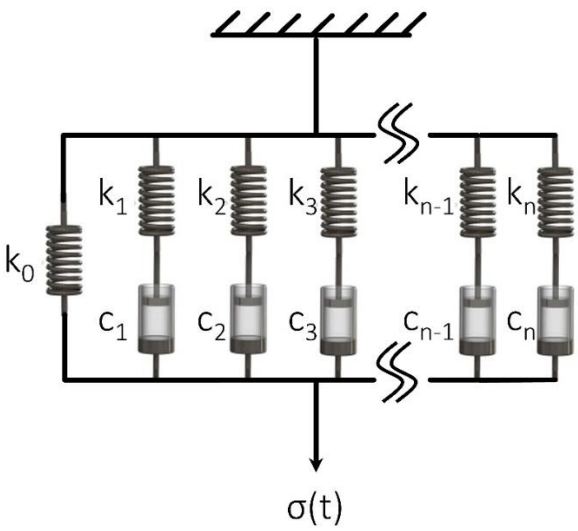

Figure 3.31: An illustration of Wiechert model, consisting of n pairs of spring-dashpot arms

It is evident that the total stress applied to the Wiechert system can be expressed as:

$$\sigma(t) = \sigma_0(t) + \sum_{j=1}^{n} \sigma_j(t) \tag{3.20}$$

Where $\sigma_0(t)$ is the stress induced from the very first spring (k_0) and $\sum_{j=1}^{n} \sigma_j(t)$ is the stress induced from the sum of the n spring-dashpot pairs.

Initially, the following derivation focuses on obtaining an expression for the visco-elastic component of the model ($\sum_{j=1}^{n} \sigma_j(t)$ term in Equation (3.20)) as a function of strain. By definition, the stress induced from the spring can be expressed by:

$$\sigma_j(t) = k_j \varepsilon_j^k(t) \tag{3.21}$$

Where k_j and ε_j^k are the spring constant and strain experienced by the spring in the j^{th} pair of the spring-dashpot, respectively.

By substituting Equation (3.21) into (3.20), $\sigma(t)$ can be expressed as:

$$\sigma(t) = \sigma_0(t) + \sum_{j=1}^{n} k_j \varepsilon_j^k(t) \tag{3.22}$$

Similarly, the stress induced from the dashpot, which is same in magnitude as the stress induced from the spring in the same spring-dashpot pair, can be expressed by:

$$\sigma_j(t) = c_j \dot{\varepsilon}_j^c(t) \tag{3.23}$$

Where c_j and $\dot{\varepsilon}_j^c$ are the dashpot constant and strain rate experienced by the dashpot in the j[th] pair of the spring-dashpot, respectively.

By re-arranging Equation (3.21) and Equation (3.23):

$$c_j \dot{\varepsilon}_j^c(t) = k_j \varepsilon_j^k(t) \tag{3.24}$$

For each spring-dashpot pair, the sum of strains experienced can be expressed by the sum of strain experienced by the spring and the dashpot:

$$\varepsilon(t) = \varepsilon_j^k(t) + \varepsilon_j^c(t) \tag{3.25}$$

By taking the derivative of Equation (3.25) with respect to time and an expression for $\dot{\varepsilon}_j^c$ can be obtained:

$$\dot{\varepsilon}_j^c(t) = \dot{\varepsilon}(t) - \dot{\varepsilon}_j^k(t) \tag{3.26}$$

By substituting Equation (3.26) in to Equation (3.24):

$$c_j\left[\dot{\varepsilon}(t) - \dot{\varepsilon}_j^k(t)\right] = k_j \varepsilon_j^k(t) \tag{3.27}$$

By applying a finite difference method on Equation (3.27) and assuming small increment of time (Δt), an expression of $\varepsilon_j^k(t)$ can be obtained:

$$\varepsilon_j^k(t) = \frac{\varepsilon(t) - \varepsilon(t-\Delta t) + \varepsilon_j^k(t-\Delta t)}{\frac{k_j}{c_j}\Delta t + 1} \tag{3.28}$$

By substituting Equation (3.28) into Equation (3.22), then:

$$\sigma(t) = \sigma_0(t) + \sum_{j=1}^{n} k_j \frac{\varepsilon(t) - \varepsilon(t-\Delta t) + \varepsilon_j^k(t-\Delta t)}{\frac{k_j}{c_j}\Delta t + 1} \tag{3.29}$$

The expression or Equation (3.29) responsible for modelling the visco-elastic behaviour of the material, as a function of strain, is obtained. In order to further account for the non-linearity of the material behaviour, a second order polynomial is assumed for the spring (k_0):

$$\sigma_0(t) = k_0^1 \varepsilon(t) + k_0^2 \varepsilon(t)|\varepsilon(t)| \tag{3.30}$$

By substituting Equation (3.30) in to Equation (3.29), the following is obtained:

$$\sigma(t) = k_0^1\varepsilon(t) + k_0^2\varepsilon(t)|\varepsilon(t)| + \sum_{j=1}^{n} k_j \frac{\varepsilon(t) - \varepsilon(t-\Delta t) + \varepsilon_j^k(t-\Delta t)}{\frac{k_j}{c_j}\Delta t + 1} \quad (3.31)$$

Where k_0^1 and k_0^2 are the coefficients of the second order polynomial.

Equation (3.28) and Equation (3.31) are the relationships that constitutive of Wiechert model, which relates the strain experienced by the non-linear, visco-elastic to the stress. Therefore, at any time instance, given the measured strain of a material in loading direction, stress can be calculated.

The Wiechert Model was adopted to characterise the signals generated from the pressure and shear sensor system. This was achieved by assuming that the change in captaincy signal is proportional to the strain experienced by the sensor frame or $\Delta C(t) \propto \varepsilon(t)$. Therefore, the applied stress to the sensor frame was linked to the change in capacitance. By re-writing Equation (3.28) and Equation (3.31), the following expressions can be obtained:

$$\Delta C_j^k(t) = \frac{\Delta C(t) - \Delta C(t-\Delta t) + \Delta C_j^k(t-\Delta t)}{\frac{k_j}{c_j}\Delta t + 1} \quad (3.32)$$

and

$$\sigma(t) = k_0^1\Delta C(t) + k_0^2\Delta C(t)|\Delta C(t)| + \sum_{j=1}^{n} k_j \frac{\Delta C(t) - \Delta C(t-\Delta t) + \Delta C_j^k(t-\Delta t)}{\frac{k_j}{c_j}\Delta t + 1} \quad (3.33)$$

3.4.4 Performance of the sensor system

The material model described in the previous section was subsequently applied to both static and dynamic test data from the sensor system (Section 3.4.2). Key parameters, linearity, resolution, drift and hysteresis were chosen for the evaluation of the performance of the TRIPS sensor system.

Linearity

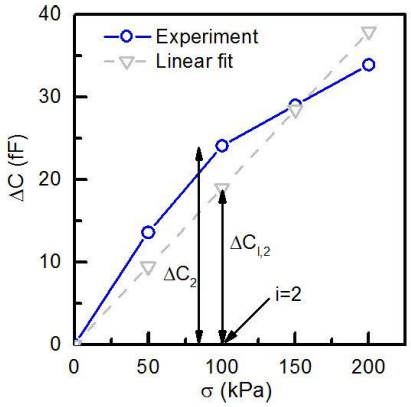

Figure 3.32: Illustration of linearity error calculation on exemplary data.

To illustrate the calculation of linearity error, Figure 3.16 presents exemplary outcome from a static sensor calibration test, whereby each loading step, i, corresponds to the capacitive signals from the sensor (ΔC_i). The data is plotted with a linear model ($\Delta C_{l,i}$). Accordingly, sensor sensitivity is evaluated as the slope of that model, while linearity error is the maximum difference in the output between the experiment and the linear model and expressed as percentage of the latter, see Equation (3.34):

$$Linearity\ Error = \frac{\left|\Delta C_i - \Delta C_{l,i}\right|_{max}}{\Delta C_{l,i}} \times 100\% \tag{3.34}$$

Figure 3.33 presents a typical response of an individual sensor to static loading. Linear models were fitted to the pressure and two shear channels of the sensor system output. Accordingly, the linearity errors for each of the channels were calculated according to Equation (3.34). For this particular sensor, pressure signal exhibits up to 11% of linearity error (Figure 3.33a). This was inevitable due to thin profile of the sensor, which promotes non-linear sensor response. However, 11% of linearity error is up to two times lower than those polymer based sensors [184-187]. Shear signal exhibits up to 2% linearity error and is symmetrical about the centre of the co-ordinate system (Figure 3.33b).

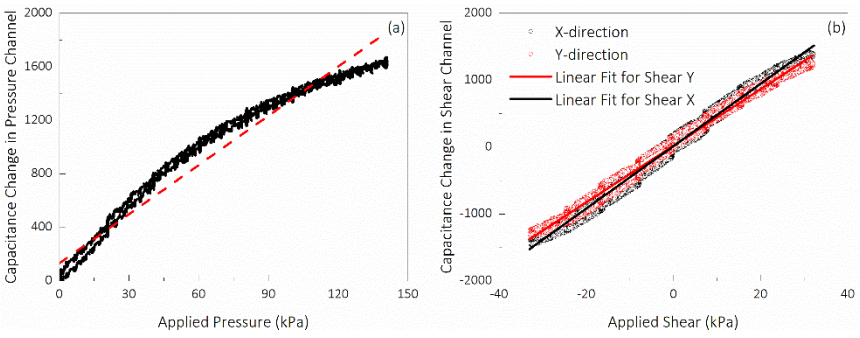

Figure 3.33: Static response of the sensor system fitted with linear models

Noise based resolution

The sensor system resolutions were evaluated by calculating root mean square of noise of the capacitance signal. Subsequently, the resolution in capacitance units was converted, via the signal-processing model, to stress with a unit of kPa. By using the results obtained in Figure 3.33a and b, 3kPa, 3kPa and 2kPa of resolution were obtained in pressure, shear X and shear Y channels without any filtering, respectively.

Drift Error

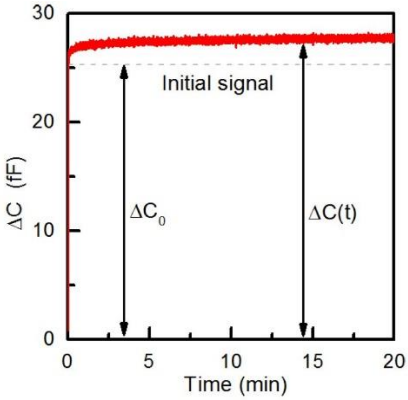

Figure 3.34: Illustration of drift error calculation on exemplary data.

Drift error at time was calculated as the difference between the signal recorded immediately after the load application (ΔC_0) and the signal at time t (ΔC (t)) (Figure 3.34) and expressed as percentage of the latter, see Equation (3.35):

$$Drift\ Error = \frac{|\Delta C_0 - \Delta C_t|}{\Delta C_t} \times 100\% \qquad (3.35)$$

Figure 3.35 shows the sensor system response under constant load, as a function of time. Based on Figure 3.35, drift errors in both pressure and shear channels can be calculated using Equation (3.35).

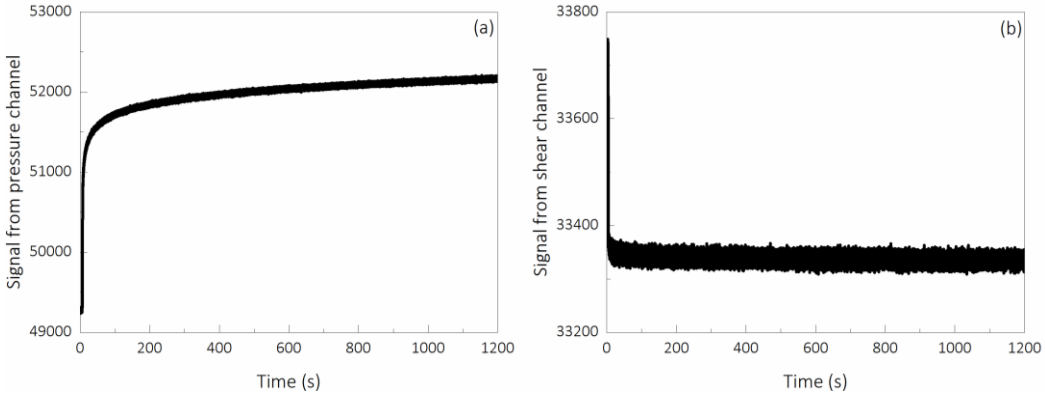

Figure 3.35: Sensor system response under constant load.

The outcomes of the drift evaluations (Table 3.1) suggest that in pressure channel, up to 15% and 4% of drift error was presented in the pressure and shear channels of the sensor system under 20min of constant loading. The sensor system drift is half that of the commercially available TekScan™ system [182]. It is also noteworthy that further improvement of the drift characteristics is possible and may be achieved using appropriate signal processing techniques.

Table 3.1: Drift error of the sensors

Time (min)	Drift error (%)		
	Pressure	Shear X	Shear Y
5	8	3	4
10	11	3	4
15	14	3	4
20	15	3	4

Hysteresis

The hysteresis error was estimated from the hysteresis loops (Figure 3.36) as the maximum difference in output between loading and unloading parts of the cycle, expressed as percentage of the smaller of the two, see Equation (3.36).

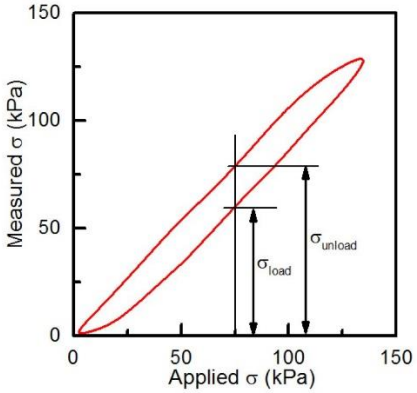

Figure 3.36: Illustration of hysteresis error calculation on exemplary data.

$$Hysteresis\ Error = \frac{|\sigma_{load} - \sigma_{unload}|}{\sigma_{load}} \times 100\% \quad (3.36)$$

Figure 3.37a and Figure 3.37b shows the sensor system dynamic response under dynamic loading with the loading profile described in Page 101. Based on the dynamic response of the sensor system, Equation (3.36) was used to calculate the hysteresis error. Based on 300 cycles of loading at 1Hz, hysteresis errors of up to 17% and 12% were measured in pressure and shear channels, respectively. When comparing to the hysteresis measured on TekScan™ system, an improvement of 29% in hysteresis error was evident.

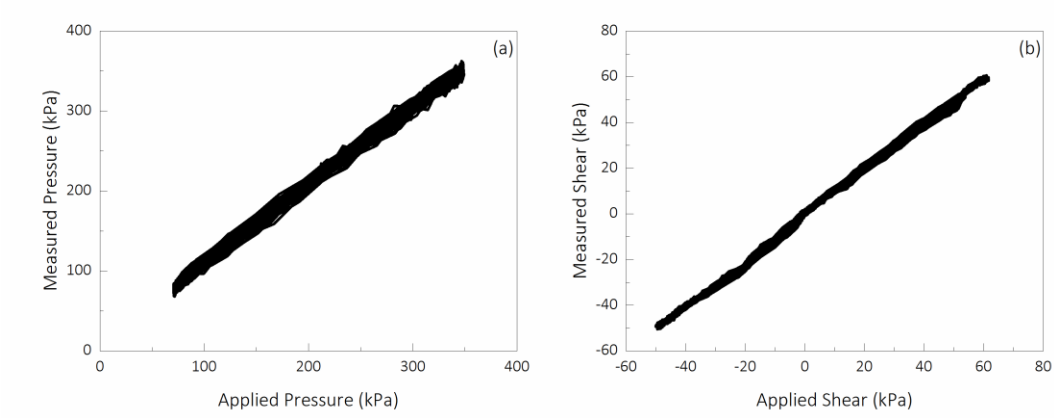

Figure 3.37: Sensor system response under cyclic load.

The TRIPS sensor system shows a greater performance in terms of linearity error, drift error and hysteresis. This is due to the application of a visco-elastic material model, compensating the sensor system performance in both static and dynamic conditions.

Repeatability analysis

Up to five sensors units were randomly selected for the assessment of intra-sensor repeatability. The sensor unit was first mounted on a compression platen (Figure 3.25). The orientation of the sensor unit was approximately fixed at the same direction with the aid of the alignment jig (Figure 3.38). Static pressure tests were carried out on each sensor unit with applied pressure profile illustrated in Figure 3.39a. The test was repeated five times. The sensor unit was removed from the platen and allowed to rest for 10 minutes between each of the tests. 10 minutes was chosen as it represents the time needed for the baseline signal to recover to zero values. It is worth noting that the shear test was not repeated due to the relatively higher risk in damaging the sensor in this type of test.

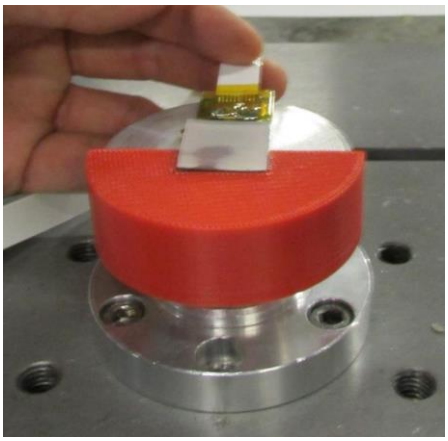

Figure 3.38: A photo showing the sensor alignment jig (red).

Figure 3.39 illustrates the change in capacitance in a typical sensor unit, obtained from the sensor system, with five repeated mechanical calibration tests. A total of ten loading steps was performed, followed by 10 unloading steps. The measured capacitance was subsequently converted to the pressure values in kilopascals, based on the signal processing model (Section 3.4.3). The largest separation in the pressure values, measured in each step, was identified using the results obtained from five repeated tests. The largest separation in pressure values, per sensor, was then identified ($\Delta P_{max.}$) with its corresponding capacitance $\Delta C_{max.}$. As an example, $\Delta P_{max.}$ of 5kPa unit was found in the 2nd step. Same analysis was applied to both Shear X channel and Shear Y Channel.

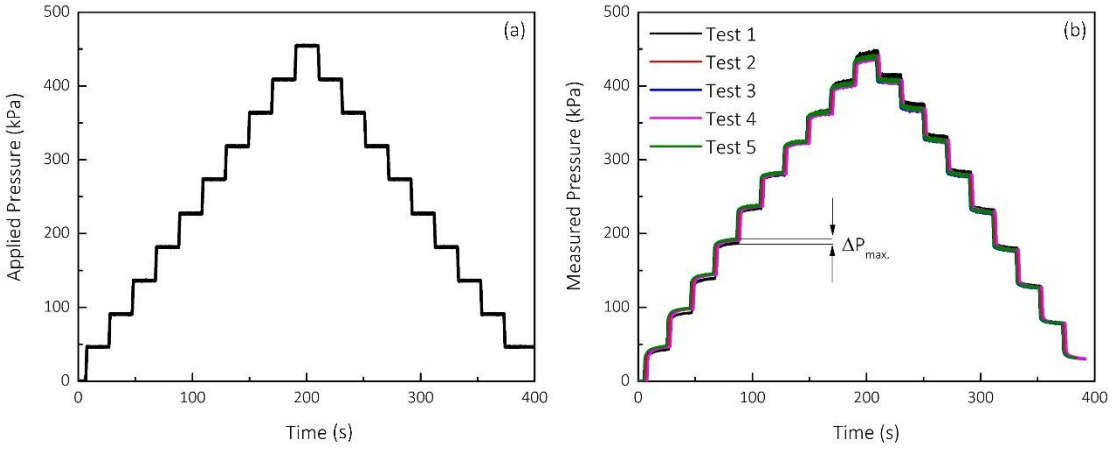

Figure 3.39: (a) Applied pressure and (b) measured pressure a function of time.

Table 3.2 shows the value of $\Delta C_{max.}$ and $\Delta P_{max.}$, obtained from five repeated test, for all five sensors. In the worst case scenario, $\Delta C_{max.}$ of up to 80 capacitance units was measured from Sensor 1. This corresponds to pressure value of approximately 5kPa. The worst case intra-sensor repeatability of 5kPa among the five sensor units, was smaller than the value obtained on FSRs (approximately 8kPa) [232]. It is worth noting that only three repeated tests were conducted on one FSR-based sensor by other researchers. The average intra-sensor repeatability performance of FSR is still not clear at different loading conditions.

Table 3.2: Intra-sensor repeatability based on five repeated tests of five sensors.

Sensor No.	Pressure	
	$\Delta C_{max.}$	$\Delta P_{max.}$
1	80	5kPa
2	62	4kPa
3	60	4kPa

4	72	5kPa
5	63	3kPa

Instead of using one set of visco-elastic parameter for the signal processing, for each of the sensor unit, both static and dynamic mechanical tests were performed. Subsequently, a signal-processing model was fitted on the sensor output from mechanical tests. Therefore, a bespoke set of visco-elastic parameter was assigned to the signal processing model for each of the sensor unit. This is to minimise the inter-sensor variability contributed from the sensor unit manufacturing process (Section 3.3.2).

3.4.5 Synchronisation between motion capture and sensor system

Having introduced the 3D motion capture system and the TRIPS sensor system, in this section, the synchronisation of the data streamed from the two pieces of equipment will be introduced. The purpose of obtaining the synchronous measurement between the two systems is to investigate the association between the motion of the key lower limb landmarks and the stress profile at the socket interface.

In order to obtain simultaneous measurements of the interface stresses and 3D coupling motion during the same walking test, a synchronisation device was designed. The schematics are shown in Figure 3.40 and the corresponding PCB shown in Figure 3.41a. When acquisition of the marker position started, a 5V trigger pulse was issued from the motion analysis system. Subsequently, this pulse was received by the sensor system controller via the synchronisation device, which marks the start of the data acquisition in the sensor system. The motion analysis system is chosen as the master device to trigger the start of the sensor system as oppose to the other way. The TRIPS sensor system can also be used to trigger the start of the motion analysis system. However, it is not recommended by the Senior Hardware Engineer in Codamotion, due to the noticeable latency in the motion analysis system.

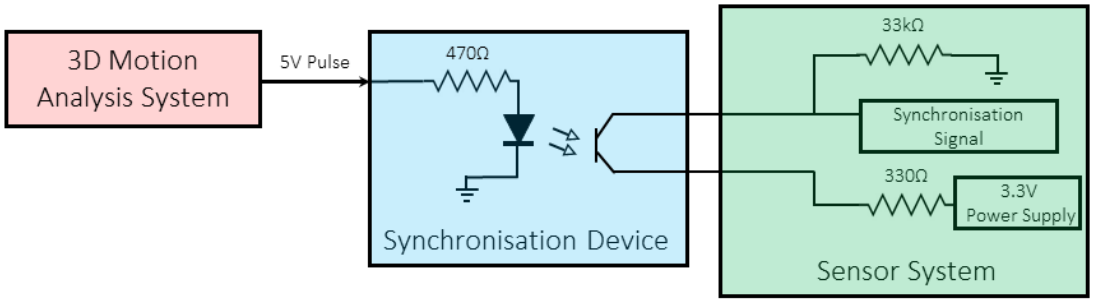

Figure 3.40: Schematics showing the circuitry of the synchronisation device, linking the 3D motion analysis system and sensor system

It is worth noting that, an optocoupler (PC367NTJ000F, SHARP Corporation, Osaka, Japan) was used to separate the circuitry on the motion analysis system from the one on TRIPS sensor system. This serves the purpose to protect the both electronic system from the excessive current flow. Appropriate sets of resistors on the motion analysis system side and the sensor system side were selected, such that there is an 11mA of current flowing between the synchronisation device (blue section in Figure 3.40), which is significantly lower that the manufacturer specified safety limit (24mA). On the sensor system side (green section in Figure 3.40), 10mA is measured during operation, which is equivalent to the sensor system operating current. Two sets of data, one from the 3D motion analysis system and one from the stress sensor system, can then be temporally synchronised using their corresponding start time. Figure 3.41b illustrates the physical connection between the motion analysis system and the TRIPS sensor system.

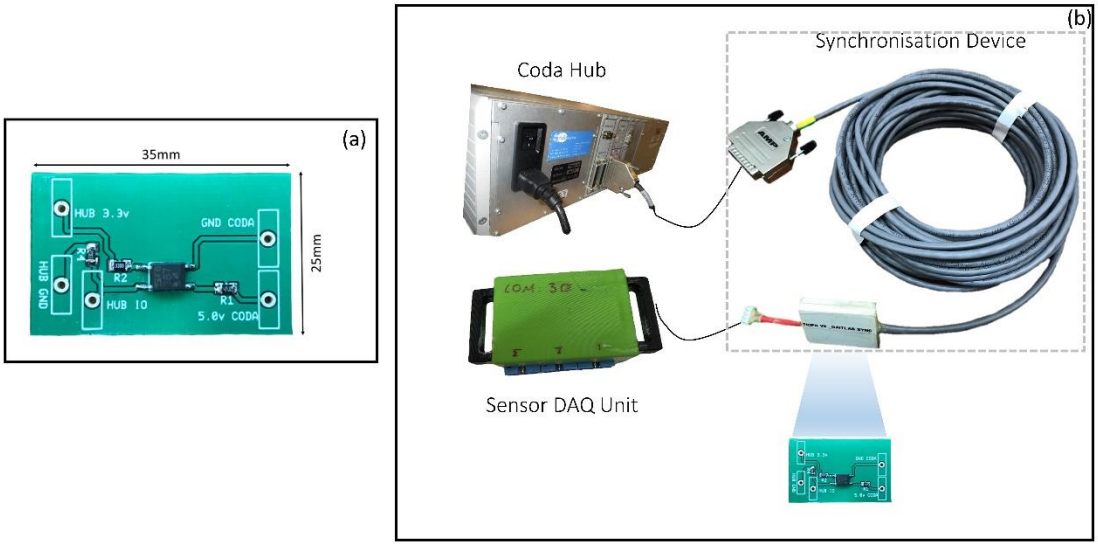

Figure 3.41: A schematic showing the connection between the 3D motion capturing system and the sensor system via a synchronisation device.

A 5V DC power supply (72-8690A, TENMA) was used to emulate the motion analysis system. Subsequently, it was connected to the synchronisation device. An oscilloscope (DS2072A, RIGOL) was used to monitor the duration between switching 5V power supply on and the record of the first data by the DAQ. 90ns was measured and this value is significantly lower that the sample period of both system (10ms for TRIPS sensor system, 10ms for marker data and 2ms for GRF). This means that the device is suitable for aligning the data from motion analysis system and TRIPS sensor system together.

3.5 Participant and research activities

3.5.1 Able-bodied participants

One able-bodied participant (denoted AB1) participated the study, approved by the University of Southampton Ethics and Research Governance Committee (ID: 12058). Table 3.3 shows the age, body mass and height of the able-bodied participant. No musculoskeletal dysfunction was reported by the participant and he is able to walk without any assistance repeatedly on both level and ramped walkway.

Table 3.3: Age, body mass, height and the body mass index of the able-bodied participant.

	AB1
Age (years)	27
Body mass (kg)	75
Height (cm)	178
Body mass Index (kg/m^2)	23.6

3.5.2 Amputee participants

Three amputee participants participated this PhD project (Table 3.4). The institutional ethical application (ID: 12058) also covers the usage of the amputee test data.

Table 3.4: Age, body mass and height of the amputee participants

	Trans-tibial 1	Trans-tibial 2	Trans-tibial 3	Knee-disarticulation
Age (years)	42	53	38	30
Body mass (kg)	49	70	81	79
Height (cm)	165	178	183	177
Body mass index (kg/m^2)	17.9	22.0	24.1	25.2
Activity level	K3	K3	K3	K3
Side of amputation	Right	Left	Right	Right
Time since amputation	5	24	18	Congenital

The Trans-tibial 1 participant has residuum length of 114cm (Figure 3.42a) and has been using prosthetic limbs since 2011. He was fitted with a TSB suction socket with silicone sleeve, one thick sock, Silcare Breathe liner and an Elan prosthetic foot^{TM}. It is worth noting here the Elan foot was in participant's habitual setting (Dorsi-flexion hydraulic ankle resistance of grade 5 and Plantar-flexion hydraulic ankle resistance of grade 5).

Trans-tibial 2 participant was involved in a traffic accident, which caused the amputation on the left side. He had a stump length of 14cm, measured from the patella to the distal end of

the stump (Figure 3.42b). A TSB suction socket was prescribed by the prosthetist. It is worth noting that, excessive pain was reported at fibula head by the participant and a circular hole was cut around fibula head location of the socket. A silicone liner (Apls Corporation, perforation liner, 3mm) was worn the socket is suspended using the silicone suction sleeve. Echelon foot is his habitual prosthetic foot with plantar-flexion and dorsi-flexion hydraulic ankle resistance both set to 5.

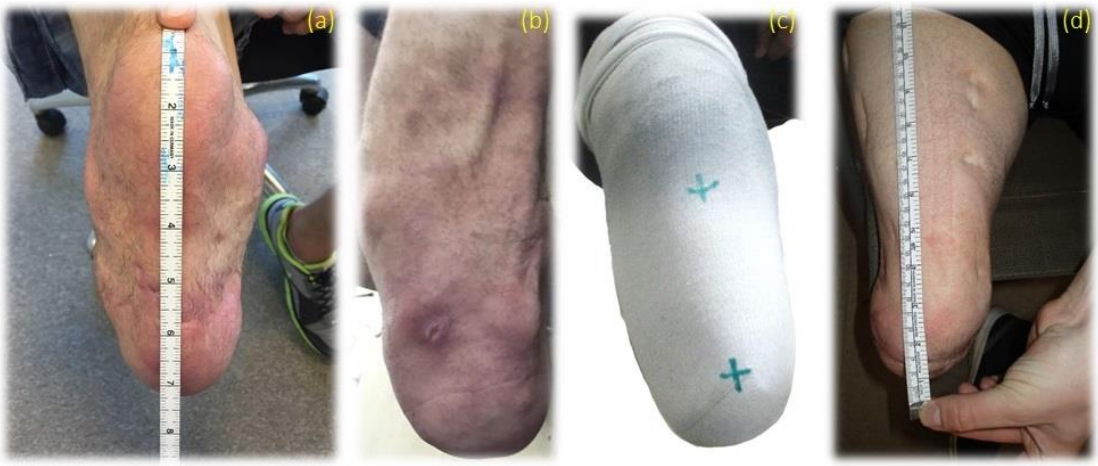

Figure 3.42: Photos showing the stumps of (a)-(c) the trans-tibial amputees and (d) the knee disarticulation amputee.

Trans-tibial 3 participant suffered from trauma, which is the major cause of his amputation on the right side. After 18 years post-amputation, he has a stable residuum (Figure 3.42c), free from infection. He is prescribed with Elan prosthetic foot, a carbon fibre TSB socket with suction suspension, a 3mm silicone gel liner and two 3mm socks.

The knee disarticulation amputee suffered from birth-defect complications. His residuum length was 440mm, from the greater trochanter to distal end of the residuum (Figure 3.42d). He was fitted with a supra-condylar suspension socket, one thick sock, a Pelite liner, a KX06 prosthetic knee and an Echelon^{TM} prosthetic foot. The prosthetic components mentioned here are his habitual ones. It is also worth noting that the Echelon^{TM} foot was in his habitual setting (Dorsi-flexion hydraulic ankle resistance of grade 5 and Plantar-flexion hydraulic ankle resistance of grade 7).

3.5.3 Research activities

AB1, Trans-tibial 1 and knee disarticulation participants involved in the study to assess the lower limb joint mechanics. This study aims to understand the difference in load transfer at lower limb joints in both able-bodied and amputee participants with different amputation level.

Having understood the load transfer at both distal and proximal location of the interface, an interface kinematic model was developed to assess the 3D motion of the residuum, relative to the socket. Trans-tibial 1, Trans-tibial 2 and knee disarticulation participants involved in the study to assess the repeatability and sensitivity of the model.

The corresponding interface kinetics will be assessed using the TRIPS sensor system. In this set of study, Trans-tibial 1, Trans-tibial 3 and knee disarticulation participants were involved. The repeatability and the sensitivity of the interface stresses measurements were studied. The detailed research activities is presented in Figure 3.43.

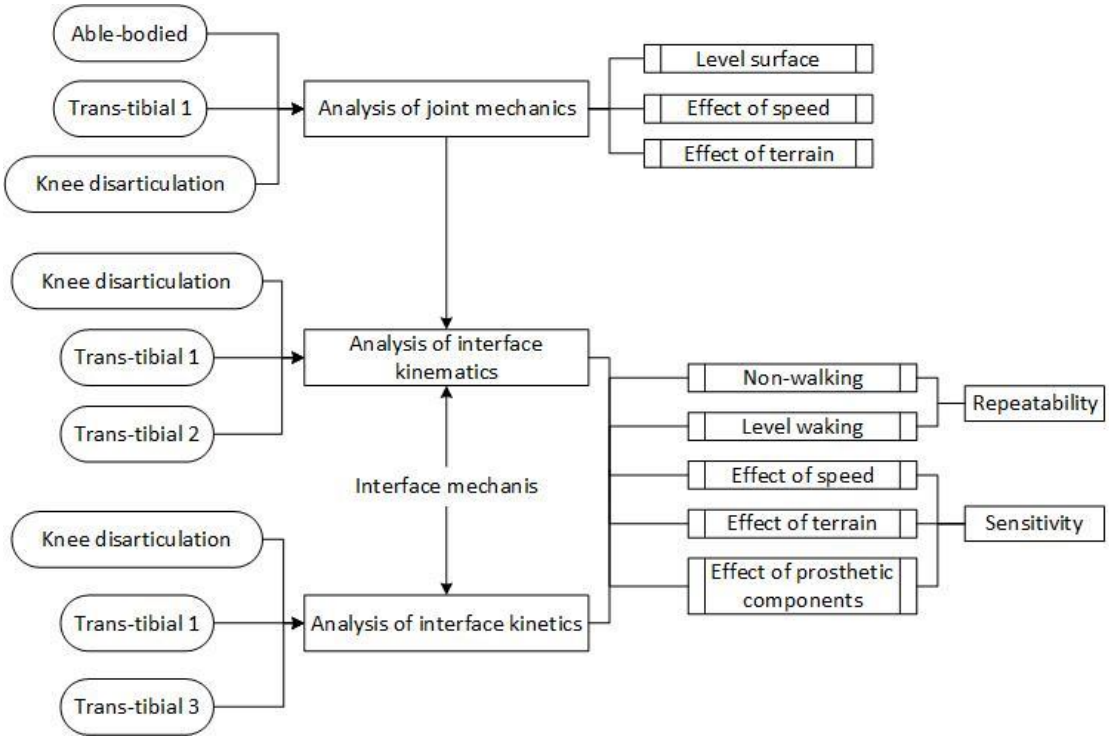

Figure 3.43: Overview of the research activities.

Chapter 4 Human lower limb joint mechanics

Human locomotion has been extensively studied in the past 40 years. 3D motion capture using infrared cameras and optical markers, combined with force plate(s), have been commonly used in gait laboratories. As reviewed in Section 2.4, socket interface biomechanics is intricately linked with limb motion and inverse dynamics during ambulation (Section 2.5). Thus, comprehensive studies of interface biomechanics must be underpinned by in-depth understanding of lower limb amputee gait. In particular, the characteristic difference between amputee gaits and able-bodied gait. The comparison of typical gait parameters between able-bodied and amputee participants was undertaken and the effects of walking speed and terrain were also studied. This is because speed and terrain are two of the main factors, which may affect gait patterns (Section 2.5.3). Consequently, the importance of socket interface biomechanics to gait stability, safety and efficiency is highlighted in the context of overall amputee gait patterns. Furthermore, the suitability of 3D motion capture markers for interface dynamics is discussed. An illustrative schematic of the work associated with this chapter is shown in Figure 4.1.

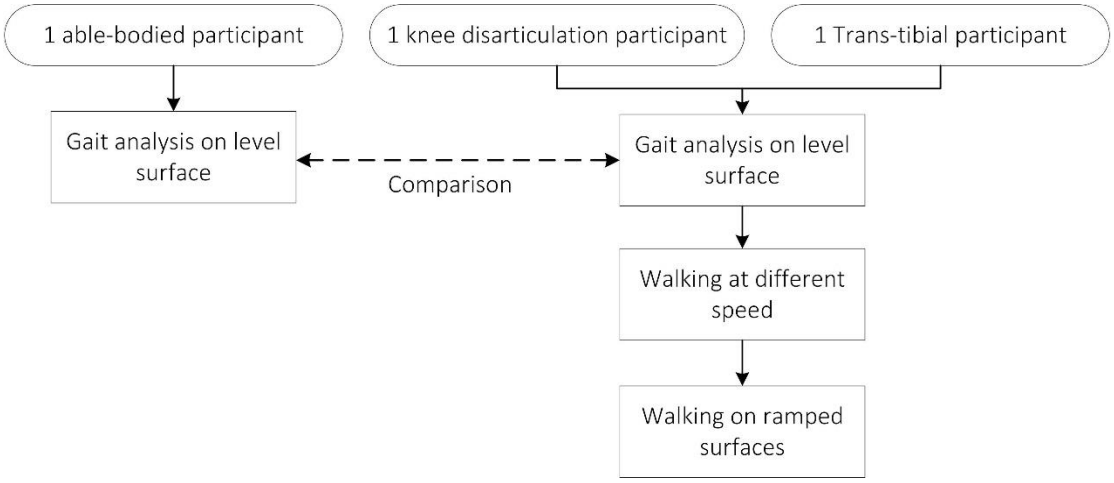

Figure 4.1: A flow chart showing the research activities involved in the abled-bodied and amputee gait analysis.

4.1 Method

4.1.1 Experimental protocol

Upon arrival in the gait laboratory in Endolite research centre (Chas A Blatchford & Sons Ltd.), the able-bodied participant, as well as the amputee participants (trans-tibial 1 and knee disarticulation) were first asked to change into Lycra. Subsequently, a total of 28 markers were placed at key anatomical landmarks based on a 6DoF maker model (Odin User Manual, 2016). The details of the marker placement protocol, for both able-bodied and amputee participants

can be found in Section 3.2.1. It is worth noting there that only one investigator, the author of this thesis, was involved in the marker placement process.

Four sessions of walking trials were performed, including:

A1: Level walking tests

In this set of tests, a reference set of gait analysis data will be collected on the able-bodied participant and amputee participants. Comparison will be made, in terms joint kinematics and kinetics, to highlight the need for a separate assessment of residuum/socket interface mechanics.

The able-bodied participant and two amputee participants were asked to walk on a 10m level walkway at self-selected waking speed. In each of the trial, the participant was asked to make contact with the force platform with prosthetic side. At least ten successful trials were performed by each of the participants. A successful trial occurred when a 'clean' contact by the prosthetic foot was made on the force platform without any observable targeting or changes in stride pattern. A clean contact is defined as one in which all the key markers were visible combined with a complete single foot contact with the force platform.

A2: Level walking tests with different walking speed

The knee-disarticulation amputee was asked to perform three sessions of level walking trials on the 10m walkway. Walking cadence was controlled by a metronome beeping at 80 beats per minute (BPM) for slow speed, 100BPM for self-selected speed and 120 BPM for fast walking speed. Based on previous tests conducted on the knee disarticulation amputee, his level walking cadence is estimated at approximately 102BPM. Therefore, 100BPM was used as his self-selected walking cadence. In each of the trial, the participant was asked to make contact with the force platform with prosthetic side. At least ten successful trials were performed.

A3: Walking tests on ramped surfaces

This session of tests were conducted on the trans-tibial and the knee disarticulation amputees. In this session, both participants were asked to walk on a descending surface and an ascending surface. As mentioned in Section 3.1, the ramp has an angle of inclination of 5° and length of 8m. Both participants were asked to walk at their self-selected speed for up to ten successful trials with their prosthetic side in contact with the force platform.

4.1.2 Data collection and analysis

The collection of marker and GRF data can be found in Section 3.1.4. It is worth noting here; at least eight steps worth of data were captured in a single trial. Among those eight steps, data contained in a single step was extracted for further analysis. For the able-bodied participant, the single step corresponds to the step with the right side making full contact with the force platform. For amputee participants, the single step corresponds to the one with prosthetic side making contact with the force platform.

Subsequently, the timing for IC was defined as the point when the vertical component of GRF was above 20N. Similarly, the timing for TO was defined as the point when the vertical component of GRF was below 20N. The end of the GC, or the IC of the next GC, was defined kinematically. This is because only one force platform was available in the gait laboratory. The timing of the peak hip extension of the contra-lateral limb was used as the timing for the second IC [233].

Equation (2.1)-Equation (2.3), described in the literature review, were used in Odin software to calculate the joint kinetics, including joint moment and joint power, as a function of time. Data in the time domain were subsequently normalised to percentage of gait cycle. Zero percent of gait cycle is defined as the timing of the IC and the 100% of GC is defined the timing when the 2nd IC occurs. The software then saves the raw marker data, GRF data, joint kinematic and joint kinetic in the form of Microsoft Excel spreadsheet. Matlab 2016a was subsequently used to calculate the mean and one standard deviation (SD) of the GRF data, joint kinematic and joint kinetic data, including joint moment and power.

Minitab 17 statistical software was used to perform statistical analysis. For all parameters e.g. mean peak values and ROM, normality of the data was first check using Anderson-Darling test with p value of 0.05 set as the threshold. Paired t-tests were performed when comparing the difference between two the mean values, under different test conditions. The level of significance was also set at $p<0.05$.

4.2 Joint mechanics on level surface

Clinical evidence showed that the tissue viability might be compromised for lower limb amputees, resulting in pressure ulcers and friction blisters. From load transfer point of view, the formation of the tissue damage can be traced back to the prolonged and cyclic loading of tissue, as well as the biological behaviour of it. The loads, experienced at the residuum/socket interface, originated from the ground interface and further transfer through the prosthesis to the socket interface. Therefore, understanding the load experienced at both prosthetic joint

and biological joint becomes critical. The purpose of this section is to understand the difference in joint mechanics obtained from both the able-bodied group and amputee group with the aim to highlight the need for the direct assessment of socket interface mechanics.

4.2.1 Ground reaction force

As mentioned in Section 2.4.4, the GRF obtained on amputee group was significantly different from the able-bodied group, in terms of peak values. This was primarily due to the lack of load bearing capability at the socket interface, with the presence of bony prominences and the biological behaviour of the residuum tissue. The first step to understand the interface biomechanics is to investigate the load transfer at the ground interface. In this section, results were obtained from protocol A1, as mentioned in Section 4.1.1.

Figure 4.2 shows the three components of GRF, obtained from the abled-bodied, trans-tibial and knee disarticulation participants, over a GC. Table 4.1 shows the peak value of the GRF, at early and TS of GC.

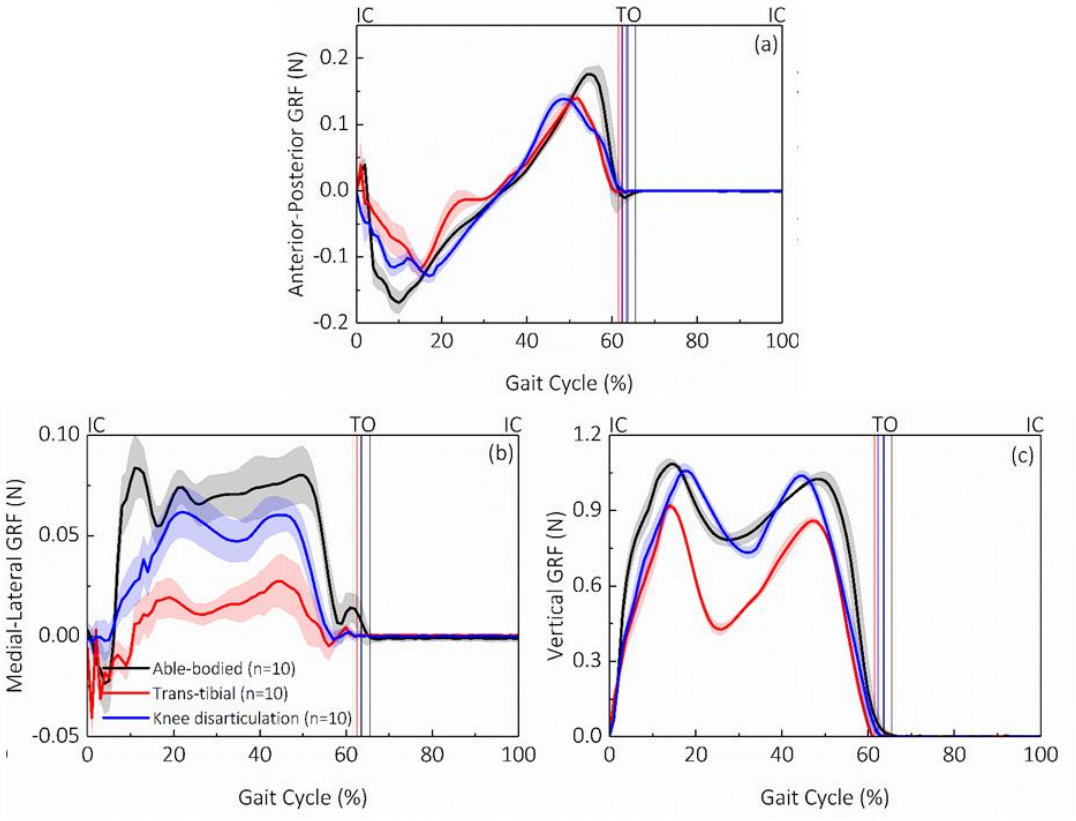

Figure 4.2: Normalised (a) anterior-posterior, (b) medial-lateral and (c) vertical component of GRF, obtained over a GC on able-bodied, trans-tibial and knee-disarticulation participant.

According to Table 4.1, the peak anterior-posterior GRF at early and TS were reduced (up to 35%) on amputee participants, comparing to the value obtained on able-bodied participants.

With regards to the peak medial-lateral GRF, a reduction (up to 75%) was evident on the amputee participants. In early stance phase, a reduction in peak vertical GRF was evident on the amputee participants, comparing to those from the able-bodied participant. Little difference was revealed in the peak vertical GRF in TS, between the knee disarticulation participant and the able-bodied participant. However, the trans-tibial participant showed reduction of peak vertical GRF in TS (up to 23%), comparing to the value obtained for the able-bodied participant.

Table 4.1: Peak value of GRF obtained on able-bodied, trans-tibial and knee-disarticulation amputee participants.

	Anterior – posterior GRF (N)		Medial – lateral GRF	Vertical GRF (N)	
	Early stance	TS	(N)	Early stance	TS
Able-bodied	-0.17±0.02	0.18±0.02	0.08±0.03	1.07±0.02	1.04±0.02
Trans-tibial	-0.11±0.01	0.14±0.02	0.06±0.03	0.90±0.01	0.80±0.01
Knee disarticulation	-0.13±0.01	0.14±0.02	0.02±0.02	1.05±0.01	1.05±0.03

In general, based on the data collected in this study, a reduction in peak GRF was evident in amputee participants when comparing to the value obtained from the able-bodied participants. With comparison to the values reported in the literature, up to 12%, 50% and 35% reduction in peak GRF was found in anterior-posterior GRF, medial-lateral GRF and vertical GRF [114, 234]. Therefore, the findings reported in this study are consistent with the literature (Section 2.4.4).

The reduction in the peak vertical GRF could be potentially associated with the impaired capability of weight bearing on the prosthetic side. It is also well known that the residuum tissue, biologically, is not suitable to be loaded or to distribute load. This would increase the risk of residuum tissue damage under prolonged loadings. Therefore, monitoring the load distribution at the socket interface, during dynamic gait, is critical to improve the socket comfort. The reduction in the peak braking force (Figure 4.2a) in early stance phase may potentially result in the increased risk of instability, during loading response. Muscles activation, together with tibial posterior movement against the socket may be evident to maintain the stability. Understanding the kinetics of the muscle and the kinematics movement of the tibia in socket is then critical to evaluate the walking stability for lower limb amputees.

4.2.2 Ankle joint biomechanics

The loss of a biological ankle can result in the lack of lower limb shock absorbing capability and controlled tibia advancement for both trans-tibial and knee disarticulation amputee (Section 2.4.4). Therefore walking stability may be compromised due to the irregular centre of mass movement, in comparison to the able-bodied group. Further, for the trans-tibial amputee in

particular, the load transfer from a prosthetic ankle, through the pylon, can be directly associated with load experienced at the socket interface. In this section, ankle joint biomechanics will be studied, including ankle joint angle, moment and power.

Ankle angle

From IC to approximately 10% of GC, an increased plantar-flexion angle was evident on amputee participants (9°), comparing with the value (6°) obtained for the able-bodied participant (Figure 4.3a). This finding is inconsistent with the values reported in the literature [116, 117], as reduced ankle plantar-flexion motion was evident. This could be attributed to the design of the prosthetic ankle. In previous studies, the measured ankle plantar flexion motion during the early stance phase was primarily due to heel compression, with no hydraulic ankle unit presented in the foot design. For the present work, the feet of the amputee participants were composed of carbon-fibre leaf springs and a hydraulic ankle unit, which may be regarded as a prosthetic articulated joint. As the heel strikes the ground, the heel carbon fibre spring compresses, the hydraulic ankle rotates into plantar-flexion, enabling more forefoot contact on the ground. In the swing phase, little ankle movement was evident on amputee participants, while up to 15° of dorsi-flexion movement was observed on able-bodied participant. As the prosthetic feet are passive, no movement was expected unless they are loaded.

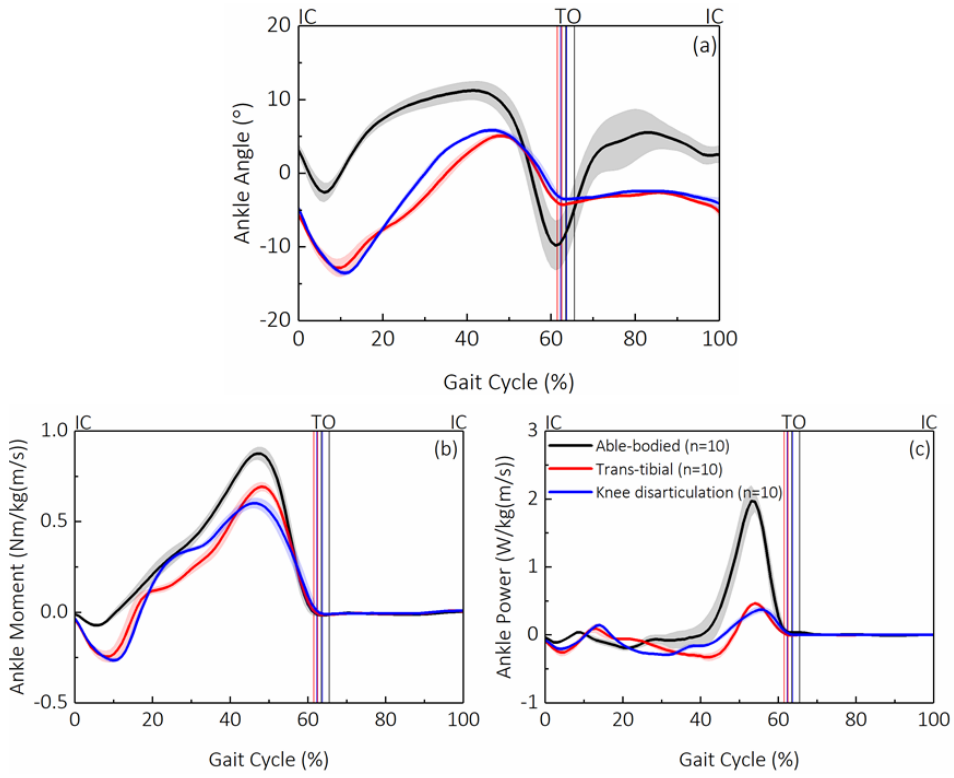

Figure 4.3: (a) Ankle angle, (b) ankle moment and (c) ankle power, obtained over a GC on able-bodied participant, trans-tibial participant and knee disarticulation participant.

Ankle moment

Greater dorsi-flexion moment (0.25Nm/kg(m/s)) was seen on the amputee participants to control the rate of ankle plantar-flexion, comparing the value obtained on the able-bodied participant (0.05Nm/kg(m/s)) (Figure 4.3b.) This may be attributed to the lack of control to achieve limb stability during loading response, as indicated in the previous reported study [120], therefore greater loads are needed for compensation. In addition, the location of the prosthetic ankle differs from the biological ones, which can induce a change in moment arm and transition time of the bending moment.

Indeed, longer dorsi-flexion duration was also evident (up to 11% of GC on amputee participants and up to 8% of GC on able-bodied person). Similar findings were also reported in other studies [120]. The peak plantar-flexion moment in TS phase, was lower in amputee participants (0.75Nm/kg(m/s)), compared to that of the able-bodied participant (1.3Nm/kg(m/s)). Literature [235] suggested up to 60-70% of reduction and it likely due to the absence of the ankle plantar flexors.

The effect of ankle mechanics on the residuum/socket interface can be assessed using ankle angle and moment. The ankle plantar-flexion motion that occurs during the loading response phase of walking assists in absorbing shock as load is rapidly transferred from the trailing to the leading leg. A greater ankle plantar-flexion movement was evident with a hydraulic ankle for amputee participant, compared with the able-bodied. This could mean that the hydraulic ankle offers an enhanced shock absorbing capability. However, a greater dorsi-flexion moment was evident on amputee participants, which could lead to an increased stress at anterior region of the residuum. This may potentially increase the risk of tissue damage. Therefore, analysis of interface mechanics with the effect different prosthetic foot technology is needed. This could potentially affect the prosthetic foot design in terms of the stiffness of the toe and heel spring, as well the resistance of the hydraulic ankle.

Ankle power

Peak ankle concentric power of 0.49W/kg(m/s) was obtained on amputee participants in the TS phase, while 2.0W/kg(m/s) of ankle power was obtained on the able-bodied participants, representing a five-fold decrease in the ankle power generation with the amputee participant (Figure 4.3c). This finding is consistent with four times reduction previously reported [235]. This result is likely due to the lack of active ankle plantar-flexion that limits the ability to generate push-off during pre-swing.

4.2.3 Knee joint biomechanics

As mentioned in Section 2.4.2, for trans-femoral amputee in particular, little knee joint motion was observed, as opposed to approximately 20° of knee flexion motion observed for the able-bodied group. The abnormal load transfer was also reflected on the knee joint moment and is directly linked to the loading profile at the socket interface. In this section, the knee joint biomechanics will be presented, including knee joint angle, moment and power.

Knee angle

It can be seen that, for the knee-disarticulation amputee, there was little knee flexion during the early stance phase (Figure 4.4a) which is consistent with previous studies [101]. The early stance phase knee flexion proved difficult for the knee-disarticulation amputee to achieve, as it was associated knee buckling and potential falling. Up to 12° and 18° of knee flexion in early stance phase were observed on the trans-tibial and able-bodied participant, respectively. Similar findings were previously reported (up to 9°) [106].

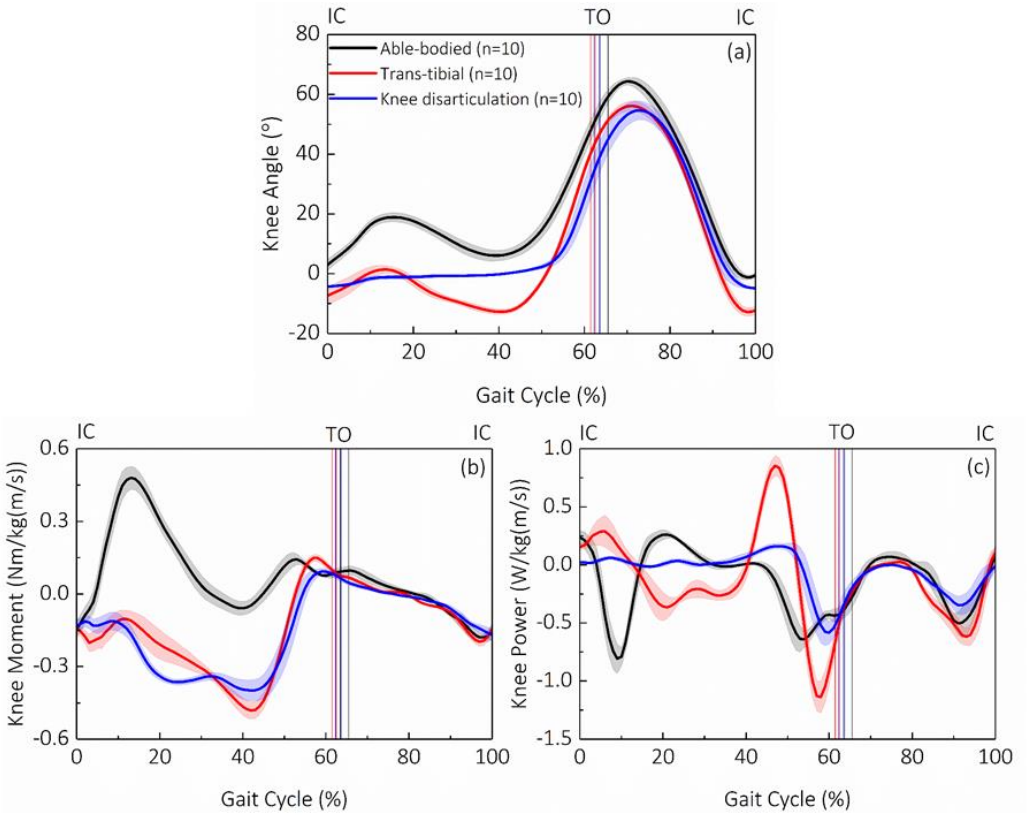

Figure 4.4: (a) Knee angle, (b) knee moment and (c) knee power, obtained over a GC on able-bodied participant, trans-tibial participant and knee disarticulation participant.

Knee moment

The greatest differences in knee moments occurred during early stance phase (Figure 4.4b). The able-bodied participant rely on the knee extensors to control knee flexion during weight acceptance. In contrast, the moment data obtained from amputee participants revealed negligible knee extensor moment with knee flexor moment dominating the stance phase. It is reported by Powers et al [106] that up to six times reduction of the knee moment was observed in amputee group comparing to the value obtained for an able-bodied group, which is consistent with the present study. The reduction of the peak knee joint moment could be associated with the presence of a biological knee joint, enclosed by a rigid socket in a non-linear, visco-elastic environment. However, results should be treated cautiously as Powers et al [106] also found there is a discrepancy between the moment data and the EMG results. This indicates mechanical measures of knee extensor demand and the actual physiologic response are not consistent. Either calculation of the energy flow and direct measuring of the load transferred through the prosthetic/body interface is needed to facilitate understanding of the overall limb biomechanics.

With an absence of the knee flexion in stance phase, the conceptualised interface pressure can be estimated based on knee moment only. For a uniaxial free knee fitted on a knee disarticulation amputee, high pressure may be observed at anterior-proximal region and posterior-distal region due to the period of the knee extensor moment (0-10% of GC). From 10%-40% of GC, knee flexion moment was evident. This could result in high pressure regions at posterior-proximal and anterior-distal locations. The pressure profile was proved to be different based on the socket design and different prosthetic knee technology. Therefore, the analysis of interface stress distribution in the plane of walking id critical for the design of the prosthetic knee.

Knee Power

A significant reduction in knee power absorption during the early stance phase was observed with the knee disarticulation participant (Figure 4.4c). This is due to the restricted knee flexion during the stance phase. This finding supports a previous study in which a 63% reduction of knee power absorption was reported during the loading response on the prosthetics limb [173]. It is suggested that for both trans-tibial and knee disarticulation amputees, the use of the hip joint is an alternative means of shock absorption, as well as the compensating mechanism on the contralateral side. In the TS phase, power generation was revealed on the trans-tibial amputee (0.8W/kg(m/s)), while power absorption was evident just before TO (-1.1W/kg(m/s)).

4.2.4 Hip joint biomechanics

Hip joint biomechanics are often used as parameter to assess the performance of the prosthetic components as it is the only intact biological joint on both trans-tibial amputee and knee disarticulation amputee [101]. Further, for knee disarticulation amputees the motion and the loading at hip joint centre can be directly associated with the interaction between the residuum and the socket. Therefore, studying the hip joint biomechanics between the able-bodied group and amputee group may facilitate the discussion on the interface biomechanics, particularly for non-trans-tibial amputees.

Hip angle

Increased hip ROM (Figure 4.5b) was observed with the amputee participants compared with the able-bodied participants (able-bodied: 36°, knee-disarticulation: 43° and trans-tibial: 40°). The finding is inconsistent with previous findings [122], as increased hip ROM (up to 15%) was evident on the amputee participant. This could be potentially explained by the lack of ability to control the limb due to the loss of muscle after amputation.

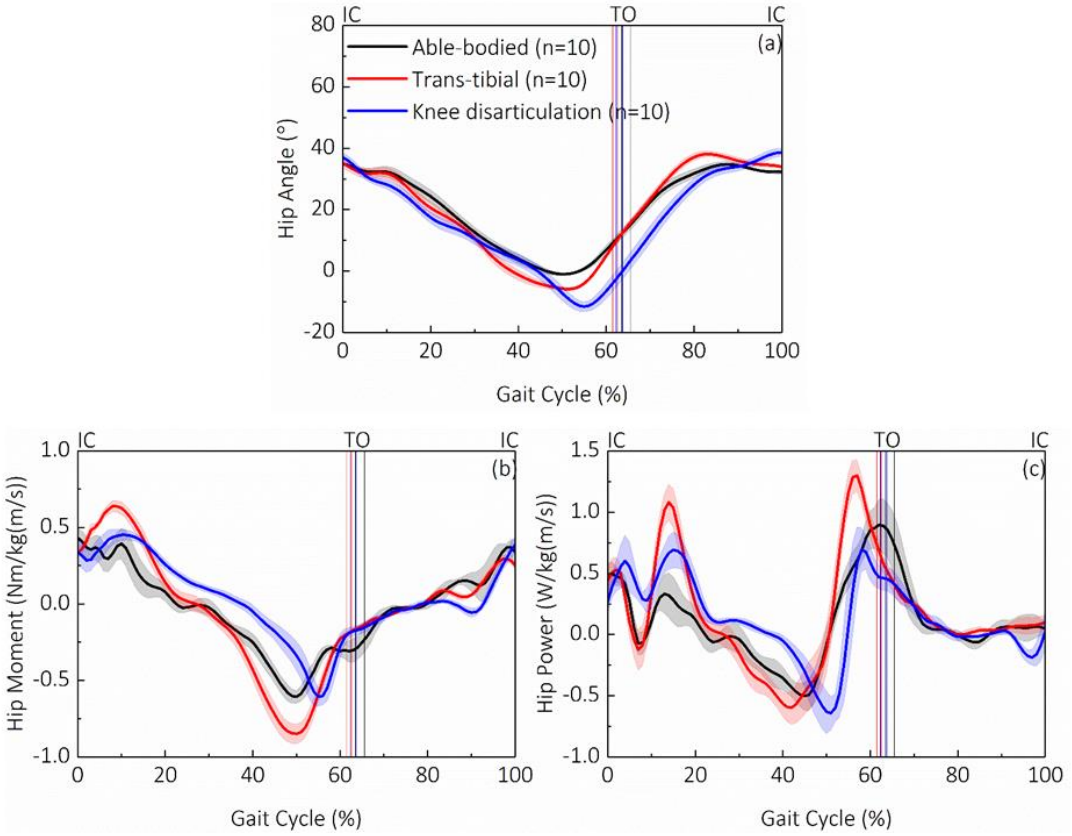

Figure 4.5: (a) Hip angle, (b) hip moment and (c) hip power, obtained over a GC on able-bodied participant, trans-tibial participant and knee disarticulation participant.

Hip moment

The mean peak hip extensor moment observed on amputee participant (up to 0.7Nm/kg(m/s)) in early stance phase (Figure 4.5b) was higher than that on the able-bodied participant (up to 0.3Nm/kg(m/s)), supporting previous findings [115, 120]. The knee disarticulation participant did not provide any active control of ankle and knee joints, the greater extension moment generated during early stance phase at the hip was probably to assist the forward progression of the limb. In TS phase, the highest hip flexion moment was evident on the trans-tibial amputee (0.8Nm/kg(m/s)), compared to those on the other two groups.

Hip power

Values of up to 1.1, 0.7 and 0.25W/kg(m/s) of hip power generation (Figure 4.5c) were obtained on the knee-disarticulation, trans-tibial and the able-bodied participant, respectively. This suggests that the amputee participants have a greater hip concentric power in early stance phase. In TS phase, up to 1.3 and 0.9W/kg(m/s) of hip power generation were obtained on the knee-disarticulation and able-bodied participant, respectively. Again, higher concentric hip power was generated by the amputee participant, both findings confirming previous data [119, 120, 123]. This finding is likely attributed to the fact that for knee-disarticulation amputee, the hip is the only available biological joint to control the limb movement and maintain the stability at the same time.

It is evident that, greater hip ROM, hip flexion moment and peak hip power was revealed for amputee participants, compared with the value obtained on the able-bodied participant. It is worth noting that, for non-trans-tibial amputees, a greater volume of tissue was presented on the residuum. This would result in a relatively lower tissue stiffness compared with tissue presented on trans-tibial amputee. A reduction in the stiffness, combined with a greater loading, would result in a greater movement between the residuum and socket. This might explain the reason why the suspension and the proprioception of the trans-femoral and knee disarticulation amputee is a major issue. This may be further linked to the Hi-Fi socket design mentioned in the literature review (Section 2.1.3), as it stabilised the soft tissue by applying compressive force at certain locations.

4.3 Effect of walking speed on amputee joint mechanics

As mentioned in Section 2.5.3, walking speed has a significant impact on the knee joint and hip joint force and moment. The investigation of the knee joint biomechanics and hip joint biomechanics within the socket, for trans-tibial amputee and knee disarticulation amputee, is critical for the understanding of the socket interface biomechanics. In this section, the results

obtained using protocol A2 was presented, in terms of GRF, joint angle, joint moment and joint power.

4.3.1 Ground reaction forces

As indicated in Figure 4.6a, up to 128±13N, 128±8N and 131±15N of anterior-posterior component of GRF was obtained, indicating little difference in the peak braking force, in early stance phase. However, in the TS phase, up to 111±5N, 126±8N and 149±9N propulsive force was obtained when walking at slow, self-selected and fast speed, respectively. It is then evident that the increase in walking speed led to higher propulsive force, at ground interface, in anterior-posterior direction.

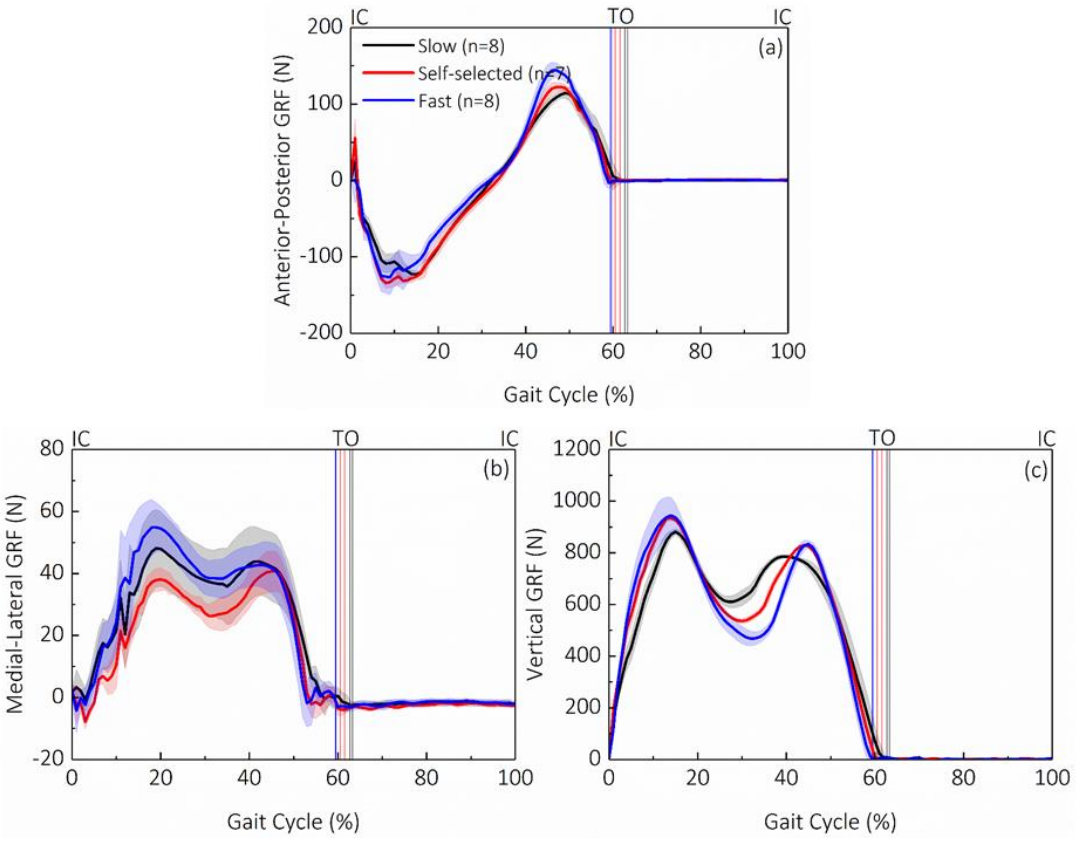

Figure 4.6: (a) Anterior-posterior, (b) medial-lateral and (c) vertical component of GRF, obtained over a GC on the knee-disarticulation participant, when walking at slow, self-selected and fast speed, respectively.

In early stance phase, highest medial-lateral (54N±11) GRF was observed when walking at fast speed, this was followed by 48N±10N obtained when walking at slow speed and 39N±4N obtained when walking at self-selected speed (Figure 4.6b). Up to 41N of medial-lateral component of GRF was obtained at TS phase, regardless of walking speed.

It is evident that, in the mid-stance, up to 643±20N, 556±10N and 488±25N of vertical component of GRF was obtained when walking at slow, self-selected and fast walking speed

(Figure 4.6c). It is hence evident that the increase in walking speed led to the decrease of vertical component of GRF at this time instant. This finding is consistent with the reported study on able-bodied participants [236]. With the transfer of the force from the ground interface to proximal locations, i.e. the socket, higher force could be experienced by the residuum. This may potentially lead to an increased axial movement between the residuum and the socket, as well as a higher chance of internal tissue breakdown.

4.3.2 Ankle joint biomechanics

At about 35% of GC (Figure 4.7a), up to 0.00±0.00°, -0.89±0.30° and -2±0.50° of ankle angle was obtained at ankle dorsi-flexion process. It is evident that the increase in walking speed led to reduction in ankle angle. Figure 4.7b shows the peak ankle bending moment of 0.68±0.02Nm/kg(m/s), 0.62±0.01Nm/kg(m/s) and 0.55±0.02Nm/kg(m/s) obtained when walking at slow, self-selected and fast walking speed, respectively. This suggested that the increase in walking speed also led to the decrease in ankle bending moment. Between 20-35% of GC, the increase in walking speed has led to the increase of negative power while between 35-45% of GC, the increase in walking speed has led to the decrease in negative power (Figure 4.7c).

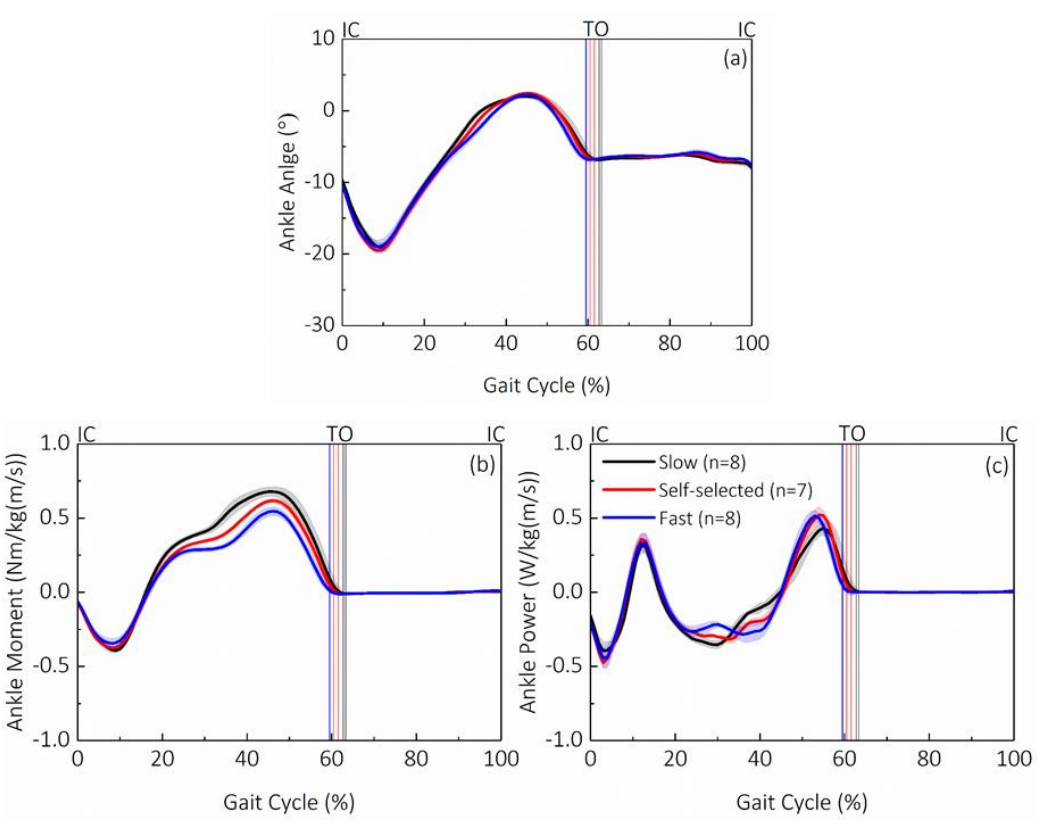

Figure 4.7: (a) Ankle angle, (b) ankle moment and (c) ankle power obtained over a GC on the knee-disarticulation participant, when walking at slow, self-selected and fast speed, respectively.

4.3.3 Knee joint biomechanics

In early stance, little knee flexion is observed (Figure 4.8a). From TS phase to mid-swing phase, up to 32±4°, 44±2° and 49±2° of knee flexion ankle was obtained when walking at slow, self-selected and fast walking speed. In other words, the increase in walking speed led to the increase in the peak knee flexion angle.

Peak knee extension moment of -0.34±0.03Nm/kg(m/s), -0.27±0.02Nm/kg(m/s) and -0.22±0.02Nm/kg(m/s) were obtained when walking at slow, self-selected and fast walking speed (Figure 4.8b), respectively. It is evident that the increase in walking speed led to the decrease of magnitude of the knee flexion moment.

The peak prosthetic knee power (Figure 4.8c) showed up to -0.55±0.1W/kg(m/s), -0.89±0.1W/kg(m/s) and 0.89±0.1W/kg(m/s) when walking at slow, self-selected and fast walking speed, respectively. When comparing the peak prosthetic knee power at slow speed to the value obtained at self-selected and fast speed, up to 62% of increase was observed. However, little difference was found in peak prosthetic knee power when walking at self-selected and fast speed.

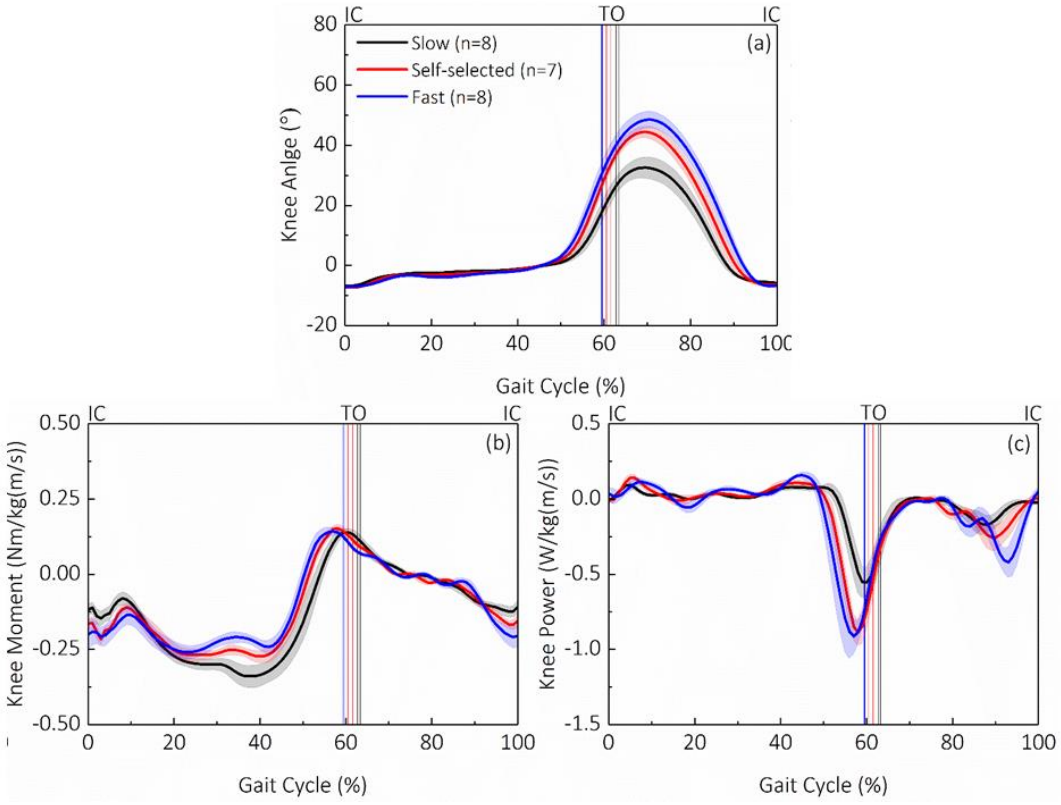

Figure 4.8: (a) Knee angle, (b) knee moment and (c) knee power, obtained over a GC on the knee-disarticulation participant, when walking at slow, self-selected and fast speed, respectively.

4.3.4 Hip joint biomechanics

When comparing the hip ROM obtained three different walking speed (Figure 4.9a), little difference was found (slow: 50±0.5°, self-selected 50±0.3° and fast: 51±0.5°). Figure 4.9b shows the hip joint moment as a function of GC. At TS phase, hip flexion moment of up to -0.50±0.08Nm/kg(m/s), 0.65±0.04Nm/kg(m/s) and 0.70±0.08Nm/kg(m/s) were obtained when walking at slow, self-selected and fast walking speed. It is evident that the increase in walking speed has led to the increase in the peak hip flexion moment at TS phase. Eccentric hip flexor activity (negative power in Figure 4.9c) was observed in the TS phase (approximately 50% of GC) and the increase in walking speed led to the increase in eccentric hip power (slow: -0.57±0.12W/kg(m/s), self-selected -0.97±0.17W/kg(m/s), and fast: -1.24±0.12W/kg(m/s)).

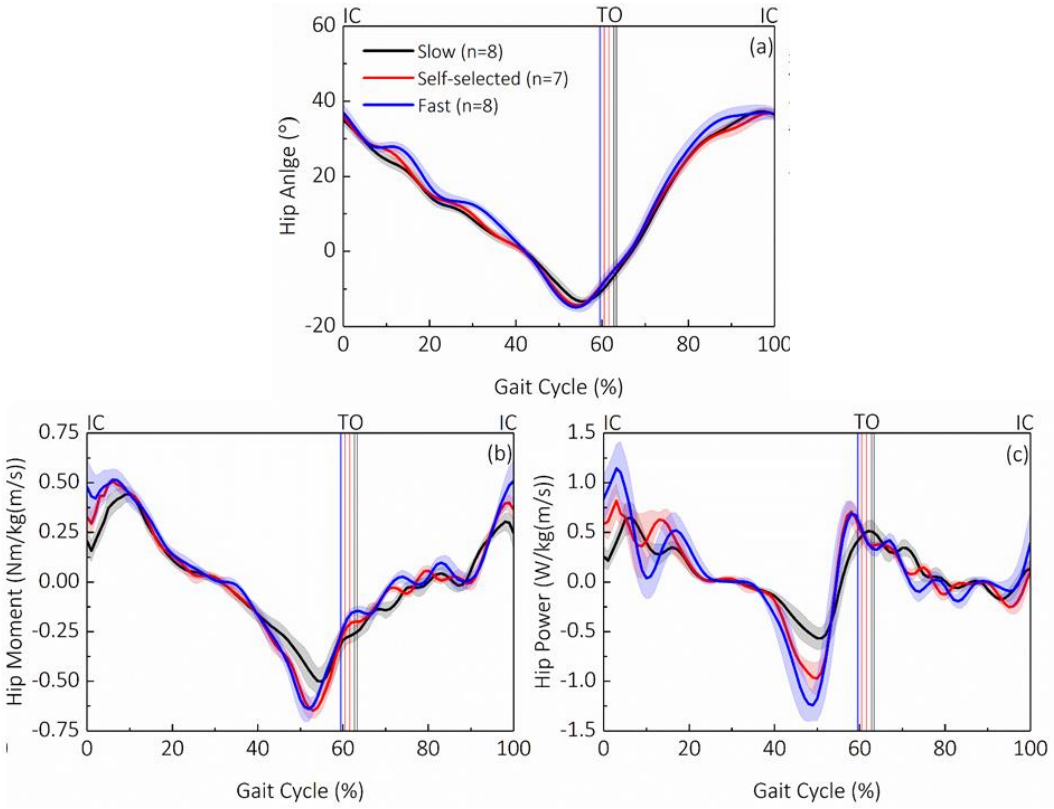

Figure 4.9: (a) hip angle, (b) hip moment and (c) hip power, obtained over a GC on the knee-disarticulation participant, when walking at slow, self-selected and fast speed, respectively.

4.4 Effect of terrain on amputee joint mechanics

The ability of lower limb amputee to negotiate ramped surfaces is severely affected by the loss of ankle joint and foot as well as the muscle associated with it. In addition, inclination surfaces increase the risks to stumble when the prosthetic limb is mobile above the ground. Therefore, maintaining the residuum stability and health inside the socket when engaging ramped surface is critical. In this section, the joint mechanics will be studied as a function of terrain for both trans-tibial and knee disarticulation participants. This is to gain understanding of the joint

mechanics to facilitate the further discussion on the interface mechanics when walking on different terrains.

4.4.1 Ground reaction force

Figure 4.10 and Figure 4.11 show the GRF as a function of GC, obtained for the trans-tibial and the knee disarticulation amputee participants, respectively. Table 4.2 illustrates the peak GRF values at early and TS of the GC.

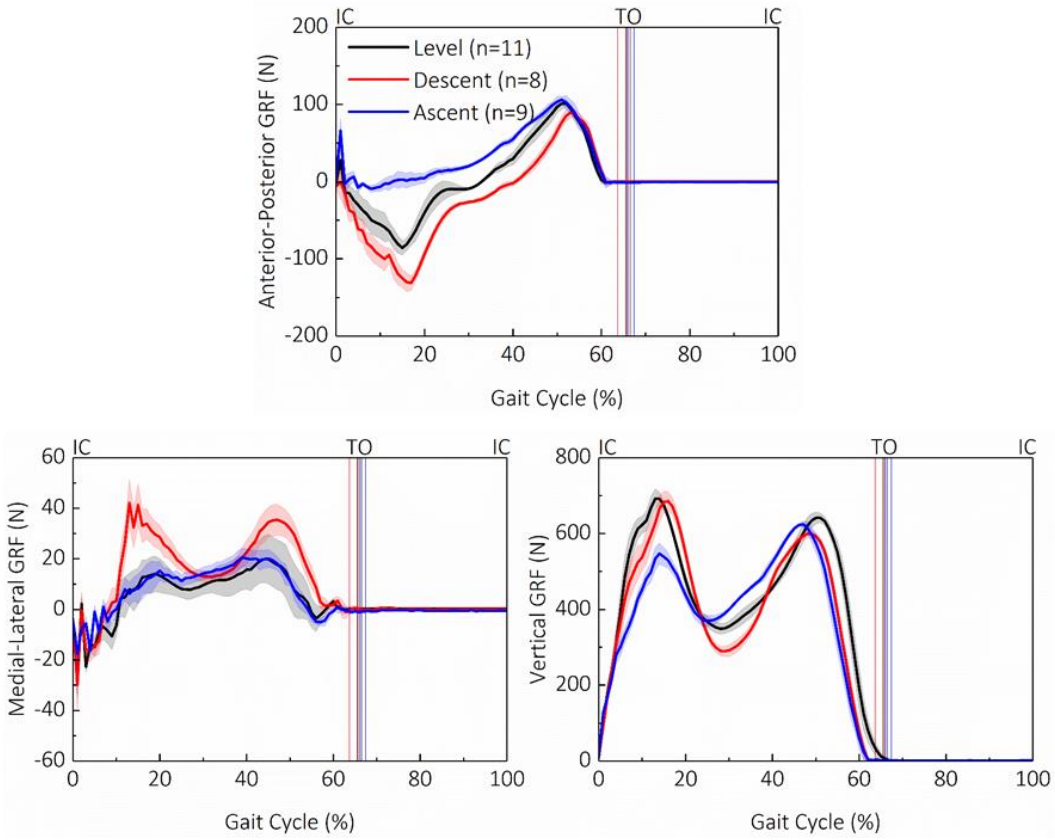

Figure 4.10: (a) Anterior-posterior, (b) medial-lateral and (c) vertical component of GRF, obtained over a GC on a trans-tibial participant, walking on level, descending and ascending surface.

An increase of early stance braking force was evident on both knee disarticulation (up to 37N) and trans-tibial amputee participant (up to 45N) on the descending ramp, compared with the value obtained on the level surface. While the in TS phase, a decrease of propulsive force was measured on both knee disarticulation (up to 21N) and trans-tibial amputee participant (up to 12N), compared with the value obtained on the level surface. When walking on the ascending ramp, a decrease in braking force was observed on both knee disarticulation (up to 88N) and trans-tibial amputee participants (up to 120N), in early stance phase. While in TS, an increase in propulsive force was observed on both participants (knee disarticulation: up to 88N, trans-tibial: up to 17N).

When walking on descending ramp, the increase in braking force in early stance phase may be associated with the need of a greater braking force to oppose the components of the body weight acting down the ramp. When walking on the ascending ramp, the increase in propulsive force may be associated with the demand for a greater force to overcome the component of body weight acting down the ramp. It can be estimated that the greater braking force on the descending surface and the greater propulsive force on the ascending surface, could potentially lead to the greater relative movement and loading at the residuum/socket interface.

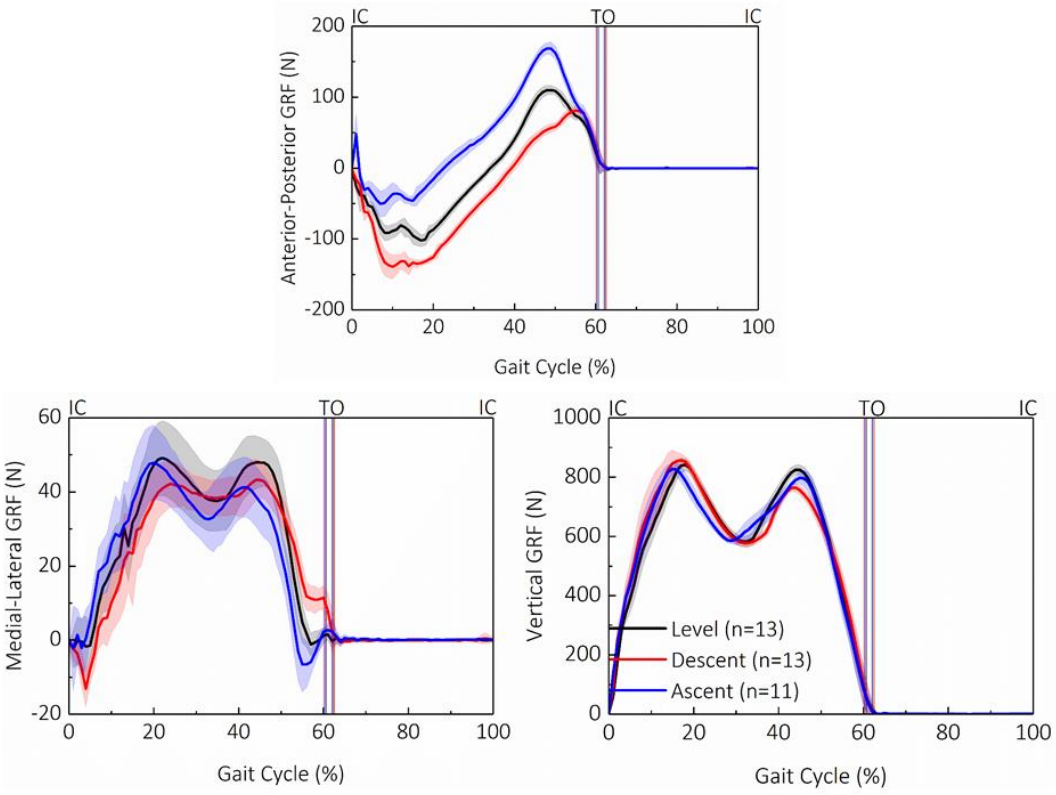

Figure 4.11: (a) Anterior-posterior, (b) medial-lateral and (c) vertical component of GRF, obtained over a GC on the knee disarticulation participant, when walking on level, descending and ascending surface.

The highest medial-lateral components of GRF were observed when walking on the descending ramp and level surface, for the trans-tibial and knee disarticulation amputee participant, respectively. This was probably resulted from the lack of stability in frontal plane when walking on the descending ramp and could be potentially reflected on the residuum/socket interface as well.

Table 4.2: Peak value of GRF obtained on the trans-tibial and the knee-disarticulation participant.

	Anterior – posterior GRF (N)		Medial – lateral GRF	Vertical GRF (N)	
	Early stance	TS	(N)	Early stance	TS

Trans-tibial					
Level	-86±10	101±5	20±9	692±9	642±11
Descent	-131±10	89±7	35±6	685±25	599±11
Ascent	-9±4	106±4	20±3	547±27	625±7
Knee disarticulation					
Level	-102±9	110±6	49±10	841±20	825±16
Descent	-139±13	81±6	42±6	857±22	764±14
Ascent	-51±19	169±7	48±9	828±16	797±20

In early stance phase, vertical GRF showed similar peak value on the trans-tibial participant when walking on level and descending surfaces. For the knee disarticulation amputee, the highest peak vertical GRF was observed when walking on descending ramp (857N). It is estimated that greater axial movement of residuum could be revealed, with a greater vertical load exerted on the prosthetic side. In TS phase, the highest peak GRF value was obtained when walking on level surface for both participants.

4.4.1 Ankle joint biomechanics

Figure 4.12 and Figure 4.13 show ankle joint biomechanics, as a function of GC for the trans-tibial and knee disarticulation participant, respectively. Using the value obtained at IC as a reference, the ankle plantar-flexion and dorsi-flexion angle obtained at early stance phase and TS phase is presented in Table 4.3.

It is evident that the greatest value for ankle plantar-flexion was obtained when walking on the descending ramp. This is likely attributed to the need for full foot contact with the walkway in early stance phase, when walking on a descending ramp, to ensure limb stability. The greatest value for ankle dorsi-flexion was obtained when walking on the ascending ramp, as rapid advancement of the shank is needed for an energetic propulsion in TS.

Table 4.3: Prosthetic ankle plantar-flexion and dorsi-flexion angle obtained on the trans-tibial and knee disarticulation participant.

	Trans-tibia participant			Knee disarticulation participant		
	Level	**Descent**	**Ascent**	**Level**	**Descent**	**Ascent**
Plantar-flexion (°)	7.1±0.5	11.1±0.5	9.0±0.4	8.8±0.2	10.2±0.3	7.2±0.3
Dorsi-flexion (°)	11.1±0.5	8.4±0.4	11.3±0.4	10.7±0.3	11.1±0.3	11.9±0.3

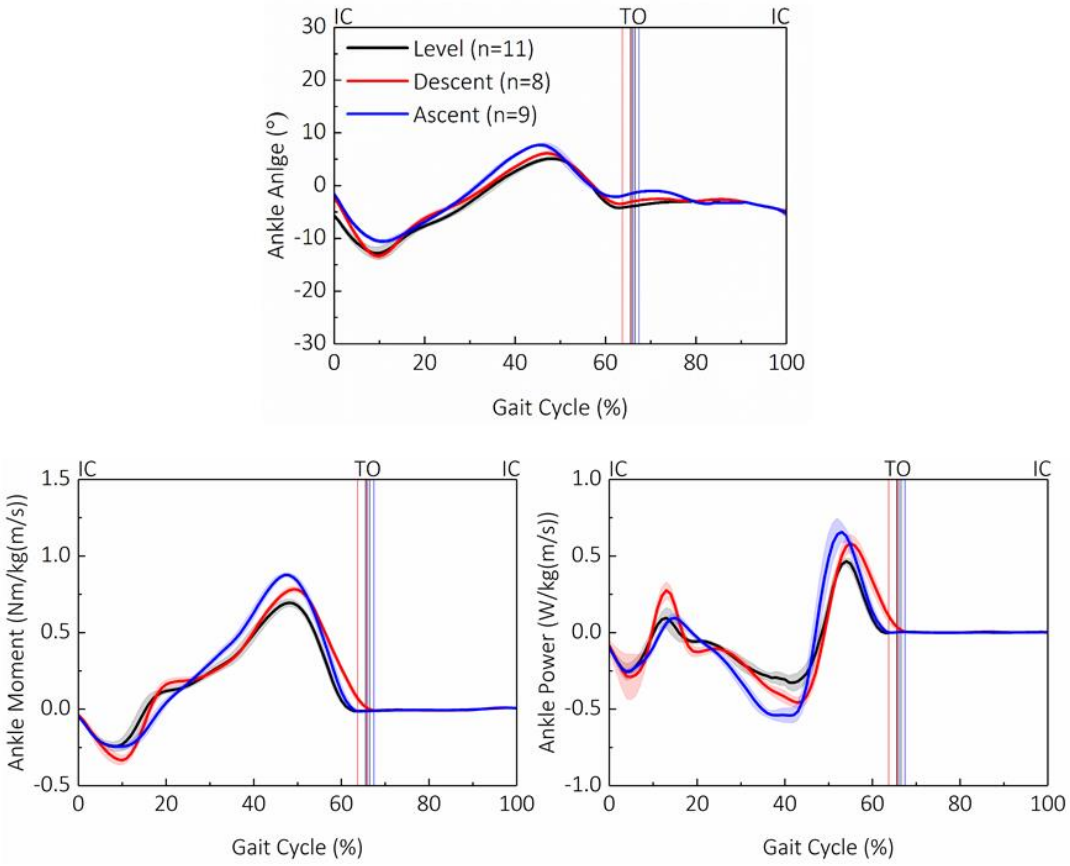

Figure 4.12: (a) Ankle angle, (b) ankle moment and (c) ankle power, obtained over a GC on a trans-tibial participant, when walking on level, descending and ascending surfaces.

Figure 4.12b and Figure 4.13b show ankle bending moment obtained for the trans-tibial and the knee disarticulation amputees, respectively. Peak ankle bending moments, including ankle dorsi-flexion in early stance phase and ankle plantar-flexion in TS, are presented in Table 4.4. Highest dorsi-flexion moment was achieved when walking on the descending ramp to lower the foot down to the surface, achieving limb stability. This could further lead to an increase pressure in anterior region of the residuum, as the dorsi-flexor tends to stop the prosthetic pylon from advancing forward. In addition, the greatest plantar-flexion moment was observed when walking on the ascending ramp to achieve an upward and forward 'push-off'.

Table 4.4: Prosthetic ankle bending moment obtained on the trans-tibial and knee disarticulation participant.

	Trans-tibia participant			Knee disarticulation participant		
Unit: Nm/kg(m/s)	Level	Descent	Ascent	Level	Descent	Ascent
Dorsi-flexion	-0.24±0.03	-0.33±0.03	-0.24±0.01	-0.26±0.02	-0.31±0.02	-0.30±0.01
Plantar-flexion	0.69±0.02	0.78±0.02	0.88±0.01	0.60±0.03	0.59±0.01	0.55±0.02

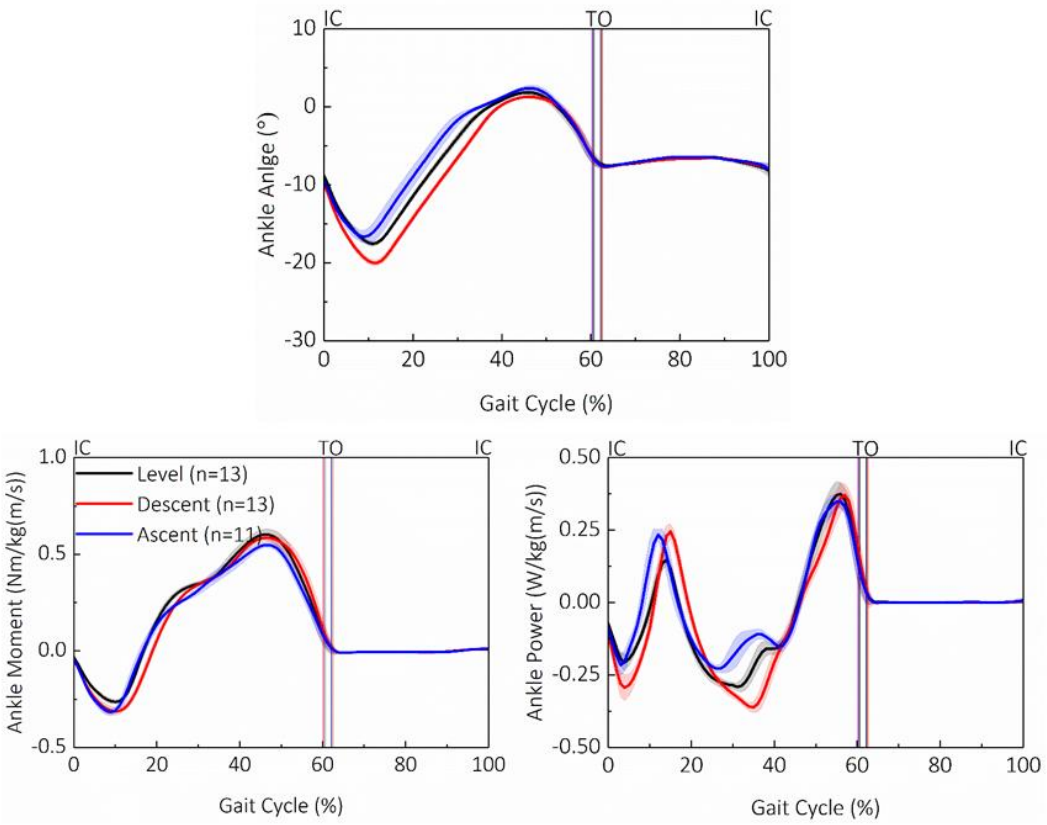

Figure 4.13: (a) Ankle angle, (b) ankle moment and (c) ankle power, obtained over a GC on a knee disarticulation participant, walking on level, descending and ascending surfaces.

With particular focus on the power generation in TS, for the trans-tibial amputee (Figure 4.12c), the highest ankle power (0.73± 0.02W/kg(m/s)) was observed when walking on the ascending ramp. This is followed by the value generated when walking on descending and level surfaces. For the knee disarticulation amputee (Figure 4.13c), a mean power generation of up to 0.38± 0.02W/kg(m/s) was obtained when walking on all terrains.

4.4.2 Knee joint biomechanics

For the trans-tibial amputee, in early stance phase, knee flexion movement was observed when walking on both level and descending surface, while knee extension movement was evident when walking on the ascending ramp (Figure 4.14a). By contrast for the knee disarticulation participant, minimal knee flexion was observed (Figure 4.15a), supporting findings from previous studies [27, 237]. When comparing the knee ROM, it is clear from Table 4.5 that the highest ROM was observed when walking on the descending ramp for both trans-tibial and knee disarticulation participants.

Table 4.5: Knee ROM obtained on the trans-tibial and knee disarticulation participant.

	Trans-tibia participant			Knee disarticulation participant		
	Level	Descent	Ascent	Level	Descent	Ascent
Knee ROM (°)	68.8±0.9	73.4±1.0	69.5±0.5	59.4±0.5	64.6±0.6	59.4±0.6

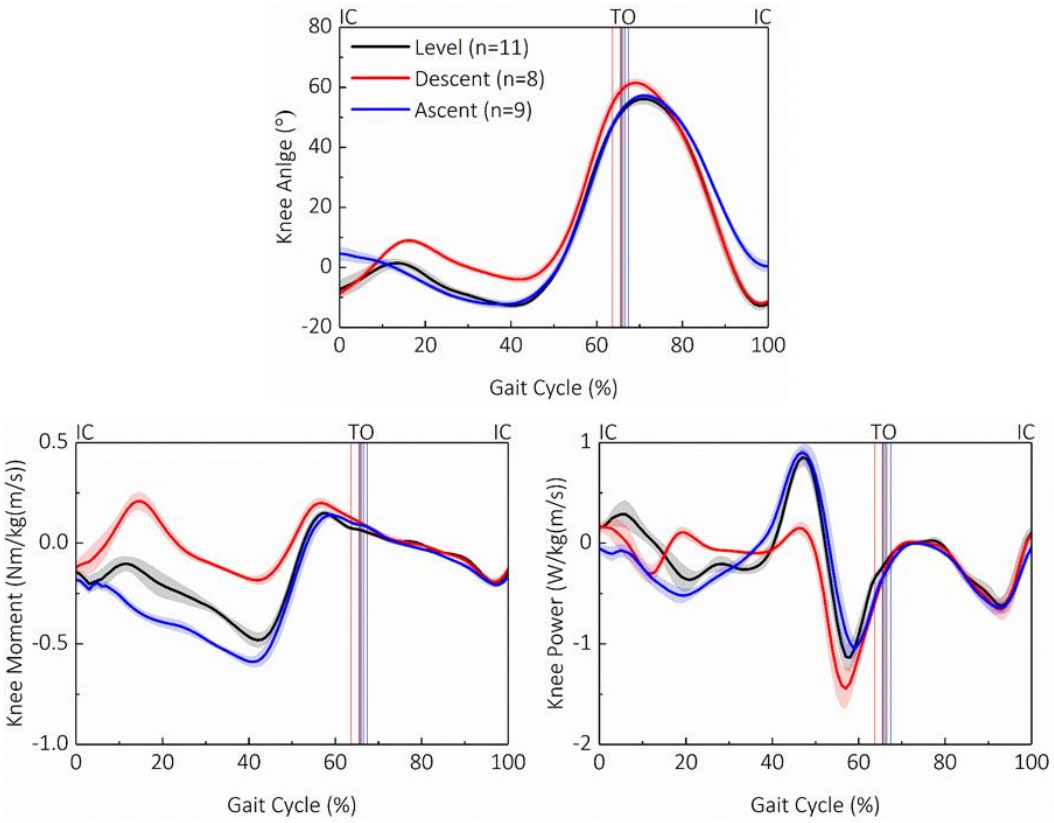

Figure 4.14: (a) Knee angle, (b) knee moment and (c) knee power, obtained over a GC on the trans-tibial participant, when walking on level, descending and ascending surfaces.

The major difference in knee moment between both amputees was during the early stance phase. For the trans-tibial participant, a positive moment (knee extension in Figure 4.14b and Figure 4.15b) was evident which was absent for the knee disarticulation amputee, a finding previously reported by Segal et al [101]. The knee extension moment observed in early stance phase supports the knee from buckling, especially when walking on the ascending ramp. Therefore, higher pressure may be experience at the anterior region of the residuum. It was also evident that the highest flexion moment, observed at 40-50% of GC, was obtained when walking on the ascending ramp, followed by the value obtained when walking on level and descending surfaces.

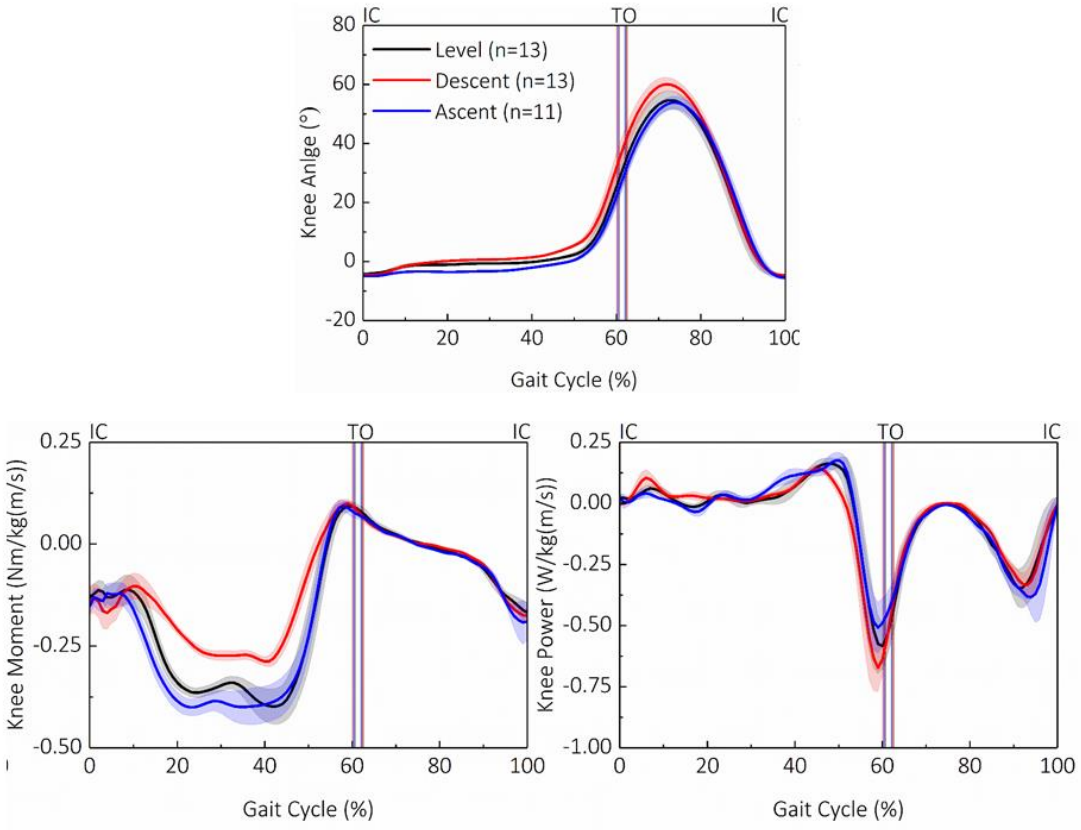

Figure 4.15: (a) Knee angle, (b) knee moment and (c) knee power, obtained over a GC on a knee disarticulation participant, walking on level, descending and ascending surfaces.

Highest power generation was observed at TS phase when walking on ascending ramp for both trans-tibial (0.90±0.07W/kg(m/s) in Figure 4.14b) and knee disarticulation amputees (0.18±0.08W/kg(m/s) in Figure 4.15b).

4.4.3 Hip joint biomechanics

At IC, the hip joint is at a more extended angular position (trans-tibial: 31° and knee disarticulation: 49° in Figure 4.16) when walking on the ascending ramp, while it is aligned at a more flexed angular position (trans-tibial: 17° and knee disarticulation: 36°) when walking on the descending ramp, compared to the values obtained during level walking (trans-tibial: 21° and knee disarticulation: 43°). The hip ROM, as presented in Table 4.6, revealed the highest values when walking on the ascending ramp and the lowest when walking on the level surface.

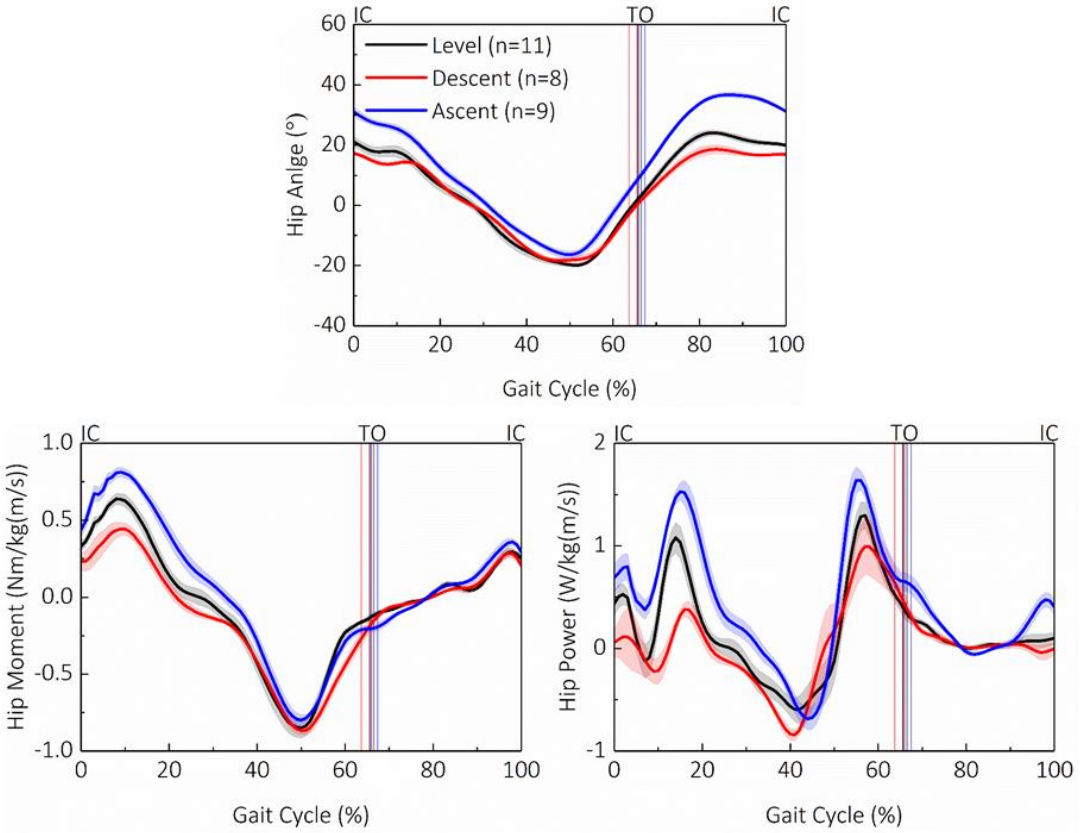

Figure 4.16: (a) Hip angle, (b) hip moment and (c) hip power, obtained over a GC on a trans-tibial participant, walking on level, descending and ascending surfaces.

Table 4.6: Hip ROM obtained on the trans-tibial and knee disarticulation participant.

	Trans-tibia participant			Knee disarticulation participant		
	Level	Descent	Ascent	Level	Descent	Ascent
Hip ROM (°)	44.0±1.0	36.9±0.8	53.1±0.9	50.3±1.2	46.2±1.0	52.9±0.6

It is evident that during most of the stance phase (0-40% of GC), highest hip joint moment was obtained when walking on the ascending ramp, followed by the value obtained on the level and descending surfaces (Figure 4.16b and Figure 4.17b). Just prior to TO, the peak hip joint moment was unaffected by the nature of the terrain (TT: -0.86±0.04Nm/kg(m/s) and TF: -0.60±0.06Nm/kg(m/s)).

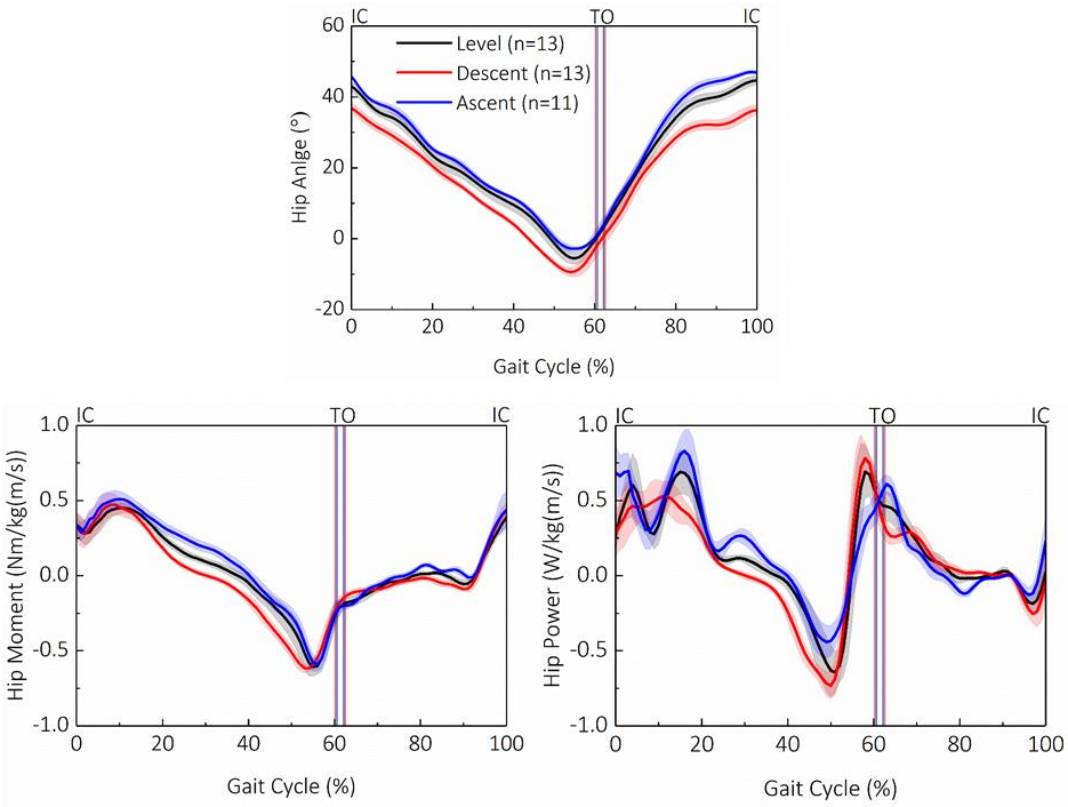

Figure 4.17: (a) Hip angle, (b) hip moment and (c) hip power, obtained over a GC on a knee disarticulation participant, walking on level, descending and ascending surfaces.

The highest concentric hip extensor activity, just before 20% of GC, occurred when walking on the ascending ramp (TT: 1.53±0.08W/kg(m/s) in Figure 4.16c and TF: 0.81±0.1W/kg(m/s) in Figure 4.17c). By contrast, during TS (40-50% of GC), the highest eccentric hip flexor power was observed when walking on the ascending ramp (TT: 0.69±0.08W/kg(m/s) and TF: 0.44±0.09W/kg(m/s)).

It has been demonstrated that there was clear differences in joint mechanics, when comparing between the able-bodied group and the amputee group. This reflects on the reduction in peak GRF, peak ankle dorsi-flexion moment and the absence of the knee extensor for the knee disarticulation amputee. The load transfer schematics described in Section 2.5.1 suggests that the interface biomechanics is highly dependent on the load transfer distal to the socket. Indeed, the load transferred from the ground interface, through the prosthetic limb was significantly different, comparing to able-bodied group. The understanding of the amputee joint biomechanics could further facilitate and explain the interface biomechanics.

The capability of the 3D motion analysis system has also been demonstrated. The gait analysis results obtained on the able-bodied participant was comparable to the values reported in the literature. The sensitivity of the system has been demonstrated using the difference observed

in joint mechanics when walking on difference walking speeds and terrains. This suggested that the 3D motion analysis system could be appropriate to use for the evaluation of interface kinematics.

The joint kinetics obtained when walking at different walking speed and on different terrain, may be further used to facilitate the discussion of residuum/socket interface biomechanics. For example, a higher dorsi-flexion moment was achieved when walking on the descending ramp, compared with the value obtained on the ascending ramp. This could further lead to an increase pressure in anterior region of the residuum, as the dorsi-flexor tends to stop to the prosthetic pylon from advancing forward. It is therefore evident that it is critical to understand the residuum/socket interface biomechanics as it could make a positive impact on the socket interface, in terms of stability, mobility and tissue health. Furthermore, the understanding of the interface mechanics could shed lights on the mechanics of the extra joint form by the residuum and the socket, which conventional gait analysis does not consider.

Chapter 5 3D motion of the lower limb residuum

As reviewed in Chapter 2, the assessment of the residuum motion in socket has long been recognised to be important for socket designs (Section 2.1.3), gait stability and safety (Section 2.2.2), stump tissue health (Section 2.2.3) and overall rehabilitation outcomes. Despite the known need and reported studies using large facilities such as SXCT and DRSA, the lack of an easy and potentially clinically accessible means still hinders biomechanical studies in this area.

This chapter aims to address this challenge by developing a novel method using 3D motion capture system with a view to characterising residuum motion during ambulation. As compared with reported method in the literature (Section 2.6.1), this assessment exploits standard gait laboratory facilities such as 3D motion capture system, which are available in some rehabilitation clinics. A first of its kind interface kinematic model was developed to provide quantitative assessment of residuum angular and axial movement relative to socket as a function of GCs. A knee-disarticulation and a trans-tibial participant have been involved in the walking tests for the preliminary evaluation of the method in terms of its effectiveness, repeatability and sensitivity. Figure 5.1 provides an overview of the research activities involved.

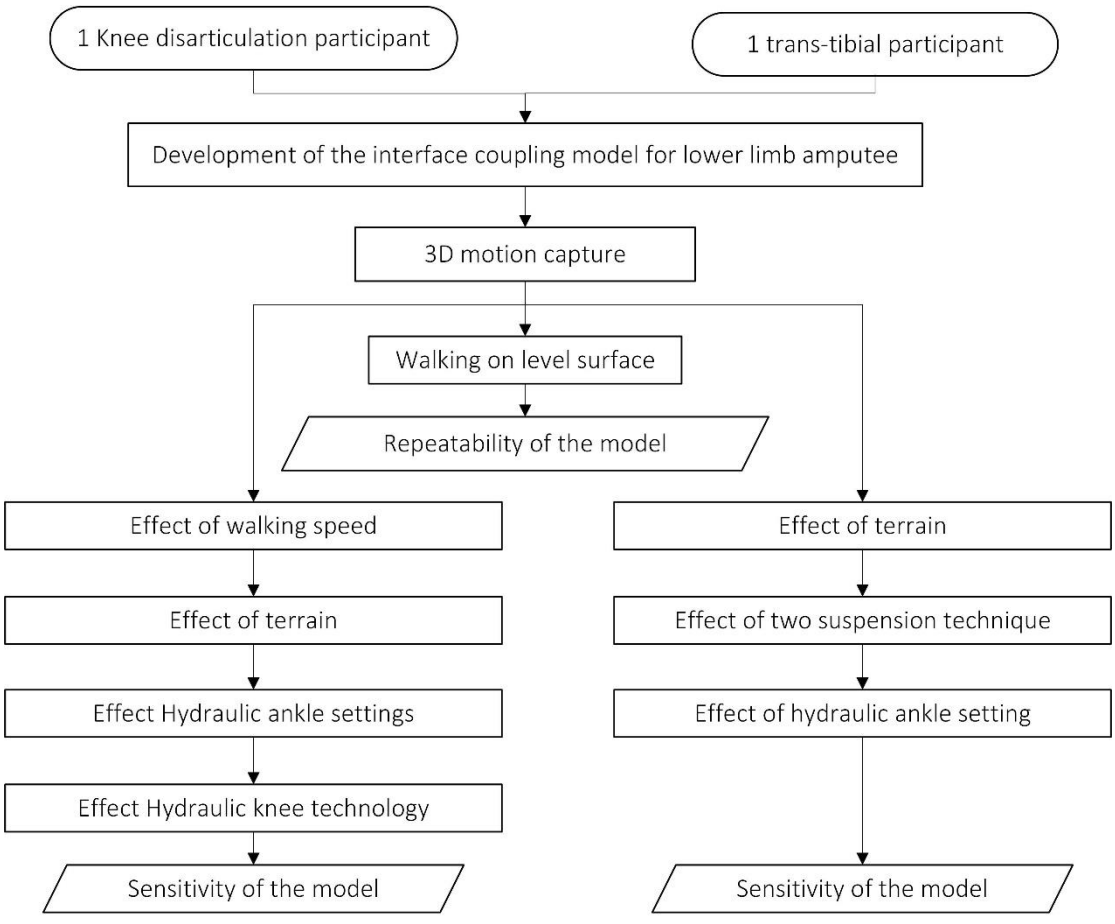

Figure 5.1: A flow chart to overview the research activities.

5.1 Development of the interface kinematic model for knee disarticulation amputee

A knee-disarticulation participant was first chosen in this study as, in general, the relative stump motion for trans-femoral amputee is greater than that of trans-tibial amputee. This is largely due to presence a greater volume of residuum tissue at the interface, which may result in a greater residuum movement inside the socket. This may further lead to the lack of proprioception of the limb and gait stability may be compromised. In this section, the details of the interface kinematic model is presented, which uses the 3D position of infra-red-based markers (Section 3.1.1) as inputs. In particular, segment definition, angular motion and axial motion are included below.

5.1.1 Segment definition

A VRS was formed by linking HJC and KPC (Figure 5.2a – red dashed line). The VRS co-ordinate system with an origin located at KPC was defined using a method described by Cappozzo [127] which is commonly used for thigh segment models on abled-bodied participants. The z-axis (Z_{VRS}) represents the vector connecting KPC to HJC. The x-axis (X_{VRS}) was perpendicular to Z_{VRS}, lying in the plane formed by HJC, LKP and MKP, with the lateral direction defined as positive. The Y-axis (Y_{VRS}) was defined as the orthogonal axis to the x–z plane, with the anterior direction defined as positive.

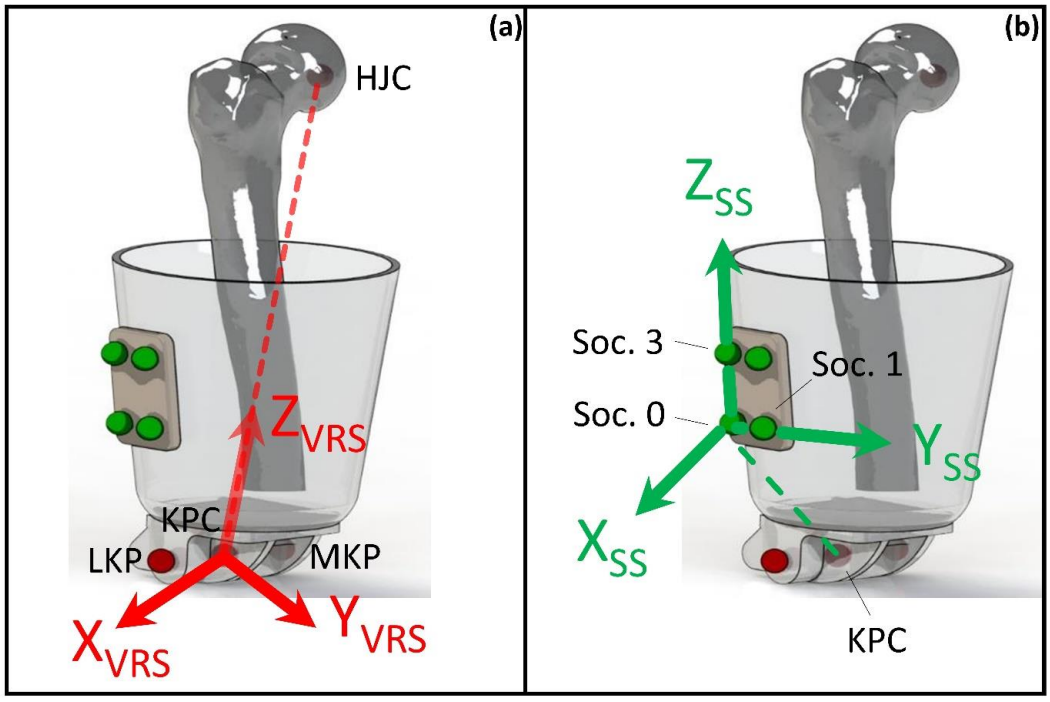

Figure 5.2: (a) Definition of Virtual Residuum Segment (VRS), (b) Socket Segment (SS) with their local co-ordinate systems

The socket cluster, which was previously used to determine the orientation of a rigid segment, allowed construction of SS and its local co-ordinate system. The SS was defined by linking KPC and the Soc. 0 marker on the socket cluster (Figure 5.2b – green dashed line), with its co-ordinate system constructed with reference to three markers on the socket cluster. The Y-axis (Y_{SS}) was in the direction of the vector from the origin, Soc. 0 to Soc. 1. The z-axis (Z_{SS}) was in the direction of the vector from Soc. 0 to Soc. 3. The x-axis (X_{SS}) was orthogonal to the y–z plane, with the lateral direction defined as positive.

5.1.2 3D angular motion between VRS and SS

Due to the dynamic nature of the SS, quasi-anatomical planes (Figure 5.3) were defined. Y_{SS} and Z_{SS} created the quasi-sagittal plane, X_{SS} and Z_{SS} created the quasi-coronal plane and X_{SS} and Y_{SS} created the quasi-transverse plane. The SS co-ordinate system was chosen as the reference frame to describe the relative motion of the VRS co-ordinate system. The VRS angular motion in the sagittal plane (α in Figure 5.3b), angular motion in the coronal plane (β in Figure 5.3c) and the transverse plane (γ in Figure 5.3d) were evaluated by using Carden angle. The step by step calculation of α, β and γ are described below.

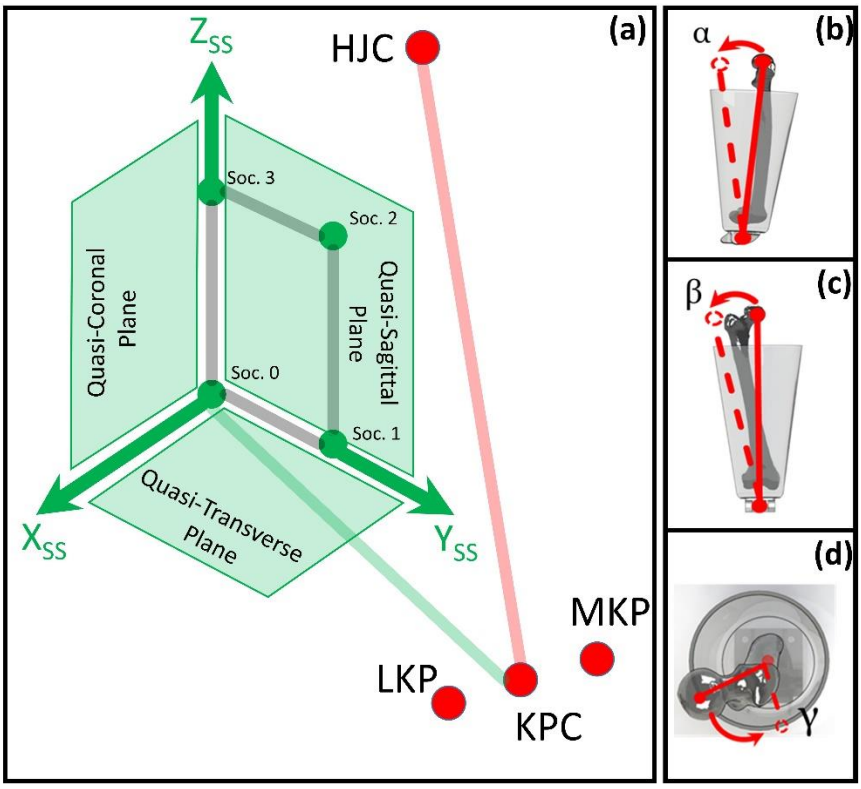

Figure 5.3: (a) Definitions of quasi-anatomical planes, (b) angular motion in quasi-sagittal plane, (c) angular motion in quasi-coronal plane and (d) angular motion in quasi-transverse plane.

Equation (5.1) describes the rotational relationship between the VRS local co-ordinate system and SS local co-ordinate system in the particular time frame of a GC.

$$\begin{bmatrix} x_{VRS} \\ y_{VRS} \\ z_{VRS} \end{bmatrix} = R \cdot \begin{bmatrix} x_{SS} \\ y_{SS} \\ z_{SS} \end{bmatrix} \tag{5.1}$$

Where the rotational matrix R [238] can be expressed by Equation (5.2),

$$\begin{bmatrix} R_{11} & R_{12} & R_{13} \\ R_{21} & R_{22} & R_{23} \\ R_{13} & R_{23} & R_{33} \end{bmatrix} = \begin{bmatrix} cos\beta \cdot cos\gamma & cos\gamma \cdot sin\beta \cdot sin\alpha - cos\alpha \cdot sin\gamma & sin\gamma \cdot sin\alpha - cos\gamma \cdot sin\beta \cdot cos\alpha \\ -sin\gamma \cdot cos\beta & cos\alpha \cdot cos\gamma - sin\alpha \cdot sin\beta \cdot sin\gamma & sin\gamma \cdot sin\beta \cdot cos\alpha + cos\gamma \cdot sin\alpha \\ sin\beta & -cos\beta \cdot sin\alpha & csoa \cdot cos\beta \end{bmatrix} \tag{5.2}$$

By multiplying the inverse of $\begin{bmatrix} x_{SS} \\ y_{SS} \\ z_{SS} \end{bmatrix}$ or $\begin{bmatrix} x_{SS} \\ y_{SS} \\ z_{SS} \end{bmatrix}^{-1}$ to both left and right hand side of the Equation (5.1), we obtain Equation (5.4):

$$\begin{bmatrix} x_{VRS} \\ y_{VRS} \\ z_{VRS} \end{bmatrix} \begin{bmatrix} x_{SS} \\ y_{SS} \\ z_{SS} \end{bmatrix}^{-1} = R \cdot \begin{bmatrix} x_{SS} \\ y_{SS} \\ z_{SS} \end{bmatrix} \begin{bmatrix} x_{SS} \\ y_{SS} \\ z_{SS} \end{bmatrix}^{-1} \tag{5.3}$$

It is evident that Equation (5.4) can be simplified to:

$$\begin{bmatrix} x_{VRS} \\ y_{VRS} \\ z_{VRS} \end{bmatrix} \begin{bmatrix} x_{SS} \\ y_{SS} \\ z_{SS} \end{bmatrix}^{-1} = R \tag{5.4}$$

The left hand side part of Equation (5.4) can be obtained based on the marker output from the 3D motion capture system, using the definitions described in Section 5.1.1. Here, we define:

$$\begin{bmatrix} x_{VRS} \\ y_{VRS} \\ z_{VRS} \end{bmatrix} \begin{bmatrix} x_{SS} \\ y_{SS} \\ z_{SS} \end{bmatrix}^{-1} = \begin{bmatrix} T_{11} & T_{12} & T_{13} \\ T_{21} & T_{22} & T_{23} \\ T_{13} & T_{23} & T_{33} \end{bmatrix} = R \tag{5.5}$$

By re-arranging Equation (5.2) and Equation (5.5):

$$\begin{bmatrix} T_{11} & T_{12} & T_{13} \\ T_{21} & T_{22} & T_{23} \\ T_{13} & T_{23} & T_{33} \end{bmatrix} = \begin{bmatrix} cos\beta \cdot cos\gamma & cos\gamma \cdot sin\beta \cdot sin\alpha - cos\alpha \cdot sin\gamma & sin\gamma \cdot sin\alpha - cos\gamma \cdot sin\beta \cdot cos\alpha \\ -sin\gamma \cdot cos\beta & cos\alpha \cdot cos\gamma - sin\alpha \cdot sin\beta \cdot sin\gamma & sin\gamma \cdot sin\beta \cdot cos\alpha + cos\gamma \cdot sin\alpha \\ sin\beta & -cos\beta \cdot sin\alpha & cos\alpha \cdot cos\beta \end{bmatrix} \tag{5.6}$$

By equating the elements on the 3rd row, 1st column of the left and right side of the Equation (5.6):

$$T_{13} = sin\beta \tag{5.7}$$

By taking the inverse sin on both sides of Equation (5.7), an expression for the angular motion in coronal plane β can be obtained:

$$\beta = sin^{-1}(T_{13}) \tag{5.8}$$

By manipulating the 3rd row, 2nd and 3rd elements on both side of Equation (5.6):

$$\frac{T_{23}}{T_{33}} = \frac{-cos\beta \cdot sin\alpha}{cos\alpha \cdot cos\beta} = -\frac{sin\alpha}{cos\alpha} = -tan\alpha \tag{5.9}$$

Therefore, the angular motion in the sagittal plane α, can be obtained using Equation (5.10):

$$\alpha = -tan^{-1}(\frac{T_{23}}{T_{33}}) \tag{5.10}$$

By manipulating the 1st column,1st and 2nd elements on both side of Equation (5.6):

$$\frac{T_{21}}{T_{11}} = \frac{-sin\gamma \cdot cos\beta}{cos\beta \cdot cos\gamma} = -\frac{sin\gamma}{cos\gamma} = -tan\gamma \tag{5.11}$$

Therefore, the angular motion in transverse plane γ, can be obtained using Equation (5.12):

$$\gamma = -tan^{-1}(\frac{T_{21}}{T_{11}}) \tag{5.12}$$

It is worth noting, the calculation process of α, β and γ at a particular time frame during gait, will be repeated for the whole dynamic GC.

5.1.3 Axial length between VRS and SS

The residuum/socket axial length, L, defined as the magnitude of the vector from KPC to HJC (Figure 5.4), was calculated at each timeframe of the dynamic motion capture, using Equation (5.13). The change in the residuum/socket axial length refers to the degree of attachment and suspension of the socket to the residuum. The decrease and increase in the axial length can be associated with the compressive and tensile loads applied to the residuum/socket interface.

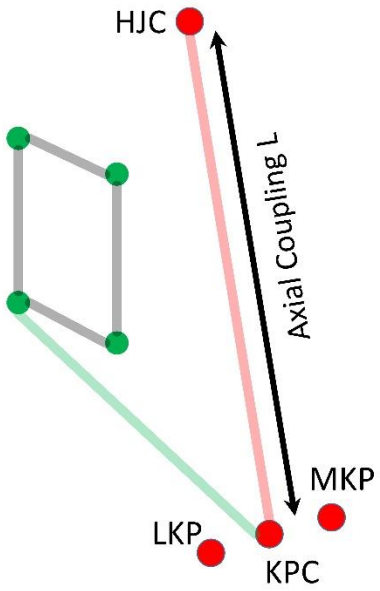

Figure 5.4: Definition of axial length, L

$$L = \sqrt{(HJC_x - KPC_x)^2 + (HJC_y - KPC_y)^2 + (HJC_z - KPC_z)^2} \quad (5.13)$$

5.2 Development of the interface kinematic model for trans-tibial amputee

A socket interface kinematic model for trans-tibial amputee was subsequently developed. For trans-tibial amputee, the evaluation of the residuum movement can be directly associated with the assessment of the socket design (Section 2.1.3) and fit. Further, the kinematic interaction between the truncated bone and the soft tissue may be further associated with the deep tissue damage (Section 2.2.3). In this section, an interface kinematic model will be described. In particular, segment definition, angular and axial length are included below.

In total, nine virtual markers were used in the interface kinematic model (Figure 5.5a). Six of them are used to construct the VRS, including MAP, LAP, APC, MFE, LFE and KJC (Figure 5.5b). With the repeat use of MAP, LAP and APC virtual markers, together with MSP, LSP and SPC virtual markers, SS were constructed.

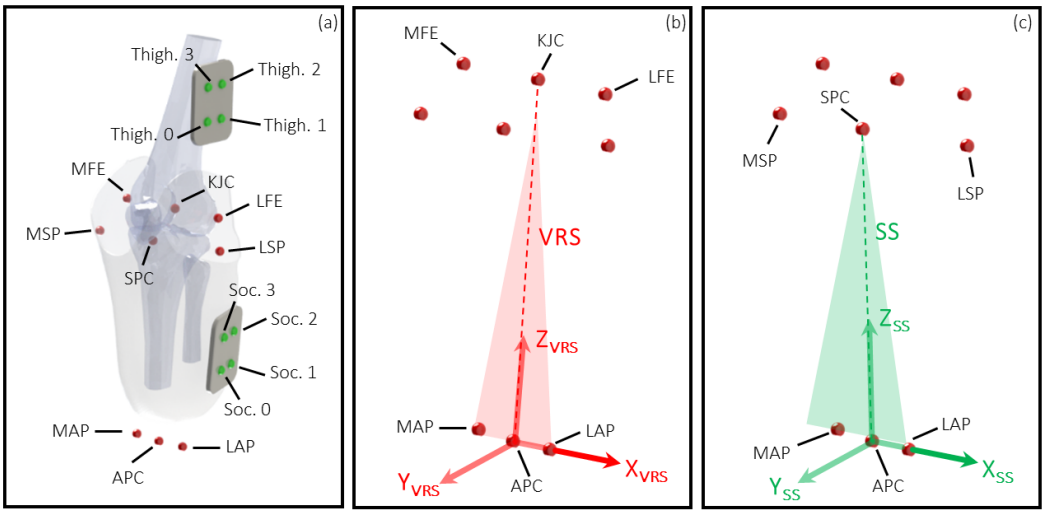

Figure 5.5: (a) key landmarks involved in the interface kinematic model, (b) definition of VRS and its local co-ordinate system and (c) definition of the SS and its local co-ordinate system.

5.2.1 Segment definition

VRS, on a trans-tibial residuum/socket interface, is defined by connecting APC to KJC. The z-axis of the VRS local co-ordinate system or Z_{VRS} is defined as unit vector starting from the APC, pointing towards the KJC. The y-axis of the VRS local co-ordinates system or Y_{VRS} is defined as the unit vector normal to the plane (red plane highlighted in Figure 5.5b) formed MAP, LAP and KJC virtual markers, in an anterior direction. Finally, the x-axis of the VRS local co-ordinate system or X_{VRS} is defined as the unit vector orthogonal to both Z_{VRS} and Y_{VRS}.

SS, on the trans-tibial residuum/socket interface, is defined by connecting APC to SPC. The z-axis of the SS local co-ordinate system or Z_{SS} is defined as unit vector starting from the APC, pointing towards the SPC. The y-axis of the SS local co-ordinates system or Y_{SS} is defined as the unit vector normal to the plane (green plane highlighted in Figure 5.5c) formed MAP, LAP and SPC virtual markers, in the anterior direction. Finally, the x-axis of the SS local co-ordinate system or X_{SS} is defined as the unit vector orthogonal to both Z_{SS} and Y_{SS}.

5.2.2 3D angular motion between VRS and SS

Due to the dynamic nature of the SS, reference planes (Figure 5.6a) were defined. Y_{SS} and Z_{SS} created the sagittal plane, X_{SS} and Z_{SS} created the coronal plane and X_{SS} and Y_{SS} created the transverse plane. The SS co-ordinate system was chosen as the reference frame to describe relative motion of the VRS co-ordinate system. The VRS movement was chosen for analysis, relative to SS, as it aligns with the 'thigh' segment defined in the conventional gait analysis. The VRS angular motion in sagittal plane (α in Figure 5.6b), angular motion in coronal plane (β in

Figure 5.6c) and angular motion in transverse plane (γ in Figure 5.6d) was evaluated by using the Carden angle (Section 5.1.2).

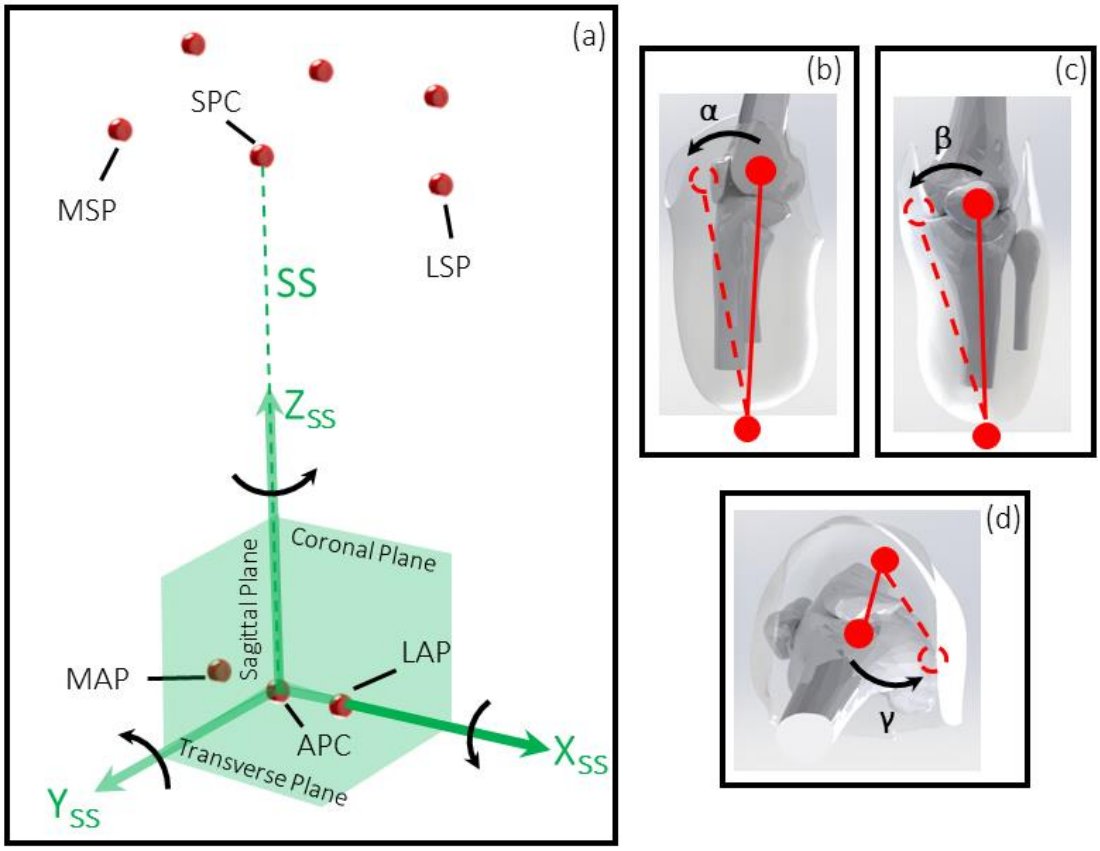

Figure 5.6: (a) Definitions of reference planes, (b) angular motion in sagittal plane, (c) angular motion in coronal plane and (d) angular motion in transverse plane.

5.2.3 Axial length between VRS and SS

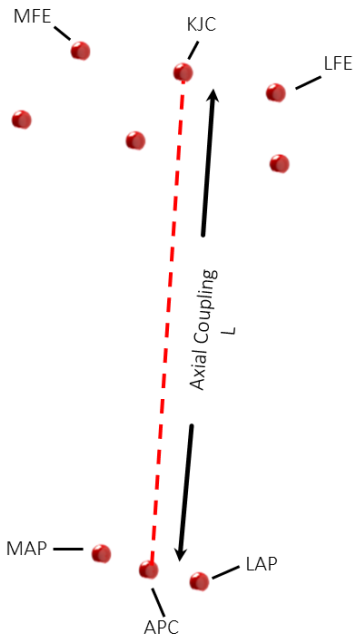

Figure 5.7: Definition of axial length, L

The residuum/socket axial length, L, defined as the magnitude of the vector from KPC to HJC (Figure 5.7), was calculated at each timeframe of the dynamic motion capture, using Equation (5.14). The residuum/socket axial length refers to the degree of attachment and suspension of the socket to the residuum. The decrease and increase in the axial length may be associated with the compressive and tensile loads applied to the residuum/socket interface, namely,

$$L = \sqrt{(APC_x - KJC_x)^2 + (APC_y - KJC_y)^2 + (APC_z - KJC_z)^2} \quad (5.14)$$

5.3 Method

The aim of amputee walking tests here is to evaluate the effectiveness of the interface kinematic model, intra- and inter-session repeatability and sensitivity. Therefore, three amputee participants are recruited in this study, briefly representing the trans-femoral and trans-tibial amputee cohorts. However, it is worth noting most of the studies have been based on the knee disarticulation amputee due to the relatively larger residuum motion, comparing to that on trans-tibial participants.

5.3.1 Experimental protocol

Knee disarticulation participant

Amputees perform varies daily living activities [239] such as standing, sit-to-stand, shifting weight and swing etc. These above-mentioned activities are also commonly included in the physiotherapy exercises and in prosthetic socket fitting process [240, 241]. The quality of socket fit when performing these activities was largely based on the observation from the prosthetist and amputee feedback. Understanding the interactions between the residuum and the socket could potentially aid with socket rectification, providing an evidence based adjustment of socket fit in addition to feedback from the amputee. Four non-walking activates were perform by the knee disarticulation amputee as listed below.

Among the four non-walking activities, four of them involve weight bearing. Simple weight bearing activities were performed first because they represent the instances experienced in the stance phase of a complex GC. The biomechanics at socket interface maybe relatively easier to understand with the aid of simple weight bearing activities. It is worth noting that, when performing non-walking activities, the participant was wearing an Echelon prosthetic foot with hydraulic ankle resistance set at his habitual settings.

- A1: weight bearing on both limbs

The participant was told to use his prosthetic limb making contact with the force platform (Figure 5.8a) statically for a period of approximately five seconds. Five seconds was chosen as it represents the time for the participant for reach a stable posture.

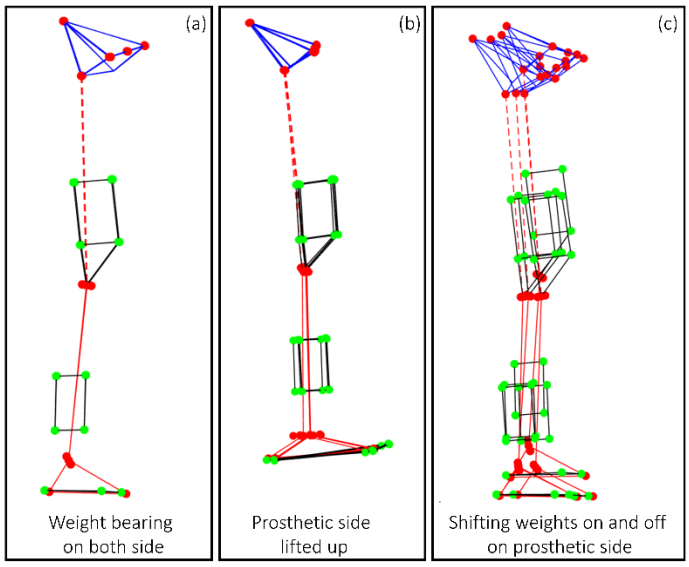

Figure 5.8: (a) weight bearing on both limb, (b) full weight bearing on contra-lateral side, i.e. lifting the prosthetic limb and (c) shifting the weight on and off.

- A2: non-weight bearing

With an aid of a crutch, the participant was asked to lift his prosthetic limb away from the ground. In the meantime, the contra-lateral side still remains statically on the floor. Once the prosthetic side clears from the ground, then the participant was told to remain at this posture for approximately five seconds.

- A3: full-weight bearing

With an aid of a crutch, the participant was told to lift this contra-lateral limb off from the floor. In the meantime, the prosthetic limb remains statically on the ground. The participant remains at this posture for approximately five seconds.

- A4: sit-to-stand

Various muscles and joints needs to co-ordinate in a synergistic manner, in order to conduct sit-to-stand activity for able-bodied group. For amputee group, this is particularly challenging due to the loss of thigh muscle, a biological knee joint and an ankle joint. The performance of the socket interface during this activity becomes particularly important as it may affect the subsequent initiation of ambulation.

A chair was prepared and the participant was asked to remain the seated position. Then the participant was given the verbal instruction of 'stand up' with his normal pace until a stable posture was reached (Figure 5.9).

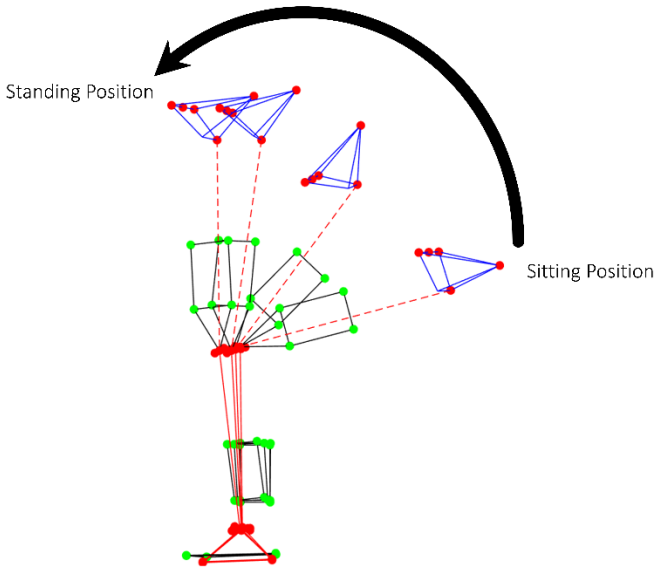

Figure 5.9: Participant performing sit-to-standing activity

- A5: Level walking

Level walking activities were performed at controlled walking speed. In each of the level walking trial, the participant was told to use their prosthetic side making contact with the force platform. Up to 10 trials were performed in each session.

For the knee disarticulation amputee, in order to evaluate the intra-session repeatability of the interface kinematic kinematic model, up to 10 sessions of level walking tests were conducted. A 10-sessions-study was designed based on the precision-based sample size calculation. The designed sample size also served purpose of analysing interface kinematic difference obtained between two years.

$$2 \times SD \times \sqrt{\frac{1}{n_1} + \frac{1}{n_2}} = \Delta \tag{5.15}$$

In Equation (5.15), the numerical number 2 was obtained from the 95% confidence interval based on the normal distribution. SD represents the standard deviation that of the measurement obtained from previously reported studies or by conducting a pilot study. n_1 and n_2, represent the sample size required for a short-term study and a long-term study. Here, it is assumed that the sample size required for both study is equal to each other. Δ represents the minimal difference that needs to be detected with 95% confidence interval. SD value of 0.75° was selected as it was the value reported by Childress and Siebert [169] for angular motion measured by Vicon 3D motion capture system. Δ value of 0.6° was selected as it was the minimal angular movement reported by Covnery and Murray [8] when walking on difference

terrains. By substituting SD value and Δ value into Equation (5.15). Sample size of five was need for the in each year.

In each of the session, the knee disarticulation participant worn exactly the same prosthetic components, i.e. Echelon VT prosthetic foot, KX06 prosthetic knee, supra-condylar suspension carbon fibre socket, Pelite liner and one thick sock. The alignment of the prosthetic components was examined by a senior prosthetist at the beginning of each session. It is also worth noting that the time of start for conducting data collection sessions were approximately between 11:00am to 11:30am. This is to minimise the variation of socket fit quality at different of the day. In addition, in each of the level walking session, walking speed is controlled by a metronome at 100BPM.

- A6: Level walking with different speed

Followed by level walking data collection session, two more level walking data collection sessions were performed by the knee disarticulation participant. There are three days in between the two sessions.

In each of the session, the participant was asked to walk at slower and faster walking speed with respect to the self-selected. Walking cadence was controlled by a metronome at 80BPM (slow walking cadence), 100BPM (self-selected walking cadence) and 120BPM (fast walking cadence). 20% increase of walking cadence was selected, as it is the fastest cadence without compromising the safety of the participant during level walking. The detailed protocol was illustrated in Figure 5.10.

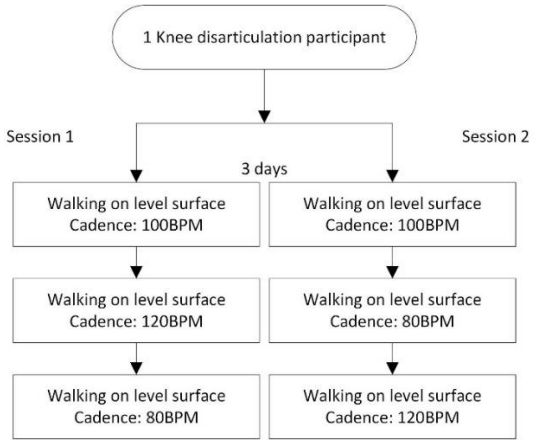

Figure 5.10: Experimental protocol for investigating the effect of walking speed on interface kinematics.

- A7: Walking on different terrains

In this session, all of the walking tests were conducted on both level and ramped surfaces as mentioned in Section 3.1, with all walking cadence controlled with a metronome at 100BPM. The detailed test protocol is illustrated in Figure 5.11.

Two repeated sessions were performed with Echelon hydraulic ankle resistance set to the habitual value (plantar-flexion resistance of 5 and dorsi-flexion resistance of 7). It is worth noting that, in both test sessions, there was no alteration of prosthetic components and the prosthetic alignment was verified by a senior prosthetist. In test Session 1, the participant was asked to walk on level surface, followed by walking on a descending ramp and subsequently on an ascending ramp. In order to minimise the effect of bias on the order of the test protocol, the order of the protocol, on ramped surface, was switched in test Session 2 (see Figure 5.11).

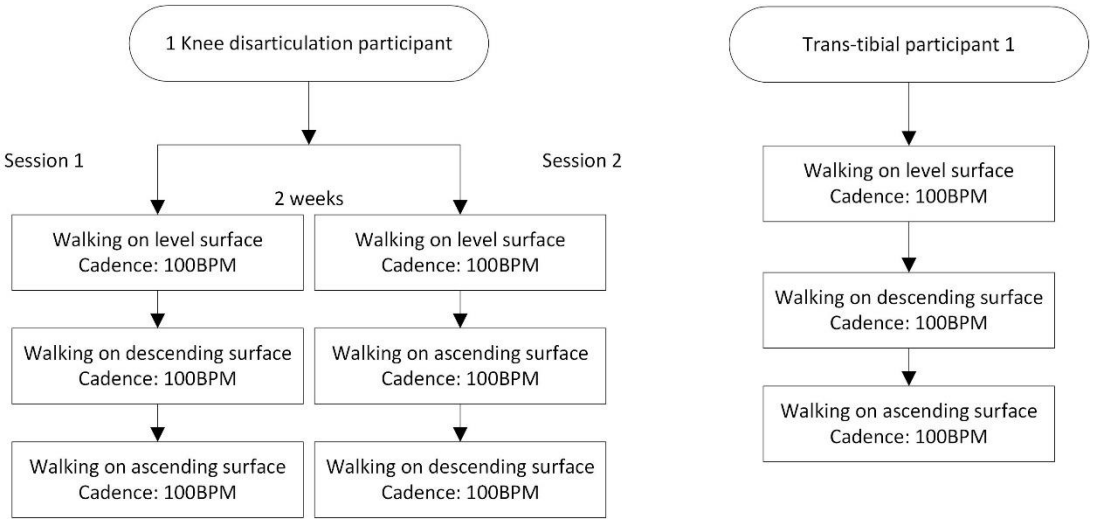

Figure 5.11: Experimental protocol for investigating the effect of terrain on interface kinematics.

- A8: Walking activities with different hydraulic ankle setting

The detailed experimental protocol for both participants is illustrated in Figure 5.12. The test started with walking on the level surface with self-selected walking speed. The hydraulic ankle resistance was set to the habitual value (plantar-flexion resistance of 5 and dorsi-flexion resistance of 7). The protocol is followed by walking on the descending ramp with the same ankle resistance setting used during level walking. Next, the hydraulic resistance setting was tuned by a senior prosthetist to brake mode. The data collection session is repeated by walking on the descending ramp at self-selected speed. Subsequently, the hydraulic ankle resistance was tuned back to the habitual setting and the participant was asked to walking on the ascending ramp. Finally, the hydraulic ankle resistance was adjusted to assist mode. Walking session is then repeated on the ascending ramp. The same study was repeated in a week time.

However, the protocol started with level walking and followed by ramp ascending and ramp descending. This is to minimise the bias resulted from the order of the protocol.

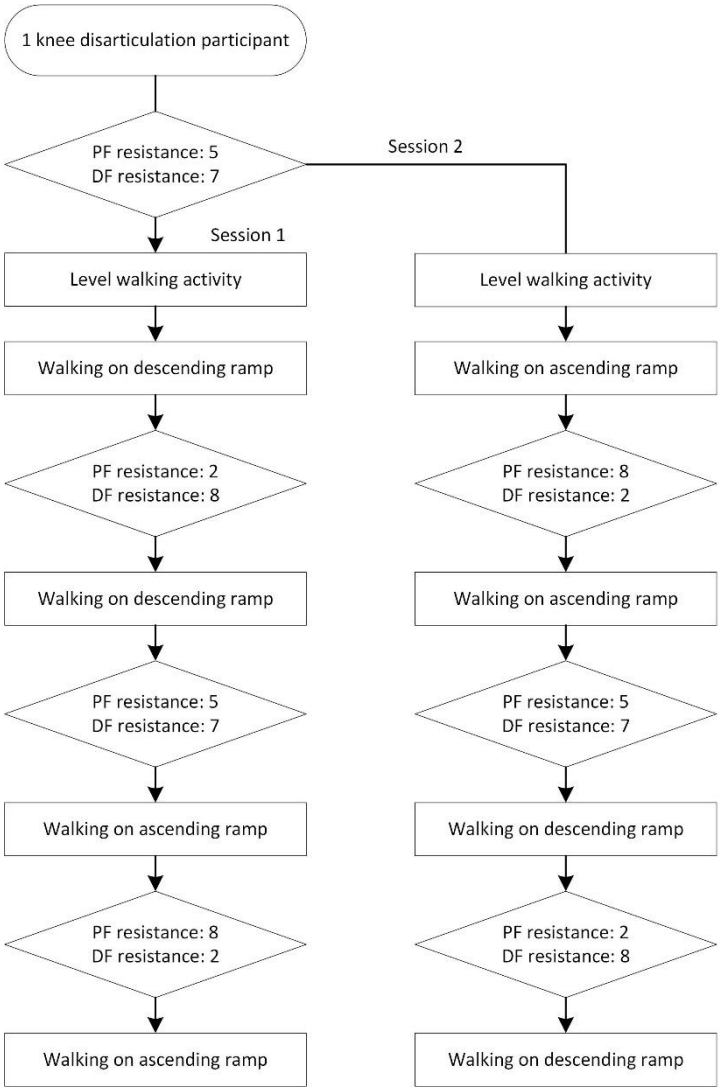

Figure 5.12: Experimental protocol for investigating the effect of hydraulic ankle resistance setting to interface kinematics.

- A9: Walking activities with different prosthetic limb technology

This case study aims to evaluate the effect of two different prosthetic knee technologies on the residuum/socket interface kinematic motion. The knee disarticulation participant took part in the study and was fitted with an Echelon foot, KX06 polycentric knee (Figure 5.13a) and a supracondylar suspension socket. In order to eliminate the potential effect of axial and torsional shock absorber, the VT unit is removed and the length of the prosthetic pylon is re-adjusted to accommodate absence of the VT unit. As the prosthetic component is no longer the habitual ones, a senior prosthetist verified the alignment of the prosthetic components and

the fit of the socket prior to testing. Participant was then asked to walk on the level walkway with walking cadence at 100BPM.

Figure 5.13: (a) The knee-disarticulation participant fitted with (a) a KX06 polycentric knee and (b) Orion 3 knee.

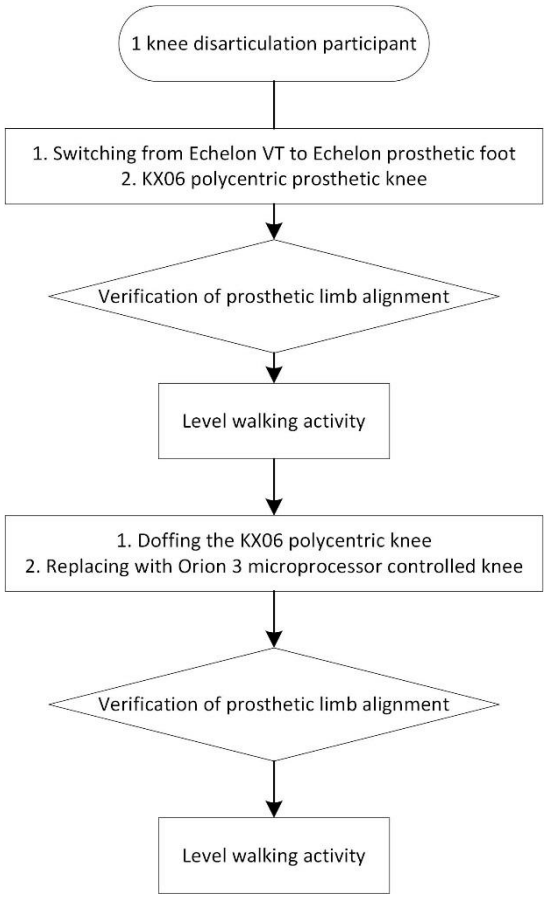

Figure 5.14: Experimental protocol for investigating the effect of prosthetic knee to interface kinematics.

At the end of the first level walking test, participant was asked to rest with prosthesis, worn below the socket, doffed. This process removes the influence of donning/doffing of the socket on the residuum/socket interface mechanics. At the same time, the senior prosthetist switched the polycentric KX06 knee (Figure 5.13a) to the microprocessor controlled Orion 3 knee (Figure

5.13b). With attention to re-produce the alignment and height of the prosthesis, an extra prosthetic female adapter was fitted at the bottom of the socket. Then the participant was asked to perform the same level walking activity with walking cadence controlled at 100BPM. The detailed experimental protocol can be found in Figure 5.14.

Trans-tibial participants

- B1: level walking activities

For trans-tibial 1 participant, two level walking data collection sessions were conducted. During each of the session, participant's habitual prosthetic components were worn. A metronome, set at 120BPM, was used to control the walking cadence. The metronome settings were close to their self-selected walking cadence. Two level walking sessions were conducted on this participant and there is one week between session 1 and session 2. Similarly, the starting time of the data collection sessions were approximately fixed at 10:30am. For trans-tibial 2 participant, only one level walking session was conducted. The participant was asked to walk at self-selected walking speed with his habitual prosthetic components. Both participants were wearing their habitual prosthetic foot (Echelon foot for Trans-tibial 1 and Elan foot for Trans-tibial 2 participant) in all subsequent studies. It is worth noting that the Elan and Echelon both incorporates a hydraulic ankle unit, however, the hydraulic resistance was controlled by microprocessor for the Elan foot.

- B2: Walking on different terrains

A single data collection session was performed with trans-tibial 1 amputee. The Elan hydraulic ankle resistance was set to the habitual value (plantar-flexion resistance of 5 and dorsi-flexion resistance of 5). The participant was first asked to walk on the level surface, followed by walking on the descending and ascending ramps.

- B3: walking with two suspension techniques

Trans-tibial 1 participant took part in the study. Instead of using his habitual prosthetic components, he was asked to use Echelon Vac prosthetic foot. In this study, only level walking activity is involved. It is worth noting that, without adjust the hydraulic setting on the Echelon Vac foot, it has the same functionality compared with the Elan prosthetic foot (habitual prosthetic foot) when walking on the level surface. Therefore, it minimises the effect of the change in prosthesis to the gait of the participant. To start with, the tube links the Echelon Vac prosthetic foot and the valve mounted on socket was disconnected by a senior prosthetist,

such that no active vacuum is allowed to build inside the socket. Participant was subsequently told to perform level walking activity at self-selected speed.

The tube was subsequently re-connected between the Echelon Vac foot and the valve mounted on the socket, allowing vacuum to build at the interface. Prior to the data collection session, the participant was told to walking along the gait laboratory for two minutes until vacuum was build inside the socket. Subsequently, he was asked to walk along the level walkway at self-selected speed. The detail protocol of this study is illustrated in Figure 5.15.

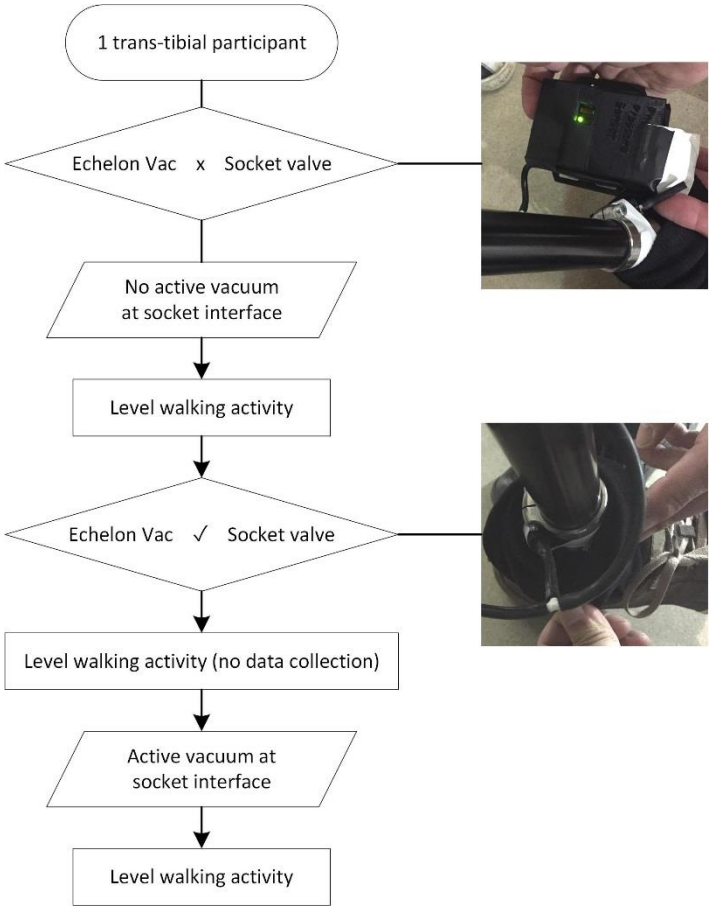

Figure 5.15: Experimental protocol for investigating the effect of socket suspension to interface kinematics.

5.3.2 Data collection and analysis

Data collection and processing

The method for raw real marker and virtual marker data collection was the same as previous studies and can be found in Section 4.1.2. Using the raw real marker and virtual marker data, VRS and SS segment with their local co-ordinate system (Section 5.1.1) were first construction using Matlab 2016a. Subsequently, angular motion and axial length were calculated for each of walking trials using the equations described in Section 5.1.2 and Section 5.1.3, respectively. The

mean and one SD values for each of the angular and axial length, over a GC, were calculated from all clean trials. The detailed Matlab scripts for the calculation of angular and axial length can be found in Appendix A4.

Statistical analysis

The waveform repeatability was analysed using coefficient of multiple correlation (CMC). The CMC analysis was performed on both results obtained within each session and across all 10 test sessions. CMC analysis was chosen as it was previously used to study the waveform repeatability of the joint kinematics, obtained from motion analysis systems [242].

For the analysis of waveform repeatability within a test day, Equation (5.16) was used.

$$R_{Intra}^2 = 1 - \frac{\sum_{i,j,t}^{M,N,T}\left(Y_{ijt} - \overline{Y_{it}}\right)^2 / MT(N-1)}{\sum_{i,j,t}^{M,N,T}\left(Y_{ijt} - \overline{Y_i}\right)^2 / (NMT-1)} \tag{5.16}$$

where Y_{ijt} is the t[th] time point of the j[th] trial on the i[th] test day. $\overline{Y_{it}}$ is the average at time poing ton the i[th] test day, namely,

$$\overline{Y_{it}} = \frac{1}{N}\sum_{j=1}^{N} Y_{ijt} \tag{5.17}$$

$\overline{Y_{it}}$ is the mean on the i[th] day and is given by,

$$\overline{Y_i} = \frac{1}{NT} - \sum_{j,t=1}^{N,T} Y_{ijt} \tag{5.18}$$

For the analysis of waveform repeatability across different test days, Equation (5.19) was used.

$$R_{Inter}^2 = 1 - \frac{\sum_{i,j,t}^{M,N,T}\left(Y_{ijt} - \overline{Y_t}\right)^2 / T(NM-1)}{\sum_{i,j,t}^{M,N,T}\left(Y_{ijt} - \overline{Y}\right)^2 / (NMT-1)} \tag{5.19}$$

where $\overline{Y_t}$ is the average at time point t over NM GCs, namely,

$$\overline{Y_t} = \frac{1}{NM}\sum_{i,j=1}^{M,N} Y_{ijt} \tag{5.20}$$

and $\overline{Y}$ is the mean over time and given by

$$\overline{Y} = \frac{1}{NMT}\sum_{i,j,t=1}^{M,N,T} Y_{ijt} \tag{5.21}$$

The calculation of R_{Intra}^2 and R_{Inter}^2 was performed in Matlab 2017b.

Minitab 17 statistical software was used t. For all parameters, normality of the data was first check using Anderson-Darling test with p value of 0.05 set as threshold. Paired t-test was performed when comparing difference between two the mean values, under different test conditions. The level of significance was also set at $p<0.05$.

5.4 3D residuum motion results - knee disarticulation amputee

5.4.1 Non-walking activities

- Static weight bearing activities (A1-A3)

Three static weight bearing activities were performed by the knee disarticulation amputee. These corresponds to A1, A2 and A3 activities described in Section 5.3.1.

Up to 492±0.5mm of axial length is obtained over a period of five seconds during when the weight was borne on both limb (A1, black line in Figure 5.16a). When the weight was borne on both limb, up to 446N (dotted line in Figure 5.16b) and 340N (Dash-dot line in Figure 5.16b) of vertical GRF was measured on the contra-lateral and prosthetic side, respectively. Therefore, a greater load (up to 106N) was experienced on the contra-lateral side than the prosthetic side. When the same test was repeated with both limb making contact with the force platform, up to 789N of vertical GRF was measured and this is equivalent to the sum of the two forces experienced on the prosthetic and contra-lateral side. It is envisaged that, when loading symmetry of the GRF changes, the axial length of the interface would change accordingly, which could affect the overall length of the limb on the prosthetic side. The axial length obtained can then provide measurement to the prosthetist to assist the adjustment of the prosthetic limb length.

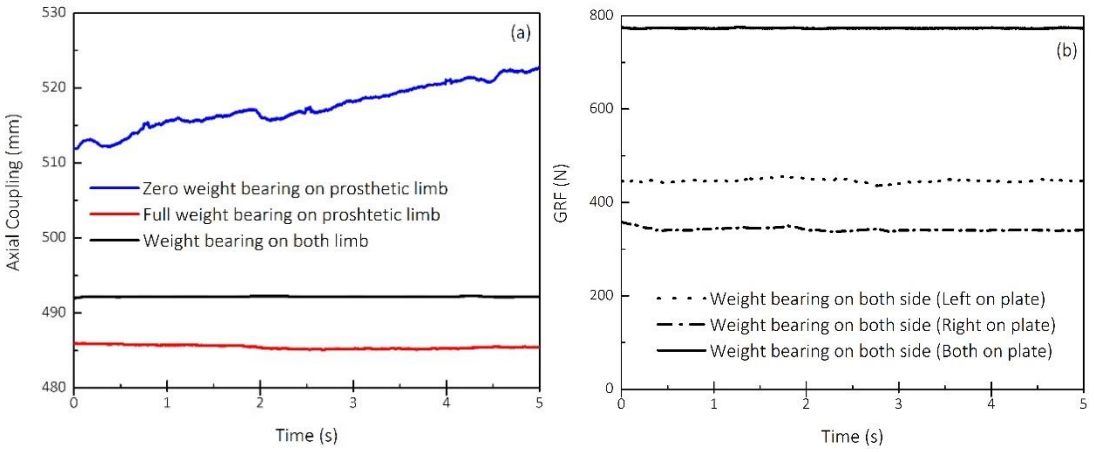

Figure 5.16: (a) Axial length and (b) GRF as a function of time, obtained from three weight bearing trials

Approximately 486±1.0mm of axial length was obtained when performing full-weight bearing trial (A2, red line in Figure 5.16a). Fluctuation between 2s-3s was observed as well as the greater SD. The participant, with the crutch assisting, was trying to keep himself balanced during the five-second of data collection period.

When shifting the whole body weight to the contra-lateral limb (A3, blue line in Figure 5.16a), approximately 512mm of axial length was obtained and it kept increasing during the five-second data collection period, reaching roughly 523mm at the end of the trial. This is equivalent to an 11mm lengthening of the residuum during this activity. It is worth noting that the lengthening process of the residuum was also visually evident. As reported by the participant, he did not feel secure due to the dropping of the prosthesis and also claimed that the muscles were fired up order to keep the socket attached to the residuum. The supra-condylar suspension socket, together with the rest of the prosthesis, was designed to be suspended at the medial and lateral femoral epicondyles. When the residuum was under tensile force, due to the weight of the socket and the rest of the prosthesis, the residuum was pulled away from the socket. This may induce a reduction in proprioception and the participant tends to regain the proprioception by firing the muscle. By performing this simple trial, socket suspension and the prosthetic limb stability, under tensile force, can be assessed.

When comparing the values obtained from three weight bearing trials. Shortest axial length was obtained during full weight bearing trial (486mm), this followed by the value obtained during weight bearing on both limb (492mm) and none weight bearing on prosthetic limb (512mm). This is likely due to the compressive and tensile force experienced during three weight bearing activities. A compressive force could shorten the axial length, as the residuum is 'pushed into' the socket. A tensile force (main contributed from the gravitational force of the prosthesis) could lengthen the axial length, as the residuum is 'pulled-out' of the socket.

- A4: Sit-to-stand

During the sit to standing transition (Figure 5.17a), the angular motion in sagittal plane decreased from 0° (0s) to -8° (0.32s). It subsequently increased to +7° (1.2s). This is equivalent to a 15° ROM in sagittal plane during sit-to-stand transition. The decrease of the angular motion could be associated with the residuum engagement with anterior region of the socket, when trying to stand up. In addition, the increase of the angular motion may be associated to the needs of posterior support during weight bearing. During standing period (from 1.2s to approximately 4s), the angular motion in sagittal plane remain steady with a fluctuation of less than 1°. The ROM of angular motion in coronal and transverse plane are both approximately

within 1° (Figure 5.17a). Convery and Murray reported 13° of angular motion in sagittal plane (Figure 2.41), which is comparable to the value obtained in the current study. However, a significantly higher value was reported in coronal plane (15° in Figure 2.41), compared with the current study. This is likely contributed from difference in level of amputation (trans-femoral amputee and knee disarticulation amputee). For the knee disarticulation amputee, distal end of the femur was commonly used as a pivot point and the non-rigid angular motion was evident at femoral head (proximal part). However, the trans-femoral QUAD socket design, used in Convery and Murrays's, study tends to give a larger medial-lateral movement at distal end of the femur, as reported in literature (Figure 2.7c).

Sit-to-stand trial is a simple action that frequently performed by amputee during daily life. It is envisaged that such activity can be used for prosthetic limb assessment. It has the potential to inform the prosthetists the stability of the socket interface via angular motion value and degree of control of prostheses via the time take to finish the activity.

It is evident that, in this particular trial, the angular motion is dominated by the motion in sagittal plane. This aligns with the magnitude of forces experienced at the ground interface, as higher peak anterior-posterior GRF (-126N at 0.31s in Figure 5.17b) was measured comparing to that the medial-lateral of GRF (-16N in Figure 5.17b). It is also worth noting that, the timing at which the peak angular motion in sagittal plane (0.32s) occurs, matches well with the in anterior-posterior GRF (0.31s). This suggests that there may be a correlation between the forces experienced at ground interface and kinematic motion experienced at residuum/socket interface.

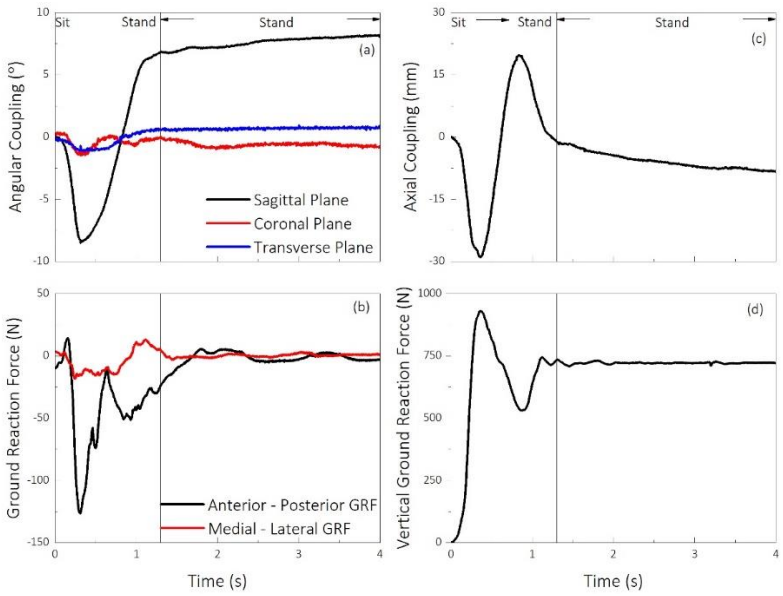

Figure 5.17: (a) Angular motion, (b) anterior-posterior and medial-lateral component of GRF, (c) axial length and (d) vertical component of GRF, obtained during sit-to-standing activities

Relative to the value observed at time zero, axial length decreased from 0mm (t=0s) to -28mm (t=0.32s), as shown in Figure 5.17c. It is followed by the increase of axial length from -28mm (t=0.32) to +20mm (t=0.84s). Then it decrease from +20mm back to value close to zero at the end of the sit-to-stand transition. It is worth noting that increase and decrease of axial could be associated with the residuum 'push-into' the socket and 'pull-out' of the socket.

Similar pattern is observed in vertical component of GRF, as shown in Figure 5.17d. The vertical component of GRF increase from 0N (t=0) to approximately 931N (t=0.33s) or 128% of BW, suggesting the vertical force, greater than body weight, is required by this subject to change from a sitting positon to standing position. This increase in vertical GRF also matches well with the decrease in axial length as the residuum was loaded. As the vertical GRF decreases from 931 (t=0.33s) to 531N (t=0.86s), during which the residuum is off-loaded slightly, the axial length restores. The final increase of vertical GRF during the end of sit-to-stand transition period may be associated with the weight balancing of the amputee, which also aligns with the further decrease in axial length. During standing period, there is a slight decrease of axial length (approximately 3mm) during a period of 2.8s.

5.4.2 Level walking activities

The section presents the results obtained by performing protocol A5 (Section 5.3.1).

An estimation of the mean (±1SD) residuum/socket angular coupling in the sagittal plane is presented in Figure 5.18a. During the stance phase, there was a general increase in angular motion from 0° at 0% of GC to a maximum value of 12° at approximately 60% of GC. This

increase in angular motion indicates the anti-clockwise rotation of the VRS relative to the SS according to Figure 5.3b, engaging with posterior-proximal region of the socket. By contrast, in the swing phase, the angular motion was restored to the original value observed at 0% of GC. This suggests a clockwise rotation of the VRS relative to SS, engaging with anterior-proximal region of the socket.

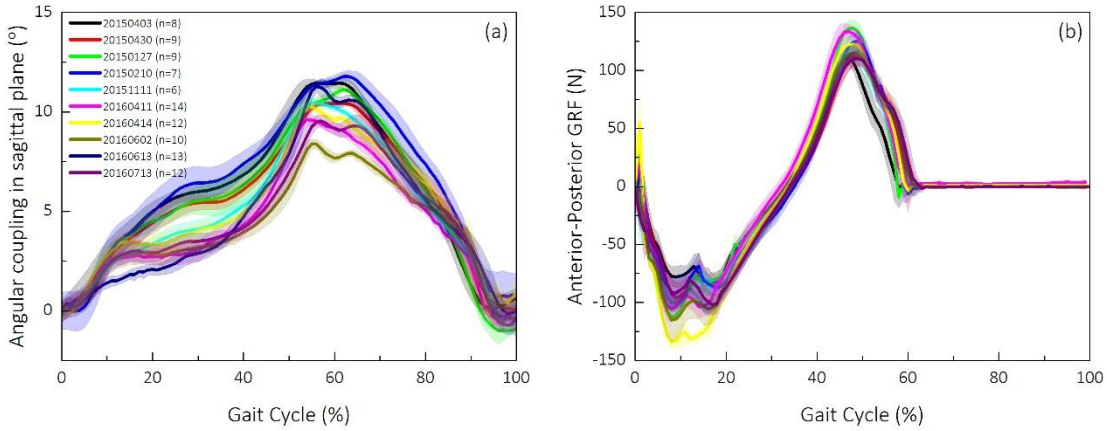

Figure 5.18: (a) Angular motion in sagittal plane (b) anterior-posterior component of GRF, obtained from the knee disarticulation participant across 27 months.

To facilitate the explanation of the residuum/socket interface angular biomechanics in sagittal plane, anterior-posterior component of GRF (Figure 5.18b) was used as it represents the principle load experienced at the ground interface. From 0% of GC to mid-stance, the prosthetic knee and socket can be treated as a relatively rigid segment as they remained extended to support the stance phase of walking [243]. At the same time, the anterior-posterior component of GRF decreased from approximately 0N (0%) to about 75N (at 20% of GC). This suggests that the GRF in the direction opposing the body progression was acted on the prosthetic foot. The combination of these phenomenon resulted in the VRS rotation in anti-clockwise direction relative to the SS, prior to mid-stance.

During the transition from 20% of GC to 30% of GC, the anterior-posterior component of GRF diminished. Thus, the angular displacement of the residuum relative to the socket, stayed relatively constant. During TS phase, with the HJC behind the socket in the sagittal plane, hip flexion began to occur. Simultaneously, the femur within the residuum propels the prosthetic forward, initiating swing phase. In swing phase, the residuum decelerated, meaning the prosthesis has a greater angular velocity than the residuum. This causes the residuum to rotate in clockwise direction, relative to the socket.

It is clear that from 0% to about 20% of the GC, the angular motion in coronal plane increased from 0° to a maximum value of 4.5° (Figure 5.3b). This is equivalent to that the VRS consistently

rotated in anti-clockwise direction according to Figure 5.3b, suggesting the residuum was engaging with the medial side of the socket. Beyond this point, there was a divergence of responses until TS phase (45% of GC), such that six sessions indicated a plateau in the angular displacement, while the other indicated the continued rotation until late stance phase. From this point onwards, the angular motion in sagittal plane increase until approximately 60% of GC, suggesting an anti-clockwise rotation of the residuum relative to socket according to Figure 5.3b. In swing phase, the angular motion was restored to the original value observed at 0% of GC.

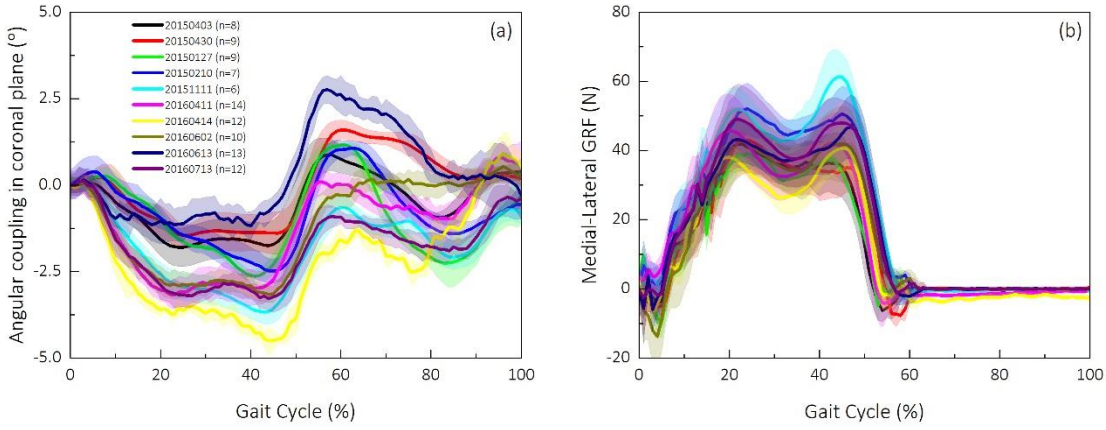

Figure 5.19: (a) Angular motion in coronal plane, over a GC across 27 months (b) medial-lateral component of GRF, obtained from the knee disarticulation participant.

To facilitate the biomechanical explanation of the angular motion in coronal plane, medial-lateral component of GRF (Figure 5.19b) was used, as it represents the principle loading the coronal plane at ground interface. As shown in Figure 5.19, the medial-lateral GRF increases from 0N at 0% of GC to a peak value of approximately 42N at 20% of GC, acting medially to the foot. This medial-directed force was further transferred proximally to the prosthetic, which caused the anti-clockwise rotation of the socket. In relative terms, the residuum rotated clockwise, so its proximal end was closer to the medial side of the socket brim. From TS phase to the end of the stance, the increase of the angular motion in coronal plane could be explained by the decrease of the of the medial-lateral component of GRF. This in effect, acts to restore the residuum angular position relative to the socket.

Up to 1.5° of residuum angular displacement relative to socket was observed in transverse plane, as shown in Figure 5.20. During most of the stance phase, the angular motion stayed at a value close to zero and it only began to change during wing phase. It is worth noting that the angular motion in transverse plane, contained in 10 data collection sessions, were small, comparing to that in the sagittal plane and coronal plane.

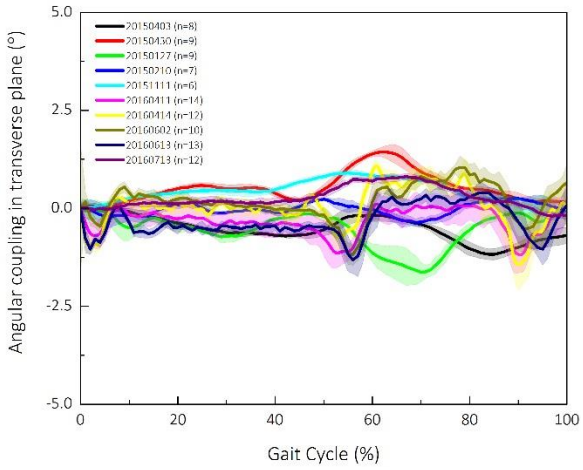

Figure 5.20: Angular motion in transverse plane, over a GC across 27 months

From 0% of GC to approximately 20% of GC, there is a decrease in axial length, suggesting the residuum has been 'pushed into' the socket (Figure 5.21). It is followed by restoration of the axial length from 20% of GC to approximately 30% of the GC (mid-stance). As the gait progresses from mid-stance to TS (50% of GC), the axial length further decrease, suggesting the residuum has been further 'pushed-into the socket. During the rest of the GC, the axial length recovers to its original length seen at 0% of GC. During a complete cycle, a maximum peak to peak value of 35mm was obtained over a period of two years (10 sessions).

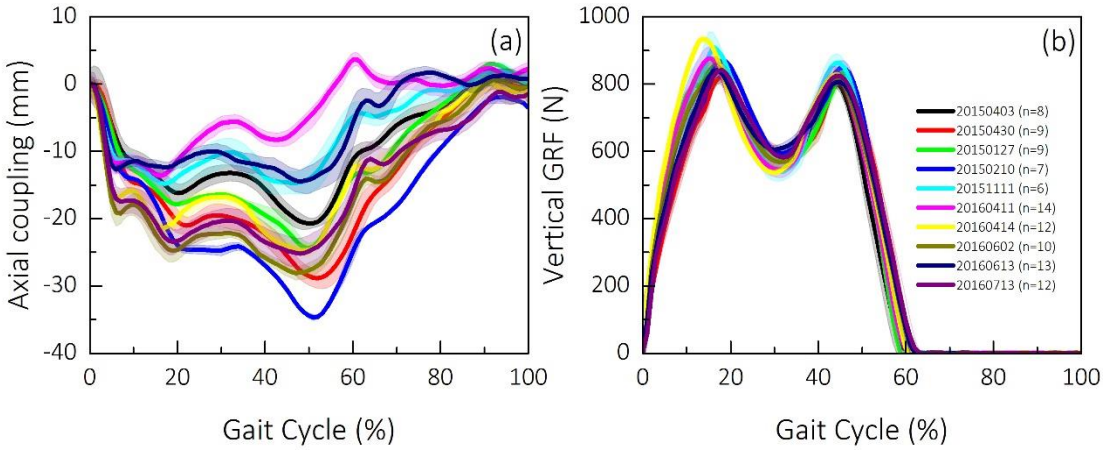

Figure 5.21: Axial length in transverse plane, over a GC across 27 months

The dynamic axial length (Figure 5.21) profile loosely resembles the shape of vertical component of GRF. As gait initiated, the axial length shortened as the participant's centre of mass dropped rapidly, reflecting on the increase of vertical component of GRF from 0N to approximately 850N. This created a greater force between KPC and HJC, acting to shorten the axial length. The restoration of the axial length between 20%-30% of GC may be associated with the decrease of vertical GRF. During TS phase (30-50% of GC), the axial length shortens

further as vertical GRF further increase to aid the heel rise and limb propulsion. It started to recover in late stance phase as the vertical component of GRF diminished rapidly, preparing for swing phase. In swing phase, the angular acceleration of the prosthetic, acts to pull it away from the residuum, resulting in an increased axial length of the VRS.

Table 5.1: Mean (SD) of peak to peak values of angular motion and axial length from 10 data collection sessions, over a span of 27 months.

Session No.	Angular Motion (°)			Axial Length (mm)
	Sagittal Plane	Coronal Plane	Transverse Plane	
1 (n=8)	11.5 ± 0.6	2.7 ± 0.6	0.7 ± 0.2	22 ± 1.0
2 (n=9)	10.4 ± 0.4	3.1 ± 0.5	1.4 ± 0.4	32 ± 1.2
3 (n=9)	10.9 ± 0.5	3.9 ± 0.5	1.5 ± 0.4	27 ± 1.1
4 (n=7)	11.8 ± 0.6	3.5 ± 0.5	0.5 ± 0.4	35 ± 1.1
5 (n=6)	10.5 ± 0.2	3.7 ± 0.6	1.1 ± 0.5	17 ± 0.5
6 (n=14)	9.6 ± 0.5	4.0 ± 0.6	1.2 ± 0.2	18 ± 0.8
7 (n=12)	10.3 ± 0.3	5.5 ± 0.4	1.5 ± 0.3	24 ± 0.8
8 (n=10)	8.8 ± 0.4	3.7 ± 0.4	2.0 ± 0.2	29 ± 0.5
9 (n=13)	11.3 ± 0.4	3.7 ± 0.5	1.3 ± 0.4	14 ± 0.4
10 (n=12)	9.3 ± 0.5	3.4 ± 0.8	1.2 ± 0.4	25 ± 0.6

Intra-session repeatability

Table 5.1 shows the mean and SD of peak to peak values of angular and axial length, over a GC, obtained from 10 data collection sessions. Up to 0.6°, 0.6° and 0.5° of intra-session SD were obtained for angular motion in sagittal, coronal and transverse plane, respectively. While up to 1.2mm of intra-session, SD was obtained for axial length. Up to 0.75° and 1.08mm of intra-session SD was obtained on the angular motion and axial length, respectively, by Childress and Siebert [169]. Therefore, the absolute SD value is comparable to the only study using 3D motion capture system.

Table 5.2: Intra-session CMC for residuum motion obtained on level surface.

Session No.	R^2_{Intra}			
	Angular motion			Axial Length
	Sagittal plane	Coronal plane	Transverse plane	
1	0.998	0.986	0.786	0.994
2	0.988	0.980	0.771	0.996
3	0.995	0.985	0.745	0.994
4	0.991	0.980	0.793	0.992

Session No.	R^2_{Intra}			
	Angular motion			Axial Length
	Sagittal plane	Coronal plane	Transverse plane	
5	0.991	0.982	0.766	0.993
6	0.988	0.988	0.765	0.994
7	0.993	0.981	0.764	0.994
8	0.994	0.983	0762	0.994
9	0.992	0.982	0.759	0.996
10	0.989	0.980	0.756	0.994

With regards to the inter-session repeatability, Table 5.2 illustrates the R^2_{Intra} values, obtained in each of the test session. R^2_{Intra} value of at least 0.988, 0.980 and 0.859 were obtained for angular motion in sagittal, coronal and transverse plane, respectively. R^2_{Intra} value of at least 0.996 was obtained for axial length. Kutner et al. [244] suggested that the for the CMC value greater than 0.9, strong association can be found in the waveform. For the CMC value greater than 0.5 and less than 0.9, the correlation between each of the waveform can be defined as moderate. Therefore, strong correlation is found in the angular motion in sagittal and coronal plane. The appropriate intra-session repeatability observed for the angular motion in the sagittal plane may be attributed to a higher level of control. This was likely exercised by the remaining muscle in the residuum and at the hip, since the direction of progression is along the sagittal plane.

A reduction in CMC values were found in transverse plane, however, they were still above 0.5 threshold. In addition, strong correlation was also revealed in axial length in each of the session. Further comparison was made on the R^2_{Intra} obtained in this study and joint kinematics obtained in previous work. The highest R^2_{Intra} (up to 0.995) was reported in hip flexion-extension angle, which is comparable to 0.998 obtained for the angular motion in sagittal plane. The lowest R^2_{Intra} (up to 0.845) was reported in hip transverse rotation in previously work [242] and this matches well with the lowest value obtained for angular motion in transverse plane, obtained in this study. It is then evident that the repeatability of the 3D motion obtained at residuum/socket interface was comparable to those obtained for joint kinematics [242].

Inter-session repeatability

Up to 10.4°±0.9°, 3.7°±0.7° and 1.2°±0.4° of inter-session mean and SD were obtained across all data collection sessions for angular motion (Figure 5.22) in sagittal, coronal and transverse plane, respectively. While an inter-session mean (±1SD) of 24mm±6mm were obtained for axial

length across 10 data collection sessions. It is worth noting that some of the inter-session SD is higher than the intra-session SD. This is particular evident in sagittal and coronal plane of angular motion, as well as axial length. This is likely due to the variation in socket fitting induced from the change in stump volume.

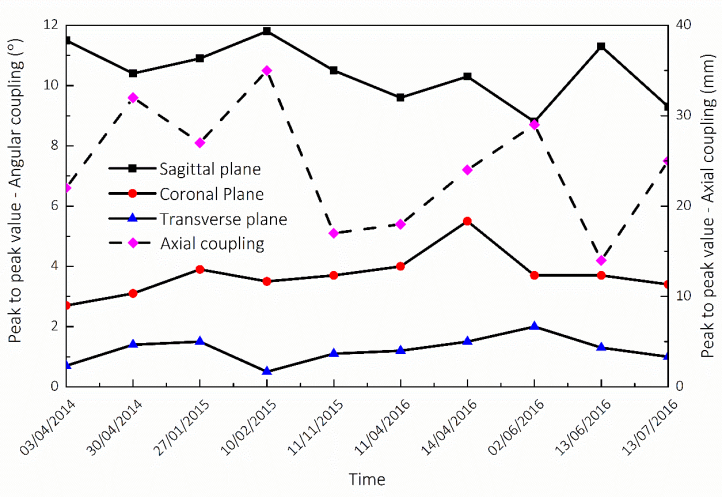

Figure 5.22: Peak to peak value of residuum/socket interface angular motion and axial length.

Approximately 0.991 of inter-session CMC value (Table 5.3) was obtained in sagittal plane, which is comparable with the intra-session CMC value. It should be noted that the intra-session repeatability was not affected by the error in marker placement. With same level of repeatability achieved in the inter-session results, this demonstrates the inconsistency in marker placement, across different session, was minimal. In addition, the angular motion value obtained in sagittal plane is robust by using the technique proposed.

Table 5.3: Inter-session CMC for 3D motion at residuum/socket interface obtained on level surface.

*Angular motion in coronal plane results from session 3, 4 and 6 were removed.

** Axial length results from session 5, 6 and 9 were removed

Total No. Session	R^2_{Inter}			
	Angular motion			Axial Length
	Sagittal plane	Coronal plane	Transverse plane	
10	0.991	0.753	0.481	0.755
7*	0.991	***0.976***	0.475	0.765
7**	0.992	0.797	0.469	***0.924***

A reduction in inter-session CMC value was obtained for the angular motion in coronal and transverse plane (first row of Table 5.3), compared with the intra-session CMC. In order to investigate the possible cause of this. Two more analysis of inter-session repeatability were

performed (2nd and 3rd row of Table 5.3). Results obtained in Session 3, 4 and 6 were removed and inter-session CMC was re-calculated. This was to investigate the reason causing the reduction in CMC for angular motion in coronal plane. The CMC value increased to 0.976 (highlighted with Bold in Table 5.3) with the removal of results from the three sessions. Similarly, the inter-session CMC value for axial length has increased from 0.755 to 0.924 with the removal of three sessions' results. Mathematically, it can be explained by the existence of two distinctive waveforms in both angular motion in coronal plane and axial length, as detailed in the results section (Figure 5.19a and Figure 5.21a). Inter-session CMC values of up to 0.987, 0.871 were obtained for hip joint angle in sagittal and coronal plane [242]. This is comparable to the value obtained in the current study.

Inter-session CMC value less than 0.5 was obtained in transverse plane, suggesting the poor waveform repeatability when comparing the results across different sessions. Similar findings were obtained in hip joint angle in transverse plane [242], as mentioned in the previous study (CMC value of 0.529). The low CMC value in transverse plane could be potentially explain by its lower value and lack of consistent pattern of the waveform. In addition, for the Codamtoion motion analysis system, the Y co-ordinate (or the medial-lateral component) was calculated based on triangulation which would potentially be subjected to error due to lighting etc. in the gait laboratory (Section 3.1.1). So far, the appropriate intra- and inter-session repeatability has been demonstrated on the overall waveform.

Analysing the change in residuum motion over time

Table 5.4 illustrates the mean and SD value of the 3D motion obtained in 2015 and 2016. It is worth noting that no significant difference was found when comparing both angular and axial motion obtained between the two years. It should be noted that the participant was using the same prosthetic limb during all tests. Prior to any test, a senior prosthetist verified the alignment of the prosthetic limb and each test conducted on approximately similar time of the day. The similar test condition mentioned above could potentially attributed to the similar results obtained between 2015 and 2016.

Table 5.4: Mean and SD of the 3D motion obtained in 2015 and 2016.

Year	Angular motion			Axial Length
	Sagittal plane	Coronal plane	Transverse plane	
2015	11.0±0.6	3.4±0.5	1.0±0.4	26.6±7.3
2016	9.9±0.9	4.1±0.8	1.4±0.3	22.0±6.0

Year	Angular motion			Axial Length
	Sagittal plane	Coronal plane	Transverse plane	
p value	0.0526	0.1357	0.1114	0.3081

It is worth noting that the knee disarticulation participant has gained 10kg of weight from early 2015 to late 2016. However, this has been reflected on the neither angular motion, nor axial length results. Further to this, the limb volume fluctuation during the course of a may also contributed to the change in the 3D motion at the socket interface.

5.4.3 Walking with different speeds

As mentioned Section 2.5.3, the optimal performance of the prosthetic device, in terms of joint loading, is walking speed dependent. If excessive relative motion exist between the residuum and socket, extra energy expenditure may be spent as a result of this motion. Therefore, the in-depth understanding of the residuum motion, at different walking speed, is critical. The section presents the results obtained by performing protocol A6 (Section 5.3.1).

Walking speed

To sessions were carried out to investigate the effect of walking speed on the residuum/socket interface kinematics. Figure 5.23 shows the walking speed obtained in the two sessions. Walking speed of up to 1.16±0.02m/s, 1.38±0.01m/s and 1.62±0.02m/s were obtained when walking cadence is controlled at 80BPM, 100BPM and 120BPM, respectively. It is also worth noting that when comparing each of the two walking speed, the differences obtained in each of the two walking speed are statistically significant (all p=0.00).

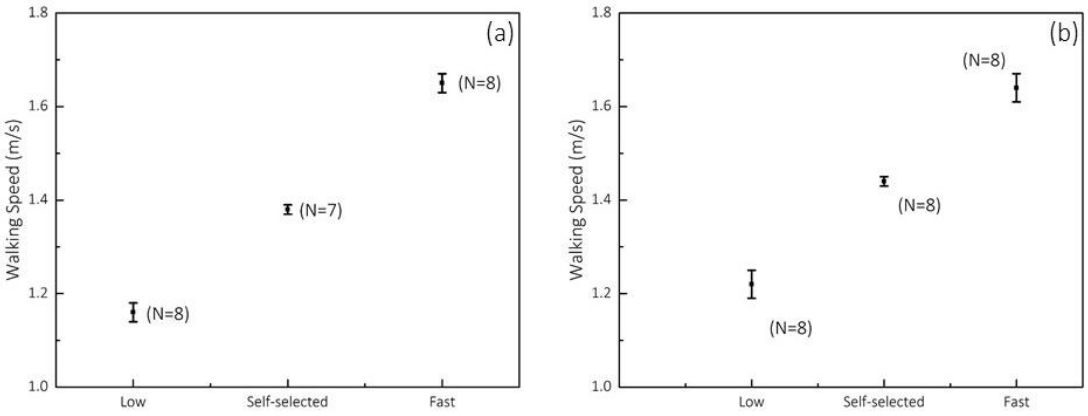

Figure 5.23: Mean and one SD of the three different walking speeds observed in Session 1 and Session 2.

Interface angular motion

It is worth noting that the generic trend, the increase of angular motion during stance and the restoration in swing phase, was observed in Figure 5.24a and Figure 5.25a matches with the test results presented in Figure 5.18a.

It is evident that, in early stance phase to mid-stance phase of the GC (approximately 10-30% of GC), a reduction of angular motion was observed as walking speed increases in both test sessions, as shown in Table 5.5. In the meantime, peak braking forces (Figure 5.24b) of up to -115N±8N, -105±12N, -121±19N in session 1 and 123N±5N, 134N±7N, 126N±23N in session 2, were obtained for slow, self-selected and fast walking speed, respectively. These findings imply that an increase in walking speed did not affect the peak braking force in early stance phase. Therefore, no direct association was found between peak braking force measured at the ground interface and residuum socket interface angular motion during 10-30% of GC. It is likely that, when walking at either slow or unnatural speeds, more effort may be needed to control stability during early stance to achieve foot flat.

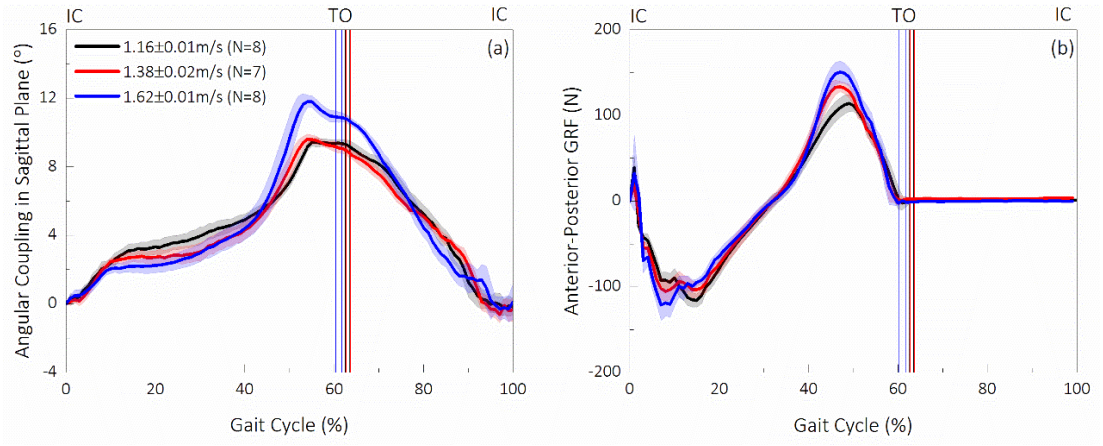

Figure 5.24: (a) Residuum/socket interface angular motion in sagittal plane, over a GC and (b) anterior-posterior component of GRF, over a GC, obtained when walking at slow, self-selected and fast walking speed in session 1.

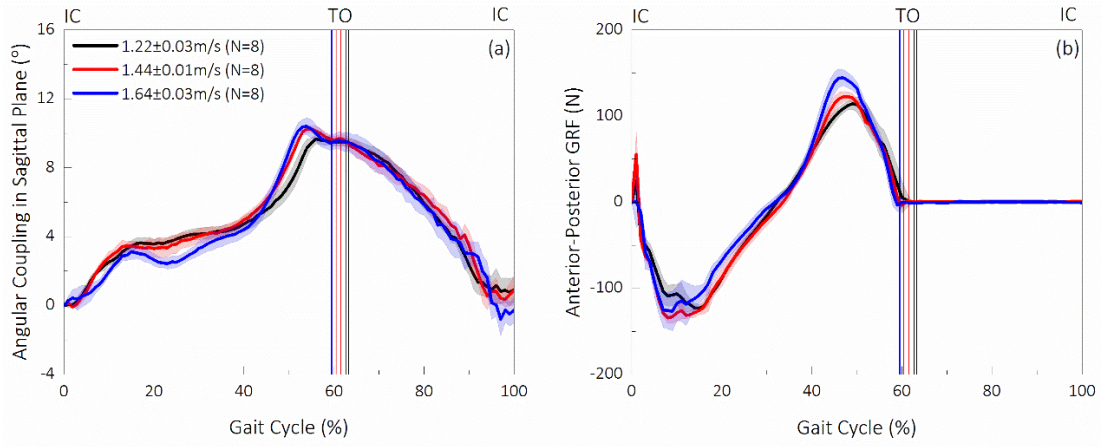

Figure 5.25: (a) Residuum/socket interface angular motion in sagittal plane, over a GC and (b) anterior-posterior component of GRF, over a GC, obtained when walking at slow, self-selected and fast walking speed in session 2.

As gait progress to late stance phase, a peak to peak value was reached at approximately 55% of GC and the increase in walking speed led to the increase of this peak to peak value in both sessions, shown in Table 5.5. In the meantime, up to 114N±9N, 133N±7N, 150N±13N (Session 1) and 114±5N, 122±5N, 144±9N (Session 2) of peak propulsion force was obtained at ground interface when walking at slow, self-selected and fast walking speed. This suggests that the increase in walking speed led to the increase in peak propulsion force in late stance phase. Therefore, association may exist between the peak force obtained at ground interface and peak residuum/socket interface angular motion. This is likely due to the extra hip muscle activation to propel the limb forward to initiate the swing phase.

Table 5.5: Residuum socket angular motion obtained during 10-30% of GC and peak to peak value obtained over a GC.

Session No.	10-30% of GC (°)			Peak to peak value (°)		
	Slow	Self-selected	Fast	Slow	Self-selected	Fast
1	3.3 ± 0.2 (n=8)	2.7 ± 0.3 (n=7)	2.2 ± 0.2 (n=8)	9.4 ± 0.3	9.6 ± 0.4	11.8 ± 0.2
2	3.6 ± 0.3 (n=8)	3.3 ± 0.3 (n=8)	2.7 ± 0.2 (n=8)	9.5 ± 0.2	10.3 ± 0.2	10.4 ± 0.3

The angular motion in coronal plane (Figure 5.26a and Figure 5.27a) decreased from 0-20% of GC, while between 20-45% of GC there were two distinct responses, namely, one in which the angular motion remained constant while the other continue to decrease. It is evident that the temporal profile observed in coronal plane matches well with that shown in Figure 5.19.

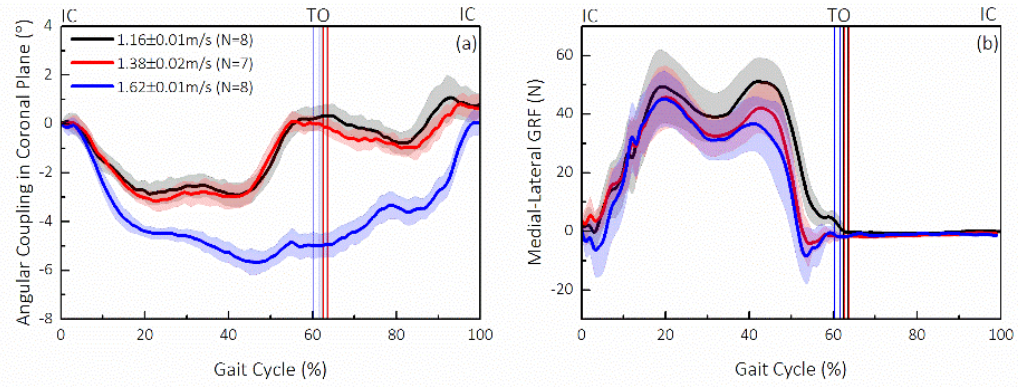

Figure 5.26: (a) Residuum/socket interface angular motion in coronal plane, over a GC and (b) medial-lateral component of GRF, over a GC, obtained when walking at slow, self-selected and fast walking speed in session 1.

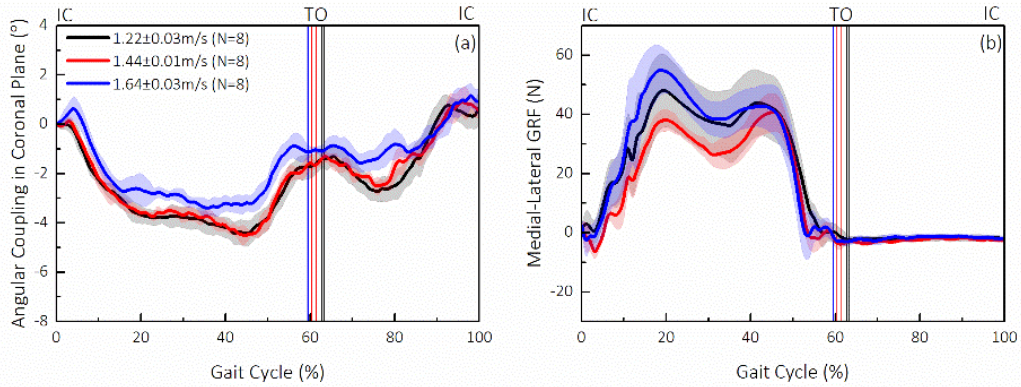

Figure 5.27: (a) Residuum/socket interface angular motion in coronal plane, over a GC and (b) medial-lateral component of GRF, over a GC, obtained when walking at slow, self-selected and fast walking speed in session 2.

In data collection session 1, as shown in Table 5.6, the increase in walking speed resulted in an increase in the peak to peak value of angular motion in coronal plane. However, in data collection session 2, there was little difference in the angular motion in coronal plane when walking at slow and self-selected speeds. In addition, when walking at the fast speed, a decrease in angular motion was observed. Therefore, in this case, it is not clear whether the increase or decrease in walking speed would affect the angular motion in the coronal plane. More investigations are needed as the Session 1 results do not fully align with those in Session 2.

Regarding to the forces experienced at ground interface, as shown in Table 5.6, the increase in walking speed has led to the decrease of peak medial-lateral GRF and increase in angular motion in coronal plane, in session 1. No association was identified between the walking speed and peak medial GRF in session 2. It is worth noting that, neither walking speed, nor ground reaction force magnitude has a marked effect on the peak to peak angular motion in coronal plane.

In session 1, the increase in walking speed has led to the increase in angular motion in coronal plane. This is like due to the design of the knee disarticulation socket. The supra-condylar socket was designed to suspend the residuum at both medial and lateral femoral epicondyle and distal region of the residuum, such that the distal end acts like a pivot point for the femur. In addition, in the proximal region, there was no design features, such as the higher or lower socket brim, built on the socket. Therefore, the femoral movement at proximal region is not restricted. Based on these factors, the control of the residuum, in the medial-lateral plane, sometimes relies on voluntary control. It is also worth noting that the increase in walking speed did not lead to the increase in angular motion in coronal plane, this is likely due to the change in socket fit, limb height and change in gait.

Table 5.6: Residuum socket angular motion obtained during 10-30% of GC and peak to peak value obtained over a GC.

Session No.	Peak to peak value of angular motion (°)			Peak medial GRF (N)		
	Slow	Self-selected	Fast	Slow	Self-selected	Fast
1	2.9 ± 0.5 (n=8)	3.0 ± 0.4 (n=7)	5.7 ± 0.3 (n=8)	51 ± 8	46 ± 10	45 ± 9
2	4.5 ± 0.4 (n=8)	4.6 ± 0.4 (n=8)	3.4 ± 0.4 (n=8)	48 ± 12	41 ± 6	55 ± 8

In general, the increase in walking speed has resulted in the increase in angular motion in both sagittal and coronal plane with the exception of session 2 in coronal plane. It is known that socket was fitted and fabricated based on statically capturing the residuum shape and volume. During the socket fitting process, the muscle activation pattern, compared with the activation pattern during dynamic walking is different. When walking at increased speed, increased muscle activation together with the increased joint range of motion could results in the increase angular engagement of the residuum with the socket. To author's best knowledge, this is the first study investigating the residuum motion relative to socket under different walking speed condition. In addition, it is envisaged that such socket performance under varied walking speed could be used to aid the development of adaptive socket system, stabilising the residuum inside the socket.

Axial length

It is worth noting that zero axial length was defined using the absolute axial length (distance between the hip joint centre and prosthetic knee pivot centre) obtained at IC (Figure 5.28a and Figure 5.29a). This eliminates the effect of data baseline variation caused by the variability in socket alignment [73]. Using values at IC for normalisation is also consistent with gait analysis kinematics reporting convention [51] and could also provide natural separation of the loads experienced by the residuum during the stance and the swing phase. Despite these advantages, the state of the residuum in axial direction relative to socket was not informative (whether it is in compressive state or a tensile state). Therefore, in each of these figures, dot-dash lines are plotted together with the dynamic data to indicate the axial length measured during standing, in relation to the values measured at IC. Researchers and prosthetist could then use the value obtained at standing (a known weight bearing state) to evaluate the axial length during dynamic walking.

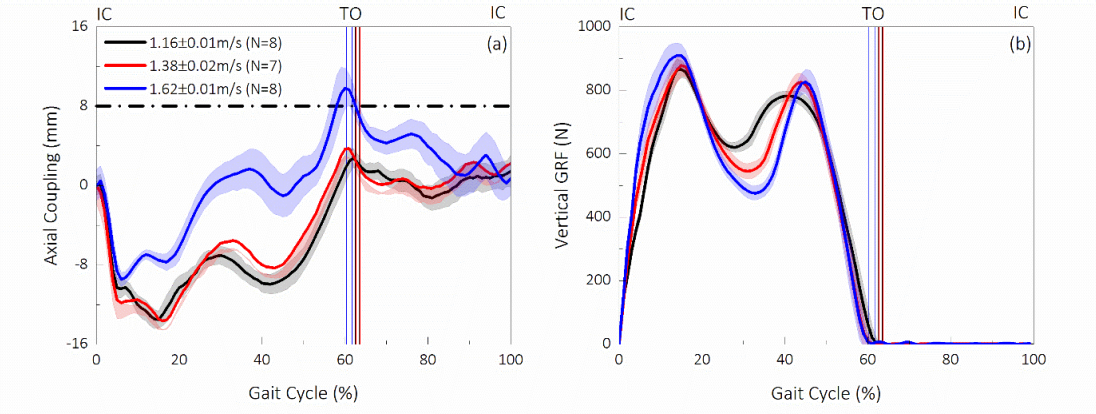

Figure 5.28: Residuum/socket interface axial length, over a GC and (b) vertical component of GRF, over a GC, obtained when walking at slow, self-selected and fast walking speed in session 1.

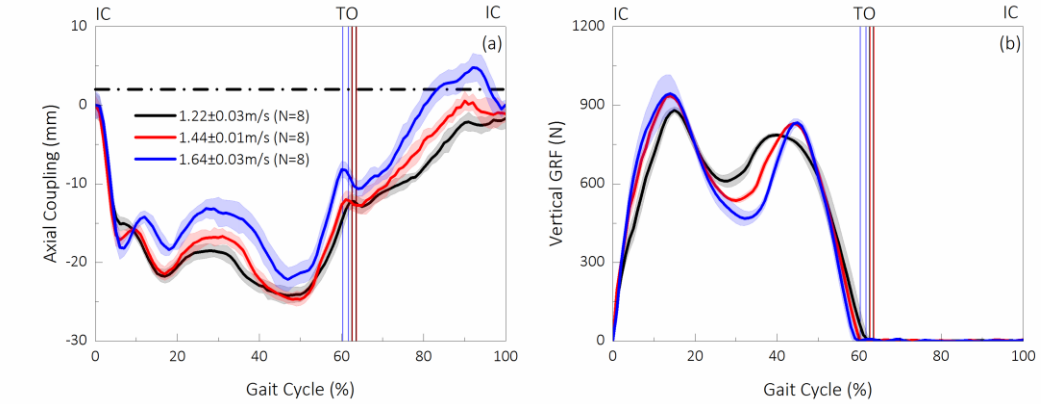

Figure 5.29: Residuum/socket interface axial length, over a GC and (b) vertical component of GRF, over a GC, obtained when walking at slow, self-selected and fast walking speed in session 2.

There was a general decrease in axial length during most of the stance phase until approximately 45-50% of GC where it was returned. However, in the two sessions, a divergence in response during swing phase. In the first session, as shown in Figure 5.28, when walking at slow and self-selected walking speeds, the axial length was stabilised whereas it decreased when walking at the fast speed. In the second session, as shown in Figure 5.29a, the axial length continued to decrease during the swing phase. Table 5.7 shows the peak to peak axial length and vertical component of GRF when walking at slow, self-selected and fast walking speed. Regardless of walking speed, higher axial length was obtained in Session 2 compared with the value obtained in Session 1, in all walking speed (p=0.00). This is likely due to the change in socket fitting over the period between Session 1 and Session 2.

Table 5.7: Residuum socket axial length obtained and peak vertical component of GRF, obtained over a GC.

Session No.	Peak to peak value of axial length (mm)			Peak vertical GRF		
	Slow	Self-selected	Fast	Slow	Self-selected	Fast
1	17 ± 1 (N=8)	18 ± 1 (N=7)	19 ± 1 (n=8)	866 ± 27	877 ± 34	909 ± 35
2	24 ± 1 (n=8)	25 ± 1 (n=8)	26 ± 1 (n=8)	881 ± 12	934 ± 10	944 ± 40

It is also worth noting that the increase in walking speed resulted in an increase in axial length, as well as the peak vertical component of GRF (Table 5.7). As the vertical component of GRF increased, there was a transfer from ground interface to socket interface, resulting in more compressive force would be exerted by the socket to the residuum. This in turn, 'pushed' the residuum more into the socket. In addition, the increase in axial length when walking speed could also be reflected on the knee joint angular and hip joint angular in sagittal plane. As shown in Figure 4.8, the increase in walking speed has led to the increase in knee flexion angle (pre-swing phase), whereas little change in hip joint angle was observed (Figure 4.9). The increased knee joint kinematics could potentially result in the tensile load exerted on the socket interface. Indeed, an increased axial couple was observed during swing phase.

During mid-stance phase of GC (approximately 30% of GC), axial length values of up to -7mm, -6mm and 1mm were obtained in Session 1, with corresponding Session 2 values of up to -19mm, -17mm, and -14mm were obtained in Session 2, when walking at slow, self-selected and fast walking speed, respectively. Therefore, the increase in walking speed resulted in a decrease in axial length at mid-stance phase. This can be explained by examining, the corresponding vertical component of GRF with values of up to 631N, 547N and 492N in Session 1, and 625N, 535N and 482N in Session 2. Therefore, the increase in walking speed led to the decrease in vertical component of GRF in mid-stance, suggesting reduced vertical force is transferred to the residuum/socket interface. This in turn, could have potentially contributed to the decrease in axial length, during mid-stance.

At approximately 60% (Session 1) and 92% (Session 2) of GC, axial length was higher than the value obtained during standing. This corresponds to the lengthening of the residuum compared with the state experienced at standing. For Session 1 particularly, the lengthening of the residuum could results in the reduction of toe clearance with the ground, thereby increase the risk of trip. By monitoring the axial length towards the end of the stance phase, it is envisaged that, control strategy could be applied to actively adapt the movement of the socket such that

there is enough clearance between the prosthetic foot and the ground. Therefore, limb safety could be improved when walking at different speed.

5.4.4 Walking on different terrains

As mentioned in Section 4.4, walking on different terrains have led to the change in knee joint moment in mid-stance phase, hip joint moment and power change in the early stance phase. These could potentially affect the socket interface kinematics as the knee joint and the hip joint forms the distal and proximal end of the socket interface, respectively. The section presents the results obtained by performing protocol A6 (Section 5.3.1).

As a general trend exhibited on all terrains, relative to the value observed at IC, the angular motion gradually increase to peak values of approximately 9°, followed by the decrease in swing phase, which was subsequently restored back to 0° for the next IC (Figure 5.30a - Figure 5.32a).

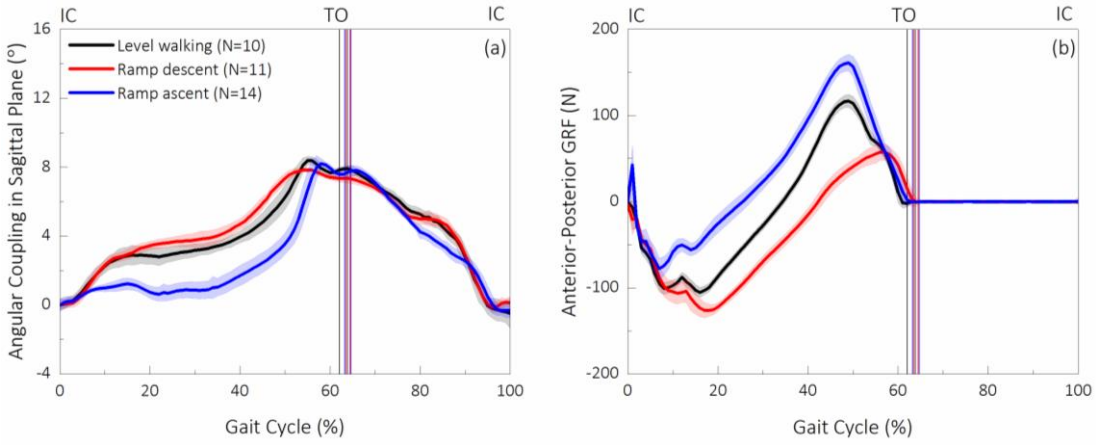

Figure 5.30: (a) Residuum/socket interface angular motion in sagittal plane, over a GC and (b) anterior-posterior component of GRF, over a GC, obtained when walking on level, descending and ascending surfaces, in session 1.

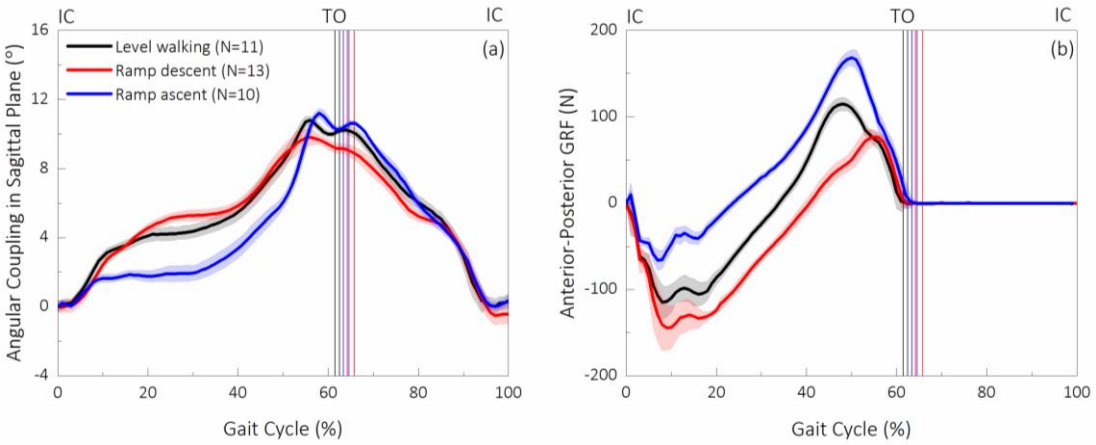

Figure 5.31: (a) Residuum/socket interface angular motion in sagittal plane, over a GC and (b) anterior-posterior component of GRF, over a GC, obtained when walking on level, descending and ascending surfaces, in session 2.

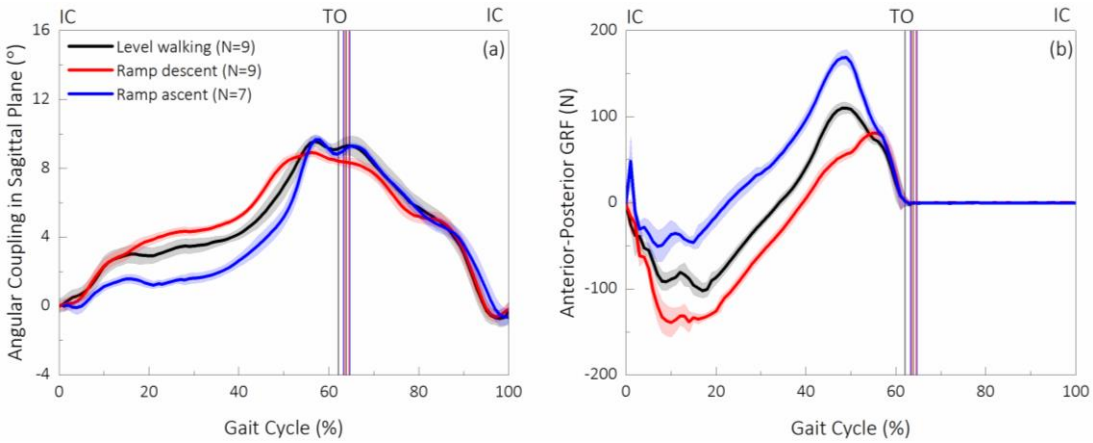

Figure 5.32: (a) Residuum/socket interface angular motion in sagittal plane, over a GC and (b) anterior-posterior component of GRF, over a GC, obtained when walking on level, descending and ascending surfaces, in session 3.

Two critical phases during GC, namely, early stance and TS phase, were chosen to explain the biomechanics at the residuum/socket interface in sagittal plane. Table 5.8 illustrates the amount of angular motion sagittal plane, during both critical phases, across the three test sessions. During early stance phase, in comparison to values obtained during level walking, there was an increase of approximately 1° of angular motion (p=0.00) and a decrease of up to 2° while walking on the descending ramp and the ascending ramp (p=0.00), respectively. After mid-stance phase, there was a decrease of angular motion (up to 1°) when walking on the descending ramp with corresponding increase of angular motion (up to 4°) on the ascending ramp.

Table 5.8: Amount of angular motion in sagittal plane, obtained in early stance and TS phase of the GC.

Session No.	Angular Motion (°) Early stance			Angular Motion (°) TS		
	Level	Descent	Ascent	Level	Descent	Ascent
1	3 ± 0.3	4 ± 0.3	1 ± 0.2	5 ± 0.1	4 ± 0.2	7 ± 0.2
2	3 ± 0.3	4 ± 0.3	0 ± 0.3	6 ± 0.2	5 ± 0.2	9 ± 0.3
3	3 ± 0.2	4 ± 0.3	2 ± 0.3	5 ± 0.2	4 ± 0.2	7 ± 0.3

As a general trend observed on all terrains, the anterior-posterior GRF (Figure 5.30b - Figure 5.32b) decreased from values close to zero at IC to a peak negative value during early stance phase, suggesting a braking force was exerted from the ground interface to the foot. In mid-stance phase to TS phase, there is an increase in anterior-posterior GRF and a peak was reached in TS phase, suggesting that a propulsive force was exerted by the ground to the foot.

The peak braking and propulsive obtained when walking on level, descending and ascending surfaces, across three sessions are illustrated in Table 5.9. When walking on level surface, no statistical difference as found in peak braking and propulsive force ($p>0.05$). This suggests that, with controlled walking cadence, the peak anterior-posterior GRF was consistent over three test sessions. When walking on the descending ramp, statistical difference were found in both peak braking and propulsive force in test Session 1 & 2 ($p=0.00$) and Session 1 & 3 ($p=0.00$). When walking on the ascending ramp, statistical difference was found in peak braking force between each of the two sessions ($p=0.00$), however, no statistical difference was found in peak propulsive force ($p>0.05$). The differences in peak anterior-posterior GRF found, when walking on non-level surface, could be potentially explained by the change in socket fit due to volume fluctuation.

When compare to level walking, in early stance phase, there was an observed increase in peak braking force (up to 38N) was observed on the descending ramp ($p=0.00$), with a corresponding decrease in peak propulsive force (up to 59N) on the ascending ramp ($p=0.00$). The former finding could potentially contribute to the increased amount of angular motion in the sagittal plane (up to 1°), due to the extra effort needed at the residuum/socket interface to achieve foot-flat, achieving limb stability. The decrease in the braking force, when walking on the ascending ramp could then be associated with the decreased angular motion (up to 2°), as less effort is needed during the early stance phase.

Table 5.9: Peak braking and propulsion force obtained when walking on level, descending and ascending surfaces, across three sessions.

Session No.	Peak braking force (N) Early stance			Peak propulsion force (N) TS		
	Level	Descent	Ascent	Level	Descent	Ascent
1	-105 ± 6	-126 ± 8	-78 ± 13	+117 ± 7	+58 ± 9	+161 ± 10
2	-115 ± 20	-145 ± 26	-66 ± 11	+115 ± 7	+77 ± 8	+169 ± 9
3	-102 ± 9	-140 ± 5	-46 ± 8	+110 ± 6	+81 ± 6	+169 ± 8

In addition to the observation on the GRF, an increased ($p=0.01$) concentric knee joint power (0.13W/kg(m/s)) was observed when walking on the descending ramp, compared with the value obtained on the ascending ramp (0.03W/kg(m/s)) (Figure 4.15c). Similar finding was obtained on the hip joint power (Figure 4.17c), in early stance phase, as a greater ($p=0.00$) concentric hip joint power was observed when walking on descending ramp, compared with the value obtained on the ascending ramp. This further confirms that at the knee and hip joint,

more work is done in early stance phase to stabilise the limb when walking on the descending ramp, comparing work need when walking on ascending ramp. Both could potentially lead to the increase in angular motion in when walking on descending ramp in early stance phase.

In TS phase, in comparison to the values obtained during level walking, a decrease (p=0.00) in peak braking force (up to 94N) and a corresponding increase (p=0.00) in propulsive force (up to 103N) when walking on ascending ramps, respectively. The former could potentially contribute the reduction in the angular motion (up to 1°), as less effort is need in propel the limb for the initiation of the swing phase. By contrast, the increase in the peak propulsive force could potentially results in the increase amount of angular motion in the sagittal plane, as extra effort is needed to propel the limb forward when walking up the ramp, initiating the swing phase.

With respect to the results obtained in gait analysis, in the transition between the braking and propulsive phase (at approximately 30% of GC), higher (p=0.00) knee joint power was observed when walking on the ascending ramp, compared with the value obtained on the descending ramp. Same findings was observed in hip joint power, as a greater hip joint power was observed at approximately 30% of GC when walking on ascending ramp, compared with the value obtained when walking on the descending ramp. Both findings in joint powers confirmed that more work was done at both knee and hip joint level, which could lead to the increased angular motion in sagittal plane when walking on ascending ramp after mid-stance phase.

At IC, as a general trend, the angular motion in coronal plane (Figure 5.33a - Figure 5.35a) gradually decreased and reached a negative peak value at approximately 20-50% of GC, suggesting the residuum had engaged with the medial region of the socket. It was then restored over the remainder of the GC and reached values seen at IC. The medial-lateral component of GRF (Figure 5.33b - Figure 5.35b) increased from IC to a peak positive value at approximately 20% of GC and maintained during 20-45% of GC. It then deceased and reached zero at TO. It is evident that positive forces were observed during most of the stance phase, suggesting a medial – directed forced was exerted from the ground interface to the residuum/socket interface, pushing the socket to rotate towards the medial region of the residuum.

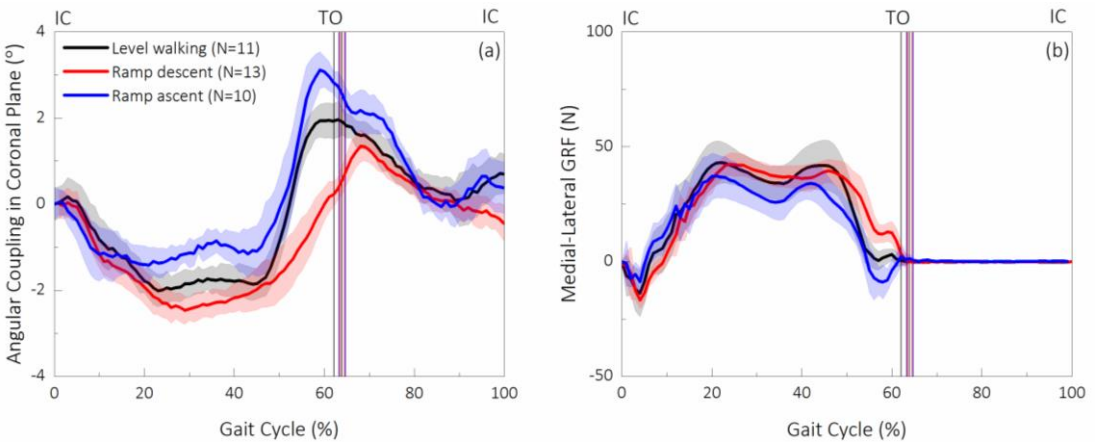

Figure 5.33: (a) Residuum/socket interface angular motion in coronal plane, over a GC and (b) medial-lateral component of GRF, over a GC, obtained when walking on level, descending and ascending surfaces, in session 1.

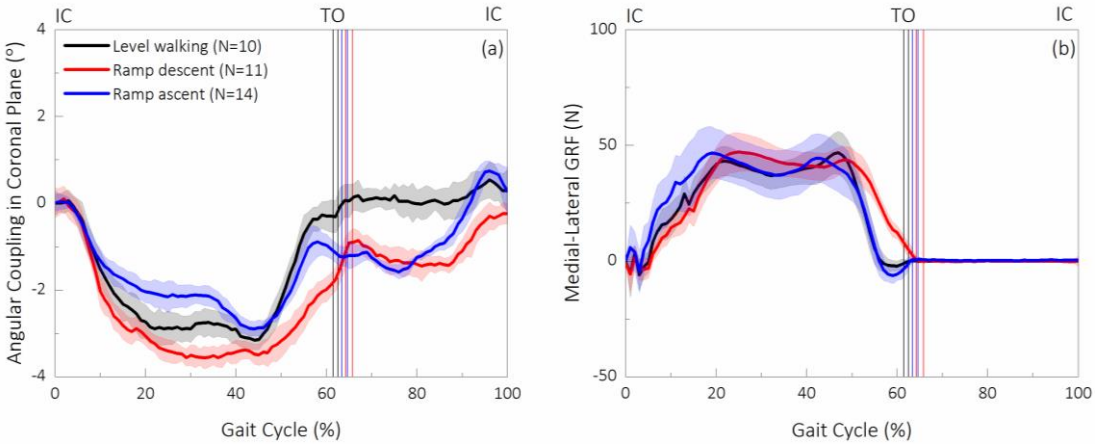

Figure 5.34: (a) Residuum/socket interface angular motion in coronal plane, over a GC and (b) medial-lateral component of GRF, over a GC, obtained when walking on level, descending and ascending surfaces, in session 2.

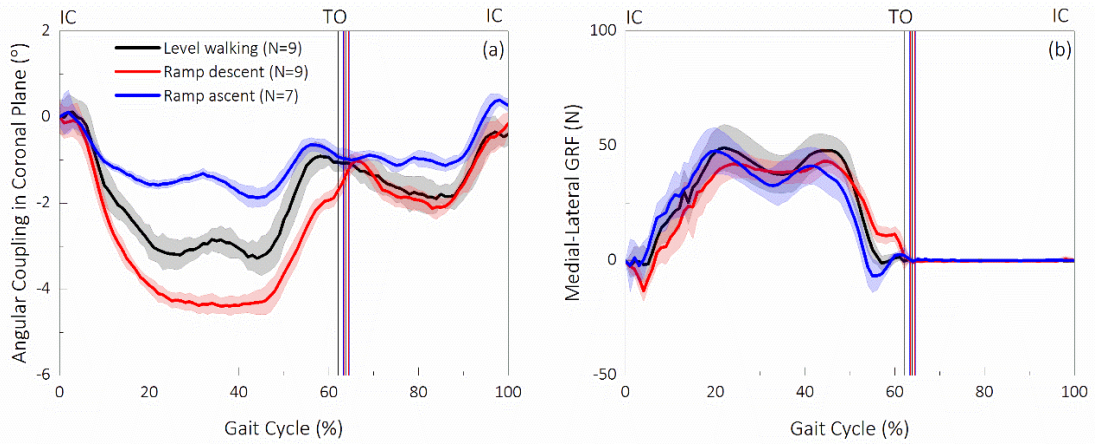

Figure 5.35: (a) Residuum/socket interface angular motion in coronal plane, over a GC and (b) medial-lateral component of GRF, over a GC, obtained when walking on level, descending and ascending surfaces, in session 3.

Table 5.10: Peak to peak value of angular motion in coronal plane and medial-lateral component of GRF, obtained when walking on level, descending and ascending surfaces, across three sessions

Session No.	Angular Motion (°)			Peak vertical GRF (N)		
	Level	Descent	Ascent	Level	Descent	Ascent
1	4 ± 0.3	4 ± 0.2	3 ± 0.3	43 ± 7	42 ± 8	37 ± 11
2	3 ± 0.3	4 ± 0.2	4 ± 0.2	47 ± 7	47 ± 8	46 ± 11
3	3 ± 0.3	4 ± 0.1	2 ± 0.2	50 ± 8	43 ± 5	48 ± 9

In general, up to 4° of angular motion was observed in the coronal plane when walking on level, ascending and descending surfaces (Table 5.10). It is worth noting that, no significant difference ($p>0.05$) in angular motion was found between each of the two sessions when walking on the descending ramp. When walking level surface, higher peak to peak angular motion was found in session 1, comparing to the value obtained in Session 2 ($p=0.00$) and Session 3 ($p=0.00$). In addition, no difference was found in angular motion between Session 2 and Session 3 ($p>0.05$). When walking on the ascending ramp, difference was found in angular motion between each of the two sessions ($p<0.05$). Therefore, it can be summarised that, more inter-session variation was observed when walking on the ascending ramp, than the variation observed on the descending ramp.

It is also worth noting that, in two out of three test sessions (Session 1 and Session 3), a greater ($p=0.00$) angular motion in coronal plane was observed when walking on descending ramp, compared with the value obtained on the ascending ramp. In test Session 2, no significant difference ($p>0.05$) was observed in angular motion in coronal plane when walking on the descending and ascending ramp.

When comparing the medial-lateral GRF in Session 1, a greater ($p=0.00$) peak medial-lateral GRF was evident when walking on the descending ramp, compared with that on the ascending ramp. In addition, no difference was found in the peak medial-lateral GRF in Session 2, when comparing the value obtained on the ascending and descending ramp. Both findings match with the peak to peak value observed in angular motion, namely, higher peak to peak angular motion was observed when walking on descending ramp, compared to the value obtained on ascending ramp in Session 1; no difference found in the angular motion when walking on ascending and descending ramp in Session 2.

With respect to the temporal profile observed between 40% and 60% of GC, two distinctive wave pattern was observed between test Session 1 and Session 2 & 3. In Session 1, the angular

motion increases and passed beyond the zero point to a positive region on the graph. In both test Session 2 and 3, the angular motion also increases, however to a value just below the zero reference point. This is likely due to the effect of donning of the socket and volume fluctuation of the residuum, which both could in turn influence the capability of the femoral rotation of coronal plane relative to the socket. Furthermore, in Session 3, two peaks (at 24% and 44% of GC on level surface and at 20% and 44% of GC on descending surface) in the angular motion profile were evident in Figure 5.35a. Correspondingly, two peaks in the temporal profile of the medial-lateral GRF was also evident when walking on level and descending ramp. A plateau region was observed between 20% and 46% of GC when walking on the ascending ramp. Correspondingly, the angular motion temporal profile remained unchanged between 24% and 46% of GC. These findings suggest that the motion of residuum relative to socket in coronal plane could be associated with the forces experienced at ground interface.

Axial length

As a general trend for each terrain, the axial length (Figure 5.36a - Figure 5.32a) decreased during the first 20% of GC and subsequently recovered as gait progresses to mid-stance phase. It was followed by a further decrease of the axial length during 30-55% of GC. During the remainder of the GC, it restored to its original value seen at IC at 100% of GC. The vertical component of GRF obtained when walking on each of the three terrains is presented in Figure 5.36b - Figure 5.32b, across the three test sessions.

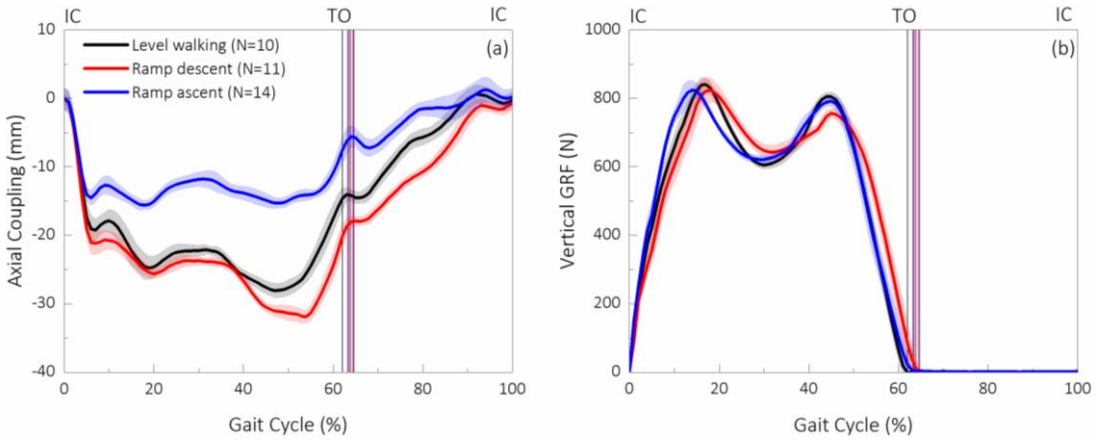

Figure 5.36: (a) Residuum/socket interface axial length, over a GC and (b) vertical component of GRF, over a GC, obtained when walking on level, descending and ascending surfaces, in session 1.

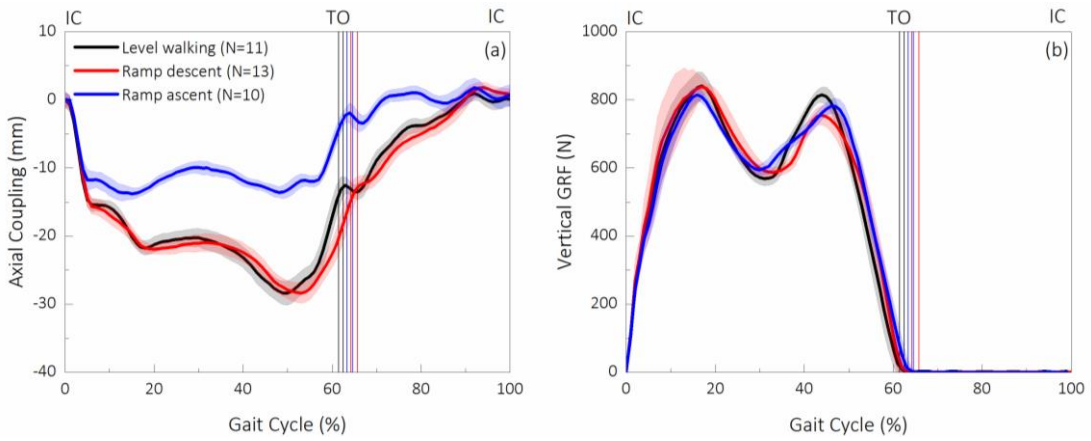

Figure 5.37: (a) Residuum/socket interface axial length, over a GC and (b) vertical component of GRF, over a GC, obtained when walking on level, descending and ascending surfaces, in session 2.

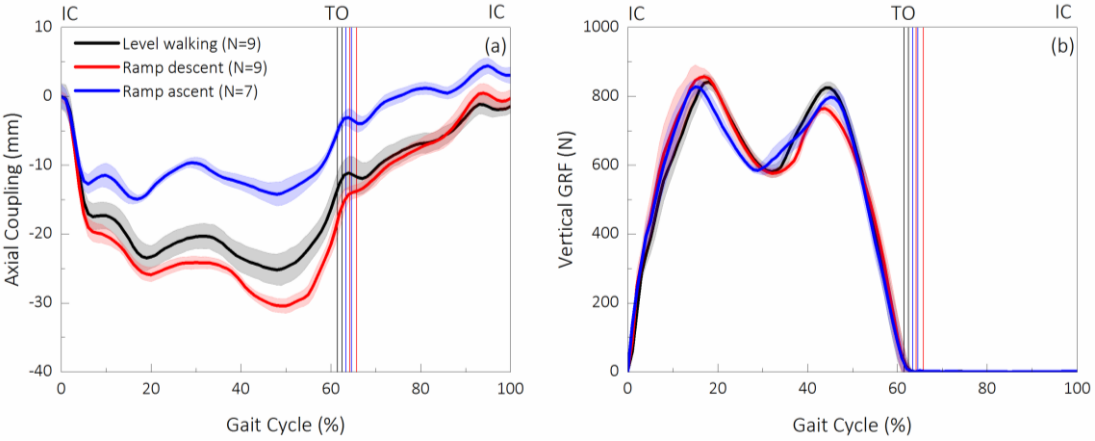

Figure 5.38: (a) Residuum/socket interface axial length, over a GC and (b) vertical component of GRF, over a GC, obtained when walking on level, descending and ascending surfaces, in session 3.

When evaluating the inter-session repeatability from Table 5.11, no significant difference ($p>0.00$) was found in axial length between test Session 1 and Session 2 on level surface, also test Session 1 and Session 3 on ascending surface. Apart from the two above-mentioned scenario, significant differences (all $p=0.00$) were found in each of the two session, on different terrains. With respect of the effect of terrain on the axial length, a greater ($p=0.00$) axial length was observed when walking on the descending ramp, compared with the value obtained on the ascending ramp, in all sessions.

Table 5.11: Peak to peak value of axial length and peak value of vertical component of GRF, obtained when walking on level, descending and ascending surfaces.

Session No.	Axial Length (mm)			Peak vertical GRF (N)		
	Level	Descent	Ascent	Level	Descent	Ascent
1	28 ± 1	32 ± 1	15 ± 0	841 ± 20	824 ± 34	824 ± 28
2	28 ± 1	28 ± 1	12 ± 0	840 ± 40	837 ± 29	815 ± 18
3	25 ± 2	30 ± 0	15 ± 1	841 ± 20	856 ± 23	828 ± 19

As previously mentioned, the decrease of axial length in most of the stance phase could be associated with the compressive force exerted from the ground interface to the residuum socket interface. With respect to peak to peak values, comparing the value obtained when walking on level surface, an increase in axial length values up to 5mm were observed when walking on the descending ramp, with corresponding decrease of up to 18mm on the ascending ramp. It is also clear in Table 5.11, in comparison to the peak vertical component of GRF obtained during level walking, reductions of the vertical component of GRF were observed in session 1 and 2 when walking on both descending and ascending surfaces. This suggests that the magnitude of the axial length was not directly associated with the peak value of GRF.

With respect to the effect of terrain on joint kinetics observed on the descending surface (Figure 4.17), a greater hip eccentric power and concentric was observed at approximately 50% and 58% of GC, respectively, compared with values obtained on ascending surface. This suggests that a greater work was produced at hip joint level to propel the limb forward and initiate the swing. This may explain the greater axial movement of the residuum when walking on descending ramp during TS phase, compared with the movement on ascending ramp. In addition, other factors should be considered such as anterior-posterior component of GRF, interface friction properties and variation in muscle activation when walking on different terrains etc.

5.4.5 Walking with different prosthetic ankle settings – hydraulic resistance

Study has shown the link between the increased socket comfort and the adaptation of prosthetic ankle on ramped surface (Section 2.5.3). The in-depth understanding of the mechanism behind this relationship would benefit from the study of interface biomechanics. The section presents the results obtained by performing protocol A7 (Section 5.3.1).

Walking on a descending ramp

It is evident that the temporal profile of the angular motion in sagittal plane (Figure 5.39 and Figure 5.40) aligns with the profile obtained in previous walking sessions (Section 5.4.4).

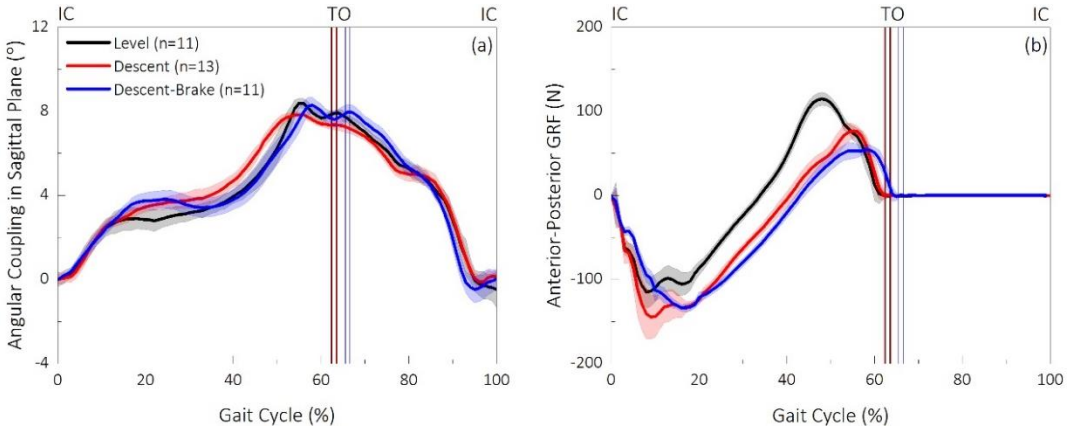

Figure 5.39: (a) Residuum/socket interface angular motion in sagittal plane and (b) anterior-posterior component of GRF, over a GC, obtained when walking on the descending ramp in session 1. Elan foot was set to normal and braking mode.

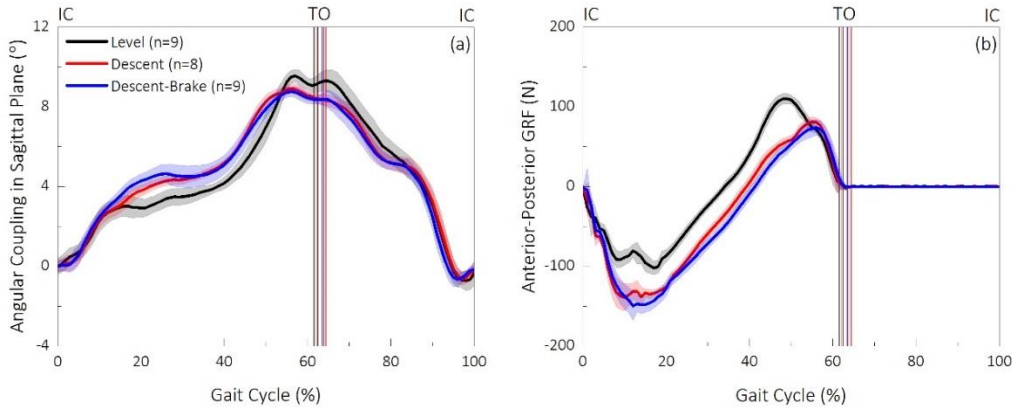

Figure 5.40: (a) Residuum/socket interface angular motion in sagittal plane and (b) anterior-posterior component of GRF, over a GC, obtained when walking on the descending ramp in session 2. Elan foot was set to normal and braking mode.

It is worth noting that, no significant difference ($p>0.05$) was found in angular motion obtained in the two test sessions (Table 5.12). It is therefore evident that both temporal profile and peak to peak value of angular motion was consistent over the two test sessions. However, higher ($p=0.00$) angular motion was obtained, regardless of the foot setting, in test Session 2 compared with the values obtained in test Session 1. This suggested that a greater variability was evident when walking on a descending ramp, over the two test sessions.

It is evident that, in both sessions, a greater angular motion in sagittal plane was evident ($p<0.05$) when braking setting was activated, comparing to the value obtained when the brake setting was de-activated. It is worth noting that the difference mentioned here is low (up to 0.5°), therefore it should be treated cautiously when try to interpret it clinically. When

comparing the peak braking force achieved in early stance phase, a higher value was obtained when brake was de-activated in session 1 compared with the value obtained when the brake was de-activated. A greater residuum motion relative to socket, with braking setting, may suggest the increased involvement of prosthetic limb, comparing to the value obtained with normal setting. This could potentially lead to the increase of loading symmetry. Using this teaches, the prosthetic component can be assessed based on the biomechanics at the socket interface.

Table 5.12: Peak to peak value of angular motion and peak value of braking force, obtained when walking on level surface, descending surface with brake setting de-activated and activated.

Session No.	Angular motion (°)			Peak braking force (N)		
	Level	Descent	Descent--Brake	Level	Descent	Descent--Brake
1	2.9 ± 0.2	3.6 ± 0.2	3.9 ± 0.2	-118 ± 7	-145± 9	-140 ± 10
2	3.0 ± 0.1	4.3 ± 0.1	4.8 ± 0.2	-101 ± 7	-135 ± 8	-153 ± 9

It is evident that the temporal profile of the angular motion in coronal plane (Figure 5.41 and Figure 5.42) aligns with the profile obtained in previous walking sessions (Section 5.4.4).

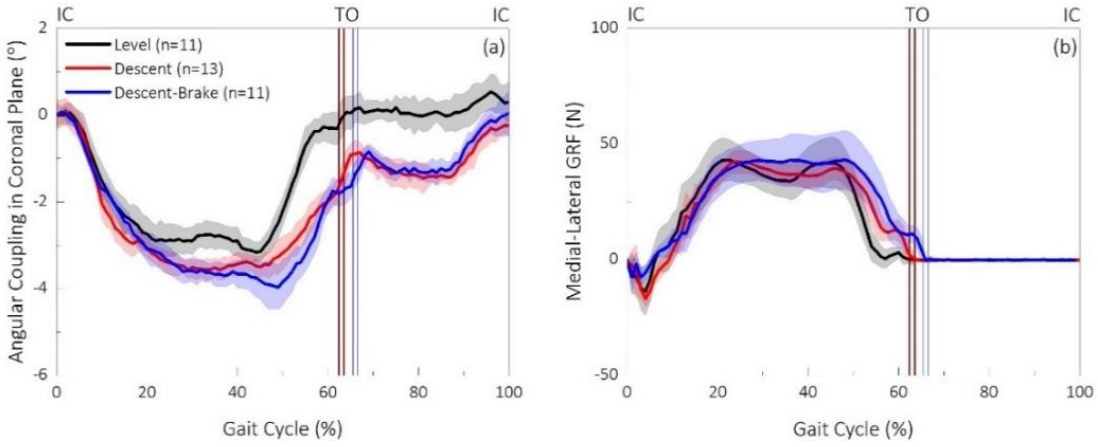

Figure 5.41: (a) Residuum/socket interface angular motion in coronal plane and (b) medial-lateral component of GRF, over a GC, obtained when walking on the descending ramp in session 1. Elan foot was set to normal and braking mode.

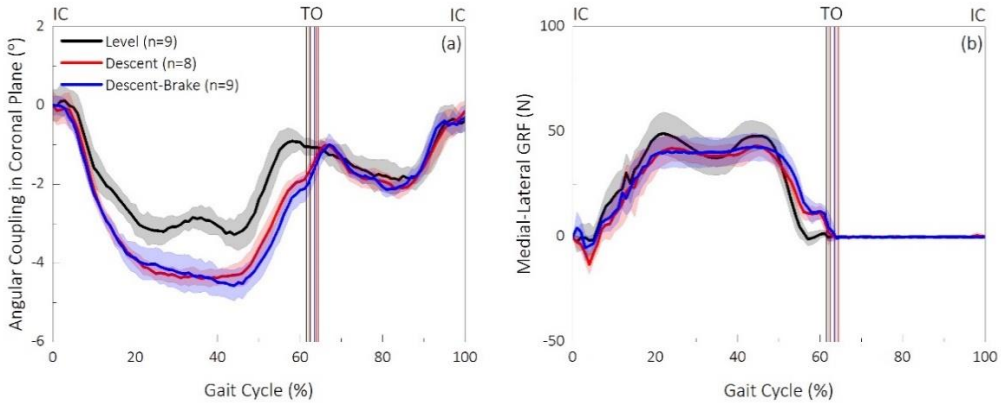

Figure 5.42: (a) Residuum/socket interface angular motion in coronal plane and (b) medial-lateral component of GRF, over a GC, obtained when walking on the descending ramp in session 2. Elan foot was set to normal and braking mode.

Regardless of terrain and hydraulic foot settings, higher angular motion in coronal plane (Table 5.13) was obtained in Session 2, compared with the values obtained in Session 1.This level of variation could potentially result from the design of the socket. No feature was built on the socket to restrict the motion of the residuum in coronal plane. With the test sessions conducted on different days, this could results in a larger variation in the residuum in coronal plane. It is also worth noting, under each test condition there was no statistical difference between the medial-lateral GRF obtained in both test sessions. Socket designs for knee disarticulation amputee is particularly challenging. It requires the stabilisation of the LFE and MFE at distal region, at the same time, moderate restriction needs to be applied at proximal regions to maintain the stability in coronal plane. Using this technique, the stability in coronal plane could be potentially correlated to the angular motion in coronal plane, providing prosthetist guidance at socket fitting stage.

Table 5.13: Peak to peak value of angular motion and peak value of medial-lateral GRF, obtained when walking on level surface, descending surface with brake setting de-activated and activated.

Session No.	Angular motion (°) – coronal plane			Peak medial-lateral GRF (N)		
	Level	Descent	Descent--Brake	Level	Descent	Descent--Brake
1	3.0 ± 0.3	3.4 ± 0.3	4.0 ± 0.3	42 ± 5	42± 5	42 ± 8
2	3.4 ± 0.4	4.9 ± 0.3	5.2 ± 0.4	46 ± 5	41 ± 6	41 ± 5

Greater peak to peak angular motion in coronal plane was observed when brake setting was activated in both sessions ($p<0.05$), comparing to the value obtained with brake de-activation. When comparing the peak medial-lateral GRF, no significant change was observed when comparing the value obtained in both foot settings ($p>0.05$).

It is evident that the temporal profile of the axial length (Figure 5.43 and Figure 5.44) aligns with the profile obtained in previous walking sessions. It is also worth noting that, from IC to TO, similar axial length values were obtained with both foot settings, as indicated by the peak values in Table 5.14.

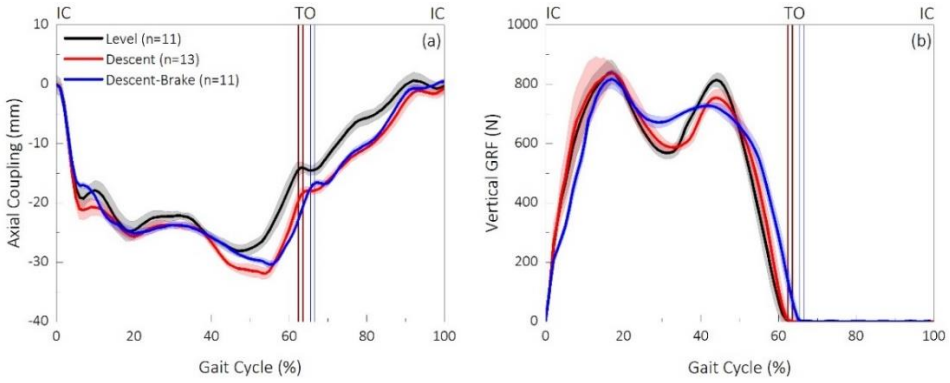

Figure 5.43: (a) Residuum/socket interface axial length and (b) vertical component of GRF, over a GC, obtained when walking on the descending ramp in session 1. Elan foot was set to normal and braking mode.

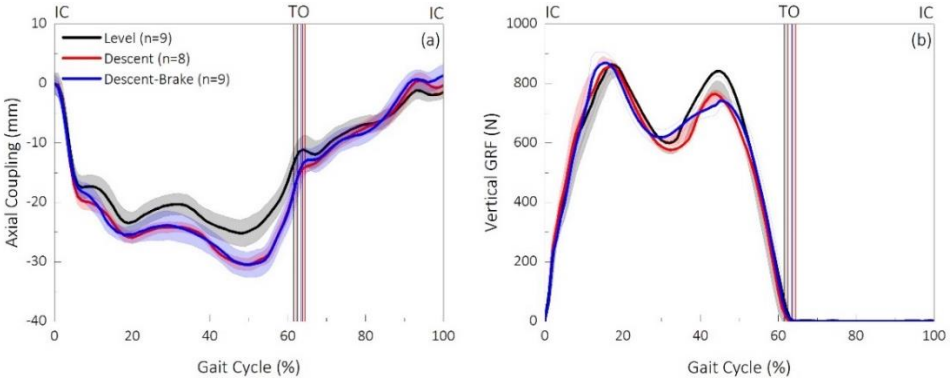

Figure 5.44: (a) Residuum/socket interface axial length and (b) vertical component of GRF, over a GC, obtained when walking on the descending ramp in session 2. Elan foot was set to normal and braking mode.

Table 5.14: Axial length and peak value of medial-lateral GRF at TS, obtained when walking on level surface, descending surface with brake setting de-activated and activated.

Session No.	Axial length (mm)			Vertical GRF (N)		
	Level	Descent	Descent--Brake	Level	Descent	Descent--Brake
1	27 ± 1	30 ± 1	31 ± 1	821 ± 20	782 ± 11	775 ± 10
2	23 ± 1	30 ± 1	30 ± 1	850 ± 15	781 ± 13	762 ± 11

When walking on a descending ramp with two hydraulic ankle settings, little change was observed in peak-to-peak axial length in stance phase (up to 0mm and 1mm in Table 5.14). However, it is not the case for the vertical GRF values, with brake activated, reduced ($p<0.05$) vertical GRF was observed comparing to the value obtained when the brake was de-activated. This may further suggest that, the increase in the vertical GRF (up to 19N), may not necessarily

induce the corresponding increase in axial length. This could potentially explained by the non-linear behaviour of the residuum tissue. The rate of increase in strain may not match the corresponding rate of increase in stress. In other word, a much greater load needs to be applied to the residuum to induce the same amount of tissue deformation at higher strains, comparing to that at lower strains. Therefore, when applying 780N of load (vertical GRF in Table 5.14) to the residuum, an additional 19N (induced from the braking setting) did not necessarily lead to the increase in the axial length. This may inform that, for a particular socket interface, there might be a threshold of the maximum axial movement under compression. This threshold can then be used as a parameter to assess the overall biomechanical performance of the socket interface.

When walking on an ascending ramp

It is evident that the temporal profile of the angular motion (Figure 5.45a and Figure 5.46a) matches well with the data obtained in Section 5.4.4. It is also worth noting that the hydraulic ankle setting did not change in peak to peak value of the angular motion value in sagittal plane (approximately 8°). When comparing the values obtained from IC to mid-stance phase (Table 5.15), assist setting has led to greater angular motion. Higher peak braking GRF was obtained assist setting was applied, comparing to the value obtained when assist setting was de-activated (Table 5.15). It is likely that the higher angular motion value in early stance phase, obtained when assist setting was applied, can be explained by the slight higher peak braking GRF.

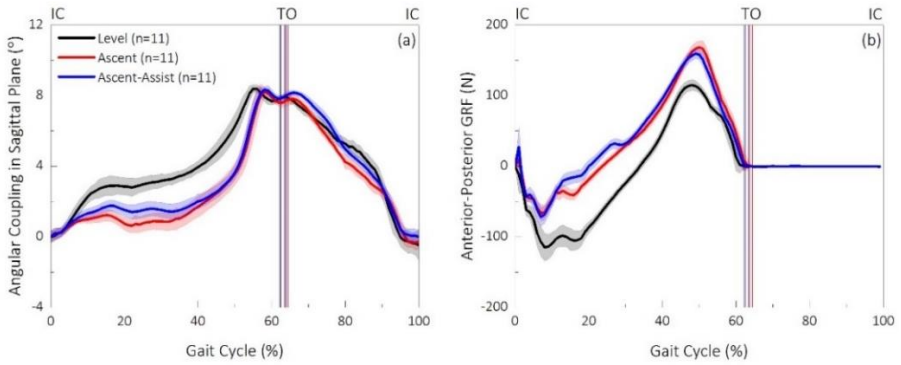

Figure 5.45: (a) Residuum/socket interface angular motion in sagittal plane and (b) anterior-posterior component of GRF, over a GC, obtained when walking on the ascending ramp in session 1. Elan foot was set to normal and braking mode.

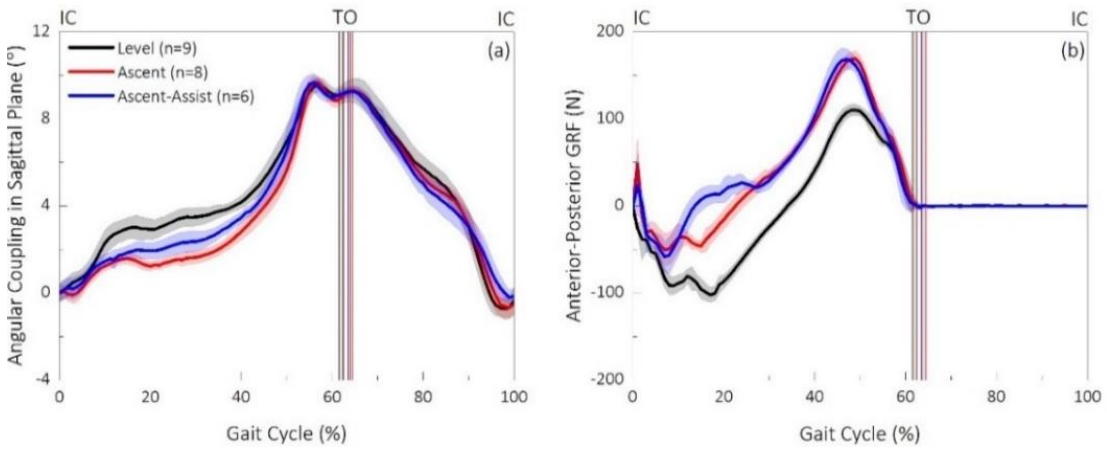

Figure 5.46: (a) Residuum/socket interface angular motion in sagittal plane and (b) anterior-posterior component of GRF, over a GC, obtained when walking on the ascending ramp in session 2. Elan foot was set to normal and braking mode.

Table 5.15: Peak to peak value of angular motion and peak value of braking force, obtained when walking on level surface, ascending surface with assist setting de-activated and activated.

Session No.	Angular motion (°) – sagittal plane			Peak braking GRF (N)		
	Level	Ascent	Ascent - Assist	Level	Ascent	Ascent - Assist
1	3.6 ± 0.2	1.0 ± 0.2	2.0 ± 0.3	99 ± 5	76 ± 9	70 ± 10
2	3.9 ± 0.3	2.5 ± 0.2	3.0 ± 0.2	118 ± 20	56 ± 8	46 ± 9

It is evident that the temporal profile of the angular motion in coronal plane (Figure 5.47a and Figure 5.48a) aligns with the profile obtained in previous walking sessions (Section 5.4.4).

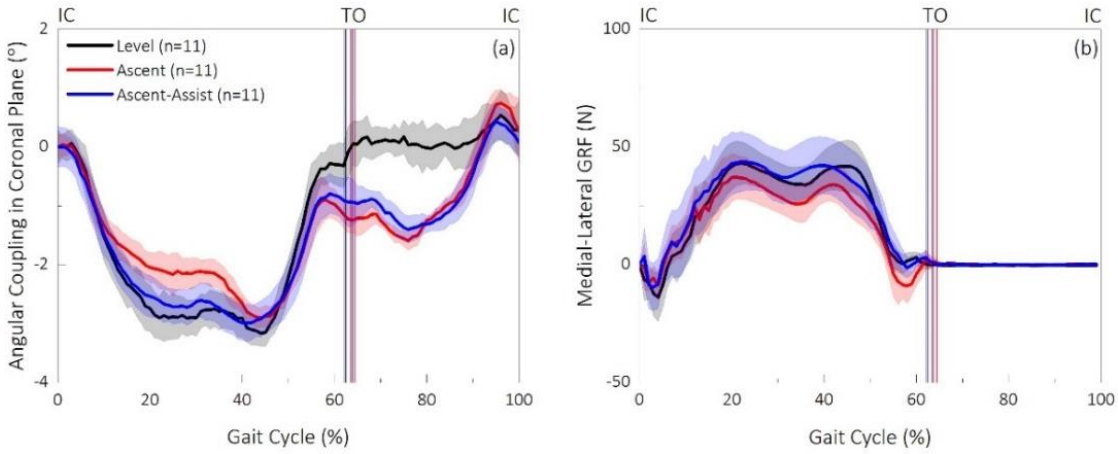

Figure 5.47: (a) Residuum/socket interface angular motion in coronal plane and (b) medial-lateral component of GRF, over a GC, obtained when walking on the ascending ramp in session 1. Elan foot was set to normal and braking mode.

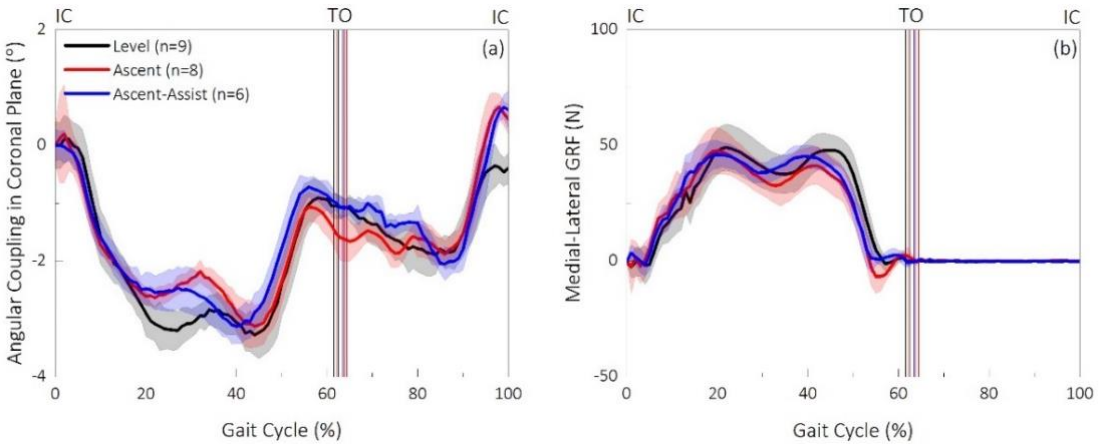

Figure 5.48: (a) Residuum/socket interface angular motion in coronal plane and (b) medial-lateral component of GRF, over a GC, obtained when walking on the ascending ramp in session 2. Elan foot was set to normal and braking mode.

Table 5.16: Peak to peak value of angular motion and peak value of medial-lateral GRF, obtained when walking on level surface, ascending surface with brake setting de-activated and activated.

Session No.	Angular motion (°) – coronal plane			Peak medial-lateral GRF (N)		
	Level	Ascent	Ascent-- Assist	Level	Ascent	Descent--Assist
1	3.1 ± 0.2	2.9 ± 0.2	3.0 ± 0.3	45 ± 5	32 ± 5	45 ± 4
2	3.3 ± 0.3	3.2 ± 0.1	3.2 ± 0.2	51 ± 5	49 ± 5	48 ± 4

It is evident that there is little difference found in the angular motion in coronal plane when assist was activated and de-activated (Table 5.16). However, when comparing the value obtained just before TS phase (approximately 36% of GC), an increase of up to 0.5° was found in the angular motion when assist setting was activated, comparing the value obtained the assist setting was de-activated. This phenomenon is particularly evident for the result obtained in session 1. This could be potentially explained by the greater medial-lateral GRF obtained when assist setting was activated (Table 5.16).

It is evident from Table 5.17 that a significant reduction in peak to peak axial length value was obtained when walking on the ascending terrain ($p<0.05$), comparing to the value obtained when walking on level surface. Walking on the ascending terrain has led to a decrease of peak vertical GRF ($p<0.05$), comparing to the value obtained when the assist setting was de-activated.

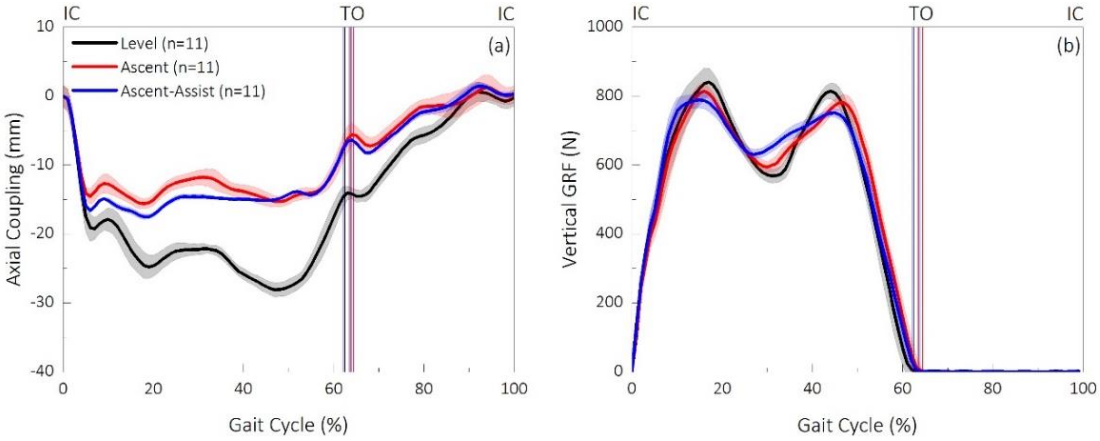

Figure 5.49: (a) Residuum/socket interface axial length and (b) vertical component of GRF, over a GC, obtained when walking on the ascending ramp in session 1. Elan foot was set to normal and braking mode.

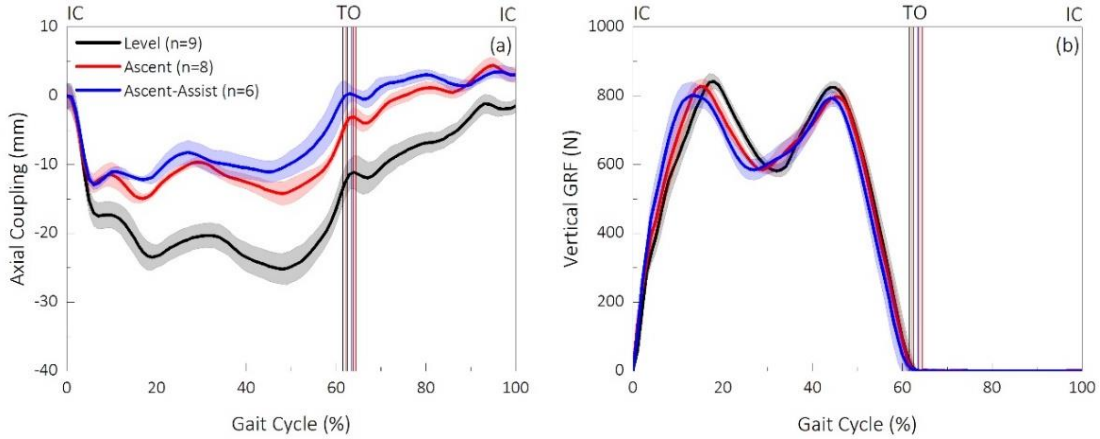

Figure 5.50: (a) Residuum/socket interface axial length and (b) vertical component of GRF, over a GC, obtained when walking on the ascending ramp in session 2. Elan foot was set to normal and braking mode.

Table 5.17: Axial length and vertical GRF obtained over a GC, when walking on level surface, ascending surface with assist setting de-activated and activated.

Session No.	Peak-to-peak axial length (mm)			Vertical GRF (N)		
	Level	Ascent	Ascent -- Assist	Level	Ascent	Ascent -- Assist
1	28 ± 1	17 ± 1	14 ± 1	849 ± 20	829 ± 11	799 ± 10
2	26 ± 1	14 ± 1	10 ± 1	852 ± 15	844 ± 13	815 ± 11

When comparing the peak to peak axial length obtained with two assist settings, no consistent trend was observed (Table 5.17) between session 1 and session 2. However, when comparing the value obtained at mid-stance phase of the GC, as shown in Table 5.18, greater axial length value was obtained when assist setting was applied, comparing to the value when assist setting was de-activated. It is also evident that, for session 1 in particular, greater vertical GRF was obtained when assist setting was applied, comparing to the value when it is de-activated. It is

likely that the increase in axial length could be associated with the greater loads in the axial direction.

Table 5.18: Axial length and vertical GRF obtained at mid-stance of GC, when walking on level surface, ascending surface with assist setting de-activated and activated.

Session No.	Axial length (mm) – mid-stance			Vertical GRF (N) – mid-stance		
	Level	Ascent	Ascent -- Assist	Level	Ascent	Ascent -- Assist
1	22 ± 1	12 ± 1	14 ± 1	583 ± 20	602 ± 11	654 ± 10
2	20 ± 1	9 ± 1	10 ± 1	601 ± 15	599 ± 13	598 ± 11

5.4.6 Walking with different prosthetic knees

As mentioned in 2.5.3, a greater knee flexor moment was achieved with a MKP, comparing with a mechanical knee, which could in turn alter the interface biomechanics. The section presents the results obtained by performing protocol A9 (Section 5.3.1).

From IC to just before TO, the angular motion in sagittal plane (Figure 5.51a) increases to up to 11° and 8°, respectively. During swing phase, the angular motion decreased such that it had restored to the value seen at IC.

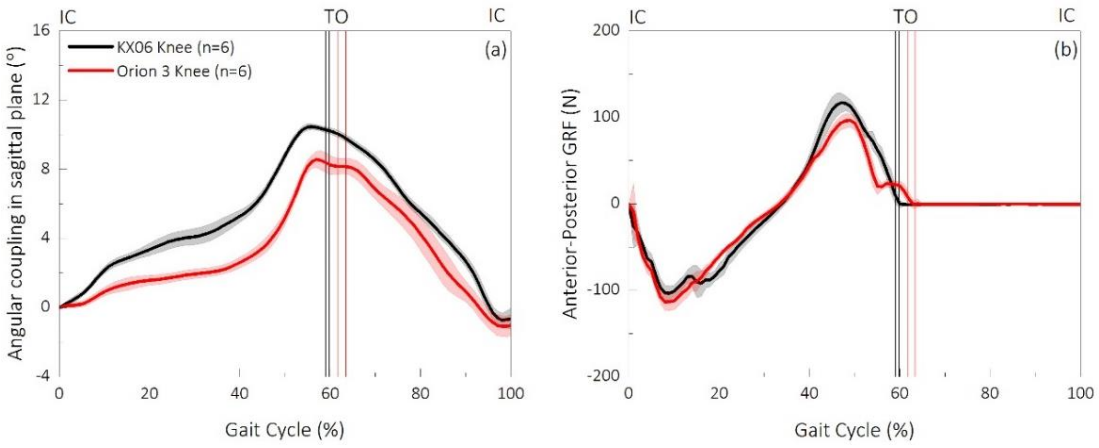

Figure 5.51: (a) Angular motion in sagittal plane and (b) anterior-posterior component of GRF, obtained over a GC. Participant was fitted with a polycentric and microprocessor controlled knee.

During early stance phase (approximately 10% of GC), peak braking forces of up to 103N and 97N were obtained when participant was fitted with a polycentric knee and MPK (Figure 5.51b), respectively. This suggested that similar braking forces were observed during early stance. At TS phase, peak propulsive forces were up to 117N and 96N. Comparing the value obtained when fitted with a polycentric knee, a reduction in peak to peak values of angular motion of up to 3° were observed, when fitted with a MPK. This may be associated the reduction in the anterior-posterior component of GRF in the TS phase.

From IC to approximately 20% of GC, the angular motion in coronal plane (Figure 5.52a) decreased from 0° to up to -2° and -3° when fitted with a polycentric knee and MPK, respectively. After 20% of GC, there was a divergence of response, with angular motion continuing to decrease until a peak value of -4° was obtained at about 43% of GC, when fitted with the polycentric knee. By contrast, the angular motion maintained a value of -2° from 20-50% of GC, when fitted with the MPK. This was followed by an increase of angular motion for the remainder of the stance phase. During swing phase, approximately 1° of fluctuation was observed.

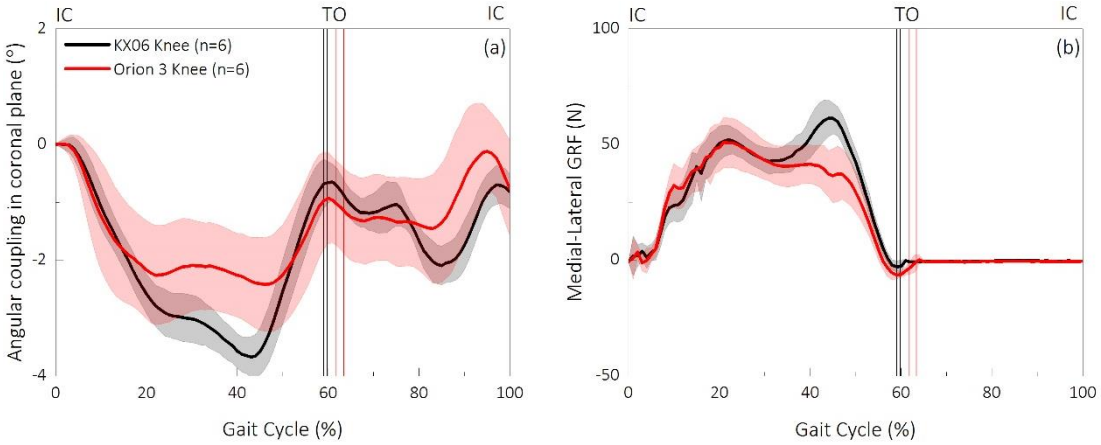

Figure 5.52: (a) Angular motion in coronal plane and (b) medial-lateral component of GRF, obtained over a GC. Participant was fitted with a polycentric and microprocessor controlled knee.

There was an increase of up to 49N in the medial force at approximately 20% of GC with a small decrease between 20-30% of GC (Figure 5.52b). From 30-50% of GC, when fitted with polycentric knee, the medial-lateral component of GRF increased to up to 61N. However, when fitted with a MPK, the medial-lateral component of GRF yielded a small decrease to a value of approximately 30N. During the remainder of the stance phase, the GRF decreased reaching zero at TO.

It is evident that, with the higher medial forces obtained at approximately 45% of GC (61N with polycentric knee and 30N with MPK), there was a corresponding higher angular motion (-4° with polycentric knee and -2° with MPK). This also suggests that the reduction in GRF may be associated with a reduction in angular motion in coronal plane.

From IC to approximately 20% of GC, axial length (Figure 5.53a) decreased from 0mm to approximately -15mm and -10mm when fitted with a polycentric and MPK, respectively. This was followed by an increase in axial length during 20-40% of GC. As gait progressed to the TS phase, the axial length further decreased with values of up to -15mm and -5mm obtained at 50% of GC. During the swing phase, the axial length restored to the value seen at IC. Peak to

peak values of up to 17mm and 10mm were obtained when the participant was fitted with polycentric and MPK, respectively.

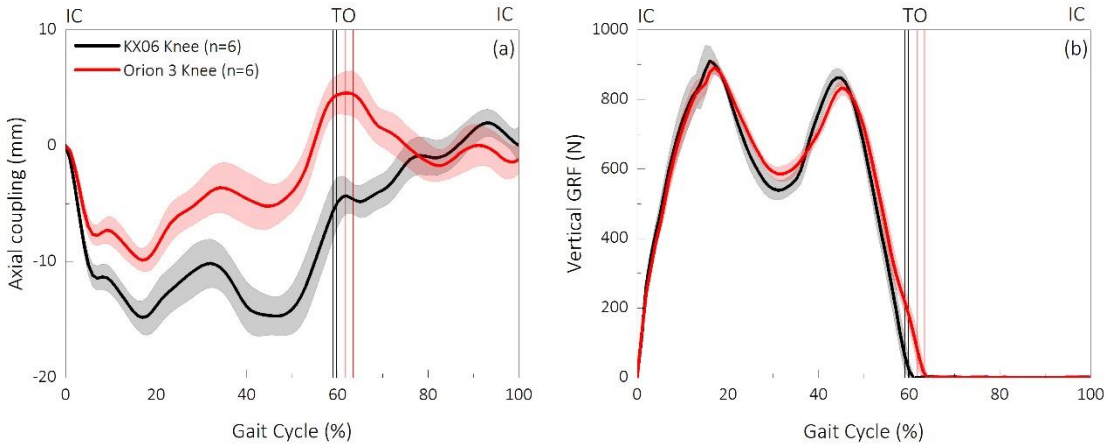

Figure 5.53: (a) Axial length and (b) vertical component of GRF, obtained over a GC. Participant was fitted with a polycentric and microprocessor controlled knee.

Similar peak vertical GRF ($p>0.05$) were obtained during early stance phase (907N±20N with polycentric knee and 911N±15N with MPK in Figure 5.53b). However, there was an increase in the vertical component of GRF during stance phase when fitted with the MPK (586N), when compared with the polycentric knee (539N).

It is evident that although similar vertical GRF was obtained in early stance phase, more axial length was obtained when fitted with the polycentric knee when compared with the MPK. It is believed that the change in the prosthetic alignment when switching the test prosthesis needed to be compensated by the increased residuum movement against the socket. In addition, the MPK with control stance support would give an enhanced residuum stability inside the socket compared with a polycentric knee.

Advantage of using MPK was previously reported in both qualitative measures (e.g. Prosthesis Evaluation Questionnaire) and quantitative measure (Time Up and Go test). In addition, based on this case study, a reduction in the 3D motion at residuum/socket interface was evident, which is critical in improving the overall prosthetic limb stability during dynamic gait. In additions to this, in order to further reduce the 3D motion at residuum/socket interface, active control algorithm can be built into the existing microprocessor in the MPK. This could, thereby, lead to a patient-specific active controlled prosthesis.

5.5 3D residuum motion results – trans-tibial amputee

Section 5.4 presents the interface kinematics on a knee-disarticulation amputee. For trans-tibial amputee, especially, the stiffness of the socket interface can be associated with the fit

[245]. Further, the stiffness of the socket interface is comprised of the relative motion and the force experience at the interface. Therefore, in this section, the residuum motion at socket interface will be studied.

5.5.1 Level walking activity

This section presents the results obtained from protocol B1 (Section 5.3.1).

From IC to approximately 18% of GC, there is a general decrease of angular motion (Figure 5.54a and Figure 5.54b). This corresponds to the VRS movement towards anterior direction, as indicated in Figure 5.6b. This finding aligns well with the conceptualised movement mentioned in the literature (Figure 2.49) as the knee is forced to extend due to the external load exerted by the socket. The angular motion maintained at this level until approximately 40% of GC, showing a further decrease. It reached a local minimum point just after TO. The further anterior movement of VRS could help to create a moment about the prosthetic ankle, aiding the loading of the prosthetic forefoot for propulsion purpose. During the rest of the GC, it recovers to the value obtained at IC. This corresponds the VRS movement towards anterior direction. It is worth noting that, majority of the motion in sagittal plane occurs in swing phase. When comparing the temporal profile obtained in two sessions, repeatable patterns were evident.

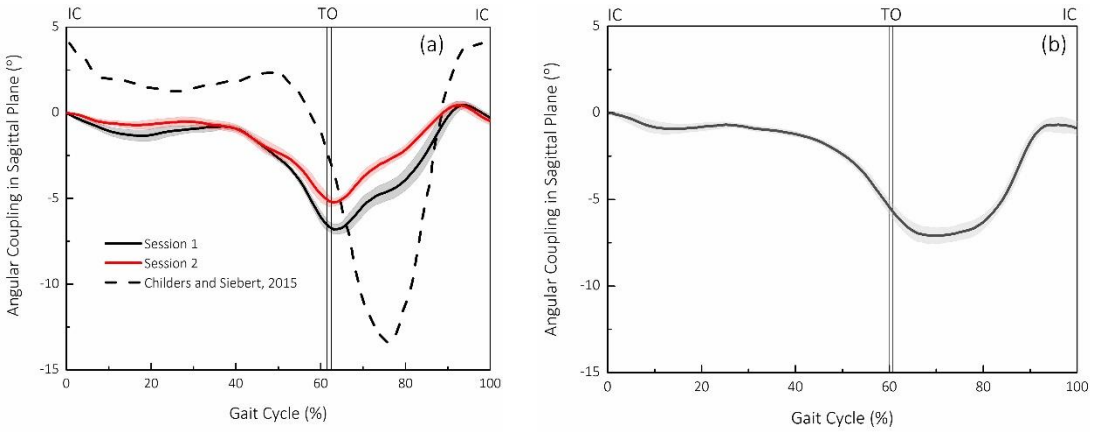

Figure 5.54: Residuum motion at socket interface in sagittal plane for (a) participant 1 and (b) participant 2, respectively.

The temporal profile of the angular motion in sagittal plane was then compared with the results obtained by Childers and Siebert [169]. In stance phase, the two temporal profiles align with each other. However, in swing phase, the timing at which the minimum value occurs, obtained by Childers and Siebert, was further shifted to a later stage of GC. This could likely attributed to the difference in gait, as no information was provided by Childer and Sieberts. Peak to peak value of up to 4.9 ± 0.3° and 7.3 ± 0.3° in sagittal plane, was obtained by participant 1 in session 1 and session 2, respectively, with higher value seen in Session 2 (p=0.00). Peak to peak value

of approximately 7.3 ± 0.3° in sagittal plane was obtained by participant 2. When comparing the peak to peak value obtained by Childers and Siebert (up to 17°), the results obtained from the current study (from two participants) was approximately halved. This may attributed to the different socket fit between the participants.

For both participant, up to 2° of angular motion was obtained in coronal plane in stance phase (Figure 5.55a and Figure 5.55b). In swing phase, approximately 4° of angular motion was obtained in the coronal plane. The increase of angular motion in coronal plane corresponds to the VRS movement towards lateral side of the socket. Lower value obtained in stance phase could be potentially explained by the socket design as medial-lateral 'wings' were built on socket to reduce the coronal plane movement. In swing phase, as the interaction between the residuum and socket is dominated by inertia, a greater movement was evident. It is worth noting that the only previous study that reports the dynamic interaction between the residuum and socket did not include the coronal plane motion.

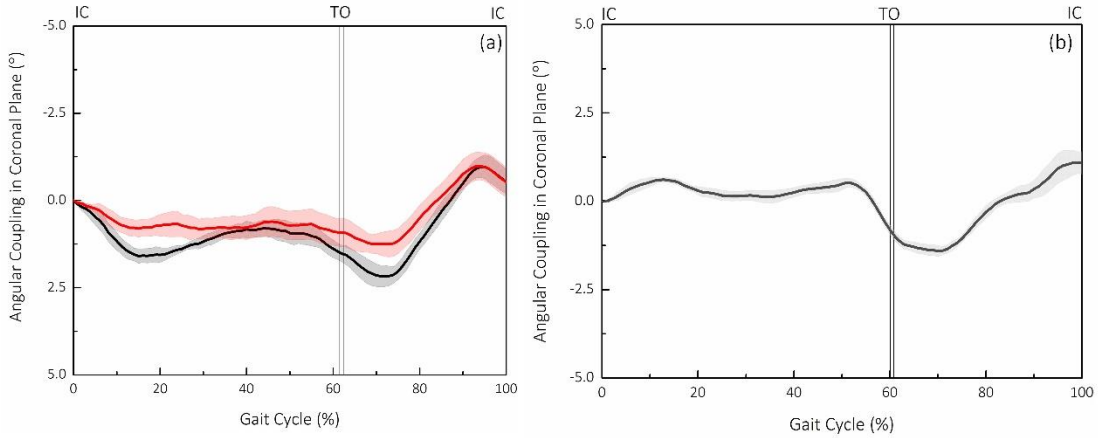

Figure 5.55: Residuum motion at socket interface in coronal plane for (a) participant 1 and (b) participant 2, respectively.

Similarly, repeatable pattern was obtained between session 1 and session 2 for participant 1 (Figure 5.56a). The temporal profile obtained from participant 2 (Figure 5.56b) also aligns with the results obtained from participant 1. Little angular movement in transverse plane was evident in stance phase. However, up to 1.2° and 1° of angular motion was obtained in transverse plane, which is significant lower than the value obtained in sagittal and coronal plane.

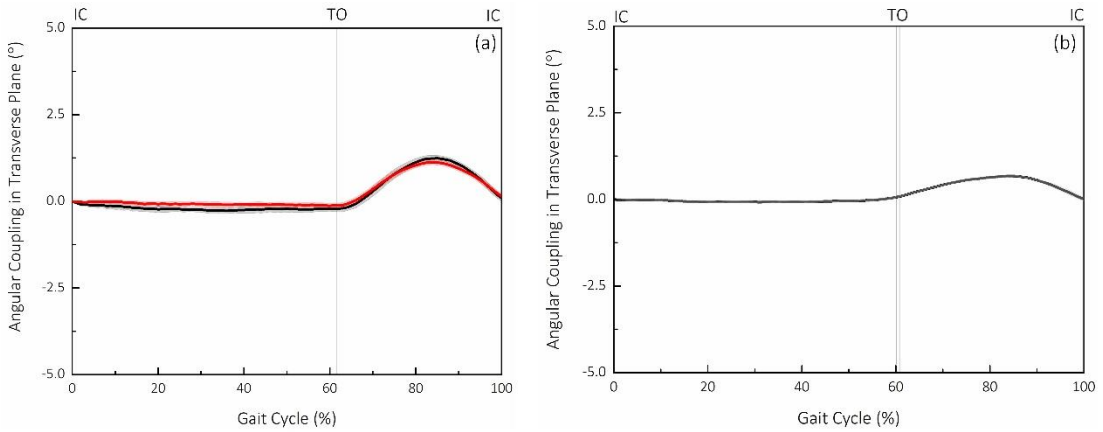

Figure 5.56: Residuum motion at socket interface in transverse plane for (a) participant 1 and (b) participant 2, respectively.

From IC to approximately 18% of GC, there is a general decrease of axial length, indicating the residuum was pushed into the socket (Figure 5.57a and Figure 5.57b). From 18% of GC to approximately 40% of GC, the axial length increases, restoring to the value seen at IC. From 40% of GC to approximately 58% of GC, there is a further decrease in axial length, meaning residuum was sinking into the socket during TS phase. During rest of the stance phase, axial length increase as swing phase starts to initiate. The lengthening and the shorten of the axial length could be potentially associated with the force transferred from the ground interface. During loading response, there is an increase in vertical GRF, which pushes the residuum into the socket. As vertical GRF reduces, reaching mid-stance, axial length restores. In TS, the limb was loaded again to generate an energetic push-off, the residuum was again pushed into the socket.

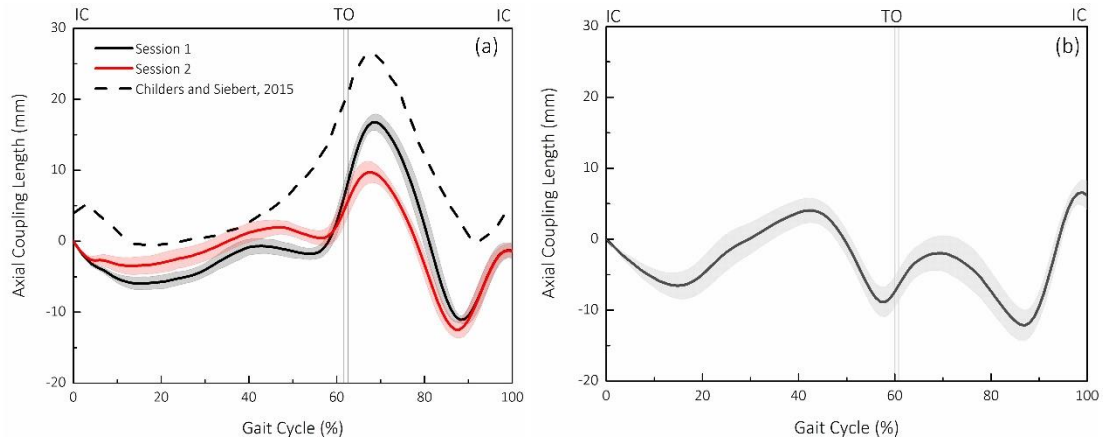

Figure 5.57: Residuum axial length at socket interface for (a) participant 1 and (b) participant 2, respectively.

Between approximately 62-65% of GC, axial legnth continues to increase, reaching a value greater than that observed at IC. This corresponds the pull-out of the residuum out of the socket. It is likely that the phenomenon could be associated with the inertial effect as the limb swings forward. Between approximately 65-88%, axial length further decreases. This may

attributed by a number of factors, including the recoil of residuum tissues in combination with the recoil related to the mechanical stiffness of the suspension system, which overcomes inertial and gravitation forces related to swing dynamics of the prosthetic limb. In the rest of the swing phase, the axial length recovers to the value obtained at IC. It is worth noting that, similar temporal profile was also obtained by Childers and Siebert. In terms of peak to peak axial length value, up to 27mm and 20mm were obtained from participant 1 in session 1 and session 2, respectively. For participant 2, up to 21mm of peak to peak axial length was obtained. This value (ranges from 20-27mm) aligns well with previous reported studies (0 - 41.7mm, Section 2.6.2).

It is worth noting that the axial length obtained on the two trans-tibial amputee (up to 5mm), in stance phase, was significantly reduced comparing to the value obtained on the knee-disarticulation amputee (up to 32mm). There are two possible explanations associated with this finding. First, although the force experience at the interface in stance phase is typically greater than the value in swing phase, the mechanical behaviour of the interface under compressive force (stance phase) can be significantly different from that during tensile force (phase). Further, muscles were activated during stance phase to control the rate of the knee motion, ensuing the stability of the limb (Section 4.2.3). The contraction of the muscle could result in a stiffer interface. With the same load applied to the interface, less axial length can be induced with a stiffer interface.

5.5.2 Walking on different terrains

As demonstrated in Section 4.4.2, walking on different terrain resulted in a change in knee joint angle and moment in early stance, for trans-tibial amputee. However, the effect of altered joint mechanics on the socket interface biomechanics is not well understood, which may be associated with the safety and stability when walking on a descending ramp. This is particularly the case for trans-tibial amputee, as the knee was contained in this socket. In this section, results obtained from protocol B2 will be presented (Section 5.3.1).

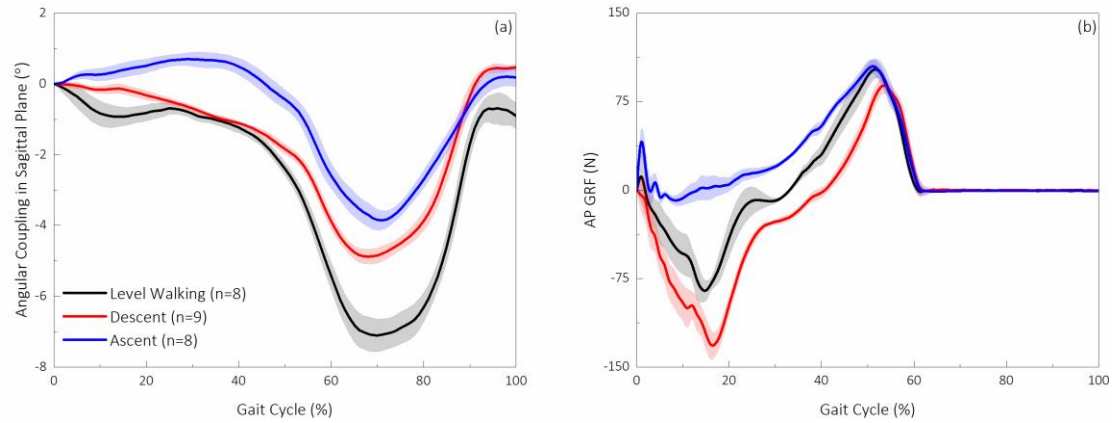

Figure 5.58: (a) Residuum/socket interface angular motion in sagittal plane obtained on different terrains, over a GC. (b) Anterior-posterior component of GRF, obtained on different terrains, over a GC

When walking on a descending ramp, there is a decrease of angular motion from IC to 40% of GC (Figure 5.58a). However, when walking on the ascending ramp, an increasing trend of angular motion was evident. Up to -135N of braking force was obtained when walking on the descending ramp at 18% of GC, while a positive value (up to +40N) was obtained at first 5% of GC when walking on the ascending ramp (Figure 5.58b). This may explain the decreasing and increase trend of angular in sagittal plane from 0-40% of GC, when walking on descending and ascending ramp, respectively. From 40% of GC, angular motion in sagittal plane decreases and reached a peak minimum point at mid-swing phase of GC (approximately 70% of GC). Similar to the previous study (Section 5.5.1), majority of the residuum motion relative to the socket occurs during swing phase.

When comparing the peak to peak value of angular motion in sagittal on different terrains. Up to 7.2 ± 0.5°, 5.5 ± 0.3° and 4.7 ± 0.3° of peak to peak value was obtained when walking on level, descending and ascending surface, respectively. It is worth noting that unlike the experimental protocol used for the knee disarticulation participant, walking speed is not controlled during data collection. The participant was walking at self-selected speed so that safety is ensured, especially when walking on the descending ramp. The difference in peak to peak value obtained in this study should be treated cautiously as walking speed may affect the residuum motion relative to socket.

Regardless of terrain, up to 1° of angular motion in coronal plane was obtained on the trans-tibial participant in stance phase (Figure 5.59a). Highest medial-lateral GRF (Figure 5.59b) was obtained when walking on descending surface (40N ± 8N), followed by the value obtained on level (22 ± 4N) and ascending surface (21 ± 11N). Though difference was found in medial-lateral GRF when walking on different terrains, little change in angular motion value was observed. As mentioned previously, this is likely due to the tight media-lateral wing and this would restrict

the movement in coronal plane. In this swing phase, up to 2.5 ± 0.2°, 1.8 ± 0.3° and 2.2 ± 0.2° of residuum motion relative to socket was obtained (Figure 5.59a).

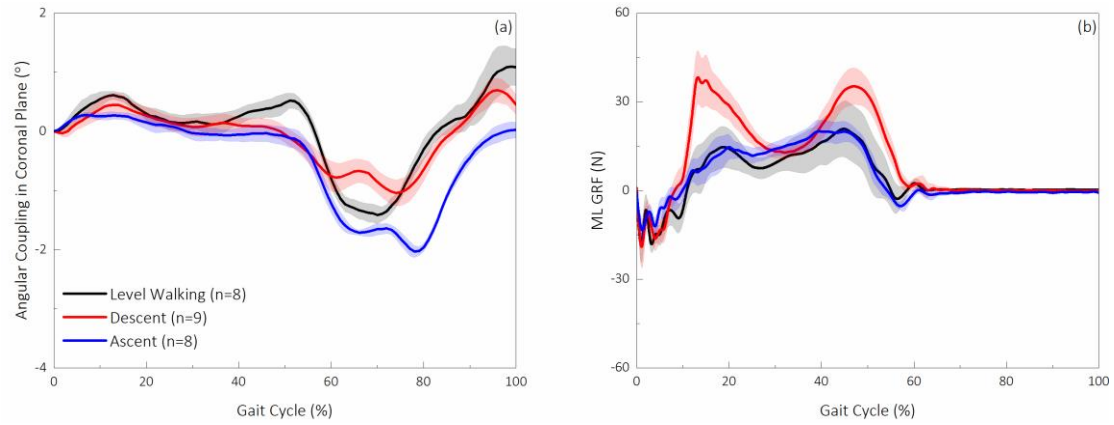

Figure 5.59: (a) Residuum/socket interface angular motion in coronal plane obtained on different terrains, over a GC. (b) Anterior-posterior component of GRF, obtained on different terrains, over a GC

From IC to approximately 18% of GC, there is a general decrease of axial length when walking on level and descending surfaces (up to -7mm in Figure 5.60a). However, this finding is not particularly evident when walking on the ascending surface, as less than 1mm of decrease in axial length was obtained at 5% of GC. Up to 683 ± 12N, 694 ± 20N and 568 ± 20N was obtained in early stance phase, when walking on level, descending and ascending surface, respectively. This decrease of axial length at this stage of GC may be attributed to the increase of vertical GRF, pushing the residuum into the socket. Lowest vertical GRF was obtained when walking on ascending surface, which may explain the reduction of axial length obtained, comparing to the values obtained on level and descending surfaces.

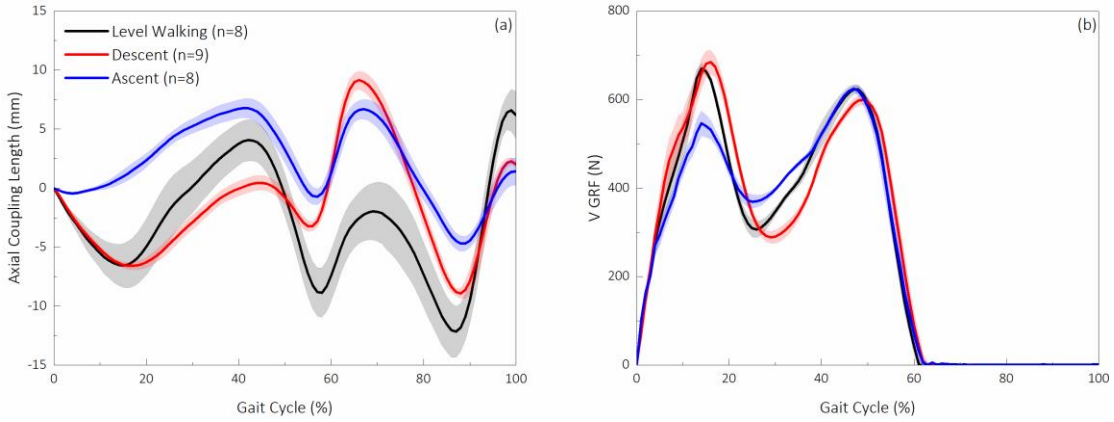

Figure 5.60: (a) Residuum/socket interface angular coupling in transverse plane obtained on different terrains, over a GC. (b) Anterior-posterior component of GRF, obtained on different terrains, over a GC

From 28% of GC, axial length increases regardless of terrain. At approximately 45% of GC, up to 11mm, 8mm and 6mm of axial length restoration were obtained when walking on level,

descending and ascending surfaces a, respectively. It is worth noting that, the timing at which the mid-stance valley occurs in vertical GRF (ranges from 25% to 30% of GC) does not match the timing of the end of restoration (45% of GC). It is believed that the axial length change during this period may have an influence from the knee rotation in sagittal plane. From 45% of GC to 65% of GC, axial length increases, meaning the residuum was pulled out of the socket, due to inertial effect. Up to 19mm, 16mm and 17mm of peak to peak axial length were obtained over a GC, when walking on level, descending and ascending surface, respectively. For this particular trans-tibial amputee, when walk on non-level surface, a reduction was found on the peak to peak interface kinematic motion, comparing to the value obtained when walk on level surface.

5.5.3 Walking with different suspension technique

The attachment between the socket and the residuum can be either achieved by a pin-lock liner suction or vacuum-assisted techniques (Section 2.1.4). The application of different techniques would inevitably alter the mechanical behaviour of the interface, such as compliance (Figure 2.12), which will in turn affect the interface kinematic motion. The choice of attachment technique on different amputee would benefit from the bespoke understanding of the interface kinematics. This section presents the results obtained from protocol B3 (Section 5.3.1).

It is evident that the temporal profiles (Figure 5.61a and Figure 5.61b) obtained in this session is similar comparing to the profile obtained in previous level walking studies (Section 5.5.1). Table 5.19 illustrates the peak to peak angular motion value obtained, over a GC. When the Echelon Vac setting is 'On' or the tube is connected to the socket, a greater angular motion value was obtained in both sagittal and coronal plane ($p<0.05$).

To be specific, with vacuum built at the socket interface, a greater angular motion in sagittal plane was observed in the swing phase (Figure 5.61a). This may be associated with a greater swing speed as adequate attachment between the residuum and the socket, resulting in more confidence in gait [68, 79]. Furthermore, with vacuum built at the socket interface, a greater angular motion in coronal plane (up to 0.3°) was observed in early stance phase, comparing with value obtained without vacuum. However, this finding needs to be treated with cautious, as 0.3° of difference may not be clinically significant. The overall increase in angular motion with vacuum presented at the interface may be associated with the increased usage of the residuum, engaging more with the socket in angular directions. The increase usage of residuum was one of the key design criteria of the modern prosthetic components. This serves the

purpose of reducing load on the contra-lateral side thus, reducing the risk of musculoskeletal disorder.

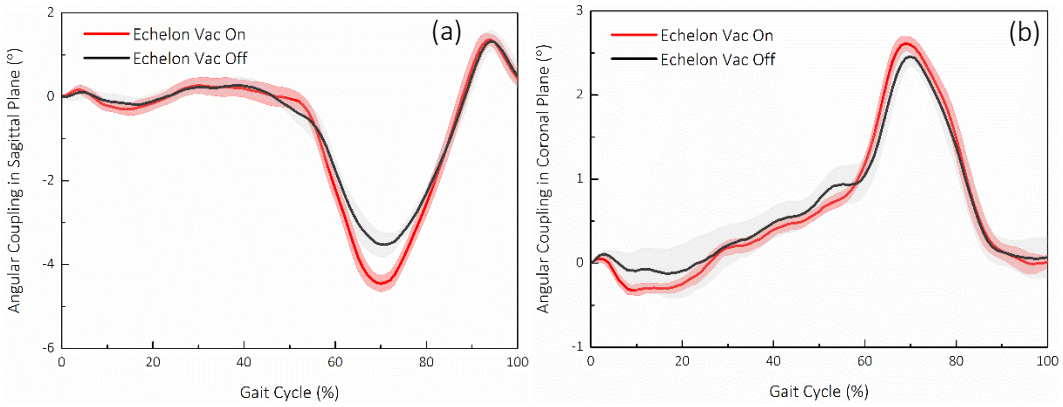

Figure 5.61: Residuum/socket interface angular motion in (a) sagittal plane and (b) coronal plane obtained with two suspension techniques, over a GC.

Table 5.19: Peak to peak value of angular motion with two Echelon Vac setting, over a GC.

Echelon Vac status	Angular motion (°)	
	Sagittal plane	Coronal plane
Off	5.0 ± 0.2	2.1 ± 0.1
On	6.1 ± 0.2	2.6 ± 0.2

Up to 21mm and 11mm of peak to peak axial length (Figure 5.62) was obtained when Echelon Vac setting was On and Off, respectively. This shows an overall reduction in axial movement of the residuum, relative to the socket when suction was built at the interface. When investigating the axial length in stance and swing phase separately, more axial movement was evident when Echelon Vac was On (up to 7mm), comparing to the value when Echelon Vac was set to Off mode (up to 3mm). In the swing phase, up to 18mm and 10mm of axial movement was obtained when Echelon Vac was set to Off and On mode, respectively.

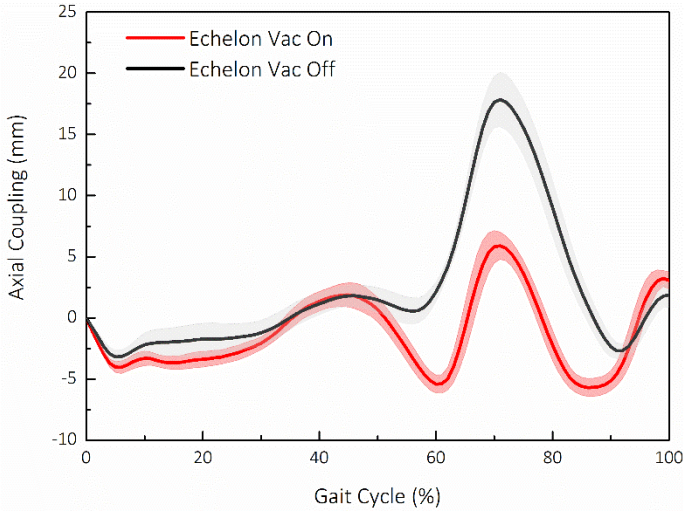

Figure 5.62: Residuum/socket interface axial length obtained with two suspension techniques, over a GC.

As reported in previous study the normal cushion liner promotes the axial movement of the residuum relative to socket in stance phase (up to 3mm), comparing to a suction liner. In swing phase, a suction liner reduces the axial moment of the residuum relative to socket (up to 4mm), comparing to a cushion liner [168, 216, 246]. It is believed that the introduction of vacuum at the socket interface could potentially results in the increase in interface stiffness in axial direction. With same inertial force applied to the socket interface, in swing phase, a stiffer interface will produce less movement. However, this is not the case for angular motion, as illustrated in Figure 5.61a. The vacuum presented at socket interface has led to an increase in angular motion in sagittal plane. It is worth noting that, although the vacuum was presented at the socket interface, the stiffness in angular direction remain unchanged. The increase in swing speed or shank angular velocity could potentially lead to the increase in angular motion. Various reports in literature [68, 79, 168, 216, 246] made a general statement as a suction socket can produce less axial motion between the residuum and the socket. This statement should be treated cautiously, as vacuum presented at socket interface may lead to increase in residuum motion in stance phase. This also shows that the proposed interface kinematic model has produced extra biomechanical understanding at socket interface, comparing to previous reported studies in this field.

This chapter presents the assessment of the residuum/socket interface kinematics for lower limb amputee. A residuum/socket interface kinematic model was developed based on a conventional 6-DoF musculoskeletal model (Section 5.1 and Section 5.2). The model enables the study of both dynamic angular motion and axial length with the aid of the 3D motion capture system. The repeatability of the model was assessed on both trans-tibial and knee disarticulation participants. Intra-session SD values of up to 0.6° and 1.2mm was obtained on

angular motion and axial length, respectively. Acceptable intra-session waveform repeatability was also obtained (R^2 value of up to 0.988). Inter-session SD values of up to 0.9° and 6mm was obtained on angular motion and axial length, respectively. In addition, acceptable waveform repeatability was achieved with R^2 values of up to 0.991. The sensitivity of the model was assessed by altering the walking speed, terrain and prosthetic components. As an example, up to 96% and 12% of increased in angular and axial length was obtained, respectively, when walking from slow to fast speed (Section 5.4.3). When walking descending surface, an increase of up to 3° of angular motion was achieved in early stance phase, comparing the value obtained when walking on ascending surface. In addition, a reduction of 3° of angular motion was evident when switching from a polycentric knee to a MPK. Therefore, potential sensitivity of interface kinematic model has been demonstrated with a series of case studies.

Chapter 6 Interface stresses of the lower limb residuum

While residuum motion has been evaluated (Chapter 5), it is important to study the mechanical loading at the socket interface as this kinetic function is intricately linked during amputee ambulation. Comprehensive understanding of these loading patterns and profiles is essential for evaluation of socket fit (Section 2.1.3), residuum tissue health for both trans-tibial and trans-femoral amputees. In particular, the socket interface is subject to multi-directional mechanical stresses i.e. pressure (perpendicular to skin surface), longitudinal shear (axial direction) and circumferential shear (transverse direction). The prolonged exposure of these interface stresses can potentially lead to discomfort (Section 2.2.1), skin ulcer and even deep tissue injuries, affecting rehabilitating outcomes and quality of lives. Despite many reported interface sensors (Section 2.7.1), the unmet need of a tri-axial pressure and shear sensors system remains which can be comfortably applied at residuum/socket interface during walking.

A novel TRIPS sensor system was developed as part of a previous PhD project by Dr. Piotr Laszczak in Prof. Liudi Jiang's team (Section 2.7.2). Although promising, the previous TRIPS sensor system faced technical issues of noise and signal processing difficulties. Clinically, only one session of amputee level walking test have been conducted. No trans-tibial amputee tests have been performed. Thus, comprehensive biomechanical studies based on trans-tibial and trans-femoral tests were needed. In this chapter, experimental protocol will be explain separately for the knee-disarticulation amputee and two trans-tibial amputees. The interface stresses obtained from a series of walking tests will be presented subsequently. Last but not the least, the interface biomechanics will be assessed using the combined kinetic and kinematic assessment.

6.1 Walking test protocol

Figure 6.1 shows a series of amputee walking tests conducted.

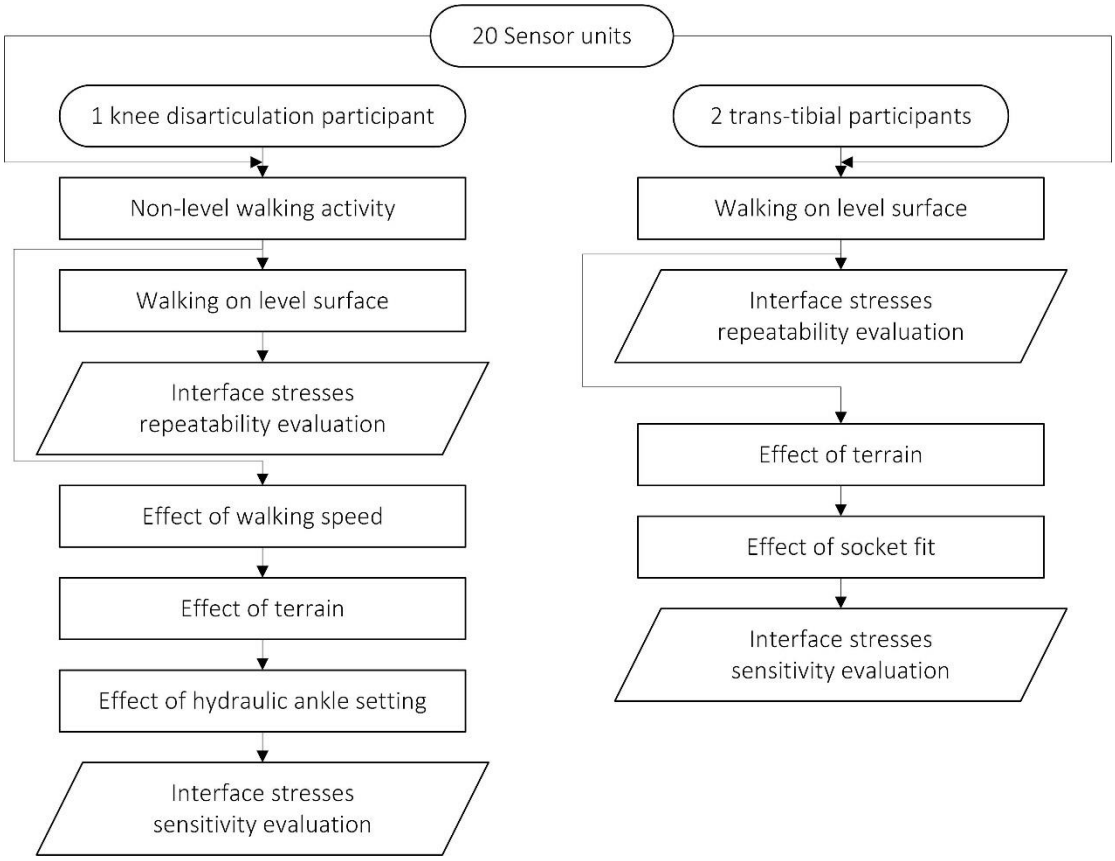

Figure 6.1: A flow chart for amputee walking tests.

6.1.1 Sensor Placement

Sensor placement on the knee disarticulation amputee

The preliminary aim of this study was to capture interfacial loading during ambulation in sagittal plane. The sagittal plane was chosen as it is the main plane where major forces and moments are transferred from ground to support the residuum/socket interface and enable the advancement of the limb (Section 2.4 and Section 4.2). Therefore, the sensors were placed at anterior and posterior regions of the socket. For this particular knee-disarticulation participant, three sensors were placed at anatomical locations of posterior-proximal (PP), anterior proximal (AP) and anterior distal (AD) respectively. The rationale of the sensor placement was based on the conceptualised knee disarticulation socket biomechanics; a majority of the load may be observed at proximal locations. AD region, also termed as 'kick-point', was also selected as a region of interest as it acts as a pivot point, especially for knee disarticulation amputee.

Prior to the placement of the sensor, the subject was asked to sit down and the Pelite liner (Figure 6.2a), worn by the participant, was doffed for inspection. At AP and PP region of the Pelite liner, signs of contact or wear were identified as shown in Figure 6.2b and Figure 6.2c. These signs of wear due to long-term use of the Pelite liner were revealed as darker regions compared to the surrounding area. At the AD region of the Pelite liner, an indent feature (dashed circle in Figure 6.2d) was identified for sensor placement.

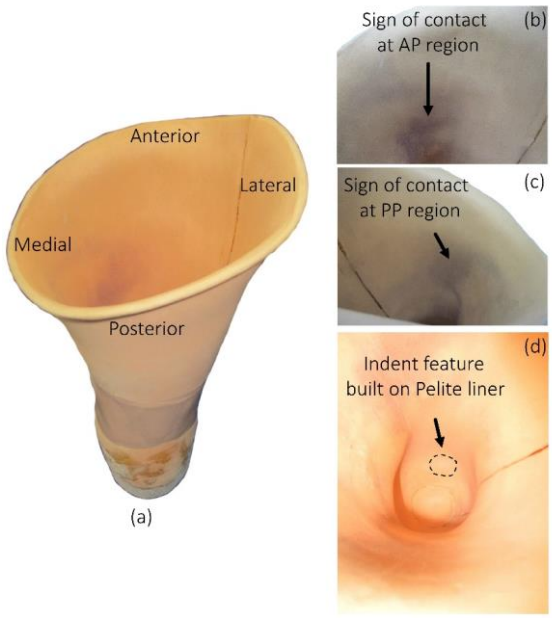

Figure 6.2: (a) A photo of the Pelite liner worn by the knee-disarticulation participant, (b) sign of contact on the AP region of the Pelite liner, (c) sign of contact on the PP region of the Pelite liner and (d) an indent feature built on the Pelite liner

Three sensors units, marked as 'Sensor 1', 'Sensor 2' and 'Sensor 3' in Figure 6.3a, were mounted on the inner surface of the Pelite liner at PP, AP and AD location, respectively, using double sided tape. The exact locations of the three sensor units were further measured using a tape measure, such that:

- Sensor placed at PP location: approximately 170mm from the medial trim line of the Pelite liner and approximately 60mm distal to the posterior brim of the Pelite liner (Figure 6.3b).
- Sensor placed at AP location: approximately 100mm from the medial trim line of Pelite liner and approximately 90mm from the anterior brim of the Pelite liner (Figure 6.3c)
- Sensor placed at AD location: 220mm distal to the anterior brim of the Pelite liner (Figure 6.3c), medial to the sensor placed at AP location of the Pelite liner.

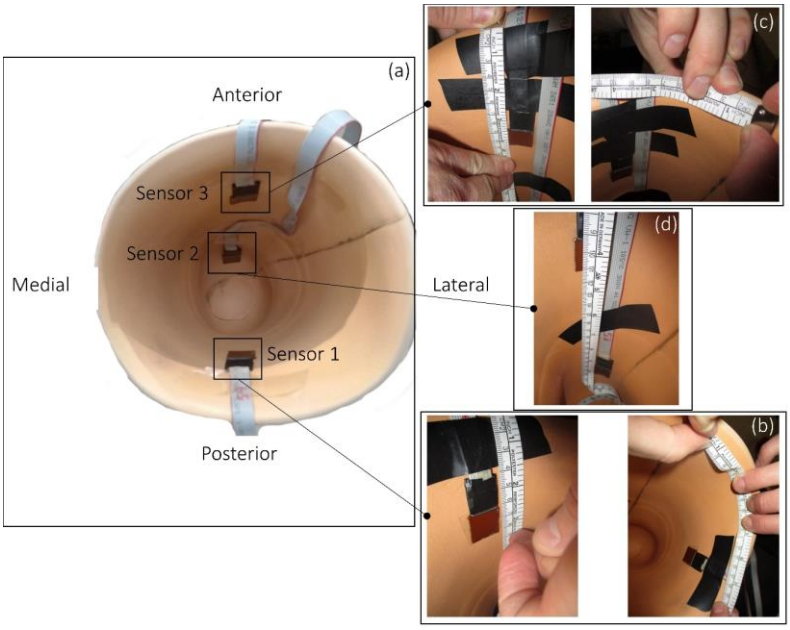

Figure 6.3: (a) Sensor placement on the inner surface of the Pelite liner and identification of sensor location on the (b) PP location, (c) AP location and (d) AD region of the Pelite liner

Once all three sensor units were mounted on the inner surface of the Pelite liner, the subject put on one thick sock and donned the liner onto the residuum. Subsequently, the socket with the rest of the prosthesis was attached. In some cases, the sensor placed at the AD location could cause discomfort on the residuum due to the sensitive nerve and scar tissue within this region of the residuum. The location of the AD sensor was then re-adjusted and moved to a more distal location.

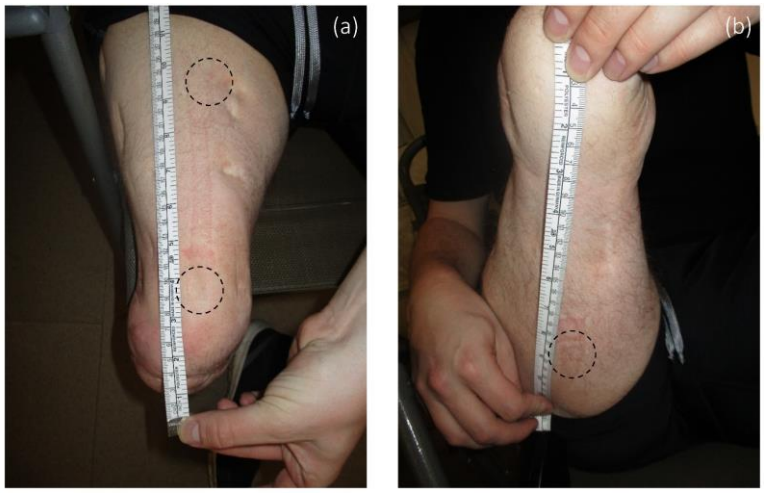

Figure 6.4: Marks transferred from the sensor unit to (a) AP, AD location and (b) PP location of the residuum

The participant was then asked to stand up and walk along the Gait Laboratory for several minutes, making sure that the socket was properly donned and no further discomfort had developed. During the first data collection session, the participant was asked to doff the socket

and the Pelite liner immediately after the walking, the locations of all three sensor units were re-measured with the tape measure again, to ensure that no slip had occurred between the sensor and the Pelite liner. In addition, in order to check the sensor was correctly placed on the residuum, visual inspection on the marks transferred from the sensor unit to the residuum were inspected, as shown in Figure 6.4. For example, by palpating the mark left by the AD sensor (Figure 6.4a), the researcher was able to feel the distal region of the femur.

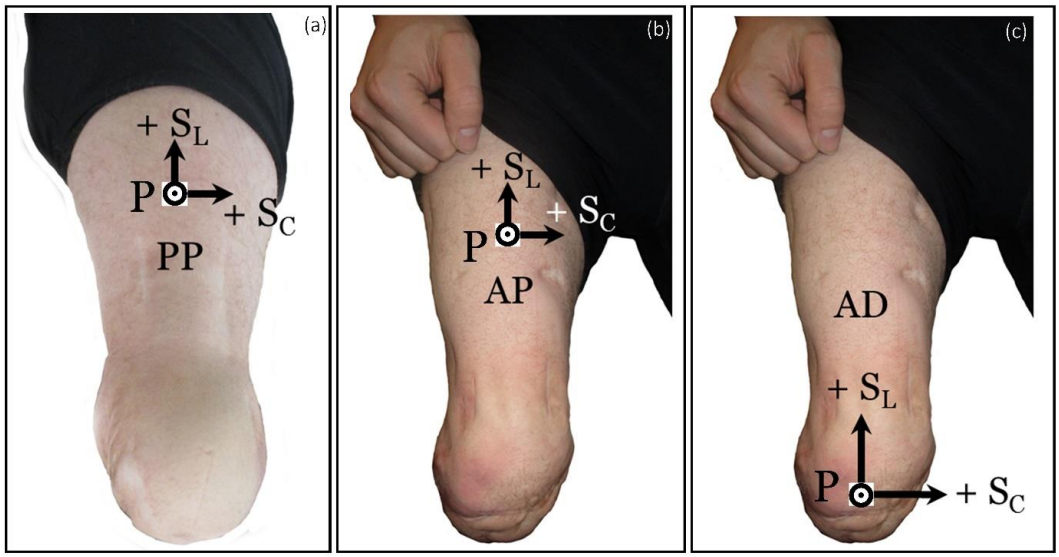

Figure 6.5: Positive directions of pressure, S_C and S_L at (a) PP, (b) AP and (c) AD location of the residuum.

Figure 6.5 shows the positive direction of the pressure, S_C and S_L measured at the PP, AP and AD locations of the residuum, respectively. Positive pressure was defined as the pressure acting perpendicular to the surface of the sensor unit. At PP region (Figure 6.5a), a positive S_C was defined as the shear stress acting on the residuum, pointing laterally; while a positive S_L was defined as the shear stress acting on the residuum, pointing proximally. At the AP region (Figure 6.5b), positive S_C was defined as the shear force, acting on the residuum, pointing medially while a positive S_L was defined as the shear force, acting on the residuum, pointing proximally. At the AD region (Figure 6.5c), positive S_C was defined as the shear force, acting on the residuum, pointing medially, while a positive S_L was defined as the shear force, acting on the residuum, pointing proximally.

Sensor placement on the trans-tibial participants

Three sensor units was attached to the inner surface of the socket, using double-sided tape. They are at the equivalent location of the patella tendon, distal location (or 'kick point') and superior popliteal fossa (SPF) of all three trans-tibial participants, as shown in Figure 6.6-Figure 6.7, respectively, with positive directions of pressure and shear stresses also illustrated. It is

worth noting that the positive directions of circumferential shear stresses are in opposite directions for left and right-sided amputees. Positive direction of longitudinal shear stresses is pointing towards proximal aspects of the stump.

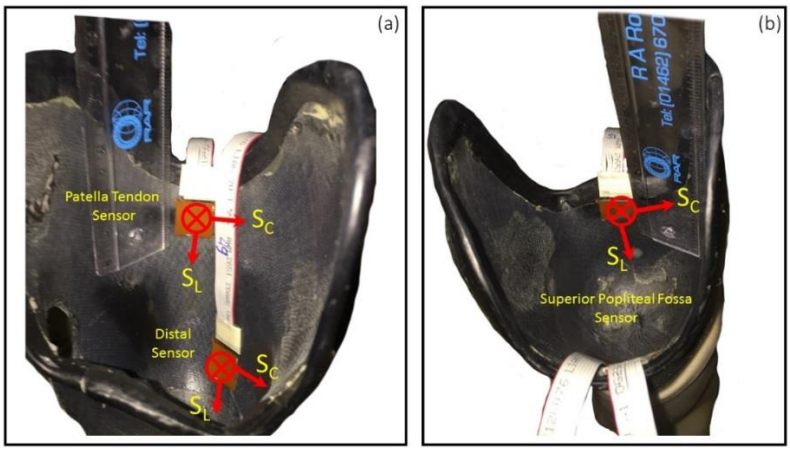

Figure 6.6: (a) sensor placement on the patella tendon location and distal location of the socket and (b) sensor placement at SPF location of trans-tibial 1 participant.

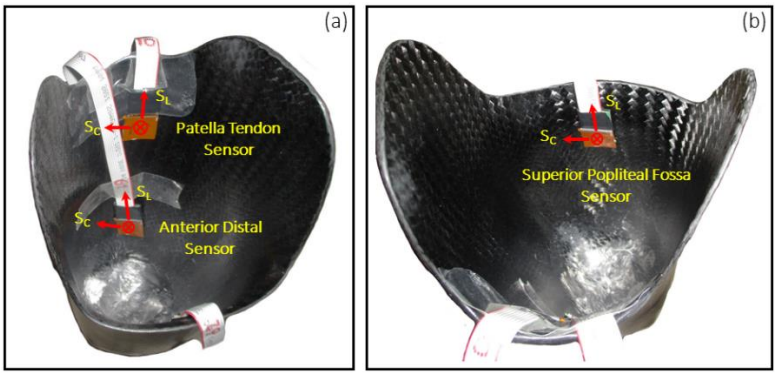

Figure 6.7: (a) sensor placement on the patella tendon location and distal location of the socket and (b) sensor placement at SPF location of trans-tibial 3 participant.

6.1.2 Experimental protocol

Knee disarticulation participants

- A1: Effect of donning of the socket

The knee disarticulation participant was asked first to remain in a seated position (Figure 6.8), subsequently, he was instructed to doff the socket and the investigator taped up to three-sensor unit to the inner socket wall and the location of each of the sensor can be found in Section 6.1.1. Once the sensor units are in position, the investigator started the data collection of the sensor system and a baseline zero was defined when the socket is doffed. Then, the participant was told to don the socket and during the donning process, the participant remained in the seated position. Once the socket is fully donned, the investigator stopped the

data acquisition of the sensor system. The whole process was repeated four times to check the repeatability of the donning process and investigate the variation in the interfacial stresses due to donning.

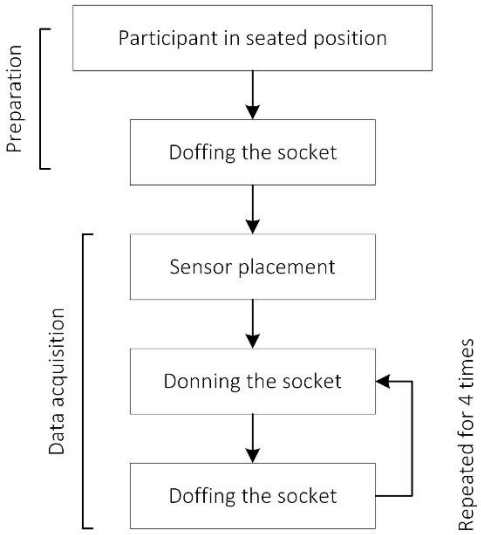

Figure 6.8: A flow chart showing the experimental protocol for capturing the interface kinetics with the effect of socket donning/doffing on the knee disarticulation participant.

- A2: Standing

Prior to this trial, the participant was asked to remain in standing position at the location of one step away from the force platform (Position A in Figure 6.9) for three seconds. Once a verbal instruction is given to the knee disarticulation participant, he took a step forward and lands his prosthetic limb on the force platform reaching Position B (Figure 6.9). The participant was told to remain in Position B, in a standing posture, for approximately four seconds. During the entire process, interfacial stresses were recorded at all three locations of the residuum.

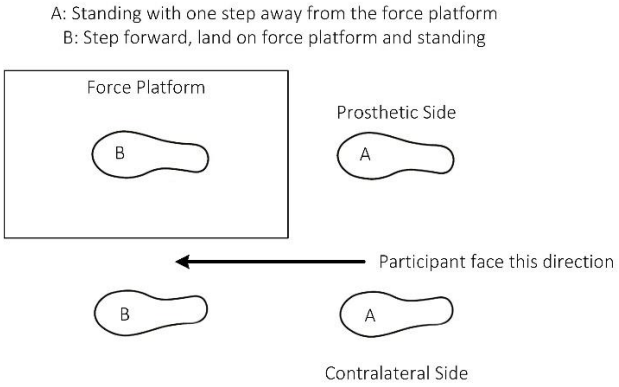

Figure 6.9: A schematics showing the experimental protocol for capturing the interface kinetics during standing on the knee disarticulation participant.

- A3: Weight shifting

Followed by the standing trial, the participant was subsequently asked to perform weight shifting trials. The detailed description of the weight shifting trial protocol can be found in Section 5.3.1. Up to five cycles of weight shifting trial were performed.

- A4: Level walking activities

In total of four separate sessions were conducted on different days (Figure 6.10). There are 3 days, 49 days and 41 days of separation between each of the data collection session. This enables the investigation on the both short and long-term change of the kinetics at the residuum/socket interface. The same level walkway and 3D motion capture system (Section 5.3.1) was used. Level walking speed was controlled by a metronome with cadence was controlled at 100BPM.

- A5: Level walking with different speed

Same experimental protocol was used in this study (See Section 5.3.1).

- A6: Walking on different terrains

The participant was asked to first walk on the level walkway with walking cadence controlled at 100BPM. Up to 12 repeated trials were conducted. Straight after the level walking session, the participant was asked to walk on the descending ramp with walking cadence controlled at approximately 100BPM. Up to 10 trials were performed. The protocol is followed by walking on the ascending ramp with cadence controlled at 100BPM. Up to 10 trials were collected. In all of the walking trials, the participant was asked to contact the force platform with their prosthetic side.

- A7: Walking activities with different hydraulic ankle setting

The protocol involved in this study is similar to the one mentioned in Section 5.3.1. However, only one session was conducted on the descending ramp.

Trans-tibial participants

- B1: Level walking activities

For the trans-tibial 1 participant, in total of three sessions of level walking tests were conducted on the same day (Figure 6.10).

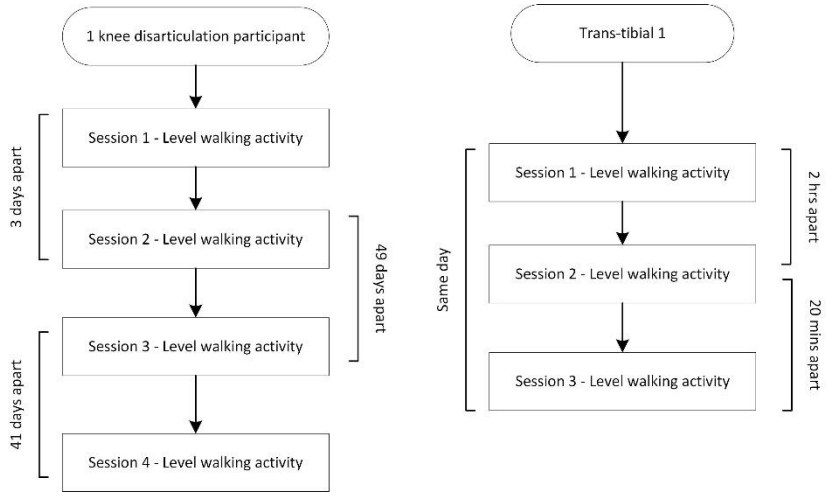

Figure 6.10: Experimental protocol for investigating the interface stresses when performing level walking activities.

- C1: Walking on different terrains

Trans-tibial 3 participant took part in the study and the experimental protocol was the same as the on the knee disarticulation amputee (A6).

- C2: Walking activities with different socket fit

In this study, the Trans-tibial 3 participant took part. The study started with level walking activity with two socks worn over the stump. As mentioned previously, the participant claims that 2 socks fitting is optimum during most of the day. Upon completion of the first level walking activity, the participant was asked to doff the socket and remove one sock from the stump. Subsequently, the same level walking session was repeated. Straight after the second level walking session, the participant doffed the socket and two thick socks were put on, on top of the one sock fit. Finally, same level walking activity was performed. It is worth noting that, for all level walking test conducted in this study, walking cadence was controlled at 100BPM.

Interface biomechanical assessment – knee disarticulation amputee

- D1: Level walking activity

Same test protocol was followed as activities A4 in this section. Instead of conducting multiple sessions, only one test session was performed.

- D2: Level walking with different speed

Same test protocol was followed as activities A5 in this section.

- D3: Walking on different terrains

Same test protocol was followed as activities A6 in this section.

6.1.3 Data collection and analysis

Data collection

Before conducting any test, a synchronisation device (Section 3.4.5) was plugged into both motion analysis system and TRIPS sensor system. This enables the alignment of the data from the motion analysis system with the data from TRIPS sensor system. The pressure and two components of shear stress were collected simultaneously at a rate of 100Hz. The data collection protocol for the motion analysis system was detailed in Section 4.1.2.

Data analysis

The data from motion analysis system, e.g. the GRF, was first reduced using linear interpolation, such that GRF data has the same sampling frequency as the ones from TRIPS sensor system. Subsequently, the GRF data and TRIPS sensor system data was synchronised by aligning their corresponding first data points. Next, both set of data was normalised with respect to a GC. The normalisation process was first performed on GRF as detailed in Section 4.1.2. Same process was performed on the TRIPS sensor results. The data analysis was followed by the calculation of mean and one SD for both GRF data and TRIPS sensor data.

To facilitate the interface biomechanical assessment, the pressure difference between posterior-proximal and anterior-proximal location of the residuum, thus indicating the residuum rotational movement in sagittal plane, Equation (6.1) is used.

$$\Delta P_{Abs} = P_{PP} - P_{AP} \tag{6.1}$$

The absolute pressure difference (ΔP_{Abs}), is then normalised by the value obtained at the IC (Equation (6.1)) to indicate the relative pressure difference thus eliminating the effect of donning/doffing, socket alignment and socket fitting.

$$\Delta P = \Delta P_{Abs} - \Delta P_{Abs\_0\%} \tag{6.2}$$

The interface biomechanics in axial direction was assessed by associating the axial length motion of the residuum with the longitudinal shear stresses obtained at PP location of the residuum. PP location was chosen as a point for analysis as it provides the highest reading from pilot amputee tests at the two proximal locations, described in Section 2.7.2.

6.2 Interface stresses for the knee disarticulation amputee

6.2.1 Non-walking activities

- A1: Effect of donning of the socket

This section presents the results obtained from the activity A1, the detailed protocol of A1 can be found in Section 6.1.2.

Figure 6.11a shows, from 0s to approximately 15s, pressure increased to 5kPa and 3kPa at PP and AP region, respectively. However, the pressure value at AD location was negligible during the donning process. Figure 6.11b reveals approximately 3kPa change in S_C at AP location, while the S_C at PP and AD location remains negligible. The donning of the socket also results in an increase in S_L (Figure 6.11b) at the PP location (up to 3kPa) and decrease in S_L at AP and AD location (approximately 3kPa).

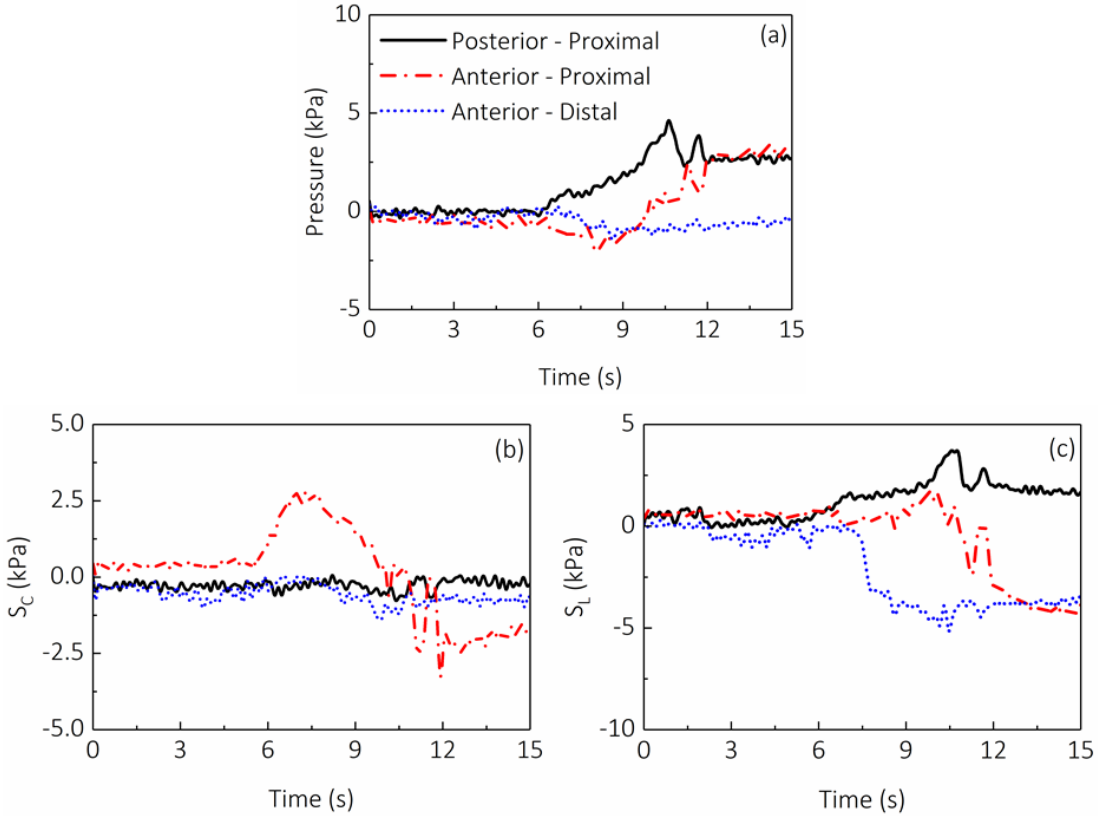

Figure 6.11: (a) Pressure, (b) circumferential and (c) longitudinal shear stresses measured during donning of the socket, as a function of time.

The change in the interfacial pressure, S_C and S_L measured after donning of socket, across four test sessions is illustrated in Table 6.1. Up to 11±4kPa and 4±1kPa were obtained at PP and AP location, respectively. When performing a 2-sample t test, higher pressure was obtained at the PP location than the value in AP location ($p=0.033$). It is worth noting that, pressure value obtained at AD location ranges from 0-10kPa, with 0kPa representing no contact between the residuum and the socket. When comparing the pressure value obtained at AD location with the value obtained at two proximal location, no statistical difference was observed ($p>0.05$ for both cases).

Up to 4kPa of change in S_C was obtained at the two proximal locations and up to 6kPa of change in S_C was observed at AD locations. When comparing the S_C obtained at all three locations, no statistical significance was found (all $p>0.05$). S_L in a range of 3-11kPa, -4-2kPa and -3-3kPa was observed at PP, AP and AD locations, respectively. Higher S_L was obtained at PP location than that in AP location ($p=0.033$), whereas no statistical difference was observed in the S_L obtained at AP and AD locations ($p>0.05$).

Table 6.1: Change in interfacial pressure, S_C and S_L due to the donning of the socket

Session NO.	Pressure (kPa)			S_C (kPa)			S_L (kPa)		
	PP	AP	AD	PP	AP	AD	PP	AP	AD
1	5	3	6	0	-2	0	3	-3	-3
2	10	6	0	3	4	0	8	0	0
3	15	4	10	4	2	6	11	2	3
4	12	4	5	4	4	5	6	-4	-1
Mean	11	4	5	3	4	3	7	-2	-2
SD	4	1	4	2	3	3	3	2	2

To the best of my knowledge, there has only been one reported work in literature that investigated the effect of the donning of the socket on the interface stresses for non-trans-tibial amputee using FEA [195]. Up to 1.4kPa, 0.4kPa and 0.6kPa of pressure, S_C and S_L were reported at PP location of the residuum. These values aligned with the sensor measurements obtained in this work although a reported value from the FEA study was lower. This may be due to the incapability of simulating muscle activation during donning process in a finite element package. In addition, the whole donning process was simplified by applying displacement in axial direction only in finite element model. However, in the real scenario, the participant has to wiggle the socket in the medial-lateral direction to aid the donning process.

In general, regions around distal end for a knee disarticulation amputee is commonly regarded as the pivot point around which femoral rotation is observed during walking (Section 2.7.3). The AD location of the socket, also designed to be the point of suspension for the weight of the prosthesis, is critical for maintaining the residuum stability inside the socket and the overall proprioception of the limb. In the four repeated stress measurement sessions conducted in this study, stress obtained in one of the session is negligible (Session 2 in Table 6.1). This indicates that the residuum was not in contact with the socket at AD location, which may affect the limb stability.

One SD of up to 4kPa, 3kPa and 3kPa was observed for pressure, S_C and S_L values. Such variations induced simply by donning of the socket across different session could be caused by a variety of practical factors. For example, for each of the donning process the entry angle of the residuum into the socket could be slightly different. In addition, muscle needs to be activated to aid the residuum to reach the appropriate location of the socket. Both could influence how residuum tissue is displaced inside socket during donning process. Nonetheless, these variations are relatively small as compare to the expected peak values in our pilot test results (Section 2.7.2).

- A2: Standing

This section presents the results obtained from the activity A2, the detailed protocol of A2 can be found in Section 6.1.2.

In 'standing phase 2' (Figure 6.12), or the stabilisation period, up to -12N and 0N of anterior-posterior GRF was obtained on the prosthetic and contra-lateral side respectively. Up to 30N and 20N of medial-lateral GRF was obtained on prosthetic side and contra-lateral side, respectively. Up to 376N and 476N of vertical GRF on prosthetic side and contra-lateral side, respectively. It is evident that higher frictional force as achieved on the prosthetic side, which may be associated with the seeking of stability as the anterior-posterior and medial-lateral GRF provides the adequate friction force at ground interface. A greater weight bearing (vertical GRF) was experienced on the contra-lateral side. This could be potentially associated with the compensatory mechanism as the prosthetic limb was less capable of weight bearing.

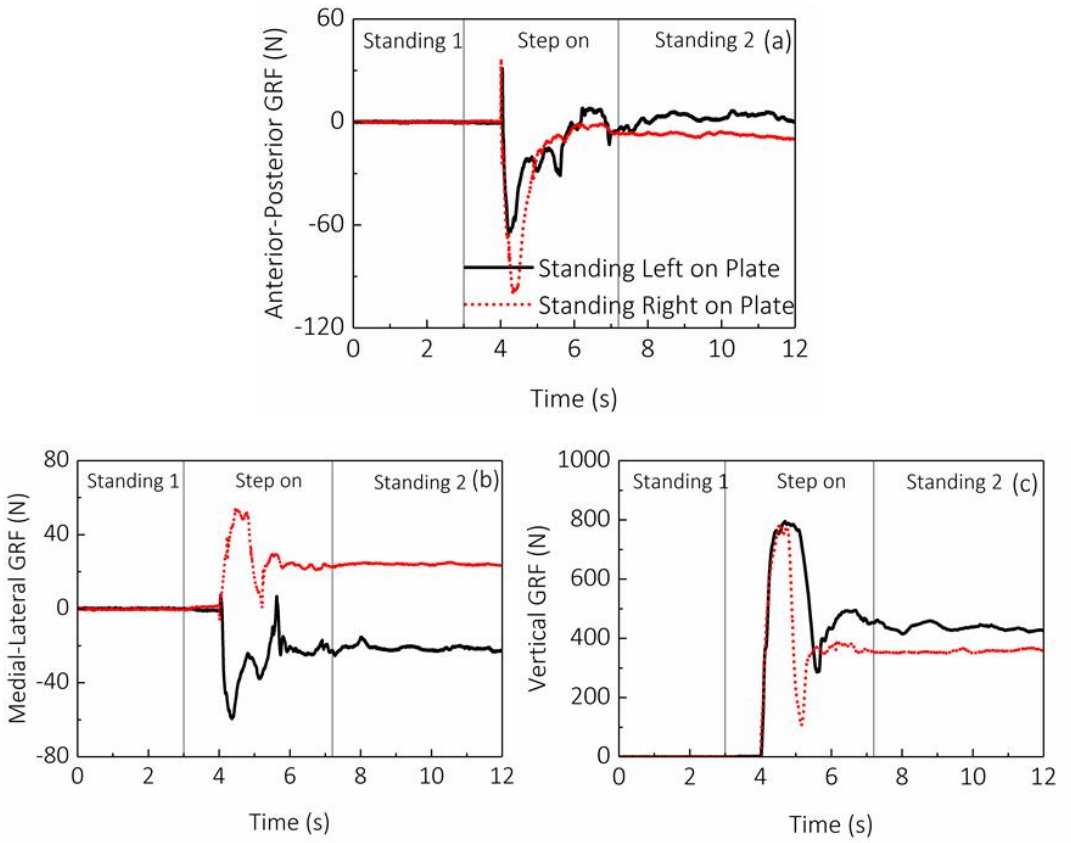

Figure 6.12: (a) Anterior-posterior, (b) medial-lateral and (c) vertical component of GRF as a function of time, during standing.

During the 'standing 1' phase, pressure (Figure 6.13a), S_C (Figure 6.13b) and S_L (Figure 6.13c) values were constant at approximately 24kP, 0kPa and 2kPa, respectively. During the 'step on' phase of the trial, pressure increased to approximately 44kPa. By contrast, S_C decreased to approximately -2kPa while S_L increased from 3kPa to 6kPa. During the 'standing 2' phase of the trial, when both limbs were stabilised, pressure, S_C and S_L were constant at approximately 29kP, -1kPa and 4kPa, respectively. By switching to the prosthetic limb contacting the force platform, up to 4kPa and 2kPa of change in the pressure and shear stresses were obtained during the two 'standing' phases, respectively.

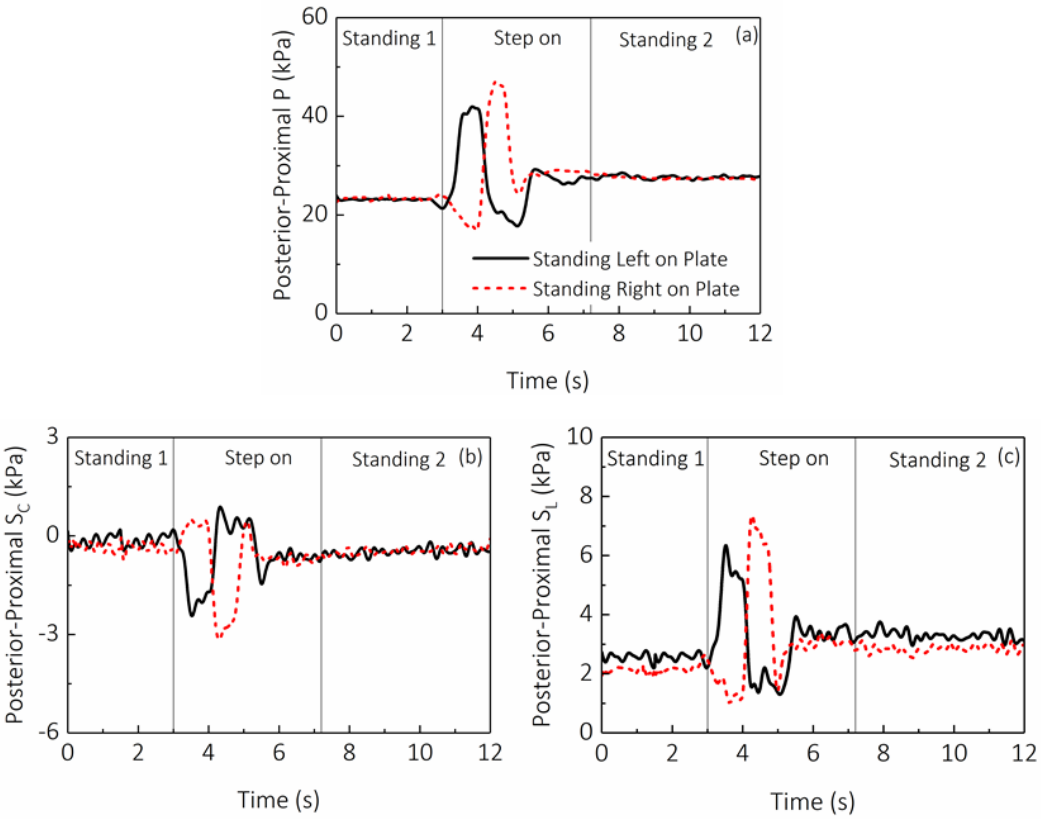

Figure 6.13: (a) Pressure, (b) circumferential and (c) longitudinal shear stresses measured at PP location of the residuum, as a function of time, during standing.

During 'standing 1' phase, pressure (Figure 6.14a), S_C (Figure 6.14b) and S_L (Figure 6.14c) values were constant at approximately 16kP, -4kPa and 4kPa, respectively. When intact limb made contact with the force platform, there was an increase in pressure and S_L to approximately 29kPa and 10kPa, respectively, whereas S_C decreased to -10kPa. During the second phase of 'standing', the pressure and S_C were restored to the value seen at the first 'standing' phase with an exception of slight increase of 1kPa in S_L. By switching to prosthetic making contact with the force platform, there was no change in peak pressure and S_C, whereas a slight decrease of 1kPa was observed in S_L.

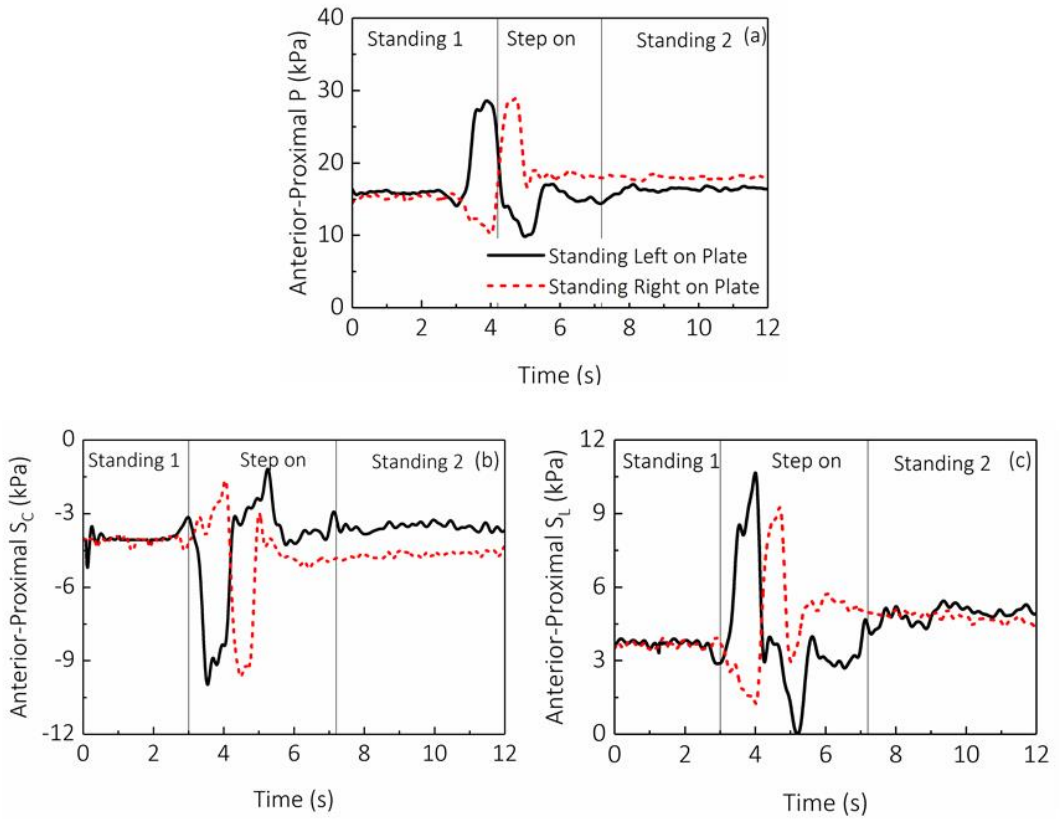

Figure 6.14: (a) Pressure, (b) circumferential and (c) longitudinal shear stresses measured at AP location of the residuum, as a function of time, during standing.

During the 'standing 1' phase, pressure (Figure 6.15a), S_C (Figure 6.15b) and S_L (Figure 6.15c) maintained at 12kPa, -1kPa and 0kPa, respectively. The 'step on' action has resulted in an increase in pressure to approximately 25kPa, a decrease of S_C to -2kPa and a decrease of S_L to -2kPa. During 'standing 2' phase, the S_C and S_L values were restored to approximately the value seen during the first 'standing' phase, whereas an increase of pressure to 16kPa was evident.

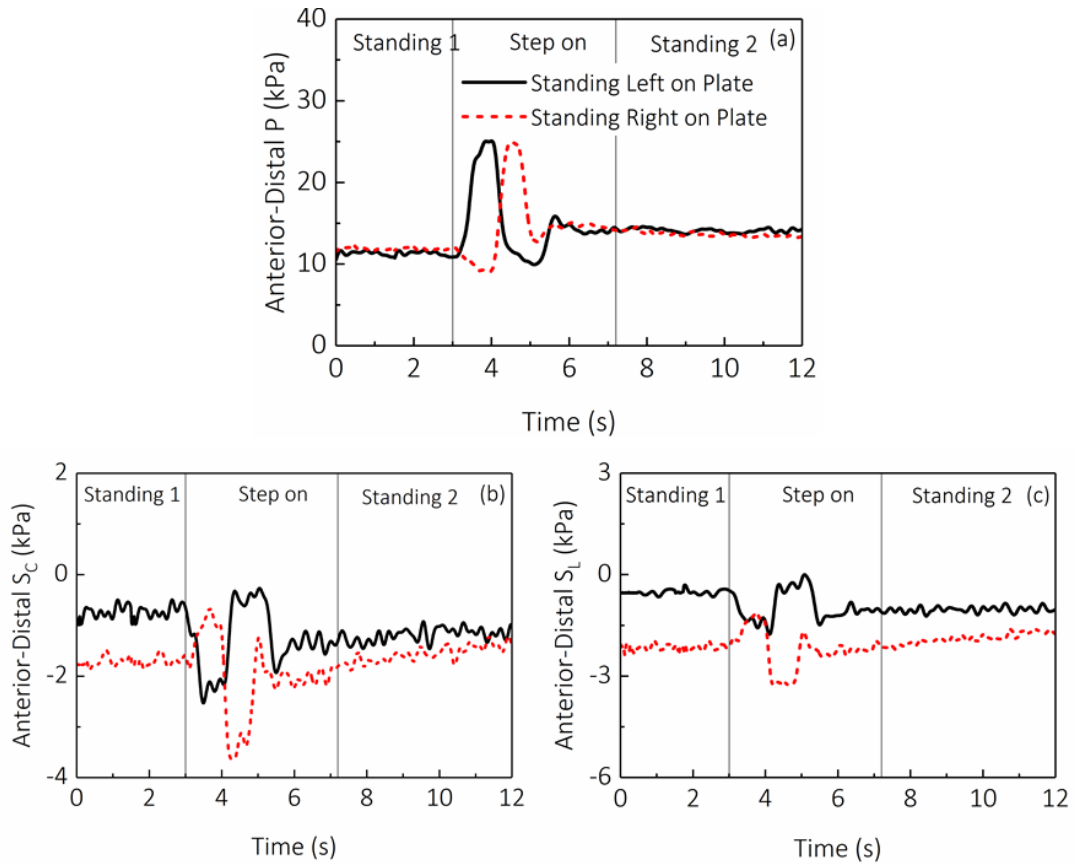

Figure 6.15: (a) Pressure, (b) circumferential and (c) longitudinal shear stresses measured at AD location of the residuum, as a function of time, during standing.

During quiet standing, pressure values of up to 29kPa, 16kPa and 16kPa of pressure were measured at PP, AP and AD location of the residuum. This suggests that higher pressure was obtained at PP location, comparing the values measured at AP and AD locations. In addition, S_C of up to -1kPa, 0kPa -2kPa were obtained, while S_L of approximately 7kPa, 0kPa and 0kPa were measured at PP, AP and AD location of the residuum, respectively. This suggests that is S_L measured at PP location, is a dominant parameter for supporting the residuum inside of the socket.

Interfacial stresses measured during standing, could be potentially used as an indicator for the quality of socket fit. As an example, significant variation of pressure levels at distal end, could be used to give indication of the socket contact at the distal end. Similarly, loading profile across specific load bearing region of the residuum could be quantitatively evaluated by measuring interfacial pressure and shear stresses. In this study, higher pressure was obtained at the PP location, comparing with the value at AP location. This indicates the main weight-bearing location at the proximal end. A prosthetist could potentially use this information as a guide, to perform rectification and achieve better socket fit.

- A3: Weight shifting

This section presents the results obtained from the activity A3, the detailed protocol of A3 can be found in Section 6.1.2.

During the first 3.5s, subject was one step away from the force plate, preparing for stepping on the force plate (marked as 'preparation' in Figure 6.16c). From approximately 3.5s to 15s, four weight shifting cycles were conducted (marked as '4 cycles' in Figure 6.16c). During those four weight shifting cycles, pressure (Figure 6.16a), S_C (Figure 6.16b) and S_L (Figure 6.16c) showed cyclic patterns.

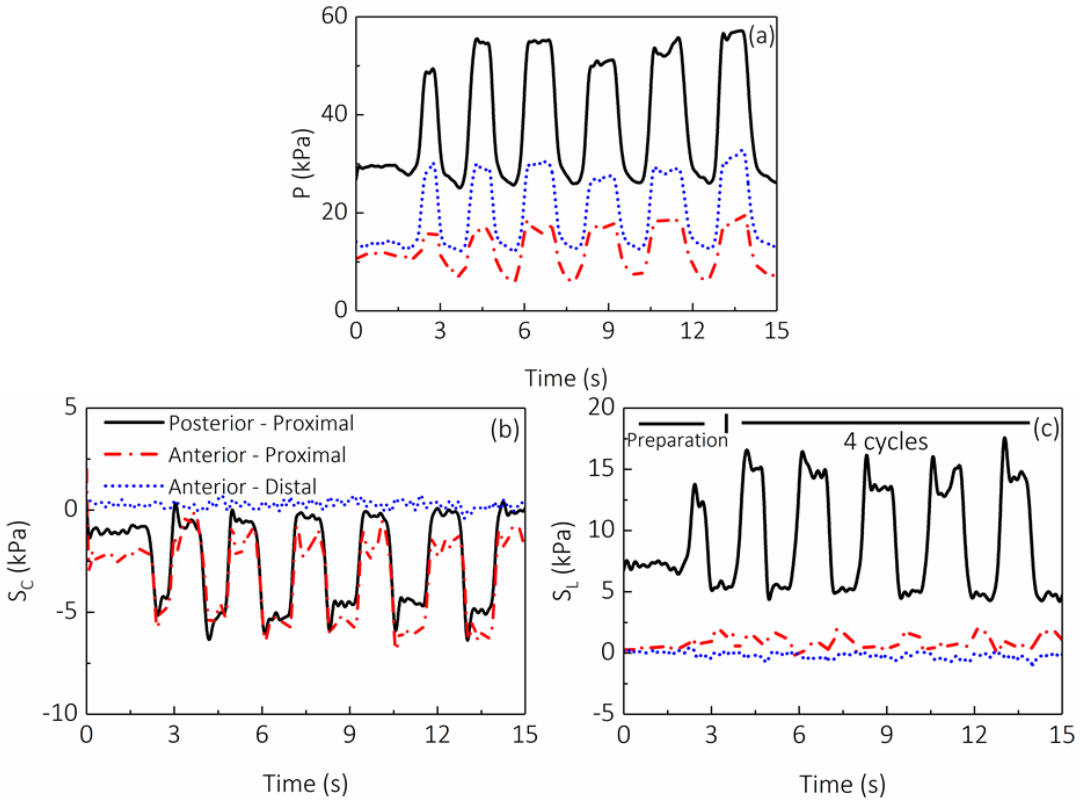

Figure 6.16: (a) Pressure, (b) circumferential and (c) longitudinal shear stresses measured during the weight shifting trial, as a function of time.

In order to facilitate the biomechanical explanation during the weight shifting activity, one cycle (started from 5.70s, ended at 7.80s) were extracted and re-plotted in Figure 6.17. Three separate phases are defined within one cycle. Weight Transfer phase were defined between 5.70s and 6.15s, during which the weight of the participant gradually transferred to the prosthetic limb. The moment when all body weight is transferred to the prosthetic side, signifies the start of the second phase, the Weight Bearing phase. During Weight Bearing phase, body weight is maintained on the prosthetic limb until time reached 7.00s. As the participant started to remove the weight from his prosthetic limb (t = 7.00s), the body weight started to

transfer to his intact side with prosthetic limb suspended in the mid-air, until time reached 7.80s. The activities perform between 7.00s and 7.80s, is then defined as Weight Removal phase.

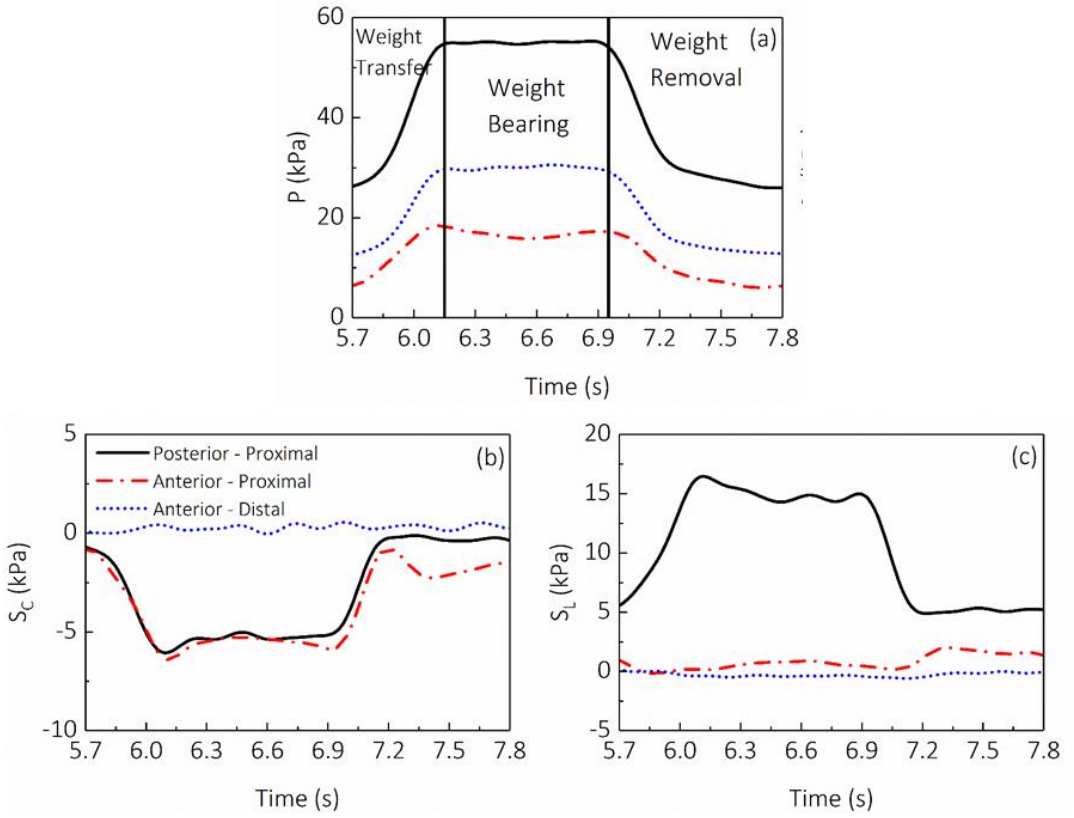

Figure 6.17: (a) Pressure, (b) circumferential shear and (c) longitudinal shear, as a function of time, extract from one of the four cycles

During Weight Transfer phase, as shown in Figure 6.17a, there are general increases of pressure from 28kPa to 55kPa, 8kPa to 18kPa and 16kPa to 30kPa at PP, AP and AD location, respectively. S_C at PP and AP region decreases from -1kPa to approximately 6kPa (Figure 6.17b), while S_C at AD region remains at roughly 0kPa. Little change was observed in S_L at AP and AD location (Figure 6.17c), while S_L at PP location increased from 6kPa to 17kPa during Weight Transfer phase.

During Weight Bearing phase, pressure, S_C and S_L all maintained roughly at the value seen at the end of the Weight Transfer phase. As the Weight Removal phase started, there are general decreases of pressure from its peak value to the value observed at the start of the cycle. Similarly, there are general increases of S_C from its peak negative value to the value seen at the start of the cycle at PP and AP location, while the S_C measured at AD location, remains at the value close to 0kPa throughout the cycle. In addition, there is a general decrease of SL during Weight Removal phase from 30kPa to 16kPa.

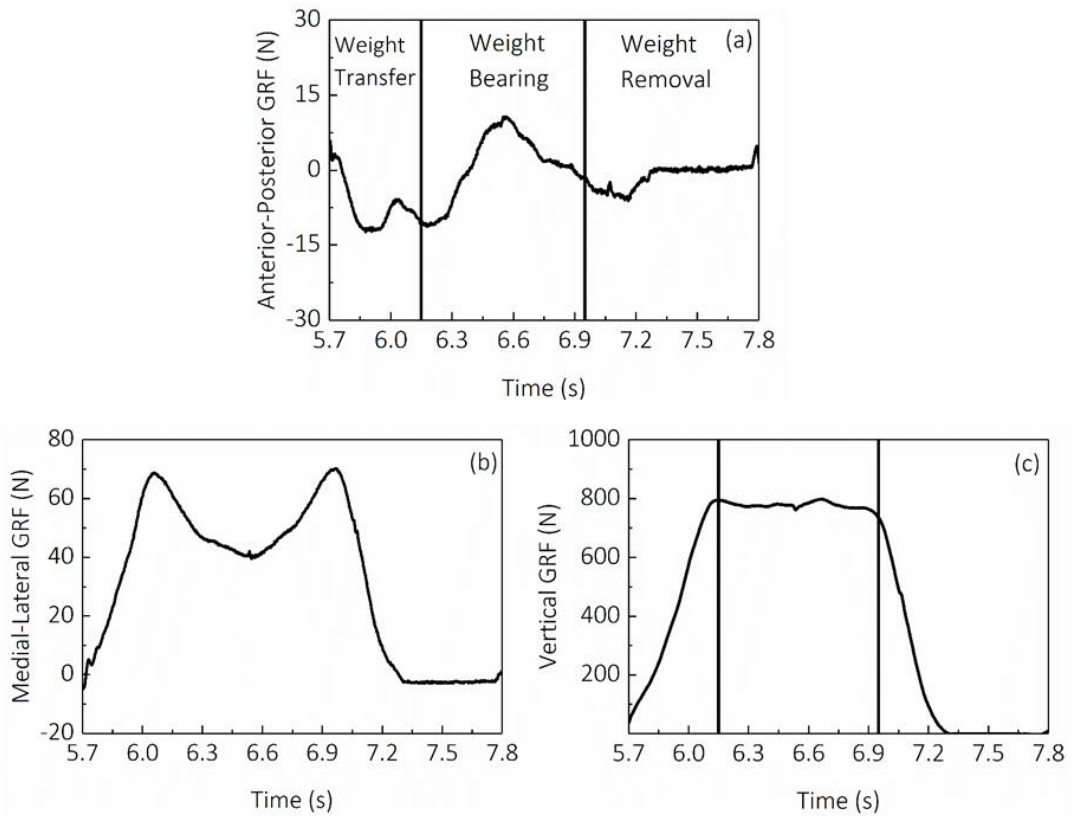

Figure 6.18: (a) anterior-posterior component, (b) medial-lateral component and (c) vertical component of GRF, as a function of time, extract from one of the four cycles

During the 'Weight Transfer' phase, there is decrease of anterior-posterior GRF (Figure 6.18a) from a value close to 0N to a peak negative value of approximately -12N. As the full body transferred to the prosthetic limb, there is an increase in the anterior-posterior GRF to approximately 13N. This is followed by the reduction in the anterior-posterior GRF to approximately -6N at the end of the 'Weight Bearing' phase. During the 'Weight Removal' phase, the anterior-posterior GRF restores to 0N as the prosthetic limb lifted from the force plate.

During the 'Weight Transfer' phase, medial-lateral GRF (Figure 6.18b) increases from a value close to 0N to up to 70N, pointing medially. It decreased from the start and reached approximately 44N by the mid 'Weight Bearing' phase. It further increases during the second half of the 'Weight Bearing' phase by the starting point of the 'Weight Removal' phase, it reached to approximately 71N. During the Weight Removal phase, the medial-lateral GRF reduces to 0N as the prosthetic limb lifted off from the force plate.

During the 'Weight Transfer' phase, there is a rapid increase in vertical GRF (Figure 6.18c) to a peak value of 800N. Then the vertical GRF is maintained at approximately 800N throughout the

'Weight Bearing' phase, until the start of 'Weight Removal' phase. During the 'Weight Removal' phase, the vertical GRF returned to 0N as prosthetic limb lifted off from the force plate.

As expected, the vertical GRF dominates the load transfer comparing with anterior-posterior and medial-lateral GRFs. As the vertical GRF increases during the 'Weight Transfer' phase (Figure 6.18a), increases in interface pressure (at all locations, Figure 6.17a) and S_L (at PP location, Figure 6.17c) were also evident. The time when peak pressure and S_L was reached (6.10s) was also at 6.1 s, aligning briefly with that of the vertical GRF (6.15s). The slight 0.05s shift could be attributable to the visco-elastic mechanical behaviour at the interface caused by combination of socket fit, residuum tissue, liner elastomer properties etc. This time shift was also reported in previous studies (Section 2.7.3). In addition, pressure at all locations maintained at their peak values (Figure 6.17a) during the 'Weight Bearing' phase when almost constant vertical GRF were also observed (Figure 6.18c).

Negative S_C obtained at PP and AP locations were observed in 'Weight Transfer' and 'Weight Bearing' phase (Figure 6.17b), suggesting the shear stress was acting medially to the residuum at PP location and laterally at AP location. This can then be translated to the potential clock-wise rotation of the residuum in relation of the socket, which may contributed to the medially-directed GRF (Figure 6.18b). Positive S_L obtained at PP location suggests the shear stress was acting proximally to the residuum. This could be linked to the 'push-in' motion of the residuum into the socket as the residuum was loaded under body weight.

6.2.2 Level walking activity

This section presents the results obtained from the activity A4, the detailed protocol of A4 can be found in Section 6.1.2.

Temporal profile of the interface stresses

A double-hump pressure profile (Figure 6.19a) was observed across all four test sessions. At IC, pressure increased from a value close to 20N to a peak of approximately 60N at 10% of GC (1st peak). It was followed by a small decrease in pressure to approximately 30% of GC, as gait progressed to mid-stance phase. From mid-stance to TS phase (45% of GC), pressure further increased and a 2nd peak was reached (up to 55kPa). During the remainder of the stance phase and swing phase, pressure decreased until it restored to the value at IC.

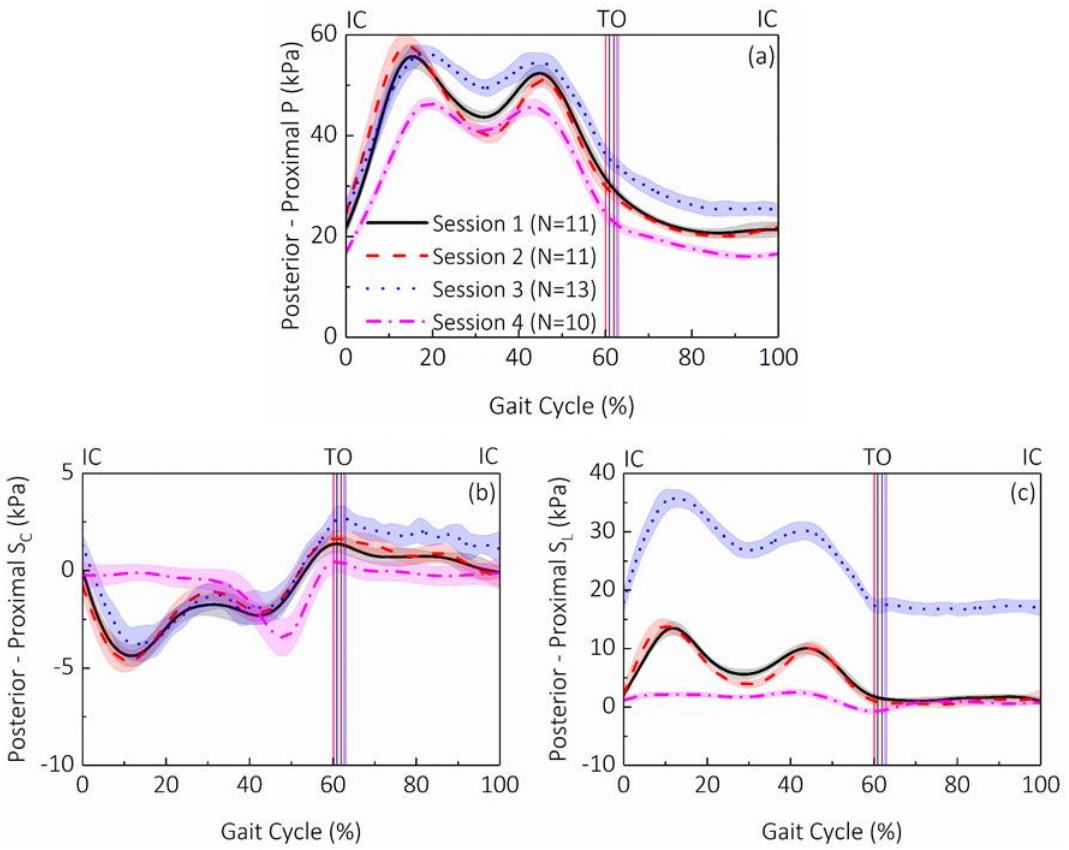

Figure 6.19: (a) Pressure, (b) S_C and (c) S_L measured at PP location of the residuum, over a GC, across four data collection sessions

S_C (Figure 6.19b) deceased from a value close to 0kPa at IC to a peak value of up to 5kPa at 10% of GC. This is followed by an increase of S_C from 10% of GC to mid-stance phase, attaining a value of approximately -2kPa. It is worth noting that, in the 4th data collections session, little change in S_C (less than 0.5kPa) was observed between IC and mid-stance phase of the GC. In the transition between mid-stance to TS phase, a slight decrease was observed in the S_C values from the first three data collection sessions. During the remainder of the stance, an increase of S_C was evident until at TO, it restored to the value seen at IC. A change in S_C of up to 1kPa was observed during swing phase in all four sessions.

During the first three test sessions, a double-hump S_L (Figure 6.19c) profile was observed, however little change in S_L (up to 2kPa) was observed during the 4th data collection session. Clearly, a value of S_L of approximately 20kPa was measured at the PP location in test Session 3, compared to values of approximately 2kPa in Sessions 1, 2 and 4. From IC to approximately 10% of GC, there was a general increase of S_L, which was followed by the decrease between 10% of GC to approximately 30% of GC. As gait progressed from mid-stance to TS phase, a further increase of S_L was evident. During the remainder of the stance phase, S_L decreased to attain the value seen at IC. In the swing phase, little change was evident in S_L. It is worth noting that

a double-hump pressure profile was observed in all test session. However, the temporal profile of the both shear stresses (S_C and S_L) observed in test Session 4 was different from the ones from the other sessions. This may suggest that the residuum was in contact with the PP location of the socket, however, the friction behaviour has changed in test Session 4 comparing to the other sessions. The change in frictional behaviour could due to several reasons. As an example, when the coefficient of friction decreases at the interface, a reduction of shear stress may occur with the same magnitude of pressure, which may explain the reduction in the magnitude of S_L at PP in test Session 4. In addition, if relative motion e.g. pistoning motion or slip, occur between the residuum and the socket, shear force may not be transferred to the sensor unit.

Pressure (Figure 6.20a) revealed a double-hump profile during stance phase. At IC, a pressure value of approximately was measured and this increased to a peak value of up to 33kPa at approximately 15% of GC. There was a subsequent decrease of pressure to 30% as gait progressed to the mid-stance phase. Pressure further increased from mid-stance to TS with peak value of up to 30kPa. For the remainder of the GC, during data collection 1, 2 and 3, pressure decreased and was restored to the value seen at IC. However, in test Session 4, the value of pressure reached 4kPa which was lower than the one at IC. In swing phase, an increase in pressure of up to 5kPa was evident. This difference observed in the temporal profile could be potential resulted from the lack of contact at AP location during TS phase. The lack of contact in TS may to the reduction in the proprioception of the limb. This further explains the subsequent increase of pressure in swing phase as the muscle could be activated to regain the control of the socket.

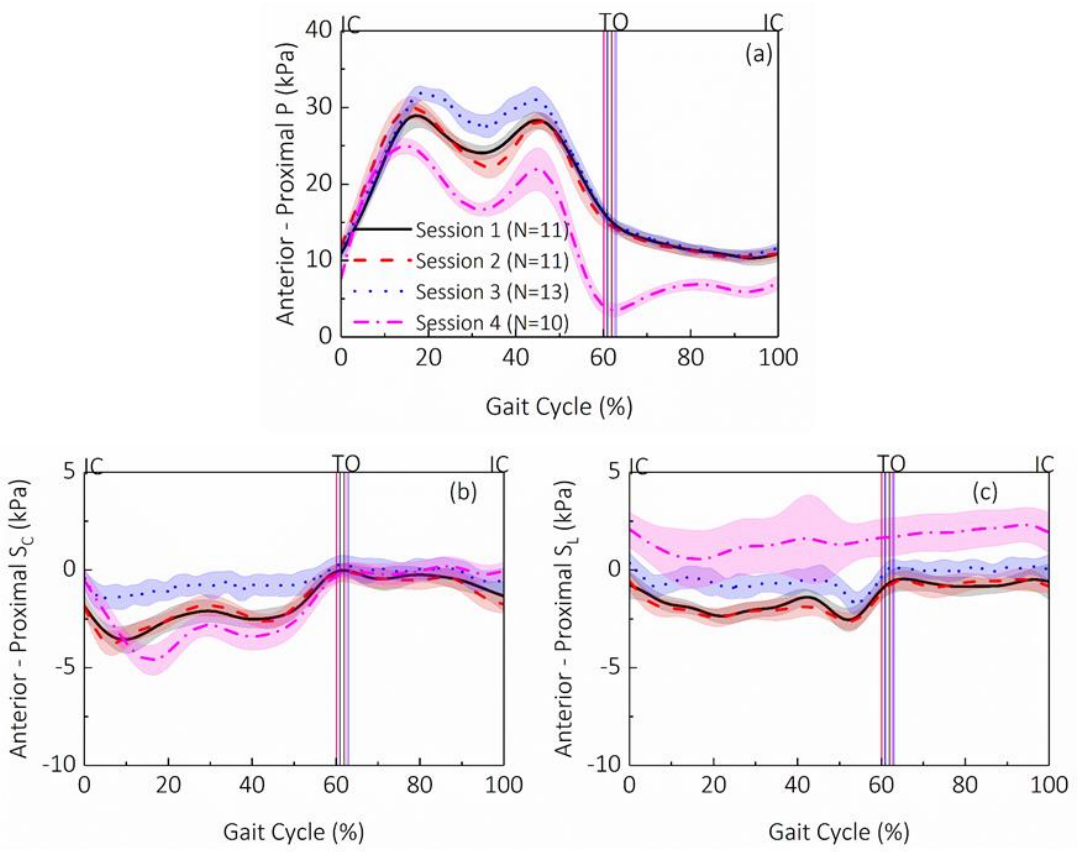

Figure 6.20: (a) Pressure, (b) S_C and (c) S_L measured at AP location of the residuum, over a GC, across four data collection sessions

It is first worth noting that the response in test Session 3 was clearly different to the other with a very small S_C (Figure 6.20b) of less than 1kPa. By contrast, a double-hump profile was clearly observed in test Session 1, 2 and 4. Therefore, it is evident that higher pressure may not lead to a corresponding higher shear stress, as other factors such as interface friction may play a critical role in the mechanical behaviour of shear stress. Similar to the S_C observed at PP location, S_C at AP decreased from IC to a negative peak of up to -5kPa during 10-20% of GC. It was then recovered to approximately 30% of GC. As gait progressed from mid-stance to TS phase, S_C further decreased to up to -3kPa. During the remainder of the stance phase, it increased until it eventually was restored to the value seen at IC. In addition, during swing phase, S_C revealed negligible change (less than 1kPa). During the first three test sessions, S_L (Figure 6.20c) values of up to -2kPa of S_L were measured. While in the last data collection, S_L values of up to +2kPa of S_L were measured at IC, with negligible change over the GC.

It is worth noting here the abnormal sensor outputs were observed in Session 3 as the participant reported after Session 3 that the AD sensor location was particular sensitive to loading due to the presence of the nerve endings. Thus, this may cause abnormal muscle

contraction locally. Thus, only results obtained session 1-3 was included and discussed as shown in Figure 6.21.

In session 1, 2 and 4, a double-hump profile for pressure was measured at AD location (Figure 6.21a). By contrast, in test Session 3, during TS phase (55% of GC), an abrupt increase of pressure was evident. It is worth noting here that, the abrupt peak observed at 55% of GC can be also associated with the verbal confirmation from the participant. The participant reported that the anterior-distal aspect of the femur was in contact with the socket when initiating the swing phase. In addition, according the participant, this location is also sensitive to loading due to the presence of the nerve endings. Intra-session differences were noted with a pressure value of approximately 25kPa at IC for session 4, with a corresponding value of approximately 9kPa of pressure obtained in test Session 1, 2 and 3.

In session 1, 2 and 4, pressure increased to its first peak at approximately 15% of GC. It was followed by a slight decrease during the transition between 15% of GC to 30% of GC (mid-stance). It then further increased as gait progressed to the TS phase. Unlike the pressure profile observed at PP and AP locations, at TO, pressure at AD was not restored to its value at IC. Instead, pressure continued to decrease throughout the swing phase and reached the value approximately seen at IC, at 100% of GC. This is likely due to the design of the socket. For a supra-condylar suspension socket, the weight of the prosthesis was suspended at the distal end of the socket. The presence of pressure during the entire GC may suggest that the residuum was always in contact with the socket. This parameter, namely, whether the residuum is always making contact with the socket, could be further developed as a clinical parameter for monitoring the quality of the suspension during dynamic gait.

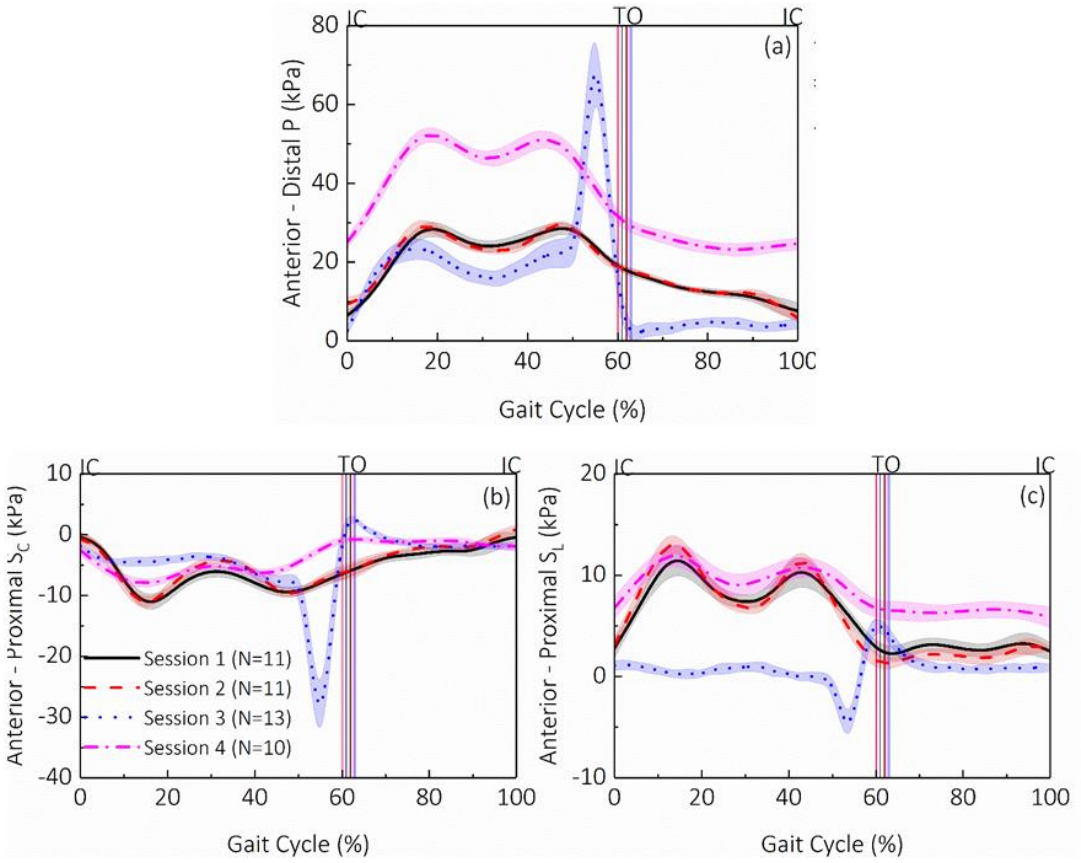

Figure 6.21: (a) Pressure, (b) S_C and (c) S_L measured at AD location of the residuum, over a GC, across four data collection sessions.

A double-hump profile in S_C (Figure 6.21b) was observed in test Session 1, 2 and 4. In these sessions, S_C decreased from 0kPa at IC to a negative peak of -11kPa at 15% of GC. Subsequently, S_C increased and reached approximately -5kPa at 30% of GC. However, in test Session 3, S_C revealed negligible change from IC to mid-stance phase. After mid-stance phase, in all sessions, S_C increased and reached the second peak at the TS phase. During the remainder of the GC, S_C was restored to the value seen at IC.

A double-hump-profile again evident in test Session 1, 2 and 4 (Figure 6.21c). S_L with a well-defined increase from IC to approximately 15% of GC. Then, the S_L decreased from early stance phase into mid-stance. During the transition from the mid-stance phase to the TS phase, there was an increase in S_L, reaching it 2nd peak in stance phase. During the remainder of the stance phase, S_L was restored to the value seen at IC. It is worth noting that, in session 3, negligible changes in S_L were observed for most of the stance phase while changes were only evident until the TS phase of the GC. In swing phase, negligible change was observed.

Peak values, in both WA phase and TS phases, for pressure, S_C and S_L are illustrated in Table 6.2.

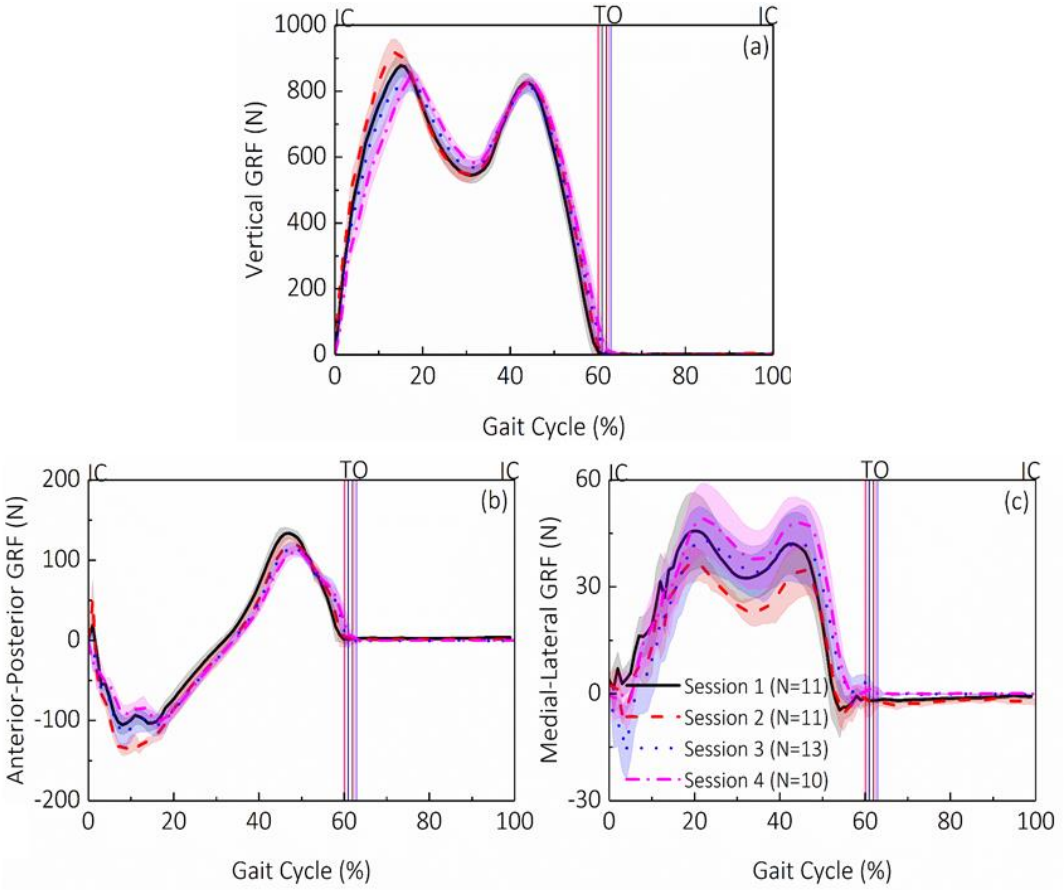

Figure 6.22: Three component of GRF, obtained across four data collection sessions.

It is envisaged that the interface kinetics can be directly associated with the load transfer from the ground interface, as illustrated Section 2.5.1. GRFs were collected in order to facilitate the discussion of the interface kinetics. Figure 6.22 compares GRFs obtained across four test sessions. The vertical GRF (Figure 6.22a) showed a typical double-hump profile across all four data collection sessions. The anterior-posterior GRF (Figure 6.22b) revealed a peak negative force occurring at approximately 15% of GC and a peak positive force at approximately 46% of GC. A positive medial-lateral GRF was observed in most of the stance phase with two peaks at approximately 20% of GC and 45% of GC. Peak values extracted from the three components of GRF were illustrated in Table 6.3.

Table 6.2: Peak pressure, S_C and S_L observed as Weight Acceptance (WA) phase and TS phase of the GC, across four sessions.

Session No.	Pressure (kPa)						Sc (kPa)						SL (kPa)					
	PP		AP		AD		PP		AP		AD		PP		AP		AD	
	WA	TS	WA	TS	WA	TS	WA	TS	WA	TS	WA	TS	WA	TS	WA	TS	WA	TS
1	56 ± 2	52 ± 2	29 ± 1	28 ± 1	28 ± 2	29 ± 1	-4 ± 1	-4 ± 1	-4 ± 0	-3 ± 1	-11 ± 1	-9 ± 1	13 ± 1	10 ± 1	-2 ± 0	-2 ± 0	11 ± 1	10 ± 1
2	57 ± 2	51 ± 1	30 ± 1	28 ± 0	29 ± 1	29 ± 0	-5 ± 1	-2 ± 1	-4 ± 1	-3 ± 1	-11 ± 1	-8 ± 1	14 ± 1	10 ± 1	-2 ± 0	-3 ± 0	13 ± 1	11 ± 1
3	57 ± 2	54 ± 1	31 ± 1	31 ± 1	23 ± 2	67 ± 5	-4 ± 1	-2 ± 1	Note[a]	Note[a]	Note[b]	-28 ± 5	36 ± 1	30 ± 1	Note[c]	Note[c]	Note[d]	Note[d]
4	46 ± 1	45 ± 1	25 ± 0	22 ± 1	52 ± 2	51 ± 2	Note[e]	-3 ± 1	-5 ± 2	-3 ± 1	-8 ± 1	-5 ± 1	Note[f]	Note[f]	Note[g]	Note[g]	12 ± 1	11 ± 1

Note:

[a]*Negligible change in S_C at AP location of the residuum was observed, during session 3, therefore, no clear peak at WA and TS was observed.*
[b]*Negligible change in SC at AP location of the residuum at WA, during session 3.*
[c]*Negligible change in S_C at AP location of the residuum was observed, during session 4, therefore, no clear peak at WA and TS was observed.*
[d]*No double-hump profile was observed in SL at AD location, during session 3. Instead, S_L only showed an abrupt change from -5kPa to 5kPa during 50%-60% of GC.*
[e]*No clear S_C peak at WA were observed, during session 4, at AP location.*
[f]*No double-hump profile was observed in S_L at PP location, during session 4.*
[g]*No double-hump profile was observed in S_L at AP location, during session 4.*

Table 6.3: Peak values obtained from three component of GRF at WA and TS phase of GC.

Session No.	Anterior-Posterior GRF (N)		Medial-Lateral GRF (N)		Vertical GRF (N)	
	WA	TS	WA	TS	WA	TS
1	-105 ± 12	+133 ± 7	47 ± 9	42 ± 8	878 ± 34	825 ± 27
2	-136 ± 8	+119 ± 8	37 ± 3	33 ± 8	956 ± 39	826 ± 6
3	-114 ± 8	+114 ± 8	43 ± 9	42 ± 8	840 ± 40	810 ± 25
4	-102 ± 8	+110 ± 6	49 ± 10	48 ± 6	841 ± 30	825 ± 16

Intra-session repeatability of the stress measurement

Intra-session SD reveals a value in the range of 0-2kPa for the three parameters, pressure, S_C and S_L for each of three locations of the residuum. However, higher SD values of up to 5kPa were evident in pressure and S_C for Session 3. These findings should be compared to the variability reported in the previous studies, namely a SD for pressure measurements of between 20kPa [247]-194kPa [9]. With regards to the interfacial shear a SD of up to 35kPa [203] has been reported. It is evident that the present intra-session repeatability with the tri-axial sensors represents a significant improvement to those previously used. However, some caution is needed as it is often difficult to directly compare data on intra-session repeatability when using different measurement devices, test protocols and investigators.

It is worth noting that the intra-session repeatability presented in this study was based on the stress measurement collected over a period of one hour. Future work may need to evaluate the stress variation during the course of a day without doffing the socket. It is estimated that, a greater SD value, due the change in socket fit, may be expected when evaluating the data collected during the course of a day. Therefore, one could envisage that the change in SD value, for example, measured in hourly base, can be used as one of control criteria for a shape-adaptive socket, maintain the optimum fit for the socket.

Inter-session repeatability of the stresses measurement

It was important to investigate further the inter-session repeatability of pressure and shear measurement. Two scenarios were chosen, a relatively short-term test and a long-term test. When comparing the values obtained from test Session 1 and Session 2 (3 days apart), both pressure and shear showed a double-hump waveform (Figure 6.19-Figure 6.21), suggesting a high degree of waveform repeatability. In terms of peak values obtained at WA and TS (Table 6.3), up to 1kPa and 2kPa difference was found in pressure and shear measurement between the two sessions, respectively. There is no statistical difference ($p>0.05$) found the in the pressure and shear obtained in the test Session 1 and Session 2. This suggested a reasonable degree of repeatability. It is worth noting that, for test Session 1 and Session 2, the starting time of the two data collections was approximately 11:00 a.m. In addition, the participant ensured that he had undertaken no intensive activities prior to the test session. This suggested that the residual limb volume and residuum/socket interface may have remained relatively stable between test sessions. The similar test and interface condition as explained above may contributed the good repeatability in measured pressure and shear obtained during the two sessions.

The long-term inter-session repeatability was assessed by using the pressure and shear measurements obtained with 49 days apart (the 2nd and the 3rd Session). The two sets of the measurements are approximately two months apart. When comparing these measurements, there were little difference in the peak pressure at PP and AP, with values of up to 3kPa at WA and TS phase. However, a higher pressure value (67kPa) was obtained at the AD location during TS in the latter session, compared with 29kPa measured in the former session. In terms of S_C measured between the two sessions, similar peak values and waveform were observed at the PP location. However, negligible change of S_C (up to -1kPa) as found at AP location in the latter session, comparing to the former session. At AD location, higher S_C (-28kPa) were obtained at TS phase in the latter session, in comparison to the former session (-8kPa).

There were clear differences (p=0.00) between the S_L measured at the PP location, with values of 15kPa and 2kPa obtained at IC. The difference presented at IC could resulted from the effect of donning and doffing of the socket. As mentioned in the previous section, up to 8kPa of S_L difference was observed due to doffing and donning of the socket. Furthermore, although both of the test session was conducted at similar time of the day, the residuum volume may be different on the two testing days. At the AD location, in the former session, a double-hump profile was evident, while the S_L only began to change just before the TO with no double-hump profile presented.

It is clear that there are marked differences in both waveform patterns and peak values for pressure and shear across 49 days. A similar observation was reported by Sanders et al. [190] whereby no significant change of interface stresses was reported diurnally. However, difference of up to approximately 1.6 times those of diurnal changes in pressure and shear values were reported when compared with pressure and shear values measured over the 20-week interval. The large variation could be caused by various factors, notably the variation in residuum volume, gait patterns and prosthetic alignment (Section 2.5.3) etc. Thus, for future applications, it would be advantageous to undertake interface stresses evaluations on the same day if different socket fitting or socket types needs to be compared and/or evaluated for a particular amputee.

In this study, interface stress obtained a short-term period and a long term were analysed on a single participant. Future work is needed to investigate the repeatability on a large cohort of participants and across a longer period of time. The investigation of the change in interfacial stress in both short-term and long-term intervals could potentially help to determine whether

an intervention is need at certain time of the year. This could also assist clinicians to predict lifetime of the socket i.e. when a new socket might need to be fitted.

Interface kinetics

Interface stresses at PP and AP locations follow similar profile of the corresponding vertical GRF. The timing of the two pressure peaks aligns well with the peaks observed in the vertical GRF (WA peak at 15%, TS peak at 45%, approximately). Pressure values of up to 57kPa were measured at PP location and pressure values of 31kPa were obtained at AP location. These peak pressure values obtained at PP and AP locations match well with those reported by Lee et al [194] on two trans-femoral amputees. In their study, at seven out of eight sites of the residuum, less than 60kPa of pressure were reported at PP location. Similarly, the highest pressure was measured at PP location of the residuum on the knee-disarticulation participant. Higher pressure values at PP location as compared with pressure at AP location in stance phase aligns with the conceptualised estimation of residuum movement relative to socket proposed by Hughes [192]. Hughes et al. proposed that, hip extensor moment would dominant the early stance phase to stabilise the prosthetic limb. This corresponds to the gluteus maximus muscle activation at posterior-proximal region of the thigh. This could further lead to the increase in pressure at PP location. At the AD location, pressure values of up to 67kPa were measured, significantly higher than the values (20-30kPa) recorded by Lee et al. This could potentially explain the stress concentrations at the AD location of the residuum on the knee-disarticulation amputee, resulting from the presence of prominences like LFE and MFE.

Negative S_C, in the both absolute value and the direction of change, were measured at all three locations of the residuum. According to Figure 6.5, a negative change in S_C, at PP location, can then be translated as a circumferential shear stress acting medially to the residuum tissue. However, a negative change in S_C, at AP and AD locations, is equivalent to circumferential shear stress acting laterally to the residuum tissue. Accordingly, the lateral force at anterior location and the medial force at posterior location could create a torque which rotates the residuum in the clockwise direction, relative to the socket. It is also worth noting that, a medial directed GRF was observed at ground interface. In theory, this medial directed GRF will be further transferred from the ground to the bottom of the socket, resulting in the circumferential shear stress acting laterally to residuum. This mechanism aligns with the direction of the circumferential shear stress (pointing laterally) observed at AP location, although it is not consistent with the S_C direction, namely pointing medially, at the PP location. This suggests that the stresses acting at the residuum/socket interface behaved in a more complex than predicted

by conventional theory. The conventional theory involves the calculation of loads transferred to the distal socket without taking the residuum muscle activation and socket designs etc.

Positive S_L values with double-hump profiles were observed at both PP and AD location in three out of four sessions. The positive S_L, in the stance phase, suggested that the longitudinal shear stress acted proximally to the residuum tissue. In effect, the residuum was moving distally relative to the socket. This could explain by the increase of vertical GRF at WA and TS phase of the GC, pushing the socket in the proximal direction, in relation of the residuum.

In this section, the repeatability of interface kinetics was assessed by performing walking test on level surface with controlled cadence. In the next section, the interface kinetics will be assessed by walking on level surface with different walking speed.

6.2.3 Walking at different speeds

As reviewed in Section 2.5.3, by walking at different speed, the load transfer mechanism through the prosthetic limb may be altered, which may result in the change in interface kinetics. This section presents the results obtained from the activity A5, the detailed protocol of A5 can be found in Section 6.1.2.

Walking speed obtained in the two sessions

Two sessions were carried out to investigate the effect of walking speed on the residuum/socket interface kinematics. Figure 6.23 shows the walking speed obtained in the two sessions. Walking speed of up to 1.20±0.03m/s, 1.40±0.01m/s and 1.65±0.03m/s were obtained when walking cadence is controlled at 80BPM, 100BPM and 120BPM, respectively. It is also worth noting that when comparing each of the two walking speeds, the difference obtained in the two walking speeds are statistically significant (all p=0.00).

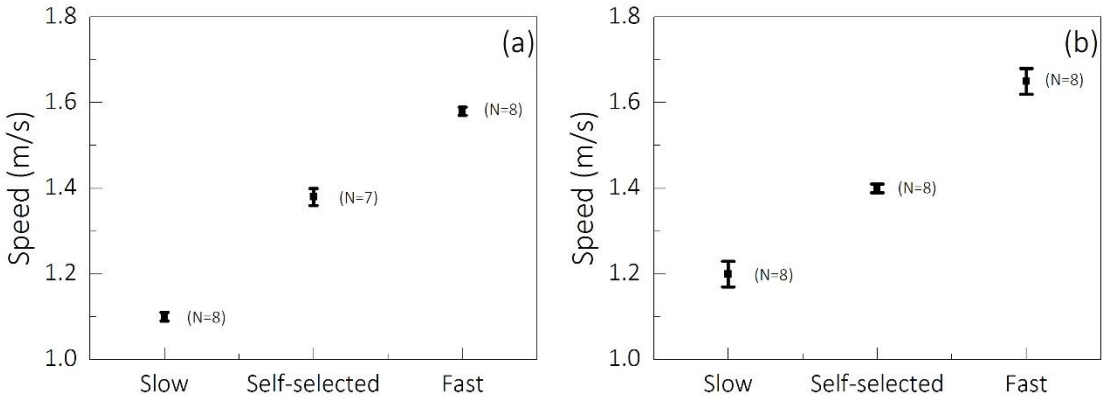

Figure 6.23: Mean and one SD of the three different walking speeds obtained in Session 1 and Session 2, when investigating the residuum/socket interface kinetics.

GRF

With regards to the vertical GRF (Figure 6.24a and Figure 6.25a), higher WA peak (p=0.00) was measured when walking at self-selected speed in Session 1, compared with the values in Session 2 (Table 6.4). However, no statistical difference (p>0.05) was found in WA peak when walking at slow and fast speed, between the two sessions. The increase in walking resulted in no significant (p>0.05) change in WA peak of vertical GRF in Session 1. In Session 2, a decreased WA peak of vertical GRF (p=0.00) was evident when walking at slow speed, compared with the value at self-selected speed. No significant difference (p>0.05) was found in WA peak of vertical GRF when walking at fast speed, compared with the value at self-selected speed. Therefore, the increase in walking speed resulted little change in the WA peak of vertical GRF, with the exception of the value obtained in Session 2 when walking at slow and self-selected speed. This finding is not consistent with the study conducted on both able-bodied group [248] and amputee group [249], as the WA peak of vertical GRF increase linearly with walking speed. This is likely attributed from the little change in the body centre of mass acceleration at WA.

Peak values at mid-stance and TS phase reveal no statistical difference (p>0.05) in both sessions, regardless of walking speed. However, the increase in walking speed resulted in an increase (all p=0.00) in mid-stance peak of vertical GRF, in both sessions. This is likely due to a more rapid deceleration of body centre of mass as walking speed increase in mid-stance. In addition, higher TS peak (p=0.00) was measured in vertical GRF when walking at self-selected speed, compared with the value at slow speed, in both sessions. Whereas no significant difference (all p>0.05) was revealed in TS peak of vertical GRF when walking at fast speed, comparing to the value at self-selected speed, in both sessions. It is worth noting, the timings at which mid-stance and TS peak occur were delayed, as walking speed increases.

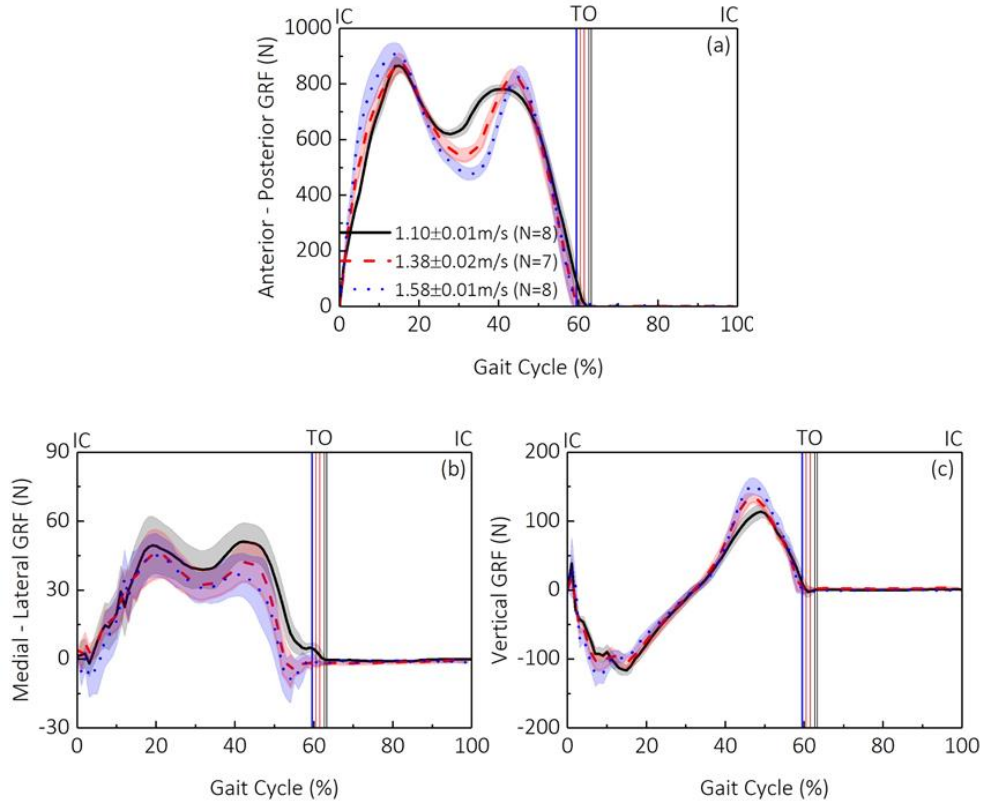

Figure 6.24: (a) vertical component, (b) medial – lateral component and (c) anterior – posterior component of GRF measured in session 1, over a GC, when walking at slow, self-selected and fast walking speed.

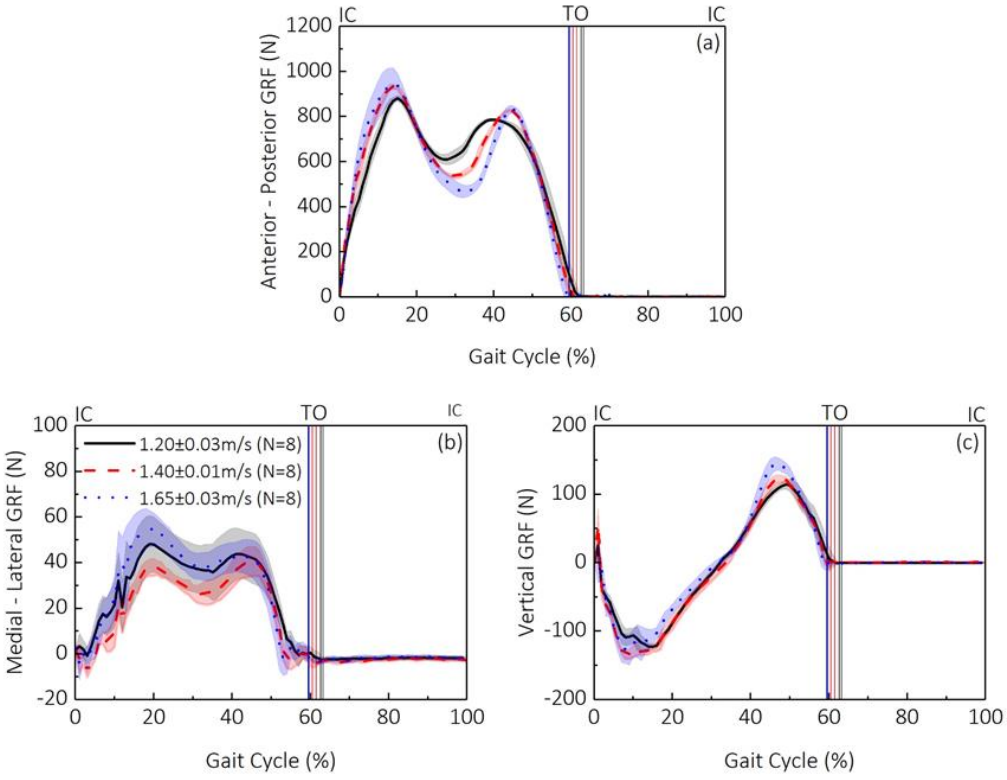

Figure 6.25: (a) vertical component, (b) medial – lateral component and (c) anterior – posterior component of GRF measured in session 2, over a GC, when walking at slow, self-selected and fast walking speed.

There is no consistent trend in the medial-lateral GRF. This may be explained by the lack of medial-lateral stability for the knee disarticulation participant. In addition, there was no feature designed on the socket to control the medial-lateral stability.

With regards to the anterior-posterior GRF, no significant difference ($p>0.05$) was found in peak braking force when walking at slow and fast speed. However, when walking at self-selected speed, a greater braking force ($p=0.00$) was measured in Session 2, compared with the value in Session 1. There is no consistent trend observed in peak braking force, with the increase in walking speed. With regards to the peak propulsive force, the increase in walking speed resulted in the increase in a greater propulsive force in both sessions (all $p<0.05$). This is consistent with the previous study [249] and may be associated with a greater anterior-posterior acceleration of the foot.

At mid-stance phase, as shown in Table 6.4, the increase in walking speed led to the decrease of vertical GRF (23% in both sessions). In addition, the timing, at which the mid-stance peak occurred, shifted to a later phase of the GC (5% in both session). This could possibly explain the decrease of pressure at PP and AP location at mid-stance and timing shift towards later phase of GC.

At TS phase of GC, as shown in Table 6.4, the increase in walking speed led to the shift (up to 6% of GC) of the timing at which TS peak of vertical GRF occur. This could potentially explain the delayed peak at TS, observed in S_L measurement at PP and AD location.

Temporal profile of the interfacial stress

Double-hump profiles were observed in pressure, S_C and S_L in both sessions (Figure 6.26 and Figure 6.27). As shown in Figure 6.26a and Figure 6.27a, pressure values increased from approximately 20kPa (at IC) to a WA peak at 10-20% of GC. This was followed by a decrease of pressure, reaching a local minimum value at mid-stance phase. During the transition to TS, pressure further increased, reaching the second peak at TS. During the remainder of the GC, pressure decreased to be restored to the value measured at IC.

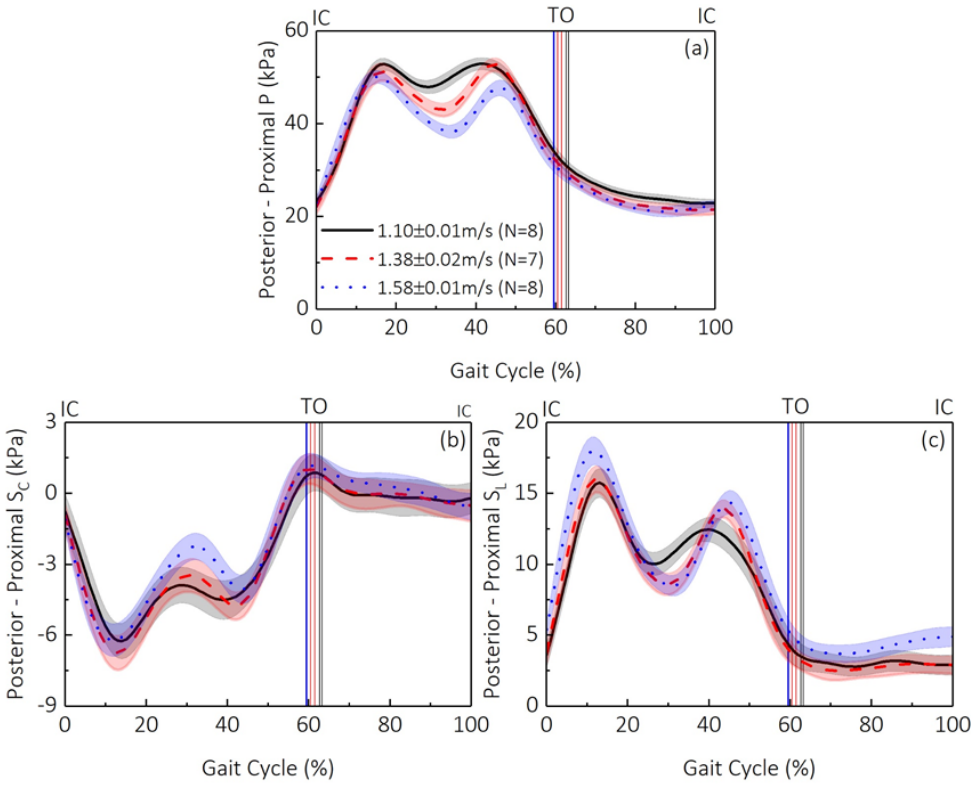

Figure 6.26: (a) Pressure, (b) S_C and (c) S_L measured at PP location of the residuum in session 1, over a GC, when walking at slow, self-selected and fast walking speed.

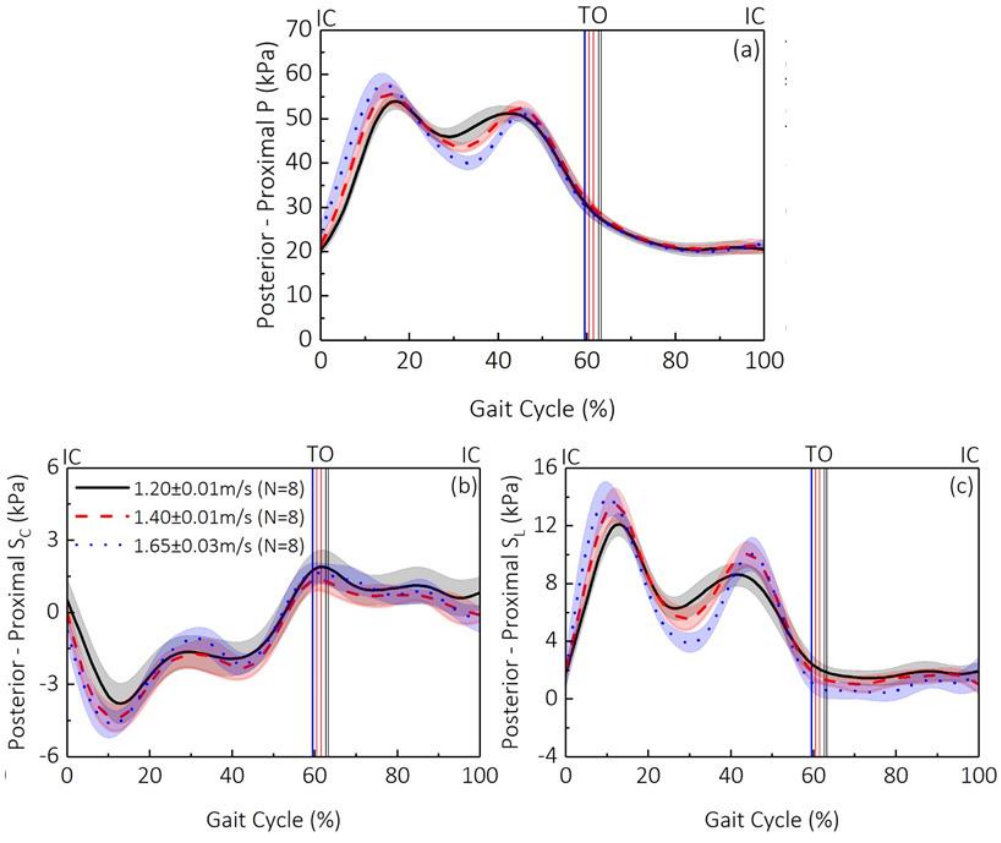

Figure 6.27: (a) Pressure, (b) S_C and (c) S_L measured at PP location of the residuum in session 2, over a GC, when walking at slow, self-selected and fast walking speed.

From IC to approximately 16% of GC (WA), S_C decreased to a peak negative value (Figure 6.26b and Figure 6.27b). S_C then increased, reaching a local maximum at mid-stance phase. Subsequently there was an increase of S_C until TO. In swing phase, S_C stabilised reaching the value measured at IC.

S_L increased from IC to approximately 13% of GC, reaching its WA peak (Figure 6.26c and Figure 6.27c). This was followed by a decrease in S_L in mid-stance phase, reaching a local minimum value. After mid-stance, it further increased until TS phase. During the remainder of the stance phase, S_L decreased and was restored to the value measured at IC. In swing phase, a change in S_L of approximately 1kPa was measured in Session 2. It is worth noting during the swing phase of Session 1, when walking at fast speed, an increase of S_L of up to 2kPa was measured. The fast walking speed could result in a greater inertial force, pulling the prosthesis away from the residuum. This may influence the proprioception of the prosthetic limb and could potentially lead to an unstable IC for the next GC. In order to counter act this tensile force, muscle may be fired in order to pull the prosthesis back. However, little difference was found in the hip power generation in swing phase obtained from gait analysis study (Figure 4.9) when walking at three different speeds. By contrast, axial length (Figure 5.29) showed a greater recovering trend in both magnitude and rate when walking at fast walking speed, compared with the ones obtained with normal and slow walking speeds. This shows that the two techniques force the evaluation of interface kinematics and kinetics have the potential to offer a more localised mechanics comparing to conventional gait analysis technique.

Double-hump profiles were only evident in pressure in both sessions (Figure 6.28 and Figure 6.29). pressure increases from IC to approximately 17% of GC, reaching its WA peak (Figure 6.28a). This was followed by a decrease to mid-stance phase and subsequent increase in TS phase. During the remainder of the GC, pressure decreased and reached the value measured at IC.

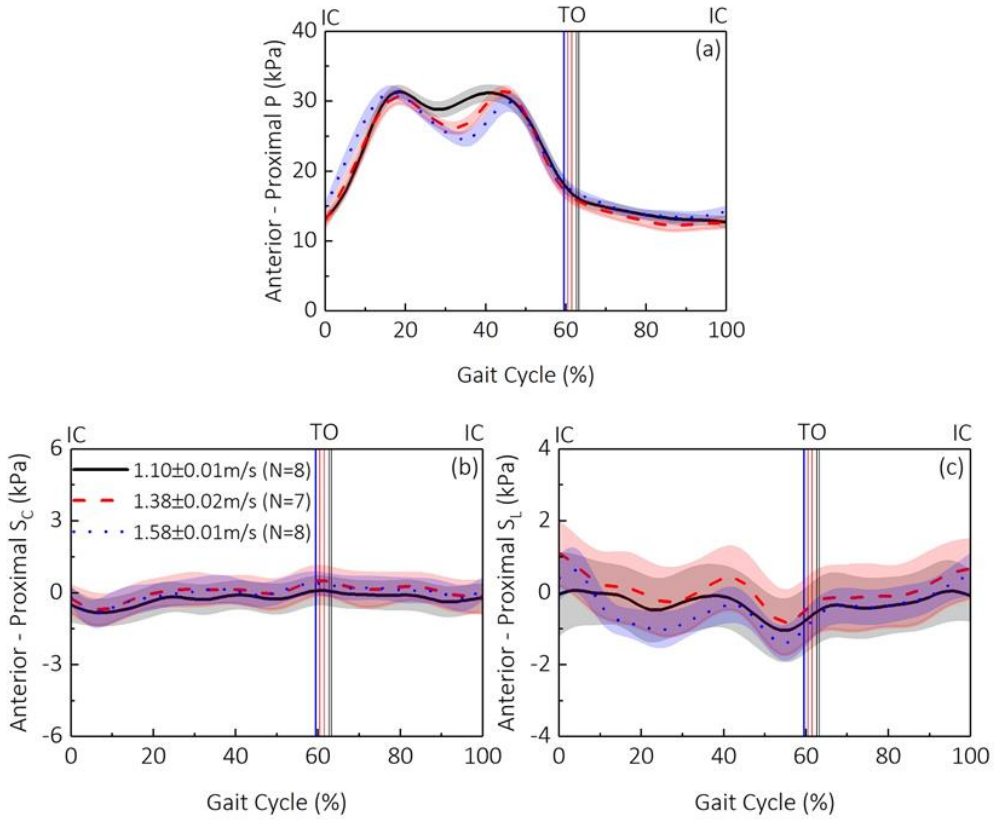

Figure 6.28: (a) Pressure, (b) S_C and (c) S_L measured at AP location of the residuum in session 1, over a GC, when walking at slow, self-selected and fast walking speeds.

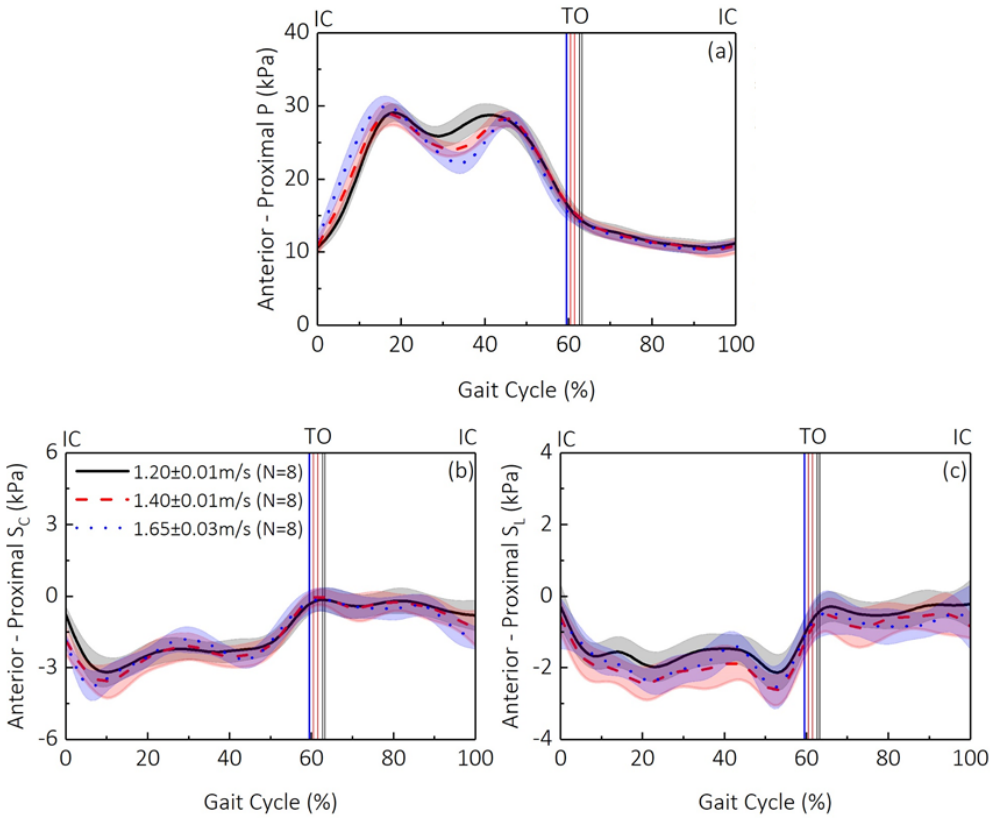

Figure 6.29: (a) Pressure, (b) S_C and (c) S_L measured at AP location of the residuum in session 2, over a GC, when walking at slow, self-selected and fast walking speeds.

In Session 1, a value of less than 1kPa of S_C was measured, while a corresponding value during Session 2 was 3kPa (Figure 6.28b and Figure 6.29b). Negligible S_L values were measured during both sessions (up to 3kPa), as shown in Figure 6.28c and Figure 6.29c.

Double-hump profiles were evident in most of the pressure, S_C and S_L measurements, in both sessions. Pressure increased from IC to approximately 19% of GC reaching a WA peak (Figure 6.30a and Figure 6.31a). This was followed by a decrease in its value up to mid-stand phase. A further increase in pressure value was evident up to TS phase. From TS phase to TO, pressure decreased reaching a value higher than that measured at IC at the end of the stance phase. In the swing phase, the pressure value was gradually restored to the value measured at IC. When comparing the pressure values measured in the two sessions, higher 2nd peak (TS peak of up to 15kPa) was measured, compared with the 1st peak (up to 12kPa) in Session 1. By contrast, similar 1st and 2nd peak of pressure was measured in Session 2. This is likely due the donning of the socket. When distal end of the femur was in appropriate contact of the sensor unit, higher pressure value will be obtained during TS because of the presence of the bony prominence. The forces experienced at AD location would a result of the combination of vertical and anterior-posterior component of GRF. However, when the distal end of the femur was in a more distal location compared with the sensor unit, a double-hump profile may occur was it resembles more like the vertical components of GRF. This is because of the less contribution of the anterior-posterior GRF to the force experienced at AD location.

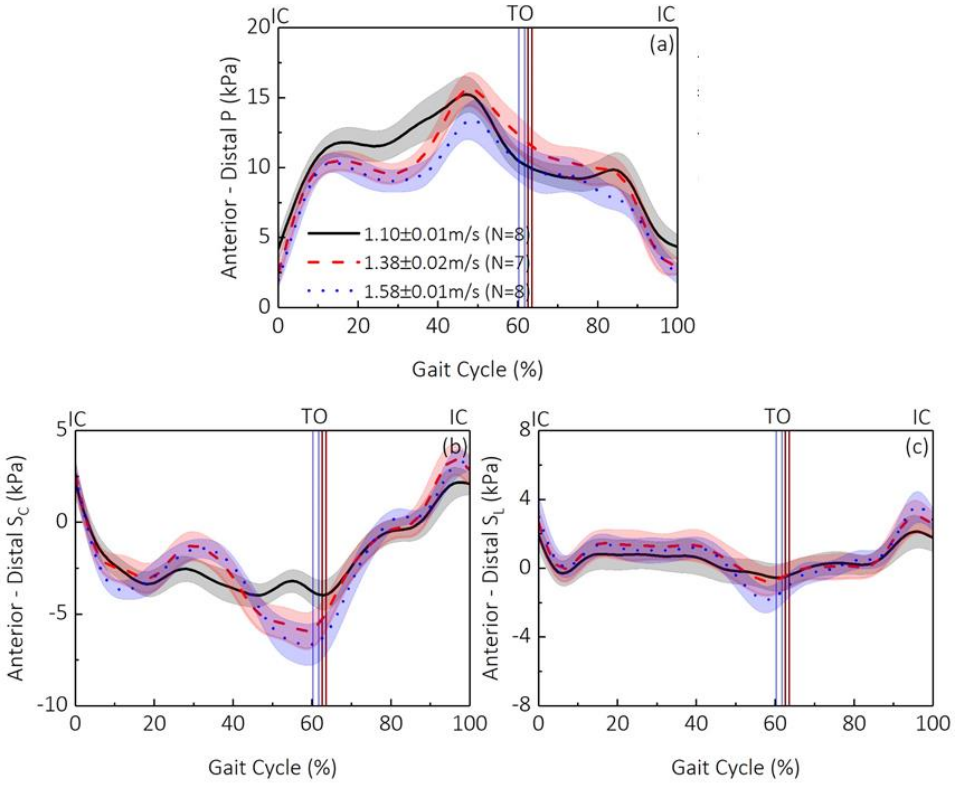

Figure 6.30: (a) Pressure, (b) S_C and (c) S_L measured at AD location of the residuum in session 1, over a GC, when walking at slow, self-selected and fast walking speeds.

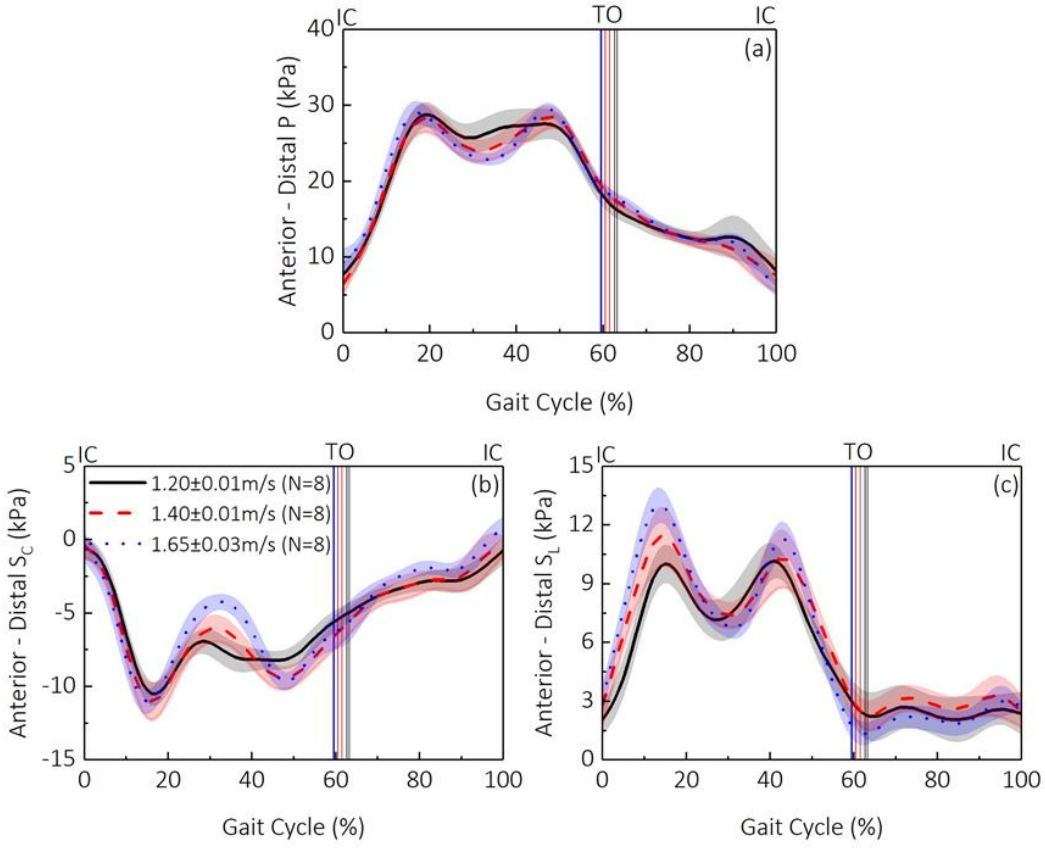

Figure 6.31: (a) Pressure, (b) S_C and (c) S_L measured at AD location of the residuum in session 2, over a GC, when walking at slow, self-selected and fast walking speeds.

S_C decreased from IC to approximately 17% of GC, reaching a WA peak (Figure 6.30b and Figure 6.31b). Thereafter the two sessions yielded different responses. In Session 1, when walking at the slow speed, S_C maintained the WA peak during most of the stance phase. By contrast, in Session 2, S_C increased reaching a local maximum at mid-stance. S_C further decreased reaching a 2nd peak at TO, in session 1 while, in Session 2, the value of the S_C decreased to TS. During the swing phase, an increase in S_C was evident as its value was restored to the measured at IC.

In session 1 (Figure 6.30c), a value of up to 2kPa of S_L was measured. In session 2 (Figure 6.31c), S_L increased to approximately 15% of GC, reaching a WA peak. This was followed by a decrease of S_L to mid-stance. A further increase of S_L was evident up to TS, reaching a TS peak. Subsequently, S_L decreased during the remainder of stance phase, reaching the value measured at IC. During the swing phase, fluctuation of S_L of up to 1kPa was evident.

Effect of walking speed on WA peak

During the WA phase, no significant change in peak pressure value was measured at the PP location with an increase in walking speed (Table 6.5), in session 1. By contrast, in session 2, the increase in walking speed resulted in an increase in peak pressure at the PP location (up to 7%), with a corresponding timing shift to an earlier phase the GC (up to 3% of GC). No consistent trends were observed in pressure at AP and AD locations due the change in walking speed (Table 6.5). With respect to S_L, an increase in walking speed resulted in an increase in the WA peak at PP (up 17%) and AD locations (up to 33%) in session 2, as shown in Table 6.5. No clear WA peaks were observed at the AP location.

Effect of walking speed on the mid-stance valley

At mid-stance, the increase in walking speed resulted in a decrease in pressure values at both PP (19% in Session 1 and 13% in Session 2) and AP (11% in Session 1 and 12% in Session 2) locations. The corresponding timings at which mid-stance peak occurred was delayed by up to 7% (session 1) and 8% (session 2), at both locations. No conclusive trend was observed in pressure at the AD location due to the increase in walking speed, in terms of either magnitude or timing of the events. Similarly, no consistent trend was observed with S_C at each location, as shown in Table 6.6. When compared to the peak S_L at mid-stance phase, the increase in walking speed resulted in its decrease of S_L at PP (up to 20% in Session 1 and up to 33% in Session 2) and AD (approximately 33% in Session 2) locations, as shown in Table 6.6. The timing at which the mid-stance peak occurred was delayed to values of approximately 5% at the PP location in both sessions and 7% at the AD location in Session 2.

Effect of walking speed on TS peak

During TS phase of the GC, no consistent trend was observed in pressure at both PP and AP locations when walking speed was increased. However, the timing of the events was delayed to a later phase of GC (up to 4% at the PP location and up to 6% at AP location, respectively). The increase in walking speed resulted in minimal effects on pressure at AD location (Table 6.7). In a similar manner, there was no consistent trend observed in S_C at TS when the walking speed was increased. With respect to S_L measured at each location, in session 2, an increase in walking speed resulted in minimal changes (Table 6.7). However, the timing at which the TS peak occurred was delayed to a later phase of GC (up to 5% at PP location and up to 3% at AD location).

Table 6.4: Magnitude and timings of peak GRF obtained at WA, mid-stance and TS phase of the GC, when walking at slow, self-selected and fast walking speeds, across two sessions

Session No.		Vertical GRF						Medial-Lateral GRF						Anterior-Posterior GRF			
		WA		Mid-stance		TS		WA		Mid-stance		TS		WA		TS	
Session 1	Slow	866 ± 27	15	620 ± 16	28	782 ± 15	41	49 ± 13	19	39 ± 8	32	51 ± 8	42	-116 ± 8	15	+113 ± 10	48
	Self-selected	877 ± 35	15	545 ± 24	31	826 ± 26	44	46 ± 10	20	32 ± 7	32	42 ± 8	43	-105 ± 12	8	+133 ± 6	47
	Fast	909 ± 25	15	477 ± 22	33	826 ± 39	45	45 ± 9	20	31 ± 6	32	37 ± 9	42	-120 ± 15	9	+150 ± 13	47
Session 2	Slow	882 ± 11	15	610 ± 22	27	785 ± 7	39	48 ± 12	19	36 ± 12	35	44 ± 10	42	-122 ± 4	14	+114 ± 7	49
	Self-selected	934 ± 10	14	536 ± 9	30	829 ± 5	44	38 ± 3	20	26 ± 4	31	41 ± 6	45	-133 ± 8	9	+122 ± 5	48
	Fast	945 ± 45	14	468 ± 8	32	833 ± 14	45	55 ± 7	19	38 ± 6	31	43 ± 7	43	-126 ± 13	9	+144 ± 9	47

Table 6.5: Magnitude and timings of pressure, S_C and S_L obtained at WA phase of the GC, when walking at slow, self-selected and fast walking speeds, across two sessions.

		Pressure						S_C						S_L					
		PP		AP		AD		PP		AP		AD		PP		AP		AD	
	Speed	Pressure (kPa)	% of GC	Pressure (kPa)	% of GC	Pressure (kPa)	% of GC	S_C (kPa)	% of GC	S_C (kPa)	% of GC	S_C (kPa)	% of GC	S_L (kPa)	% of GC	S_L (kPa)	% of GC	S_L (kPa)	% of GC
Session 1	Slow	53 ± 1	17	31 ± 1	18	12 ± 1	16	-6 ± 1	14			Note[b]		16 ± 1	12				
	Self-selected	51 ± 2	16	31 ± 1	18	11 ± 1	16	-7 ± 1	13	Note[a]		-3 ± 1	17	16 ± 1	12	Note[c]		Note[d]	
	Fast	51 ± 1	16	31 ± 1	17	10 ± 1	16	-6 ± 1	13			-4 ± 1	12	18 ± 1	12				
Session 2	Slow	54 ± 1	17	29 ± 1	18	29 ± 1	19	-4 ± 1	13	-3 ± 1	10	-11 ± 2	17	12 ± 1	13			10 ± 1	16
	Self-selected	56 ± 1	15	29 ± 1	18	28 ± 2	19	-4 ± 1	12	-4 ± 1	10	-11 ± 1	16	13 ± 1	12	Note[c]		11 ± 1	15
	Fast	58 ± 2	14	30 ± 1	16	28 ± 2	17	-5 ± 1	11	-4 ± 1	7	-11 ± 1	16	14 ± 1	10			13 ± 1	14

Note:

[a]The S_C at AP location showed less than 1kPa of change in session 1.
[b]No double-hump profile was observed on the S_C measurement at AD location in session 1.
[c]The S_L at AP location showed less than 2kPa of change in session 1 and 2.
[d]The S_L at AD location showed less than 2kPa of change in session 1.

Table 6.6: Magnitude and timings of pressure, S_C and S_L obtained at mid-stance phase of the GC, when walking at slow, self-selected and fast walking speeds, across two sessions.

		Pressure						S_C						S_L					
		PP		AP		AD		PP		AP		AD		PP		AP		AD	
	Speed	Pressure (kPa)	% of GC	Pressure (kPa)	% of GC	Pressure (kPa)	% of GC	S_C (kPa)	% of GC	S_C (kPa)	% of GC	S_C (kPa)	% of GC	S_L (kPa)	% of GC	S_L (kPa)	% of GC	S_L (kPa)	% of GC
Session 1	Slow	47 ± 1	28	28 ± 1	28	11 ± 1	23	-3 ± 1	28	Note[a]		-11 ± 1	17	10 ± 1	27	Note[b]		Note[c]	
	Self-selected	43 ± 1	33	26 ± 1	33	9 ± 1	29	-3 ± 1	32			-11 ± 1	16	9 ± 1	32				
	Fast	38 ± 1	35	25 ± 1	36	9 ± 1	30	-2 ± 1	34			-11 ± 1	15	8 ± 1	33				
Session 2	Slow	46 ± 1	28	26 ± 1	30	25 ± 1	31	-2 ± 1	29	-2 ± 1	29	-7 ± 1	28	6 ± 1	26	Note[b]		28 ± 1	26
	Self-selected	43 ± 1	34	24 ± 1	32	24 ± 1	32	-2 ± 1	31	-2 ± 1	30	-6 ± 1	31	6 ± 1	30			34 ± 1	24
	Fast	40 ± 1	35	23 ± 1	36	23 ± 1	35	-1 ± 1	33	-2 ± 1	32	-4 ± 1	33	4 ± 1	31			33 ± 1	23

Note:

[a]*The S_C at AP location showed less than 1kPa of change in session 1.*
[b]*The S_L at AP location showed less than 2kPa of change in session 1 and 2.*
[c]*The S_L at AD location showed less than 2kPa of change in session 1.*

Table 6.7: Magnitude and timings of pressure, S_C and S_L obtained at TS phase of the GC, when walking at slow, self-selected and fast walking speeds, across two sessions.

		Pressure						S_C						S_L					
		PP		AP		AD		PP		AP		AD		PP		AP		AD	
	Speed	Pressure (kPa)	% of GC	Pressure (kPa)	% of GC	Pressure (kPa)	% of GC	S_C (kPa)	% of GC	S_C (kPa)	% of GC	S_C (kPa)	% of GC	S_L (kPa)	% of GC	S_L (kPa)	% of GC	S_L (kPa)	% of GC
Session 1	Slow	53 ± 1	42	31 ± 1	41	15 ± 1	47	-5 ± 1	39			Note[b]		12 ± 1	40				
	Self-selected	53 ± 1	45	31 ± 1	45	16 ± 1	48	-5 ± 1	42	Note[a]		-6 ± 1	58	14 ± 1	43	Note[c]		Note[d]	
	Fast	48 ± 1	46	30 ± 1	47	13 ± 1	49	-4 ± 1	43			-7 ± 1	59	14 ± 1	45				
Session 2	Slow	51 ± 1	43	29 ± 1	41	28 ± 1	47	-2 ± 1	40	-2 ± 1	37	-8 ± 1	46	9 ± 1	42			10 ± 1	41
	Self-selected	52 ± 1	44	28 ± 1	45	28 ± 1	48	-2 ± 1	42	-3 ± 1	40	-9 ± 1	47	10 ± 1	44	Note[c]		10 ± 1	44
	Fast	51 ± 0	46	28 ± 1	46	29 ± 1	47	-2 ± 1	41	-3 ± 1	44	-10 ± 1	48	10 ± 1	45			11 ± 0	43

Note:

[a]*The S_C at AP location showed less than 1kPa of change in session 1.*

[b]*No double-hump profile was observed on the S_C measurement at AD location in session 1.*

[c]*The S_L at AP location showed less than 2kPa of change in session 1 and 2.*

[d]*The S_L at AD location showed less than 2kPa of change in session 1*

6.2.4 Walking on different terrains

As mentioned in Section 2.5.3, one of the key parameter that affects the load transfer through prosthesis is the terrain. As an example, for trans-femoral or knee disarticulation amputee, little knee flexion motion was observed to prevent buckling in stance phase (Section 4.2.3), which may significantly affect the kinetics at the socket interface. This section presents the results obtained from the activity A6, the detailed protocol of A6 can be found in Section 6.1.2.

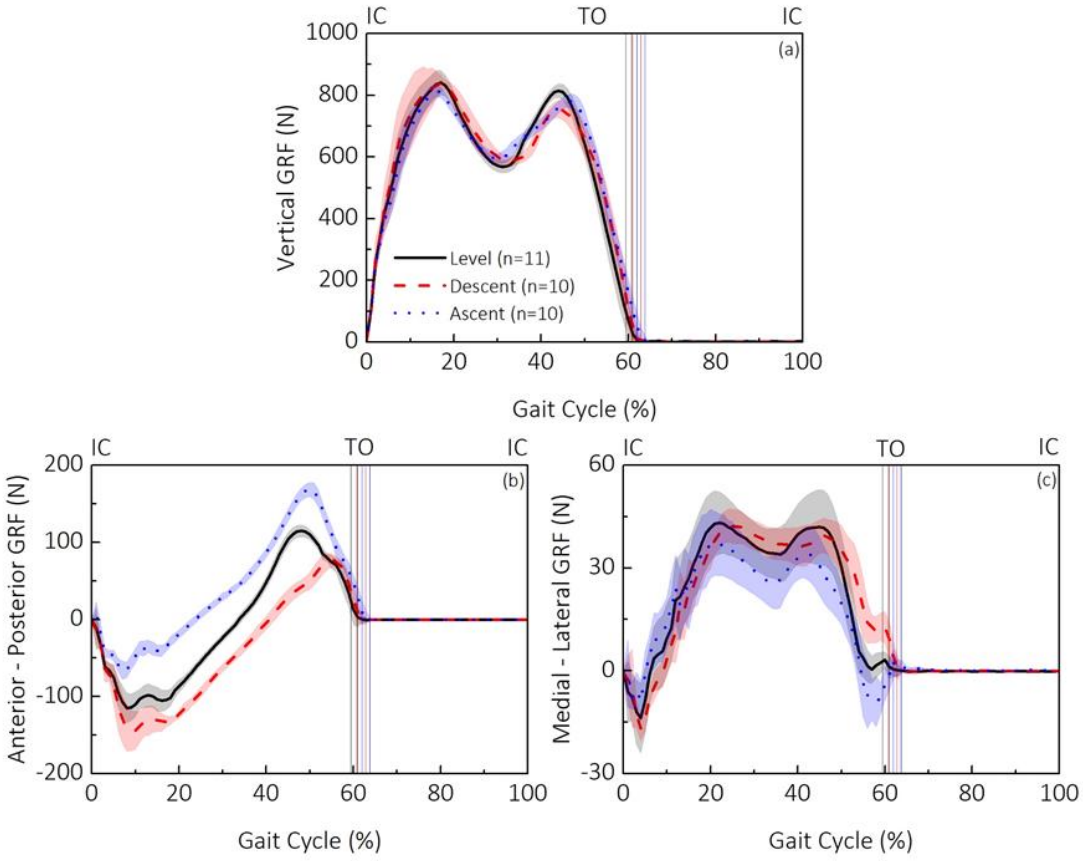

Figure 6.32: (a) Vertical, (b) anterior - posterior and (c) medial-lateral component of GRF, over a GC.

Vertical, anterior-posterior and medial–lateral component of GRF, as a function of GC, obtained when walking on different terrains are shown in Figure 6.32. Vertical component of GRF (Figure 6.32a) shows typical double-hump shaped profiles with mean peak forces of approximately 840N, 837N and 814N in early stance phase (10-20% of GC), and 814N, 754N and 781N in TS (40-60% of GC) during level, descent and ascent walking, respectively. It is worth noting that the obtained GRF on level surface is equivalent to 105% of BW and is consistent with previous study [250].

Anterior-posterior component of GRF (Figure 6.32b) shows mean peak forces of approximately -115N, -145N and -66N in early stance phase, and +115N, +77N and +169N in the TS during

level, descent and ascent walking, respectively. It is evident that the GRF from ramp descent (Figure 6.32b) shows the greater anterior-posterior braking force F_X in early stance phase (10-20% of GC) when compared to that for level walking. This may be associated with the need of a greater braking force to oppose the component of the body weight acting down the slope. By contrast, GRF results obtained from ramp ascending (Figure 6.32b) reveals greater propulsive force in the anterior-posterior direction at TS when compared to that from level waking. This may be associated with the demands of a greater propulsive force to oppose the component of the body weight acting down the slope.

Medial-lateral component of GRF (Figure 6.32c) shows that mean peak forces of +42N, +40N and +37N during level, descent and ascent walking, respectively. This suggests that a medial force was acting on the foot during the stance phase (Figure 6.32c).

pressure showed a double-hump profile with the early stance peak values of approximately 32kPa, 32kPa and 33kPa, with TS peak values of 30kPa, 29kPa and 36kPa for level, descent and ascent walking (Figure 6.33a), respectively. The corresponding values for S_C (Figure 6.33b) and S_L (Figure 6.33c) were minimal with less than 2kPa across all terrains.

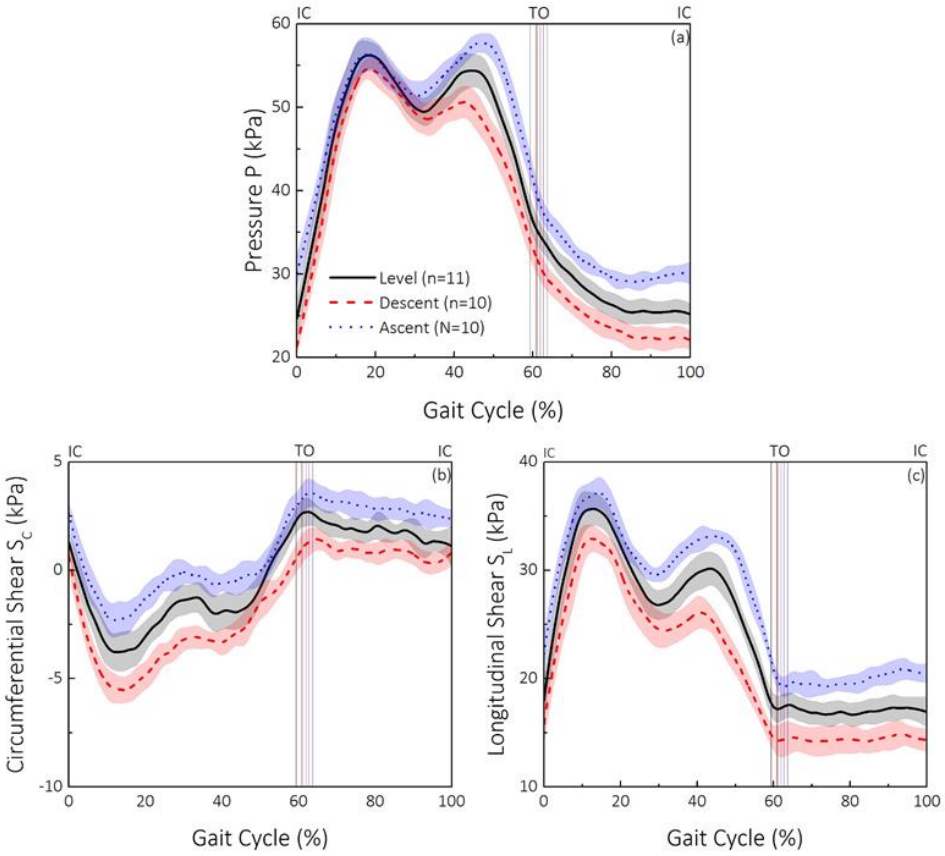

Figure 6.33: (a) Pressure, (b) circumferential shear and (c) longitudinal shear measured at anterior – proximal (AP) location of the residuum on level, ascent and descent surfaces, over a GC.

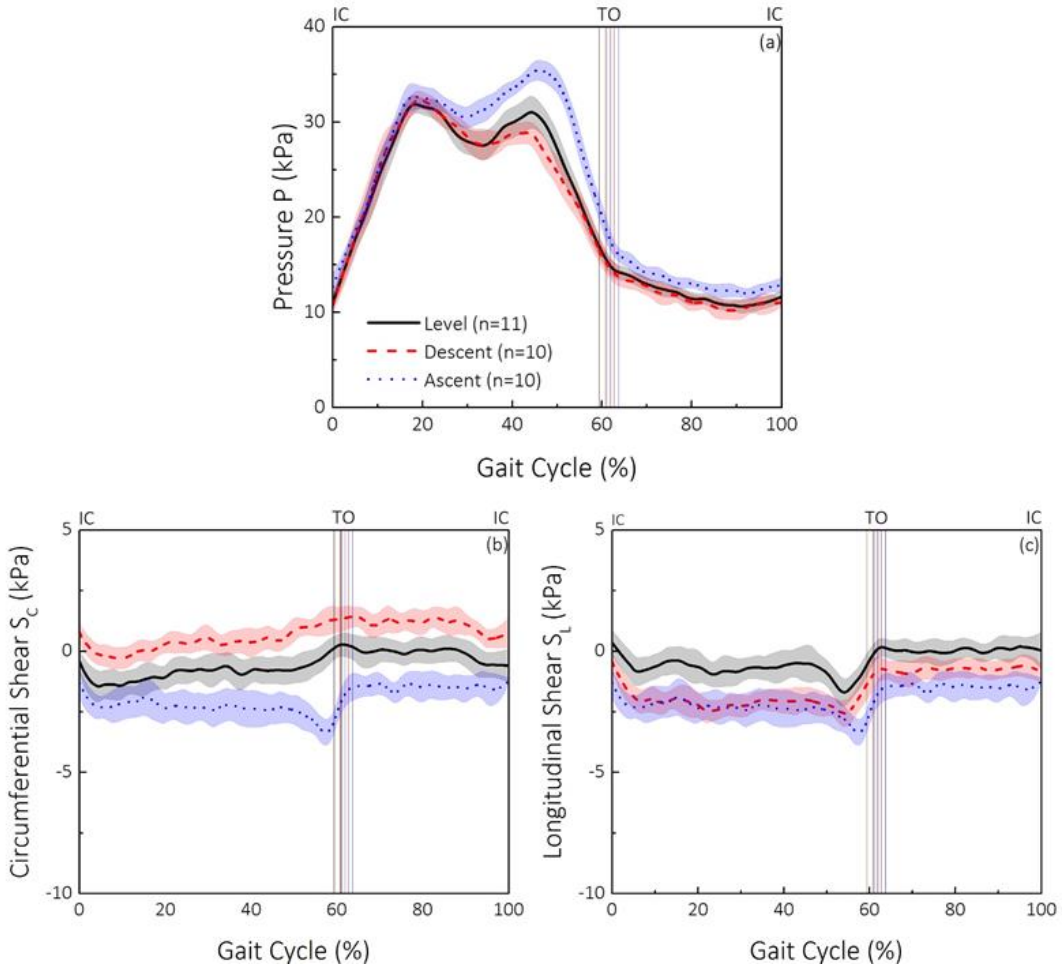

Figure 6.34: (a) Pressure, (b) circumferential shear and (c) longitudinal shear measured at posterior – proximal (PP) location of the residuum on level, ascent and descent surfaces, over a GC.

At the PP location, Figure 6.34a shows a typical double-hump shape for pressure in stance phase. At IC, up to 25±2kPa, 21±2kPa and 30±2kPa of pressure were measured when walking on level, descending and ascending surfaces, respectively. This may be associated with the direction of the GRF vector in relation of the position of the prosthetic knee joint centre. The GRF vector passed anteriorly in relation of the prosthetic knee joint centre. This resulted in a higher bending moment on the socket (Figure 4.15) at knee joint level, when walking on ascending ramp, compared with the value on level surface. This means higher load could be exerted on the PP and AD region of the residuum, compared with the values at AP and posterior-distal region. When walking on a descending ramp, a reduction in bending moment was evident compared with the value on level surface. Therefore, a reduction in pressure value may be evident at PP and AD location.

In particular, a peak pressure of approximately 56kPa was obtained in early stance phase for all tests, but in TS, peak pressure of 53±2kPa, 50±1kPa and 58±1kPa were obtained for level, descent and ascent walking, respectively. A decrease in pressure (p=0.00) at TS was measured

when walking on the descending surface whereas an increase in pressure (p=0.00) was evident when walking on ascending surface, compared with the value obtained on level surface.

Two $+S_L$ peaks in Figure 6.34c also showed a double-hump profile during stance phase, with peak values in the early stance of 36kPa, 33kPa and 37kPa and peak values in the TS of 30kPa, 26kPa and 33kPa for level, descent and ascent walking, respectively. It is also noted the pressure, S_C and S_L at the PP locations are in general are higher than those measured at the AP location. It is worth noting that the highest vertical GRF, at both early stance and TS, was measured when walking on level surface. However, higher vertical GRF did not correspond well with the higher S_L. This is likely due to the slip between the residuum and the socket. The presence of slip would mean the frictional behaviour has been shifted from the static regime to dynamic regime.

During ramp descent, higher pressure at the PP and AP locations were obtained in early stance phase, comparing to that at TS. This finding could be potentially associated with the greater braking force observed in anterior-posterior GRF. By contrast, when walking on the ascending ramp, higher pressure at the PP and AP locations were obtained at TS.

At the AD location (Figure 6.35), there was a dramatic change in pressure and shear profiles, especially in TS. Peak pressure of approximately 70±6kPa, 55kPa±4kPa and 50kPa±4kPa were observed (Figure 5g) during TS for level, descent and ascent walking, respectively. Compared with pressure obtained on level surface, a reduction was obtained when walking on both descending (p=0.00) and ascending (p=0.01) surfaces. In addition, higher pressure (p=0.01) at AD location was measured on ascending ramp, compared with the value measured on descending ramp. This matches well with the previous discussion as higher knee joint bending flexor moment was evident when walking on the ascending ramp, compared with the value on descending ramp. The peak values for S_C are approximately -26kPa, -15kPa and -24kPa (Figure 6.35b), also during TS, while low S_L (Figure 6.35c) peak values of -5kPa - 5kPa were measured.

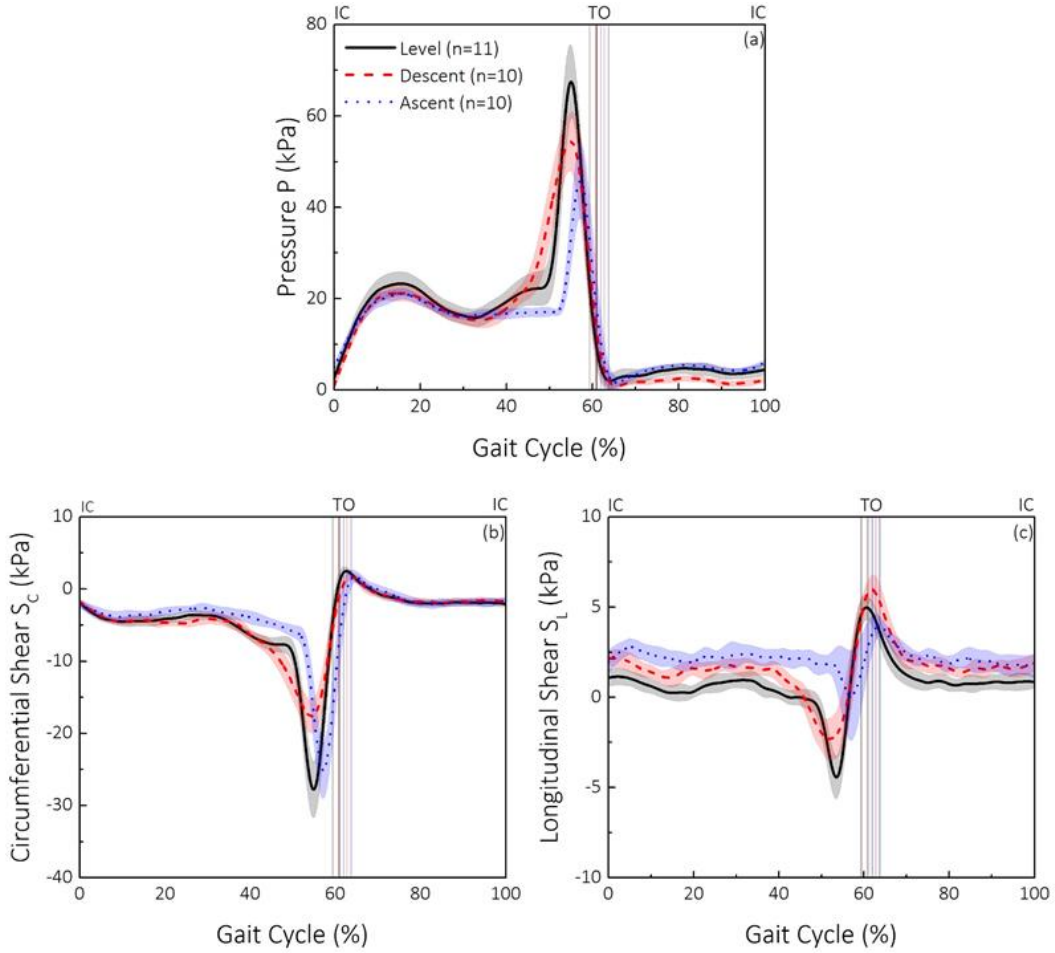

Figure 6.35: (a) Pressure, (b) circumferential shear and (c) longitudinal shear measured at anterior – distal (AD) location of the residuum on level, ascent and descent surfaces, over a GC.

Significant changes in stresses were observed at the AD location of the residuum during the TS (Figure 6.35). This can be explained by the fact that the AD location acted like a kick point, as the amputee tried to propel the prosthesis forward in preparation for the swing phase. As a result, rotation between the residuum and socket could occur during this process. Indeed, an S_C of up to −26kPa was measured acting laterally on the residuum.

In this study, the sensitivity of TRIPS sensor system has been evaluated with the effect of terrain on a knee-disarticulation socket interface. This preliminary study revealed higher peak pressure and shear value when walking on descending ramp in early stance, whereas higher pressure and shear was evident in TS when walking on ascending ramp. Both findings could be potentially associated with the change in GRF when walking on ramped surfaces. It is well known that, when walking on descending ramp, improving stability and safety is one of critical criteria for the design of the modern prosthetists. It is envisaged that, the measured stresses at residuum/socket interface could be used as indicators to trigger the actuation of the prosthetic knee and foot. When the socket fit deviates from the optimum, which will be

reflected on the interface stresses, mechanisms in the prosthetic knee and foot can be activated to provide more support of the prosthetic limb when walking on descending ramp.

6.2.5 Walking with different prosthetic ankle settings – hydraulic resistance

As mentioned in Section 2.5.3, different type of prosthetic foot (a hydraulic ankle versus a fixed ankle) has significant impact on the load transfer mechanism on prosthetic limb. However, to-date, there is no study evaluates the relationship between hydraulic ankle resistance and the socket interface kinetics, which could further aid the prosthetic component design. This section presents the results obtained from the activity A7, the detailed protocol of A7 can be found in Section 6.1.2.

Regardless of prosthetic ankle setting, up to -141N and +86N of peak braking force and propulsive force was obtained (Figure 6.36a), respectively. Peak medial-lateral GRF of up to 52 ± 5N and 44 ± 6N was obtained with brake on and off setting (Figure 6.36b), respectively. It is hence evident that a greater medial-lateral GRF was obtained when brake setting was applied, comparing to the normal setting. The early stance peak of vertical GRF with two different ankle settings showed similar values (approximately 904N, Figure 6.36c). However, a significant reduction ($p<0.05$) in TS peak of vertical GRF was observed when brake setting was applied (708N), comparing to the value obtained with normal foot setting (795N).

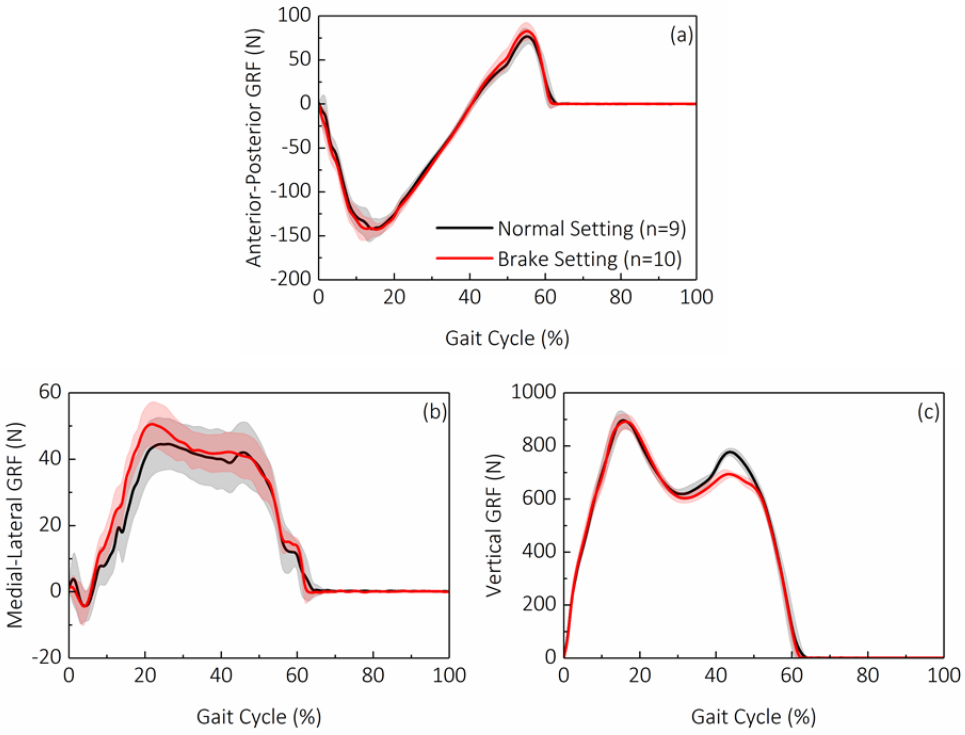

Figure 6.36: (a) Vertical, (b) anterior - posterior and (c) medial-lateral component of GRF obtained when walking on descending ramp, over a GC.

pressure (Figure 6.37a), S_C (Figure 6.37b) and S_L (Figure 6.37c) at PP location showed double-hump temporal profile. Regarding to the pressure obtained at PP, at TS phase, up to 49 ± 1kPa and 53 ± 1kPa was obtained with brake and normal setting, respectively. Peak S_C of up to 6 ± 1kPa and 7 ± 1kPa was obtained with brake and normal setting, respectively. In addition, peak S_L of up to 8 ± 1kPa and 13 ± 1kPa was obtained at TS phase with brake setting and normal setting, respectively. All three components of stress showed reduction in peak values when brake setting was applied, comparing to normal ankle setting. This could result from the reduction in peak vertical GRF in TS phase.

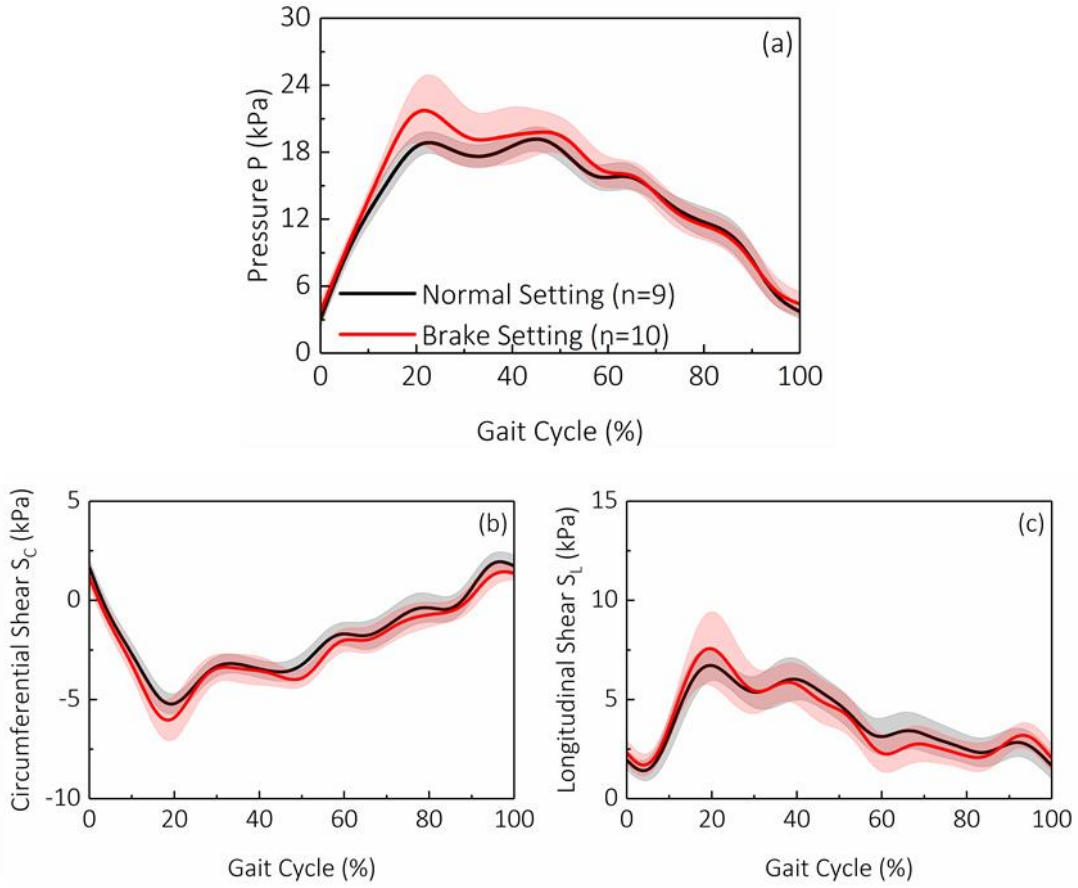

Figure 6.37: (a) Pressure, (b) circumferential shear and (c) longitudinal shear measured at posterior – proximal (PP) location of the residuum on descending surface, over a GC.

In early stance phase, pressure showed similar values (approximately 28kPa, Figure 6.38a), regardless of the ankle settings. In TS phase, up to 28 ± 1 kPa and 26 ± 1 kPa of pressure was obtained when brake and normal setting was applied. Up to 3 and 2kPa of shear stresses (Figure 6.38b and Figure 6.38c) was obtained in circumferential and longitudinal direction, respectively. In general, stresses in all three directions, at AP location, showed lower values comparing to the values obtained at PP location.

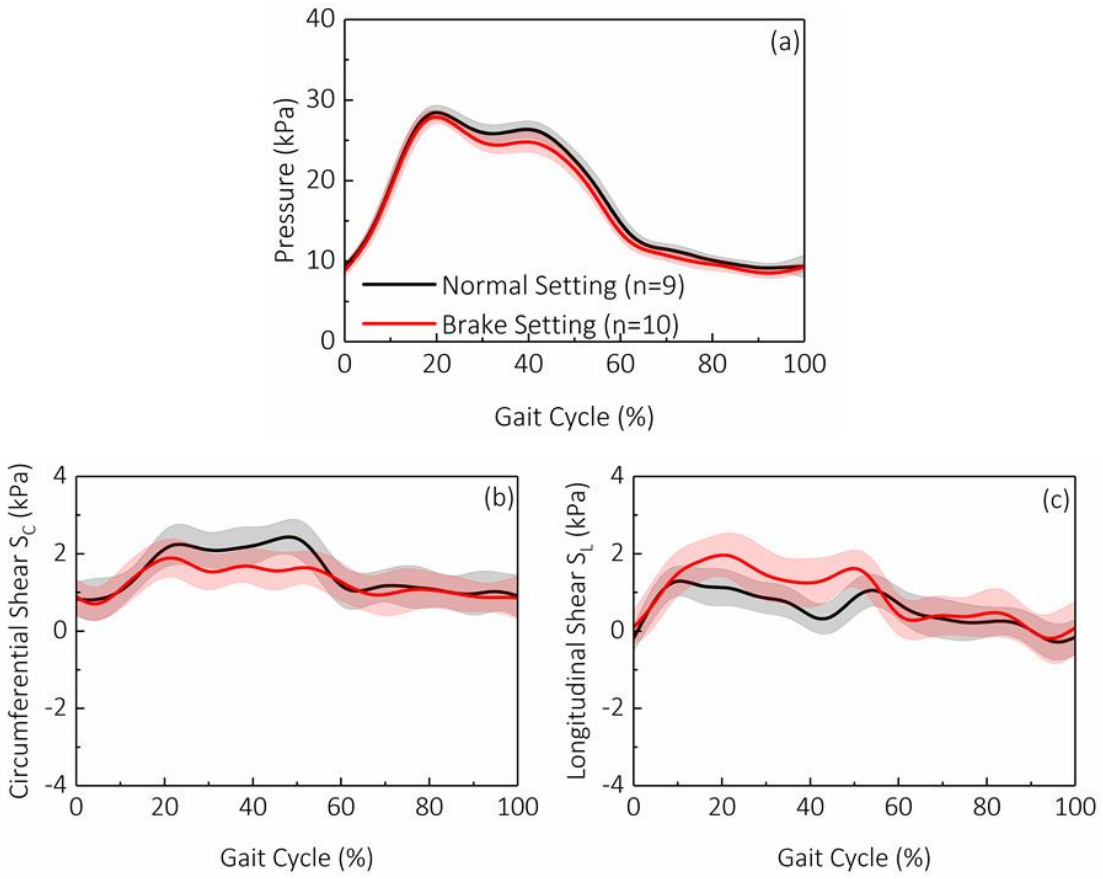

Figure 6.38: (a) Pressure, (b) circumferential shear and (c) longitudinal shear measured at anterior – proximal (AP) location of the residuum on descending surface, over a GC.

When analyse the biomechanics at the two proximal regions, higher pressure was obtained as PP location, comparing to AP location. This finding is consistent with previous results (Section 6.2.4). The application of brake setting has led to a reduction in pressure, S_C and S_L at proximal regions, with an exception of S_L at AP location (up to 1kPa of increase).

Double-hump temporal profile is not evident on the stresses obtained at AD location (Figure 6.39). Instead, pressure did not decrease to the value obtained at IC until the end of the GC, suggesting AD location of the residuum was always in contact with the socket (Figure 6.39a). The application of brake setting has led to the increase of 4kPa, 1kPa and 1kPa of increase in pressure, S_C and S_L in early stance phase, comparing to the value obtained with normal ankle setting (Figure 6.39). This increase of AD stress may be associated with the braking effect of prosthesis, stopping the rapid advancement of the prosthetic against the residuum.

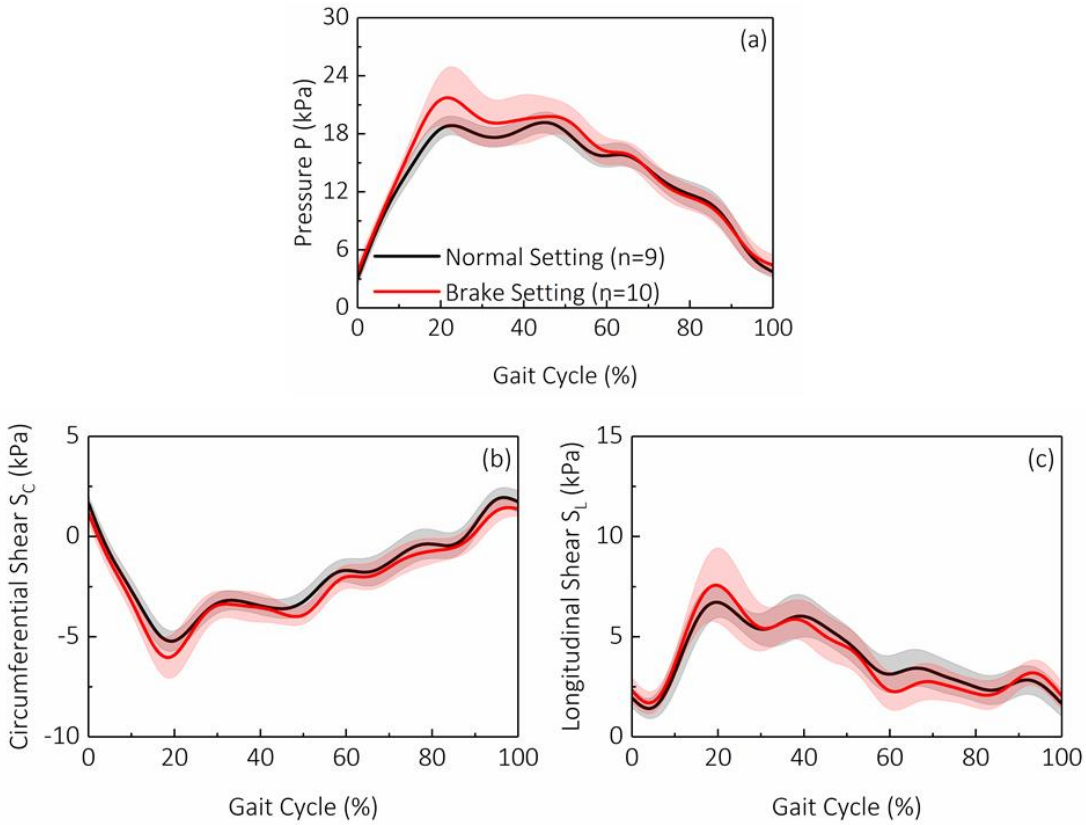

Figure 6.39: (a) Pressure, (b) circumferential shear and (c) longitudinal shear measured at anterior – distal (AD) location of the residuum on descending surface, over a GC.

When investigating the pressure at all three locations when brake setting was applied, when walking on descending ramp. Compared with the value obtained with normal foot setting, a decrease in pressure was evident in early stance phase at distal location, while a reduction in pressure was observed at two proximal locations in TS phase. This could be potentially explain by the active distal femoral motion against the socket during early stance phase to achieved brake. While at the two proximal location, less effort was required to propel the limb in TS phase. The largest difference in shear stresses was observed at the PP location, a reduction in S_L was evident when brake setting was applied, comparing with the value obtained with normal setting. This may indicate a more stable residuum in relation to the socket when brake setting was applied, comparing that with normal setting.

6.3 Interface stresses on the trans-tibial amputees

As mentioned in Section 2.7.3, the interface stresses for trans-tibial amputees can be distinctively different from those from trans-femoral and knee disarticulation amputees. The interface biomechanics may be related to the anatomical structure of a trans-tibial residuum, which contain more distinct bonny prominences as compared with non-trans-tibial residuum. From the prosthesis components aspect, the lack of prosthetic knee is also likely to play a role in load transfer profile over the residuum. Thus, the in-situ stresses exerted on a trans-tibial residuum during ambulation deserved in-depth studies.

6.3.1 Level walking activity

This section presents the level walking results obtained from the activity B1, the detailed protocol of B1 can be found in Section 6.1.2.

Trans-tibial 1 participant

- Results

From IC, pressure at patella tendon increased and a peak value was reached at approximately 45% of GC. It was followed by a sharp decrease (Figure 6.40a) of pressure until approximately 65% of GC. During the rest of the GC, pressure gradually returned to the value obtained at IC. From early to TS, S_C of up to 4kPa was measured in all three sessions (Figure 6.40b). There was an increase of S_C from approximately 55% of GC to 70% of GC. It was followed by a decrease of S_C until approximately 90% of GC. During the remainder of the GC, S_C fluctuated and returned to the value measured at IC. From IC to 20% of GC, a decreasing trend of S_L was seen at patella tendon (Figure 6.40c). It was followed by the sharp increase of S_L and a peak positive value was reached at approximately 45% of GC. During the rest of the stance phase, S_L at patella tendon returns to the value see at IC. In swing phase, S_L showed little change from 60% to 90% of GC. During the rest of the GC, S_L increased and reached the value obtained at IC.

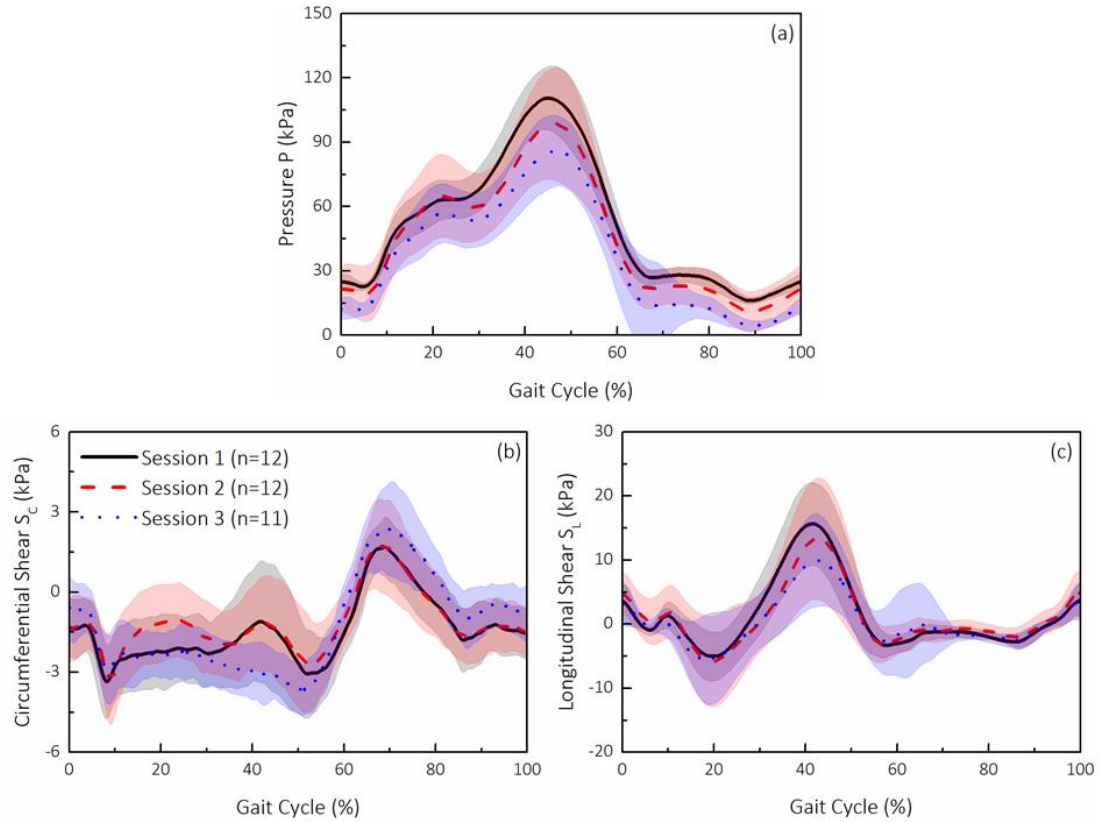

Figure 6.40: (a) Pressure, (b) circumferential shear and (c) longitudinal shear measured at patella tendon location of the residuum from three repeated sessions, over a GC.

This evident that the temporal profiles of the three components of stress showed repeatable patterns, over three data collection sessions. In addition, Table 6.8 lists the peak Pressure and shear obtained over a GC, over three sessions. It worth noting that peak Pressure and S_L decrease, over time (from session 1 to session 3, Table 6.8). Similar S_C was obtained over three sessions.

The three components of stress all showed double-hump temporal profiles (Figure 6.41). Pressure at distal location showed non-zero values (Figure 6.41a), over the entire GC, suggesting the distal region of the residuum was always in contact with the socket. Negative medial-lateral S_C was obtained in most of the stance phase (Figure 6.41b), suggesting a medial directed load was exerted on the distal location of the residuum. As the sensor unit was place on the distal region with its orientation slightly tilted towards anterior aspect of the socket, S_L showed double-hump temporal profile as well. Positive S_L (up to 40kPa) was observed during most of the stance phase (Figure 6.41c).

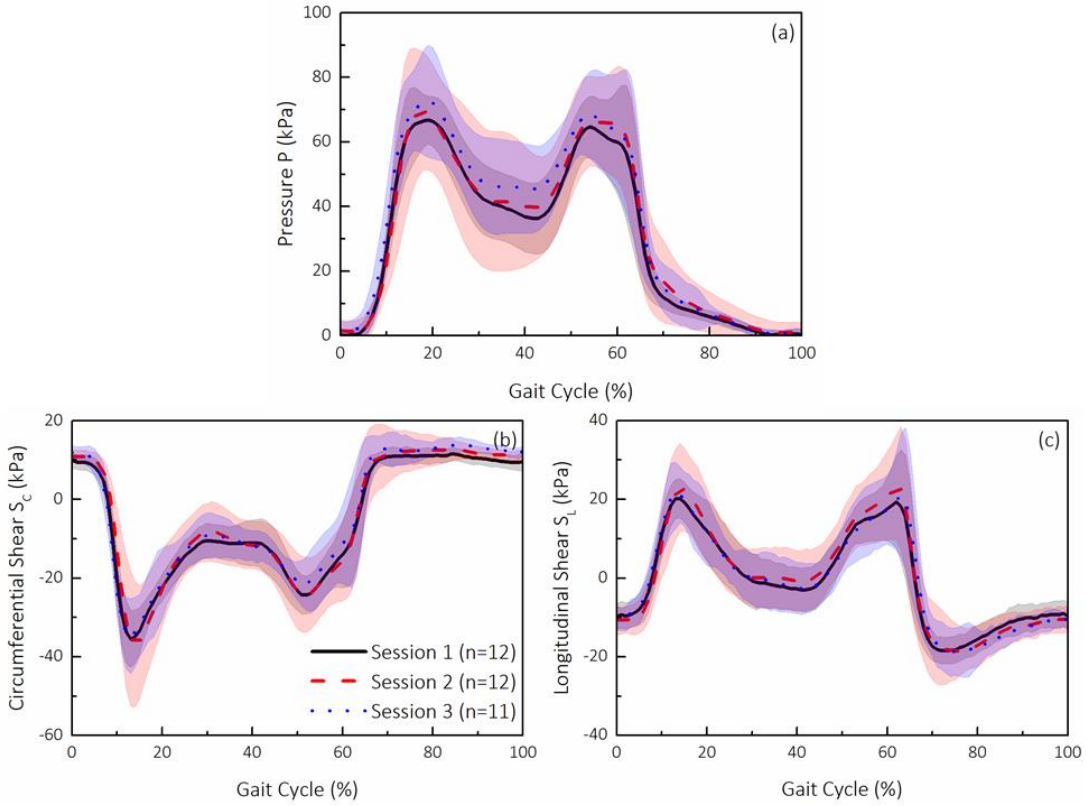

Figure 6.41: (a) Pressure, (b) medial-lateral shear and (c) anterior-posterior shear measured at distal location of the residuum from three repeated sessions, over a GC.

When comparing the value over three repeated sessions, Pressure at distal location showed a decreasing trend while S_C and S_L showed little change over time (Table 6.8). As mentioned previously, the Pressure at PTB location showed an increasing trend over time. Combining the two finings, it may suggest that the stump was lifted up higher in the socket, resulting in the higher pressure at proximal location (PTB) and lower pressure at distal location.

Double-hump temporal profile was evident on pressure (Figure 6.42a) and S_C (Figure 6.42b) at SPF location. There was no clear pattern observed in the temporal profile of S_L at SPF location. pressure profile at SPF location showed a loading delay from 0% to approximately 8% of GC (Figure 6.42a). A peak positive value was observed at TS phase.

Negative S_C was observed in most of the stance phase, suggesting loads were exerted towards the lateral direction of the SPF location (Figure 6.42b). It is worth noting in Figure 6.42c that the greater SD was observed in S_L (up to 20kPa) in session 2, over a GC, comparing to the value obtained in session 1 (up to 10kPa) and session 3 (up to 5kPa). The temporal profile of S_L in stance over three sessions was not clear, however, all of them showed an increasing trend from 70% to the end of the GC.

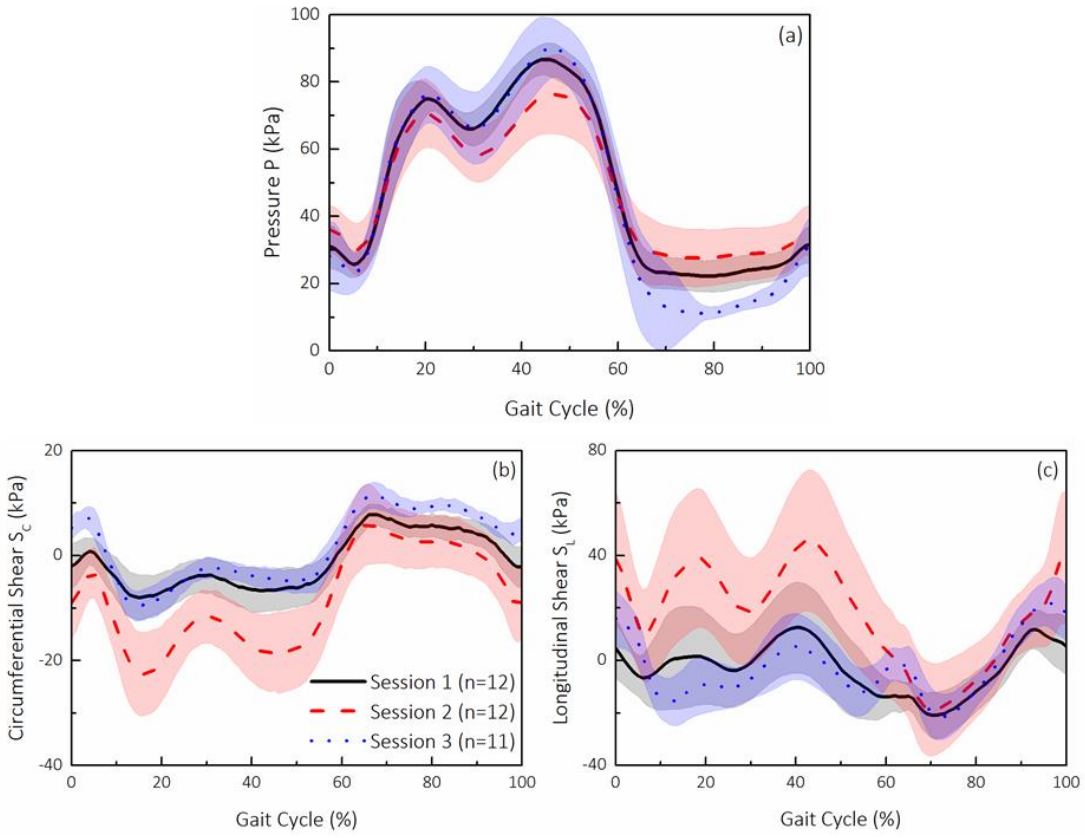

Figure 6.42: (a) Pressure, (b) circumferential shear and (c) longitudinal shear measured at SPF location of the residuum from three repeated sessions, over a GC.

- Interface kinetics

pressure at all locations did not start to increase until 5% of GC, suggesting a delay of loading. This observation is consistent with the loading delay presented in Figure 2.50 and the amount of delay was in the range reported in previous studies (4-12% of GC). The cause of the loading delay may be explained by the axial motion of the residuum relative to the socket. To be specific, the inertial force experienced in the swing phase can results in the slight detachment of the residuum relative to socket, at the distal end. When the foot just start to make contact with the ground, vertical load is then transferred to the socket interface to close the gap between the residuum and the socket, before making contact with the distal end.

In stance phase, typical double-hump temporal profile was observed on all components of stresses at distal location (Figure 6.41) and pressure and S_C at SPF locations (Figure 6.42). However, double-hump temporal profile was not evident on the stresses obtained at patella tendon location. Instead, pressure at patella tendon showed an increasing profile throughout the stance phase. This finding was consistent with previous report [9]. There may be two reasons associated with this observation. The stress, especially pressure, experienced at a distal location may resemble more like the vertical load transferred from the ground interface,

resulting in a double-hump profile. With regards to pressure at patella tendon , as outlined by Radcliffe, higher pressure is expected at anterior-proximal location (or patella tendon) and posterior-distal location to reduce the effect of buckling. In TS, the activation of the muscle work contributes the increase in pressure in TS phase. It is reported that the pressure measurement when muscle is fired was almost twice as the value obtained in a relaxed state [9].

With regards to the S_C measured at distal location, negative value (Figure 6.41b) was presented in stance phase suggesting a lateral force (Figure 6.7) was exerted on the residuum. This aligns well with the medially-directed GRF in stance phase. The medial force, experienced at ground interface was subsequently transferred proximally, resulting in a lateral force exerted on the residuum tissue, through the socket. Positive S_L was measured in stance phase, suggesting the residuum was pushed in to the socket. It is also worth noting that, from approximately 70% to the end of GC, S_L increases, indicating the residuum was gradually pulled back into the socket over the swing phase.

- Intra-session and inter-session repeatability

Up to 24kPa, 17kPa and 12kPa of one SD values were obtained for pressure measured at patella tendon , distal and SPF location, respectively. Up to 1kPa, 17kPa and 4kPa of SD values were obtained for S_C measured at patella tendon , distal and SPF location, respectively. Up to 8kPa, 8kPa and 20kPa of S_L was obtained at patella tendon , distal and SPF location, respectively. One SD values of up to 76kPa was obtained in the resultant peak stress by Sanders et al [203], which is significantly higher than the ones obtained in this study. This is likely due stress concentration resulted from the rigid strain-gauge based sensor (Section 2.7.1) used in their study. It is worth noting that the intra-session repeatability, in terms of SD values, may be dependent on the both location of measurement and the component of stress (whether it is pressure, S_C or S_L). This is largely due to the dynamic change in load transfer profile, the anisotropic mechanical behaviour of the residuum tissue and the presence of bony prominences.

Table 6.8: Peak stresses obtained on the trans-tibial amputee from three repeated sessions.

Session	pressure (kPa)			S_C (kPa)			S_L (kPa)		
	Patella tendon	Distal	SPF	patella tendon	Distal	SPF	patella tendon	Distal	SPF
1	111±14	67±7	87±4	2±1	-35±7	-8±4	16±6	20±5	
2	100±24	70±17	76±12	2±1	-37±17	-18±4	14±8	22±8	No clear peak
3	86±15	75±10	90±8	3±1	-35±10	-10±4	10±7	21±7	

Up to 25kPa, 8kPa and 14kPa of change in peak pressure (Table 6.8) was evident between three sessions at patella tendon, distal and SPF location, respectively. Minimal change in peak S_C was observed at patella tendon and distal locations across the three sessions, while up to 10kPa of change in peak S_C was observed at SPF location. Up to 6kPa change in S_L was observed at distal location among three sessions. In general, the pressure, S_C and S_L difference induced from the different test sessions were larger than that obtained on the knee-disarticulation amputee (Section 6.2.2).

A decrease and increase of pressure was evident between session 1 and session 3 ($p<0.05$), at patella tendon and distal location, respectively. This may be explained by the sinking of the residuum inside the socket, resulting in higher pressure at a more distal location. The decrease of pressure at proximal location (patella tendon) may be explain by the fact that patella tendon of residuum may not be in proper contact with patella tendon feature designed on the socket. It is worth noting that, no significant change in S_C (all $p>0.05$) was observed at all locations between each of the two sessions.

6.3.2 Walking on different terrains

As mentioned in Section 2.5.3, one of the key parameter that affects the load transfer through prosthesis is the terrain. The change in load transfer mechanism was primarily reflected on the knee joint moment, which may directly alter the interface kinetics as it is contained in the socket. Further, understanding the joint kinetic when walking on different terrain could also be associated with the interface and limb stability, especially when walking on a descending ramp.

This section presents the results obtained from the activity C1, involving walking on different terrains, the detailed protocol of C1 can be found in Section 6.1.2.

As shown in Figure 6.43a, in the early stance phase (approximately 16%-18% of GC), the anterior-posterior component of GRF showed up to -198±11N, -296±11N and -115±10N when walking on level, descending and ascending surfaces, respectively. In the TS phase (50-55% of GC), anterior-posterior component of GRF of up to 174±7N, 127±10N and 223±19N were obtained, when walking on level, ascending and descending surfaces, respectively. It is evident that up to 69N of medial-directed force was obtained in early stance phase and this value is similar when walking on different terrains Figure 6.43b. In the TS phase, highest medial force was obtained walking on the descending ramp (60N±20), this is followed by the value obtained when walking on ascending and level surfaces.

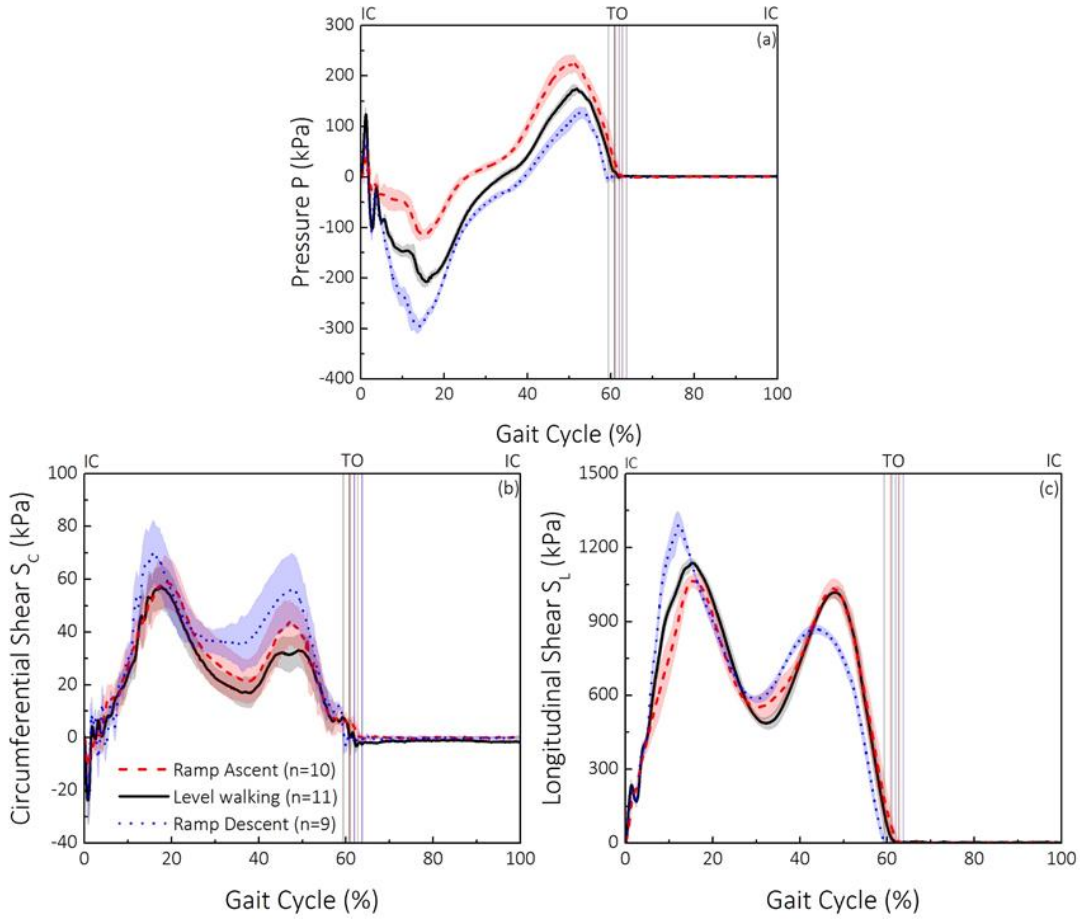

Figure 6.43: (a) Vertical, (b) anterior - posterior and (c) medial-lateral component of GRF, over a GC.

In early stance phase, up to 1137±17N, 1292±46N, 1067±30N of vertical GRF were obtained when walking on level, ascending and ascending surfaces (Figure 6.43c), respectively. In TS phase, vertical component of GRF of up to 1018±25N, 869±18N and 1034±39N were obtained when walking on level, descending and ascending surfaces, respectively.

It is evident that, double hump profile was observed in pressure (Figure 6.44a) and S_C (Figure 6.44b) over a GC. In early stance phase, up to 76kPa, 74kPa and 107kPa were obtained when walking on level, descending and ascending surfaces (Figure 6.44a). In TS phase, up to 106kPa, 76kPa and 122kPa was observed in when walking on level, descending and ascending surface. Lower pressure was obtained when walking on descending surface comparing to the value obtained during level walking. In contrast, when walking on an ascending surface, higher pressure values were obtained comparing the value obtained on level surface. In addition, regardless of the terrain, higher pressure was obtained during TS phase than that in the early stance phase. Up to 21kPa of S_C (Figure 6.44b) was observed at patella tendon location, in early stance phase. In the TS phase, up to 25kPa, 29kPa and 19kPa were obtained, when walking on

level, descending and ascending surfacesUp to -5kPa and 3kPa of S_L were obtained at early stance phase and TS (Figure 6.44c), respectively.

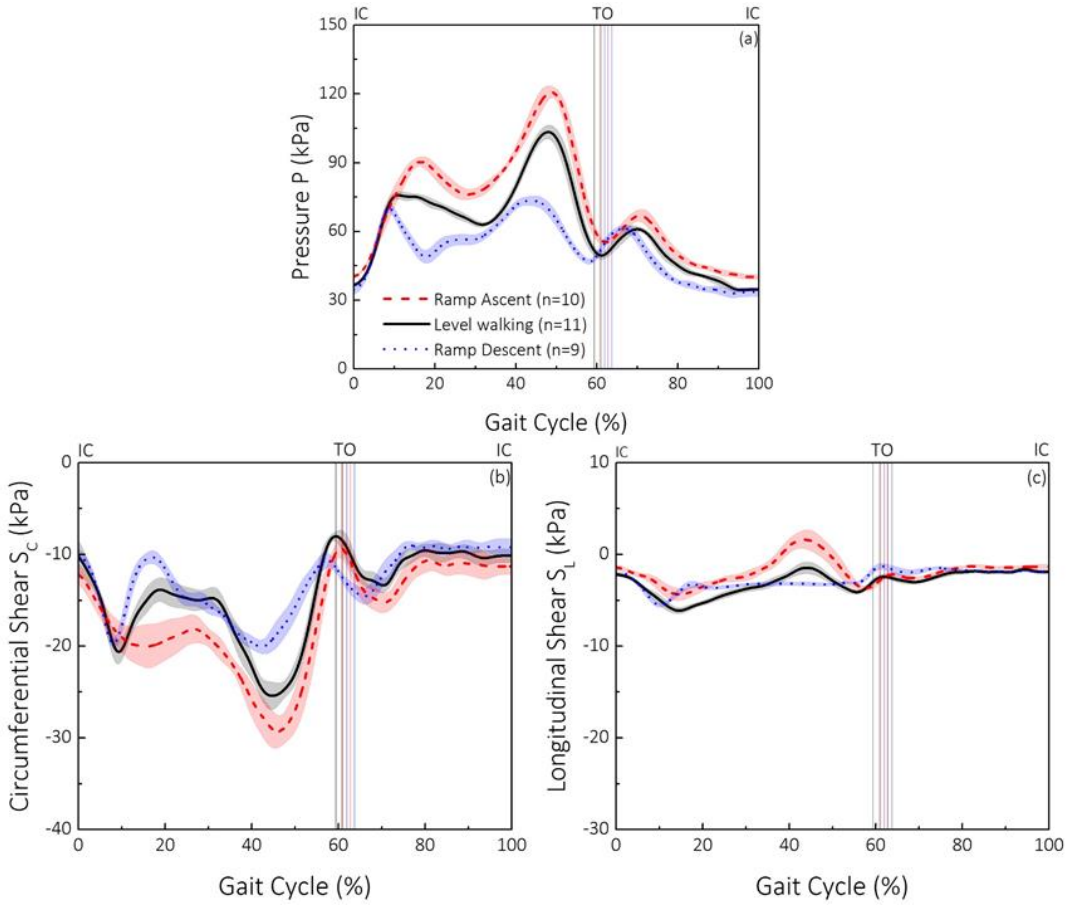

Figure 6.44: (a) Pressure, (b) circumferential shear and (c) longitudinal shear measured at patella tendon location of the residuum on level, ascent and descent surfaces, over a GC.

It is worth noting that, at IC, up to 98kPa, 44kPa and 34kPa were obtained for pressure (Figure 6.45a), S_C (Figure 6.45b) and S_L (Figure 6.45c). This may suggest the tight socket fit at distal location of the socket. The pressure at distal location (Figure 6.45a), in early stance phase, showed up to 344kPa, 373kPa and 249kPa when walking on level, descending and ascending surfaces. In TS phase, pressure values of up to 200kPa, 242kPa and 160ka were obtained when walking at level, descending and ascending surfaces, respectively. In general, highest pressure values were observed when descending the ramp, followed by the value obtained during level walking and ramp ascent. However, the pressure profile showed the reverse trend at patella tendon location. Figure 6.45b shows the S_C at distal location, over a GC. Up to 136kPa and 98kPa of S_C was obtained at early stance and TS phase (Figure 6.45b), respectively. Highest S_L value was observed in early stance phase (175kPa), this is followed by the value obtained when walking on level surface (125kPa) and ascending surface (98kPa) (Figure 6.45c). Positive S_L also indicates the residuum movement towards distal direction, relative to the socket.

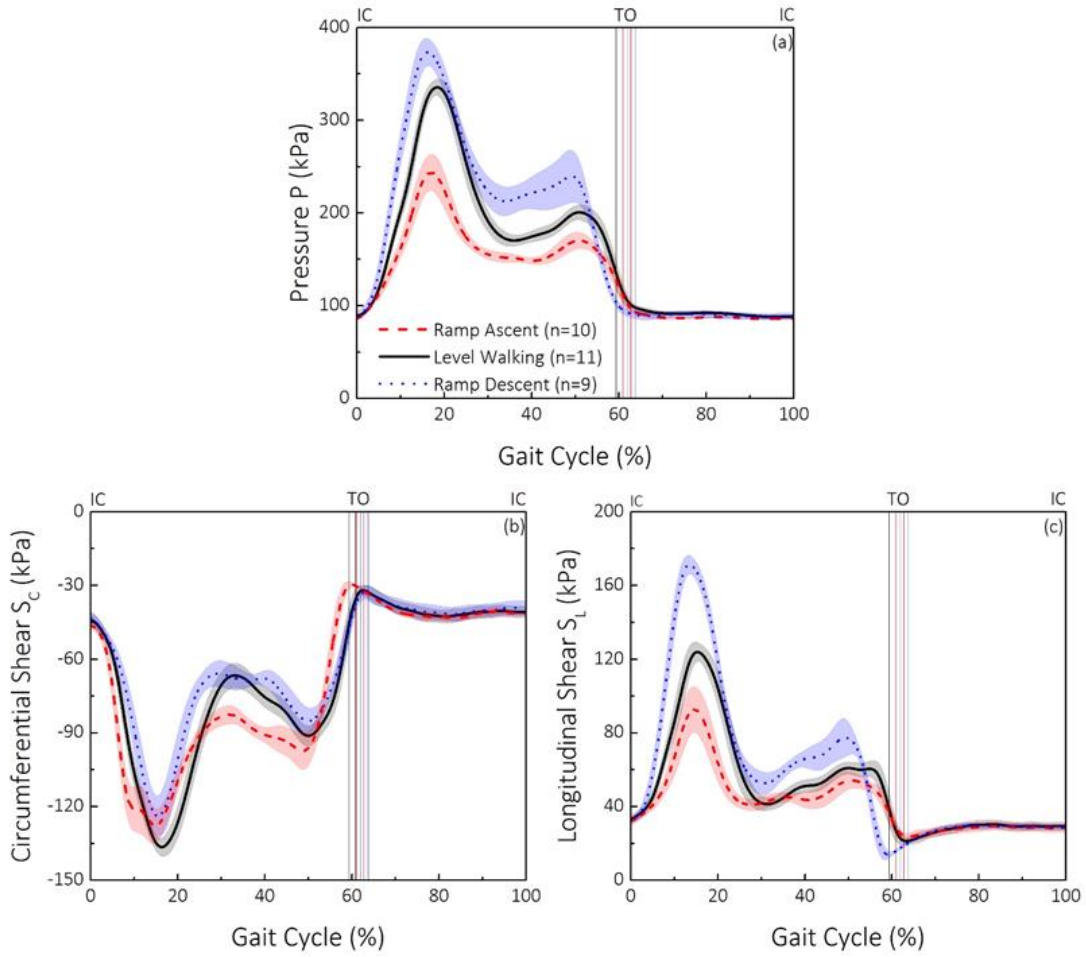

Figure 6.45: (a) Pressure, (b) circumferential shear and (c) longitudinal shear measured at anterior distal location of the residuum on level, ascent and descent surfaces, over a GC.

It is evident that similar peak pressure values (94kPa in early stance and 105kPa in TS phase) and profile was observed when walking at level and ascending surfaces (Figure 6.46a). However, lower pressure (75kPa) was observed in TS phase were observed at TS phase. This could be associated with the lower anterior-posterior component of GRF when walking on the descending ramp, comparing to the value obtained on level and ascending surface. Up to 35kPa and 26kPa of S_C was observed at early stance and TS phase, respectively, as walking on different terrain did not lead to the change in both peak S_C and profile of the S_C (Figure 6.46b).

It is worth noting that at IC, up to 10kPa of S_L was observed at SPF (Figure 6.46c) when walking on both ascending and descending ramp. However, approximately 0kPa of S_L was observed at IC when walking on level surface. This could potentially reflect on the residuum location relative to the socket. When walking on ascending and descending ramp, in this particular session, the residuum was at a more distal location, comparing to that during level walking. In early stance phase, S_L of up to 19kPa, 48kPa and 36kPa were measured when walking on level, descending

and ascending surfaces. Highest S_L was observed when walking on descending ramp in early stance phase, which could be explained by the increased anterior-posterior and vertical component of GRF.

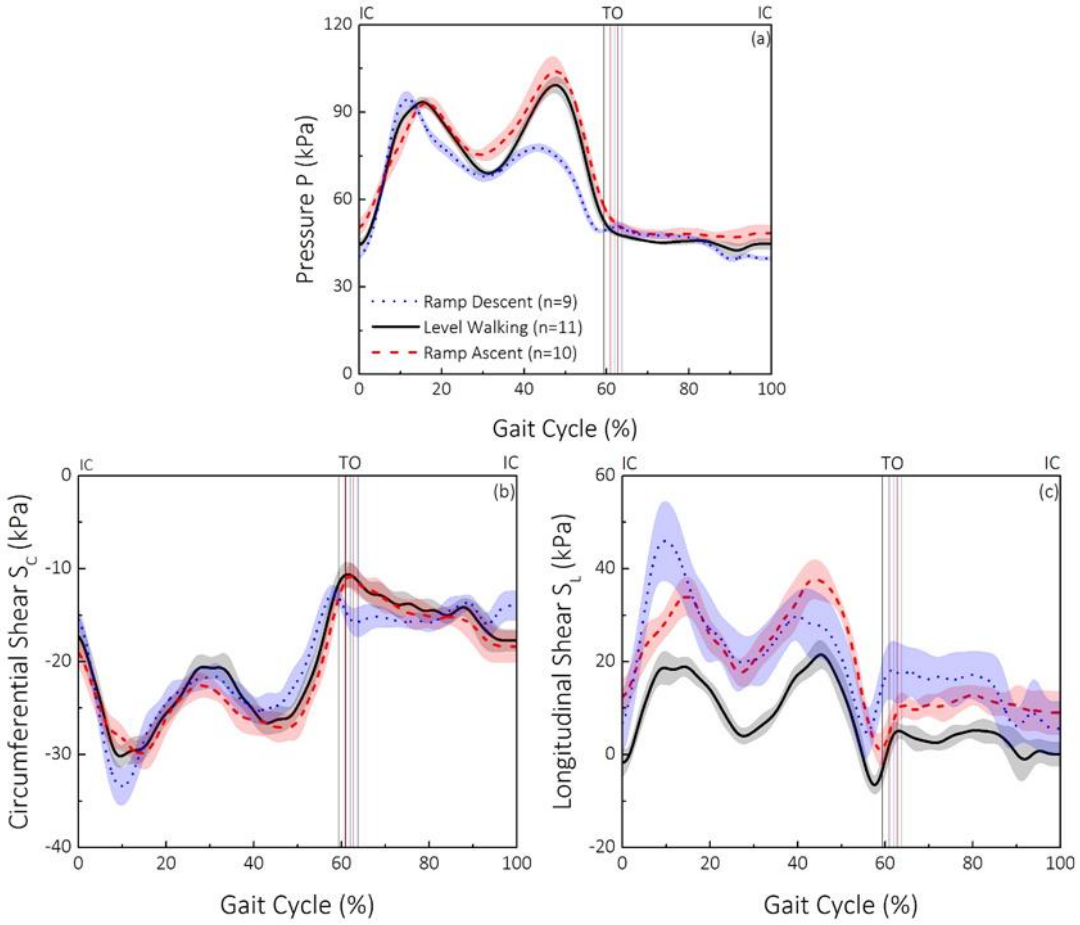

Figure 6.46: (a) Pressure, (b) circumferential shear and (c) longitudinal shear measured at SPF location of the residuum on level, ascent and descent surfaces, over a GC

Based on the three sensor measurements, two placed at the proximal locations and one placed at distal location, several key biomechanical findings can be summarised here. At two proximal locations, pressure obtained at TS phase is always higher than that obtained at early stance phase when walking on the ascending ramp, comparing the value obtained when walking on the descending ramp. This could be potentially explained by the higher anterior-posterior GRF obtained at TS phase, comparing to that obtained at early stance phase. However, this is not always the case when looking at the pressure at distal location. Regardless of the terrain, higher pressure was observed at early stance phase than that in TS phase with no clear association to the GRF. The sensor placed at distal location, equivalent to the kick point, was used to measure the change of interfacial stress due to the movement of the cut end of the tibia, hence there may not be direct correlation between the GRF and the stresses at DISTAL location. Instead, the temporal profile may be associated to the movement of tibia inside the socket.

Walking on different terrain did not seem to lead to their circumferential or longitudinal shear stresses (Figure 6.44b - Figure 6.46b) as no distinctive difference was observed in the medial-lateral component of GRF. Positive S_L was observed at distal and SPF location, suggesting there was a downward movement of the residuum relative to the socket during most of the stance phase. Apart from the positive value of S_L, double hump S_L profile was also observed at both DISTAL and SPF location as vertical GRF is the dominant force transferred from the ground interface. When walking on descending surface, higher S_L was observed in early stance phase at both Distal and SPF location. This could potentially due to the extra effort spent for braking when engaging with a descending ramp, this is also reflected on the increased anterior-posterior and vertical component of GRF when walking down the ramp. Furthermore, up to 20kPa of fluctuation of S_L was evident at SPF location, while little S_L was observed at patella tendon and distal location during swing phase. This could be associated with the muscle activation at SPF location, during swing phase, to control counter-act the inertial force exerted by the rest of the prosthesis.

6.3.3 Walking with different socket fit

As mentioned in Section 2.5.3, the load transfer from ground interface can be affected by the change in socket interface mechanical properties, such as liner thickness and coefficient of friction. Further, the change in interface mechanical properties can also be associated with socket fitting in clinical settings. Therefore, in this section the interface kinetics will be assessed as a function of socket fit. This section presents the results obtained from the activity D1, involving walking on different terrains, the detailed protocol of D1 can be found in Section 6.1.2.

In early stance phase (approximately 16%-17% of GC), up to -212N of anterior-posterior component of GRF was obtained (Figure 6.47a). There was no statistically difference (all $p>0.05$) revealed in the peak braking force for wearing 1, 2 and 3 socks. However, the was a slight delay in the timing of peak braking force when wearing three socks (Table 6.9), compared with the value obtained with two socks. In TS phase, highest propulsive force was observed when wearing 2 socks, compared with the value obtained with 1 ($p=0.00$) and 3 ($p=0.02$) socks. In addition, the adding of the socks has led to the increase of the time delay, at which the peak propulsive force was measured.

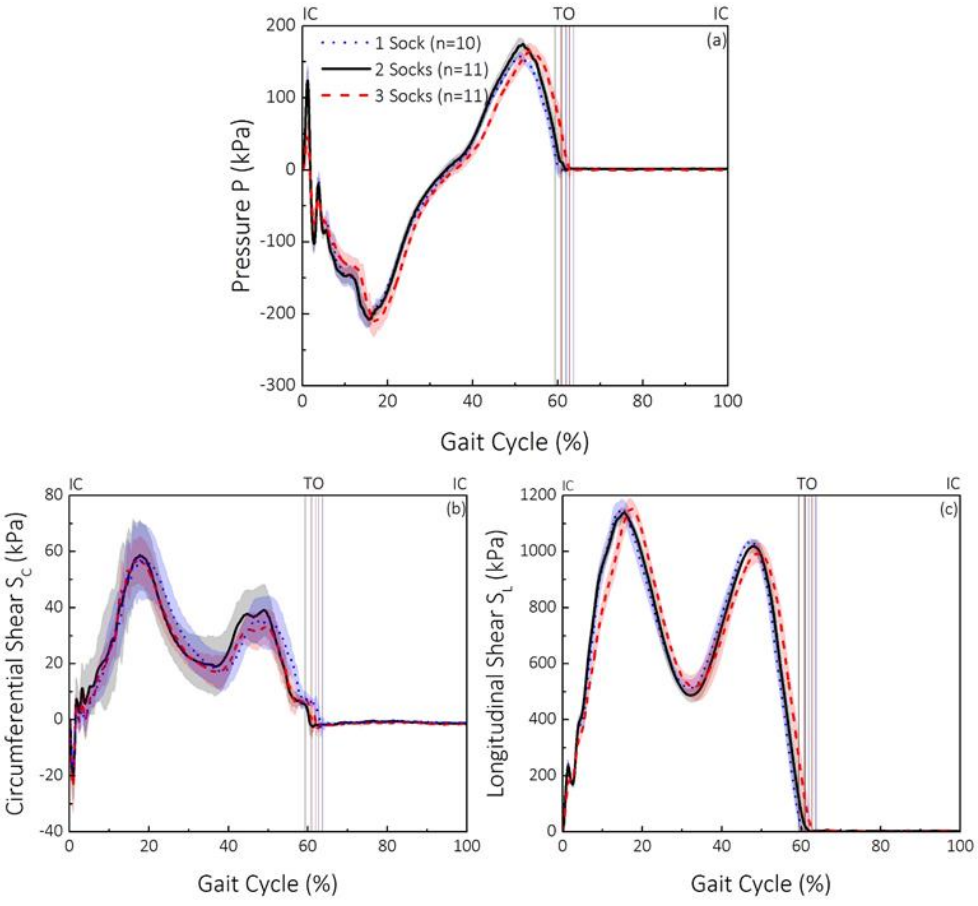

Figure 6.47: (a) Vertical, (b) anterior - posterior and (c) medial-lateral component of GRF, over a GC

Table 6.9: The mean peak value (SD) and timing for the three components of GRF, obtained from the trans-tibial amputee wearing different number of socks.

	Anterior-posterior GRF				Medial-lateral GRF		Vertical GRF			
	Braking		propulsive		Peak value		Early stance		TS	
No. Socks	N	%GC	N	%GC	N	%GC	N	%GC	N	%GC
1	-207±11	16	158±4	51	59±20	18	1149±34	15	1034±9	47
2	-208±20	16	175±6	52	57±8	18	1137±17	15	1013±23	48
3	-212±16	17	165±11	54	57±23	18	1154±33	17	995±35	49

It is evident that the adding or removal of socks didn't seem to affect both peak value of the medial-lateral GRF and the timing of which the peak value occurred (Figure 6.47b). There was no significant difference between the vertical component of GRF between each of the two conditions (Figure 6.47c). However, a higher SD value was obtained when wearing 1 and 3 sockets, compared with the value obtained with 2 socks. In addition, there was a delay in the timing, of which the early stance phase occurred when wearing 3 socks, compared with the values obtained with 1 and 2 socks. In the TS phase, the removal of one sock, from the two sock condition has led to an increase in the peak vertical GRF ($p=0.01$). A reduction in the mean value of vertical GRF was also reveal in when adding one sock, based on a two sock fit. However, this change is not statistically significant ($p>0.05$).

To author's best knowledge, this is the first study investigated the change GRF when altering the number of socks on a trans-tibial amputee. Based on this preliminary case study, significant change was revealed during the TS phase of the GC. For both anterior-posterior and vertical component of GRF, highest value was evident in an optimum socket fit (2-socks), in the TS phase. This could mean that there was a greater loading on the prosthetic side with an optimum socket fit, compared with those with a sub-optimal fit, indicating a greater involvement of the prosthetic limb during ambulation. More investigating is required to study the loading of the contra-lateral side, which could shed more lights to the asymmetry of the GRF.

Interface stresses

At IC, approximately 5±2kPa, 37±4kPa and 25±1kPa (Figure 6.48a) of pressure were obtained with 1-sock and 2-sock fit, respectively. The change from the 2-sock fit to a 1-sock fit led to approximately 32kPa of reduction in pressure. However, when adding a thick sock on top of the 2-sock fit, a reduction of pressure is also evident (up to 12kPa). According to the participant, with the 2-sock fit optimum contact can be achieved at patella tendon location. Upon removal one sock, the residuum was displaced to a more distal location, which may explain the

reduction of pressure at patella tendon bar location. Up on adding one sock at the socket interface, the residuum was held at a much proximal location in the socket. The patella tendon bar feature on the socket was no longer making contact with the patella tendon bar. In addition, more socks could result in a greater cushioning effect. Therefore, pressure at patella tendon reduces in a 3-sock fit condition, compared with those with 2-sock fit condition. It is also evident that highest pressure was obtained with a 2-sock fit in TS phase, which is consistent with the finding in both anterior-posterior and vertical component of GRF. Furthermore, regardless of the number of socks worn, up to 70kPa of change in pressure was obtained in the stance phase.

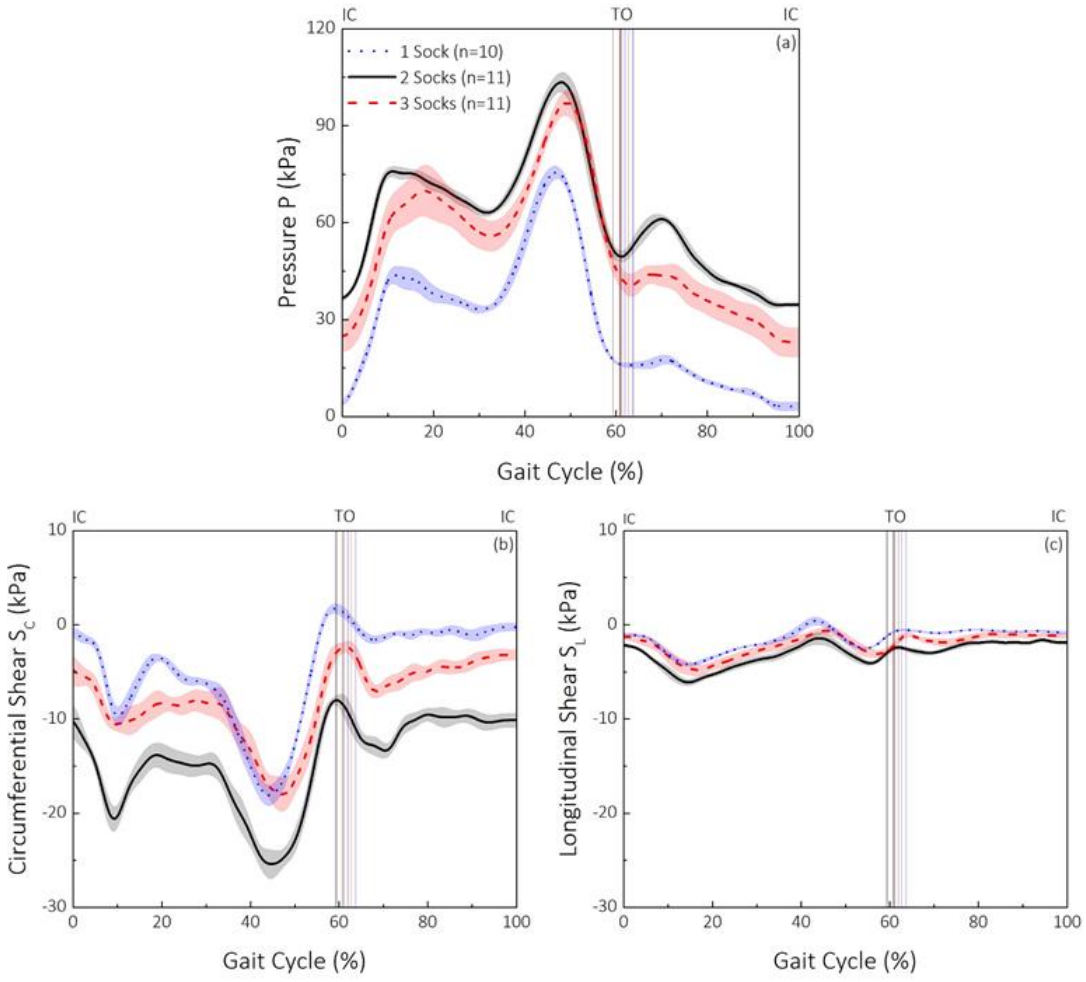

Figure 6.48: (a) Pressure, (b) circumferential shear and (c) longitudinal shear measured at patella tendon location of the residuum on level, ascent and descent surfaces, over a GC

Pressure is a critical parameter that indicates the performance of a patella tendon bearing socket. For adult amputees, the change in socket fit quality can be mitigated by adding removing socks and an optimum fit can be achieved. However, for child amputees, on top of the volume fluctuation due to activity level, the growth of residuum has a higher impact on the residuum volume change. Currently, the socket management of child amputee relies on the

frequent visit to prosthetic clinics to accommodate the rapid growth of the stump. The dramatic change in pressure with different socket fit at IC, indicates the potential for designing a self-management system for parents of the child amputees.

Apart from the difference observed at IC, up to 17±2kPa, 15±1kPa and 13±2kPa of change in S_C was observed with 1-sock fit, 2-sock fit and 3-sock fit (Figure 6.48b), respectively. Change of S_L of up to 5kPa was revealed, which is significantly less than the value obtained in circumferential direction (Figure 6.48c). Sanders et al [208], investigated the effect of weight loss on the interface stress. The study showed a reduction in both pressure and shear stress at anterior-medial-proximal location (equivalent to patella tendon location) of the stump. To aid the comparison with the current study, the reduction in weight can be approximated to have similar effect of the removal of socks. The current study suggested a decrease in shear stress when adding socks. This finding contradicts the previous study. This is likely attributed to the non-uniform change in residuum shape due to weight loss, compared with the controlled volume changed by add or removing socks.

At IC, up to 35±3kPa, 88±2kPa and 40±4kPa of pressure were observed at AD location (Figure 6.49a), with 1-sock, 2-sock and 3-sock fit, respectively. A decrease in pressure was observed at AD location when changing from a two-sock fit to a one-sock fit. This could be potentially explained by the sink of the residuum to a more distal location of the socket. AD location of the socket was no longer making contact with the 'kick-point' of the residuum, which could explain the reduction in pressure. When adding two more socks on the one-sock fit, at IC, the residuum was lifted to a more proximal location, which may cause the 'mis-match' between the AD location on the socket and the kick-point on the residuum. Two clear peaks were observed over the stance phase, with the peak in early stance phase greater than the one in TS phase. However, this does no align with Radcliffe's conceptualised stress profile described in Figure 2.49. The conceptualised stress profile revealed a lower pressure in early stance phase at anterior-distal location while a higher pressure at posterior-distal location. This was estimated based on the flexion of tibia (kinematic) against the posterior-distal location of the socket. However, the pressure change can also induced from the dorsi-flexor bending moment at the level of ankle in early stance phase.

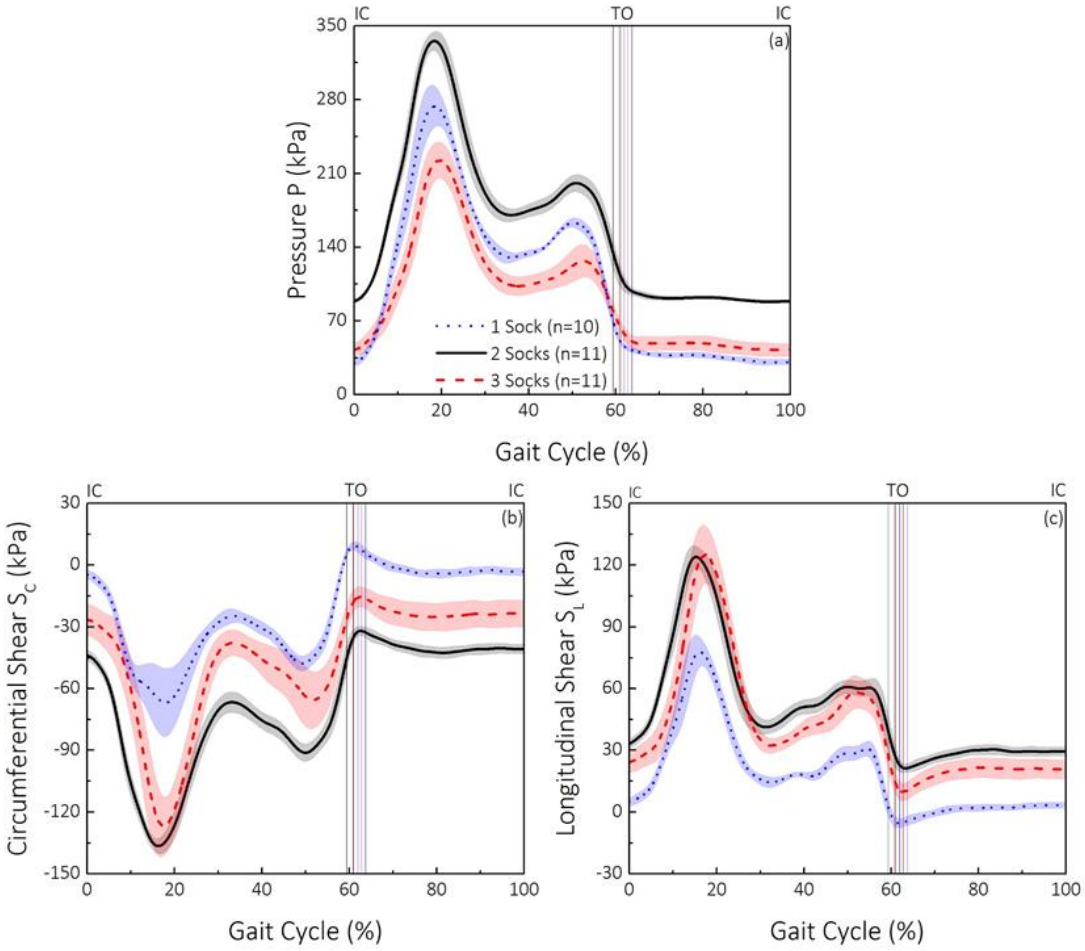

Figure 6.49: (a) Pressure, (b) circumferential shear and (c) longitudinal shear measured at anterior distal location of the residuum on level, ascent and descent surfaces, over a GC

Over the entire stance phase, up to 60±16kPa, 93±3kPa and 100kPa±8kPa of change in S_C was obtained in stance phase (Figure 6.49b). Up to 73±6kPa, 91±3kPa and 102±10kPa of change in S_L was obtained in stance phase (Figure 6.49c). It is evident that the addition of socks led to the increase in the change in both S_C and S_L at anterior-distal location. With a 3-sock fit, the residuum was lifted to a more proximal location. The truncated end of the tibia was no longer making contact with the sensor placed at the anterior-distal location of the socket. However, during dynamic walking, the vertical load transferred from the ground interface pushed the residuum more into the socket. This resulted in the proper contact between the truncated tibia and the anterior-distal sensor, hence higher shear stresses in both circumferential and longitudinal directions were revealed with more socks worn.

At IC, up to 12±3kPa, 44±1kPa and 39±5kPa of pressure were obtained with 1-sock, 2-sock and 3-sock fit (Figure 6.50a), respectively. The dramatic reduction of the pressure when changing from a 2-sock fit to a 1-sock fit may be attributed from the sinking of the residuum, when a layer of sock was removed. In stance phase, up to 53kPa, 50kPa, 47kPa change in pressure was

observed. This suggested that the addition of the sock led to the reduction in change of the pressure in the stance phase. This is likely to be explained by two possible factors. First, by adding more layer of socks, a greater cushioning was established between the residuum and the socket, which could lead to the reduction in pressure. Secondly, adding more socks could result in a tighter socket fit, constraining the interaction between the bones relative to the socket. With a 3-sock fit, pressure did not return to the value observed at IC at TO and it continued to decrease over the entire swing phase. The further strengthen the previous statement as the excessive constrain was applied to the interface with a 3-sock fit. Similarly, this feature can be potentially used as guidance to adjust socket fit in the future.

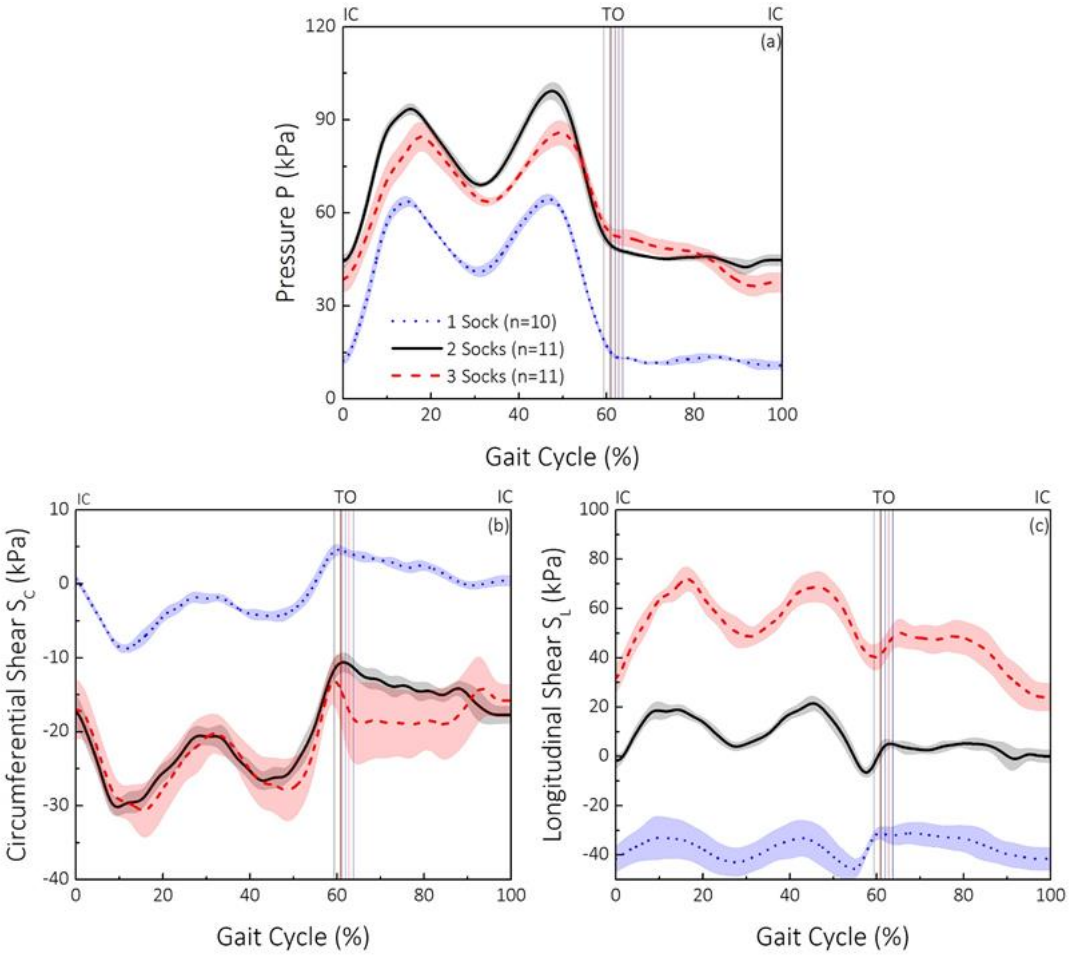

Figure 6.50: (a) Pressure, (b) circumferential shear and (c) longitudinal shear measured at SPF location of the residuum on level, ascent and descent surfaces, over a GC

At IC, 0±1kPa, 17±2kPa and 17±5kPa of S_C were obtained. S_C value of 0kPa suggested that little shear stress was transferred in the circumferential direction with 1-sock fit (Figure 6.50b). It is also worth noting that up to 6kPa of SD value was obtained over the stance phase with 3-sock fit, which is significantly higher than the value obtained with 1-sock and 2-sock fit. This may suggest that the stability in coronal plane may be compromised when excessive sock was

applied at the socket interface. The large SD value obtained with 3-sock fit also aligns well with the greatest SD value obtained in the medial-lateral GRF (Table 6.9).

At IC, -40±7kPa, 0±1kPa and 36±4kPa of S_L was obtained (Figure 6.50c). This is likely attributed the state of the residuum relative to the socket in the swing phase of the previous GC. With a loose socket fit (1-sock fit), the residuum tends to be pulled away from the socket during swing phase. This creates a longitudinal shear force towards the distal direction, resulting in a negative shear stress at IC. Similarly, due to the excessive contact between the residuum and socket during donning, a greater shear force was transferred to the residuum tissue without causing slip between the residuum and the socket, compared to the value obtained with 2-sock fit. This could result in a higher S_L at IC.

Over the entire stance phase, up to 8kPa, 10kPa and 40kPa change in S_L was observed with 1-sock, 2-sock and 3-sock fit, respectively. This suggested that the addition of sock could lead to the increase in longitudinal shear stresses. This may again be explained by the increase in static friction in the longitudinal direction with the effect of increased pressure. In theory, if the coefficient of friction remains the same, the increase in the vertical GRF could lead to the corresponding increase in the longitudinal shear stress. However, this was not the case in the current study as the greatest S_L was observed with a 3-sock fit and the corresponding vertical GRF was the lowest (Table 6.9). This lead to the hypothesis that the increase in pressure can lead to an increase in static coefficient of friction, allowing more shear force transferred to the residuum.

In this study, interface stresses were measured at key locations of a trans-tibial residuum with varied socket fit. The socket fit was controlled by either add or remove one sock from an optimal socket fit condition. This preliminary result demonstrated the potential sensitivity in interfacial stress and ground reaction forces when socket fit was altered. To author's best knowledge, this is the first study presented the change in both interfacial pressure and shear stress with the effect of socket fit.

It is clear from Table 6.9 that, highest anterior-posterior and vertical component of GRF was revealed with an optimal 2-sock fit. Either adding or removing one sock led to the decrease in the two components of GRF. In the medial-lateral direction, no significant change was revealed when socket fit was altered. A decrease in pressure at IC was evident at two proximal load bearing locations when one sock was removed from the optimal fit condition. This is likely due to the sink of residuum relative to the socket. At the distal location, either adding of removal of the sock led to the decrease of pressure at IC. A dramatic change in S_L was observed at SPF

location at IC, when socket fit was altered. With a tight socket fit, the residuum was displaced more in to the socket at initial contact, resulting in a higher longitudinal shear. With a loose fit, socket tends to be pulled away from the residuum by inertial force during swing phase, resulting in negative S_L at initial contact. From the evidence presented above, the interfacial stresses obtained at IC may be robust parameters to link with the socket fit.

Despite the two finding described above, there are limitations associated with this study. The effect of donning and doffing of the socket on the interface stress was not investigated in between the each of the socket fit conditions. The difference in absolute stresses reported at IC, or change in stresses reported over the stance may not be accurate. Cautious need to be taken when interpreting the results obtained in this case study.

This section presents the assessment of residuum/socket interface stress for both trans-tibial and knee disarticulation participants. The intra- and inter-sensor repeatability was first studied by performing mechanical tests. The sensor system, capable of measuring both pressure and shear stresses, were subsequently used to evaluate the interface kinetics. Similarly, repeatability and sensitivity studies were performed on lower limb amputee participants. Intra-session SD in a range between 0 and 2kPa was achieved in a total of four sessions. In addition, little inter-session variability, in term of peak value, was obtained between the two sessions conducted in short term. However, peak value differences of up to 67kPa and 20kPa were evident in pressure and shear measurement, respectively. This could be potentially explained by the change in socket fitting over a long period time. Adequate sensitivity was demonstrated when altering the walking speed, terrain and prosthetic components. On the knee disarticulation amputee, an increase in walking speed led to the decrease of stress at mid-stance phase and similar phenomenon was evident on the vertical GRF (Section 6.2.3). When walking on different terrains, a greater stress was measured during early stance phase on the descending ramp while a greater stress was evident during TS phase when walking on the ascending ramp (Section 6.2.4).

6.4 Analysis of interface biomechanics

Chapter 5 and Chapter 6 (Section 6.2-6.3) presented the development of means to evaluate residuum motion and stresses at socket interface, during ambulation. The effectiveness of the residuum/socket interface kinematic model (kinematics) and the TRIPS sensor system (kinetics) have been evaluated by amputee walking tests. As mentioned in Section 2.7.3, the intricate relationship between residuum motion and interface stresses have not been reported in literatures that are based on *in-situ* measurements. The novel interface kinematic model based on 3D motion capture and TRIPS sensor system enables the first-of-its-kind interface biomechanical studies. This section presents the synchronised results of residuum motions and interface stresses that have been obtained concurrently in the same walking trials of a knee disarticulation amputee. The correlation of the kinematic and kinetic information will be briefly discussed, potentially setting up a combined clinical test bed for comprehensive interface biomechanical analysis.

Figure 6.51 shows the assessment plans designed in this study.

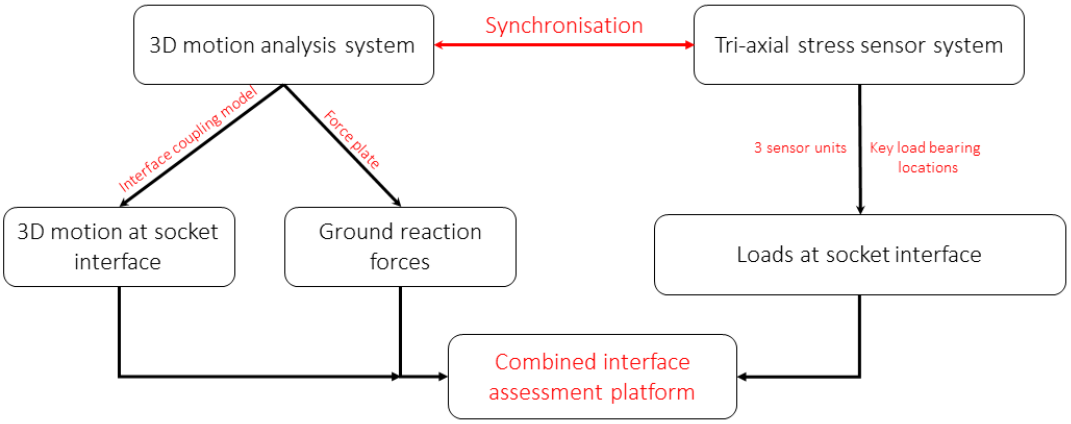

Figure 6.51: Schematics showing the interface biomechanical assessment.

6.4.1 Combined kinematic and kinetic assessment

In this series of study, socket interface biomechanics in sagittal plane and axial direction are chosen for analysis. In sagittal plane, the interface kinematic model gives an evaluation of the angular movement of the HJC in relation to the socket, in sagittal plane. It is assumed that, this angular movement can also be correlated to the proximal residuum moment relative to the socket. When the residuum segment rotates anti-clockwise, engaging with the posterior region of the socket, higher pressure will be observed at PP region of the socket (indicated by the blue rectangle in Figure 6.52a), comparing to the value at AP region. When the residuum segment rotates in the clockwise direction (Figure 6.52b), engaging with the anterior region of the socket,

higher pressure will be observed in the anterior region of the socket comparing to the value in the posterior region. In this way, the pressure measurement from the stress sensor system can be correlated to the residuum motion induced from the interface kinematic model.

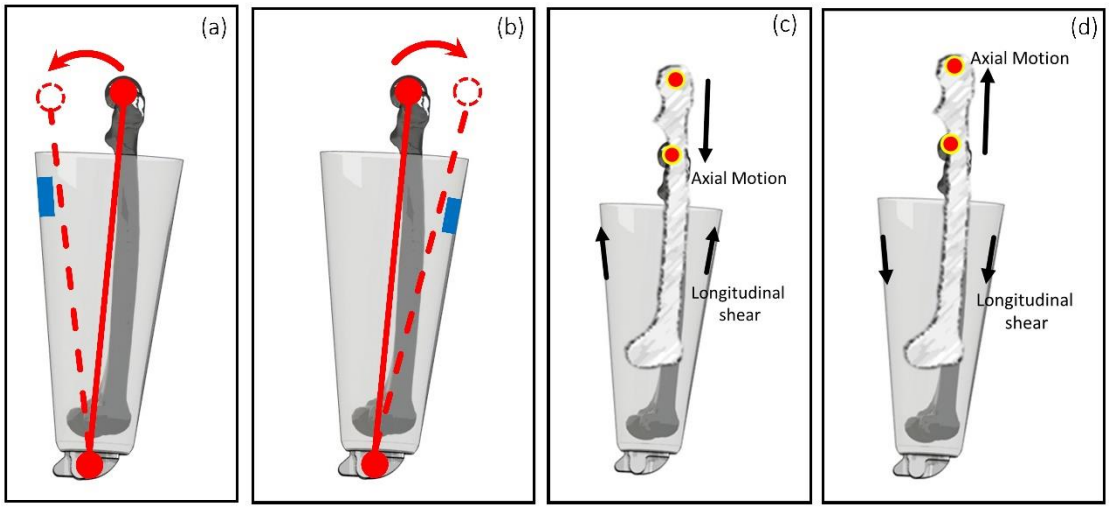

Figure 6.52: Illustration of socket interface biomechanics in (a) – (b) angular direction and (c) – (d) axial direction.

In the axial direction, the axial length induced from the interface kinematic model could be potentially associated to the longitudinal shear stresses measured from TRIPS sensor systems. A shown in Figure 6.52c, when the residuum is 'pushed' into the socket, a decrease in axial length will be evident and this could potentially leads to increase in longitudinal shear stress towards proximal direction. When the residuum is pulled out of the socket (Figure 6.52d), an increase in axial length may be observed and this could lead to an increase in axial length towards distal direction. In this way, the measured longitudinal shear stress can be correlated to the axial moment of the residuum in the socket.

6.4.2 Level walking activity

This section presents the results obtained from the activity D1, the detailed protocol of D1 can be found in Section 6.1.2.

The left axis of Figure 6.53a shows the ΔP as a function of GC and the right axis shows the angular motion in sagittal plane, as a function of GC. In general, positive ΔP (up to 17kPa) was evident in the stance phase, suggesting the pressure measured at PP location of the residuum was always higher than the value measured at AP location. In term of angular motion, an increasing trend (up to 10°) was observed in most of the stance phase, suggesting the residuum was engaging with the posterior region of the socket. Therefore, the residuum motion in the stance phase matches well with the corresponding pressure measured at two proximal locations, i.e. when the residuum engaged with the PP location of the socket, higher pressure

was also observed. In the swing phase, a decrease of ΔP was observed, suggesting the higher pressure was measure at AP location, comparing to the value at the PP location. For the angular motion in the sagittal plane, a decreasing trend was also observed, suggesting the restoration of the residuum from the stance phase, towards anterior region of the socket. Therefore, the decrease of ΔP, in the swing phase matches well the decrease of angular motion in the sagittal plane.

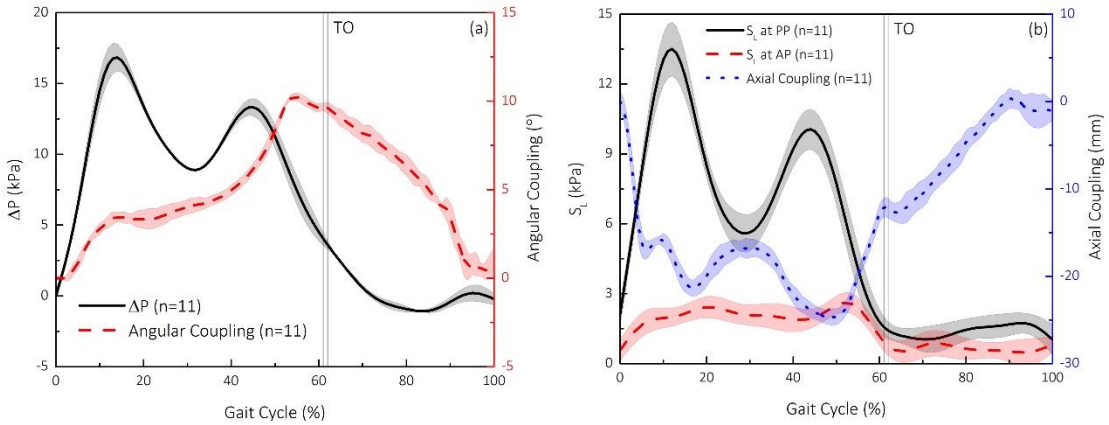

Figure 6.53: Interface biomechanics in (a) angular and (b) axial direction during level walking.

The left axis of Figure 6.53b presents the longitudinal shear stress obtained as PP and AP location, over a GC. The right axis presents the axial length values, as a function of GC. It is evident that positive S_L, in the stance phase, was measured at both PP and AP location, suggesting that the longitudinal shear force was acting on the residuum tissue towards proximal direction. Regarding to the axial length, a general decrease was observed during the stance phase, suggesting the residuum was pushed into the socket, which may induce the positive S_L acting on the residuum. In the swing phase, S_L showed little fluctuation. However, an increasing trend of the axial length was observed. This could likely contributed from the residuum slip inside the socket, during the swing phase.

It is envisaged that the biomechanical analysis at socket interface could potentially aid the prosthetist with socket design and fitting. As an example, the performance of the ischial containment socket (Figure 2.7b) on a trans-femoral amputee can be assessed by evaluating the angular motion in coronal plane and stresses at ischial seat of the socket. In addition, the performance of the Hi-Fi socket can be assessed by evaluating axial length motion and at the same time, avoiding excessive pressure along at the depression regions (Figure 2.8).

Furthermore, the intricate relationship between the interface kinematics and kinetics could potentially implemented in the monitoring system designed for lower limb amputee. As an example, for tans-femoral amputees, when the interface friction behaviour falls in static regime,

the increase in longitudinal shear stress is approximately proportional to the displacement (axial length) or strain. Socket comfort can be potentially described as a function of axial length and longitudinal stresses. When the interface friction falls in dynamic regime, i.e. slip between the residuum and the socket. The axial length will either increase or decrease depending on the direction of loading. However, when slip presents at socket interface, longitudinal shear stress ay not change at the load is not transferred to the sensor. In this case, using sensor to inform socket fit may not be appropriate. A combined kinematic and kinetic assessment is then critical in this case, especially for amputees who have reduced or loss of sensation.

6.4.3 Level walking with difference walking speeds

This section presents the results obtained from the activity D2, the detailed protocol of D2 can be found in Section 6.1.2.

The left and right axis presents the ΔP (solid lines in Figure 6.54a) and angular motion (dashed lines in Figure 6.54a), as a function of GC, respectively. To avoid the repetitive description of the results, only the effect of walking speed on the interface biomechanics will be presented and discussed here. With particular focus in the mid-stance phase of the GC, up to 11kPa, 9kPa and 6kPa of ΔP was obtained when walking at slow, self-selected and fast walking speeds, respectively. This suggested that the increase in walking speed led to the decrease of ΔP. Up to 3.0°, 2.8° and 2.4° angular motion were obtained in the mid-stance, when walking at slow, self-selected and fast walking speeds, respectively. Therefore, the increase in the walking speed led to the increase in angular motion in sagittal plane in mid-stance phase, suggesting the residuum was making more contact with the PP location of the socket. This could be potentially correlated to the ΔP pressure, as the increase in contact with PP location of the socket could results in higher ΔP. This interface biomechanics observed may be further correlate to the load transfer from the prosthetic knee joint. Knee joint was chosen as a point for analysis as it was the closest distal to the socket interface. The greater movement and stress observed in mid-stance, when walking with slow speed may be associated with the greater knee joint moment (Figure 4.8 in Section 4.3.3).

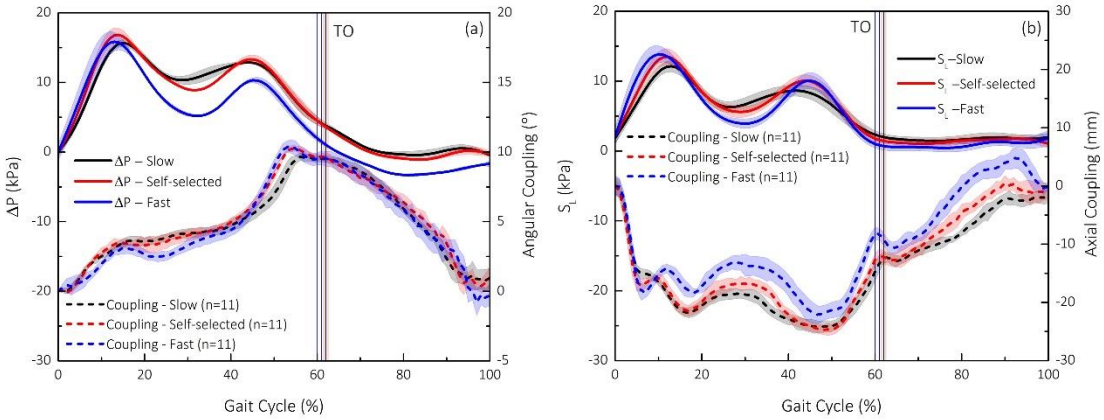

Figure 6.54: Interface biomechanics in (a) angular and (b) axial direction when walking with different speeds.

The left axis of Figure 6.54b presented the longitudinal shear stress obtained as PP location of the residuum while the right axis indicates the axial length. At mid-stance phase of the GC, up to 12kPa, 11kPa and 9kPa of S_L was obtained when walking at slow, self-selected and fast walking speeds. This suggests that the increase in walking speed led to the decrease of S_L in the mid-stance phase. When comparing the axial length obtained at mid-stance phase, up to -21mm, -18mm and -16mm was obtained when walking at slow, self-selected and fast walking speeds, respectively. This suggests that the increase in walking speed led to less axial length, which could be potentially associated with the reduction in S_L. Similarly, potential association was found between the load transfer at the ground and at the socket interface. The greatest vertical GRF was measured when walking at slow speed, followed by self-selected and fast walking speeds, at mid-stance phase (Figure 4.6 in Section 4.3.1). This could be potentially associated with the greater interfacial stress and residuum movement observed at socket interface.

In general, in mid-stance phase, the increase in walking speed does not necessarily lead to the increase in residuum motion and stresses at socket interface. Instead, when walking at slow speed, a greater mechanical interaction was evident at socket interface. This finding could be potentially implemented in the control strategy in the future intelligence prosthesis. An improvement in residuum stability can be achieved through the actuation of an adaptive socket, when walking at slow walking speed.

6.4.4 Walking on different terrains

This section presents the results obtained from the activity D3, the detailed protocol of D3 can be found in Section 6.1.2.

Anterior-posterior GRF shows mean peak forces of approximately −115 N, −145 N and −66 N in early stance phase, and +115 N, +77 N and +169 N in the TS during level, descent and ascent walking (Figure 6.55a), respectively. Vertical GRF shows typical double-hump shaped profiles with mean peak forces of approximately 840 N, 837 N and 814 N in early stance phase (10-20% of GC), and 814 N, 754 N and 781 N in TS (40-60% of GC) during level, descent and ascent walking, respectively (Figure 6.55b). Regardless of the terrain, the early stance phase peak and the TS peak in vertical GRF were separated by a mid-stance local minimum, at approximately the same point in the GC (30%). This also corresponds to the maximum vertical position of the centre of mass during stance. Therefore, this mid-stance point was chosen as a point of comparison for analysis in this work.

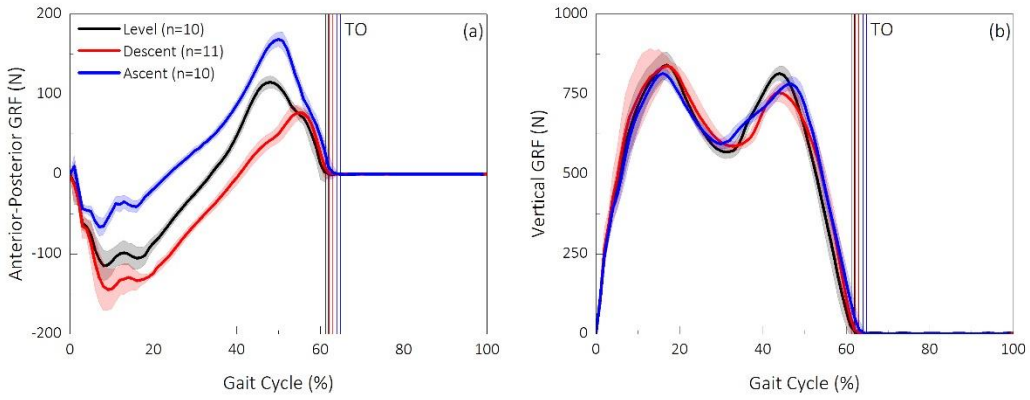

Figure 6.55: (a) Anterior-posterior GRF and (b) vertical GRF obtained when walking on different terrains.

In the sagittal plane, the kinematic movements and kinetic stresses at the interface were evaluated by characterising both the angular motion in the sagittal plane (Figure 6.56a) and the pressure at the AP and PP locations, on level, descending and ascending surfaces. Angular motion showed a 1° higher movement from IC to mid-stance when walking on descending surface (2°), compared with that on level walking (1°). This is likely due to the effort required in early stance phase to control the residuum, achieving foot-flat when descending the ramp. In addition, angular motion showed 4° more movement from mid-stance to TS when walking on ascending surface (9°) when compared to that during level walking (5°). This may be affected by the work produced by the hip in TS to propel the limb forward to initiate the swing phase. The interface kineamtics seen is mainly a result of the moment applied to the socket as a result of the anterior-posterior component of GRF. For interface kinetics, during ramp descent, higher pressure at the PP and AP locations were obtained in early stance phase, comparing to that at TS. By contrast, when walking on the ascending ramp, higher pressure at the PP and AP locations were obtained at TS.

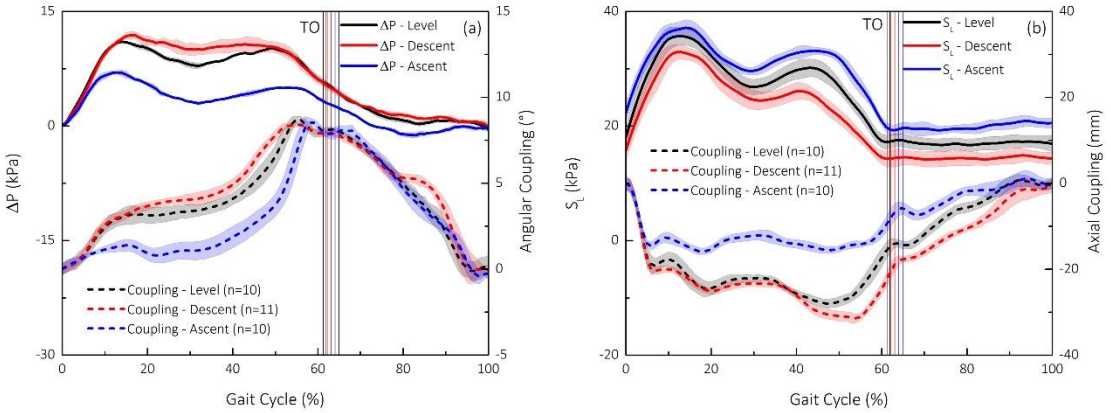

Figure 6.56: Interface biomechanics in (a) angular and (b) axial direction when walking on different terrains.

For the tests conducted on all terrains, +ve values for both angular motion and Δ*P* were obtained during the majority of the stance phase (Figure 6.56a). In particular, the increase of angular motion corresponds to the increase of Δ*P* in the early stance. This suggests that, in general, the larger the angular motion, the higher pressure at the posterior region than at the anterior region. Such an effect is illustrated by the corresponding schematic in Figure 6.52a and b, showing the VRS engagement with the posterior region of the socket, while a higher pressure was obtained at the PP location compared to that at the AP location. It is well established that the PP location of the socket provides a seating interface for the knee-disarticulation amputee, especially during stance phase of the GC, to stabilise the trunk and the prosthetic knee [2, 43]. This effect was generally observed for all terrains. However, a greater angular motion was observed during early stance phase when descending the ramp compared with the other two surfaces. This in principle corresponds to the greater anterior-posterior braking force (Figure 6.55a) during ramp decent in early stance phase, which may have resulted in a greater residuum rotation towards the posterior region of the socket from IC to mid-stance (Figure 6.56a, right axis). Indeed, at the two proximal locations, higher peak pressure were measured in early stance phase when compared to those at TS (Figure 6.56a, left axis). By contrast, when ascending the ramp, a greater propulsion force was recorded during TS (Figure 6.55q). This may explain why the increase of α occurred in between mid-stance to TS of the GC.

Figure 6.56b shows that, from approximately 0–20% of the GC, axial length shortened and the S_L at the PP location increased. As gait progresses to mid-stance, both the L and the S_L stabilise to form a plateau-like region. Axial length further shortens after mid-stance phase with a subsequent increase in the S_L at the PP location. At TS, both the axial length and the S_L started to recover. Limited S_L at the PP location was recorded during swing phase, although the recovery of axial length was evident. This may be a direct result of bony

movement inside the residuum, with minimal resulting shear transferred between the socket and the residuum. When walking on different terrains, highest peak values of S_L were obtained during the ramp ascent, followed by the values measured during level walking and ramp descent. However, the largest axial length was evident during ramp descent. This is likely a result of load dependent non-linear friction behaviour, namely, the presence of slippage at the residuum/socket interface.

This section presents a combined biomechanical assessment at residuum/socket interface using the kinematic and kinetic measurements based on two separate bioengineering techniques. Preliminary results suggest an association between the residuum movement, characterised by angular and axial length, and the pressure and shear stresses exerted at the residuum/socket interface.

This chapter presents the assessment of interface kinetics for lower limb amputees. TRIPS sensor system was used as means to provide pressure and shear at socket interface. The effectiveness of the system was evaluated primarily on a knee disarticulation amputee and a trans-tibial amputee in terms of repeatability. The sensitivities of the technique was assessed with a series of walking activities and different prosthetic components, during which the interface kinetics was also assessed. The interface biomechanics, incorporating kinematics and kinetics, is first time studied. In addition, the biomechanics evaluated at the socket interface was first time studied in conjunction with the load transfer from the ground interface, through the prosthetic limb. It is envisaged that such techniques could be potentially used to understand the biomechanical loading mechanisms at the residuum/socket interface, as well as to assist in the design and evaluation of a patient-specific prosthesis.

In the next chapter, a summary of research activities in this PhD project will be discussed.

Chapter 7 Summary and future work

7.1 Summary

This thesis thus fulfil the overall aim of project to develop a first-of-its-kind interface kinematic model and a sensor system capable of assessing multi-directional interface stresses. This has been achieved through the key objectives as stated in Section 1.2. Detailed results and analysis aligning with these objectives are presented in Chapter 5 and Chapter 6, respectively.

A residuum/socket interface kinematic model was developed to assess the kinematics at the socket interface for lower limb amputees. The model consisted of a virtual residuum segment (VRS) and a socket segment (SS) with both defined with respect to a 6-DoF lower limb musculoskeletal model This is one of the advantage, as no alteration of the well-established marker placement protocol is required, when comparing with the model proposed by Childers and Siebert [169]. The alteration of the existing marker placement protocol may introduce potential error across investigators. This technique enables the dynamic assessment of the interface kinematics in a commonly available prosthetic research laboratory without disrupting amputee's gait. This was not possible before as it either only provide static assessment or cannot be used for assessment and monitoring in daily life.

The repeatability of the model was assessed on a single knee disarticulation participant with repeated trials in the same session on the same day and in sessions across different days. In total, 10 measurement sessions were conducted over two years. Repeatable waveform (CMC values of up to 0.9) was obtained during the same measurement session and across different days. Subsequently, the same measurement technique was applied on a trans-tibial participant. Up to three measurement sessions were conducted on different day to assess both intra- and inter-session repeatability of the technique. The preliminary study also showed potential sensitivity of the interface kinematic model to walking speed, terrain and different prosthetic components. It was first evaluated by asking the knee disarticulation to perform non-walking activities, such as standing, sit-to-stand and weight shifting activities. In addition, walking speed and terrain were also selected as input parameters for the sensitivity assessment. This preliminary work suggested that the increase in walking speed could lead to a greater residuum motion inside the socket. In addition, when walking on a descending ramp, a greater coupling motion was found in early stance phase. Correspondingly, when walking on an ascending ramp, higher coupling motion was observed as terminal stance phase. Different types of prosthetic components and suspension system were chosen to evaluate the residuum motion at the interface. The preliminary study suggested that the use of MPK could potentially reduce the residuum motion inside the socket, comparing to that with a polycentric knee. In addition, an

reduction in pistoning motion was found with an active vacuum suspension, compared with a suction suspension system.

In addition to the 3D motion at the residuum socket interface, the corresponding stress profile was also examined. This involves the use of the TRIPS sensor system developed by colleagues in the University of Southampton. The sensor system proves to be clinical friendly as it involves no alteration on a socket and can be easily integrated with existing prosthetic components, resulting in minimal disruption in amputee's gait. This was not viable in previous reported studies. Up to 30 sensor units, each of which was manufactured by the author of the thesis. To ensure the performance during testing, each of sensor unit was individually calibrated and the performance was subsequently evaluated.

Three sensor units were placed on both trans-tibial and knee-disarticulation participant. Interface pressure and two orthogonal components of shear stresses were measured at each location. Before conducting the level walking test, simple non-walking activities were performed by the participant while interface stresses were acquired. These involved donning and doffing of the socket, standing and dynamic weight shifting, each of which were performed by the participant. It was demonstrated that stress at all three locations are sensitive to these simulated daily activities perform, most particularly the interface stresses at the posterior-proximal location. Up to 10kPa, 6kPa and 6kPa change in pressure, S_C and S_L was measured during four repeated measure after donning and doffing process. This is one of the first studies that evaluates the effect of donning and doffing process to the interface stresses [195]. In addition, repeatability of the measurement was assessed by performing level waking test across different days. SD values of up to 5kPa was measured in pressure, S_C and S_L when evaluating the intra-session repeatability . The corresponding inter-session repeatability reveal up to 2kPa change in stress in the short-term and 28kPa change in stress during a long-term evaluation. The intra- and inter-session repeatability was comparable to those reported by Sanders, Zachariah [190].

Interfacial stresses obtained when walking at different speeds and on different terrains were also evaluated on the knee-disarticulation amputee. Results suggested that an increase in walking speed does not necessarily lead to an increase in interfacial stress. It is also worth noting that the profile of interfacial stress seems to follow the same pattern as the vertical component of GRF at mid-stance phase. When walking on different terrains, changes in peak values were observed in both early stance phase and terminal stance phase. When walking on a descending ramp, a greater interface stress was measured in early stance phase, compared

with the value at terminal stance phase. In addition, when walking on an ascending ramp, a greater interface stress was measured in terminal stance phase, compared to the value at early stance phase. Socket fitting, representing one of most important clinical parameter was also evaluated as a function of interface stresses on a trans-tibial amputee. Sensor units were placed at both proximal location and distal location of the residuum. Socks were added or removed in order to alter the socket fitting. The preliminary results suggested that the removal of sock seems to lead to the increase the loading at distal end while reducing the load at proximal locations.

The kinematic motion and kinetic stress, obtained at the interface, was first time combined to study the interface biomechanics. A synchronisation device was developed to provide synchronous measurement of interface kinematics and kinetics. Walking speed and terrain were chosen as inputs to study in the interface biomechanics. This combined assessment further enables *in-situ* study of effect of the load transfer from the ground, through the prosthetic components, to socket interface.

7.2 Potential scientific and clinical contribution of the field

The evolution of the residuum 3D motion and stress provide *in-situ* biomechanics information during amputee walking, the use of which could be:

- The 3D residuum motion and the corresponding stress can be used as inputs to FEA for the evaluation of deep tissue damage. The assessment of the residuum internal tissue damage (Section 2.2.3) can then be assessed locally with the aid of tissue damage model, which could potentially improve overall rehabilitation outcome.
- The compliance of the socket interface can be potentially modelled with the input of residuum motion and load. The understanding of the socket interface compliance can contribute to the design of the biomimetic limb, as it requires the integration of socket interface with other mechanical (hydraulic) prosthetic components (Section 2.1.2).
- The biomechanical knowledge regarding to the linked-segment model at socket interface can then be further used to form an improved musculoskeletal model for lower limb amputee. This could potentially improve the accuracy of the estimation of joint mechanics, as to-date, the interface was treated as a rigid segment in amputee gait analysis (Section 2.5.1).
- The kinematics and kinetic measurement technique could potentially contributes to new socket designs and socket suspension techniques (Section 2.1.3). In addition, it could also provide guidance on socket alignment process (Section 2.2.1).

- The socket interface stress could also provide useful biomechanical feedback to orthopaedic surgeons. Interface stresses, as one of the rehabilitation outcome, could be associated with the existing surgical practice (Section 2.1.1). An improved surgical technique could be potentially formed with more understanding of the interface biomechanics.
- The measured socket interface kinematics and kinetics could lead to a more realistic evaluation of limb performance (ISO10328). The prosthetic limb performance is currently assessed by assuming the socket interface is rigid. Introducing a non-rigid idea for socket interface could potentially improve the accuracy and robustness of the prosthetic components assessment.
- Similar methodologies could be expanded to other application areas where relative motion and loading at body interface play important role e.g. upper limb prosthetic interface, wheelchair/special seating. The measurement of interface load at fingertip/object interface could be potentially converted to neuro signals, which could potentially help upper limb amputee to re-gain sensations.

7.3 Limitation and future work

The research presented in this thesis may be expanded in a number of ways.

In this PhD project, the study of interface biomechanics was primarily based on one knee-disarticulation amputee. The assessment of the reliability of the assessment technique can be expanded on a larger cohort of amputees, involving trans-tibial, trans-femoral and knee disarticulation amputees. This also facilitates a more in-depth understanding of the interface biomechanics involving different walking speeds, terrain, prosthetic components and interface mechanical properties.

Section 5.2 describes the interface kinematic model for trans-tibial amputee. The model was capable of estimation of the knee joint movement with respect to the socket. Similar waveform was obtained in the current study (Section 5.5.1), compared with the ones reported by Childress and Siebert . Despite the similar waveform obtained, there is a limitation regarding to the model developed for trans-tibial amputee. The tracking of the knee joint movement relies on two assumptions:

- No translational movement between the femur and truncated tibia (Figure 7.1).
- Minimal soft tissue artefact contributed from the thigh cluster markers.

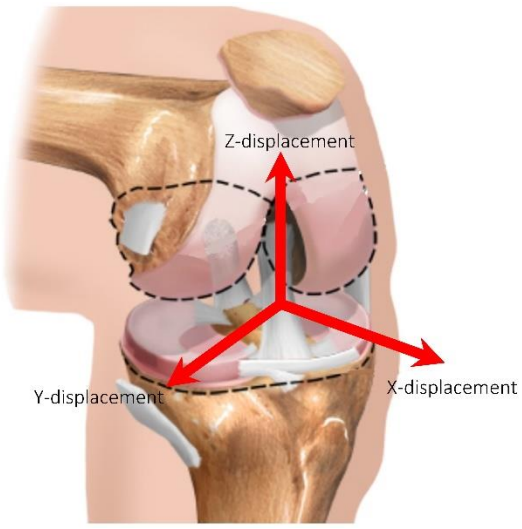

Figure 7.1: A schematic showing the translational movement between the femur and tibia.

In order to address the limitation in the interface kinematic model, developed for trans-tibial amputee, Inertial Measurement Unit (IMU) based wearable technology may be used. With millimetre sized IMU, it can be integrated with existing interface components. As an example, one IMU can be integrated with a silicone liner with the second mounted on the inner socket wall. The differential IMU signals, such as acceleration and angular velocity, obtained during dynamic ambulation can be used to derive the axial and angular movement of the residuum at socket interface. Further, the two-IMU configuration can be combined with TRIPS sensor system and subsequently applied at different locations of the interface, providing a more localised interface biomechanical assessment for lower limb amputees.

Previous studies have shown the association between limb alignment and socket reaction moment (Section 2.5.3). Different locations of the residuum may have different biological tissue behaviours. The measurement of socket reaction moment may not be adequate to guide the limb alignment process. The intricate link between the socket reaction moment and the localised dynamic stress profile and tissue viability need to be studied. This could potentially provide a means to create guidance to limb alignment process during limb fitting stage and for self-management.

A formal evaluation of the correlation between the 3D motion and stresses at measured at the socket interface can be conducted. The results presented in section 6.4 provide the basis of conducting correlation analysis, such as cross-correlation.

Translation between the kinematic and kinetic measurement to clinical outcome measure is one of the limitations of this project. Socket comfort, can be potentially interpreted as a function of interface kinematics and kinetics. Factors that affect socket comfort, such as

prosthetic alignment, suspension technique, silicone liner properties and prosthetic components, can be used as inputs to a regression model for evaluating socket comfort. The evaluation can then be translated to clinical interventions either from a prosthetist during socket fitting stage or from amputee self-management. Having identified the outcome measures, a clinical friendly user interface can be developed either via a laptop or a smartphone app. All of these could further improve the quality of the prosthetic services to lower limb amputees.

List of publications and other achievement

Journal publications

1. Tang J, McGrath M, Laszczak P, Jiang L, Bader D, Moser D, et al. Characterisation of dynamic couplings at lower limb residuum/socket interface using 3D motion capture. Med Eng Phys. 2015; 37:1162-8.
2. Tang J, McGrath M, Hale N, Jiang L, Bader D, Laszczak P, Moser D, et al. A combined kinematic and kinetic analysis at the residuum/socket interface of a knee-disarticulation amputee. Med Eng Phys. 2017; 49:131-9.
3. Laszczak P, McGrath M, Tang J, Gao J, Jiang L, Bader DL, et al. A pressure and shear sensor system for stress measurement at lower limb residuum/socket interface. Med Eng Phys. 2016; 38:695-700.
4. Valero, M, Hale, N, Tang, J, Jiang, L, McGrath, M, Gao, J, Laszczak, P, Moser, D, 2016. Interfacial pressure and shear sensor system for fingertip contact applications. Healthc Technol Lett 3, 280-283.
5. McGrath M, Gao J, Tang J, Laszczak P, Jiang L, Bader D, Moser D, Zahedi S, 2017. Development of a residuum/socket interface simulator for lower limb prosthetics. Proc Inst Mech Eng H 0, 954411917690764.
6. Hale N, Valero M, Tang J, Jiang L, Moser D. A preliminary study on characterisation of finger interface kinetics using a pressure and shear sensor system. Prosthet Orthot Int. 2017; 42:60-5.
7. Hale N, Chadwell A, Monk A, Tang J, Meng Z, Head J, Kenney L, Jiang L, 2018. Influence of electrode load and movement on the function of trans-radial myoelectric users. Clin Biomech. (Under review)
8. Tang J, Laszczak P, Hale N, McGrath M, Jiang L, Bader D, Moser D, Zahedi S. Characterisation of lower limb residuum/socket interface stiffness using 3D motion capture. Journal of the Mechanical Behaviour of Biomedical Materials. (Manuscript in preparation)

Presentations and posters in conferences

1. Tang J, Jiang L, Bader DL, McCarthy J, Bradbury R, Zahedi MS, et al. Use of gait lab 3D motion capture for dynamic assessment of amputee socket interface biomechanics – a preliminary study. Abstract published in Prosthetics and orthotics international. 2015; 39:257.
2. Tang J, McGrath M, Hale N, Jiang L, Bader D, Moser D, et al. Assessing trans-femoral residuum/socket interface coupling using 3D motion capture – Effect of terrains and walking speeds. Abstract published in Gait & posture. 2016; 49s:147.
3. Tang J, Hale N, McGrath M, Jiang L, Bader D, Laszczak P, et al. Method to assess biomechanical coupling at trans-femoral residuum/socket interface. ISPO 16th World Congress. Cape Town, ZA: International Society of Prosthetics and Orthotics; 2017.
4. Tang J, Hale N, McGrath M, Jiang L, Bader D, Laszczak P, et al. Method to assess biomechanical coupling at trans-femoral residuum/socket interface. ISPO 16th World Congress. Cape Town, ZA: International Society of Prosthetics and Orthotics; 2017.

5. Tang J, Jiang L, Bader D, Moser D, Zahedi MS, McCarthy J, et al. Influence of stump/socket relative movement on gait analysis for above knee amputees – A case study. ISPO UK Annual Scientific Meeting. London: International Society of Prosthetics and Orthotics; 2014.

6. Tang J, Jiang L, Moser D, Zahedi MS. The effect of integrated microprocessor controlled knee-foot for inclined walking - a preliminary study on LiNX. The AOPA National Assembly 2015. San Antonio: American Orthotic Prosthetic Association; 2015.

7. Tang J, Jiang L, Bader D, Laszczak P, Gao J, McGrath M, et al. Use of gait lab 3D motion capture for dynamic assessment of amputee socket interface biomechanics with validation using TRIPS sensors systems – A case study. ISPO UK Annual Scientific Meeting. Oxford: International Society for Prosthetics and Orthotics 2015.

8. Tang J, McGrath M, Hale N, Jiang L, Bader D, Moser D, et al. Assessment of socket interface kinematics and kinetics based on a trans-femoral amputee case study. International Society of Prosthetics and Orthotics UK Annual Scientific Meeting. Glasgow: International Society of Prosthetics and Orthotics; 2016.

9. Tang J, Jiang L, Bader D, McGrath M, Moser D and Zahedi MS. The influence of socket fit on the socket interface stresses – a preliminary study on a trans-tibial amputee. ISPO UK Annual Scientific Meeting. Cambridge 2017.

10. McGrath M, Gao J, Tang J, Laszczak P, Jiang L, Bader D, et al. A lower-limb stump/socket interface simulator to aid assessment of clinical interventions. Abstract published in Prosthetics and orthotics international. 2015; 39:262.

11. McGrath M, Jiang L, Bader D, Gao J, Laszczak P, Tang J, et al. Investigation into the effect of liner choice on interface stresses using a stump/socket simulator. ISPO UK Annual Scientific Meeting. Oxford: International Society for Prosthetics and Orthotics 2015.

12. McGrath M, Tang J, Hale N, Jiang L, Bader D, Laszczak P, et al. Clinical evaluation of a measurement system for loading at the lower limb stump/socket interface. International Society of Prosthetics and Orthotics UK Annual Scientific Meeting. Glasgow: International Society of Prosthetics and Orthotics; 2016.

13. Laszczak P, Jiang L, Moser D, McGrath M, Gao J, Tang J, et al. Effects of clinical interventions and everyday activities on the dynamic loading at the lower limb stump/socket interface ISPO UK Annual Scientific Meeting. Oxford: International Society of Prosthetics and Orthotics; 2015.

14. Gao J, McGrath M, Laszczak P, Tang J, Jiang L, Bader D, et al. Assessment of alignment effects on stump/socket interface and socket reaction moment using a lower-limb prosthetic simulator. Abstract published in Prosthetics and orthotics international. 2015; 39:257.

15. Gao J, Laszczak P, McGrath M, Tang J, Jiang L, Bader D, et al. A case study quantifying stump/socket interface stresses of lower-limb amputees. ISPO UK Annual Scientific Meeting. Oxford: International Society of Prosthetics and Orthotics; 2015.

16. Hale N, Valero M, Tang J, McGrath M, Laszczak P, Gao J, et al. A preliminary study on characterisation of finger interface kinetics using a pressure and shear sensor system. Trent International Prosthetic Symposium. Glasgow: International Society of Prosthetics and Orthotics; 2016.

17. Hale N, Valero M, Tang J, Jiang L, Moser D. Measuring real-time pressure and shear at the fingertip-object interface. Event: ISPO 16th World Congress. Cape Town, ZA: International Society of Prosthetics and Orthotics; 2017.

18. Valero M, Hale N, Tang J and Jiang L. A Comprehensive Mechanotransduction Model for Tactile Feedback based on Multi-Axial Stresses at the Fingertip-Contact Interface. IEEE World Haptics 2017. Munich, Germany: IEEE, 2017.

Award

1. 2014 Limbless Association prize for presentation titled: Influence of stump/socket relative movement on gait analysis for above knee amputees – a case study in the ISPO UK annual scientific meeting

2. The Best Paper Prize in the category "Advancing Technology" in the 16th World Congress of ISPO (May 2017) was awarded to the paper tilted: Method to assess biomechanical coupling at trans-femoral residuum/socket interface. This biannual conference is the most prestige in prosthetic and orthotic field, with more than 2000 delegates and expertise from over 68 countries and every continent worldwide.

Media Presence

Nelson, E., 2015. The Perfect Prosthesis? Forces TV [Online] http://forces.tv/59505755

Bibliography

[1] Pritham CH. Biomechanics and shape of the above-knee socket considered in light of the ischial containment concept. Prosthet Orthot Int. 1990;14:9-21.

[2] Radcliffe CW. Biomechanics of above knee prostheses. In: Murdoch G, editor. Prosthetic and Orthotic Practice. London: Edward Arnold; 1970. p. 191-8.

[3] Radcliffe CW. The biomechanics of below-knee prostheses in normal, level, bipedal walking. Artif Limbs. 1962;6:16-24.

[4] Levy SW. Amputees: skin problems and prostheses. Cutis. 1995;55:297-301.

[5] Kent J, Franklyn-Miller A. Biomechanical models in the study of lower limb amputee kinematics: a review. Prosthet Orthot Int. 2011;35:124-39.

[6] British Standard Institution. BS EN ISO 10328 Prosthetics - Structural testing of lower-limb prostheses - Requirements and test methods. London: BSI; 2006.

[7] Eshraghi A, Osman NA, Gholizadeh H, Karimi M, Ali S. Pistoning assessment in lower limb prosthetic sockets. Prosthet Orthot Int. 2012;36:15-24.

[8] Convery P, Murray KD. Ultrasound study of the motion of the residual femur within a trans-femoral socket during gait. Prosthetics and orthotics international. 2000;24:226-32.

[9] Pearson JR, Holmgren G, March L, Oberg K. Pressures in critical regions of the below-knee patellar-tendon-bearing prosthesis. Bull Prosthet Res. 1973;10:52-76.

[10] Williams RB, Porter D, Roberts VC, Regan JF. Triaxial Force Transducer for Investigating Stresses at the Stump Socket Interface. Medical & biological engineering & computing. 1992;30:89-96.

[11] British Society of Rehabilitaion Medicine. Amputee and prosthetic rehabilitaion - standards and guidlines. A report of the working party of the British Socity of Rehabilitaion Medicine. London: British Society of Rehabilitation Medicine; 2003.

[12] Scott H, Patel R, Hebenton J. A survery of the lower limb amputee population in Scotland 2010. Glasgow2012.

[13] Barnes Robert. Amputation Principles. In: Barnes Robert, Cox B, editors. Amputations An Illustrated Manual Philadelphia: Hanley & Belfus, Inc.; 2000. p. 1-3.

[14] World Health Organization, US Department of Defense, MossRehab Hospital U. The rehabilitation of people with amputation. Geneva: World Health Organisation; 2004.

[15] Loon H. Below knee amputation surgery. Artificial Limbs. 1962;6:86-99.

[16] Robinson KP. Skew-flap below-knee amputation. Annals of the Royal College of Surgeons of England. 1991;73:155-7.

[17] Jain SK. Skew flap technique in trans-tibial amputation. Prosthet Orthot Int. 2005;29:283-90.

[18] Subbarao KV, Bajoria S. The effect of stump length on the rehabilitation outcome in unilateral below-knee amputees for vascular disease. Clinical rehabilitation. 1995;9:327-30.

[19] Lenka P, Tiberwala D. Effect of Stump Length on Postural Steadiness During Quiet Stance in Unilateral Trans-Tibial Amputee Al Ameen J Med Sci. 2010;3:50-7.

[20] Koyel M, Lenka P, Mondal R, Triberwala D. Relation of Stump Length with Various Gait Parameters in Trans-tibial Amputees 2008;7.

[21] Tantua AT, Geertzen JH, van den Dungen JJ, Breek JK, Dijkstra PU. Reduction of residual limb volume in people with transtibial amputation. J Rehabil Res Dev. 2014;51:1119-26.

[22] Highsmith MJ, Klenow TD, Kahle JT, Wernke MM, Carey SL, Miro RM, et al. Effects of the Genium Microprocessor Knee System on Knee Moment Symmetry during Hill Walking. Technol Innov. 2016;18:151-7.

[23] Perry J, Burnfield JM, Newsam CJ, Conley P. Energy expenditure and gait characteristics of a bilateral amputee walking with C-leg prostheses compared with stubby and conventional articulating prostheses. Archives of physical medicine and rehabilitation. 2004;85:1711-7.

[24] Burnfield JM, Eberly VJ, Gronely JK, Perry J, Yule WJ, Mulroy SJ. Impact of stance phase microprocessor-controlled knee prosthesis on ramp negotiation and community walking function in K2 level transfemoral amputees. Prosthet Orthot Int. 2012;36:95-104.

[25] Wolf EJ, Everding VQ, Linberg AL, Schnall BL, Czerniecki JM, Gambel JM. Assessment of transfemoral amputees using C-Leg and Power Knee for ascending and descending inclines and steps. J Rehabil Res Dev. 2012;49:831-42.

[26] Lura DJ, Wernke MM, Carey SL, Kahle JT, Miro RM, Highsmith MJ. Differences in knee flexion between the Genium and C-Leg microprocessor knees while walking on level ground and ramps. Clinical biomechanics. 2015;30:175-81.

[27] Bellmann M, Schmalz T, Ludwigs E, Blumentritt S. Immediate effects of a new microprocessor-controlled prosthetic knee joint: a comparative biomechanical evaluation. Archives of physical medicine and rehabilitation. 2012;93:541-9.

[28] Kaufman KR, Levine JA, Brey RH, Iverson BK, McCrady SK, Padgett DJ, et al. Gait and balance of transfemoral amputees using passive mechanical and microprocessor-controlled prosthetic knees. Gait & posture. 2007;26:489-93.

[29] Schmalz T, Blumentritt S, Marx B. Biomechanical analysis of stair ambulation in lower limb amputees. Gait & posture. 2007;25:267-78.

[30] Villa C, Drevelle X, Bonnet X, Lavaste F, Loiret I, Fode P, et al. Evolution of vaulting strategy during locomotion of individuals with transfemoral amputation on slopes and cross-slopes compared to level walking. Clinical biomechanics. 2015;30:623-8.

[31] Andrysek J. Lower-limb prosthetic technologies in the developing world: A review of literature from 1994-2010. Prosthet Orthot Int. 2010;34:378-98.

[32] Campbell WB, St Johnston JA, Kernick VF, Rutter EA. Lower limb amputation: striking the balance. Annals of the Royal College of Surgeons of England. 1994;76:205-9.

[33] De Asha AR, Munjal R, Kulkarni J, Buckley JG. Walking speed related joint kinetic alterations in trans-tibial amputees: impact of hydraulic 'ankle' damping. J Neuroeng Rehabil. 2013;10.

[34] De Asha AR, Munjal R, Kulkarni J, Buckley JG. Impact on the biomechanics of overground gait of using an 'Echelon' hydraulic ankle-foot device in unilateral trans-tibial and trans-femoral amputees. Clinical biomechanics. 2014;29:728-34.

[35] Johnson L, De Asha AR, Munjal R, Kulkarni J, Buckley JG. Toe clearance when walking in people with unilateral transtibial amputation: effects of passive hydraulic ankle. J Rehabil Res Dev. 2014;51:429-37.

[36] Struchkov V, Buckley JG. Biomechanics of ramp descent in unilateral trans-tibial amputees: Comparison of a microprocessor controlled foot with conventional ankle-foot mechanisms. Clinical biomechanics. 2016;32:164-70.

[37] Cikulin K. Musculoskeletal Interventions. Physical Therapy Clinical Handbook for PTAs. Burlington, MA: Jones & Bartlett Learning; 2017. p. 178.

[38] Murphy EF, Wilson AB, Jr. Anatomical and physiological considerations in below-knee prosthetics. Artif Limbs. 1962;6:4-15.

[39] Rosenkranz G. The patellar-tendon-bearing prosthesis. Artif Limbs. 1962;6:1-3.

[40] Kahle JT. Conventional and Hydrostatic Transtibial Interface Comparison. J Prosthet Orthot. 1999;11:85-91.

[41] Reswick J, Rogers J. Experience at Rancho Los Amigos Hospital with devices and techniques to prevent pressure sores. In: Kenedi R, Cowden J, Scales J, editors. Bed sore biomechanics. London: MacMillan Press; 1976. p. 301-10.

[42] Carroll K, Baird J, Binder K. Chapter 9: Transfemoral Prosthetic Designs. In: Carroll K, Edelstein J, editors. Prosthetics and Patient Management: A Comprehensive Clinical Approach. 1st ed. Thorofare, NJ: Slack Inc.; 2006.

[43] Radcliffe CW. Functional considerations in the fitting of above-knee prostheses. Artif Limbs. 1955;2:35-60.

[44] Radcliffe CW. The Knud Jansen Lecture: above-knee prosthetics. Prosthet Orthot Int. 1977;1:146-60.

[45] Long I. Normal shape-normal alignment (NSNA) above-knee prosthesis. Clinical Prosthetics & Orthotics. 1985;9:9-14.

[46] Sabolich J. Contoured adducted trochanteric-controlled alignment method (CAT-CAM): introduction and basic principles. Clinical Prosthetics & Orthotics. 1985;9:15-26.

[47] Alley RD, Williams TW, 3rd, Albuquerque MJ, Altobelli DE. Prosthetic sockets stabilized by alternating areas of tissue compression and release. J Rehabil Res Dev. 2011;48:679-96.

[48] Geil MD. Consistency and accuracy of measurement of lower-limb amputee anthropometrics. The Journal of Rehabilitation Research and Development. 2005;42:131.

[49] Silver-Thorn MB, Childress DS. Generic, geometric finite element analysis of the transtibial residual limb and prosthetic socket. J Rehabil Res Dev. 1997;34:171-86.

[50] Amali R, Noroozi S, Vinney J, Sewell P, Andrews S. Predicting interfacial loads between the prosthetic socket and the residual limb for below-knee amputees - A case study. Strain. 2006;42:3-10.

[51] Winter D. Biomechanics and motor control of human movement. 4th ed. New Jersey: John Wiley & Sons Inc.; 2009.

[52] Lehmann JF, Price R, Okumura R, Questad K, de Lateur BJ, Negretot A. Mass and mass distribution of below-knee prostheses: effect on gait efficacy and self-selected walking speed. Archives of physical medicine and rehabilitation. 1998;79:162-8.

[53] Breakey J. Criteria For Use Of Supracondylar And Supracondylar-Suprapatellar Suspension For Below-Knee Prostheses. Orthotics Prosthet. 1973;27:14-8.

[54] Rubin G, Nitschke R, Gardner H. The supracondylar-suprapatellar PTB prosthesis. Bulletin of Prosthetics Research. 1970;10:102-6.

[55] Gholizadeh H, Abu Osman NA, Eshraghi A, Ali S. The effects of suction and pin/lock suspension systems on transtibial amputees' gait performance. PLoS One. 2014;9:e94520.

[56] Gerschutz M, Denune J, Colvin J, Schober G. Elevated Vacuum Suspension Influence on Lower Limb Amputee's Residual Limb Volume at Different Vacuum Pressure Settings. J Prosthet Orthot. 2010;22:252-6.

[57] Gerschutz M, Hayne M, Colvin J, Denune J. Dynamic effectiveness evaluation of elevated vacuum suspension. J Prosthet Orthot. 2015;27:161-5.

[58] Dickinson AS, Steer JW, Worsley PR. Finite element analysis of the amputated lower limb: A systematic review and recommendations. Medical engineering & physics. 2017;43:1-18.

[59] Sengeh D, Herr J. A variable impedance prosthetic socket for a transtibial amputee designed from mri data. J Prosthet Orthot. 2013;25:129-37.

[60] Sengeh DM, Moerman KM, Petron A, Herr H. Multi-material 3-D viscoelastic model of a transtibial residuum from in-vivo indentation and MRI data. J Mech Behav Biomed Mater. 2016;59:379-92.

[61] Zheng Y, Mak AF. Effective elastic properties for lower limb soft tissues from manual indentation experiment. IEEE Trans Rehabil Eng. 1999;7:257-67.

[62] Buis A, Dumbleton T, Murray K, McHugh B, McKay G, Sexton S. Measuring the daily stepping activity of people with transtibial amputation using the ActivPAL activity monitor. Journal of Prosthetics and Orthotics. 2014;26:43-7.

[63] Zachariah SG, Saxena R, Fergason JR, Sanders JE. Shape and volume change in the transtibial residuum over the short term: preliminary investigation of six subjects. J Rehabil Res Dev. 2004;41:683-94.

[64] Fernie G, Holliday P, Logg R. Health and Welfare Canada Final Report on Project #606-1317-41. Toronto Ontario: West Park Research, West Park Hospital; 1980.

[65] Lilja M, Johansson S, Oberg T. Relaxed versus activated stump muscles during casting for trans-tibial prostheses. Prosthet Orthot Int. 1999;23:13-20.

[66] Fernie GR, Holliday PJ. Volume fluctuations in the residual limbs of lower limb amputees. Archives of physical medicine and rehabilitation. 1982;63:162-5.

[67] Boonhong J. Correlation between volumes and circumferences of residual limb in below knee amputees. Journal of the Medical Association of Thailand. 2006;59:S1-4.

[68] Board WJ, Street GM, Caspers C. A comparison of trans-tibial amputee suction and vacuum socket conditions. Prosthet Orthot Int. 2001;25:202-9.

[69] Boone DA, Kobayashi T, Chou TG, Arabian AK, Coleman KL, Orendurff MS, et al. Influence of malalignment on socket reaction moments during gait in amputees with transtibial prostheses. Gait & posture. 2013;37:620-6.

[70] Kobayashi T, Orendurff MS, Boone DA. Effect of alignment changes on socket reaction moments during gait in transfemoral and knee-disarticulation prostheses: case series. J Biomech. 2013;46:2539-45.

[71] Kobayashi T, Orendurff MS, Zhang M, Boone DA. Effect of alignment changes on sagittal and coronal socket reaction moment interactions in transtibial prostheses. J Biomech. 2013;46:1343-50.

[72] Aulie AL, Burgess EM. Prosthetic alignment device supplementally secured by a hoop stress. Google Patents; 1992.

[73] Zahedi MS, Spence WD, Solomonidis SE, Paul JP. Alignment of lower-limb prostheses. J Rehabil Res Dev. 1986;23:2-19.

[74] Sanders JE, Daly CH. Interface pressures and shear stresses: sagittal plane angular alignment effects in three trans-tibial amputee case studies. Prosthet Orthot Int. 1999;23:21-9.

[75] Appoldt F, Bennett L, Contini R. Stump-socket pressure in lower extremity prostheses. J Biomech. 1968;1:247-57.

[76] Seelen HAM, Anemaat S, Janssen HMH, Deckers JHM. Effects of prosthesis alignment on pressure distribution at the stump/socket interface in transtibial amputees during unsupported stance and gait. Clinical rehabilitation. 2003;17:787-96.

[77] Levy SW. Skin problems of the leg amputee. Prosthet Orthot Int. 1980;4:37-44.

[78] Gholizadeh H, Abu Osman NA, Luviksdottir A, Eshraghi A, Kamyab M, Wan Abas WA. A new approach for the pistoning measurement in transtibial prosthesis. Prosthet Orthot Int. 2011;35:360-4.

[79] Street G. Vacuum suspension and its effects on the limb. Orthopadie Technik. 2006;4:1 - 7.

[80] Portnoy S, Siev-Ner I, Shabshin N, Gefen A. Effects of sitting postures on risks for deep tissue injury in the residuum of a transtibial prosthetic-user: a biomechanical case study. Computer methods in biomechanics and biomedical engineering. 2011;14:1009-19.

[81] Portnoy S, Vuillerme N, Payan Y, Gefen A. Clinically oriented real-time monitoring of the individual's risk for deep tissue injury. Medical & biological engineering & computing. 2011;49:473-83.

[82] Portnoy S, van Haare J, Geers RP, Kristal A, Siev-Ner I, Seelen HA, et al. Real-time subject-specific analyses of dynamic internal tissue loads in the residual limb of transtibial amputees. Medical engineering & physics. 2010;32:312-23.

[83] Söderberg B, Ryd L, Persson B. Roentgen stereophotogrammetric analysis of motion between the bone and the socket in transtibial amputation prosthesis: A case study. J Prosthet Orthot. 2003;15:95-9.

[84] Grevsten S, Eriksson U. Stump-socket contact and skeletal displacement in a suction patellar-tendon bearing prosthesis. The Journal of bone and joint surgery American volume. 1974;56:1692-6.

[85] Newton RL, Morgan D, Schreiber MH. Radiological evaluation of prosthetic fit in below-the-knee amputees. Skeletal radiology. 1988;17:276-80.

[86] Noll V, Eschner N, Schumacher C, Beckerle P, Rinderknecht S. A physically-motivated model describing the dynamic interactions between residual limb and socket in lower limb prostheses. Current Directions in Biomedical Engineering. 2017;3:15-8.

[87] Czerniecki JM, Morgenroth DC. Metabolic energy expenditure of ambulation in lower extremity amputees: what have we learned and what are the next steps? Disability and rehabilitation. 2015:1-9.

[88] Kristinsson O. The ICEROSS concept: a discussion of a philosophy. Prosthet Orthot Int. 1993;17:49-55.

[89] Fillauer CE, Pritham CH, Fillauer KD. Evolution and Development of the Silicone Suction Socket (3s) for Below-Knee Prostheses. J Prosthet Orthot. 1989;1:92-103.

[90] Legro MW, Reiber G, del Aguila M, Ajax MJ, Boone DA, Larsen JA, et al. Issues of importance reported by persons with lower limb amputations and prostheses. J Rehabil Res Dev. 1999;36:155-63.

[91] Husain T. An experimental study of some pressure effects on tissues with reference to the bed - sore problem. The Journal of Pathology and Bacteriology. 1953;66:347-58.

[92] Kosiak M. Etiology and pathology of ischemic uclers. Archives of physical medicine and rehabilitation. 1959;39:62-9.

[93] Salawu A, Middleton C, Gilbertson A, Kodavali K, Neumann V. Stump ulcers and continued prosthetic limb use. Prosthet Orthot Int. 2006;30:279-85.

[94] Linder-Ganz E, Engelberg S, Scheinowitz M, Gefen A. Pressure-time cell death threshold for albino rat skeletal muscles as related to pressure sore biomechanics. Journal of biomechanics. 2006;39:2725-32.

[95] Linder-Ganz E, Shabshin N, Itzchak Y, Yizhar Z, Siev-Ner I, Gefen A. Strains and stresses in sub-dermal tissues of the buttocks are greater in paraplegics than in healthy during sitting. Journal of biomechanics. 2008;41:567-80.

[96] Naylor PF. Experimental friction blisters. The British journal of dermatology. 1955;67:327-42.

[97] Sulzberger MB, Cortese TA, Fishman L, Wiley HS. Studies on blisters produced by friction. I. Results of linear rubbing and twisting technics. The Journal of investigative dermatology. 1966;47:456-65 contd.

[98] Cortese TA, Jr., Griffin TB, Layton LL, Hutsell TC. Experimental friction blisters in Macaque monkeys. The Journal of investigative dermatology. 1969;53:172-7.

[99] Winter DA. Kinematic and Kinetic Patterns in Human Gait - Variability and Compensating Effects. Hum Movement Sci. 1984;3:51-76.

[100] Burnfield JM, Powers CM. Prediction of slips: an evaluation of utilized coefficient of friction and available slip resistance. Ergonomics. 2006;49:982-95.

[101] Segal AD, Orendurff MS, Mute GK, McDowell ML, Pecoraro JA, Shofer J, et al. Kinematic and kinetic comparisons of transfemoral amputee gait using C-Leg (R) and Mauch SNS (R) prosthetic knees. J Rehabil Res Dev. 2006;43:857-69.

[102] Bateni H, Sandra O. Kinematic and Kinetic Variations of Below-Knee Amputee Gait. Journal of Prosthetics & Orthotics. 2002;14:2-10.

[103] Burke MJ, Roman V, Wright V. Bone and joint changes in lower limb amputees. Ann Rheum Dis. 1978;37:252-4.

[104] Hungerford D, Cockin J. Fate of the retained lower limb joints in Second World War amputees. British Orthopaedic Association Autumn Meeting1974.

[105] Kovac I, Medved V, Ostojic L. Spatial, temporal and kinematic characteristics of traumatic transtibial amputees' gait. Coll Antropol. 2010;34 Suppl 1:205-13.

[106] Powers CM, Rao S, Perry J. Knee kinetics in trans-tibial amputee gait. Gait & posture. 1998;8:1-7.

[107] Jarvis HL, Bennett AN, Twiste M, Phillip RD, Etherington J, Baker R. Temporal Spatial and Metabolic Measures of Walking in Highly Functional Individuals With Lower Limb Amputations. Archives of physical medicine and rehabilitation. 2017;98:1389-99.

[108] Bateni H, Olney S. Kinematic and Kinetic Variations of Below-Knee Amputee Gait. Journal of Prosthetics & Orthotics. 2002;14:2-10.

[109] Uchytil J, Jandacka D, Zahradnik D, Farana R, Janura M. Temporal-spatial parameters of gait in transfemoral amputees: Comparison of bionic and mechanically passive knee joints. Prosthet Orthot Int. 2014;38:199-203.

[110] Beyaert C, Grumillier C, Martinet N, Paysant J, Andre JM. Compensatory mechanism involving the knee joint of the intact limb during gait in unilateral below-knee amputees. Gait & posture. 2008;28:278-84.

[111] Kovac I, Medved V, Ostojic L. Ground reaction force analysis in traumatic transtibial amputees' gait. Coll Antropol. 2009;33 Suppl 2:107-14.

[112] Nissan M. The initiation of gait in lower limb amputees: some related data. J Rehabil Res Dev. 1991;28:1-12.

[113] Isakov E, Keren O, Benjuya N. Trans-tibial amputee gait: time-distance parameters and EMG activity. Prosthet Orthot Int. 2000;24:216-20.

[114] Castro MP, Soares D, Mendes E, Machado L. Plantar pressures and ground reaction forces during walking of individuals with unilateral transfemoral amputation. PM R. 2014;6:698-707 e1.

[115] Nolan L, Wit A, Dudzinski K, Lees A, Lake M, Wychowanski M. Adjustments in gait symmetry with walking speed in trans-femoral and trans-tibial amputees. Gait & posture. 2003;17:142-51.

[116] Postema K, Hermens HJ, de Vries J, Koopman HF, Eisma WH. Energy storage and release of prosthetic feet. Part 1: Biomechanical analysis related to user benefits. Prosthet Orthot Int. 1997;21:17-27.

[117] Powers CM, L T, J P, E. A. Influence of prosthetic foot design on sound limb loading in adults with unilateral below-knee amputations. Archives of physical medicine and rehabilitation. 1994;75:825-9.

[118] Isakov E, Burger H, Krajnik J, Gregoric M, Marincek C. Influence of speed on gait parameters and on symmetry in transtibial amputees. Prosthet Orthot Int. 1996;20:153-8.

[119] Sadeghi H, Allard P, Duhaime M. Muscle power compensatory mechanisms in below-knee amputee gait. Am J Phys Med Rehabil. 2010;80:25-32.

[120] McNealy LL, Gard SA. Effect of prosthetic ankle units on the gait of persons with bilateral trans-femoral amputations. Prosthet Orthot Int. 2008;32:111-26.

[121] Goujon-Pillet H, Sapin E, Fode P, Lavaste F. Three-dimensional motions of trunk and pelvis during transfemoral amputee gait. Archives of physical medicine and rehabilitation. 2008;89:87-94.

[122] Rabuffetti M, Recalcati M, Ferrarin M. Trans-femoral amputee gait: socket-pelvis constraints and compensation strategies. Prosthet Orthot Int. 2005;29:183-92.

[123] Seroussi RE, Gitter A, Czerniecki JM, Weaver K. Mechanical work adaptations of above-knee amputee ambulation. Archives of physical medicine and rehabilitation. 1996;77:1209-14.

[124] Kadaba MP, Ramakrishnan HK, Wootten ME. Measurement of lower extremity kinematics during level walking. Journal of orthopaedic research : official publication of the Orthopaedic Research Society. 1990;8:383-92.

[125] Marika K, Issam F, David E, Salim G. What are the gains and losses when using a non-six degree of freedom skin marker set for clinical gait analysis? Gait & posture. 2006;24:S121-S2.

[126] de Leva P. Adjustments to Zatsiorsky-Seluyanov's segment inertia parameters. J Biomech. 1996;29:1223-30.

[127] Cappozzo A, Catani F, Croce UD, Leardini A. Position and orientation in space of bones during movement: anatomical frame definition and determination. Clinical biomechanics. 1995;10:171-8.

[128] Jia X, Zhang M, Lee WC. Load transfer mechanics between trans-tibial prosthetic socket and residual limb--dynamic effects. J Biomech. 2004;37:1371-7.

[129] Jia X, Zhang M, Li X, Lee WC. A quasi-dynamic nonlinear finite element model to investigate prosthetic interface stresses during walking for trans-tibial amputees. Clinical biomechanics. 2005;20:630-5.

[130] Prince F, Winter D, Sjonnesen G, Wheeldon R. New technique for the calculation of the energy stored, dissipated, and recovered in different ankle-foot prostheses. IEEE Transaction on Rehabilitation Engineering. 1994;2:247.

[131] Geil MD, Parnianpour M, Quesada P, Berme N, Simon S. Comparison of methods for the calculation of energy storage and return in a dynamic elastic response prosthesis. J Biomech. 2000;33:1745-50.

[132] Dillon MP, Barker TM. Comparison of gait of persons with partial foot amputation wearing prosthesis to matched control group: observational study. J Rehabil Res Dev. 2008;45:1317-34.

[133] Dillon MP, Barker TM, Pettet G. Effect of inaccuracies in anthropometric data and linked-segment inverse dynamic modeling on kinetics of gait in persons with partial foot amputation. J Rehabil Res Dev. 2008;45:1303-16.

[134] Sjodahl C, Jarnlo G, Soderberg B, Persson B. Kinematic and kinetic gait analysis in the sagittal plane of trans-femoral amputees before and after special gait re-education. Prosthet Orthot Int. 2002;26:101-12.

[135] Sanders JE, Miller RA, Berglund DN, Zachariah SG. A modular six-directional force sensor for prosthetic assessment: a technical note. J Rehabil Res Dev. 1997;34:195-202.

[136] Berme N. A Shorter Pylon Transducer for Measurement of Prosthetic Forces and Moments during Amputee Gait. Engineering in Medicine. 1975.

[137] Dumas R, Cheze L, Frossard L. Loading applied on prosthetic knee of transfemoral amputee: comparison of inverse dynamics and direct measurements. Gait & posture. 2009;30:560-2.

[138] Fiedler G, Slavens B, Smith RO, Briggs D, Hafner BJ. Criterion and construct validity of prosthesis-integrated measurement of joint moment data in persons with transtibial amputation. J Appl Biomech. 2014;30:431-8.

[139] Frossard L, Beck J, Dillon M, Evans JH. Development and preliminary testing of a device for the direct measurement of forces and moments in the prosthetic limb of transfemoral amputees during activities of daily living. J Prosthet Orthot. 2003;15:135-42.

[140] Koehler SR, Dhaher YY, Hansen AH. Cross-validation of a portable, six-degree-of-freedom load cell for use in lower-limb prosthetics research. J Biomech. 2014;47:1542-7.

[141] Neumann ES, Brink J, Yalamanchili K, Lee JS. Use of a load cell and force-moment curves to compare transverse plane moment loads on transtibial residual limbs: A preliminary investigation. Prosthet Orthot Int. 2014;38:253-62.

[142] Schwarze M, Hurschler C, Seehaus F, Oehler S, Welke B. Loads on the prosthesis-socket interface of above-knee amputees during normal gait: validation of a multi-body simulation. J Biomech. 2013;46:1201-6.

[143] Kobayashi T, Orendurff MS, Arabian AK, Rosenbaum-Chou TG, Boone DA. Effect of prosthetic alignment changes on socket reaction moment impulse during walking in transtibial amputees. J Biomech. 2014;47:1315-23.

[144] Fey NP, Klute GK, Neptune RR. The influence of energy storage and return foot stiffness on walking mechanics and muscle activity in below-knee amputees. Clinical biomechanics. 2011;26:1025-32.

[145] Vrieling AH, van Keeken HG, Schoppen T, Otten E, Halbertsma JP, Hof AL, et al. Uphill and downhill walking in unilateral lower limb amputees. Gait & posture. 2008;28:235-42.

[146] Fradet L, Alimusaj M, Braatz F, Wolf SI. Biomechanical analysis of ramp ambulation of transtibial amputees with an adaptive ankle foot system. Gait & posture. 2010;32:191-8.

[147] Nickel E, Sensinger J, Hansen A. Passive prosthetic ankle-foot mechanism for automatic adaptation to sloped surfaces. J Rehabil Res Dev. 2014;51:803-14.

[148] De Asha AR, Johnson L, Munjal R, Kulkarni J, Buckley JG. Attenuation of centre-of-pressure trajectory fluctuations under the prosthetic foot when using an articulating hydraulic ankle attachment compared to fixed attachment. Clinical biomechanics. 2013;28:218-24.

[149] Kobayashi T, Orendurff MS, Zhang M, Boone DA. Individual responses to alignment perturbations in socket reaction moments while walking in transtibial prostheses. Clinical biomechanics. 2014;29:590-4.

[150] Boutwell E, Stine R, Hansen A, Tucker K, Gard S. Effect of prosthetic gel liner thickness on gait biomechanics and pressure distribution within the transtibial socket. The Journal of Rehabilitation Research and Development. 2012;49:227.

[151] Astrom I, Stenstrom A. Effect on gait and socket comfort in unilateral trans-tibial amputees after exchange to a polyurethane concept. Prosthet Orthot Int. 2004;28:28-36.

[152] Commean PK, Brunsden BS, Smith KE, Vannier MW. Below-knee residual limb shape change measurement and visualization. Archives of physical medicine and rehabilitation. 1998;79:772-82.

[153] Commean PK, Smith KE, Vannier MW. Lower extremity residual limb slippage within the prosthesis. Archives of physical medicine and rehabilitation. 1997;78:476-85.

[154] Erikson U, James U. Roentgenological study of certain stump-socket relationships in above-knee amputees with special regard to tissue proportions, socket fit and attachment stability. Upsala J Med Sci. 1973;78:203-14.

[155] Grevsten S, Erikson U. A roentgenological study of the stump-socket contact and skeletal displacement in the ptb-suction prosthesis. psala Journal of Medical Sciences. 1975;80:49-57.

[156] Lilja M, Johansson T, Oberg T. Movement of the tibial end in a PTB prosthesis socket: a sagittal X-ray study of the PTB prosthesis. Prosthet Orthot Int. 1993;17:21-6.

[157] Seeber J, Magilner A, Reyes T. Radiological technique to evaluate patellar-tendon-bearing prosthesis. Archives of physical medicine and rehabilitation. 1972;53:65-9.

[158] Tanner JE, Berke GM. Radiographic comparison of vertical tibial translation using two types of suspensions on a transtibial prosthesis: A case study. J Prosthet Orthot. 2001;13:14-6.

[159] Vannier MW, Commean PK, Brunsden BS, Smith KE. Visualization of prosthesis fit in lower-limb amputees. Ieee Comput Graph. 1997;17:16-29.

[160] Selvik G. Roentgen stereophotogrammetry. A method for the study of the kinematics of the skeletal system. Acta Orthop Scand Suppl. 1989;232:1-51.

[161] Papaioannou G, Mitrogiannis C, Nianios G, Fiedler G. A new method for assessing residual limb skin-tissue strain during above-knee amputee high speed movement. 55th Annual Meeting of the Orthopaedic Research Society. Las Vegas, NV, USA: Orthopaedic Research Society; 2009.

[162] Papaioannou G, Mitrogiannis C, Nianios G, Fiedler G. Assessing residual bone-stump-skin-socket interface kinematics of above knee amputees with high accuracy biplane dynamic roentgen stereogrammetric analysis. 55th annual Meeting of Orthopaedic Research Society. Las Vegas, USA: Orthopaedic Research Society; 2009.

[163] Papaioannou G, Mitrogiannis C, Nianios G, Fiedler G. Assessment of Vacuum-assisted trans-tibial amputee socket dynamics. 9th International Conference on Information Technology and Applications in Biomedicine. Larnaca, Cyprus: IEEE Engineering in Medicine and Biology Society; 2009.

[164] Papaioannou G, Mitrogiannis C, Nianios G, Fiedler G. Assessment of amputee socket-stump-residual bone kinematics during strenuous activities using Dynamic Roentgen Stereogrammetric Analysis. Journal of biomechanics. 2010;43:871-8.

[165] Papaioannou G, Mitrogiannis C, Nianios G, Fiedler G, Wood J. Effects of assisted vacuum TT socket design on the relative motion at the stump/socket interface. 56th Annual Meeting of the Orthopaedic Research Society. New Orleans, LA, USA: Orthopaedic Research Society; 2010.

[166] Convery P, Murray KD. Ultrasound study of the motion of the residual femur within a trans‐femoral socket during daily living activities other than gait. Prosthetics and orthotics international. 2001;25:220-7.

[167] Murray KD, Convery P. The calibration of ultrasound transducers used to monitor motion of the residual femur within a trans‐femoral socket during gait. Prosthetics and orthotics international. 2000;24:55-62.

[168] Gholizadeh H, Osman NA, Kamyab M, Eshraghi A, Abas WA, Azam MN. Transtibial prosthetic socket pistoning: static evaluation of Seal-In((R)) X5 and Dermo((R)) Liner using motion analysis system. Clinical biomechanics. 2012;27:34-9.

[169] Childers WL, Siebert S. Marker-based method to measure movement between the residual limb and a transtibial prosthetic socket. Prosthet Orthot Int. 2016;40:720-8.

[170] Sanders JE, Karchin A, Fergason JR, Sorenson EA. A noncontact sensor for measurement of distal residual-limb position during walking. J Rehabil Res Dev. 2006;43:509-16.

[171] Childers WL, Perell-Gerson K, Gregor RJ. Measurement of motion between the residual limb and the prosthetic socket during cycling. J Prosthet Orthot. 2012;24:19-24.

[172] Muro-de-la-Herran A, Garcia-Zapirain B, Mendez-Zorrilla A. Gait analysis methods: an overview of wearable and non-wearable systems, highlighting clinical applications. Sensors (Basel). 2014;14:3362-94.

[173] Tao W, Liu T, Zheng R, Feng H. Gait analysis using wearable sensors. Sensors (Basel). 2012;12:2255-83.

[174] Bocobo CR, Castellote JM, MacKinnon D, Gabrielle-Bergman A. Videofluoroscopic evaluation of prosthetic fit and residual limbs following transtibial amputation. J Rehabil Res Dev. 1998;35:6-13.

[175] Burgess EM, Moore AJ. A study of interface pressures in the below-knee prosthesis (physiological suspension: an interim report). Bull Prosthet Res. 1977;14:58-70.

[176] Appoldt A, Bennett L. A preliminary report on dynamic socket pressures. Bull Prosthet Res. 1967;10:20-55.

[177] Rae J, Cockrell J. Interface pressure and stress distribution in prosthetic fitting. Bull Prosthet Res. 1971;8:64-111.

[178] Pearson JR, Grevsten S, Almby B, Marsh L. Pressure variation in the below-knee, patellar tendon bearing suction socket prosthesis. J Biomech. 1974;7:487-96.

[179] Appoldt F, Bennett L, Contini R. Socket pressure as a function of pressure transducer protrusion. Bull Prosthet Res. 1969;10-11:236-49.

[180] Patterson RP, Fisher SV. The accuracy of electrical transducers for the measurement of pressure applied to the skin. IEEE transactions on bio-medical engineering. 1979;26:450-6.

[181] Tekscan Inc. Medical Sensor 9811E. Boston2016.

[182] Polliack AA, Sieh RC, Craig DD, Landsberger S, McNeil DR, Ayyappa E. Scientific validation of two commercial pressure sensor systems for prosthetic socket fit. Prosthet Orthot Int. 2000;24:63-73.

[183] TekScan I. Flexifore sensor user manual. Boston: RTekScan, Inc.,; 2010.

[184] Sundara-Rajan K, Bestick A, Rowe G, Klute G, Ledoux W, Mamishev A. Capacitive Sensing of Interfacial Stresses. Sensors. Kona2010. p. 2569 - 72.

[185] Sundara-Rajan K, Bestick A, Rowe GI, Klute GK, Ledoux WR, Wang HC, et al. An interfacial stress sensor for biomechanical applications. Measurement Science and Technology. 2012;23:085701.

[186] Sundara-Rajan K, Rowe G, Bestick A, Mamishev A, Klute G, Ledoux W. Capacitive Sensing of Interfacial Forces in Prosthesis. 2010 IEEE International Workshop on Medical Measurements and Applications. Ottawa: IEEE; 2010. p. 73 - 6.

[187] Sundara-Rajan K, Rowe GI, Simon AJ, Klute GK, Ledoux WR, Mamishev AV. Shear Sensor for Lower Limb Prosthetic Applications. 2009 First Annual Ornl Biomedical Science & Engineering Conference: Exploring the Intersections of Interdisciplinary Biomedical Research2009. p. 61-4.

[188] Laszczak P, McGrath M, Tang J, Gao J, Jiang L, Bader DL, et al. A pressure and shear sensor system for stress measurement at lower limb residuum/socket interface. Medical engineering & physics. 2016;38:695-700.

[189] Sanders JE, Daly C. Measurement of stresses in three orthogonal directions at the residual limb-prosthetic socket interface. IEEE Trans Rehabil Eng. 1993;1:79-85.

[190] Sanders JE, Zachariah SG, Jacobsen AK, Fergason JR. Changes in interface pressures and shear stresses over time on trans-tibial amputee subjects ambulating with prosthetic limbs: comparison of diurnal and six-month differences. J Biomech. 2005;38:1566-73.

[191] van Pijkeren T, Naeff M, Kwee HH. A new method for the measurement of normal pressure between amputation residual limb and socket. Bull Prosthet Res. 1980;17:31-4.

[192] Hughes J. Biomechanics of the through-knee prosthesis. Prosthet Orthot Int. 1983;7:96-9.

[193] Appoldt FA, Bennett L, Contini R. Tangential pressure measurements in above-knee suction sockets. Bull Prosthet Res. 1970;10:70-86.

[194] Lee VSP, Solomonidis SE, Spence WD. Stump-socket interface pressure as an aid to socket design in prostheses for trans-femoral amputees - A preliminary study. P I Mech Eng H. 1997;211:167-80.

[195] Lacroix D, Patino JF. Finite element analysis of donning procedure of a prosthetic transfemoral socket. Ann Biomed Eng. 2011;39:2972-83.

[196] Zhang L, Zhu M, Shen L, Zheng F. Finite element analysis of the contact interface between trans-femoral stump and prosthetic socket. 2013 35th Annual International Conference of the IEEE Engineering in Medicine and Biology Society (EMBC)2013. p. 1270-3.

[197] Sanders JE, Daly CH, Burgess EM. Clinical measurement of normal and shear stresses on a trans-tibial stump: characteristics of wave-form shapes during walking. Prosthet Orthot Int. 1993;17:38-48.

[198] Sanders JE, Zachariah SG, Baker AB, Greve JM, Clinton C. Effects of changes in cadence, prosthetic componentry, and time on interface pressures and shear stresses of three trans-tibial amputees. Clinical biomechanics. 2000;15:684-94.

[199] Katz K, Susak Z, Seliktar R, Najenson T. End-bearing characteristics of patellar-tendon-bearing prosthesis--a preliminary report. Bull Prosthet Res. 1979;16:55-68.

[200] Winarski DJ, Pearson JR. Least-Squares Matrix Correlations between Stump Stresses and Prosthesis Loads for Below-Knee Amputees. J Biomech Eng-T Asme. 1987;109:238-46.

[201] Engsberg J, Julie M, Springer J, Harder J. Quantifying Interface Pressures in Below-Knee-Amputee Sockets. Journal of the Association of Children's Prosthetic-Orthotic Clinics. 1992;27:81.

[202] Sanders JE, Daly CH, Burgess EM. Interface shear stresses during ambulation with a below-knee prosthetic limb. J Rehabil Res Dev. 1992;29:1-8.

[203] Sanders JE, Lam D, Dralle AJ, Okumura R. Interface pressures and shear stresses at thirteen socket sites on two persons with transtibial amputation. J Rehabil Res Dev. 1997;34:19-43.

[204] Zhang M, Turner-Smith AR, Tanner A, Roberts VC. Clinical investigation of the pressure and shear stress on the trans-tibial stump with a prosthesis. Medical engineering & physics. 1998;20:188-98.

[205] Convery P, Buis AW. Socket/stump interface dynamic pressure distributions recorded during the prosthetic stance phase of gait of a trans-tibial amputee wearing a hydrocast socket. Prosthet Orthot Int. 1999;23:107-12.

[206] Sanders JE, Bell DM, Okumura RM, Dralle AJ. Effects of alignment changes on stance phase pressures and shear stresses on transtibial amputees: measurements from 13 transducer sites. IEEE Trans Rehabil Eng. 1998;6:21-31.

[207] Beil TL, Street GM, Covey SJ. Interface pressures during ambulation using suction and vacuum-assisted prosthetic sockets. J Rehabil Res Dev. 2002;39:693-700.

[208] Sanders JE, Fergason JR, Zachariah SG, Jacobsen AK. Interface pressure and shear stress changes with amputee weight loss: case studies from two trans-tibial amputee subjects. Prosthet Orthot Int. 2002;26:243-50.

[209] Chou Y-L, Shi S-S, Huang G-F, Lin T-S. Interface pressure and gait analysis in different walking speeds on the below-knee amputees with multiple axis prosthetic foot prothesis. Biomed Eng Appl Basis Comm. 2003;15.

[210] Goh JC, Lee PV, Chong SY. Static and dynamic pressure profiles of a patellar-tendon-bearing (PTB) socket. Proc Inst Mech Eng H. 2003;217:121-6.

[211] Goh JC, Lee PV, Chong SY. Stump/socket pressure profiles of the pressure cast prosthetic socket. Clinical biomechanics. 2003;18:237-43.

[212] Beil TL, Street GM. Comparison of interface pressures with pin and suction suspension systems. J Rehabil Res Dev. 2004;41:821-8.

[213] Dou P, Jia X, Suo S, Wang R, Zhang M. Pressure distribution at the stump/socket interface in transtibial amputees during walking on stairs, slope and non-flat road. Clinical biomechanics. 2006;21:1067-73.

[214] Dumbleton T, Buis AW, McFadyen A, McHugh BF, McKay G, Murray KD, et al. Dynamic interface pressure distributions of two transtibial prosthetic socket concepts. J Rehabil Res Dev. 2009;46:405-15.

[215] Wolf SI, Alimusaj M, Fradet L, Siegel J, Braatz F. Pressure characteristics at the stump/socket interface in transtibial amputees using an adaptive prosthetic foot. Clinical biomechanics. 2009;24:860-5.

[216] Ali S, Osman NA, Mortaza N, Eshraghi A, Gholizadeh H, Wan Abas WA. Clinical investigation of the interface pressure in the trans-tibial socket with Dermo and Seal-In X5 liner during walking and their effect on patient satisfaction. Clinical biomechanics. 2012;27:943-8.

[217] Sewell P, Noroozi S, Vinney J, Amali R, Andrews S. Static and dynamic pressure prediction for prosthetic socket fitting assessment utilising an inverse problem approach. Artificial intelligence in medicine. 2012;54:29-41.

[218] Ali S, Abu Osman NA, Eshraghi A, Gholizadeh H, Abd Razak NA, Wan Abas WA. Interface pressure in transtibial socket during ascent and descent on stairs and its effect on patient satisfaction. Clinical biomechanics. 2013;28:994-9.

[219] Yeung LF, Leung AK, Zhang M, Lee WC. Effects of long-distance walking on socket-limb interface pressure, tactile sensitivity and subjective perceptions of trans-tibial amputees. Disability and rehabilitation. 2013;35:888-93.

[220] Shirazi S, Fatouraee N, Safaeepour Z. The need for stump-socket interface pressure measurment during bidirectionally perturbed stance in transtibial amputees: A case study. 2014 21th Iranian Conference on Biomedical Engineering (ICBME). Tehran: IEEE; 2014. p. 220-3.

[221] Eshraghi A, Abu Osman NA, Gholizadeh H, Ali S, Abas WA. Interface stress in socket/residual limb with transtibial prosthetic suspension systems during locomotion on slopes and stairs. Am J Phys Med Rehabil. 2015;94:1-10.

[222] Safari MR, Tafti N, Aminian G. Socket Interface Pressure and Amputee Reported Outcomes for Comfortable and Uncomfortable Conditions of Patellar Tendon Bearing Socket: A Pilot Study. Assist Technol. 2015;27:24-31; quiz 2-3.

[223] Gholizadeh H, Abu Osman NA, Eshraghi A, Arifin N, Chung TY. A comparison of pressure distributions between two types of sockets in a bulbous stump. Prosthet Orthot Int. 2016;40:509-16.

[224] Wu G, Siegler S, Allard P, Kirtley C, Leardini A, Rosenbaum D, et al. ISB recommendation on definitions of joint coordinate system of various joints for the reporting of human joint motion--part I: ankle, hip, and spine. International Society of Biomechanics. J Biomech. 2002;35:543-8.

[225] Bell AL, Brand RA, Pedersen DR. Prediction of Hip-Joint Center Location from External Landmarks. Hum Movement Sci. 1989;8:3-16.

[226] Bell AL, Pedersen DR, Brand RA. A Comparison of the Accuracy of Several Hip Center Location Prediction Methods. J Biomech. 1990;23:617-21.

[227] Leardini A, Cappozzo A, Catani F, Toksvig-Larsen S, Petitto A, Sforza V, et al. Validation of a functional method for the estimation of hip joint centre location. J Biomech. 1999;32:99-103.

[228] Laszczak P, Jiang L, Bader DL, Moser D, Zahedi S. Development and validation of a 3D-printed interfacial stress sensor for prosthetic applications. Medical engineering & physics. 2015;37:132-7.

[229] Illinois Tool Works Inc. ElectroPuls. 2017.

[230] Laszczak P. Interfacial pressure and shear sensor system for lower limb proshteitc applications. Southampton, UK: Universtiy of Southampton; 2016.

[231] Julian V. Basic Elasticity and Viscoelasticity. Structural Biomaterial. Princeton, New Jersey: Princeton University Press; 2012.

[232] Vecchi F, Freschi C, Micera S, Sabatini AM, Dario P, Sacchetti R. Experimental Evaluation of Two Commercial Force Sensors for Applications in Biomechanics and Motor Control. 5th Annual Conference of the International Functional Electrical Stimulation Society. Aalborg, Denmark2000.

[233] De Asha AR, Robinson MA, Barton GJ. A marker based kinematic method of identifying initial contact during gait suitable for use in real-time visual feedback applications. Gait & posture. 2012;36:650-2.

[234] Cerqueira ASOd, Yamaguti EY, Mochizuki L, Amadio AC, Serrão JC. Força de Reação do Solo e atividade eletromiográfica da marcha de amputados transfemorais: uma série de casos. Revista Brasileira de Cineantropometria e Desempenho Humano. 2013;15.

[235] Su PF, Gard SA, Lipschutz RD, Kuiken TA. Gait characteristics of persons with bilateral transtibial amputations. J Rehabil Res Dev. 2007;44:491-501.

[236] Schwartz MH, Rozumalski A, Trost JP. The effect of walking speed on the gait of typically developing children. J Biomech. 2008;41:1639-50.

[237] Detrembleur C, Vanmarsenille JM, De Cuyper F, Dierick F. Relationship between energy cost, gait speed, vertical displacement of centre of body mass and efficiency of pendulum-like mechanism in unilateral amputee gait. Gait & posture. 2005;21:333-40.

[238] Robertson G, Caldwell D, Hamill J, Kamen G, Saunders W. Three-Dimensional Kinematics. Research Methods in Biomechanics , 2E. Champaign, IL: Human Kinetics; 2014. p. 35-59.

[239] Legro MW, Reiber GE, Czerniecki JM, Sangeorzan BJ. Recreational activities of lower-limb amputees with prostheses. Journal of rehabilitation research and development. 2001;38:319-25.

[240] Gailey R, Clark C. Chapter 23: Physical Therapy Management of Adult Lower-Limb Amputees. In: American Academy of Orthopaedic Surgeons, Bowker JH, Michael JW, editors. Atlas of Limb Prosthetics: Surgical, Prosthetic, and Rehabilitation Principles. 2nd ed: American Academy of Orthopaedic Surgeons; 1992.

[241] British Association of Chartered Physitherapists in Amputee Rehabilitation. Clinical guidelines for the pre and post operative physiotherapy management of adults with lower limb amputation. In: Broomhead P, Diana D, Hancock A, Unia P, Anne B, Davies V, editors. Nottingham, UK: BACPAR; 2006.

[242] Kadaba MP, Ramakrishnan HK, Wootten ME, Gainey J, Gorton G, Cochran GV. Repeatability of kinematic, kinetic, and electromyographic data in normal adult gait. Journal of orthopaedic research : official publication of the Orthopaedic Research Society. 1989;7:849-60.

[243] Schuch M. Transfemoral amputation: Prosthetic management. In: Smith D, Michael J, Bowker J, editors. Atlas of limb prosthetics: surgical, prosthetic, and rehabilitation principles. 3rd ed. Rosemont, IL: American Academy of Orthopedic Surgeons; 1992.

[244] Kutner M, Wasserman W, Neter J, Nachtsheim C. Applied Linear Statistical Models. 4th ed. New York: McGraw-Hill Education; 2004.

[245] Klasson B. Appreciation of Prosthetic Socket Fitting from Basic Engineering Principles. Glasgow: National Centre for Training and Education in Prosthetics and Orthotics; 1995.

[246] Gholizadeh H, Abu Osman NA, Eshraghi A, Ali S, Saevarsson SK, Wan Abas WA, et al. Transtibial prosthetic suspension: less pistoning versus easy donning and doffing. J Rehabil Res Dev. 2012;49:1321-30.

[247] Polliack AA, Craig DD, Sieh RC, Landsberger S, McNeal DR. Laboratory and clinical tests of a prototype pressure sensor for clincial assessment of prosthetic socket fit. Prosthet Orthot Int. 2002;26:23-34.

[248] Keller T, Weisberger A, Ray J, Hassan S, Shiavi R, Spengler D. Relationship between vertical ground reaction force and speed during walking, slow jogging, and running. Clinical biomechanics. 1996;11:253-9.

[249] Silverman AK, Neptune RR. Differences in whole-body angular momentum between below-knee amputees and non-amputees across walking speeds. J Biomech. 2011;44:379-85.

[250] Perry J, Burnfield JM. Gait analysis normal and pathological function. New Jersey: SLACK Incorporated; 2010.

Appendix

A1 Ethics and Research Governance Online (ERGO) application form

ERGO 20847

UNIVERSITY OF Southampton

ERGO application form – Ethics form

All mandatory fields are marked (M*). Applications without mandatory fields completed are likely to be rejected by reviewers. Other fields are marked "if applicable". Help text is provided, where appropriate, in italics after each question.

1. APPLICANT DETAILS

1.1 (M*) Applicant name:	Mr. Jinghua Tang, Dr. Mike McGrath, Dr. Jianliang Gao, Mr. Piotr Laszczak, Dr. Liudi Jiang
1.2 Supervisor (if applicable):	Dr. Liudi Jiang
1.3 Other researchers/collaborators (if applicable): *Name, address, email, telephone*	**Chas A. Blatchford and Sons Ltd**

2. STUDY DETAILS

2.1 (M*) Title of study:	Biomechanics of level walking in lower-limb amputees
2.2 (M*) Type of study (*e.g. Undergraduate, Doctorate, Masters, Staff*):	Doctorate
2.3 i) (M*) Proposed start date:	29/09/2014
2.3 ii) (M*) Proposed end date:	01/10/2017

2.4 (M*) What are the aims and objectives of this study?
To collect and analyse sets of biomechanical parameters which characterise walking in lower-limb amputees. To collect pilot data on a small group of healthy subjects to familiarize the researchers with the processes of data collection and processing.

2.5 (M*) Background to study (*a **brief** rationale for conducting the study*):
One of the main functions of a lower-limb prosthesis is to facilitate walking for amputees. Its success is generally determined by the transfer of load across the stump-socket interface. However, to date, neither the clinicians nor the prosthetic users receive any quantifiable means for tri-axial load profile measurements at the critical stump/socket interface. We plan to be trained and familiarized with the processes of a motion analysis gait lab available at Blatchford, who is our industry partner, to obtain essential motion and force plate data during typical normal walking of healthy participants. Similar data from lower limb amputees will be provided by Blatchford. This data can then be used for computational simulation as a means of interfacial load estimation. This data can also be exploited to evaluate the performance of an artificial stump/socket simulator which is built at TSRL in the Faculty.

This study will involve both Ph.D students (Jinghua Tang and Piotr Laszczak) and two postdoctoral researches funded by Medical Research Council (Dr. Mike McGrath and Dr. Jianliang Gao) as well as project leader (Dr. Liudi Jiang), who are also co-applicants for this ethical application.

2.6 (M*) Key research question (*Specify hypothesis if applicable*):

With a focus on the amputee gait conditions, what are the key features of an amputee's gait during level walking, and how can they be used for computational analysis? How do these features differ from our simulator performance?

2.7 (M*) Study design (*Give a **brief** outline of basic study design*)
Outline what approach is being used, why certain methods have been chosen.

This research project is outlined as follows:

Phase 1. Familiarise with gait lab hardware/software, understand the process of gait analysis by collecting pilot data from 5 healthy subjects. This will be done by training organised and conducted by/at the industrial sponsor, Chas A Blatchford & Sons Ltd.

Phase 2. Collect and analyse kinematic and kinetic gait data from lower limb amputees. This will be organised and conducted by/at the industrial sponsor, Chas A Blatchford & Sons Ltd, with UoS staff and students as observers only.

The key scientific objective of this study is oriented around phase 2, while phase 1 is meant to serve to sanction the collection and use of some pilot data to familiarize the team with the processes involved.

3. SAMPLE AND SETTING

3.1 (M*) How are participants to be *approached*? *Give details of what you will do if recruitment is insufficient. If participants will be accessed through a third party (e.g. children accessed via a school) state if you have permission to contact them and **upload any letters of agreement to your submission in ERGO**.*

For Phase 1, five healthy volunteers will be recruited through advertising around the University campus.

For phase 2, the amputee(s) needed for the data collection will be organised by Blatchford & Sons Ltd, any UoS staff and students will only be observers. Thus, this Ethics application for the collection of the data only applies to activities included in Phase 1 and the usage of data arising from Phase 2. Please note that Blatchford provides contracted prosthetic and orthotic service to over 30,000 patients in the NHS via 13 centres, also including DMRC and private clinic facilities. They are bound by terms of reference of their NHS contracts which include ethics, clinical governance, patient data protection etc.

All Blatchford data is collected with signed consent form from amputee participants, which includes the use of data for research and development (R&D), training and education purposes. Blatchford process ensures data management and security according to the data protection act. Blatchford will perform/control the process of anyonamization of all data and ensure all data passed on to the University will not be personally identifiable. Blatchford data is also provided and bound by terms of existing research agreement between University of Southampton and Blatchford and can only be used with their permission. Estimated number of amputee subjects for this study is 12 with 2-3 exemplar data per subject.

3.2 (M*) Who are the proposed sample and where are they from (e.g. fellow students, club members)? *List inclusion/exclusion criteria if applicable. NB The University does not condone the use of 'blanket emails' for contacting potential participants (i.e. fellow staff and/or students).* *It is usually advised to ensure groups of students/staff have given prior permission to be contacted in this way, or to use of a third party to pass on these requests. This is because there is a potential to take advantage of the access to 'group emails' and the relationship with colleagues and subordinates; we therefore generally do not support this method of approach.* *If this is the only way to access a chosen cohort, a reasonable compromise is to obtain explicit approval from the Faculty Ethics Committee (FEC) and also from a senior member of the Faculty in case of complaint.*
For phase 1, we aim to recruit healthy subjects through advertising around the University campus. The inclusion criteria are that participants are 18 years old or over, and they do not have any pathology that affects their ability to walk for a sustained period of time.

3.3 (M*) Describe the relationship between researcher and sample (*Describe any relationship e.g. teacher, friend, boss, clinician, etc.*)
Only a small sample is required, and it might be that those volunteers will be colleagues familiar with our research although there is no foreseeable relationship between us and the participants.

3.4 (M*) Describe how you will ensure that fully informed consent is being given: (*include how long participants have to decide whether to take part*)
The study will be advertised as described above, and each potential applicant will be provided with the participant information sheet prior to their appointment. It is made clear that they may withdraw from the study at any time without giving a reason. Upon arrival at the gait lab, at the time of their appointment, each participant will again be supplied with a copy of the participant information sheet to read and they will be given the opportunity to ask any further questions. Once the participant is happy to continue, they will be asked to read, initial, sign and date a consent form, detailing that they understand their role in the study and what is required.

4. RESEARCH PROCEDURES, INTERVENTIONS AND MEASUREMENTS

4.1 (M*) Give a brief account of the procedure as experienced by the participant *(Make clear who does what, how many times and in what order. Make clear the role of all assistants and collaborators. Make clear total demands made on participants, including time and travel).* ***Upload any copies of questionnaires and interview schedules to your submission in ERGO.***
The experiment will take place in the gait laboratory based at Chas A. Blatchford & Sons Ltd in Basingstoke. This lab is equipped with a gait analysis system including 3D motion capture cameras and force plates. The participant will be required to wear shorts and t-shirt, be barefoot and have retro-reflective markers positioned at key points on their feet (lateral malleolus, second metatarsal head and heel), legs (shank, thigh and lateral epicondyle) and pelvis (Anterior/Posterior superior iliac spines and sacrum). These markers will be attached using double sided tape. The participants will then be asked to walk along a

track of approximately 10m at their natural walking speed (which will be calculated using the marker motion data). The force plates are mounted into this track and record the applied forces in the three principle axes. The 3D motion capture cameras cover this area and will record the participant's motion and display it on a PC monitor in real-time.

The procedure is expected to be completed within 2 hours.

At the end of tests, the participant may request a summary of the projects' findings at a later date.

5. STUDY MANAGEMENT

5.1 (M*) State any potential for psychological or physical discomfort and/or distress?

Allergy induced skin irration may occur because of the usage of bandages or double-sided tapes when mounting reflective markers.

5.2 (M*) Explain how you intend to alleviate any psychological or physical discomfort and/or distress that may arise? (if applicable)

The full procedure of the tests, the activities required, and duration of the tests will be explained to the participants before they begin. Consent will be obtained before the tests. It is also made clear that the participants can choose to withdraw at any time during the test, for whatever reason, without consequence, should he/she feel the need to do so. The experimenter will inform the participants about each step as they occur throughout testing, drawing on their extensive experience in performing these tests with amputees.

5.3 Explain how you will care for any participants in 'special groups' *(i.e. those in a dependent relationship, vulnerable or lacking in mental capacity)* **(if applicable)?**

All clinical tests with amputees will be organised and conducted by Blatchford. For these tests, UoS researchers are observers only with permission from the participant and Blatchford staff.

5.4 Please give details of any payments or incentives being used to recruit participants (if applicable)?

Only travel and parking expenses up to £20 per participant will be provided.

5.5 i) How will participant anonymity and/or data anonymity be maintained (if applicable)?

Two definitions of anonymity exist:

i) Unlinked anonymity - *Complete anonymity can only be promised if questionnaires or other requests for information are not targeted to, or received from, individuals using their name or address or any other identifiable characteristics. For example if questionnaires are sent out with no possible identifiers when returned, or if they are picked up by respondents in a public place, then anonymity can be claimed. Research methods using interviews cannot usually claim anonymity – unless using telephone interviews when participants dial in.*

ii) Linked anonymity - *Using this method, complete anonymity cannot be promised because participants can be identified; their data may be coded so that participants are not identified by researchers, but the information provided to participants should*

indicate that they could be linked to their data.
Maintained through linked anonymity. We may use subjects' photographs and videos for teaching and presenting/publishing the research. There is a section on the consent form for participants to give permission for this or not if they wish. If they consent we will cover their face in any photographs and videos to keep them anonymous. All information that is collected about them during the course of this research will be kept strictly confidential and any information about them will have their name removed so that they cannot be recognised from it.

5.5 ii) How will participant confidentiality be maintained (if applicable)? *Confidentiality is defined as the non-disclosure of research information except to another authorised person. Confidential information can be shared with those who are already party to it, and may also be disclosed where the person providing the information provides explicit consent.*
For the researchers, confidentiality issues will be covered by the project agreements which have been signed by both UOS and Blatchford. For other participants, all data will be anonymous and any photographs/videos taken during testing will not identify the participant involved.

5.6 (M*) How will personal data and study results be stored securely during and after the study? *Researchers should be aware of, and compliant with, the Data Protection policy of the University. You must be able to demonstrate this in respect of handling, storage and retention of data.*
Data are securely stored on University computers/servers

5.7 (M*) Who will have access to these data?
The UoS project research team led by Liudi Jiang (this includes all four researchers included here and any further researchers may be included in the team in future). To be compliant with the agreement with Blatchford, some project data are shared with Blatchford under the confidentiality agreement, vice versa. The project team reserves the right to analyse the data and publish the results, using linked anonymity.

N.B. – Before you upload this document to your ERGO submission remember to:

1. Complete ALL mandatory sections in this form

2. Upload any letters of agreement referred to in question 3.1 to your ERGO submission

3. Upload any interview schedules and copies of questionnaires referred to in question 4.1

UNIVERSITY OF Southampton

ERGO application form – Ethics form

All mandatory fields are marked (M*). Applications without mandatory fields completed are likely to be rejected by reviewers. Other fields are marked "if applicable". Help text is provided, where appropriate, in italics after each question.

1. APPLICANT DETAILS

1.1 (M*) Applicant name:	Prof. Liudi Jiang, Dr Michael McGrath, Dr Maria Valero de Rodanas, Jinghua Tang, Nick Hale, Chikai Sun
1.2 Supervisor (if applicable):	Prof. Liudi Jiang
1.3 Other researchers/collaborators (if applicable): *Name, address, email, telephone*	**Chas A. Blatchford & Sons Ltd (CAB)**

2. STUDY DETAILS

2.1 (M*) Title of study:	Interface sensor systems for foot plantar studies
2.2 (M*) Type of study (*e.g. Undergraduate, Doctorate, Masters, Staff*):	Staff
2.3 i) (M*) Proposed start date:	01/05/2016
2.3 ii) (M*) Proposed end date:	01/10/2019

2.4 (M*) What are the aims and objectives of this study?
To develop an interface sensor system suitable for foot plantar applications, calibrated by gait lab measurements. To collect kinetic interfacial biomechanical and environmental data using sensors at the foot plantar area along with kinematic data which characterise walking in healthy subjects.

2.5 (M*) Background to study (*a **brief** rationale for conducting the study*):
The load distribution normal to the sole of the foot has long been known to be a key parameter in determining the likelihood of foot health problems. However, although the distribution of the load tangential to this interface is also widely agreed to be equally important, it has not yet been convincingly determined. Such information would be useful in foot health diagnostics, rehabilitation and sports medicine. Currently, no commercially available system can achieve this in a clinically practical manner. This is the exact focus of this project and the potential benefit from the outcomes of this research. In terms of measuring biomechanical loads, the sensor technology exists already and has been used in prosthetic applications. We intend to adapt the current design to make it more appropriate for use at the plantar surface of the foot, potentially adding further capabilities to provide data relating to motion and external stimuli,

such as temperature, so that we may fully characterise the bioenvironmental conditions that influences foot health.

A patent related to this novel sensor has been filed in 2012. It is now crucial and timely that the technology to be developed for the plantar applications, which aims at obtaining both kinetic and kinematic data.

This study will involve the project leader (Prof. Jiang), and members of her research team including postdoctoral researchers and PhD students.

2.6 (M*) Key research question (*Specify hypothesis if applicable*):

To design, develop and optimise sensor systems so that both kinetic and kinematic data collected can be used clinically for characterising the bioenvironmental conditions at the plantar surface of the foot as well as facilitating scientific studies in human locomotion.

2.7 (M*) Study design (*Give a **brief** outline of basic study design*)
Outline what approach is being used, why certain methods have been chosen.

The focus of the study will be on developing and calibrating the sensor system. The sensors and associated circuitry will be developed further and adapted to the application of measuring bioenvironmental conditions at the plantar surface. Bench tests will be performed in a research lab to validate the sensor system. Sensors will also be used to take measurements at the plantar surface of the researchers' feet. Data will be collected for various everyday activities, such as walking.

Where possible, we plan to use a gait laboratory to obtain essential motion and force plate data during typical everyday activities for healthy participants, in conjunction with our sensor system. The sensor measurements will be synchronised with the gait lab measurements and/or built in inertial measurement units (IMU) signals. This will help to provide application-specific data for calibration purposes. For this study, we plan to use the gait laboratory at Chas A. Blatchford & Sons (Basingstoke, UK), which is equipped with a gait analysis system including 3D motion capture cameras and force plates.

It is worth mentioning here that, a typical sensor system consists sensor units, which are connected to a small circuitry board via a flexible cable. The entire system will be battery powered. Only the sensor units will be placed at the plantar area, which will NEVER be in direct contact with bare skin. In fact, a silicone gel and/or fabric materials will be used in-between the sensor and the skin of any participants. Thus, abrasion to skin is completely prevented.

3. SAMPLE AND SETTING

3.1 (M*) How are participants to be *approached?* *Give details of what you will do if recruitment is insufficient. If participants will be accessed through a third party (e.g. children accessed via a school) state if you have permission to contact them and **upload any letters of agreement to your submission in ERGO**.*

The participants will be Prof Liudi Jiang and members of her research team. It is anticipated that data will be collected from up to a maximum of six researchers from the group.

3.2 (M*) Who are the proposed sample and where are they from (e.g. fellow students, club members)? *List inclusion/exclusion criteria if applicable. NB The University does not condone the use of 'blanket emails' for contacting potential*

participants (i.e. fellow staff and/or students). *It is usually advised to ensure groups of students/staff have given prior permission to be contacted in this way, or to use of a third party to pass on these requests. This is because there is a potential to take advantage of the access to 'group emails' and the relationship with colleagues and subordinates; we therefore generally do not support this method of approach.* *If this is the only way to access a chosen cohort, a reasonable compromise is to obtain explicit approval from the Faculty Ethics Committee (FEC) and also from a senior member of the Faculty in case of complaint.*
The participants will be Prof Liudi Jiang and members of her research team. It is anticipated that data will be collected from up to a maximum of six researchers from the group. All participants used will be 18 years old or over, and they will not have any pathology that affects their ability to walk for a sustained period of time.

3.3 (M*) Describe the relationship between researcher and sample (*Describe any relationship e.g. teacher, friend, boss, clinician, etc.*)
The participants will be Prof Liudi Jiang and members of her research team. It is anticipated that data will be collected from up to a maximum of six researchers from the group.

3.4 (M*) Describe how you will ensure that fully informed consent is being given: (*include how long participants have to decide whether to take part*)
Each potential participant will be provided with the participant information sheet prior to their appointment. It is made clear that they may withdraw from the study at any time without giving a reason. Before measurements are taken, each participant will again be supplied with a copy of the participant information sheet to read and they will be given the opportunity to ask any further questions. Once the participant is happy to continue, they will be asked to read, initial, sign and date a consent form, detailing that they understand their role in the study and what is required.

4. RESEARCH PROCEDURES, INTERVENTIONS AND MEASUREMENTS

4.1 (M*) Give a brief account of the procedure as experienced by the participant *(Make clear who does what, how many times and in what order. Make clear the role of all assistants and collaborators. Make clear total demands made on participants, including time and travel).* ***Upload any copies of questionnaires and interview schedules to your submission in ERGO.***
The participant will have the sensors at the plantar area of their feet, measuring interfacial loads and environmental data e.g. temperature etc. The participant will be asked to perform everyday activities, such as walking. The sensors will be transmitting its measurements to a laptop, tablet or smart phone. The circuitry board for the sensors (previously tested and validated in a research laboratory) will be housed in a small plastic box, along with batteries to power it. This box can either be carried or attached to participant e.g. around the ankle, using a Velcro strap or adhesion tapes etc., depending upon their preference. On occasions where gait lab testing is possible, the participant will be required to wear shorts and t-shirt and have gait lab markers positioned at key points on their feet, legs and pelvis. These markers will be attached using elasticated straps. A force plate will be mounted into a walking track and the participant will be required to

walk over it. It will record the applied forces in the three principle axes. The 3D motion capture cameras cover this area and will record the participant's motion and display it on a PC monitor in real-time. The procedure is expected to be completed within an hour.

5. STUDY MANAGEMENT

5.1 (M*) State any potential for psychological or physical discomfort and/or distress?
None.

5.2 (M*) Explain how you intend to alleviate any psychological or physical discomfort and/or distress that may arise? (if applicable)
The full procedure of the tests, the activities required, and duration of the tests will be explained to the participants before they begin. Consent will be obtained before the tests. It is also made clear that the participants can choose to withdraw at any time during the test, for whatever reason, without consequence, should he/she feel the need to do so. The experimenter will inform the participants about each step as they occur throughout testing, drawing on their extensive experience in performing these tests.

5.3 Explain how you will care for any participants in 'special groups' *(i.e. those in a dependent relationship, vulnerable or lacking in mental capacity)* **(if applicable)?**
There will be no participants from 'special groups'.

5.4 Please give details of any payments or incentives being used to recruit participants (if applicable)?
N/A

5.5 i) How will participant anonymity and/or data anonymity be maintained (if applicable)? *Two definitions of anonymity exist:* *i)* Unlinked anonymity - *Complete anonymity can only be promised if questionnaires or other requests for information are not targeted to, or received from, individuals using their name or address or any other identifiable characteristics. For example if questionnaires are sent out with no possible identifiers when returned, or if they are picked up by respondents in a public place, then anonymity can be claimed. Research methods using interviews cannot usually claim anonymity – unless using telephone interviews when participants dial in.* *ii)* Linked anonymity - *Using this method, complete anonymity cannot be promised because participants can be identified; their data may be coded so that participants are not identified by researchers, but the information provided to participants should indicate that they could be linked to their data.*
Maintained through linked anonymity. We may use participants' photographs and videos for teaching and presenting/publishing the research. There is a section on the consent form for participants to give permission for this or not if they wish. If they consent we will cover their face in any photographs and videos to keep them anonymous. All information that is collected about them during the course of this research will be kept strictly confidential and any information about them will have their name removed so that they cannot be recognised from it.

5.5 ii) How will participant confidentiality be maintained (if applicable)? *Confidentiality is defined as the non-disclosure of research information except to another authorised person. Confidential information can be shared with those who are already party to it, and may also be disclosed where the person providing the information provides explicit consent.*
For all participants, all data will be anonymous and any photographs/videos taken during testing will not identify the participant involved.

5.6 (M*) How will personal data and study results be stored securely during and after the study? *Researchers should be aware of, and compliant with, the Data Protection policy of the University. You must be able to demonstrate this in respect of handling, storage and retention of data.*
Data are securely stored on University computers/servers.

5.7 (M*) Who will have access to these data?
The UoS project research team led by Liudi Jiang (this includes all postdoctoral researchers and PhD students). For research sponsered/supported by Blatchford, to be compliant with the collabroation agreement with Blatchford, some project data are shared with Blatchford under the confidentiality agreement, vice versa. The project team reserves the right to analyse the data and publish the results, using linked anonymity.

N.B. – Before you upload this document to your ERGO submission remember to:

1. Complete ALL mandatory sections in this form

2. Upload any letters of agreement referred to in question 3.1 to your ERGO submission

3. Upload any interview schedules and copies of questionnaires referred to in question 4.1

A2 Calibration certificate for Kistler force plate (9286BA)

KISTLER
measure. analyze. innovate.

Kalibrierschein Kraft
Calibration Certificate Force

Type Kistler 9286BA Serial No. 4435020

Kalibriert durch Calibrated by	Datum Date
S. Mogavero	26. Mar. 2013

Referenzgeräte Reference Equipment	Typ Type	Serien-Nr. Serial-No.
Gebrauchsnormal Working Standard	Kistler 9067 Kistler 9068 Kistler 9068	474351 107070 128643
Kontrolleinheit Control Unit	Kistler 5233A1Y0386	563223
Ladungskalibrator Charge Calibrator	Kistler 5395A	605262

Umgebungstemperatur Ambient Temperature °C	Relative Feuchte Relative Humidity %
23	42

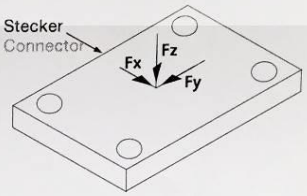

Messergebnisse Results of Measurement

Bereich Range	Kalibrierter Bereich Calibrated Range		Empfindlichkeit Sensitivity							
	Fx / Fy kN	Fz kN	1 [3] X1+2 [4] mV/N	2 [3] X3+4 [4] mV/N	3 [3] Y1+4 [4] mV/N	4 [3] Y2+3 [4] mV/N	5 [3] Z1 [4] mV/N	6 [3] Z2 [4] mV/N	7 [3] Z3 [4] mV/N	8 [3] Z4 [4] mV/N
4 [2]	0 ... 5	0 ... 20	1,966	1,945	1,938	1,957	0,892	0,886	0,886	0,890
3 [1]	0 ... 2.5	0 ... 10	3,931	3,891	3,876	3,914	1,783	1,773	1,771	1,781
2 [2]	0 ... 1.25	0 ... 5	7,862	7,782	7,751	7,829	3,566	3,545	3,543	3,561
1 [1]	0 ... 0.25	0 ... 1	39,402	38,978	38,884	39,276	17,701	17,599	17,584	17,676

Bereich Range	Kalibrierter Bereich Calibrated Range		Übersprechen Cross talk					
	Fx / Fy kN	Fz kN	Fx → Fy %	Fy → Fx %	Fx → Fz %	Fy → Fz %	Fz → Fx %	Fz → Fy %
3 [1]	0 ... 2.5	0 ... 10	-0,4	1,4	1,1	-1,3	0,0	0,2
1 [1]	0 ... 0.25	0 ... 1	-0,1	1,5	0,9	-1,3	0,1	0,2

[1] Gemessen Measured
[2] Berechnet Calculated (±0,5%)
[3] Kanalnummer Channel No.
[4] Signal Signal

Messverfahren / Measurement Procedure: Kontinuierliche Kalibrierung, Vergleichsverfahren / Continuous Calibration, Comparison Method

Kistler betreibt die SCS Kalibrierstelle Nr. 049, akkreditiert nach ISO 17025. SCS Kalibrierzertifikate sind auf Bestellung erhältlich
Kistler operates the SCS Calibration Laboratory No. 049, which is accredited per ISO 17025. SCS Calibration Certificates are available on request.

Bestätigung Confirmation

Das oben durch die Serienummer identifizierte Gerät entspricht der Vereinbarung der Bestellung und hält die Herstelltoleranzen gemäss den Spezifikationen der Datenblätter ein. Dieses Dokument erfüllt die Anforderungen von EN 10204 Abnahmeprüfzeugnis "3.1". Alle Messmittel sind auf nationale Normale rückverfolgbar Das Kistler Qualitätsmanagement System ist nach ISO 9001 zertifiziert. Dieses Dokument ist ohne Unterschrift gültig.
The equipment mentioned above and identified by Serial Number complies with the agreement of the order and meets the manufacturing tolerances specified in the data sheests. This document fulfils the requirements of EN 10204 Inspection Certificate "3.1". All measuring devices are traceable to national standards. The Kistler Quality Management System is certified per ISO 9001. This document is valid without a signature

Kistler Instrumente AG
Eulachstrasse 22
Postfach
CH-8408 Winterthur
Tel. +41 52 224 11 11
Fax +41 52 224 14 14
info@kistler.com
ZKB Winterthur BC 732
Swift: ZKBKCHZZ80A
Konto: 1132-0374.628
IBAN: CH67 0070 0113 2003 7462 8
MwSt. Nr.: 229 713
ISO 9001 zertifiziert
www.kistler.com

A3 Procedures of palpating anatomical landmarks

Palpation of pelvic landmarks

- Step 1: the subject adopts an upright standing positon.
- Step 2: the research place fingers on the anterior part of the iliac crest.
- Step 3: the anterior part of the iliac crest is followed forwards, until a bony prominence region is located.
- Step 4: confirm this location by moving the finger around and selecting the most prominent location as ASIS.
- Step 5: the tip of the Pointer is placed at the palpated location and the trigger is activated.
- Step 6: the marker visibility report (four markers on the Pointer, six markers from the pelvic frame) is checked from the Odin software.
    - If all marker is available, proceed to Step 7
    - If one or more markers can not be captured by the optical sensing unit, the orientation of the pointer was adjusted and protocol returned to Step 5

Step 7: the same process is repeated to digitise right ASIS

Palpation of knee joint landmarks

For the able-bodied group, the process for palpation of the knee joint landmarks, including lateral femoral epicondyle (LFE) and medial femoral epicondyle (MFE), can be described as:

- Step 1: the subject was required to stand and flex the knee.
- Step 2: the researcher placed the index and middle finger around the lateral side of the knee.
- Step 3: the fingers glided backwards until the lateral collateral ligament is reached.
- Step 4: the ligament was followed proximally until a tubercle is reached, which corresponds to the lateral femoral epicondyle.

Followed by the digitisation of LFE, the medial femoral epicondyle (MFE) was subsequently digitised, following the steps below:

- Step 1: the subject was required to stand and flex the knee.
- Step 2: the researcher placed the middle finger on the insertion of the Adductor Magnus muscle.
- Step 3: the thumb was placed on the distal edge of the medial condyle.

- Step 4: the index finger was placed midway between the thumb and the middle finger, and moved slightly forwards towards the patella. The index finger should locate a small tubercle, this corresponds to the MFE.

A4 Source code for calculations of residuum/socket interface coupling motion

```
% THIS IS THE MATLAB SCRIPT THAT ESTIMATE THE RESIDUUM/SOCKET COUPLING FOR
% KNEE-DISARTICULATION AND ABOVE KNEE AMPUTEES (CREATED BY JINGHUA TANG
20160602)

%% CLEAR PREVIOUS DATA, CLOSE ALL FIGURES AND TURN WARNING OFF

clc; clear all; close all;
warning('off','all');

%% READ ALL ODIN FILES AND GROUP ALL OF THEM INTO A CELL

RB_Walking_ODIN1=load('J:\SES
Research\Public\ResearchProject_SocketBiomechanics\CABData\Motion Bundles
and Trial Information\Motion Bundles from JT\2016-06-02\Odin
Output\Matlab\Level_Walkng_Right_Side\JTMM020616RBB2-
Level_024_2016_6_2.mat');
RB_Walking_ODIN2=load('J:\SES
Research\Public\ResearchProject_SocketBiomechanics\CABData\Motion Bundles
and Trial Information\Motion Bundles from JT\2016-06-02\Odin
Output\Matlab\Level_Walkng_Right_Side\JTMM020616RBB2-
Level_025_2016_6_2.mat');
RB_Walking_ODIN3=load('J:\SES
Research\Public\ResearchProject_SocketBiomechanics\CABData\Motion Bundles
and Trial Information\Motion Bundles from JT\2016-06-02\Odin
Output\Matlab\Level_Walkng_Right_Side\JTMM020616RBB2-
Level_026_2016_6_2.mat');
RB_Walking_ODIN4=load('J:\SES
Research\Public\ResearchProject_SocketBiomechanics\CABData\Motion Bundles
and Trial Information\Motion Bundles from JT\2016-06-02\Odin
Output\Matlab\Level_Walkng_Right_Side\JTMM020616RBB2-
Level_027_2016_6_2.mat');
RB_Walking_ODIN5=load('J:\SES
Research\Public\ResearchProject_SocketBiomechanics\CABData\Motion Bundles
and Trial Information\Motion Bundles from JT\2016-06-02\Odin
Output\Matlab\Level_Walkng_Right_Side\JTMM020616RBB2-
Level_028_2016_6_2.mat');
RB_Walking_ODIN6=load('J:\SES
Research\Public\ResearchProject_SocketBiomechanics\CABData\Motion Bundles
and Trial Information\Motion Bundles from JT\2016-06-02\Odin
Output\Matlab\Level_Walkng_Right_Side\JTMM020616RBB2-
Level_001_2016_6_2.mat');
RB_Walking_ODIN7=load('J:\SES
Research\Public\ResearchProject_SocketBiomechanics\CABData\Motion Bundles
and Trial Information\Motion Bundles from JT\2016-06-02\Odin
Output\Matlab\Level_Walkng_Right_Side\JTMM020616RBB2-
Level_002_2016_6_2.mat');
RB_Walking_ODIN8=load('J:\SES
Research\Public\ResearchProject_SocketBiomechanics\CABData\Motion Bundles
and Trial Information\Motion Bundles from JT\2016-06-02\Odin
Output\Matlab\Level_Walkng_Right_Side\JTMM020616RBB2-
Level_003_2016_6_2.mat');
RB_Walking_ODIN9=load('J:\SES
Research\Public\ResearchProject_SocketBiomechanics\CABData\Motion Bundles
and Trial Information\Motion Bundles from JT\2016-06-02\Odin
Output\Matlab\Level_Walkng_Right_Side\JTMM020616RBB2-
Level_004_2016_6_2.mat');
RB_Walking_ODIN10=load('J:\SES
Research\Public\ResearchProject_SocketBiomechanics\CABData\Motion Bundles
and Trial Information\Motion Bundles from JT\2016-06-02\Odin
```

```
Output\Matlab\Level_Walkng_Right_Side\JTMM020616RBB2-
Level_005_2016_6_2.mat');
RB_Walking_ODIN11=load('J:\SES
Research\Public\ResearchProject_SocketBiomechanics\CABData\Motion Bundles
and Trial Information\Motion Bundles from JT\2016-06-02\Odin
Output\Matlab\Level_Walkng_Right_Side\JTMM020616RBB2-
Level_006_2016_6_2.mat');
RB_Walking_ODIN12=load('J:\SES
Research\Public\ResearchProject_SocketBiomechanics\CABData\Motion Bundles
and Trial Information\Motion Bundles from JT\2016-06-02\Odin
Output\Matlab\Level_Walkng_Right_Side\JTMM020616RBB2-
Level_007_2016_6_2.mat');
RB_Walking_ODIN13=load('J:\SES
Research\Public\ResearchProject_SocketBiomechanics\CABData\Motion Bundles
and Trial Information\Motion Bundles from JT\2016-06-02\Odin
Output\Matlab\Level_Walkng_Right_Side\JTMM020616RBB2-
Level_008_2016_6_2.mat');
RB_Walking_ODIN14=load('J:\SES
Research\Public\ResearchProject_SocketBiomechanics\CABData\Motion Bundles
and Trial Information\Motion Bundles from JT\2016-06-02\Odin
Output\Matlab\Level_Walkng_Right_Side\JTMM020616RBB2-
Level_009_2016_6_2.mat');

RB_ODIN={RB_Walking_ODIN1,RB_Walking_ODIN2,RB_Walking_ODIN3,RB_Walking_ODIN
4,RB_Walking_ODIN5,RB_Walking_ODIN6,RB_Walking_ODIN7,RB_Walking_ODIN8,RB_Wa
lking_ODIN9,RB_Walking_ODIN10,RB_Walking_ODIN11,RB_Walking_ODIN12,RB_Walkin
g_ODIN13,RB_Walking_ODIN14};

%% DEFINE INTIAL CONTACT (IC), TOE-OFF (TO) USING ODIN FILES

% ABSOLUTE TIME IN ODIN .MAT FILES
for i=1:length(RB_ODIN)

    IC_time{i}=RB_ODIN{i}.Events.Right.IC;
    TO_time{i}=RB_ODIN{i}.Events.Right.TO;
    TSE_time{i}=RB_ODIN{i}.Events.Right.TSE;

end

% SAMPLING FREQUENCY FOR FORCE PLATE AND MARKER DATA
for i=1:length(RB_ODIN)

    marker_frequency{i}=RB_ODIN{i}.Marker.Marker.LShank2.Rate;
    force_frequency{i}=RB_ODIN{i}.Force.Force.F1.Rate;

end

% DEFINE DATA INDEX
for i=1:length(RB_ODIN)

    marker_start{i}=IC_time{i}*marker_frequency{i};
    marker_end{i}=TSE_time{i}*marker_frequency{i};

    force_start{i}=IC_time{i}*force_frequency{i};
    force_end{i}=TSE_time{i}*force_frequency{i};

end

%% DEFINE NORMALISED TIME AND ABSOLUTE TIME
```

```
% DEFINE A NORMALISED GAIT CYCLE
gait_cycle=0:100;

% DEFINE THE NON-NORMALISED TIME FOR MARKER DATA
for i=1:length(RB_ODIN)

    time_m{i}=0:(1/marker_frequency{i}):((marker_end{i}-
marker_start{i})/marker_frequency{i});

end

% DEFINE THE NON-NORMALISED TIME FOR FORCE DATA
for i=1:length(RB_ODIN)

    time_f{i}=0:(1/force_frequency{i}):((marker_end{i}-
marker_start{i})/marker_frequency{i});

end

% DEFINE NORMALISED TIME FOR MARKER DATA
for i=1:length(RB_ODIN)

    time_n_m{i}=0:time_m{i}(end)/100:time_m{i}(end);

end

% DEFINE NORMALISED TIME FOR FORCE DATA
for i=1:length(RB_ODIN)

    time_n_f{i}=0:time_m{i}(end)/100:time_m{i}(end);

end

%% EXTACT RELEVANT REAL AND VIRTUAL MARKER DATA

for i=1:length(RB_ODIN)

    % KNEE JOINT CENTRE

knee_x{i}=RB_ODIN{i}.RefPoint.RefPoint.RKnee.Data(marker_start{i}:marker_en
d{i},1);

knee_y{i}=RB_ODIN{i}.RefPoint.RefPoint.RKnee.Data(marker_start{i}:marker_en
d{i},2);

knee_z{i}=RB_ODIN{i}.RefPoint.RefPoint.RKnee.Data(marker_start{i}:marker_en
d{i},3);

knee_glb{i}=RB_ODIN{i}.RefPointFilter.RefPointFilter.RKnee.Data(marker_star
t{i}:marker_end{i},1:3);

    % 3 SOCKET MARKERS

socket0_glb{i}=RB_ODIN{i}.Marker.Marker.RThigh0.Data(marker_start{i}:marker
_end{i},1:3);
```

```
socket1_glb{i}=RB_ODIN{i}.Marker.Marker.RThigh1.Data(marker_start{i}:marker
_end{i},1:3);

socket2_glb{i}=RB_ODIN{i}.Marker.Marker.RThigh2.Data(marker_start{i}:marker
_end{i},1:3);

socket3_glb{i}=RB_ODIN{i}.Marker.Marker.RThigh3.Data(marker_start{i}:marker
_end{i},1:3);

    % HIP JOINT CENTRE

hip_x{i}=RB_ODIN{i}.RefPoint.RefPoint.RHip.Data(marker_start{i}:marker_end{
i},1);

hip_y{i}=RB_ODIN{i}.RefPoint.RefPoint.RHip.Data(marker_start{i}:marker_end{
i},2);

hip_z{i}=RB_ODIN{i}.RefPoint.RefPoint.RHip.Data(marker_start{i}:marker_end{
i},3);

hip_glb{i}=RB_ODIN{i}.RefPointFilter.RefPointFilter.RHip.Data(marker_start{
i}:marker_end{i},1:3);

    % LATERAL FEMORAL EPICONDYLE

LFE_x{i}=RB_ODIN{i}.RefPoint.RefPoint.RLateralFemoralEpicondyle.Data(marker
_start{i}:marker_end{i},1);

LFE_y{i}=RB_ODIN{i}.RefPoint.RefPoint.RLateralFemoralEpicondyle.Data(marker
_start{i}:marker_end{i},2);

LFE_z{i}=RB_ODIN{i}.RefPoint.RefPoint.RLateralFemoralEpicondyle.Data(marker
_start{i}:marker_end{i},3);

LFE_glb{i}=RB_ODIN{i}.RefPoint.RefPoint.RLateralFemoralEpicondyle.Data(mark
er_start{i}:marker_end{i},1:3);

    % MEDIAL FEMORAL EPICONDYLE

MFE_x{i}=RB_ODIN{i}.RefPoint.RefPoint.RMedialFemoralEpicondyle.Data(marker_
start{i}:marker_end{i},1);

MFE_y{i}=RB_ODIN{i}.RefPoint.RefPoint.RMedialFemoralEpicondyle.Data(marker_
start{i}:marker_end{i},2);

MFE_z{i}=RB_ODIN{i}.RefPoint.RefPoint.RMedialFemoralEpicondyle.Data(marker_
start{i}:marker_end{i},3);

MFE_glb{i}=RB_ODIN{i}.RefPoint.RefPoint.RMedialFemoralEpicondyle.Data(marke
r_start{i}:marker_end{i},1:3);

end

%% VIRTUAL RESIDUUM SEGMENT (VRS) LOCAL COORDINATE SYSTEM

% IT IS WORTH NOTING THAT THE AXIS CONVENTION USED HERE IS FROM GORDON BOOK

% VRS-Z VECTOR (DISTAL-PROXIMAL AIXS) STARTS FROM THE PROSTHETIC PIVOT
CENTRE POINTING TOWARDS HIP
```

```
% JOINT CENTRE
for i=1:length(RB_ODIN)

    VRS_Z_Vector{i}=hip_glb{i}-knee_glb{i};

end

% VECTOR STARTS FROM THE KNEE JOINT CENTRE POINTING TOWARDS LATERAL FEMORAL
% EPICONDYLES
for i=1:length(RB_ODIN)

    KJC_LFE_Vector{i}=LFE_glb{i}-knee_glb{i};

end

% VRS-Y VECTOR (ANTERIOR-POSTERIOR AXIS) CAN BE OBTAINED FROM THE CROSS
% PRODUCT OF VRS-Z VECTOR AND KJC_LFE VECTOR
for i=1:length(RB_ODIN)

    VRS_Y_Vector{i}=cross(VRS_Z_Vector{i},KJC_LFE_Vector{i});

end

% VRS-x VECTOR (MEDIAL-LATERAL AXIS) CAN BE OBTAINED FROM THE CROSS
% PRODUCT OF VRS-Y VECTOR AND VRS-Z VECTOR
for i=1:length(RB_ODIN)

    VRS_X_Vector{i}=cross(VRS_Y_Vector{i},VRS_Z_Vector{i});

end

% CONVERT VECTOR TO AXES
for i=1:length(RB_ODIN)

    for j=1:length(hip_glb{i}(:,1))


VRS_X_Axis{i}(j,1:3)=VRS_X_Vector{i}(j,1:3)/norm(VRS_X_Vector{i}(j,1:3));

VRS_Y_Axis{i}(j,1:3)=VRS_Y_Vector{i}(j,1:3)/norm(VRS_Y_Vector{i}(j,1:3));

VRS_Z_Axis{i}(j,1:3)=VRS_Z_Vector{i}(j,1:3)/norm(VRS_Z_Vector{i}(j,1:3));

    end

end

%% SOCKET SEGMENT (SS) LOCAL COORDINATE SYSTEM

% SS-Z VECTOR
for i=1:length(RB_ODIN)

    SS_Z_Vector{i}=socket3_glb{i}-socket0_glb{i};

end

% SS-Y VECTOR
```

```
for i=1:length(RB_ODIN)

    SS_Y_Vector{i}=socket1_glb{i}-socket0_glb{i};

end

% SS-X VECTOR
for i=1:length(RB_ODIN)

    SS_X_Vector{i}=cross(SS_Y_Vector{i},SS_Z_Vector{i});

end

% CONVERT VECTOR TO AXES
for i=1:length(RB_ODIN)

    for j=1:length(hip_glb{i}(:,1))


SS_X_Axis{i}(j,1:3)=SS_X_Vector{i}(j,1:3)/norm(SS_X_Vector{i}(j,1:3));

SS_Y_Axis{i}(j,1:3)=SS_Y_Vector{i}(j,1:3)/norm(SS_Y_Vector{i}(j,1:3));

SS_Z_Axis{i}(j,1:3)=SS_Z_Vector{i}(j,1:3)/norm(SS_Z_Vector{i}(j,1:3));

    end

end

%% CONSTRUCTION OF ORIENTATION MATRIX

% VRS AND SS SEGMENT ORIENTATION MATRIX
for i=1:length(RB_ODIN)

    for j=1:length(hip_glb{i}(:,1))


R_VRS{i}{j}=[VRS_X_Axis{i}(j,1:3);VRS_Y_Axis{i}(j,1:3);VRS_Z_Axis{i}(j,1:3)
];

R_SS{i}{j}=[SS_X_Axis{i}(j,1:3);SS_Y_Axis{i}(j,1:3);SS_Z_Axis{i}(j,1:3)];

    end

end

%% ROTATIONAL MATRIX

% INVERSE OF THE SOCKET ORIENTATION MATRIX
for i=1:length(RB_ODIN)

    for j=1:length(hip_glb{i}(:,1))

        Transpose_R_SS{i}{j}=transpose(R_SS{i}{j});

    end
```

```
end

% ROTATIONAL MATRIX
for i=1:length(RB_ODIN)

    for j=1:length(hip_glb{i}(:,1))

        R_Coupling{i}{j}=R_VRS{i}{j}*Transpose_R_SS{i}{j};

    end

end

%% EULER ANGLE CALCULATIONS

for i=1:length(RB_ODIN)

    for j=1:length(hip_glb{i}(:,1))

        Alpha{i}{j}=atand(-R_Coupling{i}{j}(3,2)/R_Coupling{i}{j}(3,3));
        Gamma{i}{j}=atand(-R_Coupling{i}{j}(2,1)/R_Coupling{i}{j}(1,1));

Beta{i}{j}=atand(R_Coupling{i}{j}(3,1)/(sqrt((R_Coupling{i}{j}(1,1))^2+(R_C
oupling{i}{j}(2,1))^2)));

    end

end

for i=1:length(RB_ODIN)

    Coupling_Coronal_Angle{i}=cell2mat(Beta{i});
    Coupling_Sagittal_Angle{i}=cell2mat(Alpha{i});
    Coupling_Transverse_Angle{i}=cell2mat(Gamma{i});

end

%% AXIAL COUPLING

for i=1:length(RB_ODIN)

    Coupling_Axial{i}=sqrt((knee_x{i}-hip_x{i}).^2+(knee_y{i}-
hip_y{i}).^2+(knee_z{i}-hip_z{i}).^2);

end

%% GROUND REACTION FORCES

for i=1:length(RB_ODIN)


AP_GRF{i}=RB_ODIN{i}.Force.Force.F1.Data(force_start{i}:force_end{i},1);

ML_GRF{i}=RB_ODIN{i}.Force.Force.F1.Data(force_start{i}:force_end{i},2);
    V_GRF{i}=RB_ODIN{i}.Force.Force.F1.Data(force_start{i}:force_end{i},3);

end
```

```
%% DATA NORMALISATION

for i=1:length(RB_ODIN)


Coupling_Sagittal_Angle_n(:,i)=interp1(time_m{i},Coupling_Sagittal_Angle{i}
,time_n_m{i},'linear');

Coupling_Coronal_Angle_n(:,i)=interp1(time_m{i},Coupling_Coronal_Angle{i},t
ime_n_m{i},'linear');

Coupling_Transverse_Angle_n(:,i)=interp1(time_m{i},Coupling_Transverse_Angl
e{i},time_n_m{i},'linear');

Coupling_Axial_n(:,i)=interp1(time_m{i},Coupling_Axial{i},time_n_m{i},'line
ar');

    AP_GRF_n(:,i)=interp1(time_f{i},AP_GRF{i},time_n_f{i},'linear');
    ML_GRF_n(:,i)=interp1(time_f{i},ML_GRF{i},time_n_f{i},'linear');
    V_GRF_n(:,i)=interp1(time_f{i},V_GRF{i},time_n_f{i},'linear');

end

%% DETERMINE MEAN AND SD

for l=1:101

    mean_Coupling_Sagittal_Angle(l)=mean(Coupling_Sagittal_Angle_n(l,:));
    mean_Coupling_Coronal_Angle(l)=mean(Coupling_Coronal_Angle_n(l,:));

mean_Coupling_Transverse_Angle(l)=mean(Coupling_Transverse_Angle_n(l,:));
    mean_Coupling_Axial(l)=mean(Coupling_Axial_n(l,:));
    mean_AP_GRF(l)=mean(AP_GRF_n(l,:));
    mean_ML_GRF(l)=mean(ML_GRF_n(l,:));
    mean_V_GRF(l)=mean(V_GRF_n(l,:));

    std_Coupling_Sagittal_Angle(l)=std(Coupling_Sagittal_Angle_n(l,:));
    std_Coupling_Coronal_Angle(l)=std(Coupling_Coronal_Angle_n(l,:));
    std_Coupling_Transverse_Angle(l)=std(Coupling_Transverse_Angle_n(l,:));
    std_Coupling_Axial(l)=std(Coupling_Axial_n(l,:));
    std_AP_GRF(l)=std(AP_GRF_n(l,:));
    std_ML_GRF(l)=std(ML_GRF_n(l,:));
    std_V_GRF(l)=std(V_GRF_n(l,:));

end

%% EXCEL SPREADSHEET OUTPUT

xlswrite('RB_Coupling 2016-06-02.xls', {'Gait Cycle'
'Coupling_Sagittal_Angle' 'Coupling_Sagittal_Angle + SD'
'Coupling_Sagittal_Angle - SD' 'Coupling_Coronal_Angle'
'Coupling_Coronal_Angle + SD' 'Coupling_Coronal_Angle - SD'
'Coupling_Transverse_Angle' 'Coupling_Transverse_Angle + SD'
'Coupling_Transverse_Angle - SD' 'Coupling_Axial' 'Coupling_Axial + SD'
'Coupling_Axial - SD' 'AP GRF' 'AP GRF + SD' 'AP GRF-SD' 'ML GRF' 'ML GRF +
SD' 'ML GRF-SD' 'V GRF' 'V GRF + SD' 'V GRF-SD'},'Level', 'A1');
xlswrite('RB_Coupling 2016-06-02.xls', [transpose(gait_cycle)
transpose(mean_Coupling_Sagittal_Angle)
```

```
transpose(mean_Coupling_Sagittal_Angle+std_Coupling_Sagittal_Angle)
transpose(mean_Coupling_Sagittal_Angle-std_Coupling_Sagittal_Angle),...

transpose(mean_Coupling_Coronal_Angle)
transpose(mean_Coupling_Coronal_Angle+std_Coupling_Coronal_Angle)
transpose(mean_Coupling_Coronal_Angle-std_Coupling_Coronal_Angle),...

transpose(mean_Coupling_Transverse_Angle)
transpose(mean_Coupling_Transverse_Angle+std_Coupling_Transverse_Angle)
transpose(mean_Coupling_Transverse_Angle-std_Coupling_Transverse_Angle),...
                                        transpose(mean_Coupling_Axial)
transpose(mean_Coupling_Axial+std_Coupling_Axial)
transpose(mean_Coupling_Axial-std_Coupling_Axial),...
                                        transpose(mean_AP_GRF)
transpose(mean_AP_GRF+std_AP_GRF) transpose(mean_AP_GRF-std_AP_GRF),...
                                        transpose(mean_ML_GRF)
transpose(mean_ML_GRF+std_ML_GRF) transpose(mean_ML_GRF-std_ML_GRF),...
                                        transpose(mean_V_GRF)
transpose(mean_V_GRF+std_V_GRF) transpose(mean_V_GRF-std_V_GRF)],...
                                       'Level', 'A2');
```